



University of Venda

SCHOOL OF ENVIRONMENTAL SCIENCES

DEPARTMENT OF ECOLOGY AND RESOURCE MANAGEMENT

**MINERALOGY AND GEOCHEMISTRY OF KAOLINS IN OXIDIC SOILS
DEVELOPED FROM DIFFERENT PARENT ROCKS IN LIMPOPO
PROVINCE, SOUTH AFRICA**

BY

**OYEBANJO, OMOSALEWA OMOLARA
STUDENT No: 16019766**

A THESIS SUBMITTED TO THE DEPARTMENT OF ECOLOGY AND RESOURCE
MANAGEMENT, SCHOOL OF ENVIRONMENTAL SCIENCES, UNIVERSITY OF
VENDA, IN FULFILMENT OF THE REQUIREMENTS FOR THE PHD IN
ENVIRONMENTAL SCIENCES

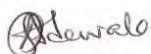
PROMOTER: SENIOR PROF. G.E. EKOSSE

CO-PROMOTER: PROF. J.O. ODIYO

AUGUST 2020

DECLARATION

I, OYEBANJO Omosalewa Omolara, Student Number 16019766, hereby declare that this thesis submitted to the Department of Ecology and Resource Management, School of Environmental Sciences, University of Venda, for the PhD in Environmental Sciences is my own work and has not been previously submitted, in whole or in part, to any university for any degree. Information derived from the published and unpublished work of others has been acknowledged in the text and a list of those references is given.



14th August, 2020

.....
Signature

.....
Date

We certify that this declaration is correct.



19th August 2020

.....
Promoter's Signature

.....
Date

Senior Professor GE Ekosse



.....

...23 August 2020...

Co-promoter's Signature

Date

Professor JO Odiyo

DEDICATION

This thesis is dedicated to God Almighty, the Author and Finisher.

ACKNOWLEDGEMENTS

Acknowledging my indebtedness is exceedingly difficult, first, I owe a debt of gratitude to my promoter, the Director of Research and Innovation, University of Venda, Senior Professor G E Ekosse for his enduring patience, attention to details and consummate professionalism throughout my period of study. My appreciation also goes to my co-promoter, the Dean, School of Environmental Sciences, University of Venda, Professor J O Odiyo without whose contributions, encouragements and support, this thesis would not have been completed.

My sincere appreciation goes to the Management of University of Venda for funding this research through its Research and Publication Committee (RPC). I am grateful to Professor J Odhiambo and Mr P. Tshidada both in the Dept. of Soil Sciences, University of Venda for allowing me to use their laboratory for sample preparation, determination of particle size distribution and colour. Special thanks to members of staff of the School of Environmental Sciences, University of Venda namely: Dr E Stam, Professor W Gitari and Dr Wasiu for allowing me to use the Ecology and Resource Management laboratory for phosphorus adsorption and Fourier transform infrared spectroscopic analyses. I acknowledge Mr G Akintola for his assistance during my fieldwork.

The following analytical laboratories are acknowledged: XRD facility, Dept. of Geology, University of Pretoria, Pretoria for my mineral phase identification and quantification; the Central Analytical Facility, Stellenbosch University for my geochemical analyses; the Mineralogy Section Laboratory, Council for Mineral Technology (MINTeK), Randburg for my petrographical, morphological and microchemical analyses; the Institute of Soil, Climate and Water, Agricultural Research Council, Pretoria for my cation exchange capacity (CEC), exchangeable cations, organic matter, and available Phosphorus analyses; and the Department of Chemistry laboratory, University of Johannesburg for my differential thermal analysis (DTA).

Special thanks to Professor T R Ajayi, Professor C A Ajayi, Professor I A Tubosun, Dr Alayande, Dr and Dr (Mrs) Edokpayi, Mr Kenny Ekanade, Dr Bankole Samson, Mr Tunde Ogunkoya, Dr Bukalo and Dr Durowoju for their unwavering support, advice and

encouragement. I express my gratitude to the Elegbeleyes, the Marshalls, Dr Anyansi and all members and leaders of Christ Tabernacle, University of Venda, for making my spiritual and academic journey a memorable one. To try to name them all would inevitably leave some unmentioned whose help is nonetheless of value even though their names escaped my memory.

I sincerely appreciate my super parents; Pastor and Deaconess Adewale and my parents-in-law for their prayers, love, encouragement and support always. To my siblings, Dr and Mrs Adebayo and Master Adetomiwa Adewale and to the Oyebanjos, the Ogbuewus and the Badmus who have all gone out of their ways to offer me a lasting affection, I am deeply grateful.

An extraordinary thank you to my diamond crown, Olaoluwatikonipekun Moses and to the Loves of my life, Afemisolaoluwatikonipekun Joshua, Morireolaoluwatikonipekun Jedidiah, and Emimololaoluwatikonipekun Joanna, for all the things you do, thank you especially for praying and pushing me to grow, for loving me when I am in a dark place, but never allowing me to stay there, thank you for asking me tough questions, thank you for showing me truth when I need it, grace when I do not deserve it and discernment when I am too confused to understand. I will always love you guys.

Above all, my enormous appreciation goes to my maker, my help in ages past and my hope for years to come, the Almighty God for bringing me to “this place” in my life. To you alone be glory, honour, and adoration forever.

ABSTRACT

Kaolin dominated soils are common in the tropical and subtropical regions. People depend on kaolin-rich soils for agricultural production of food and fiber. The most popular of all South African soils is the Hutton form which accounts for the marvelous redness of the landscape across the Country. The apedal (structureless) soils in the group are characterised by a relatively low CEC ($< 11 \text{ cmol}_c \text{ kg}^{-1}$) reflecting oxidic mineralogy with predominantly kaolinitic assemblage. The geochemical and mineralogical composition of soil kaolin has significant implications on soil fertility, geochemical exploration and engineering properties. Despite the dominance of kaolin in these soils, little is known of their properties in the medium. The nature of kaolin minerals in soils varies with parent material, degree of weathering and pedogenic environment. Most studies conducted in South Africa on kaolins are limited to reference kaolins with little or no publication on soil kaolins, hence, this study.

This research involved the evaluation of mineralogical and geochemical characteristics of oxidic soils and soil kaolins developed from four (4) selected parent rocks which were basalt, granite, arkosic sandstone, and gneiss. Soils developed from quartzite were selected as control. Representative soil samples collected from profiles developed from the different parent rocks were analysed for physico-chemical, mineralogical, and geochemical data.

The mineralogical and geochemical data obtained by x-ray diffractometry (XRD), x-ray fluorescence (XRF), and laser ablation inductively coupled plasma mass spectrometry (LA-ICPMS) were used in unraveling the influence of the provenance and degree of weathering on the soil characteristics. The mineralogical and geochemical data for soil kaolins were determined through XRD, scanning electron microscopy (SEM), Fourier transform infrared (FTIR) spectroscopy, thermogravimetric analysis and differential scanning calorimetry, XRF, and LA-ICPMS to establish their mineralogical and geochemical properties with respect to their parent rocks. Comparison between the soil kaolins and selected reference kaolins were also conducted.

The phosphorus (P) sorption data acquired photometrically were employed to evaluate the relationship between the P sorption capacities of the soils and soil kaolins. The influence of soil properties on the fertility of the soils were assessed based on the physico-chemical (pH, particle size distribution, and electrical conductivity (EC)) and chemical (organic matter (OM) content, cation exchange capacity (CEC), available P, exchangeable cations (Ca, K, Mg, Na, and Al), and P sorption) data. The mineralogical and geochemical data for the parent rocks were obtained by XRD, optical microscopy, XRF, and LA-ICPMS. Multivariate statistical analyses were also conducted.

Results showed that the dominant colour in the studied bulk soils was dusky red (31 %) followed by brown (23 %), reddish brown, yellowish red, and yellowish brown (23 %) as well as strong brown, dark brown, reddish grey, very dark greyish brown, and dark red. Soil textures were clayey to sandy loamy with OM contents between 0.41 and 4.76 %. The pH, EC, CEC, exchangeable cations, and available P values generally ranged from 5.22 to 8.38, 10.25 to 114.40 $\mu\text{S}/\text{cm}$, 2.93 to 18.30 cmol/kg , 0.03 to 13.92 cmol/kg , and <0.01 to 54.99 mg/kg , respectively. Kaolinite and quartz were the dominant phases for soils developed from basalt whereas, quartz and plagioclase were the dominant mineral phases in soils developed from granite, arkosic sandstone, and gneiss, respectively. Other minerals present in the soils were microcline, muscovite, hematite, goethite, montmorillonite, anatase, gibbsite, chlorite, and actinolite.

Geochemical compositions of the bulk soils show relative enrichment of Fe_2O_3 , TiO_2 , CaO , K_2O , MgO , MnO , and Na_2O (except for CaO , K_2O , MgO , MnO , and Na_2O in soils developed from basalt). Chemical index of alteration (CIA), chemical index of weathering (CIW), and plagioclase index of alteration (PIA) values varied between 54.92 and 99.81 % which suggest low to high degree of chemical weathering. The A-CN-K and A-CN-K-FM diagrams for the different soils also support these observations. Trace elements were generally enriched in soils developed from basalt and gneiss (except for Rb, Sr, and Ba in soils developed from basalt), but were depleted in soils developed from granite and arkosic sandstone (except for Cr and Ta). The principal

factors responsible for the mineralogical and geochemical characteristics of the soils were the parent rocks and degree of weathering.

In the soil kaolins, the dominant clay mineral was kaolinite accounting for 23 to 85 wt % followed by montmorillonite, chlorite, and gibbsite. The non-clay minerals like quartz, plagioclase, muscovite, microcline, anatase, goethite, hematite, and actinolite accounted for the remaining percentages. The soil kaolins were characterised by thin platy kaolinite particles with partially to poorly-ordered structural order. The platy kaolinite crystals have their longest dimension sizes between 0.06 and 0.25 μm . The dehydroxylation temperatures for the studied soil kaolins ranged from 425 to 475 $^{\circ}\text{C}$.

The $\text{SiO}_2/\text{Al}_2\text{O}_3$ ratio was lowest in soil kaolins developed from basalt and higher in soils developed from granite, arkosic sandstone, and gneiss which is consistent with their mineralogy since the former have more kaolinite. Higher Fe_2O_3 and CEC values were obtained relative to reference kaolins which could be attributed to the presence of more structural iron in the soil kaolins as well as their smaller crystal sizes. The presence of weatherable and accessory minerals accounted for the enrichment of Co, Ni, Cu, Zn, and Pb in the soil kaolins. The kaolinite in the soils were formed by leaching and desilication of the primary minerals in the parent rocks under suboxic conditions.

H-type P adsorption isotherms obtained for both the soils and soil kaolins indicated their high affinity for phosphorus by chemisorption. The average maximum P adsorption values were in decreasing order of soils developed from basalt > granite > arkosic sandstone > quartzite (control) > gneiss, respectively whereas, for soil kaolins is basalt > granite > quartzite (control) > arkosic sandstone > gneiss, respectively. Relative to other soils developed from different parent rocks, soils developed from basalt (with more clay content) had higher capacity and buffer power for P adsorption. The standard P requirements for the soils ranged from 7.78 to 92.91 mgP/kg and were classified as low based on the Langmuir model. Significant correlation between the P adsorption parameters for the soils and soil kaolins indicated that the later could be taken as a good predictor for P sorption dynamics in the soils.

Electrical conductivity of the soils were taken to be negligible in interfering with plant growth. The available P values were generally below the critical level of 12 – 15 mg/kg for soils developed from basalt, gneiss, and quartzite (control) but higher in soils developed from granite and arkosic sandstone. All the soil evaluation factor (SEF) average values estimated were greater than five indicating that they are not of poor soil fertility. The correlation results between the soil properties and P sorption parameters suggest that several variables can influence the P sorption dynamics of the soil. Regression analyses further indicated that CEC, pH, OM, and clay content in the soils account for 99 % bounding P energy variation whereas, Fe_2O_3 accounts for 76 % P sorption maximum variation in the soils. In addition, variations in Fe_2O_3 and sand contents in the soils account for 96 % and 95 % maximum buffering capacity and external P requirement (EPR) variations, respectively. Models to advance the interplay between the various soil properties and P sorption parameters in the soils were developed.

Mineralogical and geochemical characteristics of the soils were principally controlled by the parent rocks and degree of weathering. The soil kaolins displayed significant differences relative to reference kaolins. Langmuir model is most suited for describing P sorption in soils and soil kaolins developed from different parent rocks within the studied area. P sorption parameters for the soils can readily be obtained from the P sorption parameters of the kaolins present in them. EPR obtained and models for predicting P sorption parameters from selected soil properties developed for the various soils will improve the efficiency of routine P fertilizer applications. Iron oxide (Fe_2O_3) played the most crucial role in explaining the P sorption dynamics of the soils.

The major contributions from this study have been: better understanding of the influence of parent rock characteristics and degree of weathering on the soil characteristics, the nature of soil kaolins and its influence on soil properties as well as P sorption dynamics in soils have been better established, and improvement of the understanding on the relationship between soil properties and P sorption dynamics in the soils.

Keywords: Oxidic soils, kaolins, weathering, fertility, and properties.

TABLE OF CONTENTS

DECLARATION	ii
DEDICATION	iii
ACKNOWLEDGEMENTS	iv
ABSTRACT	vi
TABLE OF CONTENTS	x
LIST OF FIGURES	xvii
LIST OF TABLES	xxiii
LIST OF APPENDICES	xxviii
LIST OF ABBREVIATIONS	xxix
LIST OF UNITS AND SYMBOLS	xxx
CHAPTER ONE: INTRODUCTION	1
1.1 Background	1
1.2 Problem Statement	3
1.3 Motivation	5
1.4 Hypotheses	5
1.5 Objectives	6
1.5.1 Main Objective	6
1.5.2 Specific Objectives	6
1.6 Study Areas	6
1.6.1 Brief description of Study Areas	6
1.6.2 Geology of the Study Areas	8
1.7 Climate	12
1.8 Delimitations	13

CHAPTER TWO: LITERATURE REVIEW	14
2.1 Geology of South Africa	14
2.2 Soil Formation	17
2.2.1 Factors controlling Soil Formation	18
2.2.2 Formation of Kaolins in Soils	21
2.3 Kaolin in Soils	25
2.4 Properties of Soil Kaolins	30
2.4.1 Physico-chemical Properties of Soil Kaolins	30
2.4.2 Mineralogical Properties of Soil Kaolins	31
2.4.3 Geochemical Properties of Soil Kaolins	34
2.5 Occurrence of Soils in South Africa	36
2.5.1 Classification of Soils in South Africa	36
2.5.2 Kaolinitic Rich Soils in South Africa	38
2.6 Soil Kaolins related to Pedoclimatic and Pedogenetic Considerations	40
2.7 Soil Kaolins related to Soil Fertility Management	43
2.8 Research methods review	48
2.8.1 Instrumental Methods	48
2.8.2 Statistical Methods	50
2.10 Concluding Remarks	51
CHAPTER THREE: RESEARCH METHODS	52
3.1 Soil and Rock Sampling	52
3.2 Soil Sample Preparation	53
3.2.1 Separation of Clay and Silt Fractions	57
3.3 Rock Sample Preparation	58
3.4 Laboratory Analyses	58
3.4.1 Analyses of Bulk Soil Samples	58
3.4.1.1 Physico-chemical Analyses	58

3.4.1.2 X-ray Diffraction (XRD) Mineralogical Analyses	62
3.4.1.3 Chemical Analyses	62
3.4.2 Analyses of Clay and Silt Fractions	66
3.4.3 Analyses of Soil Kaolins	67
3.4.3.1 Chemical Analyses	67
3.4.3.2 Mineralogical Analyses	68
3.4.4 Analyses of Parent Rocks	71
3.4.4.1 Mineralogical Analyses	72
3.4.5 Validation of Analytical Procedures	73
3.5 Data Interpretation	73
3.5.1 Sorption Parameters and External Phosphorus Requirement (EPR)	73
3.5.2 Statistical Analyses	74
3.5.3 Weathering Indices	75
3.5.4 Elemental Ratios	76
3.5.5 Discrimination Diagrams	76
3.5.6 Assessment of Soil Fertility Status	76
3.6 Concluding Remarks	76
CHAPTER FOUR: RESULTS	77
4.1 Physico-chemical Properties of the Bulk Soils and Soil Kaolins	77
4.1.1 Colour of the bulk soils	77
4.1.2 Hydrogen Ion Concentration (pH) of the bulk soils	78
4.1.3 Electrical Conductivity (EC) of the bulk soils	79
4.1.4 Texture of the bulk soil	80
4.1.5 Cation Exchange Capacity (CEC)	83
4.1.5.1 CEC of bulk soils	83
4.1.5.2 CEC of Soil Kaolins	83
4.1.6 Available Phosphorus	84
4.1.7 Exchangeable Cations	85
4.1.7.1 Calcium (Ca)	85
4.1.7.2 Magnesium (Mg)	85

4.1.7.3 Potassium (K), Sodium (Na), and Aluminium (Al)	86
4.1.8 Organic Matter (OM)	86
4.2 Mineralogical Properties of the Studied Parent rocks, Soils and Soil Kaolins	86
4.2.1 Petrographic studies of the Parent Rocks	86
4.2.2 X-ray Diffraction (XRD) Studies	92
4.2.2.1 Qualitative Analyses	92
4.2.2.2 Quantitative Analyses	109
4.2.3 Scanning Electron Microscopy with an Energy Dispersive X-ray Spectrum (SEM-EDX) studies	115
4.2.4 Fourier Transform Infrared Spectroscopy	127
4.2.5 Thermogravimetric Analyses (TGA) and Differential Scanning Calorimetry (DSC)	135
4.3 Geochemical Studies	153
4.3.1 Geochemical Properties of Studied Parent rocks	153
4.3.1.1 Major Element Oxides	153
4.3.1.2 Trace Elements	154
4.3.1.3 Rare Earth Elements (REEs)	156
4.3.2 Geochemical Properties of the Bulk soils	157
4.3.2.1 Major Element Oxides	157
4.3.2.2 Trace Elements	159
4.3.2.3 Rare Earth Elements (REEs)	160
4.3.3 Geochemical Properties of the Silt fractions of the studied Soils	163
4.3.3.1 Major Element Oxides	163
4.3.3.2 Trace Elements	164
4.3.3.3 Rare Earth Elements (REEs)	166
4.3.4 Geochemical Properties of the Clay fractions of the studied Soils	166
4.3.4.1 Major Element Oxides	166
4.3.4.2 Trace Elements	168
4.3.4.3 Rare Earth Elements (REEs)	170
4.3.5 Geochemical Properties of Soil Kaolins	171
4.3.5.1 Major Element Oxides	171
4.3.5.2 Trace Elements	172
4.3.5.3 Rare Earth Elements (REEs)	175
4.4 Concluding Remarks	177

CHAPTER FIVE: INFLUENCE OF PROVENANCE AND DEGREE OF WEATHERING ON OXIDIC SOILS DEVELOPED FROM DIFFERENT PARENT ROCKS IN LIMPOPO PROVINCE, SOUTH AFRICA **178**

5.1	Influence of Provenance	178
5.2	Degree of Weathering	192
5.3	Statistical Analyses	203
5.4	Concluding Remarks	210

CHAPTER SIX: THE NATURE OF SOIL KAOLINS DEVELOPED FROM DIFFERENT PARENT ROCKS IN LIMPOPO PROVINCE, SOUTH AFRICA **211**

6.1	Mineralogical Characteristics	211
6.1.1	Mineral Identification and Quantification	211
6.1.2	Kaolinite Crystallinity	213
6.1.3	Kaolinite Morphology	216
6.2	Geochemical Characteristics	217
6.2.1	Major Elements	217
6.2.2	Trace Elements	220
6.2.3	Rare Earth Elements (REEs)	220
6.2.4	Statistical Analyses of Geochemical and Mineralogical Data	224
6.3	Concluding Remarks	230

CHAPTER SEVEN: PHOSPHORUS SORPTION IN SOILS AND SOIL KAOLINS DEVELOPED FROM DIFFERENT PARENT ROCKS IN LIMPOPO PROVINCE, SOUTH AFRICA **232**

7.1	Soils and Soil Kaolins Phosphorus Adsorption Isotherms Characteristics	232
7.2	Adsorption Parameters	234
7.2.1	Langmuir Adsorption Parameters for Soils	234
7.2.2	Freundlich Adsorption Parameters for Soils	238
7.2.3	Langmuir Adsorption Parameters for Soil Kaolins	242
7.2.4	Freundlich Adsorption Parameters for Soil Kaolins	246
7.3	External Phosphorus Requirements (EPR)	249

7.4 Variability of Adsorption Parameters	252
7.4.1 Correlation between Sorption parameters, Provenance, and degree of weathering	252
7.4.2 Test of Hypothesis	254
7.5 Concluding Remarks	255
CHAPTER EIGHT: PROPERTIES OF OXIDIC SOILS DEVELOPED FROM DIFFERENT PARENT ROCKS IN LIMPOPO PROVINCE, SOUTH AFRICA: IMPLICATIONS ON FERTILITY AND PHOSPHORUS ADSORPTION	256
8.1 Soil Properties and Fertility	256
8.1.1 Evaluation of the Soil Fertility Status	261
8.2 Relationship between Sorption Parameters and Soil Properties	262
8.2.1 Bounding Energy and Soil Properties	262
8.2.2 Sorption Maximum and Soil Properties	267
8.2.3 Maximum Buffering Capacity, External Phosphorus Requirements, and Soil Properties	269
8.3 Concluding Remarks	273
CHAPTER NINE: KAOLINS IN OXIDIC SOILS DEVELOPED FROM DIFFERENT PARENT ROCKS IN LIMPOPO PROVINCE, SOUTH AFRICA: INFLUENCE ON SOME SOIL FERTILITY PARAMETERS	274
9.0 Background	274
9.1 Influence of soil kaolins on some soil fertility parameters	274
9.2 Concluding Remarks	282
CHAPTER TEN: CONCLUSIONS AND RECOMMENDATIONS	284
10.1 Conclusions	282
10.2 Recommendations	287
REFERENCES	288
APPENDICES	

LIST OF FIGURES

Figure 1.1:	Map of Limpopo Province showing the locations of the Study Areas	8
Figure 1.2:	Geologic Map of the Soutpansberg Group showing the study areas	9
Figure 1.3	Geologic Map of the Southern Marginal Zone (Limpopo Belt) and Northern Sector of the Kaapvaal Craton showing the study areas	10
Figure 1.4:	Köppen-Geiger Climate classification for Limpopo Province, SA	12
Figure 2.1:	Geologic map of South Africa	14
Figure 2.2:	Simplified geological map showing the main crustal provinces	16
Figure 2.3	Soil Profile	17
Figure 2.4:	Schematic progression of basic and acidic zones through soils during soil development	19
Figure 2.5:	Relative proportions of clay minerals in surface soil horizons	22
Figure 2.6:	Pathways for the formation of kaolinite in soils	23
Figure 2.7:	Octahedral and Tetrahedral units in kaolinite	24
Figure 2.8:	Schematic diagram of kaolinite structure	25
Figure 2.9:	SEM of kaolins in soils	26
Figure 2.10:	TEM of kaolins in soils	26
Figure 2.11:	Relationship between SSA, CSD, and CEC	29
Figure 2.12:	X-ray diffraction patterns of deferated clay fraction	30
Figure 2.13:	SEM of kaolins in geophagic soil	31
Figure 2.14:	TEMs of soil kaolins and reference kaolin	31
Figure 2.15:	Distribution of the soil groups in South Africa	37
Figure 2.16:	Distribution of the soil groups in Limpopo Province	40
Figure 2.17:	The plot Langmuir maximum P retention capacity (X_m) of kaolin from tropical soils against SSA	43
Figure 2.18:	Phosphorus cycle in soil	45
Figure 2.19:	Relationship between soil pH and different forms of P fixation	45
Figure 3.1:	Soil developed from Basalt at Sibasa area	55
Figure 3.2:	Soil developed from Granite Gneiss at Muledane area	55
Figure 3.3:	Soil developed from Granite at Matoks area	56

Figure 3.4:	Soil developed from Arkosic Sandstone at Sagole area	56
Figure 3.5:	Soil developed from Quartzite at Matavhela area	57
Figure 3.6:	Laser 193 nm Excimer interfaced to the Agilent 7700 ICP-MS	66
Figure 3.7:	Zeiss EVO MA15 Scanning Electron Microscope	69
Figure 3.8:	Bruker Alpha Platinum – ATR Spectrometer	70
Figure 3.9:	Olympus BX41 Petrographic Microscope	72
Figure 4.1:	Textural ternary plot for soils developed from basalt	81
Figure 4.2:	Textural ternary plot for soils developed from granite	81
Figure 4.3:	Textural ternary plot for soils developed from arkosic sandstone	82
Figure 4.4:	Textural ternary plot for soils developed from gneiss	82
Figure 4.5:	Textural ternary plot for soils developed from quartzite	83
Figure 4.6:	Photomicrograph of basalt	86
Figure 4.7:	Photomicrograph of basalt	87
Figure 4.8:	Photomicrograph of basalt	87
Figure 4.9:	Photomicrograph of granite	88
Figure 4.10:	Photomicrograph of granite	89
Figure 4.11:	Photomicrograph of granite	89
Figure 4.12:	Photomicrograph of arkosic sandstone	90
Figure 4.13:	Photomicrograph of arkosic sandstone	90
Figure 4.14:	Photomicrograph of arkosic sandstone	91
Figure 4.15:	Photomicrograph of quartzite	91
Figure 4.16:	Mineral phases as determined by XRD of basalt rock	92
Figure 4.17:	Mineral phases as determined by XRD of granite rock	93
Figure 4.18:	Mineral phases as determined by XRD of arkosic sandstone rock	93
Figure 4.19:	Mineral phases as determined by XRD of Quartzite rock	94
Figure 4.20:	Mineral phases as determined by XRD of bulk soils developed from basalt	94
Figure 4.21:	Mineral phases as determined by XRD of bulk soils developed from granite	95
Figure 4.22:	Mineral phases as determined by XRD of bulk soils developed from arkosic sandstone	95
Figure 4.23:	Mineral phases as determined by XRD of bulk soils developed from gneiss	96

Figure 4.24: Mineral phases as determined by XRD of bulk soils developed from quartzite	96
Figure 4.25: Mineral phases as determined by XRD of silt fractions of soils developed from basalt	97
Figure 4.26: Mineral phases as determined by XRD of silt fractions of soils developed from granite	97
Figure 4.27: Mineral phases as determined by XRD of silt fractions of soils developed from arkosic sandstone	98
Figure 4.28: Mineral phases as determined by XRD of silt fraction of soil developed developed from gneiss	98
Figure 4.29: Mineral phases as determined by XRD of silt fractions of soils developed from quartzite	99
Figure 4.30: Mineral phases as determined by XRD of clay fractions of soils (S1)	99
Figure 4.31: Mineral phases as determined by XRD of clay fractions of soils (S2)	100
Figure 4.32: Mineral phases as determined by XRD of clay fractions of soils (S3)	100
Figure 4.33: Mineral phases as determined by XRD of clay fractions of soils (MAT1)	101
Figure 4.34: Mineral phases as determined by XRD of clay fractions of soils (MAT2)	101
Figure 4.35: Mineral phases as determined by XRD of clay fractions of soils (MAT3)	102
Figure 4.36: Mineral phases as determined by XRD of clay fractions of soils (SA1)	102
Figure 4.37: Mineral phases as determined by XRD of clay fractions of soils (SA2)	103
Figure 4.38: Mineral phases as determined by XRD of clay fractions of soils (SA3)	103
Figure 4.39: Mineral phases as determined by XRD of clay fractions of soils developed from gneiss	104
Figure 4.40: Mineral phases as determined by XRD of clay fractions of soils developed from quartzite	104
Figure 4.41: Mineral phases as determined by XRD of soil kaolins (S1)	105
Figure 4.42: Mineral phases as determined by XRD of soil kaolins (S2)	105
Figure 4.43: Mineral phases as determined by XRD of soil kaolins (MAT1)	106
Figure 4.44: Mineral phases as determined by XRD of soil kaolins (MAT3)	106
Figure 4.45: Mineral phases as determined by XRD of soil kaolins (SA2)	107
Figure 4.46: Mineral phases as determined by XRD of soil kaolins (SA3)	107

Figure 4.47: Mineral phases as determined by XRD of soil kaolins (MU1)	108
Figure 4.48: Mineral phases as determined by XRD of soil kaolins	108
Figure 4.49: SEM elemental map of representative soil kaolin developed from basalt	115
Figure 4.50: SEM elemental map of representative soil kaolin developed from basalt	116
Figure 4.51: SEM image of representative soil kaolin developed from basalt	117
Figure 4.52: SEM image of representative soil kaolin developed from basalt	117
Figure 4.53: SEM image of representative soil kaolin developed from basalt	117
Figure 4.54: SEM image of representative soil kaolin developed from basalt	118
Figure 4.55: SEM image of representative soil kaolin developed from basalt	118
Figure 4.56: SEM image of representative soil kaolin developed from basalt	119
Figure 4.57: SEM elemental map of representative soil kaolin developed from granite	119
Figure 4.58: SEM elemental map of representative soil kaolin developed from granite	120
Figure 4.59: SEM image of representative soil kaolin developed from granite	120
Figure 4.60: SEM image of representative soil kaolin developed from granite	121
Figure 4.61: SEM elemental map of representative soil kaolin developed from arkosic sandstone	121
Figure 4.62: SEM elemental map of representative soil kaolin developed from arkosic sandstone	122
Figure 4.63: SEM image of representative soil kaolin developed from arkosic sandstone	122
Figure 4.64: SEM image of representative soil kaolin developed from arkosic sandstone	123
Figure 4.65: SEM elemental map of representative soil kaolin developed from gneiss	123
Figure 4.66: SEM image of representative soil kaolin developed from gneiss	124
Figure 4.67: SEM elemental map of representative soil kaolin developed from quartzite	124
Figure 4.68: SEM elemental map of representative soil kaolin developed from quartzite	125
Figure 4.69: SEM image of representative soil kaolin developed from quartzite	125
Figure 4.70: SEM image of representative soil kaolin developed from quartzite	126
Figure 4.71: SEM image of representative soil kaolin developed from quartzite	126
Figure 4.72: SEM image of representative soil kaolin developed from quartzite	127
Figure 4.73: The IR spectra of soil kaolins developed from basalt between 4000 to 3500 cm^{-1}	131
Figure 4.74: The IR spectra of soil kaolins developed from basalt between 1200 to 500 cm^{-1}	131

Figure 4.75: The IR spectra of soil kaolins developed from granite between 4000 to 3500 cm^{-1}	132
Figure 4.76: The IR spectra of soil kaolins developed from granite between 1200 to 500 cm^{-1}	132
Figure 4.77: The IR spectra of soil kaolins developed from arkosic sandstone between 4000 to 3500 cm^{-1}	133
Figure 4.78: The IR spectra of soil kaolins developed from arkosic sandstone between 1200 to 500 cm^{-1}	133
Figure 4.79: The IR spectra of soil kaolins developed from gneiss between 1200 to 500 cm^{-1}	134
Figure 4.80: The IR spectra of soil kaolins developed from quartzite between 1200 to 500 cm^{-1}	134
Figure 4.81: TGA/DTG and DSC/TGA curves of S1 0-20 cm	137
Figure 4.82: TGA/DTG and DSC/TGA curves of S1 20-50 cm	138
Figure 4.83: TGA/DTG and DSC/TGA curves of S1 50-100 cm	139
Figure 4.84: TGA/DTG and DSC/TGA curves of S2 0-20 cm	140
Figure 4.85: TGA/DTG and DSC/TGA curves of S2 20-50 cm	141
Figure 4.86: TGA/DTG and DSC/TGA curves of S2 50-100 cm	142
Figure 4.87: TGA/DTG and DSC/TGA curves of MAT1 0-20 cm	143
Figure 4.88: TGA/DTG and DSC/TGA curves of MAT1 20-50 cm	144
Figure 4.89: TGA/DTG and DSC/TGA curves of MAT3 0-20 cm	145
Figure 4.90: TGA/DTG and DSC/TGA curves of MAT3 20-50 cm	146
Figure 4.91: TGA/DTG and DSC/TGA curves of SA2 0-20 cm	147
Figure 4.92: TGA/DTG and DSC/TGA curves of SA3 0-20 cm	148
Figure 4.93: TGA/DTG and DSC/TGA curves of SA3 20-50 cm	149
Figure 4.94: TGA/DTG and DSC/TGA curves of MU1 0-20 cm	150
Figure 4.95: TGA/DTG and DSC/TGA curves of CMA 0-20 cm	151
Figure 4.96: TGA/DTG and DSC/TGA curves of CMA 20-50 cm	152
Figure 5.1: Mineral abundances in the soils (A) and parent rocks (B)	181
Figure 5.2: Chondrite-normalised REE pattern of average of the soils developed from basalt and their parent rocks	190
Figure 5.3: Chondrite-normalised REE pattern of average of the soils developed from granite and their parent rocks	190
Figure 5.4: Chondrite-normalised REE pattern of average of the soils developed from	

arkosic sandstone and their parent rocks	191
Figure 5.5: Chondrite-normalised REE pattern of average of the soils developed from gneiss and their parent rocks	191
Figure 5.6: Chondrite-normalised REE pattern of average of the soils developed from quartzite and their parent rock	192
Figure 5.7: CIA ternary diagram for the soils	194
Figure 5.8: A-CN-K ternary diagram showing location of common minerals, UCC, PAAS, and possible weathering trends	196
Figure 5.9: A-CN-K ternary diagram for soils developed from basalt	196
Figure 5.10: A-CN-K ternary diagram for soils developed from granite	197
Figure 5.11: A-CN-K ternary diagram for soils developed from arkosic sandstone	197
Figure 5.12: A-CN-K ternary diagram for soils developed from gneiss	198
Figure 5.13: A-CN-K ternary diagram for soils developed from quartzite	198
Figure 5.14: A-CNK-FM ternary diagram for soils developed from basalt	200
Figure 5.15: A-CNK-FM ternary diagram for soils developed from granite	200
Figure 5.16: A-CNK-FM ternary diagram for soils developed from arkosic sandstone	201
Figure 5.17: A-CNK-FM ternary diagram for soils developed from gneiss	202
Figure 5.18: A-CNK-FM ternary diagram for soils developed from quartzite	202
Figure 5.19: Scree plot of the studied Soils developed from basalt	203
Figure 5.20: Scree plot of the studied Soils developed from granite	204
Figure 5.21: Scree plot of the studied Soils developed from arkosic sandstone	204
Figure 5.22: Scree plot of the studied Soils developed from gneiss and quartzite	205
Figure 6.1: Mineral abundances (wt %) in the soil kaolins developed from different parent rocks	212
Figure 6.2: SEM image of representative soil kaolins developed from basalt	217
Figure 6.3: Chondrite-normalised REE pattern of average of the soil kaolins	223
Figure 6.4: Scree plot of the studied soil kaolins developed from basalt	225
Figure 6.5: Scree plot of the studied soil kaolins developed from granite	225
Figure 6.6: Scree plot of the studied soil kaolins developed from arkosic sandstone, gneiss, and quartzite (control)	226

Figure 7.1: Phosphorus adsorption isotherms for soils developed from different parent rocks in Limpopo Province, South Africa	233
Figure 7.2: Phosphorus adsorption isotherms for soil kaolins developed from different parent rocks in Limpopo Province, South Africa	233
Figure 7.3: Langmuir adsorption isotherm for soils developed from basalt	234
Figure 7.4: Langmuir adsorption isotherm for soils developed from granite	235
Figure 7.5: Langmuir adsorption isotherm for soils developed from arkosic sandstone	235
Figure 7.6: Langmuir adsorption isotherm for soils developed from gneiss	236
Figure 7.7: Langmuir adsorption isotherm for soil developed from quartzite	236
Figure 7.8: Freundlich adsorption isotherms for soils developed from basalt	239
Figure 7.9: Freundlich adsorption isotherms for soils developed from granite	239
Figure 7.10: Freundlich adsorption isotherms for soils developed from arkosic sandstone	240
Figure 7.11: Freundlich adsorption isotherms for soils developed from gneiss	240
Figure 7.12: Freundlich adsorption isotherm for soil developed from quartzite	241
Figure 7.13: Langmuir adsorption isotherms for soil kaolins developed from basalt	243
Figure 7.14: Langmuir adsorption isotherms for soil kaolins developed from granite	243
Figure 7.15: Langmuir adsorption isotherms for soil kaolins developed from arkosic sandstone	244
Figure 7.16: Langmuir adsorption isotherms for soil kaolins developed from gneiss	244
Figure 7.17: Langmuir adsorption isotherm for soil kaolin developed from quartzite	245
Figure 7.18: Freundlich adsorption isotherms for soil kaolins developed from basalt	247
Figure 7.19: Freundlich adsorption isotherms for soil kaolins developed from granite	247
Figure 7.20: Freundlich adsorption isotherms for soil kaolins developed from arkosic sandstone.	248
Figure 7.21: Freundlich adsorption isotherms for soil kaolins developed from gneiss	248
Figure 7.22: Freundlich adsorption isotherm for soil kaolins developed from quartzite	249
Figure 9.1: Binary diagram between % kaolinite, exch. Mg, Ca, Na, Al, and K	277
Figure 9.2: Binary diagram showing relationship between % kaolinite, CIA, CEC, SFI, SEF, and OM	279
Figure 9.3: Binary diagram showing relationship between % kaolinite, pH, and EPR	280
Figure 9.4: PCA Scree plot of % kaolinite and some soil properties	281

LIST OF TABLES

Table 1.1: Lithostratigraphy of the Soutpansberg Group	9
Table 1.2: Lithostratigraphy of granitoid intrusions	11
Table 2.1: Stratigraphy of South Africa	16
Table 2.2: Lattice parameters for kaolin minerals	26
Table 2.3: Key to soil groups in South Africa	37
Table 3.1: Summary Information on the Study Areas	52
Table 3.2: Number of Samples collected at each location	54
Table 3.3a: Summary of the various soil analyses done	59
Table 3.3b: Summary of the various rock analyses done	60
Table 4.1: Hue, Value, Chroma, and Colour of the studied bulk soils	78
Table 4.2: pH and EC ($\mu\text{S}/\text{cm}$) of the studied bulk soils	79
Table 4.3: Textures from the particle size distribution of the studied bulk soils	80
Table 4.4: CEC (cmol/kg) in the Bulk soil and Soil kaolins developed from different Parent Rocks in Limpopo Province, South Africa	84
Table 4.5: Available phosphorus (mg/kg), Exchangeable cations (cmol/kg), and Organic matter (%) in the studied bulk soils	85
Table 4.6: Results of Quantitative analyses of minerals present (wt %) in parent rocks	109
Table 4.7: Results of Quantitative Analyses of Minerals present (wt %) in the Bulk samples of the studied Soils	112
Table 4.8: Results of Quantitative Analyses of Minerals present (wt %) in the Silt Fractions of the studied Soils	112
Table 4.9: Results of Quantitative Analyses of Minerals present (wt %) in the Clay Fractions of the studied Soils	113
Table 4.10: Results of Quantitative Analyses of Minerals present (wt %) in the Soil Kaolins developed from different parent rocks	114
Table 4.11: Elemental Percentages present in the studied Soil kaolins obtained by SEM/EDS	128
Table 4.12: DTG/DSC/TGA Endothermic and Exothermic Peak Temperatures	136
Table 4.13: Major element oxide concentrations (wt %) in parent rocks	155

Table 4.14: Trace element concentrations (ppm) in parent rocks	155
Table 4.15: Rare earth element concentrations (ppm) in parent rocks	156
Table 4.16: Major element oxide concentrations (wt %) in bulk soils	158
Table 4.17: Trace element concentrations (ppm) in bulk soils	161
Table 4.18: Rare earth element concentrations (ppm) in bulk soils	162
Table 4.19: Major element oxide concentrations (wt %) in the silt fractions	165
Table 4.20: Trace element concentrations (ppm) in the silt fractions	165
Table 4.21: Rare earth element concentrations (ppm) in the silt fractions	167
Table 4.22: Major element oxide concentrations (wt %) in the clay fractions	169
Table 4.23: Trace element concentrations (ppm) in the clay fractions	169
Table 4.24: Rare earth element concentrations (ppm) in the clay fractions	171
Table 4.25: Major element oxide concentrations (wt %) in the soil kaolins	173
Table 4.26: Trace element concentrations (ppm) in the soil kaolins	174
Table 4.27: Rare earth element concentrations (ppm) in the soil kaolins	177
Table 5.1a: Major element oxides (wt %) and CIA of Oxidic Soils developed from different parent rocks in Limpopo Province, South Africa and for average UCC	179
Table 5.1b: Major element oxides (wt %) and CIA of different Parent rocks	179
Table 5.2: Major element oxide ratios between the soils and their respective parent rocks	181
Table 5.3a: Trace element concentrations (ppm) of Oxidic Soils developed from different parent rocks in Limpopo Province, South Africa and for average UCC and Critical Concentrations	183
Table 5.3b: Trace element concentrations (ppm) of different parent rocks	184
Table 5.4: Trace element ratios between the soils and their respective parent rocks	184
Table 5.5: Ti-normalised enrichment factor of trace elements for the Oxidic soils	185
Table 5.6a: Rare earth element (REE) concentrations (ppm) and elemental ratios of the Oxidic soils	188
Table 5.6b: Rare earth element (REE) concentrations (ppm) in the different parent rocks	189
Table 5.7: Factor Loadings obtained from Principal Component Analysis of the studied Soils developed from basalt	206

Table 5.8: Factor Loadings obtained from Principal Component Analysis of the studied Soils developed from granite	207
Table 5.9: Factor Loadings obtained from Principal Component Analysis of the studied Soils developed from arkosic sandstone	208
Table 6.1: Structural order of kaolinites in soils developed from different Parent rocks using IR-N classification	215
Table 6.2: Major element oxides (wt %) of soil kaolins	218
Table 6.3: Trace elements concentrations (ppm) of soil kaolins	221
Table 6.4: Rare Earth Elements concentrations (ppm) of soil kaolins	222
Table 6.5: Factor Loadings obtained from Principal Component Analysis of the studied Soil kaolins developed from basalt	227
Table 6.6: Factor Loadings obtained from Principal Component Analysis of the studied Soil kaolins developed from granite	228
Table 6.7: Factor Loadings obtained from Principal Component Analysis of the studied Soil kaolins developed from arkosic sandstone, gneiss, and quartzite	229
Table 7.1: Phosphorus adsorption parameters for soils developed from different parent rocks in Limpopo Province, South Africa	238
Table 7.2: Redlich-Peterson (b_R) and Sips ($1/n$) model exponents for the studied soils and soil kaolins	242
Table 7.3: Phosphorus Adsorption Parameters for soil kaolins developed from different parent rocks in Limpopo Province, South Africa	245
Table 7.4: External Phosphorus Requirements (EPR) values for soils developed from different parent rocks in Limpopo Province, South Africa	250
Table 7.5: External Phosphorus Requirements (EPR) values for soil kaolins developed from different parent rocks in Limpopo Province, South Africa	250
Table 7.6: The magnitude of P adsorption in the soils studied	251
Table 7.7: Pearson Correlation Coefficients between Sorption parameters, Provenance, and degree of weathering	253
Table 7.8: T-test for significance of difference in P sorption parameters between soils soils and soil kaolins developed from different parent rocks	254

Table 8.1: Physico-chemical parameters, fertility indices (SFI), and evaluation factors (SEF) of Oxidic Soils developed from the different parent rocks	257
Table 8.2: pH requirements for plants	257
Table 8.3: Soil conductivity limits	258
Table 8.4: Pearson correlation matrix for linear relationships between parameters for Oxidic Soils developed from the different parent rocks	259
Table 8.5: Soil CEC classification	261
Table 8.6: Pearson correlation matrix for linear relationships between sorption parameters and properties of Oxidic Soils developed from the different parent rocks	262
Table 8.7: Variables entered/removed for each of the models where bounding energy is the dependent variable	264
Table 8.8: ANOVA of the models with bounding energy as the dependent variable	264
Table 8.9: Regression coefficients of the models when each soil variable was removed with bounding energy as the dependent variable	265
Table 8.10: Regression coefficients of the excluded variables for models with bounding energy as the dependent variable	266
Table 8.11: Statistics summary of each regression model with bounding energy as the dependent variable	267
Table 8.12: Variables entered/removed for the model where sorption maximum (X_m) is the dependent variable	268
Table 8.13: Regression coefficients of the excluded variables for the model with sorption maximum (X_m) as the dependent variable	268
Table 8.14: ANOVA of the model with sorption maximum as the dependent variable	269
Table 8.15: Regression coefficients of the model with sorption maximum as the dependent variable	269
Table 8.16: Statistics summary of the regression model with sorption maximum as the dependent variable	269
Table 8.17: Variables entered/removed for the models where aX_m and EPR are the dependent variables	270
Table 8.18a: Regression coefficients of the excluded variables for the models with	

aXm as the dependent variable	270
Table 8.18b: Regression coefficients of the excluded variables for the models with EPR as the dependent variable	271
Table 8.19a: Regression coefficients of the models with aXm as the dependent variable	271
Table 8.19b: Regression coefficients of the models with EPR as the dependent variable	272
Table 8.20a: Statistics summary of the regression model with aXm as the dependent variable	272
Table 8.20b: Statistics summary of the regression model with EPR as the dependent variable	273
Table 9.1: Pearson correlation matrix for linear relationships between % kaolinite and some soil properties	276
Table 9.2: Factor Loadings obtained from Principal Component Analysis of % kaolinite and some soil properties	286

LIST OF APPENDICES

Appendix 4.1: Position and assignment of IR bands of soil kaolins and theoretical kaolinite	ii
Appendix 7.1: Phosphorus adsorption raw data	iii
Appendix 7.2: Redlich-Peterson and Sips Isotherm plots	v
Research outputs	xii

LIST OF ABBREVIATIONS

AAS	: Atomic absorption spectrometry
ANOVA	: Analysis of variance
ATR	: Attenuated total reflectance
BDL	: Below detection limit
CEC	: Cation exchange capacity
CIA	: Chemical index of alteration
DTA	: Differential thermal analysis
EF	: Enrichment factor
EPR	: External phosphorus requirement
FTIR	: Fourier transform infrared
Ga	: Giga annum (Billion years)
HREE	: Heavy rare earth elements
IR	: Infrared
LA-ICPMS	: Laser ablation inductively coupled plasma mass spectrometer
LOI	: Loss on ignition
LREE	: Light rare earth elements
Ma	: Mega annum (Million years)
OM	: Organic matter
PPL	: Plain polarised light
REE	: Rare earth elements
SDGs	: Sustainable development goals
SEF	: Soil evaluation factor
SEM	: Scanning electron microscopy

SFI : Soil fertility indices
UCC : Upper Continental Crust
XPL : Cross polarised light
XRD : X-ray diffractometry

LIST OF UNITS AND SYMBOLS

Al	: Aluminium
Al ₂ O ₃	: Aluminium oxide
Å	: Angstrom
cmol/kg	: Centimoles per kilogram
cm	: Centimeter
dS/cm	: Decisiemens per centimeter
°C	: Degrees Celsius
Eu	: Europium
H	: Hertz
HCl	: Hydrogen chloride
HF	: Hydrogen fluoride
Fe ₂ O ₃	: Iron oxide
La	: Lanthanum
Lu	: Luthetium
kbar	: Kilobar
kg	: Kilogram
kg/ha	: Kilograms per hectare
km	: Kilometer
kW	: KiloWatt
kV	: KiloVolt
µm	: Micrometer
µS/cm	: MicroSiemens per centimeter
mg/kg	: Milligrams per kilogram

nA	: NanoAmperes
nm	: Nanometer
HNO ₃	: Nitric acid
ppm	: parts- per- million
%	: Percent
P	: Phosphorus
K	: Potassium
Si	: Silicon
H ₂ O	: Water
wt. %	: Weight percent

Chapter One

Introduction

This chapter gives the background, problem statement, motivation, hypotheses, objectives, study areas, climate, and delimitations of the study.

1.1 Background

Soil is the major source of nitrogen, mineral elements including potassium (K), calcium (Ca), phosphorus (P), magnesium (Mg), and silicon (Si), and water for plants. Solid materials in soils comprise about 50% of the soil volume, with the remaining volume occupied by water and air. Plant nutrients exist in soils as either anions or cations. Plants uptake these essential elements in ionic forms from the soils through their roots and from the air through their leaves (Weil and Brady, 2017). There are problems in the availability of these elements necessary for plant growth in soils. The two main chemically active components of soils (organic matter and clay minerals) have the capacity to fix ions. Soil organic matter (SOM) through its cation exchange capacity (CEC) hold nutrient cations (K, Ca, and Mg) in easily exchangeable form wherein they can be used by plants. The CEC of SOM in most agricultural soils within the pH range of 5 to 7.5 is mainly from carboxyl groups that lost hydrogen ion (H^+) and thus gained a negative (-) charge (Magdoff and Weil, 2004). Havlin *et al.*, (2014) and Kome *et al.* (2019) reported that the dominant ion exchanger in soils is the clay mineral present.

Clay minerals are a group of aluminosilicates composed of layers of silica (Si) tetrahedral and aluminium (Al) octahedral sheets. The sheet units have the chemical composition $(Al, Si)_3O_4$ (Wilson, 2013). In clays, the tetrahedral sheets are always bonded to octahedral sheets formed from small cations, such as aluminum or magnesium, and coordinated by six oxygen atoms. The ratio between Si and Al sheets determine the clay mineral type. Clay minerals exist in 1:1, 2:1, and 2:1:1 form. Kaolin is the most common 1:1 clay and is composed of one Si sheet and one Al sheet (Murray, 2007). Highly weathered soils of tropical and subtropical regions are dominated by

kaolin minerals, oxides of iron, aluminum, and titanium and resistant minerals such as quartz and zircon (Hughes *et al.*, 2009). High proportion of the world's population relies on kaolin-rich soils for agricultural production of food and fiber (ISSS, 1998).

The weathering of primary minerals present in the parent rock plays a major role in the overall soil mineralogical and geochemical characteristics. Parent rock has a marked influence on the type and nature of clay minerals in the soil profile. Heckman and Rasmussen (2011) reported vast differences in the CEC, clay content, Fe-oxides, as well as clay mineralogy between soils developed from felsic and mafic rocks. In addition, the kind of soil that develops from a parent rock would be markedly affected by the nature of the clay minerals present. Some soil properties are related, directly or indirectly, to their dominant kaolin mineralogy. Some of the soil chemical properties include low-pH and weak- pH buffering, Al toxicity, low available P and high P-fixation capacity, deficiencies of Na, Ca, Mg, K and micronutrients, and low CEC (Schwertmann and Herbillon, 1992). Soil physical processes, particularly those relating to aggregation and dispersion, may depend on the crystal properties of kaolin and some kaolinitic soils exhibit poor structure (Dixon, 1989). However, despite the dominance of kaolin in soils of the tropics, little is known of the extent to which the properties of kaolin vary in tropical soils and how this variation affects soil properties.

Based on climate and soil characteristics, only 12% of South African soils is suitable to produce rain-fed crops whereas only 3% can be considered to be truly fertile land. The population of South Africa is growing at 2% per year and is expected to attain 82 million by 2035 against its current 54 million. This implies that food production or imports must increase using the same or fewer natural resources (Stats SA, 2014). According to a report by the Department of Agriculture, Republic of South Africa (2003), most South African soils are deficient in phosphorus (P). The deficiency of P in soils have been linked to low P in the parent rocks and high sorption property of kaolin minerals present in the soils of tropical and subtropical environments and thereby making applied P unavailable to plants (Siradz, 2008). The P sorption capacity of kaolin in soils is related to its surface area where more Al-OH sites on the faces and edges are exposed; these sites are where P sorption occurs. In acidic soils, although both positive (+) and negative (-) sites exist, the kaolin mineral edge surfaces have a net (+) charge due to

excess H^+ ions associated with the exposed Si-OH and Al-OH groups at low pH. The predominance of + charges readily attracts P ions (Havlin *et al.*, 2014). Chemical fertilizers are well known for their acidity and basicity – forming effects. Both nitrogen and phosphorus based fertilizers are known for these effects.

The overuse of fertilizers to increase soil productivity contributes to environmental pollution of rivers and groundwater. Nitrogen released into the atmosphere as nitrous oxide – a greenhouse gas is 300 times more potent than carbon dioxide (EPA, 2010). Surplus P in aquatic environments can lead to excess algal growth, resulting in oxygen depletion and fish death. Hence, the study seeks to pioneer the characterisation of soil kaolins from soil profiles developed on granite, basalt, gneiss, and arkosic sandstones in South Africa, which will form the basis for developing appropriate soil fertility management procedures in several agricultural production systems.

1.2 Problem Statement

Parent rocks as a major factor in soil formation determines the mineralogical and geochemical characteristics of soils and clay minerals that forms in any given environment. The effect of the parent rocks on soil characteristics is believed to diminish as weathering intensity increases (Nesbitt and Young, 1989). Hence, unravelling the influence of provenance and weathering on soil characteristics is crucial in fertility management.

A review on soil mineralogy research in South Africa between 1978 and 2002 (Buhmann *et al.*, 2004) revealed that most articles (over 160 publications) on soil clay mineralogy usually present data on clay compositions without discussion. Despite the dominance of kaolin in soils, little is known of their properties in the medium (Yoothong *et al.*, 1997). Previous studies conducted in South Africa on kaolins are limited to standard kaolins with little or no publication on soil kaolins. The study of pure or standard clay deposit may serve as a basis in understanding kaolin in soils. Hart *et al.* (2002) and Hughes *et al.* (2009) reported that soil kaolin characteristics differ greatly when compared to standard mineral kaolin in that the former commonly have high defect structures, complex crystal morphologies, very small crystal size and appreciable structural iron. The nature of kaolin minerals varies with parent material, degree of

weathering and pedogenic environment (Watanabe *et al.*, 2006). Based on recent investigations of soil kaolins from Indonesia, Western Australia, and Thailand, Hart *et al.* (2002, 2003) observed significant differences in their properties within a single geographic region and particularly within a single profile. Till date, no attempt has been made to unravel the characteristics of soil kaolins developed on different parent rocks in South Africa leading to a great omission in the overall clay minerals body of knowledge in this part of the world. Hence, the research being proposed will be directed towards filling the gap in the knowledge of soil kaolins in Limpopo Province, South Africa. The resulting understanding will be very useful in agricultural and environmental management because the characteristics of the soil kaolins will affect the overall physical, mineralogical, and chemical properties of the soils (Singh and Gilkes, 1992).

The health of an agricultural production system for field crop, horticulture, and livestock depends largely on the quality of the soil in relation to its organic matter richness and right balance of plant nutrients (Imasuen and Onyeobi, 2013). These two qualities are greatly influenced by the clay mineral composition. Soil clay mineralogy influences organic matter dynamics in soils, sorption and ion reactions, and fixation of nutrients (Hart *et al.*, 2003). The World Bank Report on Agricultural and Rural Development in Sub-Saharan Africa identified low soil fertility and uncertainty of water availability during plant growth as the two main constraints hindering improved agricultural production in the region (Gregory and Bumb, 2006).

Low soil fertility due to certain nutrient deficiencies (P, N, and K) in some South African soils necessitated the heavy reliance on the application of fertilisers, further causing increase in input cost and environmental degradation (Meyer *et al.*, 2004). Matthews and Bernard (2015) reported that the limited freshwater surface water resources in South Africa has been greatly affected by eutrophication due to nutrient enrichment and the associated excessive plant growth in water bodies. Schoumans *et al.* (2014) concluded that agricultural phosphorus (P) losses are well documented as a major contributor to eutrophication of surface water due to excess fertilisation to increase crop yield. Population growth has excessively increased the demand for food which has necessitated the rise in the use of fertilizer to improve crop yield. The nutrient sorption capacities of soils have been linked to the sorption capacity of soil kaolins (Gilkes and

Prakongkep, 2016). Hence, understanding the sorption properties of soil kaolins in South Africa is crucial in increasing the precision in the application of fertilisers. This will minimise over-fertilisation and under-fertilisation problems in soil, reduce the influx of nutrients into freshwater systems, and optimise economic returns on the fertiliser input cost.

1.3 Motivation

Studies in soil mineralogy have been inadequate in evaluating the role of clay minerals present in predicting soil behaviour especially from agricultural and environmental points of view (Buhmann *et al.*, 2004). This study is critical at a time like this considering the new sustainable development goals (SDGs). One of the foci of the SDGs is to eradicate poverty and hunger (Food insecurity) among millions of the world's human population through increased and sustainable food production. This is hindered by low agricultural productivity in many Sub-Saharan African (SSA) countries. The low agricultural productivity has been attributed to nutrient deficiency linked directly to soil fertility which Kutu and Diko (2011) described to be related to the clay mineralogical compositions of the soils in the region.

Wiriyakitnateekul *et al.* (2010) advocated that agricultural development in tropical and subtropical countries will require the optimum utilisation of soil mineral resources which are dominated by kaolins. Costanza *et al.* (2014) argued that to achieve a prosperous, high quality of life that is equitably shared and sustainable by the end of 2030, an integrated multidisciplinary approach in all aspects of scientific research is required especially in the area of agriculture and the environment. With regards to sustainable agricultural production, the knowledge gained from this research on phosphorus sorption capacity of soil kaolins will no doubt provide an economically and environmentally sound nutrient management options in relation to the soil's geologic parent rocks.

1.4 Hypotheses

- The mineralogy and geochemistry of the soil is influenced by the degree of weathering and parent rock.

- The mineralogical and geochemical properties of soil kaolins vary systematically with parent rock.
- The phosphorus sorption capacity of soils within tropical and subtropical region equals to that of soil kaolins present in them.
- Variations in the nature of soil properties have direct implications on the soil fertility and phosphorus sorption capacity.

1.5 Objectives

1.5.1 Main Objective

The main objective of the research is to evaluate the characteristics of selected soils and soil kaolins in Limpopo Province, South Africa and their possible effects on soil fertility.

1.5.2 Specific Objectives

Specific objectives of this study are summarised below:

- To assess the influence of provenance and degree of weathering on the mineralogical and geochemical characteristics of soils developed from different parent rocks in Limpopo Province, South Africa.
- To establish the variations in the mineralogical and geochemical characteristics of the soil kaolins developed from different parent rocks in Limpopo Province, South Africa.
- To evaluate the relationship between the phosphorus sorption capacities of the soils and soil kaolins.
- To assess the degree of variability in the soil fertility and phosphorus sorption capacity in relation to the soil properties.

1.6 Study Areas

1.6.1 Brief Description of Study Areas

The study areas are located within the Vhembe and Capricorn Districts in Limpopo Province, South Africa (Fig. 1.1). The Vhembe District is located at the periphery of the South African land borders with Zimbabwe, Botswana, and Mozambique. The district is

the hub of commercial farming in the Limpopo Province with two distinct agro-systems; north of the Soutspanberg mountain range, one finds a semi-arid area that is primarily used for livestock organic ranching and where irrigation is possible, horticultural production. In the south of the Soutspanberg are subtropical and higher-rainfall areas with valleys and hillsides, where farming involves mixed cultivation, plantation forestry and fruit and nut cultivation (Hall *et al.*, 2013). The Capricorn District named after the tropic of Capricorn which passed through it is the economic hub of the Limpopo Province.

- **Study sites**

The research involved the study of four selected soil profiles developed from granite, basalt, arkosic sandstone, and granite gneiss respectively within the Limpopo Province in South Africa. These include:

1. Soils developed from basalt and granite gneiss are in Sibasa and Muledane respectively within the Thulamela Municipality of Vhembe District, Limpopo Province (Fig. 1.1). The municipality has the highest population size of 618,462 based on the 2011 census and agricultural production within the Limpopo Province. The municipality's economic strength is in agriculture and eco-tourism (Stats SA, 2017).
2. Soils developed from granite are in Matoks within the Molemole Municipality of Capricorn District, Limpopo Province (Fig. 1.1). The population size of the municipality is 108,321 which is the smallest in the Capricorn District based on 2011 census. The municipality's economic strength is in agriculture (Stats SA, 2017).
3. Soils developed on arkosic sandstone are in Sagole within the Musina Municipality of Vhembe District, Limpopo Province (Fig. 1.1). The municipality has a population size of 132, 000. The municipality is rich in natural resources such as gold, diamond, nickel, coal, and magnesium. The municipality's economic strength is in mining and tourism (Stats SA, 2017).

1.6.2 Geology of the Study Areas

The geology of the study areas is briefly described below:

- i. The soils developed from basalt and arkosic sandstone occur within the Sibasa Basalt Formation and Wyllie's Poort Formation respectively of the Soutpansberg Group (Fig. 1.2). The stratigraphy of the Group comprises of both volcanic and sedimentary succession which has been subdivided into six formations (Table 1.1) (SACS, 1980; Brandl, 1999; and Barker *et al.*, 2006).

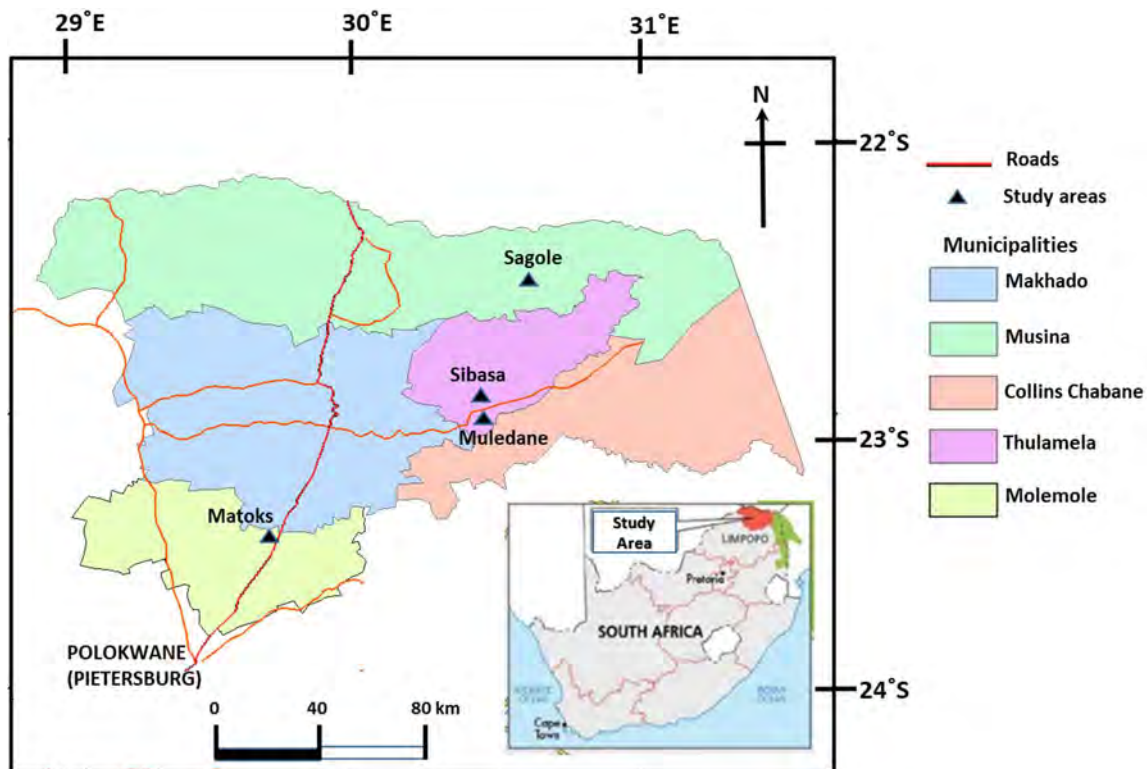


Figure 1.1: Map of Limpopo Province showing the locations of the Study Areas (Modified after Hall *et al.*, 2013).

- ii. **The Sibasa Basalt Formation:** this is a sequence composed of cyclically erupted basalts. They are generally aphanitic – fine grained with colour variation from blackish to light green depending on the degree of epidotisation. Amygdaloidal varieties have vesicles filled with quartz and chalcedony. The matrix is made up of clinopyroxene (mainly augite) and plagioclase. Interbedded clastic sediments which include quartzite, shale, and minor conglomerate locally

reach a maximum of 400 m. The formation thickness is estimated to reach about 3000 m (Barker *et al.*, 2006).

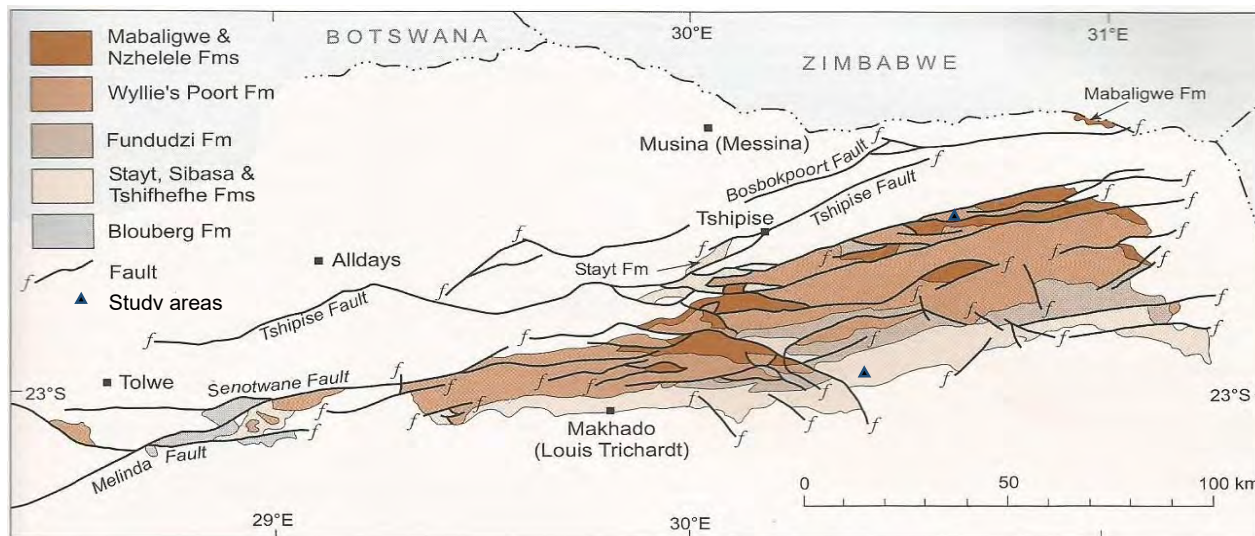


Figure 1.2: Geologic Map of the Soutpansberg Group showing the study areas (Modified after Barker *et al.*, 2006).

Table 1.1: Lithostratigraphy of the Soutpansberg Group (SACS, 1980; Brandl, 1999; and Barker *et al.*, 2006).

Formation	Lithology
Nzhelele	Red argillaceous and arenaceous sediments with thin layers of pyroclastic rocks
Musekwa	Basalts with coarse gabbroic texture
Wyllie's Poort	Quartzitic and Feldspathic (arkosic) sandstones
Fundudzi	Arenaceous and argillaceous rocks with intercalated bands of lava
Sibasa	Dominantly basalts with intercalation of quartzite, shale and minor conglomerate
Tshifhefhe	Epidotised clastic sediments including shale, greywacke, and conglomerate.

The Wyllie's Poort Formation: This formation according to Brandl (1981) underlies the major part of the more mountainous ground of the Soutpansberg Group. Its basal contact has been interpreted as a regional unconformity (Cheney *et al.*, 1990). It is medium- to coarse grained with prominent agate conglomerate at the base in some areas. Towards the eastern part of Tshipise, the uppermost portion of the Formation is

well-bedded, light coloured feldspathic (arkosic) sandstone. In addition, minor lenticular intercalations of basaltic lava and pyroclastic rocks are developed in the eastern regions. Its maximum recorded thickness is 1,500 metres.

- iii. The soils developed from granite and granite gneiss occur within the Matok Granite and Goudplaats-Hout River Gneiss Suite of the Southern Marginal Zone, Limpopo Belt (Fig. 1.3 and Table 1.2). The Southern Marginal Zone separated from the adjacent Kaapvaal Craton by the Hout River Shear Zone comprises of the Bandelierkop Complex, Goudplaats-Hout River Gneiss, Matok Granite, and Palmietfontein Granite respectively (Kramers *et al.*, 2006).

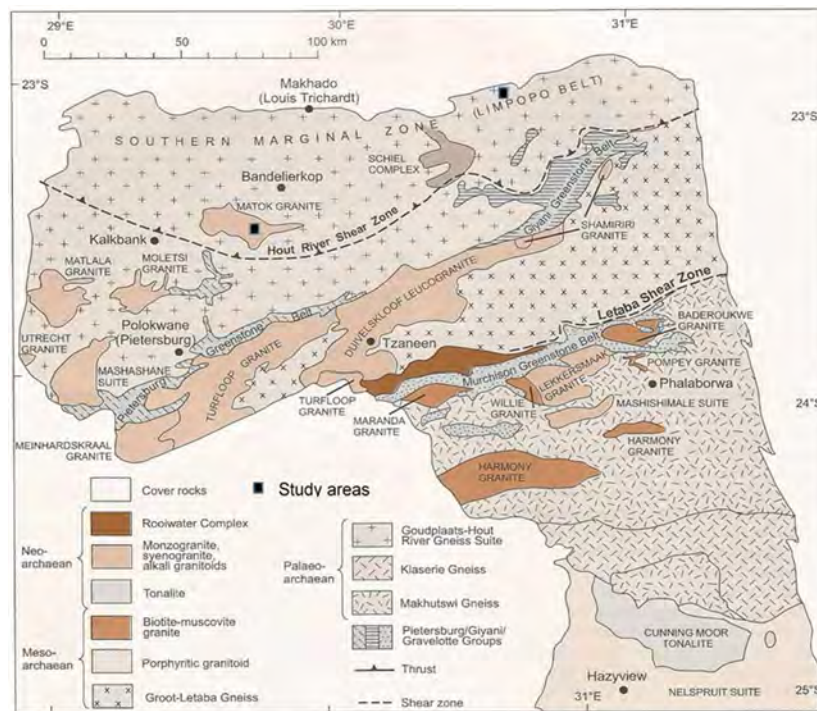


Figure 1.3: Geologic Map of the Southern Marginal Zone (Limpopo Belt) and Northern Sector of the Kaapvaal Craton showing the study areas (Modified after Robbs *et al.*, 2006).

The **Matok Granite** is emplaced north of the Hout River Shear zone. It intruded an earlier charno-enderbitic unit which occurs preferentially in the northern part of the granite body. The granite is whitish to pink in colour, medium grained to porphyritic with a range of composition from granitic to granodioritic while the charnockitic suite comprises of both enderbite and charno-enderbite. The charno-enderbitic units are fine-

to medium grained, greyish green to olive green rocks that are composed of quartz, plagioclase, orthoclase, hyperstene, and augite. Radiometric ages between 2663 and 2666 Ma from zircon U-Pb dating have been recorded for the granitic suite (Barton *et al.*, 1992).

Table 1.2: Lithostratigraphy of granitoid intrusions in the northeastern Kaapvaal Craton based on known emplacement ages (Modified after Robbs *et al.*, 2006).

Rock Unit/Locality	Lithology
Matok Granite	Granite
Uitloop Granite	Granite
Lekkersmaak Granite	Porphyritic granite
Mashishimale Suite	Peraluminous granite
Rooiwater Complex	Hornblende tonalite
Turfloop Granite	Porphyritic granodiorite
Willie Granite	Porphyritic granite
Gravelotte area	Pegmatite
Melkboomfontein Granite	Granite
Maranda Granite	Granite
Baderoukwe Granite	Trondhjemite
Makhutswi Gneiss	Tonalite gneiss
Harmony Granite	Trondhjemite
Goudplaats-Hout River Gneiss	Migmatitic tonalite gneiss

The **Goudplaats-Hout River Gneiss Suite** comprises of a wide spectrum of granitoid gneiss of various types and compositions. According to Robbs *et al* (2006), the migmatitic gneiss within the Southern Marginal Zone of the Limpopo Belt is well layered with granodioritic composition. It is composed of oligoclase, quartz, alkali feldspar, biotite, and minor hornblende. Also present is the coarse-grained to pegmatoidal leucocratic granite composed of plagioclase, quartz, perthite, and minor biotite. In places where it forms large masses, they may be discordant to the regional fabric within the gneisses. Radiometric minimum age of 2671 ± 2 Ma from multi-grain zircon U-Pb dating has been obtained for the Goudplaats-Hout River Gneiss (Barton *et al.*, 1992).

1.7 Climate of the study areas

In a broader sense, the climate of Limpopo Province, South Africa is categorised under the subtropical climate (Schulze, 1997, Maponya and Mpandeli, 2015). However, based on the Köppen Geiger Classification, the climatic conditions of the study areas within the Vhembe and Capricorn Districts of Limpopo Province varies spatially from being arid in the north (Bwh), temperate in the central areas (Cwa and Cwb), and arid in the eastern and western boundaries, with few sub-humid pockets in the centre (Fig. 1.4) (Conradie, 2012). It is characterised by hot summer months with high temperature and humidity during summer and cool mild dry windy weather in winter period.

Data from the weather base station in Thohoyandou in the last 112 years shows that the average monthly temperature is relatively warm throughout the year ranging from 15.6 °C (June) to 23.9 °C (January). Monthly average precipitation ranges between 7.6 mm (July) to 154.4 mm (February) and rainfall cycles during summer period starts from September extending to March. The weather often becomes windy during summer period (Maponya and Mpandeli, 2015).

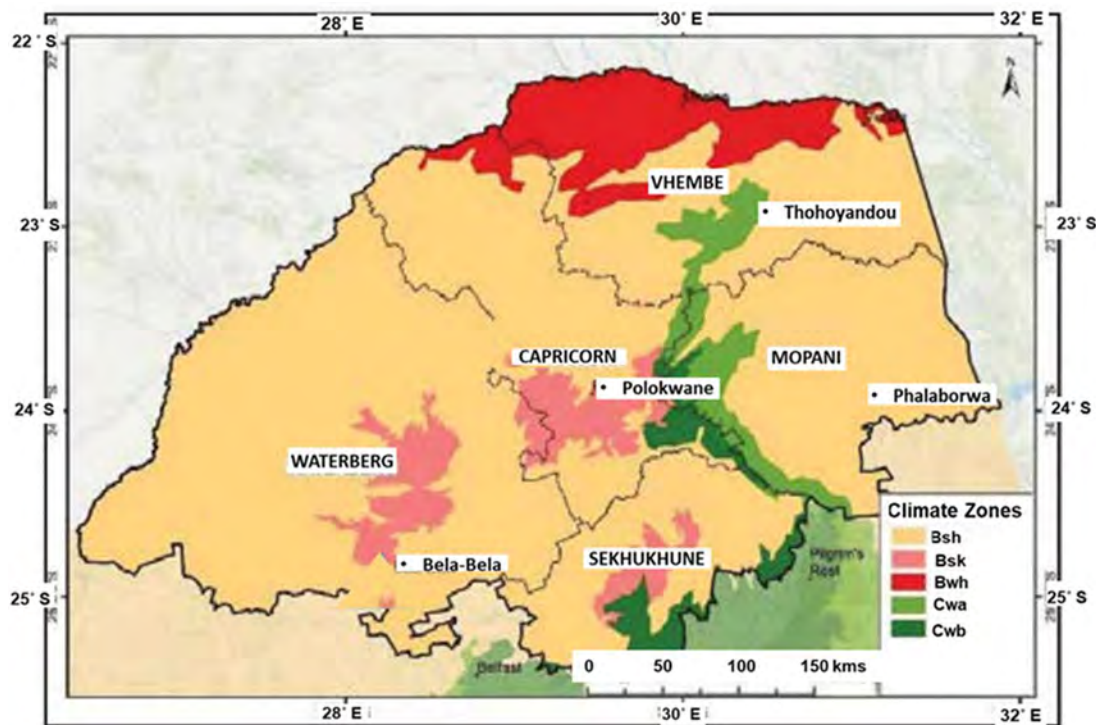


Figure 1.4: Köppen-Geiger Climate classification for Limpopo Province, South Africa (Conradie, 2012).

1.8 Delimitations

The current research focused only on soil kaolins from selected soil profiles that developed from granite, basalt, gneiss, and arkosic sandstone rocks in South Africa. Other rock types being parent rocks to soils not related to kaolins were not considered. The term 'soil kaolin' is used in this study in terms of the predominance of kaolin minerals in the soils relative to other clay minerals.

Chapter Two

Literature Review

This chapter reviews available literature on Geology of South Africa, soil formation, kaolin in soils, formation of kaolin in soils, properties of soil kaolins, distribution of kaolin-rich soils in South Africa, soil kaolins related to pedoclimatic and pedogenetic considerations, and soil kaolins related to soil fertility management.

2.1 Geology of South Africa

South Africa has a long and complex geological evolution which covers about 3.6 billion years (Ga) of Earth history (Fig. 2.1 and Table 2.1). The geology of South Africa has been divided into three Eon subdivisions, namely Archaean Eon, Proterozoic Eon, and Phanerozoic Eon. The Limpopo mobile belt falls within the Archaean Eon (Johnson *et al.*, 2006).

The Archaean Eon in South Africa can be divided into two older (>2.5 Ga) cratonic domains—the Kaapvaal and Zimbabwe Cratons in the eastern half and two younger (< 2.5 Ga) cratonic domains—the Angola and Maltahohe Cratons in the western half. Separating these cratons are mobile belts: the Limpopo Belt between the Kaapvaal and Zimbabwe Cratons, and the Damara Belt between the Angola and Maltahohe Cratons (Zhao *et al.*, 2002) (Fig. 2.2).

The Limpopo Belt is a high-grade metamorphic orogen that has an ENE–WSW elongation of about 650 km and a width of 200 km. The belt itself has conventionally been subdivided into three zones, a central zone bordered symmetrically by the northern and southern marginal zones which abut the southern edge of the Zimbabwe Craton and the northern edge of the Kaapvaal Craton, respectively. These zones are separated from each other, and from the adjacent cratons, by prominent terrane boundaries (Van Reenen *et al.*, 1990; Holzer *et al.*, 1998). The Limpopo Belt is synchronous with the deposition of the volcano-sedimentary sequences of the Dominion Group, Witwatersrand and Ventersdorp Supergroups.

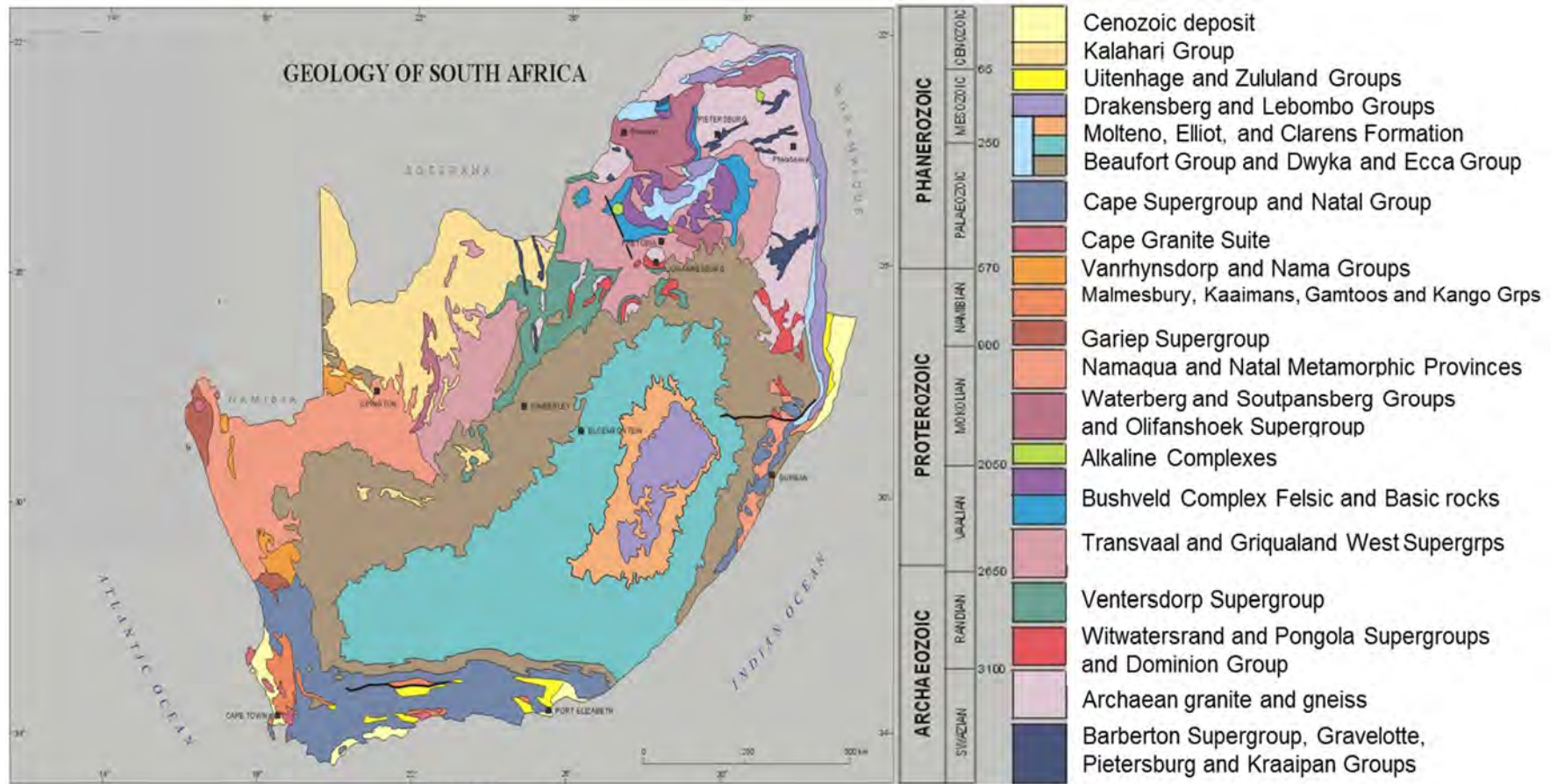
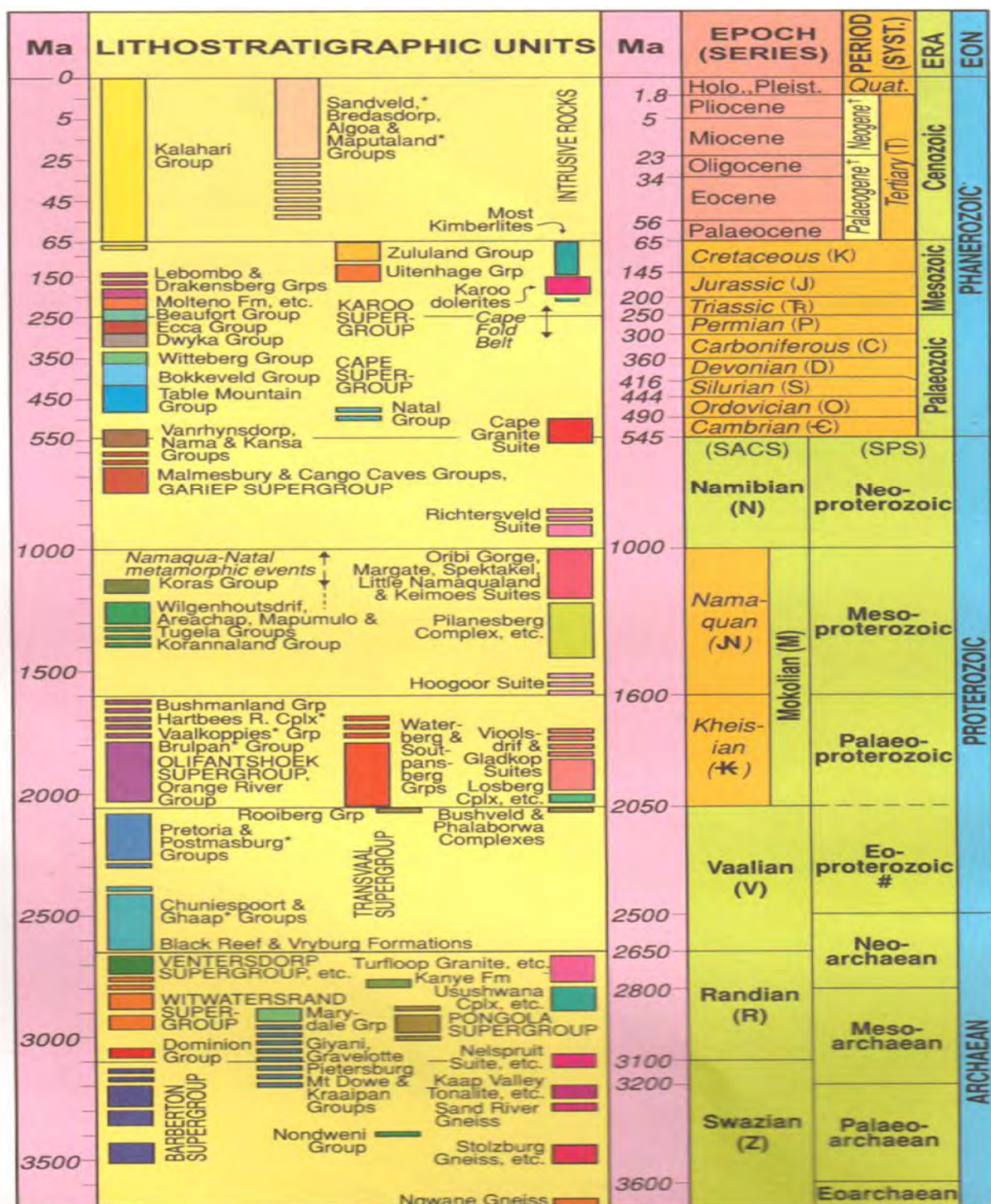


Figure 2.1: Geologic map of South Africa (Council of Geoscience, 2003).

Table 2.1: Stratigraphy of South Africa (After Johnson *et al.*, 2006).



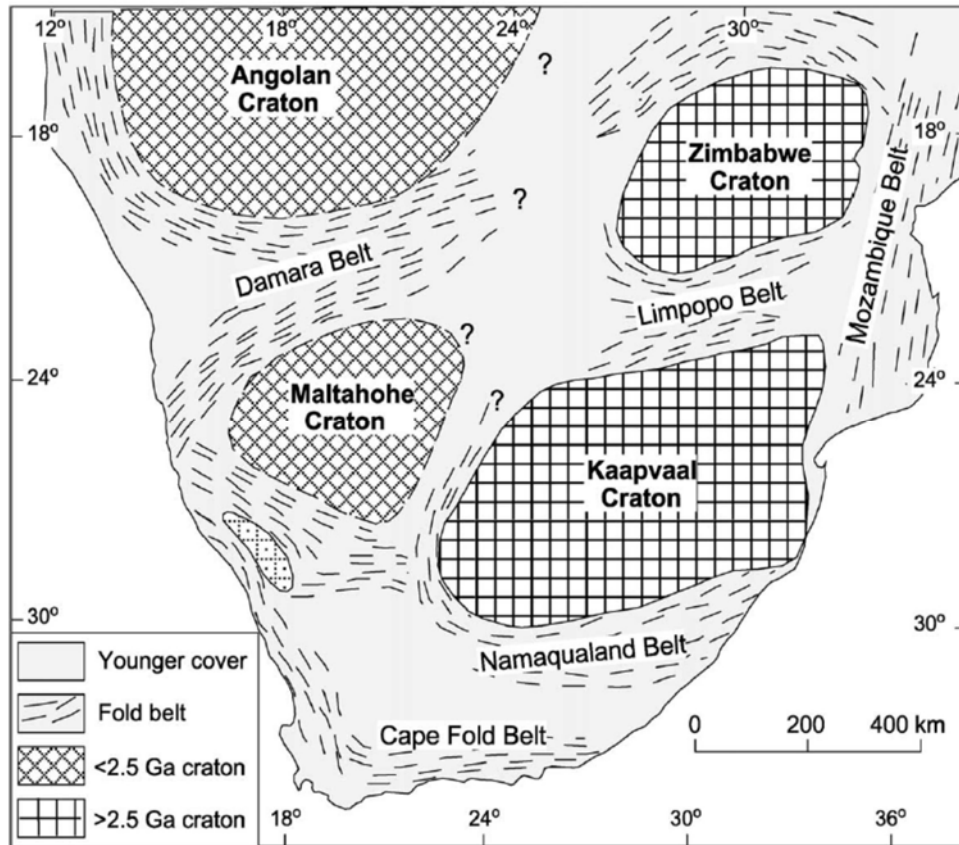


Fig. 2.2: Simplified geological map showing the main crustal provinces in South Africa, including main cratons and mobile belts (Adapted from Zhao *et al.*, 2002).

The central zone of the Limpopo Belt is dominated by metasedimentary rocks (quartzites, metapelites, calc-silicate and carbonate rocks), intruded by layered ultramafic–gabbroic-anorthositic rocks (Messina Suite). Marginal zones to the Zimbabwe Craton to the north and the Kaapvaal Craton to the South are dominated by high-grade equivalent of the granite-greenstone terrane of the adjacent cratons (Poujol *et al.*, 2003).

2.2 Soil Formation

Weathering profiles generally have in common a soil layer underlain by a layer of saprolite and bedrock (Fig. 2.3). A profile for matured soil consists of O, A, B, C, and R horizons. In all these layers, we have varying particle sizes with clay as the ultimate fine size. Velde and Meunier (2008) defined saprolite as “a nonstructure –conservative altered bedrock

with lower density”. The “O” horizon is the topmost layer of most soils composed mainly of plant litter at various levels of decomposition and humus while the “A” horizon is composed primarily of mineral particles though organic material could also mix with the mineral particles. More importantly, the “A” horizon is also known as the zone of eluviation where materials are lost to the underlying “B” horizon (zone of illuviation) with more clay particle and oxides of iron and aluminum enrichment. The “C” horizon (also referred to as saprolite in pedology) is composed of weathered parent material with particles ranging from clay to boulders. Mature soils generally display all these horizons whereas immature soils may have O, A, and C horizons (Fig. 2.3).

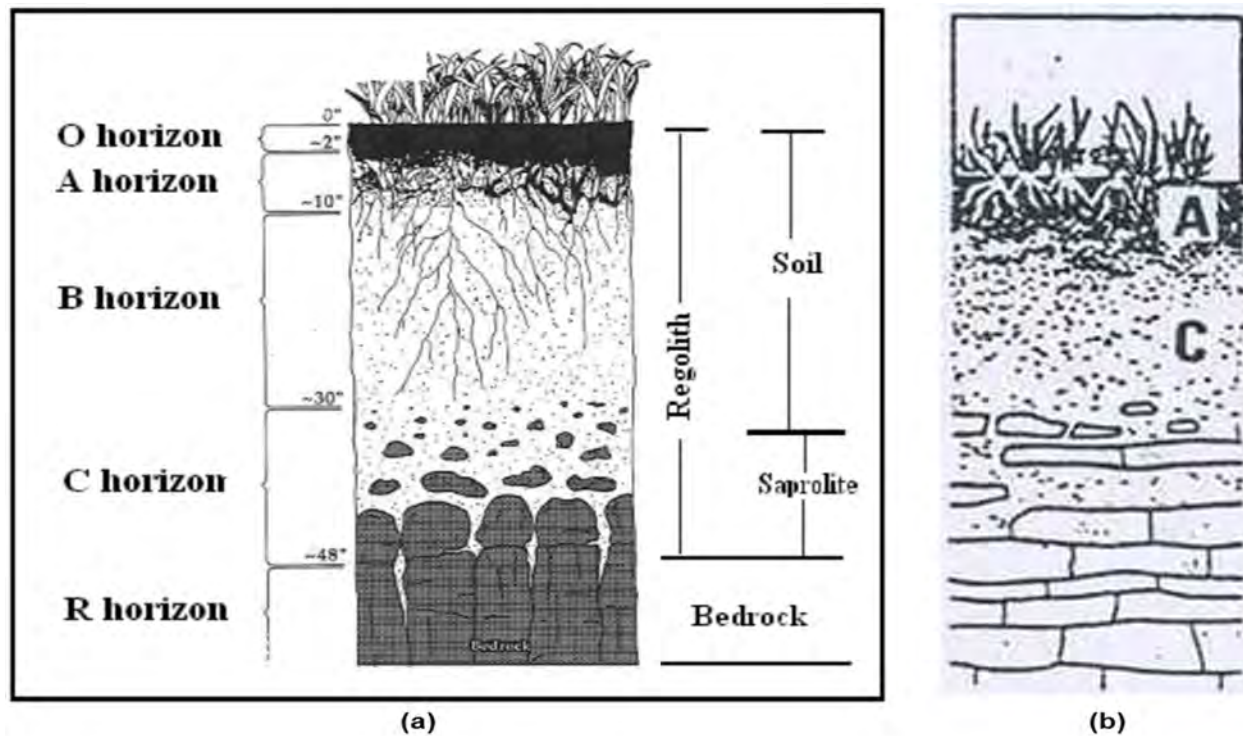


Figure 2.3: (a) A typical mature soil profile and (b) A typical immature soil profile (USDA, 2010).

2.2.1 Factors Controlling Soil Formation

There are at least five classic factors that are intertwined in the formation of a soil. These are: climate, parent material, time, organisms and topography (relief) (Reeves *et al.*, 2006). Soil scientists identify climate and organisms as “active” factors of soil formation because their influence over soil development can be directly observed. For example,

rain, heat, cold, wind, microorganisms (algae, fungi), earthworms, and burrowing animals can be directly observed influencing soil development. Time, topography, and parent material are noted as “passive” factors because their effects are not immediately observed. The passive factors can, however, control how climate and organisms affect soil development and formation.

i. Climate

The two significant pedogenetic properties of climate which affects weathering are temperature and rainfall. Climate affects the organic matter content and associated properties (notably nitrogen), reaction and base saturation. The profile depth, texture, and type of clay mineral synthesised are influenced by the climate. Tropical and subtropical conditions where there is free drainage and intense weathering leading to an acidic environment (Fig. 2.4), with depletion of bases from the soil profile and a relative depletion of silica compared with alumina favours the development of ultisols and oxisols with kaolinites that may be poorly ordered (Wilson, 2013). Pedoclimate may affect the nature of soil kaolins; for example structural order decreases as the length of the dry season decreases (Hughes and Brown, 1979).

ii. Parent Material

The composition of parent material is fundamental for the characteristics of the soils (texture, chemistry, mineralogy, and nutrient cycling) and their agricultural potentials in the tropics and subtropical environments (Jenny, 1994). Soil texture is influenced by the grain size of the parent material for instance; sand-size quartz grains will give rise to sandy soil even under intense chemical weathering conditions. Soil texture further affects the organic matter content, CEC, profile drainage, and moisture retaining capacity which all have agricultural implications (Young, 1976 and Buol *et al.*, 2011). Felsic rocks provide poor supply of calcium, potassium, iron, and manganese and a large residue of insoluble quartz. When a soil solution is low in bases, the main secondary mineral produced is 1:1 lattice clay mineral. Feldspars and other weatherable silicate minerals in soil parent rocks commonly undergo complex mineral transformations to form kaolinite in soils, with

accompanying loss of silica and bases from the soil through leaching. The weathering of feldspars to form kaolinite could be divided into two steps (Eqns. 2.1 and 2.2).

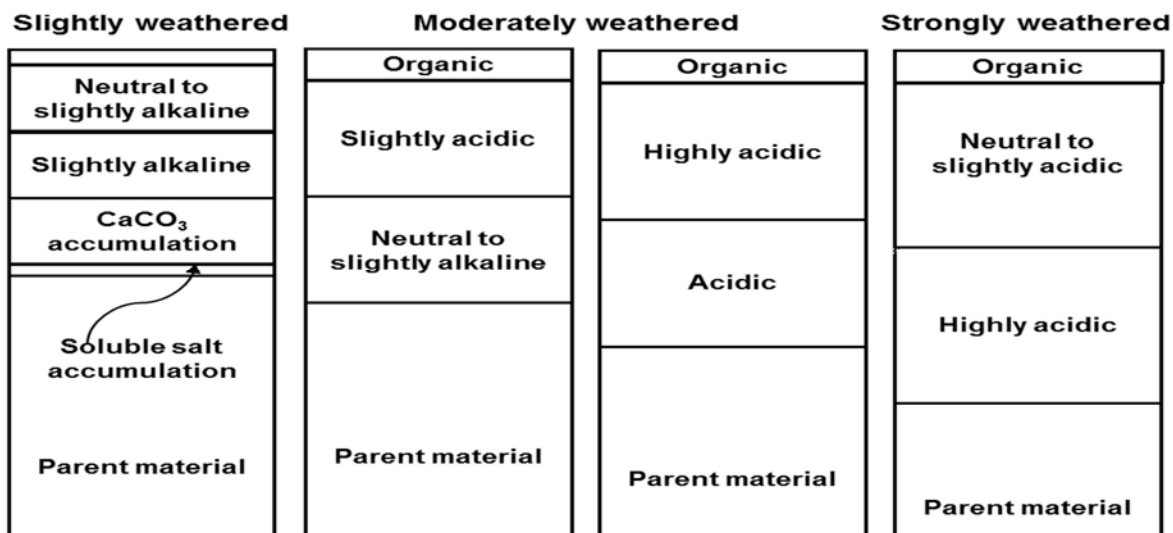
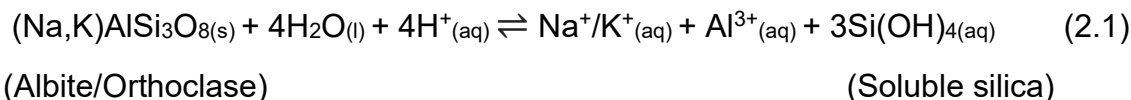
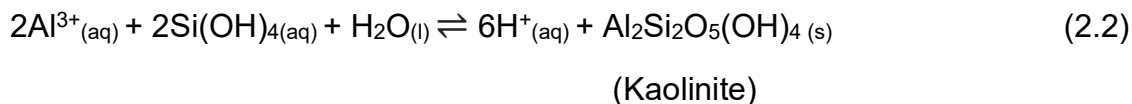


Figure 2.4: Schematic progression of basic and acidic zones through soils during soil development. This sequence also represents soil profiles from arid to humid to humid tropical regions (After Strawn *et al.*, 2015).

Step one under acidic conditions:



Step two involves the interaction of the soil solution Al^{3+} with the soluble silica to form kaolinite:



Low-defect kaolin often occurs in subsoils of well drained soils over granitic or siliceous sedimentary rocks (Kanket, 2006). Basic rocks provide a base-rich weathering environment favouring the synthesis of 2:1 lattice clay minerals. In such soils, fertility is higher because there is continuous renewal of nutrients such as calcium, magnesium, and potassium resulting from the weathering of primary minerals.

iii. Time

Time is the interval through which the effects of the other factors are integrated. Time influences soil properties not through effects on the type of processes but on the stage of soil maturity attained. The time required for the formation of kaolins in soils depends on the rate of pedogenic processes which include the dissolution of primary minerals and formation of secondary minerals (Buol *et al.*, 2011).

iv. Organisms

Soil organisms play a vital role in the degradation of organic matter and subsequent soil humus formation. There are multitudes of organisms living in the soil which include mites, snails, beetles, millipedes, springtails, worms, ground squirrels, gophers, grubs, nematodes, and microorganisms (e.g., bacteria, fungi, actinomycetes and algae). Microorganisms are the most abundant organisms in the soil. The activity of soil organisms is strongly influenced by soil temperature, acidity and soil-water relations. Their major contributions to soil are improved soil structure, nutrient transformations and fertility, aeration and enhanced productivity (Strawn *et al.*, 2015).

v. Topography (Relief)

Relief modifies the landscape distribution of moisture, and gives rise to local differences in soil wetness and dryness. Topography has a strong influence on soil development. Soils on the side of hills tend to be shallow, due to erosional losses. Soils on the tops of hills tend to be deep, but lighter in color, due to downward leaching losses. Soils in the valleys tend to be deeper, darker, and contain more horizons. This is due to increased material deposition from hillside erosion, material accumulation from downward leaching from the tops of hills, and the collection of greater quantities of water in the low lying areas.

2.2.2 Formation of Kaolins in Soils

Kaolin minerals (namely kaolinite, halloysite, nacrite, and dickite) in soils could be of primary origin formed in-situ by the alteration of feldspar-rich and aluminium-rich rocks due to surface weathering, groundwater activity, and action of hydrothermal fluids or

Wilson (1999) gave an extensive review on the three principal processes accountable for the genesis of kaolins which were earlier stated by Millot (1965). These processes include:

- i. Detrital inheritance whereby soils, kaolins are inherited/transported from pre-existing parent rock or weathered material. More often, inherited soil kaolins are extremely diverse and complex in nature reflecting both the variety of parent rocks as well as the transformation and neoformation processes that may have occurred in previous weathering environments. The presence of kaolin in soils by inheritance is prevalent where weathering is mainly physical (Reeves *et al.*, 2006).
- ii. Transformation whereby the essential silicate structure of the clay mineral is maintained but with major change in the interlayer region of the structure.
- iii. Neoformation occurs where the clay mineral forms through crystallization of gels or solutions which depends on the physicochemical conditions of the environment such as pH, composition, and concentration of the soil solutions, as well as the nature of the starting material and factors relating to the external environment like temperature, rainfall and percolation rate (Fig. 2.5). Millot (1965) described kaolinite as classical product of neoformation formed under acidic weathering conditions.

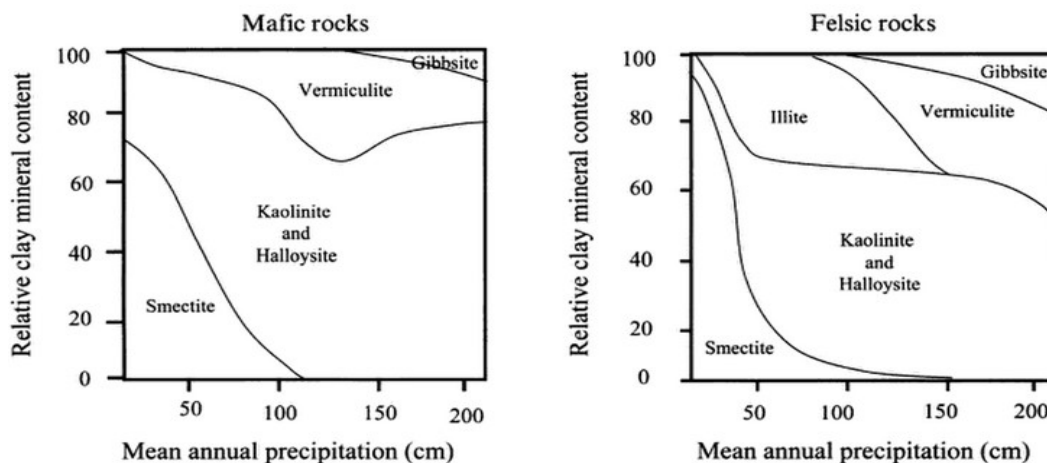


Figure 2.5: Relative proportions of different clay minerals in surface soil horizons developed on mafic (e.g basalt) and felsic (e.g granite) rocks as a function of rainfall (Reeves *et al.*, 2006). Kaolin minerals occupy much wider precipitation range and dominate above 50 cm per year.

Pedro (1982) stated that total hydrolysis of minerals through dilute solutions in the pH range 5 – 9.6 brings about the removal of all elements including silica, precipitation of gibbsite and kaolin minerals. Wilson *et al.* (1997) from his observation of kaolinite accompanying some trioctahedral micaceous clays in some alluvial soils from Nigeria concluded that there is indeed a possibility for the direct transformation of biotite → kaolinite (Eqn. 2.6) without intervening vermiculite stage in tropical soils. Therefore, soil kaolinite can either be regarded as products of neoformation primarily and secondarily through direct transformation of micas, conversion of hydroxyl-Al interlayered vermiculite or smectite and weathering of smectite through an intermediate kaolinite-smectite interstratified phase (Fig. 2.6).

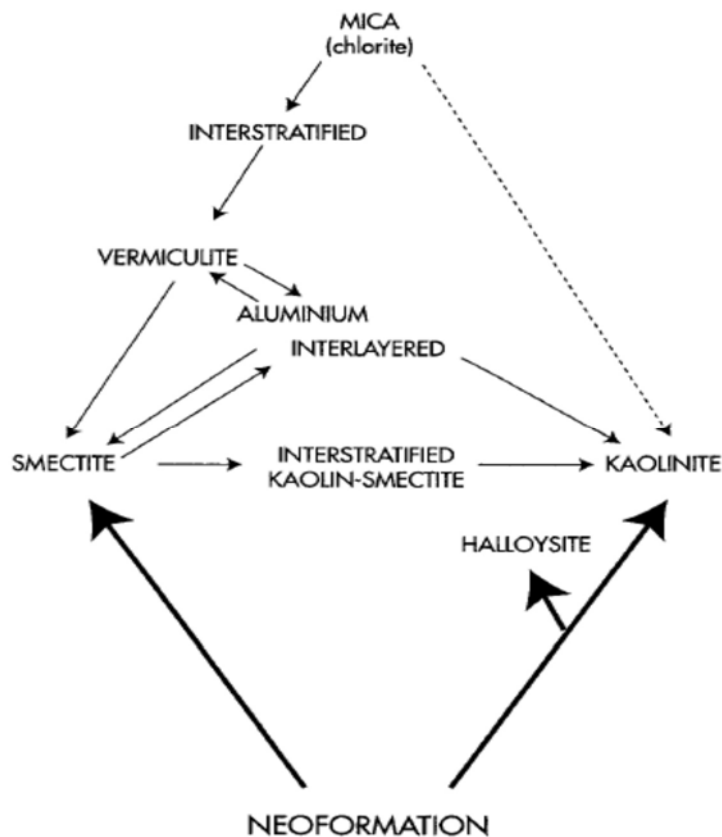
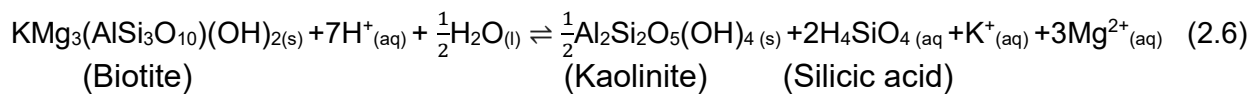


Figure 2.6: Pathways for the formation of kaolinite in soils (Wilson, 1999).

2.3 Kaolin in Soils

Kaolin minerals are composed of Al-substituted octahedral sheets and Si-substituted tetrahedral sheets in a 1:1 relationship (Fig. 2.7). The common minerals in the group are kaolinite ($\text{Al}_2\text{Si}_2\text{O}_5(\text{OH})_4$), halloysite ($\text{Al}_2\text{Si}_2\text{O}_5(\text{OH})_4 \cdot 2\text{H}_2\text{O}$), and the less common dickite ($\text{Al}_2\text{Si}_2\text{O}_5(\text{OH})_4$) and nacrite ($\text{Al}_2\text{Si}_2\text{O}_5(\text{OH})_4$) with the same ideal composition. Halloysite may be hydrated whereby water is present in its structural layers with a basal cleavage of 10.25 Å but when heated, it becomes dehydrated and the basal cleavage spacing reduces to 7.13 which is equivalent to kaolinite basal spacing (Fig. 2.8) (Murray, 2007). A summary of the lattice parameters for the kaolin minerals are given in Table 2.2. The two common ones are products of acid weathering but halloysite is more associated with volcanic origin. They are dominant in clay fraction of most oxisols and many ultisols.

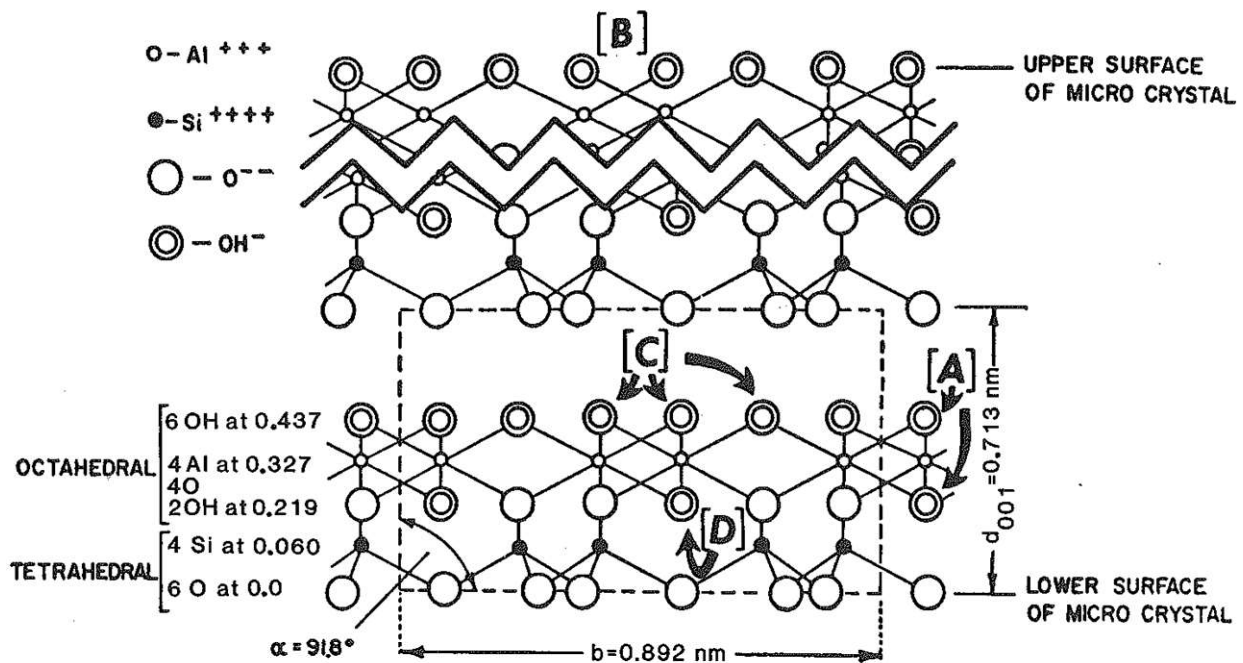


Figure 2.7: Octahedral and tetrahedral units in kaolinite. [A] and [B] shows 'outer hydroxyls'; [C] designates 'inner-surface hydroxyls'; and [D] indicates 'inner-hydroxyls' (Dixon, 1989).

Aridisols do not have kaolin as the dominant clay mineral because in the arid climates, leaching necessary for kaolin to develop is rare. Wilson (2013) expressed the complete weathering sequence of volcanic ash formed from andesitic and rhyolitic compositions as

volcanic ash → allophane → 10 Å halloysite → 7 Å halloysite → kaolinite. This transformation takes considerable time to attain the various stages. However, feldspars and biotites have also been identified as probable precursors of halloysite in deeply weathered granitic rocks (Joussein *et al.*, 2005).

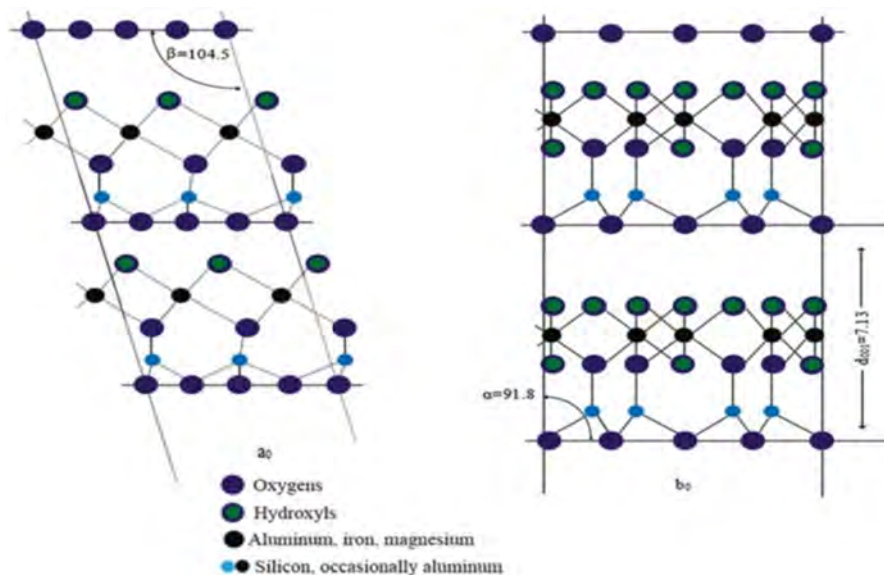


Figure 2.8: Schematic diagram of kaolinite structure (After Murray, 2007).

Table 2.2: Lattice parameters for kaolin minerals (After Haq *et al.*, 2008).

	Kaolinite		Hydrated Halloysite	Dehydrated Halloysite	Dickite	Nacrite
a	5.155 Å	a	5.14 Å	5.14 Å	5.1474 Å	8.906 Å
b	8.945 Å	b	8.90 Å	8.90 Å	8.939 Å	5.146 Å
c	7.405 Å	c	20.7 Å	14.9 Å	14.390 Å	15.664 Å
α	91.7°	β	99.7°	101.9°	96.483°	113.58°
β	104.862°					
γ	89.822°					

Kaolinite crystals have varied submicron-size usually $<2 \mu\text{m}$ and platy morphology in mature soils. The pseudo-hexagonal shape often identified as kaolinite presumed to be due to the close packing of O's and OH's in the hexagonal pattern. The particle size and crystal perfection determines the surface area, chemical and physical activity of the kaolinite. As such, soil property can adversely be modified by the cleavage of kaolinite books into thin flakes. Kaolinite morphology in soils varies as it is in rocks with best developed forms typically occurring in euhedral, hexagonal, and platy crystals stacked together as vermicular or book-like aggregates (Wilson, 2013) (Figs. 2.9 and 2.10).

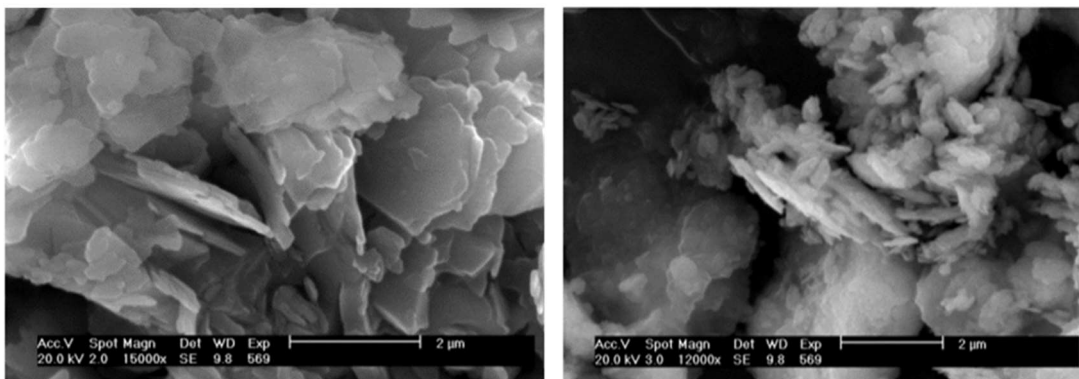


Figure 2.9: Scanning electron photomicrographs showing pseudo-hexagonal platelets of kaolinite in geophagic soil (Ekosse and Anyangwe, 2012).

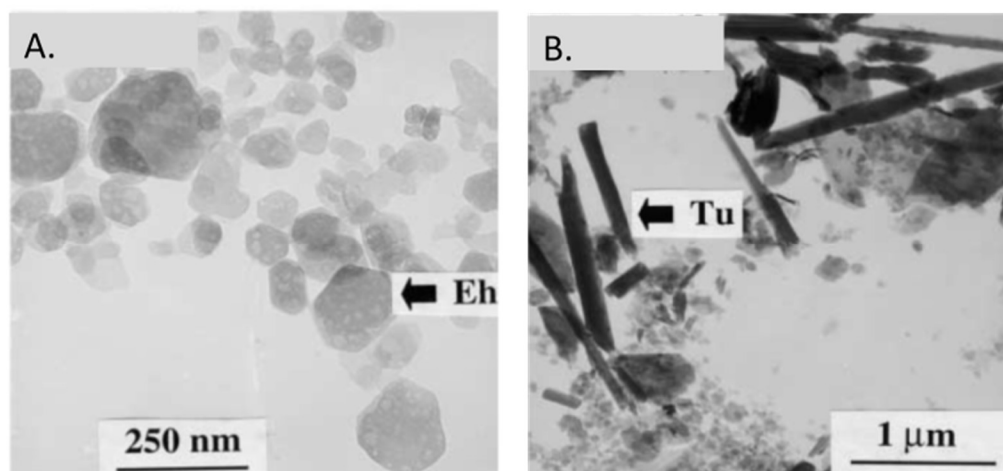
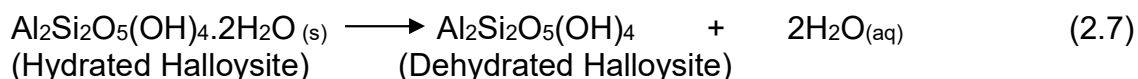


Figure 2.10: Transmission electron microscope (TEM) micrographs of kaolins from clay fractions of Brazilian soils (a) Kaolinite showing hexagonal euhedral faces and (b) Halloysite showing tubular morphology (After Melo *et al.*, 2001) developed from arkosic sandstone and granite respectively.

Soil kaolinite have 001 basal spacing values ranging from 0.713 to 0.7275 nm and 002 basal spacing values ranging from 0.357 to 0.359 nm if neither chlorite nor expanded vermiculite is present (Singh and Gilkes, 1992; Melo *et al.*, 2001; and Wiriyaakittateekul *et al.*, 2010). Chlorite may be indicated by separation of chlorite peaks at 0.354 nm from the kaolinite peak at 0.357 nm. Also, the endothermic DTA peak values between 489 and 518 °C (but generally less than 500 °C) and sharp IR absorption maxima at 3700, 3697 and 3620 cm⁻¹ are additional evidence for soil kaolinite. The lower DTA values when compared to 550 °C for standard kaolinite may be due to reduced crystal and poor crystallinity (Melo *et al.*, 2001). In differentiating between kaolinite and halloysite in soils or standard reference deposits when they are moist or air-dried, formamide intercalation expands halloysite in few minutes to 1.04 nm but will take close to 4 hrs or more to expand kaolinite (Dixon, 1989).

Halloysite can occur in two forms, namely hydrated and dehydrated halloysite. The hydrated halloysite with water between the silicate layers is unstable at room temperature and the water is lost irreversibly to form the dehydrated halloysite (Joussein *et al.*, 2005) (Eqn. 2.7).



The morphology of both the hydrated and dehydrated forms are often tubular (Fig. 2.10) but appears to be related to the iron content with the substitution of the larger Fe³⁺ for Al in the octahedral sheet which without substitution is smaller than the tetrahedral sheet (Huang *et al.*, 2011). Spheroidal forms of halloysite have been reported from weathering products of volcanic glass with a fast dissolution rate and crystallization in which case the resulting supersaturated solutions favour this particular shape (Singer *et al.*, 2004). The spheroidal halloysite had less substitution of Al by Fe than tubular halloysite, whereas the platy forms had most structural Fe among the halloysites (Papoulis *et al.*, 2004).

Studies conducted covering a range of parent rock types and climates (Churchman, 1990; Singer *et al.*, 2004; Papoulis *et al.*, 2004 and Jongkind and Buurman, 2006) showed an

apparent genetic relationship between halloysite and kaolinite in weathering profiles. There is a general trend from halloysite at depth toward kaolinite at the surface of profiles of residual rock. However, both halloysite and kaolinite at different stages could exist simultaneously with one another (Churchman *et al.*, 2010). In addition, the general trend does not imply that halloysite transform to kaolinite as weathering intensifies with time even in soil profiles because the results of Churchman and Gilkes (1989) showed tubular halloysite as dominant in the clay fraction of saprolite on dolerite from Western Australia and as the weathering intensified up profile, kaolinite began to appear as hexagonal particles.

The possibility for halloysite to transform to kaolinite in solid phase is very unlikely (Robertson and Eggleton, 1991) since the halloysite earlier described by Churchman and Gilkes (1989) progressively became dehydrated thereby causing the intercalation with the polar liquids to be more difficult. Etame *et al.* (2009) established a chemical dependence of halloysites upon parent rocks from a study on soils from nephelinite (alkali- and rare-earth-rich lava) in tropical Cameroon. Ce-rich halloysite was formed from mineral phillipsite, Fe-rich halloysite characterized the alteromorphs on clinopyroxene, Ca-rich halloysite marked alteromorphs of hauyne, and K-rich halloysite characterised alteromorphs on leucite.

Studies on nacrite have been few, probably because of the rarity of the mineral. However, studies have shown that nacrite occurs as relatively large euhedral blocky crystals based on scanning electron microscopic images and hence with a high edge to basal surface ratio compared to kaolinite (Wilson, 2013). Nacrite dehydroxylation endotherm occurs at about 660 °C and IR absorption bands at 3648 and 3629 cm^{-1} . The formation of nacrite requires higher temperatures and stress based on its occurrence on slickensided fracture surfaces in Coal Measures of the Liege Basin, Belgium (Goemaere, 2004). However, Buhmann (1988) identified nacrite forming authigenically by evaporative precipitation of pore solution on black shale walls of a water supply tunnel in South Africa with perfect hexagonal crystals formed at ambient temperatures.

Dickite is relatively more crystalline than kaolinite and occurs in bigger crystals (2.50 and 7.73 μm) with lath-like form thereby creating better opportunities for structural analyses

(Chen *et al.*, 2001). The dehydroxylation endothermic peak occurs at a higher temperature, typically at about 670 °C, as opposed to 500 – 600 °C for well-crystallised kaolinite. The IR spectra is often characterised by three absorption bands at 3704, 3653, and 3622 cm^{-1} . Dickite forms during diagenesis of sediments, principally arkosic sandstones and hydrothermal alteration of various rock types in environments with higher temperatures (150 – 300 °C) and pressures (2.7 – 4.6 kbar) than is normally associated with formation of kaolinite (Ruiz Cruz and Andrea, 1996 and Papoulis *et al.*, 2005).

2.4 Properties of Soil Kaolins

2.4.1 Physico-chemical properties of soil kaolins

The specific surface area (SSA) and cation exchange capacity (CEC) values of soil kaolins are between 10 – 90 $\text{m}^2 \text{g}^{-1}$ and 5 – 10 cmol kg^{-1} respectively (Gilkes and Prakongkep, 2016). The surface area is approximately proportional to the reciprocal of the coherently scattering domain (CSD). Hence, the ionic exchange capacity of soil kaolins is attributed to the SSA which is inversely linked to their small crystal sizes (Hughes *et al.*, 2009) (Fig. 2.11).

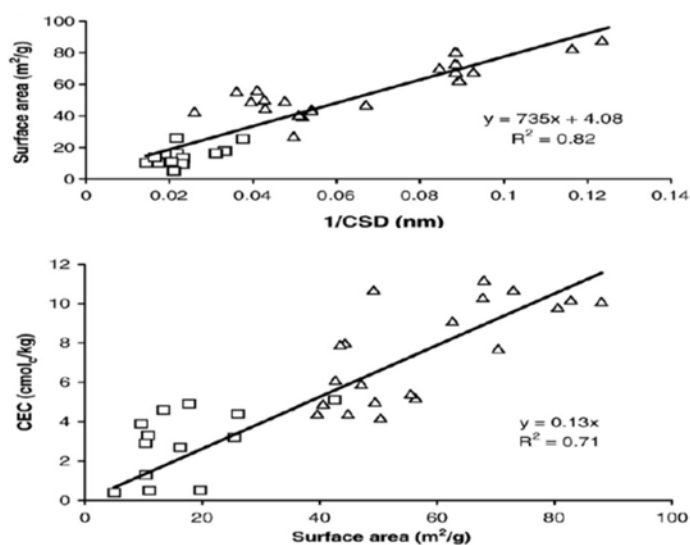


Figure 2.11: Relationship between SSA, CSD, and CEC for soil (triangles) and standard (squares) kaolins (Hughes *et al.*, 2009).

2.4.2 Mineralogical properties of soil kaolins

The most common kaolin minerals occurring in soils are kaolinite followed by halloysite (Trakoonyingcharoen *et al.*, 2006) (Fig. 2.12). Ekosse and Anyangwe (2012) identified typical flaky platelet kaolinite morphology in geophagic clayey soils from Botswana (Fig. 2.13). The size and shape of kaolin crystals in soils is highly diverse. Soil kaolins generally have smaller shapes than standard kaolins (Fig. 2.14).

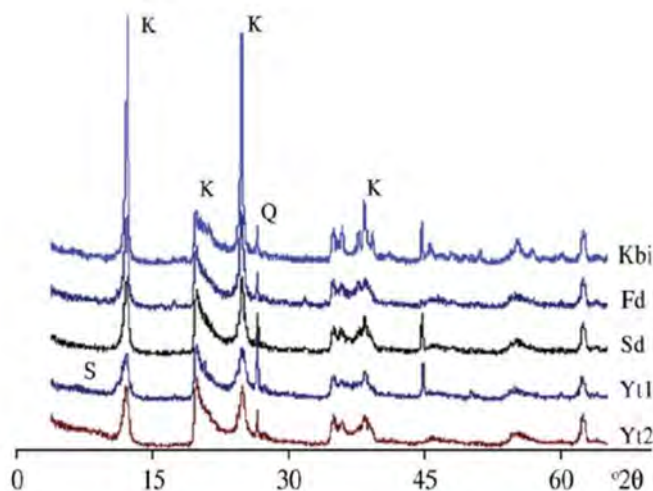


Figure 2:12: X-ray diffraction patterns of randomly oriented deferrated clay fraction of red ultisols from Thailand showing the dominance of kaolinite with no other clay minerals (K = kaolinite, Q = quartz) (After Trakoonyingcharoen *et al.*, 2006).

Hughes and Brown (1979) developed an empirical crystallinity index (CI) for soil kaolins derived from humid tropical area of Southern Nigeria. The development of CI was necessary since the common Hinckley index in assessing the degree of crystalline order by XRD seems impossible to measure for soil kaolins. The CI values obtained for the Nigerian soil kaolins suggested that the CI may be related to genetic factors (for example, rock type, rainfall, vegetation, and the presence of appreciable amounts of weatherable minerals) which could influence the environment in which the kaolin crystallized. For four (4) rock types, the mean CI values 6.9 ± 0.4 for sedimentary, 7.4 ± 2.5 for intermediate crystalline, 9.2 ± 2.2 for basic crystalline, and 10.0 ± 1.0 for acid crystalline rocks were obtained. Soils having weatherable minerals like feldspars in their fine sand fraction were categorised as 'young soils' and were observed to have lower crystallinity indices relative to the 'older' soils having quartz dominating the fine sand fraction.

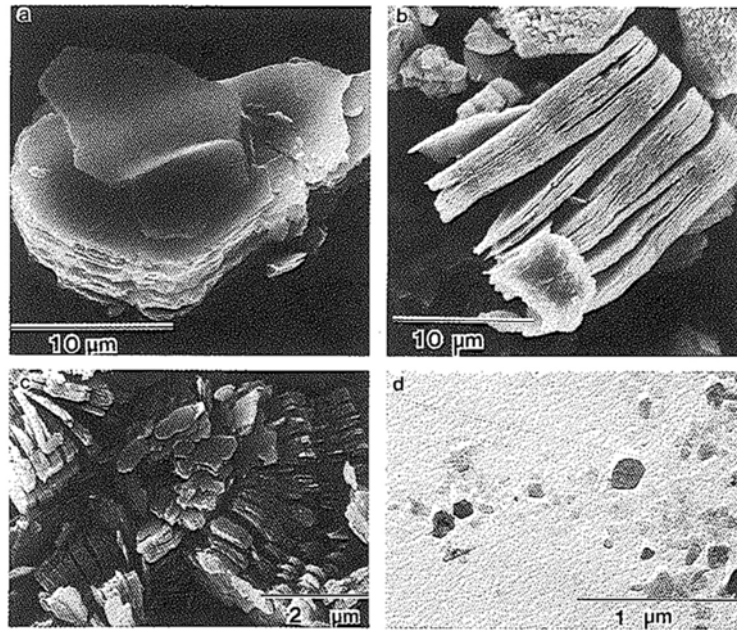


Figure 2.13: Scanning electron photomicrograph showing: (a) stack of kaolinite flakes with bent sheet; (b) book of loosely stacked kaolinite assemblages; (c) vermicular book of kaolinite with irregular edges; and (d) submicron plates of kaolinite from Falba Btgl soil (Dixon, 1989).

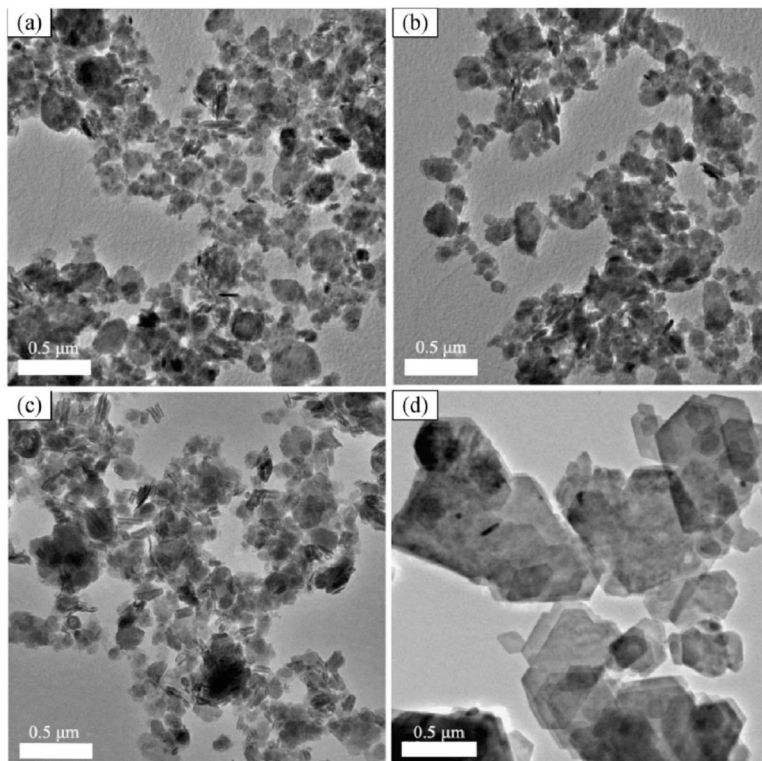


Figure 2.14: TEMs of soil kaolins (a)WA169 from Australia, (b)WA235 from Australia, (c) INC63 from Indonesia, and (d) Georgia reference kaolin G1261 (Hughes *et al.*, 2009). The much larger crystal size of the mineral kaolin is evident.

Hence, the presence of weatherable minerals in the soil hinders the crystallisation of well-ordered kaolins. The CI value of 6.2 and 8.2 for kaolinites in oxisols and ultisols from Thailand (Darunsontaya *et al.*, 2010) respectively are indicative of structural disorder and are considerably less than the range of 38 – 83 CI values obtained for standard reference kaolinite (Hughes and Brown, 1979; and Singh and Gilkes, 1992).

Chittleborough and Walker (1988) emphasised the systematic variations in soil kaolinite crystallinity to factors associated with soil formations such as profile hydrology; the more hydromorphic the soil, the lower the crystallinity. The effect of changes in the particle-size distributions in some soils from Southeastern Australia to changes in the kaolinite crystallinity using CI showed that the CI values for fine clay-size were significantly lower than that for the coarse clay-size. A decrease in the CI values was observed in the crystallinity of soil kaolinites of coarse clay-size after prolonged period of weathering of the parent material alluvium.

Current X-ray diffraction (XRD) 'crystallinity indices' cannot distinguish between different soil kaolins since almost pure kaolin samples are required. The possibility that kaolin properties are related to their susceptibility to expansion by the hydrazine–water–glycerol (HWG) intercalation procedure was investigated for soil kaolins from Indonesia, Australia, and Thailand, and some reference kaolins. The soil kaolins contained minor impurities, mostly quartz, anatase, illite, and hydroxy-interlayered vermiculite. Through the HWG test, kaolins formed by hydrothermal processes were distinguished from those formed under near surface (pedological) conditions (Hughes *et al.*, 2009).

Wiriyakitnateekul *et al.* (2010) reported that soil kaolins derived from sandstones have platy and large crystal sizes in contrast to those derived from basalt with lath and small crystal size, low crystallinity, and high specific surface area. Laths according to Chen *et al.* (2004) are a common morphological feature of kaolin pseudomorphs after mica. Sandeep and Sujatha (2014) carried out the SEM analysis of kaolin in different forest ecosystems in India. The soil kaolins from moist deciduous and evergreen forests showed hexagonal and platy kaolinite, whereas shola, grassland, and scrub jungle gave tubular halloysites along with kaolinites. The presence of halloysites which are a metastable phase in kaolinite formation was inferred to indicate a system-induced restricted

weathering in the tropics because the climatic conditions may not have provided sufficient activation energy for the temperature-dependent halloysite to kaolinite transformation.

2.4.3 Geochemical properties of soil kaolins

The geochemical composition of soil kaolin is quite variable and commonly does not conform to the ideal composition of kaolin (39.5 wt % Al_2O_3 and 46.6 wt % SiO_2). The variation based on data obtained for 176 soil kaolins from diverse localities gave a median value of 46.33 wt % for SiO_2 which coincides with the ideal composition and 36.52 wt % for Al_2O_3 which is lower than the ideal composition (Gilkes and Prakongkep, 2016). This can be attributed to the substitution of Fe for Al in the octahedral sheet of the soil kaolins which can incorporate up to 11 wt % Fe_2O_3 (Wilson, 2013; Gilkes and Prakongkep, 2016).

The mean Fe concentration values 18 gkg^{-1} and 17 gkg^{-1} obtained for kaolins in oxisols and ultisols developed from different parent materials in Thailand suggest that iron substitution in the kaolins may not be dependent on the Fe content of the parent materials (Darunsontaya *et al.*, 2010). However, average Fe_2O_3 concentrations for Indonesia (2.51 wt %) and Western Australia (2.56 wt %) were similar for kaolins from other tropical and highly weathered soils in Nigeria (1.86 wt %), Rwanda (2.32 wt %), and Cuba (1.52 wt %) (Mestdagh *et al.*, 1980; Hart *et al.*, 2002). Oxisols derived from basalt due to their higher content of iron oxides and high clay content have relatively higher contents of most elements than do soils from other parent material with the exceptions of K and Rb which are greater in soil kaolins from granite. Illite in some clay fractions explains the higher K concentration in the ultisols relative to the oxisols.

Kanket *et al.* (2005) studied the chemical and crystallographic properties of kaolins in ultisols from a range of parent materials in Thailand. The Fe_2O_3 content of the soil kaolins ranged from $12.4 - 44.8 \text{ gkg}^{-1}$ and CEC ranged from $7.2 - 23.4 \text{ cmol}_c\text{kg}^{-1}$ with appreciable amounts of Ni, Cu, Zn, Co, and Pb present in highly weathered soils. The presence of minor elements as structural ions will have significant implications for soil fertility and geochemical exploration since the properties of the ion will affect the adsorption and

desorption of plant nutrients in the soils. The $\text{SiO}_2/\text{Al}_2\text{O}_3$ ratios of the soil kaolins ranged from 1.20 – 1.76 with a mean value of 1.38 which is more than the values of 1.17 for ideal kaolin and 1.20 for standard reference Georgia kaolin. This was attributed to the presence of quartz and the replacement of Al in the soil kaolins by Fe (Kanket *et al.*, 2005). The association of Fe with soil kaolinite has been observed in several previous studies which have shown that the Fe is present in the Fe^{3+} form and substitutes for Al in the octahedral sheet of the kaolinite (Jepson and Rowse, 1975; Herbillon *et al.*, 1976; and Singh and Gilkes, 1992).

Soil kaolinites from Southern Australia have K_2O contents ranging from 0.10 – 0.29 wt % which was interpreted to indicate the presence of 1 – 2.9 wt % micaceous interlayers but the mica layers were not detected by XRD (Singh and Gilkes, 1992). Melo *et al.* (2001) reported that Ti content ranged between 0.21 – 4.70 wt % in Brazilian soil kaolins which they explained that Ti might be associated with the kaolinite by either substituting in the structure of the kaolinite or present as a discrete surface-sorbed form. The average Fe_2O_3 concentration in the kaolinite of the clay fraction (19.1 gkg^{-1}) was higher than that obtained in the silt fraction (6.6 gkg^{-1}) which may be related to much of the Fe probably substituted for Al in the octahedral site or some of the Fe present as free Fe oxides not totally removed by the dithionite-citrate-bicarbonate treatment. The smaller kaolinite particle of the clay fraction showed a lower degree of crystal order, higher K and Mg levels. Based on the strong relationship between the asymmetry index (AI) of the (001) diffraction line and the level of K in kaolinite from the younger soils, the K and Mg in the kaolinite are taken to be part of the residual micaceous layers interleaved in kaolinite crystals. This observation has been earlier stated by Lee *et al.* (1975) that the presence of K in kaolinite is due to inclusion of micaceous layers.

There is an association between iron content and poor structural order in kaolins because soil kaolins have higher iron content and lower degree of structural order when compared to the standard kaolins (St. Pierre *et al.*, 1992). Based on Mössbauer spectral parameter values of δ (chemical isomer shift) and Δ (quadrupole interaction) ranging from 0.32 – 0.34 and 0.51 – 0.58 respectively for iron in soil kaolins from Indonesia and Western

Australia, the iron is present as Fe^{3+} oxidation state and are octahedrally coordinated (Siradz, 2000).

Kaolinitic tropical soils from Brazil show that the dissolution and rate of release of Al, Si, and Fe exhibits strong pH dependence with dissolution minima occurring at 0.4-0.9 pH units and release rate order as $\text{Al} > \text{Si} > \text{Fe}$. The rapid mobilization of Al in organic solid phases in soils with decreasing pH accounts for the relatively higher release rate of Al which is very important in interpreting soil weathering mechanisms in tropical systems (Chorover and Sposito, 1995). The surface charge properties of kaolinite are not only important for adsorption reaction but also affect the dissolution behavior of kaolinites. The negative surface charge on kaolinite increases with decreasing crystallinity of kaolinite (Khawmee *et al.*, 2010).

2.5 Occurrence of Soils in South Africa

2.5.1 Classification of Soils in South Africa

South Africa is a country with great variety of soils, the mineralogical composition of which undoubtedly influences agricultural, environmental, and engineering properties (Buhmann *et al.*, 2004). The Soil Classification Working Group (1991) under the Department of Agricultural Development, Republic of South Africa established seventy-three (73) soil forms to reflect the nature of soils that occur in South Africa. The various soil forms are constituted after identifying master and diagnostic horizons and materials which are referred to by means of geographic names without any intrinsic significance. Fey (2010), due to many taxa in the previous classification and expansion of knowledge, identified the need for the development of fewer classes which covers geographic distribution, properties (including profile descriptions and analytical data), classification (including correlation with major international systems), genesis, and environmental significance. Fourteen (14) soil groups were established (Table 2.3 and Figure 2.15).

Table 2.3: Key to soil groups in South Africa (After Fey, 2010).

Differentiating principle	Soil group	Concept	Diagnostic horizon or material for identification
Soils with special topsoil characteristics	1	Organic	Wetland or montane peat
	2	Humic	Humus enrichment; free drainage; low base status; humid climate
	3	Vertic	Swelling, cracking clay; basic parent material; semi-arid to sub-humid climate
	4	Melanic	Dark, structured clay; high base status; semi-arid to sub-humid climate
Soils with special subsoil characteristics relating to pedogenic accumulation and having an orthic topsoil	5	Silicic	Cementation by amorphous silica or sepiolite; arid climate
	6	Calcic	Carbonate or gypsum enrichment; arid climate
	7	Duplex	Marked textural contrast through clay enrichment
	8	Podzolic	Metal humate enrichment; siliceous parent material
	9	Plinthic	Absolute iron enrichment; localised, hydromorphic segregation with mottling or cementation
	10	Oxidic	Residual iron enrichment through weathering; uniform colour
	11	Gleyic	Protracted reduction in an aquic subsoil or wetland
Young soils with an orthic topsoil but weakly developed subsoil	12	Cumulic	Incipient soil formation in colluvial, alluvial or aeolian sediment
	13	Lithic	Incipient soil formation on weathering rock or saprolite
	14	Anthropic	Human disturbance

Soil group	WRB correlation (IUSS Working Group 2006)
1. Organic	Histosols Gleysols
2. Humic	Umbrisols Ferralsols Acrisols Luvisols Lixisols Cambisols
3. Vertic	Vertisols Gleysols Phaeozems
4. Melanic	Chernozems Umbrisols Gleysols Phaeozems Kastanozems Luvisols Calcisols Leptosols Fluvisols
5. Silicic	Durisols
6. Calcic	Calcisols Gypsisols Luvisols Lixisols
7. Duplex	Planosols Solonetz Luvisols Albeluvisols Lixisols
8. Podzolic	Podzols
9. Plinthic	Plinthosols Ferralsols Acrisols Stagnosols Lixisols Arenosols
10. Oxidic	Acrisols Alisols Ferralsols Luvisols Lixisols Arenosols Cambisols Nitisols
11. Gleyic	Gleysols Stagnosols Planosols
12. Cumulic	Cambisols Arenosols Fluvisols Luvisols Acrisols Lixisols
13. Lithic	Leptosols Cambisols Acrisols Lixisols
14. Anthropic	Anthrosols Technosols

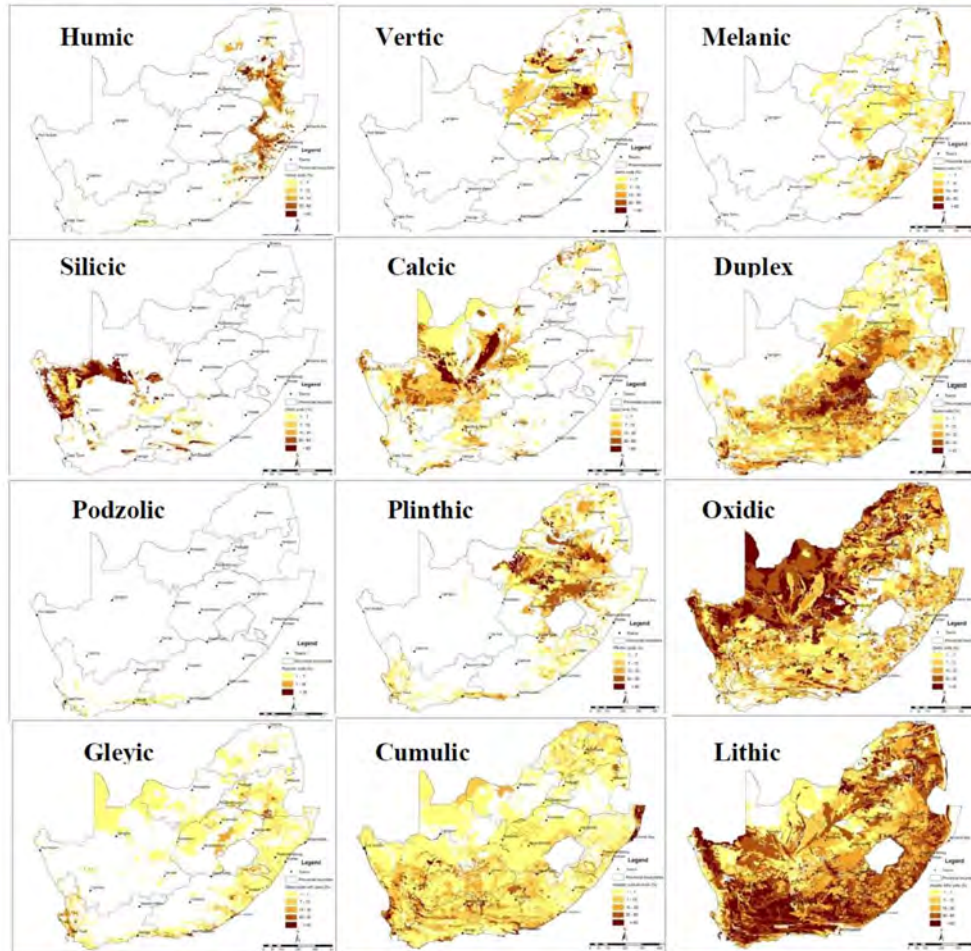


Figure 2.15: Distribution of the soil groups in South Africa (The darkest colour indicates > 60 % of soils in the mapping unit and lightest yellow colour between 1 and 7 %) (After Fey, 2010).

2.5.2 Kaolinitic rich Soils in South Africa

From his classification, the humic, plinthic, and oxidic soils have predominantly kaolinitic assemblage developed from different parent rocks under a range of climatic conditions.

- **Humic soils**

Humic soils occur in areas with high rainfall and cool temperatures with horizons marked by accumulation of humus (Fig. 2.15). Soils containing insufficient organic matter to qualify as humus but which has a low base status and sesquioxidic mineralogy are categorized under the oxidic group. Humic soils have a diagnostic humic A horizon with

more than 1.8% organic carbon and less than 4 cmol_c of exchangeable base cations. This horizon may be followed by a red apedal B as a result of advanced weathering and free drainage. The clay fraction is dominated by kaolinite, aluminous chlorite, gibbsite and iron oxides (mainly goethite and/or hematite) with low CEC, low pH and high phosphate fixing capacity. Soil Classification Working Group (1991) forms within the humic group are Kranskop, Magwa, Inanda, Lusiki, Sweetwater, and Nomanci. They are common in the eastern seaboard of South Africa, especially in Kwazulu- Natal, the Pondoland coast and along the eastern escarpment region of Mpumalanga (Bühmann *et al.*, 2004; Shange and Conradie, 2012).

- **Plinthic soils**

Where iron oxides are found segregated and concentrated in soil in the form of mottling and cementation, pedologists call this plinthite. Plinthite is broadly equivalent to what geologists call laterite when well developed (Fey, 2010). They consist of an orthic A horizon which grades into silt or hard plinthic B horizon depending on the degree of pedogenesis. Soils earlier described by the Soil Classification Working Group (1991) within the plinthic group are Longlands, Wasbank, Westleigh, Dresden, Avalon, Glencoe, Bainsvlei, and Lichtenberg respectively. The distribution and abundance of plinthic soils across South Africa (Fig. 2.15) shows that they are largely absent from regions of extremely low and high rainfall. Pronounced dry season is a prerequisite for plinthic formation coupled with sufficiently wet season to induce saturation with water and mobilization of iron in the reduced form. Specialised bacteria increase the rate of oxidation and reduction. The plinthic horizon (with low organic matter and CEC) has 25% iron by volume, humus-poor mixture of kaolinitic clay and quartz and other diluents, which changes irreversibly to a hard mass or to irregular aggregate on exposure to repeated wetting and drying with free access to oxygen (IUSS Working Group WRB, 2006).

- **Oxidic soils**

Oxidic soils have an orthic A horizon and B horizon that is uniformly coloured with red and/or yellow oxides of iron. It comprises of Pinedene, Griffin, Clovelly, Bloemdal, Hutton, Shortlands and Costanantia soil forms of the Soil Classification Working Group (1991)

respectively. The most popular of all South African soils is the Hutton form which accounts for the marvelous redness of the landscape across the Country (Fig. 2.15). The apedal (structureless) soils in the group are characterised by a relatively low CEC ($< 11 \text{ cmol}_c \text{ kg}^{-1}$) reflecting oxidic mineralogy with predominantly kaolinitic assemblage. Since CEC is low, a loss of organic matter through cultivation may have adverse effects on soil quality. In such areas, soil acidity and phosphate fixation are research priorities (Fey, 2010).

The study areas fall within the broader oxidic soil group based on Fey (2010) classification under the Hutton 35 (Hu35) soil series of the Soil Classification Working Group (1991). The Hu35 represents Hutton Form Portsmouth series which occupy about 40 % of the land area of the Limpopo Province (Fig. 2.16). The Hu35 has 15 % clay content in the eutrophic B horizon which underlies the orthic topsoils with low organic carbon content (Soil Classification Working Group, 1991). The eutrophic B horizon has high base status which could be red or yellow-brown depending on the mineralogy of the parent material. Red B apedal horizon are common in soils developed from basic parent rocks such as basalt with ferromagnesian minerals whereas yellow-brown apedal B horizon are easily formed on sandstones, granites, and granite gneisses with felsic minerals.

2.6 Soil kaolins related to pedoclimatic and pedogenetic Considerations

Kaolins occurring in soils due to pedogenesis are formed directly in response to current climatic conditions or owing indirectly to previous weathering cycle. They are commonly dominant in ultisols and oxisols formed under intense weathering with the depletion of bases from the soil profile but usually not dominant in alfisols (moderately weathered soils). Orientation relationships between the precursor minerals such as feldspars and micas may suggest the origin of the kaolin in soils (Wilson, 2013).

Origin by topotactic replacement in which the crystallographic orientation of the parent biotite crystal determines that of the product kaolinite crystals has been suggested, whereas epitaxial origin of oriented kaolinite on biotite basal surfaces have also been indicated (Gilkes and Suddhiprakarn, 1979; Singh and Gilkes, 1992).

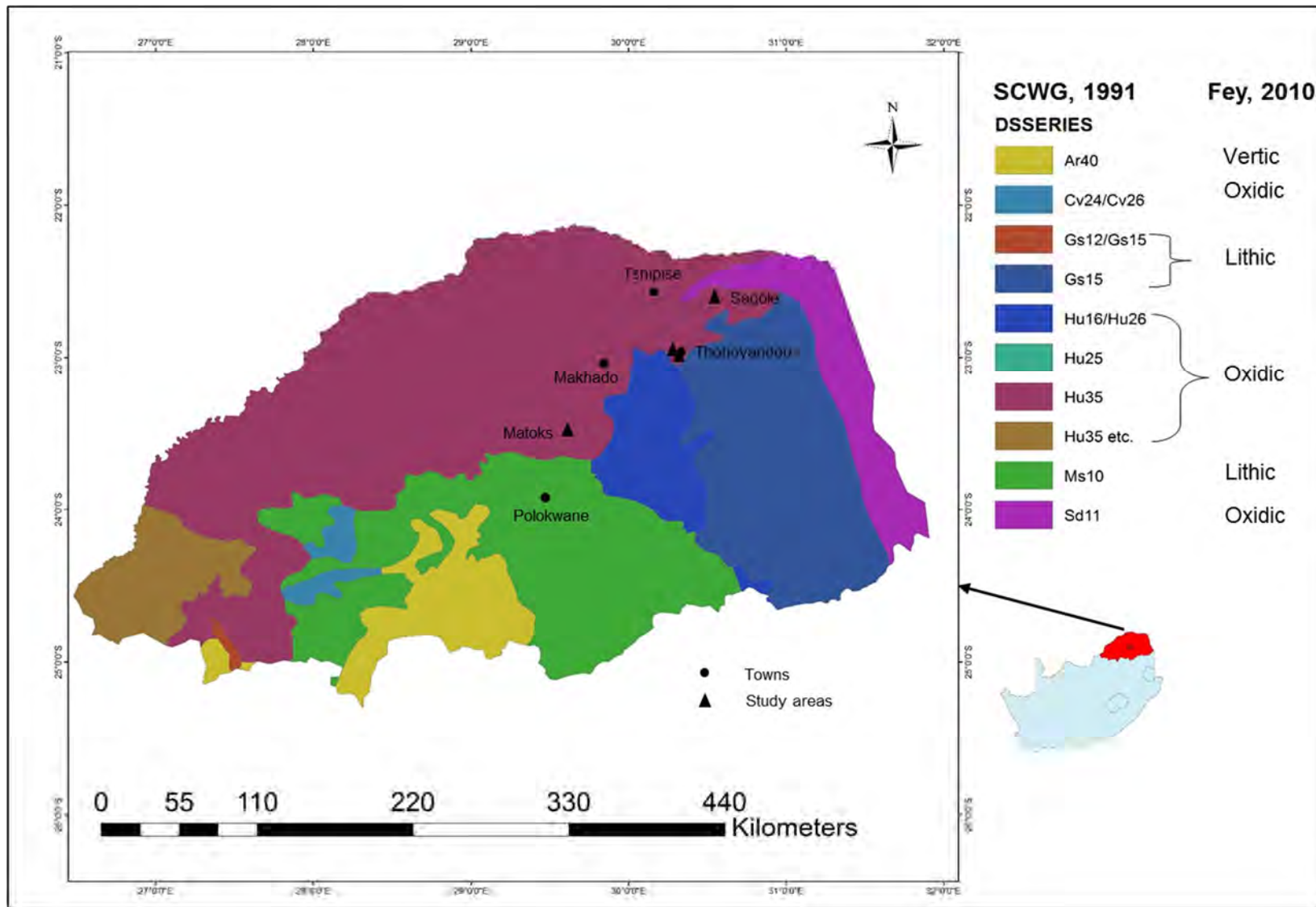


Figure 2.16: Distribution of the soil groups in Limpopo Province (ARC-ISCW, 2006).

Kaolinite in arkosic sandstones formed due to diagenesis after sediment deposition is believed to be related to flushing by acidic meteoric waters at shallow depths and at low temperatures (< 100 °C) leading to feldspar dissolution (Lanson *et al.*, 2002).

Red soils in Thailand, covering about 21 % of the country's agricultural land area, have been classified into oxisols and ultisols (Moncharroen, 1992). High TiO₂ concentration values ranging between 2.03 – 6.3 % was reported (Trakoonyinchareon *et al.*, 2006) in the kaolins from red soil developed on mafic materials relative to Fe₂O₃ and K₂O which is due to removal of large amounts of alkali ions and silica during weathering causing the concentration of TiO₂ content (Melo *et al.*, 2001).

In pedoclimatic studies, partly unrolled SEM halloysite tubes may be indicative of a shift to drier pedoclimate (Singh and Gilkes, 1992) since the length of rainfall and dry season affect crystal morphology. Trakoonyinchareon *et al.* (2006) observed that two soil kaolins developed from a single parent material basalt have different properties and the concentrations differ. One has smaller crystal size, lower percentage of euhedral crystals, and higher Fe₂O₃ than the other which they interpreted to be reflective of the prolonged moist conditions experienced by the former compared to the long dry season experienced by the latter. Varajao *et al.*, (2001) observed that less Fe is incorporated into kaolin formed under drier conditions which may have facilitated growth of euhedral crystals. The identification of mixtures of different morphologies ranging from large and small euhedral hexagonal, anhedral, tube, and lath in the red soil kaolins have been related to their cation exchange capacity (CEC) and specific surface area (SSA). This is crucial in the buffering and nutrient retention particularly in soils which have little organic matter. Conversely, parent material may exert a major influence on the crystal morphology of kaolinite based on the observation from two soils located hundreds of kilometers apart in different states in Brazil but formed from similar parent materials having similar crystal forms (Melo *et al.*, 2001).

Large variations in the mineralogical, chemical, and physical properties of purified soil kaolins from Indonesia and Western Australia using analytical transmission electron microscopy (TEM), XRD, thermogravimetric analysis (TGA), and chemical analyses have been reported (Hart *et al.*, 2002). The soil kaolins have small size and different

morphologies relative to the standard kaolins with large euhedral pseudo-hexagonal crystals. In particular, the Indonesian soil kaolins have poorly-defined tubes and subhexagonal plates while the Western Australian soil kaolins are composed mainly of anhedral plates. The molar Al/Si ratio for the bulk samples were generally <1.00 which can be attributed to the Fe substitution for Al coupled with the fact that minor amounts of contaminant quartz was observed on the XRD patterns which could as well influence this value. The Fe concentration did not show any inverse relationship with the structural order. The HB indices for Western Australia soil kaolins decreased with increasing Fe while for Indonesian soil kaolins was a reverse trend. The systematic differences in the kaolin sizes and morphological characteristics between Western Australia and Indonesia soil kaolins was interpreted to be indicative of a unique pedoenvironment. Thus, soil kaolins can provide a distinctive fingerprint for a particular pedoenvironment which can provide useful basis in the study of transported materials and paleosols.

2.7 Soil Kaolins related to Soil Fertility Management

Soils with kaolins as the dominant clay mineral usually have low chemical and physical fertility resulting in some management problems. The high specific surface area (SSA) of soil kaolins relative to standard kaolin causes a substantial cation and anion retention capacities which are important in agriculture in retaining cationic and anionic forms of plant nutrient elements against leaching under the high rainfall condition in the tropics. Fertilisers, lime, and organic matter are commonly applied to these soils and reaction of these additives with kaolin crystals enhance soil fertility and structure (Gilkes and Prakongkep, 2016). Kaolinite absorbs more P per unit surface area than 2:1 clay minerals. Kaolinite has charged crystal edges due to incomplete bonding of oxygen and Si, Al cations (Velde and Barre, 2010). These charges attract ions from aqueous solutions. It has been observed that kaolinite has an attraction of 5 – 10 milli equivalents of cation charge per 100 g of clay due to un-terminated bonds on its crystal edges (Velde, 1985). Therefore, the amount of charge and ions fixed on the surface varies as a function of the crystal size such that the small crystals have more edge sites and hence more

attracting power (Fig 2.17). Relative charges on ions as well as the residual charges on clay structures that attract ions affect the selectivity of different species (Grim, 1968).

The amount of fertilizer to be applied must optimize economic return to fertiliser inputs. Phosphate sorption is an important process affecting the availability of phosphate to plants and the effectiveness of P-fertilisers. For kaolin rich soils, it seems probable that much of the phosphate retention is by kaolin rather than by the more reactive but much less abundant sesquioxides. Adsorbed phosphate may only be sparingly available to plants due to P-fixation by kaolin thereby requiring farmers to apply large amounts of fertiliser.

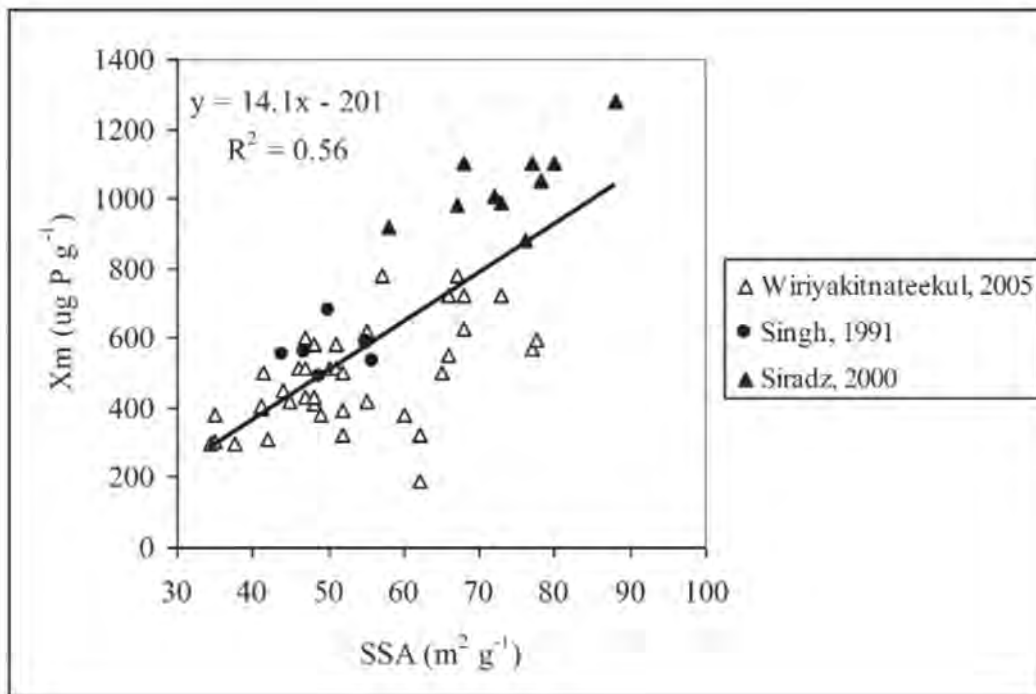


Figure 2.17: The plot Langmuir maximum P retention capacity (X_m) of kaolin from tropical soils against SSA (After Gilkes and Prakongkep, 2016).

Phosphorus in soils could either be in solution or fixed form (Fig. 2.18). Soil organic P is related to organic materials (plants and micro-organisms), whereas the inorganic P is bound to Al, Fe, Ca, Mg etc. The reactions between P and Fe-Al oxides and Ca

carbonates determine P fixation in soils (Reddy *et al.*, 1999). In soils, P is most available in the pH range of 6.5 to 7.0 (Poswa, 2016) (Figure 2.19).

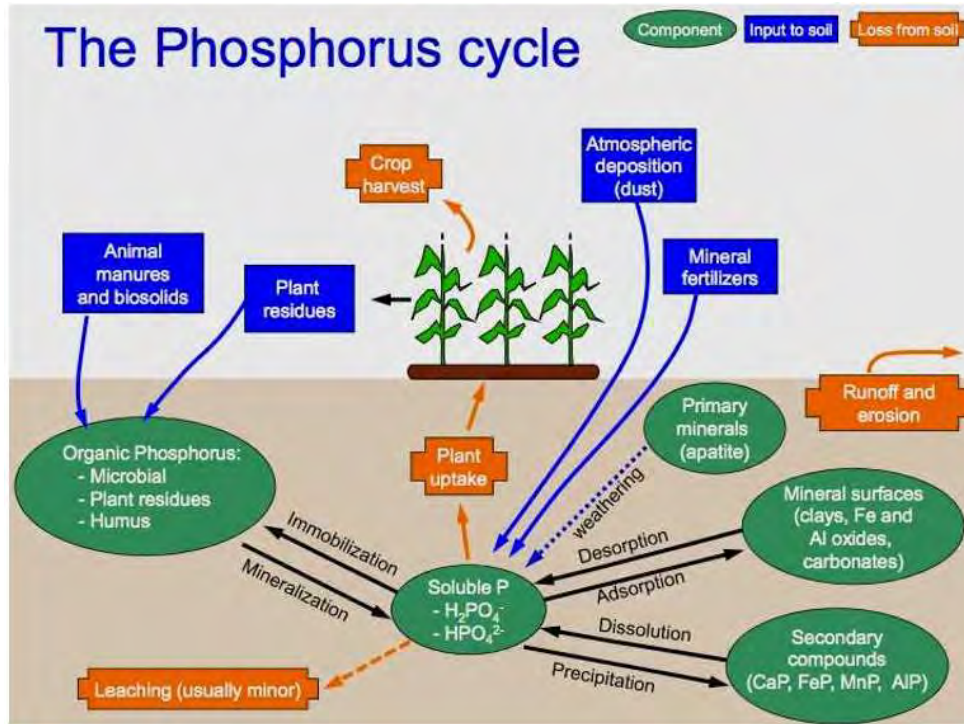


Figure 2.18: Phosphorus cycle in soil (After Filippelli, 2002).

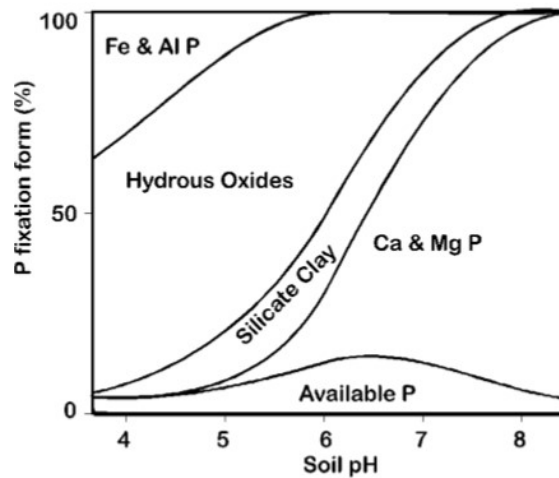


Figure 2.19: P fixation form variations with soil pH (After Poswa, 2016).

Adsorption describes sorption reactions taking place at the surface of the particles through electron donor, electron acceptor interaction, electrostatic attraction or covalent bonding. Various mathematical isotherm models have been proposed for describing the P sorption characteristics of kaolinites such as the Langmuir and Freundlich equations based on two parameters (Eqns. 2.8 and 2.9) (Wiryakitnateekul *et al.*, 2005; Singh and Gilkes, 1992).

The Langmuir isotherm assumes that maximum adsorption occurs when a saturated monolayer of adsorbate molecules is present on the adsorbent surface, the energy of adsorption is constant.

The Langmuir equation: $x = (a x_m c) / (1 + ac)$ (2.8)

Where: x = amount of P sorbed ($\mu\text{g Pg}^{-1}$ soil), c = concentration of P in equilibrium solution ($\mu\text{g Pml}^{-1}$), x_m = sorption maximum ($\mu\text{g Pg}^{-1}$ soil), and a = coefficient related to bonding energy.

Freundlich isotherm describes the multilayer adsorption of heterogeneous systems and assumes that different sites have several adsorption energies involved.

The Freundlich equation: $x = k c^b$ (2.9)

Where: x = amount of P sorbed, c = P concentration in equilibrium solution, k and b are constants. K is a measure of sorption surface and b relates to the energy of sorption.

Linear form of equation 2.8 is given as

$$c/x = (1/ax_m) + (c/x_m) \quad (2.10)$$

A plot of c/x against c should give a straight line with slope $1/x_m$ and intercept $1/ax_m$, if the data follow the Langmuir equation (Eqn. 2.10). The sorption parameters derived from the equations can be useful in predicting the maximum sorption capacity (x_m) and abundance of adsorption sites (k) for soil kaolinites which will be of interest in analysing soil fertility and other management parameters (Siradz, 2008).

Singh and Gilkes (1992) examined the P sorption characteristics of soil kaolinites from Southwestern Australia based on the Langmuir model. The P sorption maximum values for the soil kaolinites ranged from 486 – 654 μgPg^{-1} which was six times greater than that for clay fraction obtained for standard kaolin minerals which could be due to the structural disorder and higher SSA in the former whereby the soil kaolinite exposes more Al-OH site on faces and edges where P sorption is believed to occur.

Numerous studies have shown that the Redlich-Peterson and Sips isotherms were more accurate than the Langmuir and Freundlich isotherms as they contain three unknown parameters (Kumara *et al.*, 2014).

The Redlich-Peterson (R-P) isotherm is a three-parameter empirical adsorption model that incorporates elements from both the Langmuir and Freundlich isotherms (Foo and Hammed, 2010) and amends the inaccuracies. The adsorption mechanism is unique and does not follow ideal monolayer adsorption characteristics. The linear expression of the R-P isotherm model is defined as

$$\ln \left(K_R \frac{C_e}{q_e} - 1 \right) = b_R \ln C_e + \ln a_R \quad (2.11)$$

Where, K_R is the Redlich-Peterson adsorption capacity constant determined *via* trials and errors to obtain the maximum linear regression value of the isotherm graph. C_e and q_e are the equilibrium concentrations in mg/L and amount adsorbed at equilibrium (mg/g). The parameter a_R is the R-P isotherm constant and b_R is the exponent between 0 and 1. The Langmuir and Freundlich isotherms can be derived from the R-P isotherm. When $b_R = 1$, the R-P equation becomes the Langmuir isotherm equation and when $b_R = 0$, it is closer to the Freundlich equation. Hence, it can be applied to both homogenous and heterogenous systems. However, the accuracy of these interpretations strongly depends on the fitting method by varying K_R values to obtain the maximum value of the correlation coefficient for the regression in Eqn. 2.11 (Kumara *et al.*, 2014).

The Sips isotherm is derived from the limiting behavior of the Langmuir and Freundlich isotherms for predicting heterogenous system. The isotherm overcomes the drawback

associated with Freundlich model of continuing increase in the absorbed amount with increase in concentration (Foo and Hameed, 2010). When C_e approaches a low value, the Sips isotherm effectively reduces to Freundlich, while at high C_e , it predicts the Langmuir monolayer sorption characteristic. The Sips linear equation (Eqn. 2.12) model is expressed as

$$\frac{1}{q_e} = \frac{1}{Q_{\max} K_S} \left(\frac{1}{C_e} \right)^{1/n} + \frac{1}{Q_{\max}} \quad (2.12)$$

Where K_S (1/mg) and Q_{\max} (mg/g) are the Sips equilibrium constant and maximum adsorption capacity values obtained from the slope and the intercept of the plot. The Sips isotherm equation is characterised by the dimensionless heterogeneity factor, n , which can describe the system's heterogeneity when it is between 0 and 1. When $n = 1$, the Sips equation reduces to the Langmuir equation and it implies a homogeneous adsorption process (Kumara *et al.*, 2014).

2.8 Research methods review

2.8.1 Instrumental methods

The instrumental method routinely used for qualitative and quantitative mineralogical analysis of soils is X-ray diffraction (XRD). Several steps have been introduced to improve the accuracy of this method such as preliminary treatments of sample preparation as dispersion of particles, removal of organic matter, etc (Zabala *et al.*, 2007). The Rietveld method of quantitative analysis eliminates numerous instrumental and sample-related problems such as preferred orientation, separation of overlapping and broad reflections, variation in standard data with composition, etc. The Rietveld refinement approach has numerous advantages over conventional quantitative methods. The former Rietveld method uses all-reflections in pattern rather just strongest ones which minimise the uncertainty in the derived weight percentages and the effects of preferred orientation (Bish and Post, 1993). The Fourier transform infrared spectroscopy (FTIR) plays a complementary role in the interpretation of the XRD qualitative data (Ekosse, 2005;

Oyebanjo *et al.*, 2018). FTIR is a vibrational spectroscopy method which is based on absorption that emits infrared (IR) frequencies (Larkin, 2011). The use of attenuated total reflectance (ATR) has revolutionised the application of FTIR. It is now one of the most popular techniques in the analysis of soils as it is quick, non-destructive and requires no sample preparation. Typical ATR crystals used are germanium (Ge), zinc selenide (ZnSe), thallium bromiodide (KRS-5), silicon (Si) or diamond (C). These vary in their depth of penetration into the sample between approximately 0.5 and 2 μm (Smith *et al.* 2017).

Scanning Electron Microscopy with an Energy Dispersive X-ray Spectrum (SEM-EDX) is the best known and widely used for surface analytical techniques. High resolution images of surface morphologies of the sample are generated. Qualitative elemental results at a single spot can be used to create elemental map showing the distribution of elements within the area (Smith *et al.*, 2017).

The instrumental methods routinely used for the determination of major, trace, and rare earth elements in soils are atomic absorption spectrometry (AAS), X-ray fluorescence (XRF), inductively coupled plasma mass spectrometry (ICP-MS), and laser ablation – ICPMS (LA-ICP-MS) (Bulska and Ruszczynska, 2017). The flame-AAS is one of the oldest techniques, whereas the graphite furnace – AAS is an improved model of AAS. The AAS technique is a single element approach which will require 2-3 minutes per element for each sample. The XRF is ideal for rapid and accurate whole bulk major elemental analysis better than AAS, ICP-MS, and LA-ICPMS. The inductively coupled mass spectrometry (ICP-MS) is widely used in routine multielemental determination at the trace and ultratrace level in liquid samples with different matrix composition. The ICP-MS analytical procedure requires previous digestion of solid samples. However, the recent development in ICP-MS has led to the advent of the introduction of the laser ablation (LA) application. The LA-ICP-MS allows direct solid sampling which avoids wet decomposition of the sample as well as risk of contamination during sample preparation (Bulska and Ruszczynska, 2017).

2.8.2 Statistical methods

Experimental statistical procedures used in almost all scientific research are fundamental for clearer interpretation of the results of experiments conducted. However, incorrect use of these procedures can lead the researcher to incorrect or incomplete conclusions. Statistical analytical procedures are quantitative techniques used in assessing uncertainties and their effects on the interpretation of experiments and observations of natural phenomena (Zimmermann, 2004).

The term “multivariate statistics” is appropriately used to include all statistics where there are more than two variables simultaneously analysed. It involves multidimensional data with more than one dependent, Y , or outcome variable. Multivariate analysis techniques are used to understand how the set of outcome variables as a combined whole are influenced by other factors, how the outcome variables relate to each other, or what underlying factors produce the results observed in the dependent variables (Steel *et al.*, 1997). This allows the identification of the underlying structure that is presumed to exist within a set of multivariate observations (Davis, 2002). This structure is expressed in the pattern of variances and covariances between variables and the similarities between observations. Principal Components Analysis (or PCA) is a data analysis tool that is often used to reduce the dimensionality (or number of variables) from many interrelated variables, while retaining as much of the information (e.g. variation) as possible. PCA calculates an uncorrelated set of variables known as factors or principal components. These factors are ordered so that the first few retain most of the variation present in all the original variables. The factor/component analyst hopes to identify each factor/component as representing a specific theoretical/underlying factor.

Bivariate statistics involves the analysis of two variables (often denoted as X , Y), for the purpose of determining the empirical relationship between them. Bivariate statistics such as the Pearson product moment correlation coefficient and the independent groups t-test and F-test (or one-way ANOVA) are commonly used. The F-distribution is formed by the ratio of two independent chi-square variables divided by their respective degrees of freedom. The tests are designed to test if two population variances are equal by

comparing the ratio of two variances. Here, the null hypothesis (that is, no statistical difference between the variances/means) if the p-value is greater than or equal to the level of significance (0.01 or 0.05) (Davis, 2002).

Multiple regression statistics involve one continuous Y variable and two or more continuous X variables. The goal is to construct a linear model that minimises error in predicting Y. That is, to create a linear combination of the X variables that is maximally correlated with the Y variable by obtaining standardised regression coefficients. The predictors which are the independent variables may be entered all at once (simultaneous) or in sets of one or more (sequential). We may use some a priori hierarchical structure to build the model sequentially (enter first X1, then X2, then X3, etc., each time seeing how much adding the new X improves the model, or, start with all X's, then first delete X1, then delete X2, etc., each time seeing how much deletion of an X affects the model). We may just use a statistical algorithm (one of several sorts of stepwise selection) to build what we hope is the “best” model using some subset of the total number of X variables available. This method has been widely applied in modelling how soil properties' affect P sorption in soils (Umoh *et al.*, 2014). Most literatures referred to it as stepwise regression analyses (Mnthamballa *et al.*, 2015).

2.10 Concluding Remarks

This literature review chapter focused on the geological framework of South Africa with interest on the Limpopo mobile belt. The chapter examined the various factors important in soil formation such as climate, parent material, time, organisms, and topography (relief). Published works on the mineralogy and geochemistry of kaolins in soils relative to reference kaolins were also reviewed. Kaolin distribution in South African soils were also discussed with emphases on humic, plinthic, and oxidic soils. The chapter concluded by examining pedoclimatic, pedogenetic, and fertility implications from the nature of kaolins in soils, and provided a review of research methods.

Chapter Three

Research Methods

The research design adopted in this study was quantitative (Davis, 2002) to generate primary data on the mineralogical and geochemical characteristics of the soils and soil kaolins. In addition, experimental research design which also falls under the quantitative research methods was used in assessing the P sorption characteristics of the soils and soil kaolins. Statistics and relevant models were used to analyse, explain, and establish trends and relationships observed (Zimmermann, 2004). This chapter presents the methodology followed in the fieldwork, sample preparation, laboratory and data analyses, and interpretation employed for this study.

3.1 Soil and Rock Sampling

Reconnaissance visits to selected sites were made based on the geology of Vhembe and Capricorn Districts, Limpopo Province, South Africa (Fey, 2010; Hunter *et al.*, 2006) to locate parent rocks, soil profiles developed from them and identify various zones within the soil horizons. The geology, location, profile description, and climate type information for the study areas are summarised in Table 3.1. The soil type was dominantly Hutton Form Portsmouth 35 Series (Hu35) (ARC-ISCW, 2006).

Table 3.1: Summary Details on the Study Areas

S/N	Geology	Location	Profile Description ^a	Climate ^b
1.	Basalt	Sibasa	Orthic A with deep red apedal B horizon	Semi-Arid, dry hot (BSh)
2.	Granite Gneiss	Muledane	Orthic A with shallow yellow-brown apedal B horizon	Semi-Arid, dry hot (BSh)
3.	Granite	Matoks	Orthic A with shallow yellow-brown apedal B horizon	Warm temperate, winter dry, hot summer (Cwa)
4.	Arkasic Sandstone	Sagole	Orthic A with shallow yellow-brown apedal B horizon	Semi-Arid, dry hot (BSh)

^(a) - Soil Classification Working Group (1991) and Fey (2010) and

^(b) - Köppen-Geiger Climate classification for South Africa (Conradie, 2012).

Three (3) soil profiles developed from each parent rocks (basalt, granite gneiss, granite, and arkosic sandstone respectively) were selected. A control site underlain by quartzite in Matavhela village (close to Sagole village) was chosen because it does not readily contain primary minerals that can weather to form kaolins. The soil information for the control sampling site is similar to those of the arkosic sandstone in Sagole village (Table 3.1). Using judgmental sampling technique (Tan, 2011; Diko and Ekosse, 2013), representative soil samples were collected using a soil auger (Figs. 3.1 – 3.5) from depths ranging from 0 - 20, 20-50, and 50 – 100 cm depending on the depth to bedrock and labelled appropriately. Prior to sampling, the topmost part of the soil was scraped off before sample collection to reduce the effect of any external leached material and surface contamination (Deepthy, 2008). Fresh hand specimen samples of the parent rocks were collected *in situ* from each of the soil sampling sites (except for granite gneiss which could not be sampled because the exposed rocks were highly weathered). A geologic hammer was used to break the various grab rock samples collected.

A total of twenty-six (26) soil and ten (10) rock samples were collected (Table 3.2). The soil samples were coded for ease of handling as S, MAT, SA, MU, and CMA for basalt, granite, arkosic sandstone, granite gneiss, and quartzite, respectively. Numbers were added to these codes except for CMA (e.g S1, MAT1, SA1, MU1) to differentiate the soil samples associated with specific profiles from the various parent rocks.

3.2 Soil Sample Preparation

Disaggregation of air-dried samples was done gently using a mortar and pestle without grinding them so that coarse grained non-clay minerals will not be reduced to the clay-size range. This was also to ensure that the internal structures of the particles were not destroyed (Deepthy, 2008). The disaggregated samples were transferred into a nest of sieves comprising of 2 mm (top), 1 mm, 125 μm , 105 μm , 63 μm sizes and the collection plate (bottom) and placed on a vibratory Fritsch Spartan Analysette 3 – Pulverisette sieve shaker in the Soil Science Laboratory, School of Agriculture, University of Venda (UNIVEN) for 10 minutes where an electromagnetic drive causes

vertical oscillation of the sieves. The <2 mm fraction was taken as the bulk soil sample (van Reeuwijk, 2002). The <63 μm fraction (silt + clay) were collected from which the clay (<2 μm) fraction was later separated from the silt (between 2 μm and 63 μm) fraction.

The presence of organic matter in samples can affect analyses; for example, by inhibiting soil dispersion into various fractions, producing broad x-ray diffraction peaks, and increasing the background. Organic matter was removed from the samples by oxidation with 30% hydrogen peroxide (H_2O_2) as described by Jackson (1979) and Bird and Chivas (1988) in the Soil Science Laboratory, School of Agriculture, UNIVEN. Fifty grams of each bulk samples were transferred into 500 ml beakers and 20 ml of H_2O_2 were added to the samples.

Table 3.2: Number of Samples collected at each location.

Location	Coordinates	Parent Rock	Samples				Total
			Rock	Soil 0-20 cm	Soil 20-50 cm	Soil 50-100 cm	
Sibasa	22° 57' 09" S 30° 27' 10" E	Basalt	1	1	1	1	4
	22° 57' 27" S 30° 27' 51" E	Basalt	1	1	1	1	4
	22° 56' 17" S 30° 28' 13" E	Basalt	1	1	1	1	4
Matoks	23° 27' 46" S 29° 44' 03" E	Granite	1	1	1	-**	3
	23° 27' 16" S 29° 44' 48" E	Granite	1	1	1	-**	3
	23° 26' 03" S 29° 44' 49" E	Granite	1	1	1	-**	3
Sagole	22° 31' 39" S 30° 36' 16" E	Arkoscic Sst.	1	1	1	-**	3
	22° 31' 01" S 30° 36' 54" E	Arkoscic Sst.	1	1	1	-**	3
	22° 30' 20" S 30° 36' 44" E	Arkoscic Sst.	1	1	1	-**	3
Muledane	23° 01' 06" S 30° 27' 08" E	Granite Gneiss	-*	1	-**	-**	1
	23° 01' 36" S 30° 27' 41" E	Granite Gneiss	-*	1	-**	-**	1
	23° 02' 16" S 30° 27' 28" E	Granite Gneiss	-*	1	-**	-**	1
Matavhela	22° 40' 24" S 30° 33' 51" E	Quartzite (Control)	1	1	1	-**	3
	Total						36

*Highly weathered samples; **Weathered bedrock encountered at that depth.



Figure 3.1: Soil developed from Basalt at Sibasa area.



Figure 3.2: Soil developed from Granite Gneiss at Muledane area.



Figure 3.3: Soil developed from Granite at Matoks area.



Figure 3.4: Soil developed from Arkosic Sandstone at Sagole area.



Figure 3.5: Soil developed from Quartzite at Matavhela area.

To make up to 300 ml, distilled water was added to each of the beakers and placed on a sand bath for approximately four hours at a temperature of 200 °C until the supernatant was clear when all the organic matter had been decomposed. The samples were washed thoroughly with distilled water after this treatment. After the removal of organic matter from the bulk samples, they were oven-dried at 105 °C and gently crushed and packaged for mineralogical and geochemical analyses.

3.2.1 Separation of Clay and Silt Fractions

After the removal of organic matter from the <63 μm fraction, the samples were dispersed and centrifuged as described by Suslick and Price (1999) and Jakubowska (2007) in order to obtain the clay fractions. The clay fractions were obtained by ultrasonication with an energy input of 300 J m/L (1 min) using probe type ultrasonic

disintegrator UP400S equipped with 7 mm diameter sonotrode S7 in the Ecology and Resource Management Laboratory, School of Environmental Sciences, UNIVEN. After the ultrasonic irradiation, the samples were centrifuged (using a Grant-bio LMC-3000 centrifuge) at 1000 rpm for 3 mins. The floating phase (clay fraction) and the settling phase (silt fraction) were transferred into petri dishes and oven dried at 105 °C. The oven dried (using a Labotec EcoTherm Digital Oven) clay and silt fractions were gently crushed and packaged for laboratory analyses.

3.3 Rock Sample Preparation

Thin sections of the collected rock samples were prepared at the Mineralogy Section Laboratory, Council for Mineral Technology (MINTEK), Randburg. The rock samples were impregnated in blue epoxy, glued after drying onto 2.5 cm x 4.5 cm glass slides and then polished to a thickness of about 30 µm for petrographic analyses. The rock samples were also crushed in stainless steel jaw crusher and then pulverised to be a homogenous powder in the department of Mining and Environmental Geology, UNIVEN prior to mineralogical and geochemical analyses.

3.4 Laboratory Analyses

The various size fractions were analysed to generate physico-chemical, mineralogical, and chemical data (Table 3.3).

3.4.1 Analyses of Bulk Soil Samples

3.4.1.1 Physico-chemical Analyses

i. Particle Size Distribution

The determination of three fractions (sand, silt, and clay) by hydrometer followed the procedures described by van Reeuwijk (2002). The method is based on the Stoke's law (Eqn. 3.1) governing the rate of sedimentation of particles suspended in water (Gaspe *et al.*, 1994).

Table 3.3a: Summary of the various soil analyses conducted, size fractions, number of samples and laboratory where they were carried out.

S/N	Analyses		Particle size fraction	Number of samples	Laboratory where analyses were done
1.	Physico-chemical	Colour, particle size distribution (PSD), pH and EC	Bulk	26	Department of Soil Science, University of Venda (UNIVEN)
2.	Mineralogical	X-ray diffraction	Bulk	10+01**	Department of Geology, University of Pretoria (UP)
			Silt	10	
			Clay	26	
			DF Clay*	16	
		Fourier transform infrared spectroscopy	DF Clay*	26	Department of Ecology and Resource Management, UNIVEN
Thermogravimetric analysis and Differential scanning calorimetry	DF Clay*	16	Department of Chemistry, University of Johannesburg (UJ)		
Scanning electron microscopy	Clay	10	Mineralogy Section, MINTEK		
3.	Chemical	X-ray fluorescence spectroscopy (XRF) and Laser ablation inductively coupled plasma mass spectroscopy (LA-ICP-MS)	Bulk	26+01**	Central Analytical Facilities, Stellenbosch University (SU).
			Silt	10	
			Clay	10	
			DF Clay*	21	
		Energy-dispersive X-ray spectroscopy	DF Clay*	10	Mineralogy Section, MINTEK
		CEC	Bulk	13	Agricultural Research Council, Pretoria
			DF Clay*	10	
		OM	Bulk	13	Agricultural Research Council, Pretoria
Available Phosphorus	Bulk	13	Agricultural Research Council, Pretoria		
Phosphorus Adsorption	Bulk	13	Department of Ecology and Resource Management, UNIVEN		
	DF Clay*	13			

*Deferated clay fraction (Soil kaolins); **duplicate sample

Table 3.3b: Summary of the various rock analyses conducted, number of samples, and laboratory where they were carried out.

S/N	Analyses		Number of samples	Laboratory
1	Mineralogical	Petrography	10	Mineralogy Section, MINTEK
2	Chemical	XRF and LA-ICP-MS	10	Central Analytical Facilities, SU.

$$V = 2 g r^2 (d_1 - d_2) / 9\eta \quad (3.1)$$

Where V = rate of settling particles (cm/s), g is the acceleration due to gravity (981 cm/s^2), r is the radius of the particles (cm), d_1 is density of the particles g/cm^3 , d_2 is the density of fluid (water) (g/cm^3), and η is the viscosity (g/cms).

Fifty grams of dispersed sample (Section 3.2) was transferred into sedimentation cylinder and filled to 1000 ml mark with deionised water and allowed to stand overnight to equilibrate. In addition, 100 ml of 5% calgon dispersion solution was mixed with 880 ml of deionized water in a 1000 ml cylinder to prepare a blank solution. For each sample, the temperature was measured at the beginning of the experiment and the hydrometer reading of the blank was taken. The density was determined by inserting the plunger into suspension and carefully mixed for 30 secs until a uniform suspension was obtained. The hydrometer reading was taken by inserting the ASTM 152H soil hydrometer after 40 secs. This represents the amount of silt plus clay suspended since the sand has settled to the bottom of the cylinder by this time. The temperature was taken again and the hydrometer reading was measured again after 6 hours, 52 minutes. This is the amount of clay in suspension. The silt has settled to the bottom of the cylinder by this time. Temperature and density corrections were made by adding 0.2 unit to the reading for every 1°C above 20°C , and subtraction of 0.2 unit from the reading for every 1°C below 20°C . The density of the blank at each reading was subtracted from the corresponding density readings for each of the samples.

The percentages of clay, silt, and sand were determined as follows:

$$P_{\text{clay}} = (\text{corrected hydrometer reading at 6 hrs, 52 mins/ wt of sample}) \times 100 \quad (3.2)$$

$$P_{\text{silt}} = ((\text{corrected hydrometer reading at 40 secs/ wt of sample}) \times 100) - (P_{\text{clay}}) \quad (3.3)$$

$$P_{\text{sand}} = 100 \% - P_{\text{silt}} - P_{\text{clay}} \quad (3.4)$$

The P_{clay} , P_{silt} , and P_{sand} are plotted on the textural triangle to determine the sample textures.

ii. Colour Determination

Visual colour assessment provided a rapid means of simply comparing different samples but the use of a Munsell soil colour chart with separate notations for hue, value, and chroma (HVC) gave an objective assessment. These three variables represent all visible colours in equally distributed increments, represented by colour chips. Dry bulk soil samples were used since moisture can significantly affect whiteness (SSS, 2014). The HVC characteristics and colour of each sample was obtained by making visual comparison with the soil colours in the Munsell soil colour chart (Ruck and Brown, 2015).

iii. Hydrogen Ion Concentration (pH) and Electrical Conductivity (EC) Measurements

About 50 ml of water was added to 20 g of the bulk soil sample in a 100 ml polythene wide-mouth type bottle. The bottle was subsequently capped and shaken for 2 hours. Prior to the determination of the pH, the bottle was shaken by hand once or twice before opening. The pH meter electrode probe was immersed in the upper part of the suspension. Measurements were made using a Thermoscientific Orion VersaStar pH meter twice and the average recorded for each sample. Commercial buffer solutions of pH 7.0 and 4.0 were used for calibration of the pH meter. A Thermoscientific Orion VersaStar conductivity meter calibrated using a conductivity standard (1413 $\mu\text{S}/\text{cm}$ at 25 °C) electrode probe was immersed in the upper part of the suspension. The measurements were taken twice and the average recorded for each sample. These steps followed the procedures outlined by van Reeuwijk (2002).

3.4.1.2 X-ray Diffraction (XRD) Mineralogical Analyses

The samples were prepared according to the standardized Panalytical backloading system, which provides nearly random distribution of the particles. The samples were analysed using a PANalytical X'Pert Pro powder diffractometer with an X'Celerator detector and variable divergence- and fixed receiving slits with Fe filtered Co-K α radiation ($\lambda=1.789 \text{ \AA}$). Samples were scanned from $0.02^\circ 2\theta$ to $85^\circ 2\theta$ at a counting time of 0.5 secs. The diffraction peaks occur when the paths of the diffracted x-ray are equal to an integer multiple of the path difference expressed by Bragg's equation as follows:

$$n\lambda = 2d\sin\theta \quad (3.5)$$

Where; n = integer, λ = wavelength, d = interactive spacing in Angstroms (\AA), and θ = diffraction angle.

The phases were identified using X'Pert Highscore plus software and compared with data and patterns available in the mineral powder diffraction file (ICDD, 2002) for confirmation. The relative phase amounts (weight %) was estimated using the Rietveld method (Autoquan Program). The qualitative and quantitative analyses were carried out at the Department of Geology, University of Pretoria.

3.4.1.3 Chemical Analyses

i. Organic matter

The organic matter content of soil was indirectly estimated through multiplication of the organic carbon concentration by 1.724. The organic carbon was determined according to the Walkley and Black wet oxidation procedure (Walkley and Black, 1934). This involved wet combustion of organic carbon with a mixture of potassium dichromate and sulfuric acid. After reaction, the residual dichromate was titrated against ferrous sulphate (Nelson and Sommers, 1996). A weight of 0.5 g of soil was placed in a 250 ml Erlenmeyer flask. 5 ml of 1N $\text{K}_2\text{Cr}_2\text{O}_7$ was added into the flask and swirled gently to disperse the soil into suspension. Then 10 ml of concentrated H_2SO_4 was further added to the flask, swirled gently until the soil and reagents were mixed. Phosphoric acid (H_3PO_4) was then added to the flask to eliminate interferences from the ferric (Fe^{3+}) ion that may be present in the sample. The phosphoric acid forms a complex with the interfering Fe^{3+} which provides a sharper color change of the indicator. The flask was

allowed to stand with occasional swirling for 30 minutes before the addition of 30 ml of deionized water and 3-4 drops of o-phenolphthalein indicator. The solution was titrated with 1N FeSO_4 until the colour changes to a red end point.

ii. Cation Exchange Capacity (CEC)

Cation exchange capacity was measured using 0.01 M silver thiourea solution at pH 4.7 to displace the exchangeable cations (Rayment and Higginson, 1992). A weight 2 g of soil was placed into acid washed vials and 20 ml of 0.01 Ag (TU) was added and shaken for 16 hrs. 10 ml of 1% La-chloride and 5 ml of 5% HNO_3 was added to centrifuged and pipetted 1 ml of soil extraction in 100 ml volumetric flask and made up to 100 ml with deionised water. The concentration of Na, K, Ca, and Mg in solution was determined by using atomic absorption spectrophotometry (AAS). Exchangeable Al was determined according to the procedures of Non-Affiliated Soil Analysis Working Group manual (1990).

iii. Available Phosphorus Determination

The readily acid – soluble forms of phosphorus were extracted with Bray No. 1 solution as outlined by Olsen and Sommers (1982). Phosphorus in the sample was determined on an AAS (210 VGP Buck scientific) by the blue ammonium molybdate with ascorbic acid as a reducing agent. A 5 g soil was weighed into 100 ml extraction bottle and 35 ml of Bray 1 solution (0.03 M NH_4F and 0.025 M HCl) was added. The bottle was placed in a reciprocal shaker, shaken for 10 minutes and filtered through Whatman No. 42 filter paper. An aliquot of 5 ml of the filtrate was pipetted into 25 ml flask and 10 ml colouring reagent (ammonium paramolybdate) was added followed by a pinch of ascorbic acid. After mixing well, the mixture was allowed to stand for 15 minutes to develop a blue colour. The colour was measured using a Thermo/Milton Roy Spectronic 21D spectrophotometer at 660 nm wavelengths. The available phosphorus was extrapolated from a standard curve.

A standard series of 0, 1.2, 2.4, 3.6, 4.8, and 6.0 mg P/l was prepared by pipetting respectively 0, 10, 20, 30, 40 and 50 ml of 12.0 mg P/l in 100 ml volumetric flask and made to volume with distilled water.

Calculation:

$$P \text{ (mg/kg)} = ((a - b) \times d \times e \times mcf) / g \quad (3.6)$$

Where: a = mg P/l in the sample extract, b = mg P/l in the blank, g = sample weight in grams, mcf = moisture correction factor, d = volume of extraction solution (35 ml), and e = final volume of the sample solution (15 ml).

iv. X-ray Fluorescence (XRF) Spectrometry

For the major element compositions, glass disks were prepared for XRF analysis using 7 g of high purity trace element and Rare Earth Element (REE)-free flux ($\text{LiBO}_2 = 32.83\%$, $\text{Li}_2\text{B}_4\text{O}_7 = 66.67\%$, $\text{LiI} = 0.50\%$) mixed with 0.7 g of the powder sample following the procedures described by Verma *et al.* (1996). Whole-rock major element compositions were determined by XRF spectrometry on a PANalytical Axios Wavelength Dispersive spectrometer at the Central Analytical Facilities, Stellenbosch University (SU), South Africa. The spectrometer is fitted with an Rh tube and with the following analyzing crystals: LIF200, LIF220, PE 002, Ge 111 and PX1. The instrument is fitted with a gas-flow proportional counter and a scintillation detector. The gas-flow proportional counter uses a 90% Argon-10% methane mixture of gas. Major elements were analysed on a fused glass disk using a 2.4kW Rhodium tube. Matrix effects in the samples were corrected for by applying theoretical alpha factors and measured line overlap factors to the raw intensities measured with the SuperQ PANalytical software. The concentration of the control standards that were used in the calibration procedures for major element analyses fit the range of concentration of the samples. Amongst these standards were NIM-G (Bushveld Granite from the Council for Mineral Technology, South Africa) and BE-N (Basalt from the International Working Group).

The Loss on Ignition (LOI) was determined by oven-drying the samples at 105 °C overnight to remove the moisture. About 2.0 g of the samples were taken in a silica

crucible and placed inside a muffle furnace at 1000 °C for 2 hours. Then it was allowed to cool to room temperature inside a dessicator to avoid adsorption of moisture and weighed again. LOI was calculated using equation 3.7 (van Reeuwijk, 2002).

$$\text{LOI (wt \%)} = ((W_2 - W_3) / (W_2 - W_1)) \times 100 \quad (3.7)$$

Where: W_1 is the weight of the empty crucible, W_2 is the total weight of the crucible plus sample before keeping inside furnace, and W_3 is the total weight of the crucible and sample after heating to 1000 °C.

v. Laser Ablation – Inductively Coupled Plasma – Mass Spectrometry (LA-ICP-MS)

The LA-ICP-MS allows direct analysis of solid samples with minimal sample treatment using sample introduction system including laser and spark ablation (Gunther and Hattendorf, 2005). A Resolution 193 nm Excimer laser from ASI connected to an Agilent 7700 ICP-MS was used in the analysis of trace elements in the samples (Fig. 3.1). Ablation was performed in He gas at a flow rate of 0.35 L/min, then mixed with argon (0.9 L/min) and Nitrogen (0.004 L/min) just before introduction into the ICP plasma. The procedure followed the descriptions by Gunther and Hattendorf (2005). For traces in fusions, 2 spots of 100 µm is ablated on each sample using a frequency of 10 Hz and 2 mJ energy. Fusion disks prepared for XRF analysis by an automatic Claisse M4 Gas Fusion instrument and ultrapure Claisse Flux, using a ratio of 1:10 sample:flux, were coarsely crushed and a chip of sample mounted along with up to 12 other samples in a 2.4 cm round resin disk. The mount was mapped, and then polished for analysis.

Trace elements were quantified using NIST 612 for calibration and the % SiO₂ from XRF measurement as internal standard, using standard – sample bracketing. Two replicate measurements were made on each sample. The calibration standard was repeated after every 12 samples. A quality control standard was ran in the beginning of the sequence as well as with the calibration standards throughout. BCR-2 or BHVO 2G, both basaltic glass certified reference standards produced by USGS (Wilson, 1997), was used for this purpose. A fusion control standard from certified basaltic reference material (BCR-2, also from USGS) was also analysed in the beginning of a sequence to

verify the effective ablation of fused material. Data was processed using Glitter software, distributed by Access Macquarie Ltd., Macquarie University NSW 2009, USA. The analyses were carried out at the Central Analytical Facilities, SU, South Africa.



Figure 3.6: Laser 193 nm Excimer interfaced to the Agilent 7700 ICP-MS.

3.4.2 Analyses of Clay and Silt Fractions

The X-ray diffraction (XRD) was carried out to determine the mineral constituents present in the clay and silt fractions and hence be able to identify the soils having kaolins as the dominant clay mineral. The mineralogical analyses were done following the procedures earlier described in Section 3.4.1.2. The geochemical analyses of the clay and silt fractions were also carried out following the same description as earlier discussed under Section 3.4.1.3.

3.4.3 Analyses of Soil Kaolins

Organic matters were removed from selected representative soil kaolins (<2 μm) using hydrogen peroxide (H_2O_2) as described by Jackson (1979) and Bird and Chivas (1988). Free iron oxides were removed from the soil kaolins by repeated treatment with dithionite citrate bicarbonate following the procedure of Mehra and Jackson (1960). The purified soil kaolin samples were used to study various properties of the kaolins in soil using a variety of techniques.

3.4.3.1 Chemical Analyses

The chemical analyses (CEC, XRF, and LA-ICP-MS) of the soil kaolins were also carried out following the same description as earlier discussed under Section 3.4.1.3.

i. Phosphate Adsorption Capacity Analyses

Three grams of each of the bulk soil (< 2 mm) and soil kaolin (< 2 μm) samples were equilibrated in 30 mL 0.01 M CaCl_2 , containing 0, 20, 40, 60, and 80 mg L^{-1} P in 50 mL centrifuge tubes for five days at room temperature as described by Fox and Kamprath (1970). Three drops of toluene were added to each of the samples to suppress microbial growth. The suspensions were shaken mechanically using an isothermal shaker at room temperature twice daily for 30 minutes. At the end of five days, the suspension was centrifuged at 1600 rotation per minute (rpm) for 15 minutes and the supernatant was filtered. The P concentration in the filtrate was determined photometrically using MERCK Spectroquant Pharo 100 Spectrophotometer at Department of Ecology and Resource Management, UNIVEN following the Phosphate cell test manual (2016). All adsorption measurements were carried out in triplicate. The difference between the amount of P in solution before and final after equilibrium (c) were taken as the amount of P sorbed (x). Blank/control experiments were conducted using the various P concentrations without adsorbents (soil and soil kaolins). These were carried out to account for P precipitation out of solution (if any). No precipitation was observed and hence, no need for the correction of the initial P concentrations used.

3.4.3.2 Mineralogical Analyses

i. X-ray Diffraction Analysis

X-ray diffraction was used to identify minerals other than clay minerals and determine kaolinite crystallinity indices of the soil kaolins. This was done following the procedures earlier described in Section 3.4.1.2.

ii. Scanning Electron Microscopy with an Energy Dispersive X-ray Spectrum (SEM-EDX)

The morphological and microchemical analyses of the soil kaolins were carried out using a Zeiss EVO MA15 Scanning Electron Microscope (Fig. 3.7) at Mineralogy section, MINTEK with the images obtained by backscattered electron detector. The procedure followed the descriptions by Leonard *et al.*, 2012. Backscattered electron images provide a qualitative representation of composition of a sample and its phases. The brightness of a phase is proportional to the atomic mass of the phase. Therefore, a phase which appears brighter has an atomic mass greater than the surrounding or adjacent phase. Prior to imaging, the samples were mounted on aluminium stubs with double sided carbon tape. The samples were then coated with a thin (~10 nm thick) layer of gold, using an Edwards S150A Gold Sputter Coater. This is done in order to make the sample surface electrically conductive to avoid electron build-up on the sample surface which can cause electron charge. A Zeiss Back Scattered Electron (BSE) Detector (Zeiss NTS BSD) and Zeiss Smart SEM software were used to generate BSE images. The samples were further set in epoxy resin, polished and chemically quantified by semi-quantitative Bruker Energy Dispersive Spectrometry (EDS) system. Elemental maps were captured to illustrate and verify the mode of occurrence of the kaolins and other minerals associated with it. Element mapping is a procedure available on the SEM where specific selected chemical elements can be 'searched' within a microscopic field of view, and the relative concentrations of the element are illustrated with different selected colours. If one particular element is present in a particle, the specific particle is highlighted with the colour for that element.

Beam conditions during the quantitative analysis and backscattered electron image analysis on the Zeiss EVO MA15 were 20 kV accelerating voltage, 2 nA probe current. The counting time was 10 seconds live-time.



Figure 3.7: Zeiss EVO MA15 Scanning Electron Microscope.

iii. Fourier Transform Infrared (FTIR) Spectrophotometry

The FTIR in clay mineralogy can characterise the functional group in clays and fingerprint regions of very small quantities of samples (Tan, 2011). The clay size fraction

was used to minimise the dispersion of the Infrared spectra (IR) beam, scattering of radiant IR, and the distortion and broadening of absorption bands which arises from sample size heterogeneity with coarse particles causing interferences (Deepthy, 2008). The IR (400 to 4000 cm^{-1} with a resolution of 4 cm^{-1}) spectra were obtained using a Bruker Alpha Platinum – Attenuated total reflectance (ATR) Spectrometer (Fig. 3.8) at Department of Ecology and Resource Management, UNIVEN following the procedures outlined by Madejova and Komadel (2001). To achieve high quality spectra, good contact between the sample and the ATR crystal (ZnSe) was ensured. The Bruker's spectroscopy software, OPUS, allowed real time monitoring of the spectral quality after applying pressure on the sample. The IR peaks were reported based on % transmittance to given wavelengths.



Figure 3.8: Bruker Alpha Platinum – Attenuated total reflectance (ATR) Spectrometer.

The FTIR is an alternative method in the determination of kaolinite disorder (crystallinity) degree based on differences in the position and relative intensity of OH stretching and bending bands in IR spectrum (Madejova *et al.*, 1997). Vaculikova *et al.* (2011) proposed two approaches in determining the degree of structural disorder of kaolinites from IR spectra namely, empirical approach (IR-E) and numerical approach (IR-N). The IR-E is based on resolution and relative intensities of bands in OH stretching and bending region whereas IR-N is based on crystallinity indices (CI) calculated from the intensities selected vibration modes structural OH bands.

iv. Thermogravimetric Analysis and Differential Scanning Calorimetry (TGA-DSC)

The TGA-DSC techniques were the methods used in investigating the thermal characteristics of the soil kaolins. TGA measures change in weight during heating or cooling whereas DSC measures heat absorbed or liberated during heating or cooling. The endothermic and exothermic reactions occurring during the heating of the soil kaolin was recorded by a differential thermal analyzer. The operating principle is based on the Kissinger (1956) equation (Eqn. 3.8) from which the peak temperature can be calculated.

$$\ln (\Theta T_m^{-2}) = C - E (RT_m^{-1}) \quad (3.8)$$

Where: Θ = Heating rate, T_m = Peak temperature, C = Integrating constant, E = Activation energy, and R = Gas constant.

A TA instrument SDT Q600 TGA-DSC analyser in the Department of Chemistry, UJ was used for the thermal analysis. The sample (10 mg) was heated from room temperature (25 °C) to 1100 °C, at a rate of 10 °C/min (Ekosse, 2007; Diko *et al.*, 2016).

3.4.4 Analyses of Parent Rocks

The chemical analyses (XRF and LA-ICP-MS) of the parent rocks were carried out following the same description as earlier discussed under Section 3.4.1.3.

3.4.4.1 Mineralogical Analyses

i. X-ray Diffraction Analysis

X-ray diffraction was used to identify minerals present in the parent rocks. This was done following the procedures earlier described in Section 3.4.1.2.

ii. Petrographic Analysis

An Olympus BX41 Petrographic microscope with a dedicated camera was utilised in conjunction with the Stream Essentials software package at Mineralogy section, MINTEK (Fig. 3.9). The optical analysis was conducted for qualitative determination of minerals present. For proper identification of the minerals, all thin sections were studied under both plain polarised light (ppl) and cross polarised light (xpl). The ppl was to distinguish mineral characteristics, such as relief and pleochroism whereas, the xpl was used for the observation of zoning and twinning in the minerals.

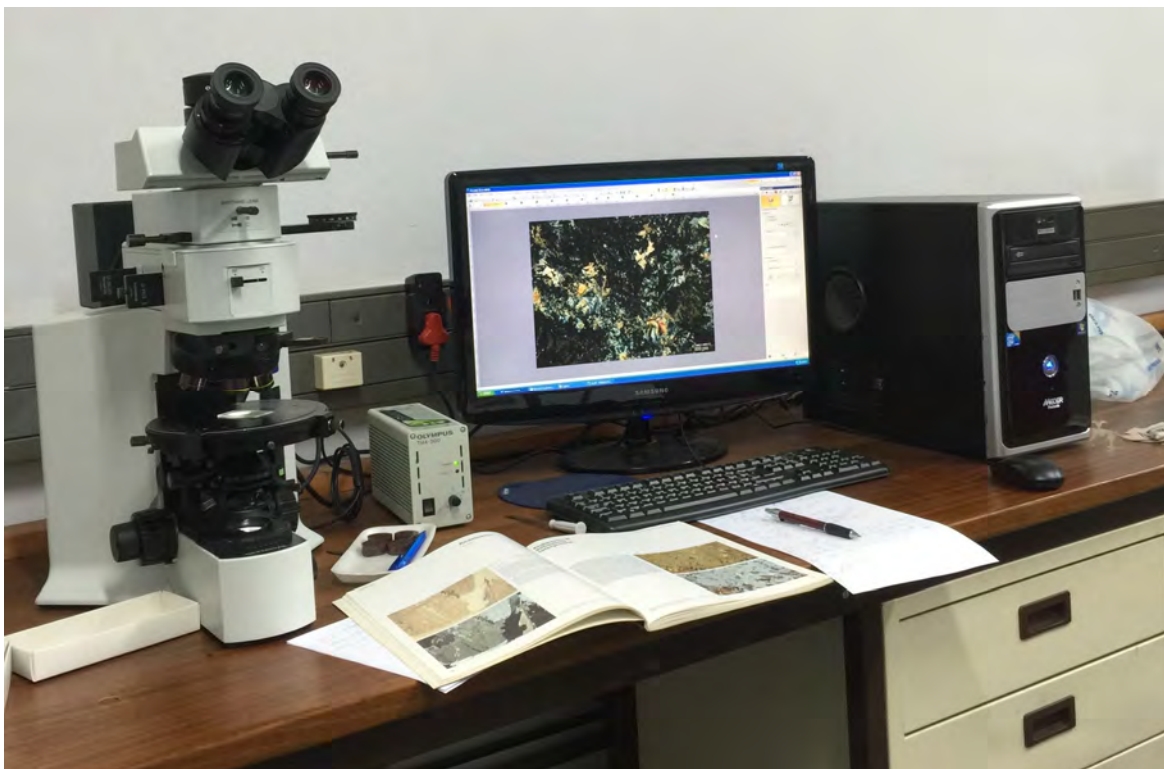


Figure 3.9: Olympus BX41 Petrographic Microscope.

3.4.5 Validation of Analytical Procedures

Validation is an important feature in any method of measurement because it is closely related to the quality of the results. Therefore, the analytical information must be of sufficient quality and accuracy. The quality of data generated in the laboratory depends on the integrity of the samples collected from the field. To avoid sample contamination, standard field precautions and procedures were followed during field sampling. During all the laboratory analyses, all apparatuses were thoroughly cleansed with distilled water and in some cases acetone to avoid sample contamination. In evaluating laboratory accuracy, duplicate samples were analysed. In addition, standard reagents and chemicals used were supplied by MERCK (Pty) Ltd., Johannesburg, South Africa.

3.5 Data Interpretation

3.5.1 Sorption Parameters and External Phosphorus Requirement (EPR)

The data obtained from phosphate adsorption capacity analyses were fitted to the (i.) **Langmuir model** (Eqn. 3.9) by plotting c/x against c which will give a straight line (if it follows the Langmuir Model) with slope $1/x_m$ and intercept $1/ax_m$. The Langmuir model will then be used to calculate different P buffer indices (i) maximum P adsorption (x_m), defined as the amount of P adsorbed when surfaces are saturated, (ii) P affinity or binding energy (a) measures comparatively how strongly the added phosphorus is adsorbed or released from the adsorbing surface. It is the reciprocal of the equilibrium P concentration at the saturation of the half of total available site (slope/intercept) (Olsen and Watanabe, 1957), and (iii) maximum buffering capacity (MBC) is a capacity factor which measures the ability of the soil to replenish phosphate ions in soil solution when they are depleted. It is the maximum slope of the Langmuir isotherm, calculated from $a \cdot x_m$ (Holford and Mattingly, 1976).

$$\text{Linear form: } c/x = (1/ax_m) + (c/x_m) \quad (3.9)$$

(ii.) **Freundlich model** (Eqn. 3.10) by plotting $\log x$ against $\log c$ with slope $(1/n)$ and intercept $(\log a)$ from which the P sorption energy (n) and sorption capacity (a) will be calculated respectively (Singh and Gilkes, 1992; Amrani *et al.*, 1999 and Hamdi *et al.*, 2014). The sorption capacity will be considered as a capacity factor, implying that a soil

having large sorption capacity value has a great absorbing capacity. It could be a measure of the heterogeneity of surface sites having different affinities for phosphate retention by the soil.

$$\text{Linear form: } \log x = \log a + 1/n \log c \quad (3.10)$$

R² values will give the goodness fit of the data to the model regression lines from the graphs.

The external phosphorus requirement (EPR) which is the amount of P that must be added to the soil to maintain a soil solution critical concentration of 0.2 mg P l⁻¹ below which crops/plants will suffer from P deficiency (Bolland *et al.*, 2003; Mnthambala *et al.*, 2015). This critical value will be substituted into the fitted Langmuir equation ($x = (a x_m c) / (1 + ac)$) and Freundlich equation ($x = k c^{1/b}$) respectively.

In addition, the Redlich-Peterson and Sips three parameter isotherms were further used to assess the ability of the two parameter isotherms to model the equilibrium sorption data (Ayawei *et al.*, 2017). The plots of $\ln(C_e/q_e)$ versus $\ln C_e$ and $\ln[q_e(X_m - q_e)]$ versus $\ln C_e$ enabled the determination of the Redlich-Peterson and Sips constants from the slopes and intercepts, respectively (Saruchi and Kumar, 2016).

3.5.2 Statistical Analyses

The advanced IBM Statistical Package for the Social Sciences (SPSS) version 23 was used in the study.

- i. The multivariate statistical approach such as factor analyses was applied in assessing the variations in the soils and soil kaolin characteristics (Davis, 2002; Kanket, 2006). All data were normalised by means of z-scores to equate the variables. The data were further transfigured into a new data set delineating the factor loading (eigenvector) and score (eigenvalues). Each of the factors/components which defined covariance relationships between the correlated variables were used to account for the data variability. Factors accounting for less than 4 % of the data variability and with eigenvalues less than 1 were not considered (Davis, 2002; Hofer *et al.*, 2013). To minimise collinearity, variables that can be understood by a linear relationship with other variables

were excluded. This was also to ensure that the ratio of sample size to number of variables is not too small (MacCallum *et al.*, 1999).

- ii. Independent T-test and F-test were used to test the significance of relationship between P adsorption at tillage depth (0-20 cm, where most root activities and fertiliser applications were generally restricted) in soils and soil kaolins developed from the various parent rocks. All tests of significance were made with probability levels of 0.05 and 0.01 respectively (Davis, 2002).
- iii. Multiple regression (stepwise regression), Analysis of Variance (ANOVA), and correlation analyses were performed to determine the influence and relationship between the P sorption parameters and soil properties at tillage depth (0-20 cm) (Umoh *et al.*, 2014). Since the sample sizes were small (three per rock type), for precise and valid statistical interpretations, the analyses were conducted by using all the samples at once (Zimmermann, 2004).

3.5.3 Weathering Indices

The indices used in the study were selected based on feldspar been one of the dominant minerals present in the parent rocks that can weather easily to clays (Price and Velbel, 2003; Hofer *et al.*, 2013). The indices that were calculated (Eqns. 3.11 – 3.13) in assessing the extent of chemical weathering/alteration based on the molecular proportions of element oxides include:

- The Chemical Index of Alteration (CIA) (Nesbitt and Young, 1982)

$$\text{CIA} = \left[\frac{\text{Al}_2\text{O}_3}{\text{Al}_2\text{O}_3 + \text{CaO}^* + \text{Na}_2\text{O} + \text{K}_2\text{O}} \right] \times 100 \quad (3.11)$$

- The Plagioclase Index of Alteration (PIA) (Fedo *et al.*, 1995)

$$\text{PIA} = \left[\frac{\text{Al}_2\text{O}_3 - \text{K}_2\text{O}}{\text{Al}_2\text{O}_3 + \text{CaO}^* + \text{Na}_2\text{O} - \text{K}_2\text{O}} \right] \times 100 \quad (3.12)$$

- The Chemical Index of weathering (CIW) (Harnois, 1988)

$$\text{CIW} = \left[\frac{\text{Al}_2\text{O}_3}{\text{Al}_2\text{O}_3 + \text{CaO}^* + \text{Na}_2\text{O}} \right] \times 100 \quad (3.13)$$

Where, CaO* represents CaO associated with the silicate fraction of the sample. McLennan *et al.* (1993) proposed that CaO values should be accepted if CaO < Na₂O and when CaO > Na₂O, it is assumed that the concentration of CaO equals that of Na₂O.

3.5.4 Elemental Ratios

Geochemical proxies used for assessing provenance include the following ratios:

Th/U, LREE/HREE, and Eu/Eu* in differentiating between felsic and mafic sources (Cullers (1994, 2000); and Cullers and Podkovyrov (2000)).

3.5.5 Discrimination Diagrams

Ternary and distribution diagrams were used in evaluating the geochemical trends such as A-CN-K and A-CNK-FM (Nesbitt and Young, 1984 and 1989).

3.5.6 Assessment of Soil Fertility Status

The overall soil fertility status of the soils was estimated using soil fertility index (SFI) (Eqn. 3.14) and soil evaluation factor (SEF) (Eqn. 3.15) by Lu *et al.* (2002).

$$\text{SFI} = \text{pH} + \text{OM} (\% \text{ dry soil}) + \text{Avai. P} (\text{mg/kg dry soil}) + \text{Exch. K} (\text{cmol/kg}) + \text{Exch. Ca} (\text{cmol/kg}) + \text{Exch. Mg} (\text{cmol/kg}) - \text{Exch. Al} (\text{cmol/kg}) \quad (3.14)$$

$$\text{SEF} = [\text{Exch. K} (\text{cmol/kg}) + \text{Exch. Ca} (\text{cmol/kg}) + \text{Exch. Mg} (\text{cmol/kg}) - \log (1 + \text{Exch. Al} (\text{cmol/kg}))] \times \text{OM} (\% \text{ dry soil}) + 5 \quad (3.15)$$

3.6 Concluding Remarks

This chapter detailed the research methods employed in the study. Fresh rock and soil samples were collected, prepared, and analysed for various physico-chemical, mineralogical, and geochemical laboratory analyses. The various data interpretation approaches taken were presented accordingly. Statistical data and model analyses conducted were also discussed.

Chapter Four

Results

This chapter presents the physico-chemical, mineralogical, and geochemical data for the parent rocks, bulk soil, silt, clay and deferrated clay fractions (soil kaolins) of the studied soils developed from different parent rocks within Limpopo Province, South Africa.

4.1 Physico-chemical Properties of the Bulk Soils and Soil Kaolins

4.1.1 Colour of the bulk soils

Soil colour is produced by minerals and organic matter present in the soil. This study shows colour variation both within and among the soils developed from the different parent rocks. Generally, the soils had shades of colour varying from dusky red (31 %), brown (27 %) to reddish brown (15 %), and yellowish brown to yellowish red (8 %), reddish grey (8 %), and dark red (4 %) (Table 4.1). Soils developed from basalt had two distinct colours, dark red (89 %) and dusky red (11 %).

Soils developed from granite had varying shades of colour from reddish brown (33 %) to yellowish red (17 %), and from brown (33 %) to strong brown (17 %). In all the soils sampled, soils developed from arkosic sandstone had the highest colour variation with colours varying from brown (32 %), dark brown (17 %) to dark reddish brown (17 %) to very dark reddish brown (17 %) to reddish grey (17 %).

Two distinct colours were observed for soils developed from gneiss. They are yellowish brown (67 %) and yellowish red (33 %). Soils developed from quartzite (control) were purely brown in colour.

Table 4.1: Hue, Value, Chroma, and Colour of the studied bulk soils.

Parent Rock	Sample ID	Hue/Value/Chroma	Colour
Basalt	S1 0-20cm	10R/3/4	Dusky red
	S1 20-50cm	10R/3/4	Dusky red
	S1 50-100cm	10R/3/4	Dusky red
	S2 0-20cm	10R/3/3	Dusky red
	S2 20-50cm	10R/3/4	Dusky red
	S2 50-100cm	10R/3/3	Dusky red
	S3 0-20cm	10R/3/3	Dusky red
	S3 20-50cm	10R/3/6	Dark red
	S3 50-100cm	10R/3/4	Dusky red
Granite	MAT1 0-20cm	5YR/5/4	Reddish brown
	MAT1 20-50cm	7.5YR/4/4	Brown
	MAT2 0-20cm	7.5YR/4/6	Strong brown
	MAT2 20-50cm	5YR/4/6	Yellowish red
	MAT3 0-20cm	7.5YR/5/4	Brown
	MAT3 20-50cm	5YR/4/4	Reddish brown
Arkosic Sandstone	SA1 0-20cm	10YR/3/3	Dark brown
	SA1 20-50cm	10R/4/1	Reddish grey
	SA2 0-20cm	10YR/5/3	Brown
	SA2 20-50cm	10YR/5/3	Brown
	SA3 0-20cm	7.5YR/7/2	Dark reddish brown
	SA3 20-50cm	7.5R/7/3	Very dark greyish brown
Gneiss	MU1 0-20cm	10YR/5/4	Yellowish brown
	MU2 0-20cm	10YR/5/4	Yellowish brown
	MU3 0-20cm	5YR/4/6	Yellowish red
Quartzite	CMA 0-20cm	10YR/5/3	Brown
	CMA 20-50cm	7.5YR/4/4	Brown

4.1.2 Hydrogen Ion Concentration (pH) of the bulk soils

The pH of soils developed from basalt was between 6.21 and 6.50 with a mean value of 6.00, whereas pH of soils developed from granite was between 5.58 and 6.12 with a mean value of 5.76. The pH of soils developed from arkosic sandstone ranged from 6.24 to 8.38 with a mean value of 7.57, whereas pH of soils developed from gneiss were between 6.49 and 7.10 with a mean value of 6.81. Soil samples formed from quartzite had a pH range of 5.11 to 5.13 with an average value of 5.12. Generally, the pH values of the studied soil samples ranged from slightly acidic to slightly basic with values between 5.11 to 8.38 (Table 4.2).

4.1.3 Electrical Conductivity (EC) of the bulk soils

The EC of soil formed from basalt were between 11.66 and 56.40 $\mu\text{S}/\text{cm}$ with a mean value of 24.14 $\mu\text{S}/\text{cm}$, whereas EC of soils formed from granite were between 10.25 and 21.60 $\mu\text{S}/\text{cm}$ with a mean value of 15.40 $\mu\text{S}/\text{cm}$. The EC of soil samples formed from arkosic sandstone varied from 40.00 to 112.00 $\mu\text{S}/\text{cm}$ with a mean value of 85.02 $\mu\text{S}/\text{cm}$, whereas EC of soils formed from gneiss were between 12.60 and 15.31 $\mu\text{S}/\text{cm}$ with a mean value of 13.72 $\mu\text{S}/\text{cm}$. Soil samples formed from quartzite have an EC between 17.80 and 62.00 $\mu\text{S}/\text{cm}$ with an average value of 39.9 $\mu\text{S}/\text{cm}$ (Table 4.2).

Table 4.2: pH and EC ($\mu\text{S}/\text{cm}$) of the studied bulk soils.

Parent Rock	Sample ID	pH	EC
Basalt	S1 0-20cm	6.50	19.90
	S1 20-50cm	6.43	13.62
	S1 50-100cm	6.41	11.66
	S2 0-20cm	5.30	56.40
	S2 20-50cm	5.36	25.09
	S2 50-100cm	5.22	47.90
	S3 0-20cm	6.41	14.96
	S3 20-50cm	6.23	12.16
	S3 50-100cm	6.21	15.56
Granite	MAT1 0-20cm	5.58	21.60
	MAT1 20-50cm	5.64	13.37
	MAT2 0-20cm	5.90	17.50
	MAT2 20-50cm	6.12	11.24
	MAT3 0-20cm	5.58	18.42
	MAT3 20-50cm	5.73	10.25
Arkosic Sandstone	SA1 0-20cm	8.17	90.3
	SA1 20-50cm	8.21	112.00
	SA2 0-20cm	6.41	40.60
	SA2 20-50cm	6.24	40.00
	SA3 0-20cm	8.00	114.40
	SA3 20-50cm	8.38	112.8
Gneiss	MU1 0-20cm	6.85	13.25
	MU2 0-20cm	6.49	15.31
	MU3 0-20cm	7.10	12.60
Quartzite	CMA 0-20cm	5.13	17.80
	CMA 20-50cm	5.11	62.00

4.1.4 Texture of the bulk soil

Soils developed on basalt predominantly had clay textures. The texture of soils developed on arkosic sandstone and quartzite was sandy loam, whereas the soils developed on granite and gneiss had textures varying from sandy loam to loamy sand (Table 4.3, Figures 4.1 - 4.5).

Table 4.3: Textures from the particle size distribution of the studied bulk soils.

Parent Rock	Sample ID	Texture
Basalt	S1 0-20cm	Clay
	S1 20-50cm	Clay
	S1 50-100cm	Clay
	S2 0-20cm	Clay
	S2 20-50cm	Clay
	S2 50-100cm	Clay
	S3 0-20cm	Clay
	S3 20-50cm	Clay
	S3 50-100cm	Clay
Granite	MAT1 0-20cm	Sandy loam
	MAT1 20-50cm	Sandy loam
	MAT2 0-20cm	Loamy sand
	MAT2 20-50cm	Sandy loam
	MAT3 0-20cm	Sandy loam
	MAT3 20-50cm	Sandy loam
Arkosic Sandstone	SA1 0-20cm	Sandy loam
	SA1 20-50cm	Sandy loam
	SA2 0-20cm	Sandy loam
	SA2 20-50cm	Sandy loam
	SA3 0-20cm	Sandy loam
	SA3 20-50cm	Sandy loam
Gneiss	MU1 0-20cm	Sandy loam
	MU2 0-20cm	Sandy clay loam
	MU3 0-20cm	Sandy loam
Quartzite	CMA 0-20cm	Sandy loam
	CMA 20-50cm	Sandy loam

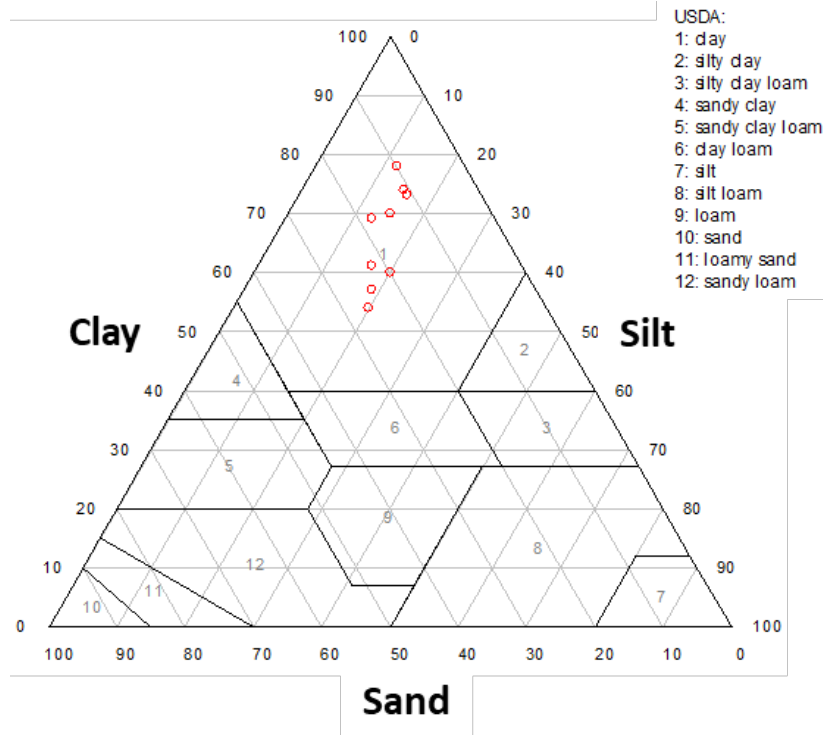


Figure 4.1: Textural ternary plot for soils developed from basalt.

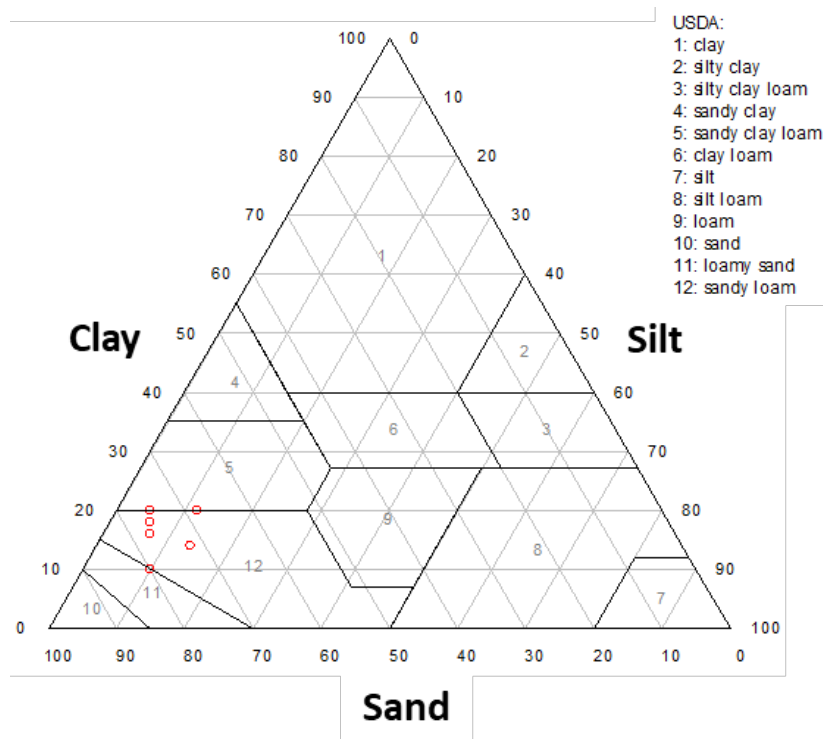


Figure 4.2: Textural ternary plot for soils developed from granite.

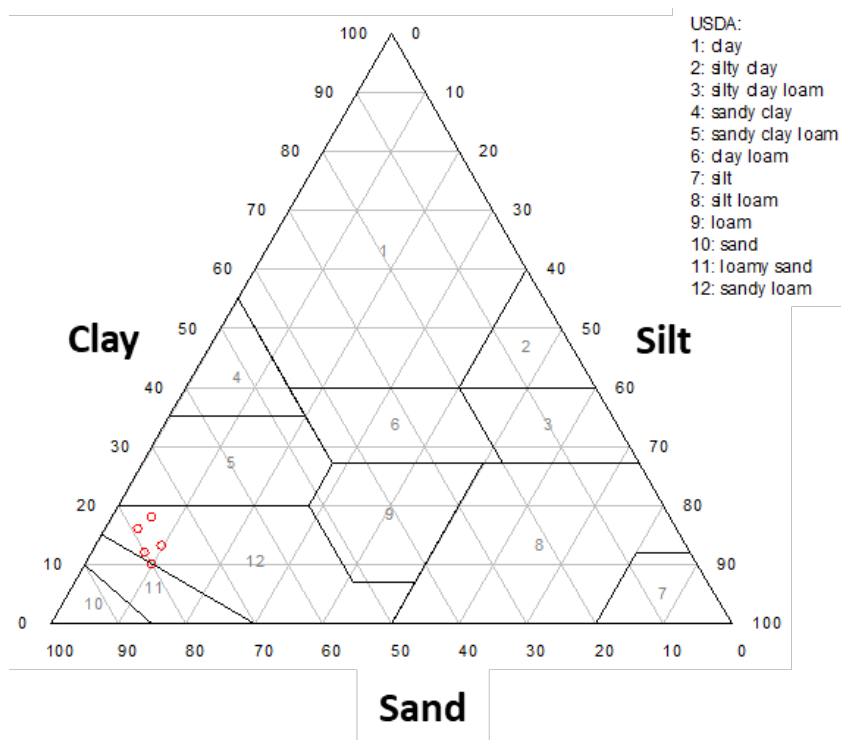


Figure 4.3: Textural ternary plot for soils developed from arkosic sandstone.

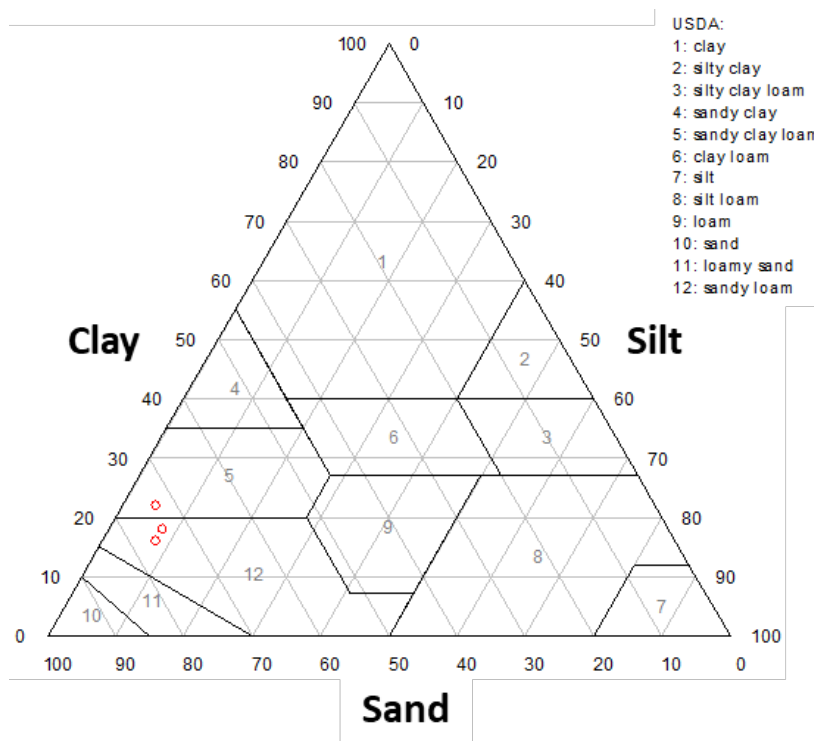


Figure 4.4: Textural ternary plot for soils developed from gneiss.

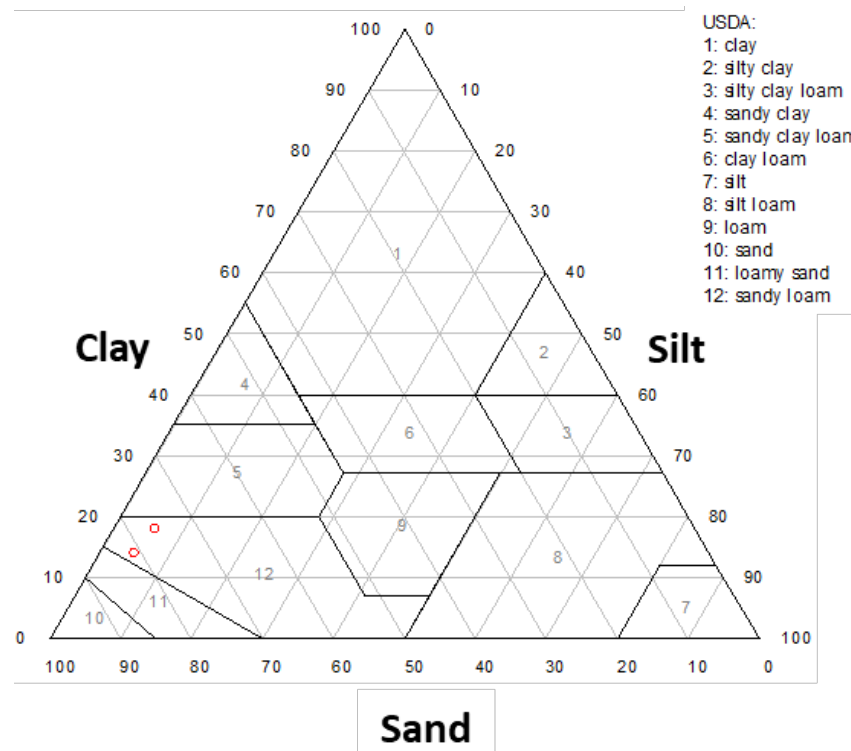


Figure 4.5: Textural ternary plot for soils developed from quartzite.

4.1.5 Cation Exchange Capacity (CEC)

4.1.5.1 CEC of bulk soils

The CEC of the soils developed from basalt ranged from 13.22 to 18.30 cmol/kg with a mean value of 15.01 cmol/kg, whereas CEC of soils developed from granite were between 2.93 and 4.12 cmol/kg with a mean value of 3.58 cmol/kg. The CEC of soils developed from arkosic sandstone ranged from 5.09 to 11.57 cmol/kg with a mean value of 9.31 cmol/kg, whereas CEC of soils developed from gneiss were between 4.87 and 10.70 cmol/kg with a mean value of 7.53 cmol/kg. Soil formed from quartzite (control) had a CEC value of 2.57 cmol/kg (Table 4.4).

4.1.5.2 CEC of Soil Kaolins

The CEC of the soil kaolins developed from basalt ranges from 6.09 to 22.98 cmol/kg with a mean value of 15.48 cmol/kg, whereas CEC of soil kaolins developed from

granite were between 7.48 and 9.88 cmol/kg with a mean value of 8.80 cmol/kg. The CEC of soil kaolins developed from arkosic sandstone ranged from 18.48 to 28.24 cmol/kg with a mean value of 28.01 cmol/kg, whereas CEC of soil kaolins developed from gneiss were between 9.69 and 19.91 cmol/kg with a mean value of 14.83 cmol/kg. Soil kaolins formed from quartzite (control) have a CEC value of 9.74 cmol/kg (Table 4.4).

Table 4.4: CEC (cmol/kg) in the Bulk soil and Soil Kaolins developed from different Parent Rocks in Limpopo Province, South Africa.

Parent Rock	Sample ID	CEC (Bulk soil)	CEC (Soil kaolins)
Basalt	S1 0-20 cm	13.50	6.09
	S2 0-20 cm	18.30	22.98
	S3 0-20 cm	13.22	17.37
Granite	MAT1 0-20 cm	4.12	7.48
	MAT2 0-20 cm	3.68	9.88
	MAT3 0-20 cm	2.93	9.03
Arkosic Sandstone	SA1 0-20 cm	11.28	28.24
	SA2 0-20 cm	5.09	18.48
	SA3 0-20 cm	11.57	37.3
Gneiss	MU1 0-20 cm	10.70	19.91
	MU2 0-20 cm	4.87	9.69
	MU3 0-20 cm	7.03	14.89
Quartzite	CMA 0-20 cm	2.57	9.74

4.1.6 Available Phosphorus

The concentration of available phosphorus in soils developed from basalt and gneiss were <0.01 mg/kg, whereas the concentration of available phosphorus in soils developed from granite ranged from 15.33 to 26.41 mg/kg with a mean value of 22.02 mg/kg. The concentration of available phosphorus in soils developed from arkosic sandstone ranged from <0.01 to 54.99 mg/kg with a mean value of 30.96 mg/kg, while the concentration of available phosphorus in soil developed from quartzite (control) was 0.97 mg/kg (Table 4.5).

Table 4.5: Available phosphorus (mg/kg), exchangeable cations (cmol/kg), and organic matter (%) in the studied bulk soils.

Parent Rock	Sample ID	Avai. P	Ca	K	Mg	Na	Al	OM
Basalt	S1 0-20 cm	<0.01	5.14	0.11	1.91	0.11	0.81	0.62
	S2 0-20 cm	<0.01	3.73	0.29	1.84	0.09	1.12	3.62
	S3 0-20 cm	<0.01	2.61	0.1	0.95	0.07	0.76	0.41
Granite	MAT1 0-20 cm	24.32	0.75	0.21	0.48	0.04	0.26	4.55
	MAT2 0-20 cm	15.33	1.06	0.23	0.68	0.04	0.17	4.03
	MAT3 0-20 cm	26.41	0.74	0.25	0.50	0.05	0.33	2.90
Arkosic Sandstone	SA1 0-20 cm	6.96	13.92	0.5	1.41	0.03	0.41	2.79
	SA2 0-20 cm	54.99	1.5	0.29	1.69	0.06	0.23	2.59
	SA3 0-20 cm	<0.01	10.28	0.63	2.29	0.07	0.37	4.76
Gneiss	MU1 0-20 cm	<0.01	7.24	0.09	3.88	0.09	0.31	4.24
	MU2 0-20 cm	<0.01	2.87	0.07	1.68	0.09	0.24	4.76
	MU3 0-20 cm	<0.01	4.99	0.07	3.17	0.2	0.18	2.79
Quartzite	CMA 0-20 cm	0.97	0.09	0.03	0.60	0.06	0.04	4.45

4.1.7 Exchangeable Cations

4.1.7.1 Calcium (Ca)

The concentration of Ca in soils developed from basalt ranged from 2.61 to 5.14 cmol/kg with a mean value of 3.83 cmol/kg, whereas the concentration of Ca in soils developed from granite ranged from 0.74 to 1.06 mg/kg with a mean value of 0.85 cmol/kg. Soils developed from arkosic sandstone had Ca concentrations between 1.5 and 13.92 cmol/kg with a mean value of 8.57 cmol/kg, whereas the concentration of Ca in soils developed from gneiss ranged from 2.87 to 7.24 cmol/kg with a mean value of 5.03 cmol/kg. In soil developed from quartzite (control), the concentration of Ca was 0.09 cmol/kg (Table 4.5).

4.1.7.2 Magnesium (Mg)

The concentration of Mg in soils developed from basalt ranged from 0.95 to 1.91 cmol/kg with a mean value of 1.57 cmol/kg, whereas the concentration of Mg in soils developed from granite ranged from 0.48 to 0.68 mg/kg with a mean value of 0.55 cmol/kg. The concentration of Mg in soils developed from arkosic sandstone ranged from 1.41 to 2.29 cmol/kg with a mean value of 1.80 cmol/kg, whereas the concentration of Mg in soils developed from gneiss ranged from 1.68 to 3.88 mg/kg with a mean value

of 2.91 cmol/kg. In soil sample developed from quartzite, the concentration of Mg was 0.03 cmol/kg (Table 4.5).

4.1.7.3 Potassium (K), Sodium (Na), and Aluminium (Al)

The concentration of Na and Al in all the soils developed from different parent rocks were generally less than 1 cmol/kg (except for S2 0-20 cm) (Table 4.5).

4.1.8 Organic Matter (OM)

Values obtained for OM were generally greater than 2.5 % in soils developed from granite, arkosic sandstone, gneiss, and quartzite (control) whereas, soils developed from basalt had values lesser than 1 % (except for S2 0-20 cm) (Table 4.5).

4.2 Mineralogical Properties of the Studied Parent rocks, Soils and Soil Kaolins

4.2.1 Petrographic studies of the Parent Rocks

Thin section observations of the fresh basalt rocks revealed the presence of pyroxene and laths of plagioclase as the major mineral constituents and possibly chlorite. The plagioclases were generally euhedral to subhedral without zoning crystals. The presence of rainbow-like coloured minerals suggests possible alteration of the pyroxene (Figs. 4.6 – 4.8).

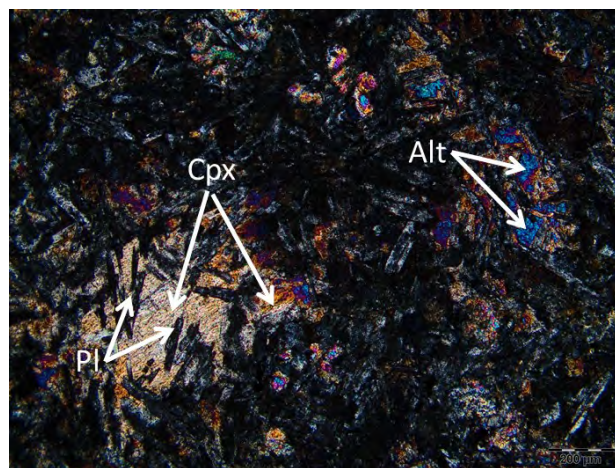


Figure 4.6: Photomicrograph of basalt showing plagioclase (Pl), clinopyroxene (Cpx), and possible alteration (Alt) of Cpx under cross-polarised light.

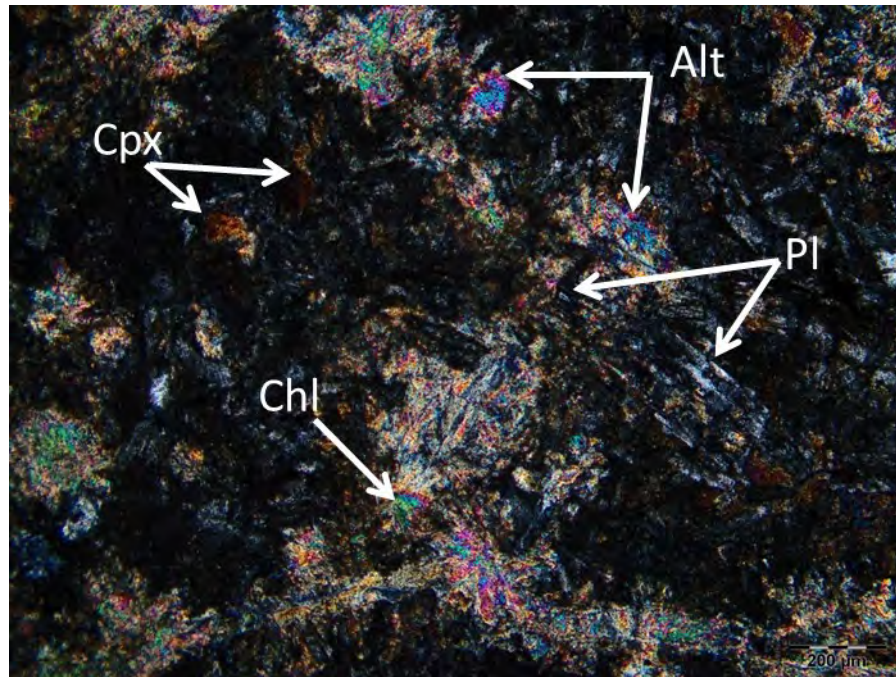


Figure 4.7: Photomicrograph of basalt showing plagioclase (Pl), clinopyroxene (Cpx), chlorite (Chl), and possible alteration (Alt) of Cpx under cross-polarised light.

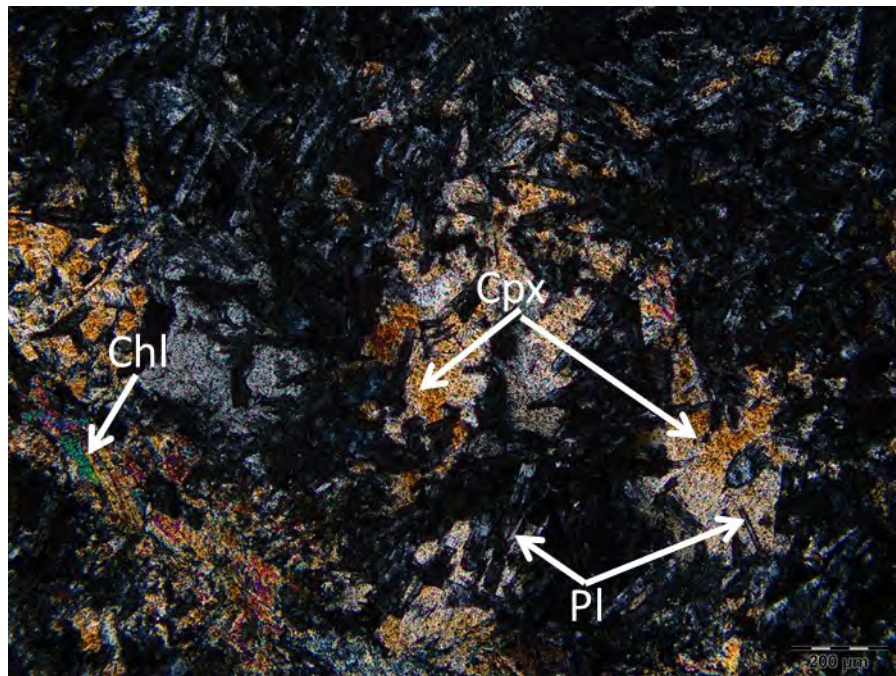


Figure 4.8: Photomicrograph of basalt showing plagioclase (Pl), clinopyroxene (Cpx), and chlorite (Chl) under cross-polarised light.

Granite samples have coarse-grained plagioclase, quartz, and muscovite minerals. The plagioclases occur as anhedral to subhedral with zoning crystals, particularly polysynthetic twinning showing continuous extinction. Carlsbad (simple) and cross-hatched twinning were absent. Quartz minerals were generally anhedral without any triple junction which could have indicated equilibrium cooling. Poikilitic plagioclase with inclusions of quartz was also observed which suggest that the plagioclase is latter than the included quartz mineral (Figs. 4.9 – 4.11).

Fresh arkosic sandstone thin section observations showed the rock mineralogically contains quartz, muscovite, and microcline. Quartz and microcline occur as anhedral to subhedral felsic phenocryst with the presence of cross-hatched twinnings (Figs 4.12 – 4.14).

Quartz was the dominant mineral component in the quartzite which occurs as rounded to subrounded and anhedral crystals. The rounded crystals suggest that the materials must have undergone prolonged and possibly multicycle transport (Xu *et al.*, 2013) (Fig. 4.15).

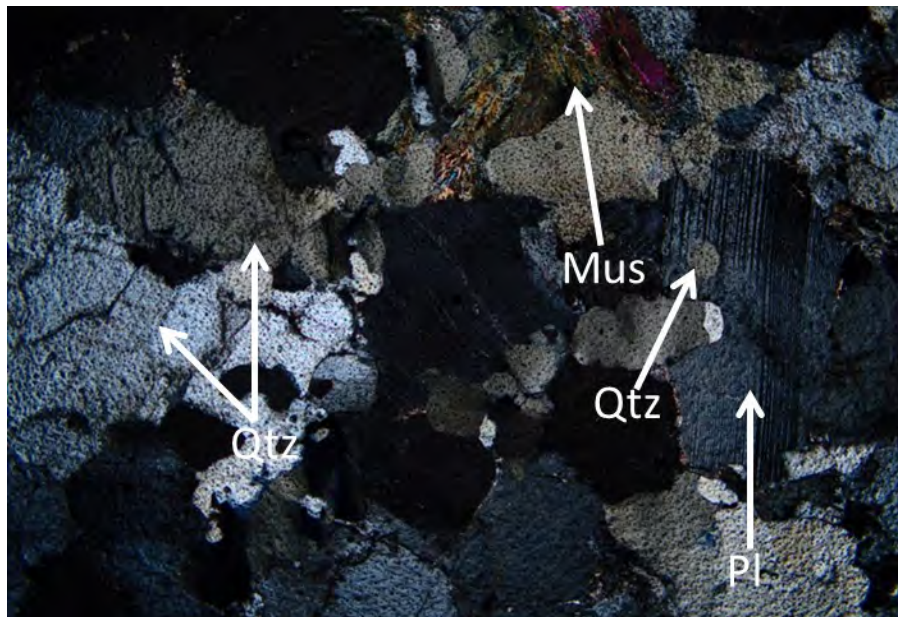


Figure 4.9: Photomicrograph of granite showing plagioclase (Pl) with inclusion of quartz (Qtz), quartz (Qtz), and muscovite (Mus) under cross-polarised light.

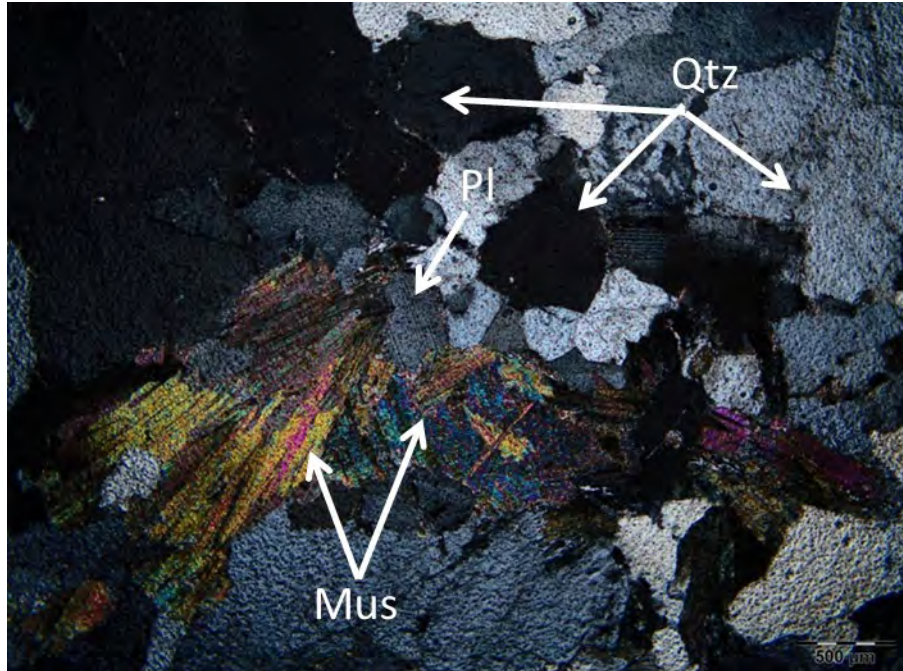


Figure 4.10: Photomicrograph of granite showing association between plagioclase (Pl), quartz (Qtz), and muscovite (Mus) under cross-polarised light.

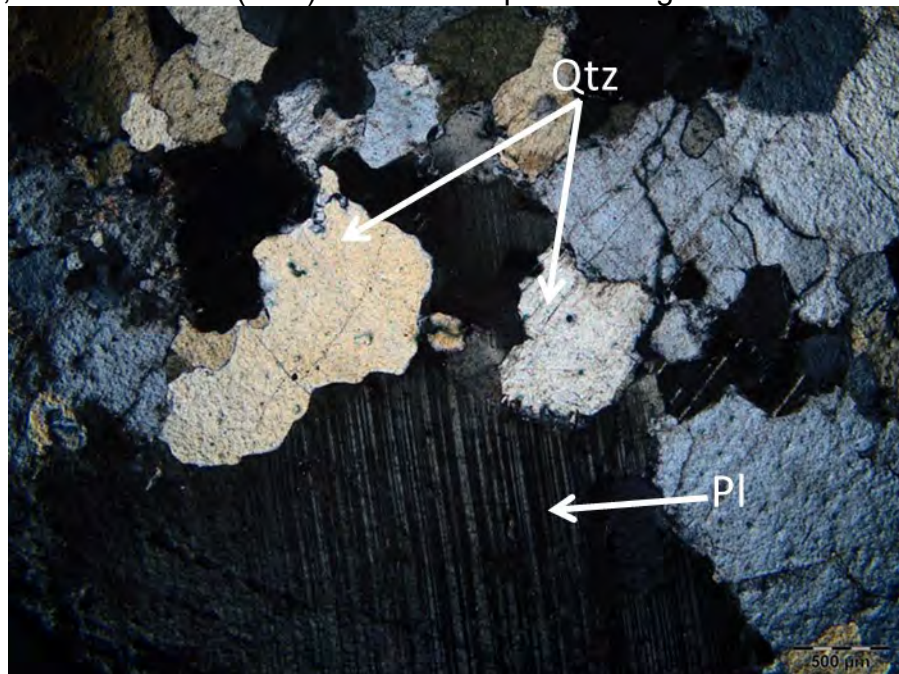


Figure 4.11: Photomicrograph of granite showing plagioclase (Pl) with inclusion of quartz (Qtz), quartz (Qtz) under cross-polarised light.

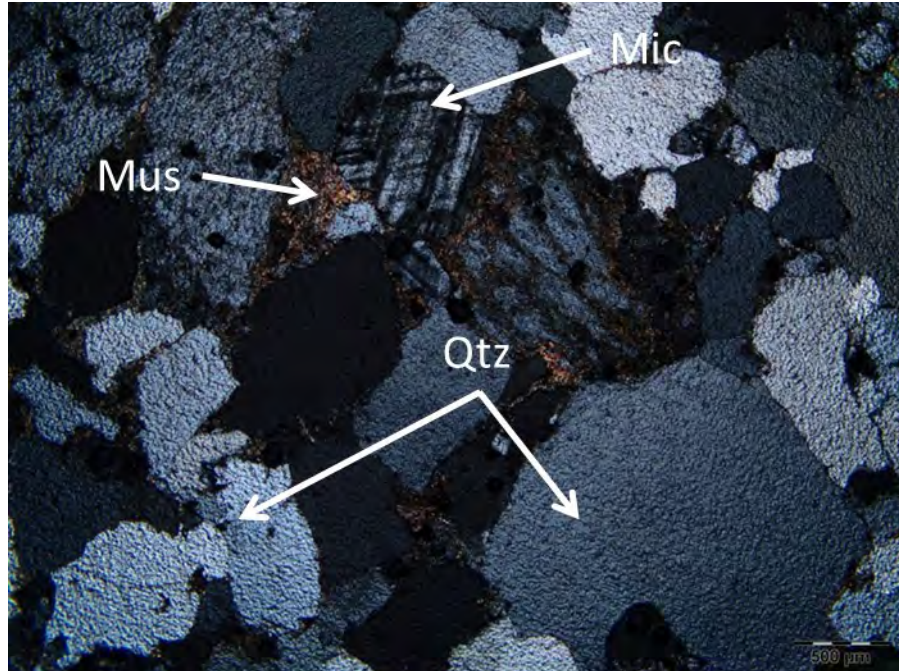


Figure 4.12: Photomicrograph of arkosic sandstone showing quartz (Qtz), microcline (Mic), and muscovite (Mus) under cross-polarised light.

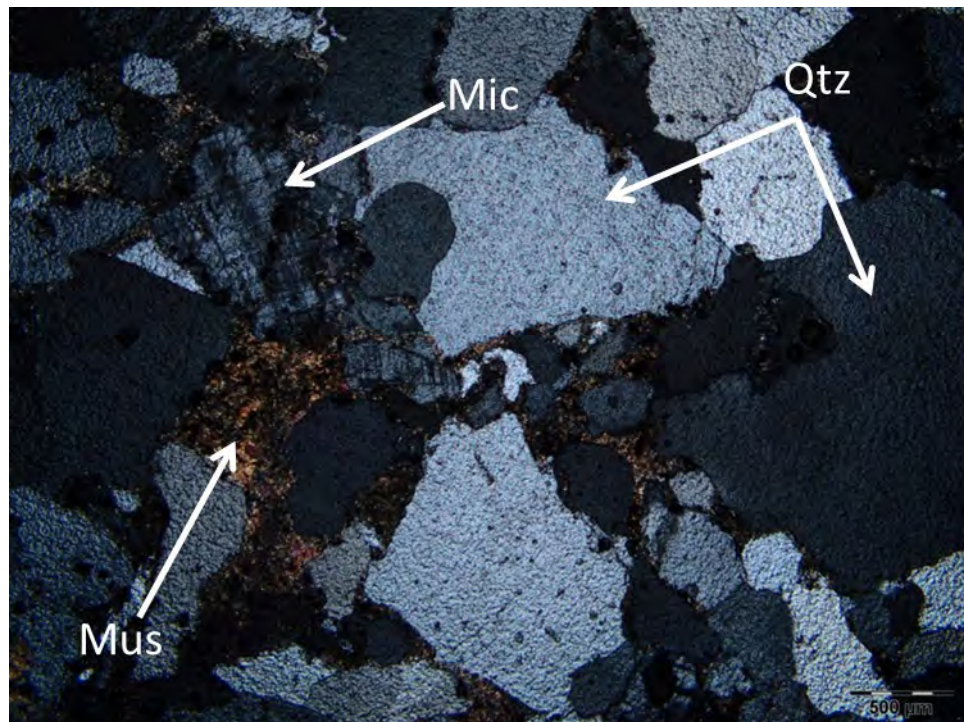


Figure 4.13: Photomicrograph of arkosic sandstone showing quartz (Qtz), microcline (Mic), and muscovite (Mus) under cross-polarised light.

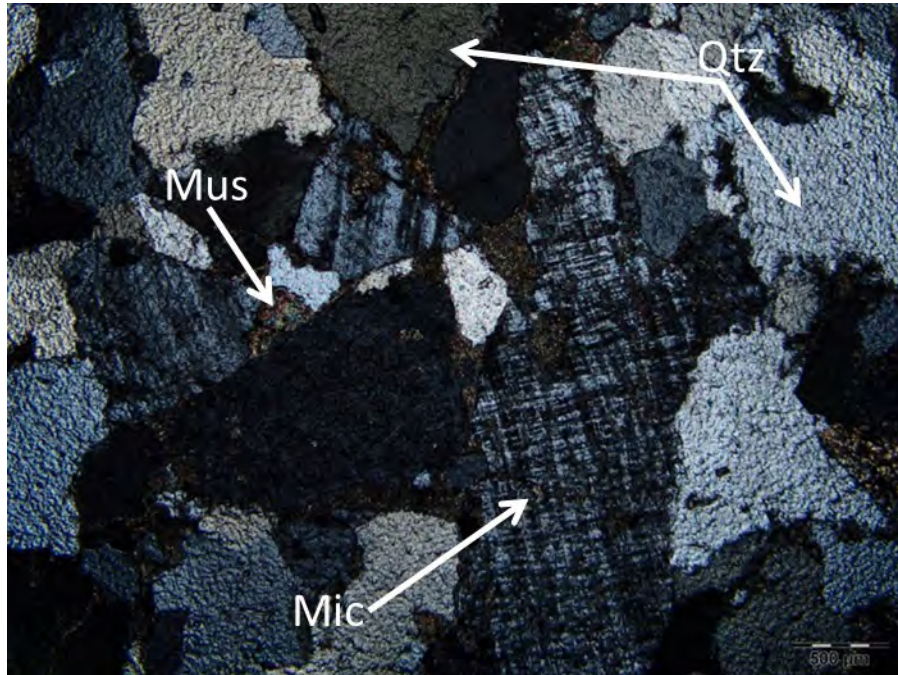


Figure 4.14: Photomicrograph of arkosic sandstone showing quartz (Qtz), larger grain of microcline (Mic), and muscovite (Mus) under cross-polarised light.



Figure 4.15: Photomicrograph of quartzite showing predominantly quartz (Qtz) under cross-polarised light.

4.2.2 X-ray Diffraction (XRD) Studies

4.2.2.1 Qualitative Analyses

The qualitative analyses of the studied parent rocks, soil fractions, and soil kaolins developed from them were based on the identification of known characteristic mineral peaks. Kaolinite peaks were observed at 7.13 Å, 4.36 Å, 4.16 Å, and 3.57 Å whereas peaks at 4.25 Å and 3.34 Å were assigned to quartz. Peaks identified at 3.18 Å and 3.19 Å were assigned to plagioclase whereas, peaks at 3.35 Å and 3.31 Å were assigned to microcline. Chlorite peaks were observed at 14.2 Å, 7.10 Å, and 3.55 Å. Peaks observed at 3.51 Å, 4.15 Å, 2.71 Å, 10.01 Å, 4.85 Å, 8.47 Å, 15.01 Å, 1.97 Å, and 2.92 Å were assigned to anatase, goethite, hematite, muscovite, gibbsite, actinolite, montmorillonite, diopside, and epidote, respectively. Figures 4.16 – 4.48 shows the X-ray diffraction patterns of the studied parent rocks, soil fractions, and soil kaolins confirming the presence of the different mineral phases.

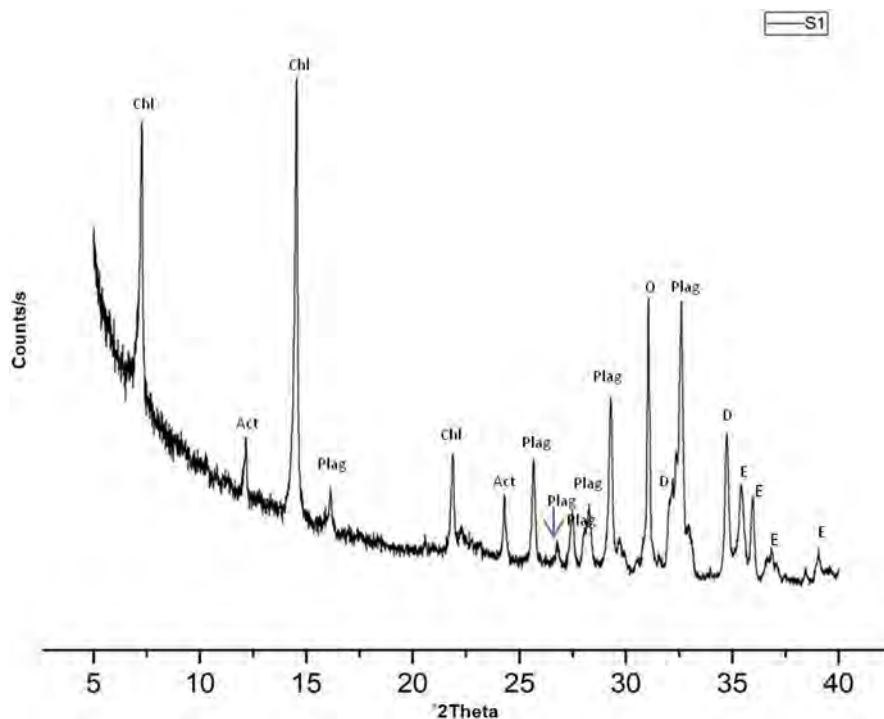


Figure 4.16: Mineral phases as determined by XRD of basalt rock: Chl = chlorite, Act = actinolite, Plag = plagioclase, Q= quartz, D = diopside, E = epidote.

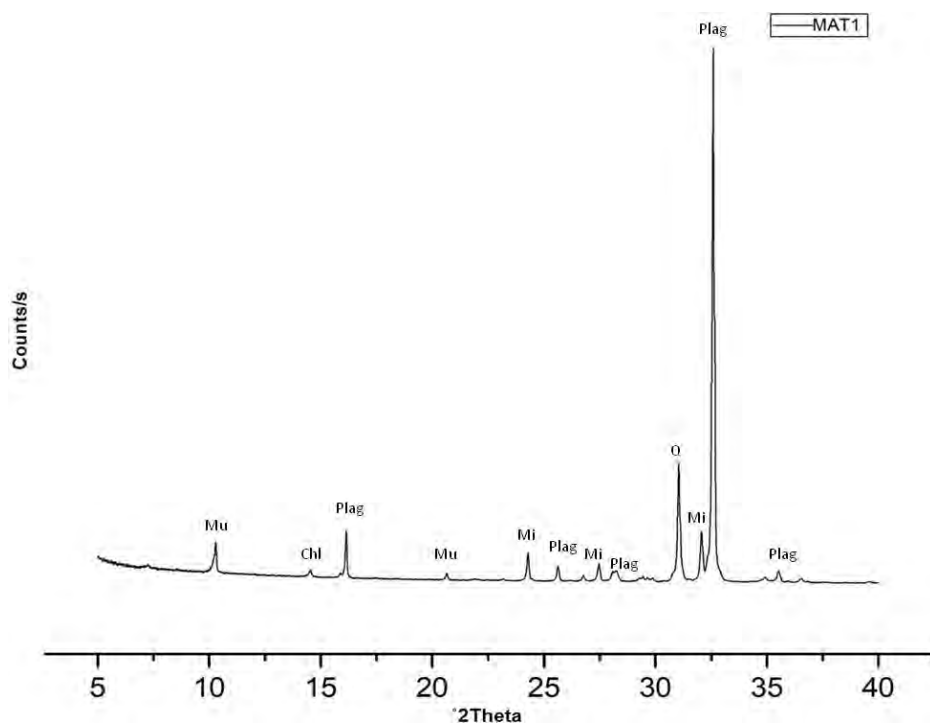


Figure 4.17: Mineral phases as determined by XRD of granite rock: Mu = muscovite, Chl = chlorite, Plag = plagioclase, Mi = microcline, Q = quartz.

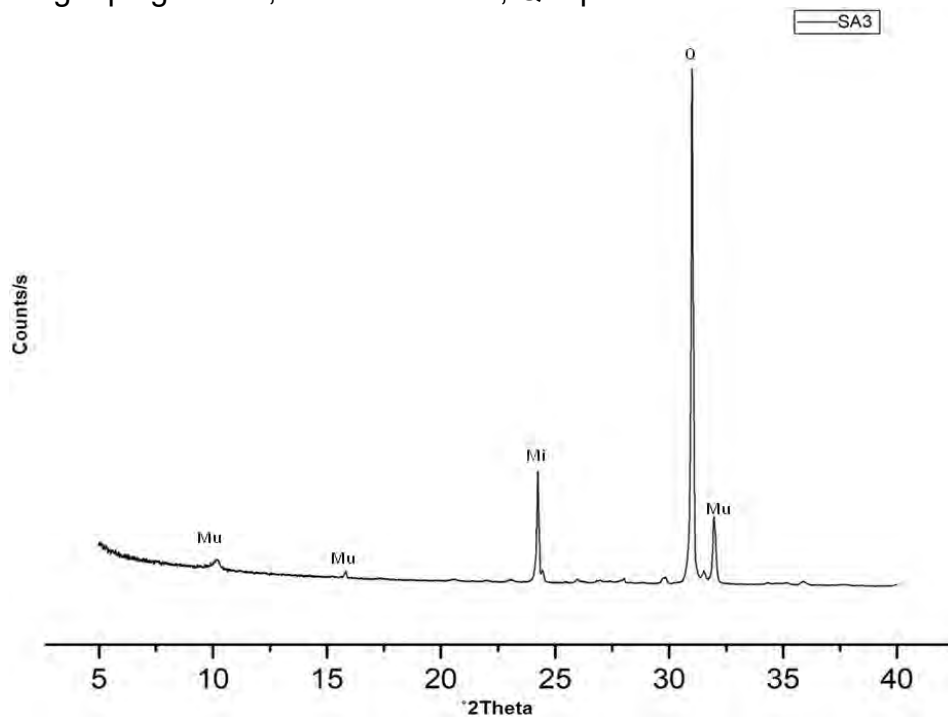


Figure 4.18: Mineral phases as determined by XRD of arkosic sandstone rock: Mu = muscovite, Mi = microcline, Q = quartz.

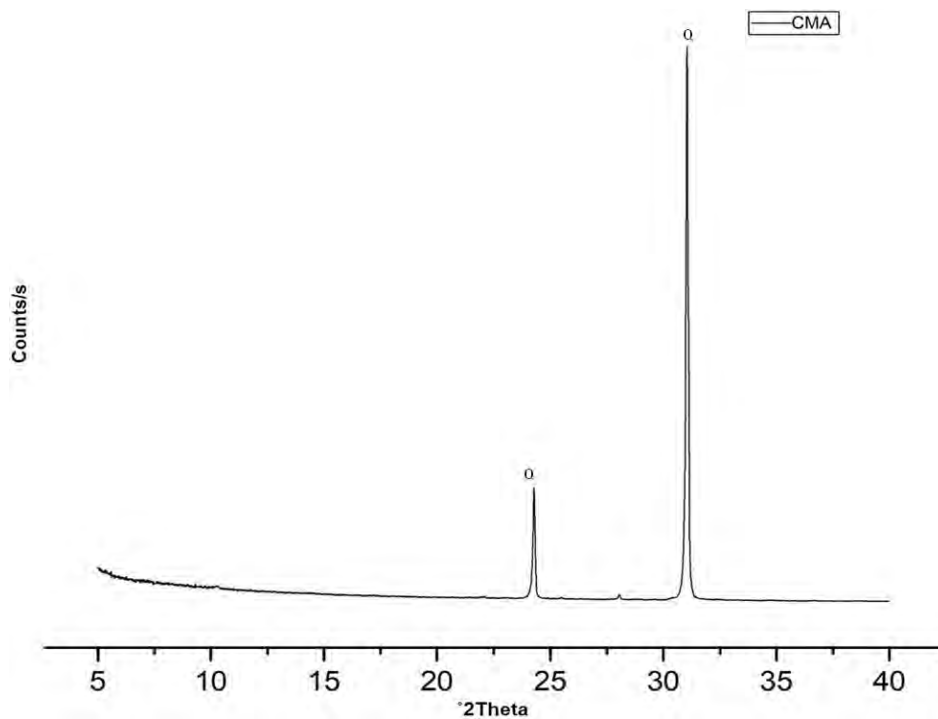


Figure 4.19: Mineral phases as determined by XRD of Quartzite rock: Q= quartz.

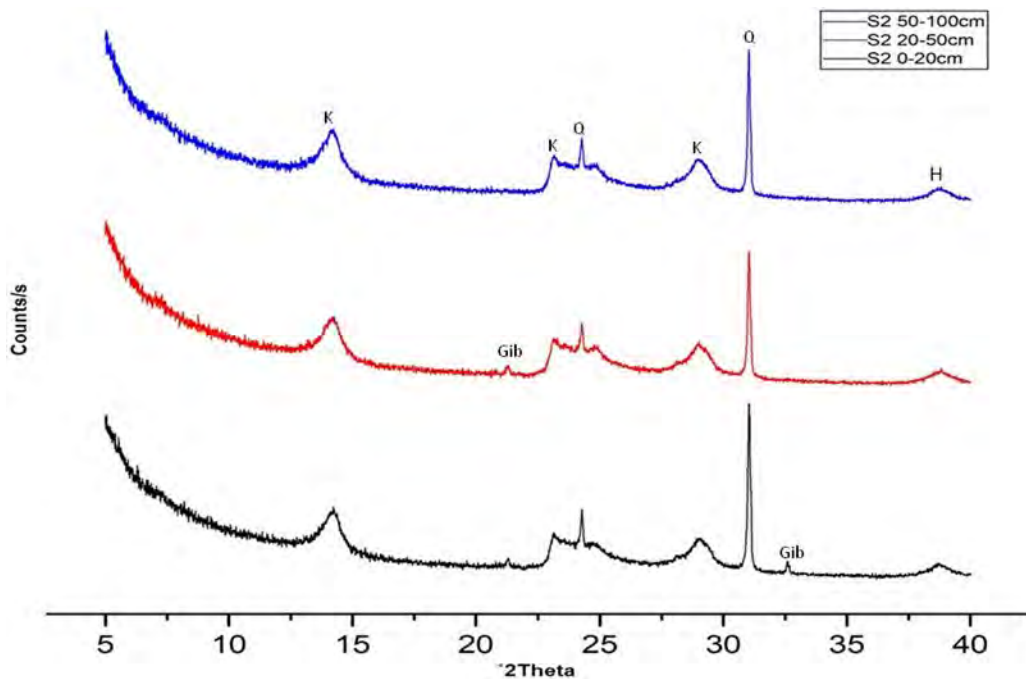


Figure 4.20: Mineral phases as determined by XRD of bulk soils developed from basalt: K= kaolinite, Q= quartz, H = hematite, Gib =gibbsite.

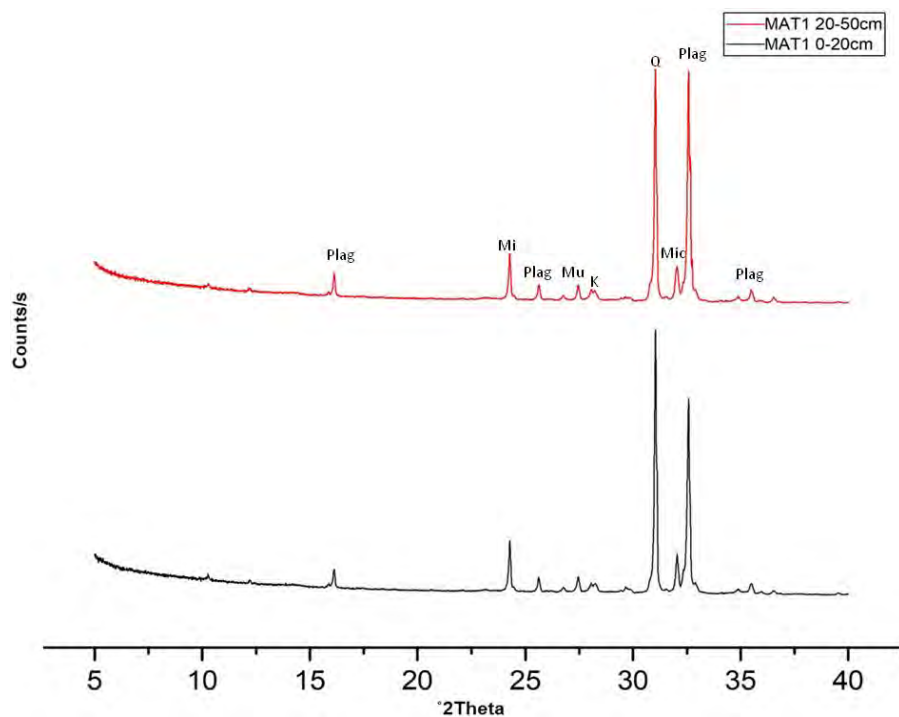


Figure 4.21: Mineral phases as determined by XRD of bulk soils developed from granite: Mu = muscovite, K = kaolinite, Plag = plagioclase, Mi = microcline, Q = quartz.

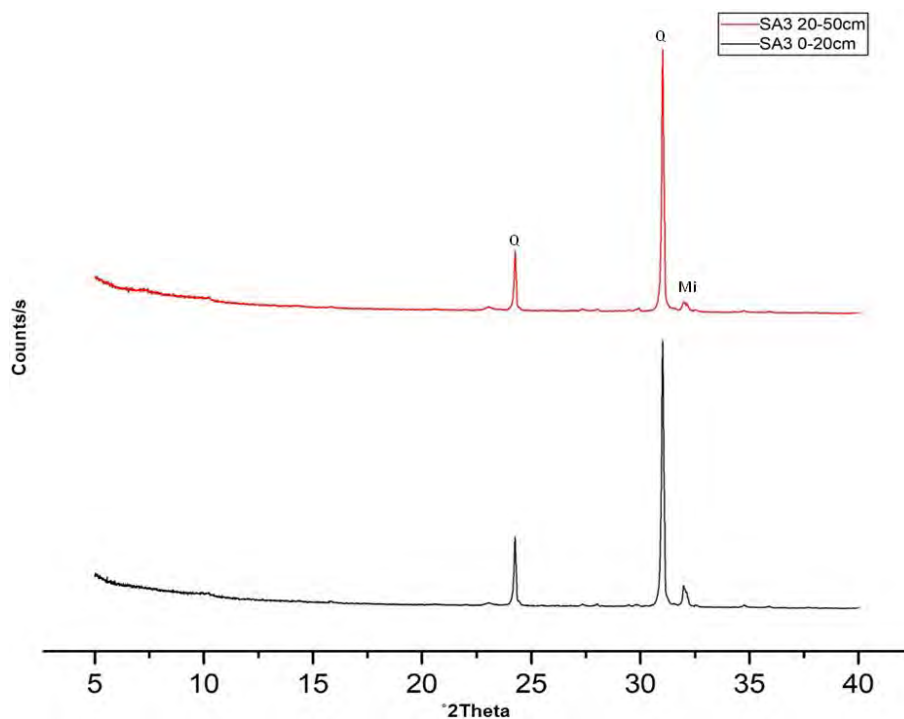


Figure 4.22: Mineral phases as determined by XRD of bulk soils developed from arkosic sandstone: Mi = microcline, Q = quartz.

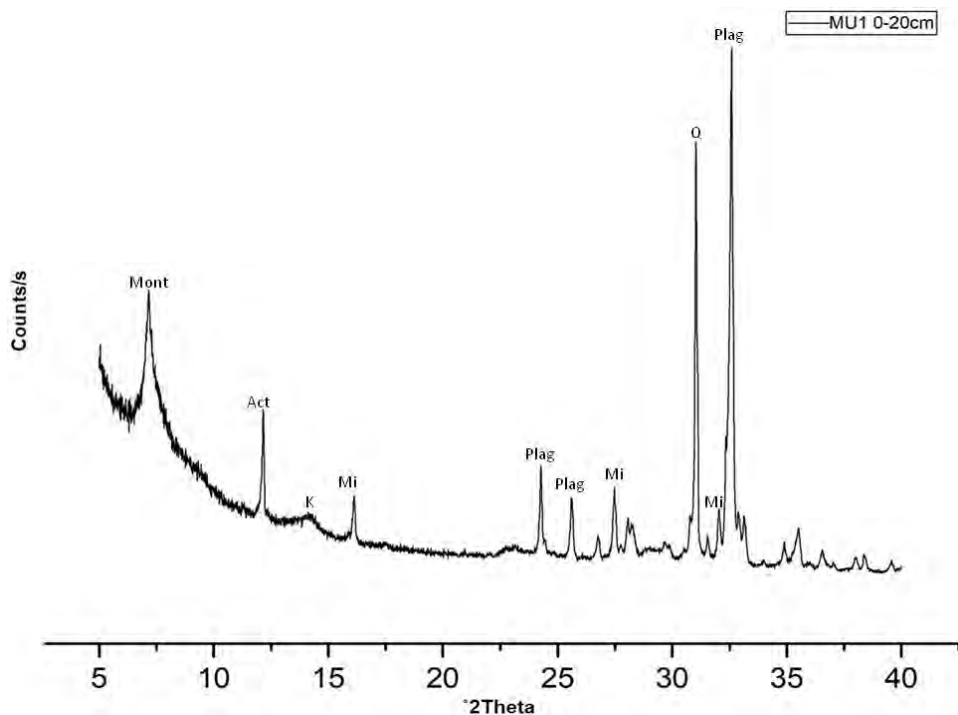


Figure 4.23: Mineral phases as determined by XRD of bulk soils developed from gneiss; Mont = montmorillonite, Act = actinolite, Plag = plagioclase, Mi = microcline, Q= quartz.

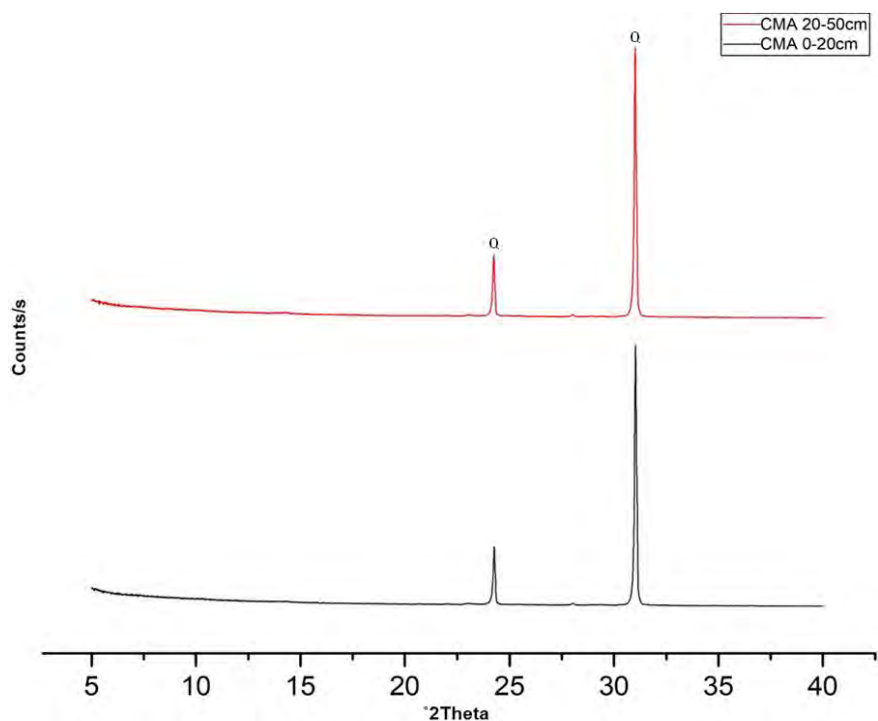


Figure 4.24: Mineral phases as determined by XRD of bulk soils developed from Quartzite; Q= quartz.

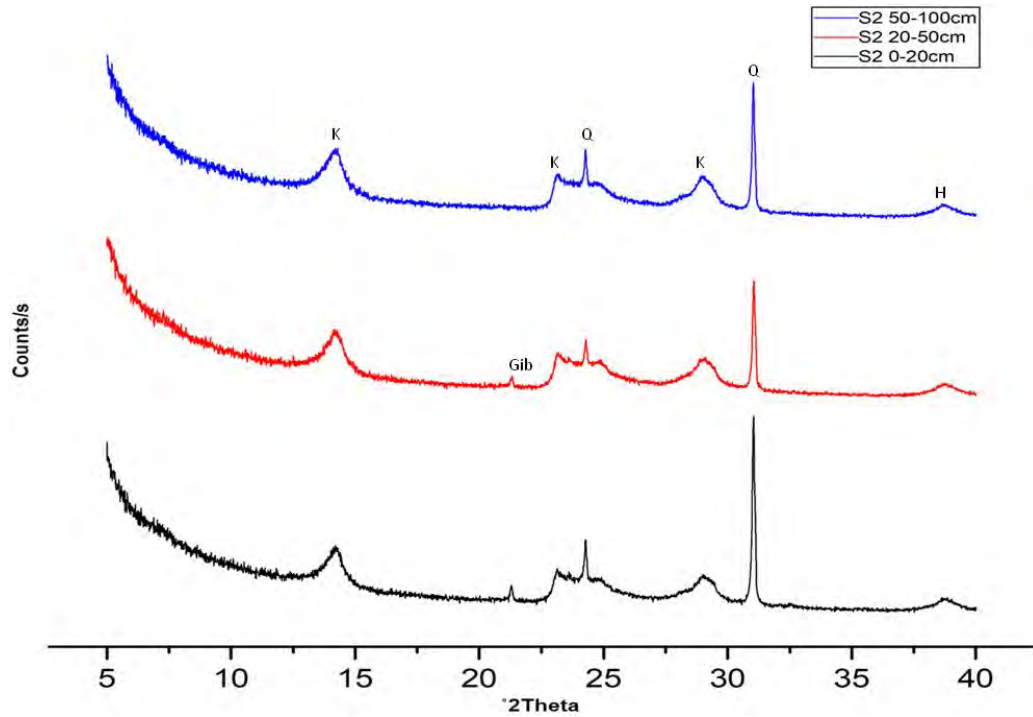


Figure 4.25: Mineral phases as determined by XRD of silt fractions of soils developed from basalt; K = kaolinite, Q= quartz, H = hematite, Gib = gibbsite.

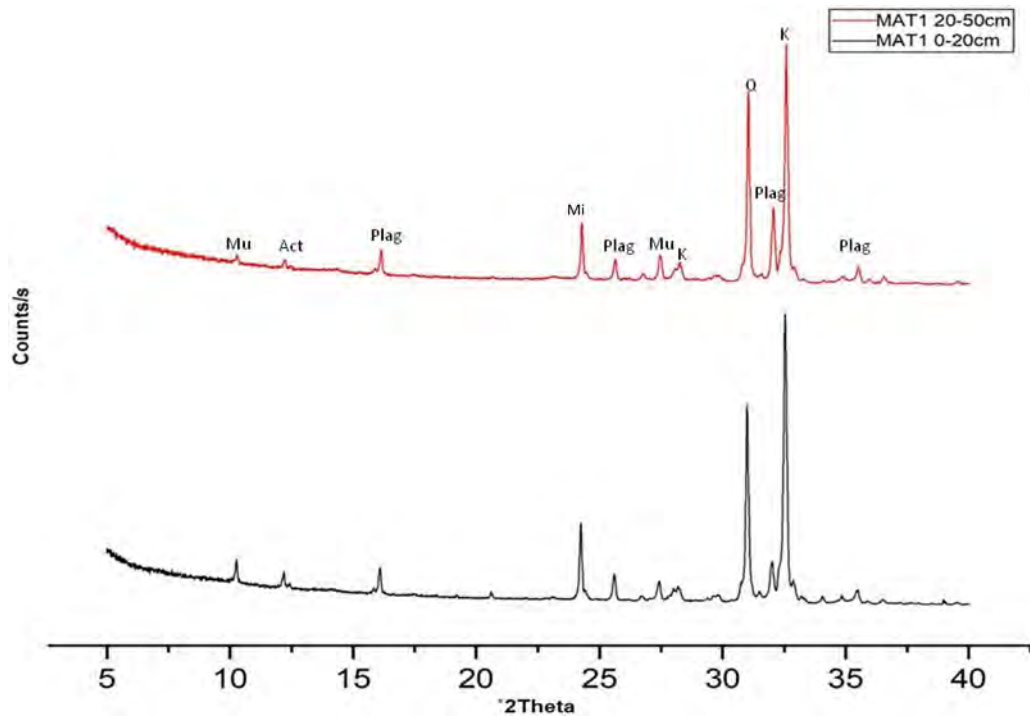


Figure 4.26: Mineral phases as determined by XRD of silt fractions of soils developed from granite; Mu = muscovite, Act = actinolite, Plag = plagioclase, Q= quartz, K =kaolinite, Mi = microcline.

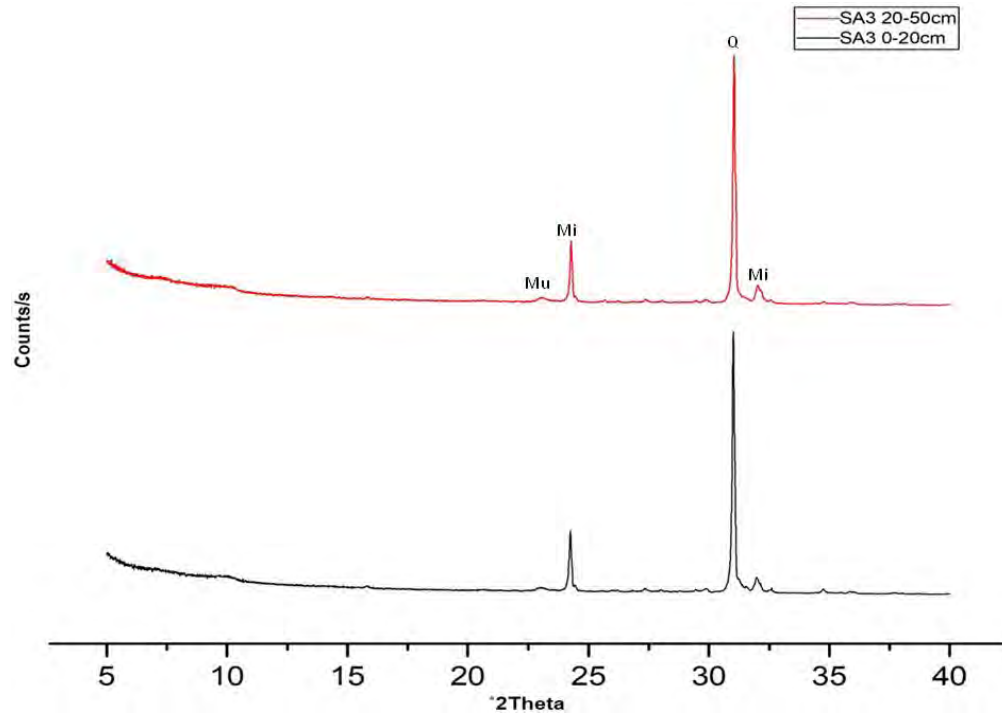


Figure 4.27: Mineral phases as determined by XRD of silt fractions of soils developed from arkosic sandstone; Mu =muscovite, Mi = microcline, Q= quartz.

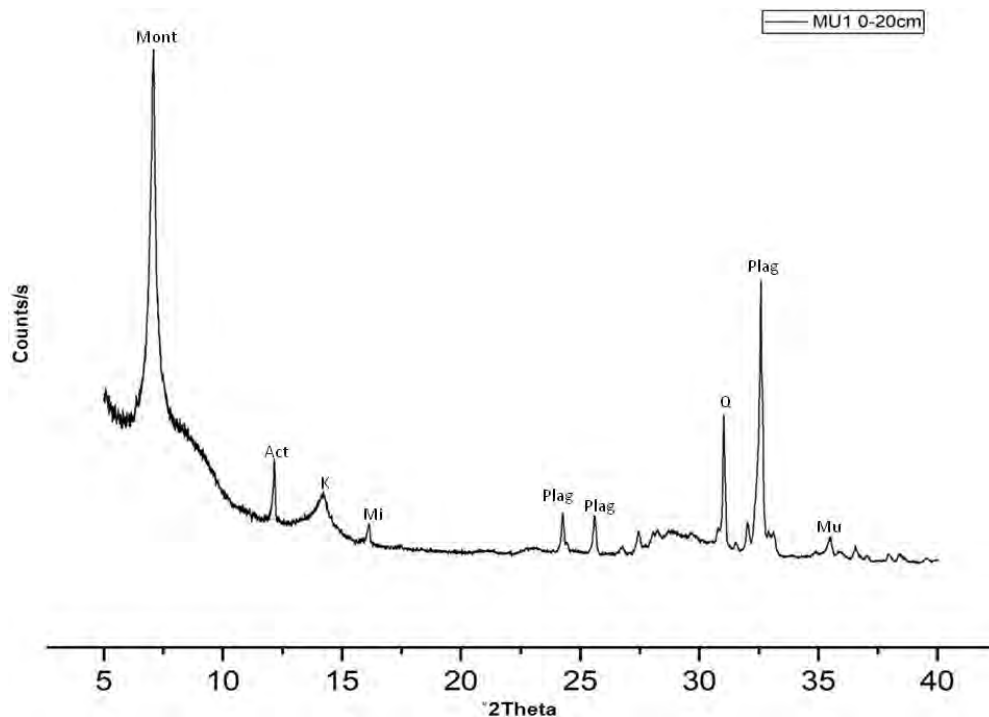


Figure 4.28: Mineral phases as determined by XRD of silt fraction of soil developed from gneiss; Mu =muscovite, Mont: montmorillonite, Act = actinolite, K = kaolinite, Plag = plagioclase, Mi = microcline, Q= quartz.

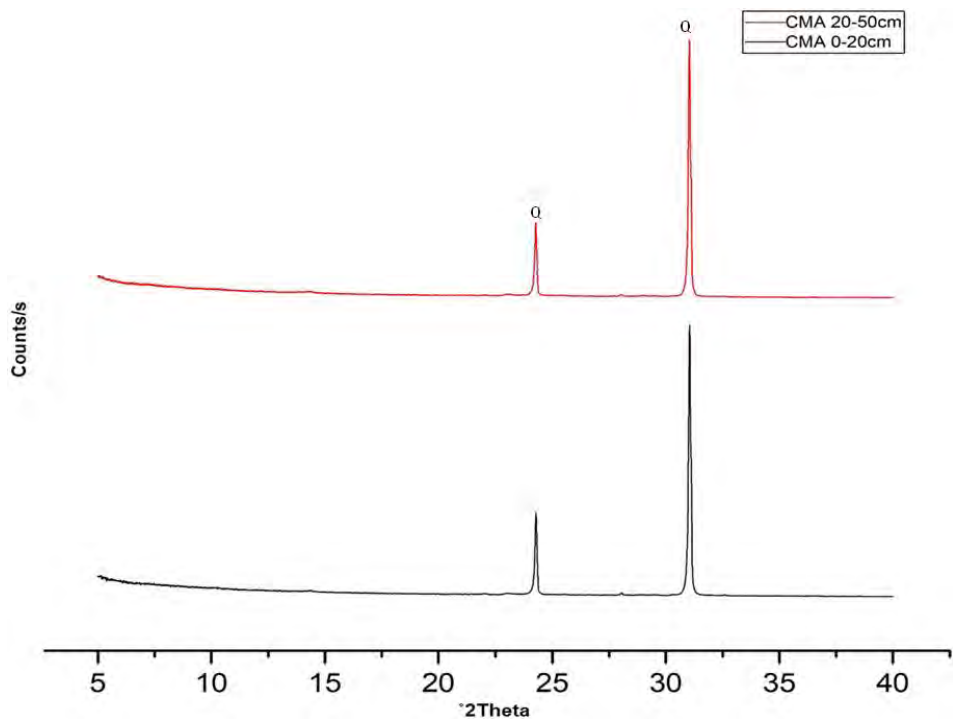


Figure 4.29: Mineral phases as determined by XRD of silt fractions of soils developed from quartzite; Q= quartz.

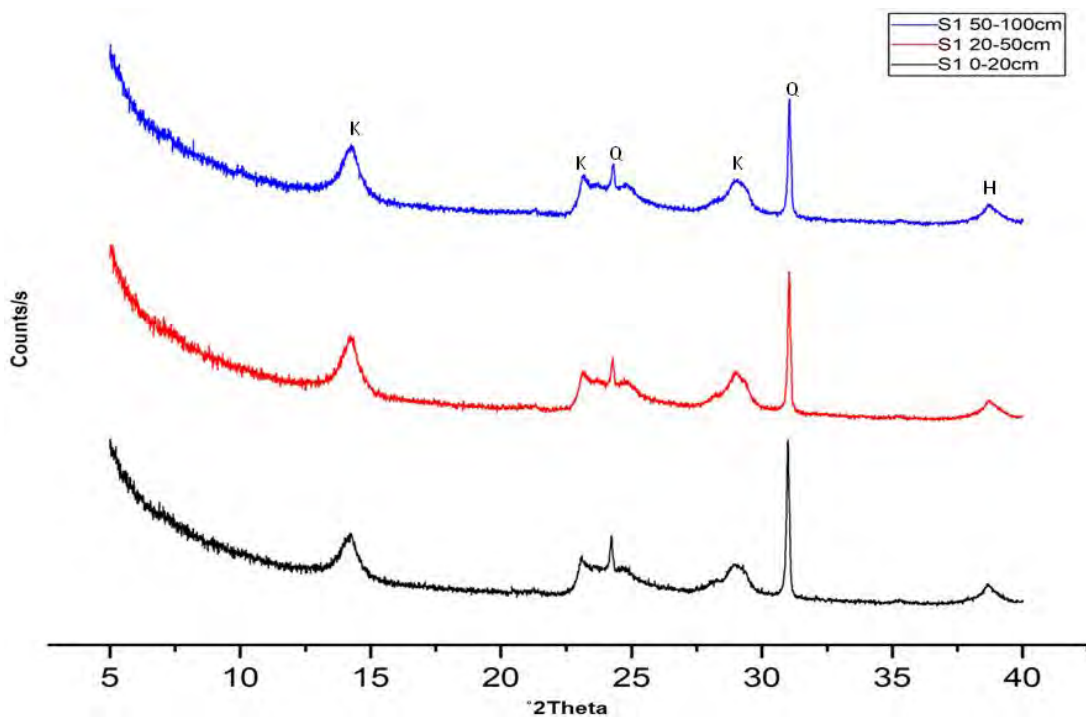


Figure 4.30: Mineral phases as determined by XRD of clay fractions of soils (S1) developed from basalt; K = kaolinite, Q= quartz, H= hematite.

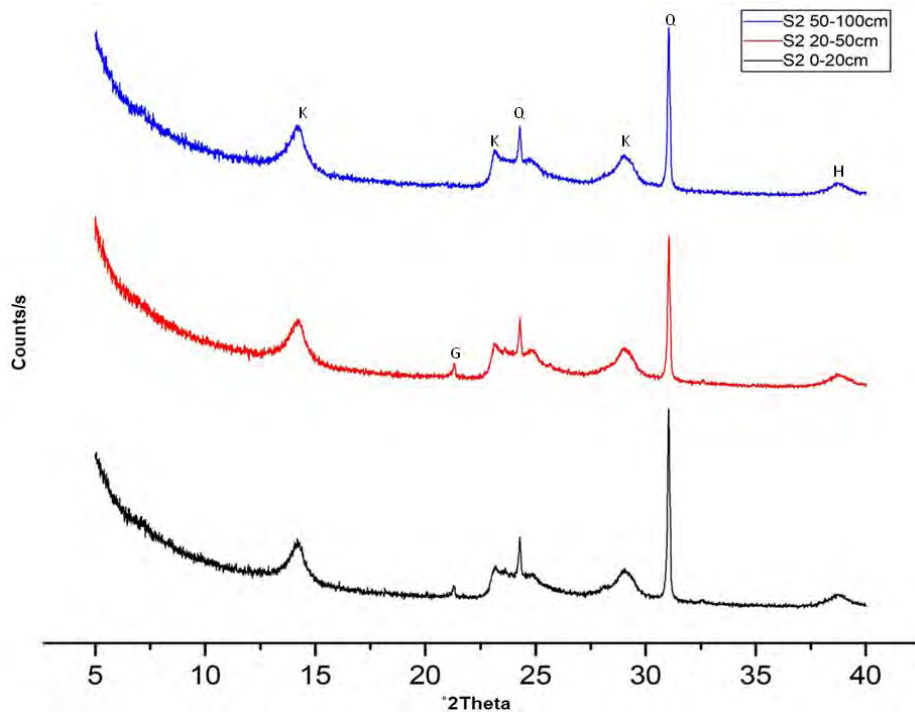


Figure 4.31: Mineral phases as determined by XRD of clay fractions of soils (S2) developed from basalt; K = kaolinite, Q= quartz, G = goethite, H =hematite.

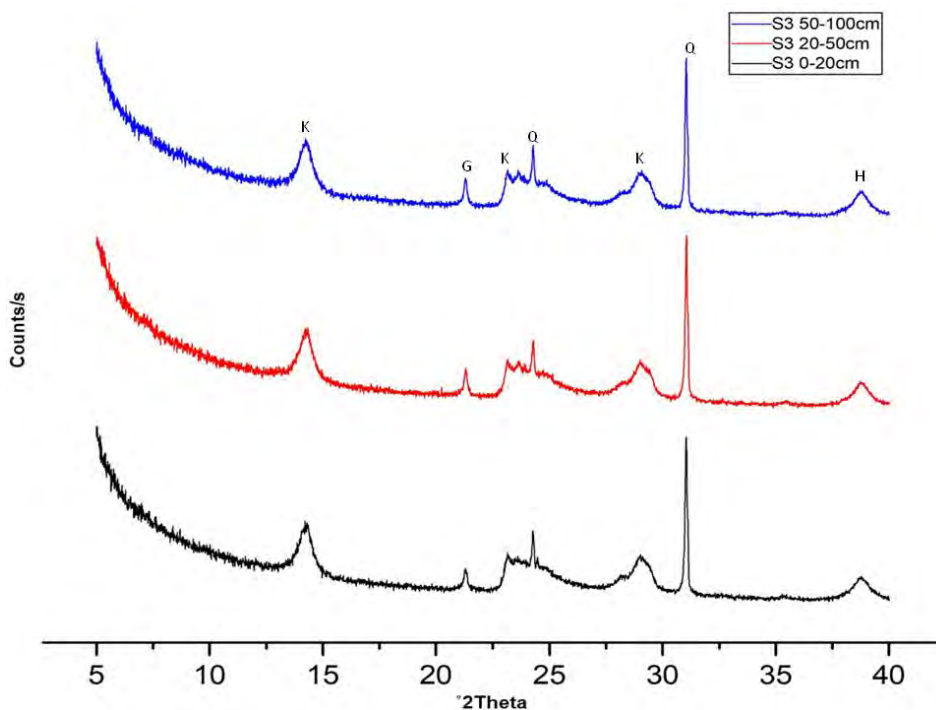


Figure 4.32: Mineral phases as determined by XRD of clay fractions of soils (S3) developed from basalt; K = kaolinite, Q= quartz, G =goethite, H= hematite.

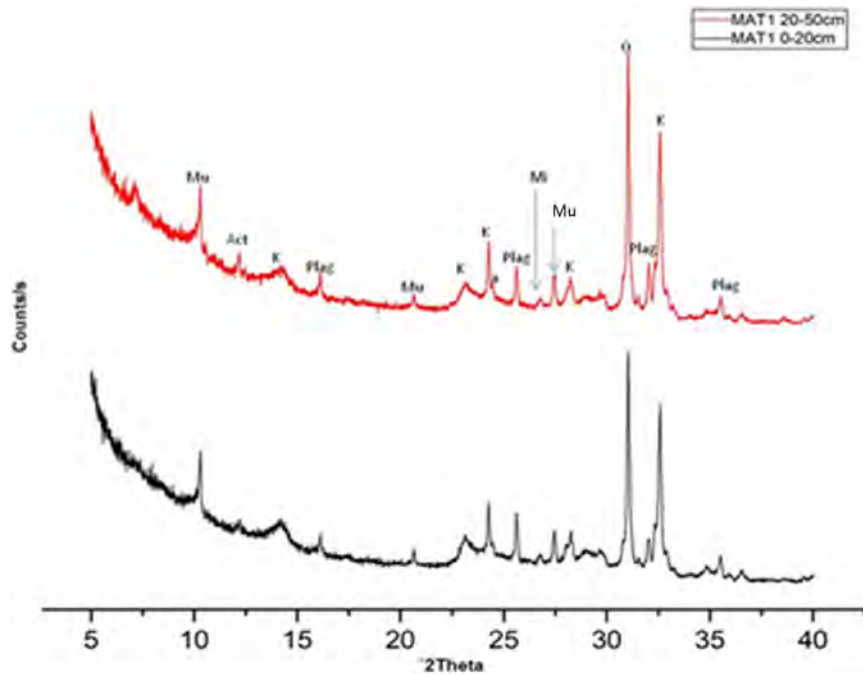


Figure 4.33: Mineral phases as determined by XRD of clay fractions of soils (MAT1) developed from granite; Mu = muscovite, Act = actinolite, K= kaolinite, Plag = plagioclase, Mi = microcline, Q = quartz.

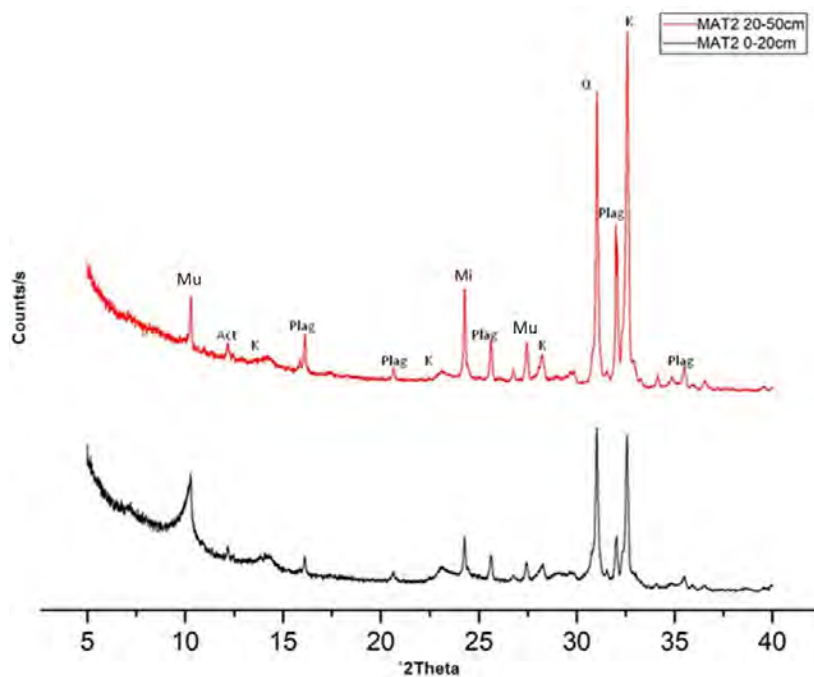


Figure 4.34: Mineral phases as determined by XRD of clay fractions of soils (MAT2) developed from granite; Mu = muscovite, Act = actinolite, Plag = plagioclase, K = kaolinite, Mi = microcline, Q= quartz.

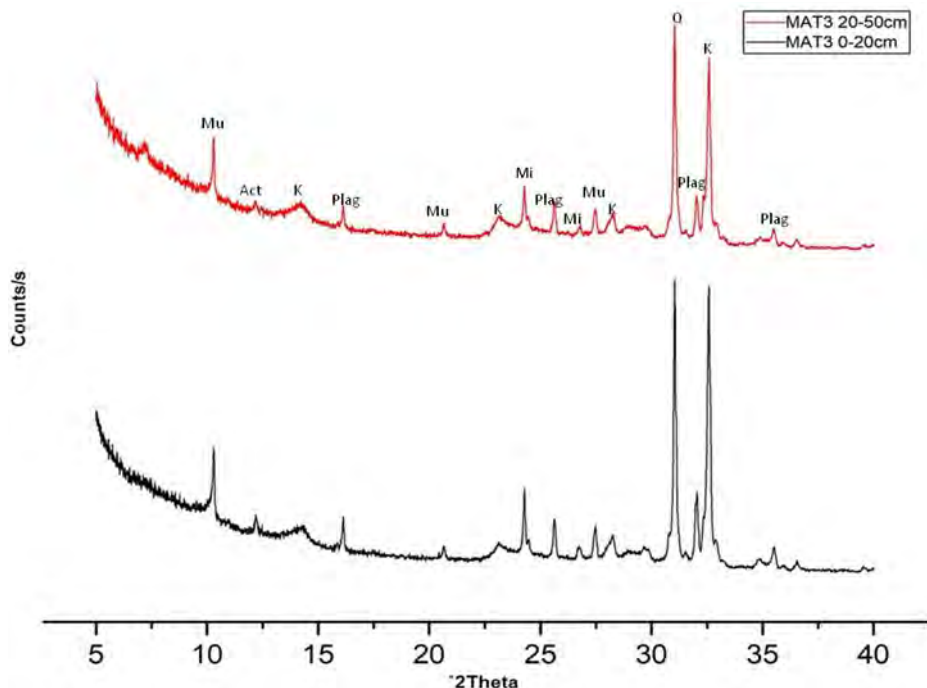


Figure 4.35: Mineral phases as determined by XRD of clay fractions of soils (MAT3) developed from granite; Mu = muscovite, Act = actinolite, Plag = plagioclase, K = kaolinite, Mi = microcline, Q= quartz.

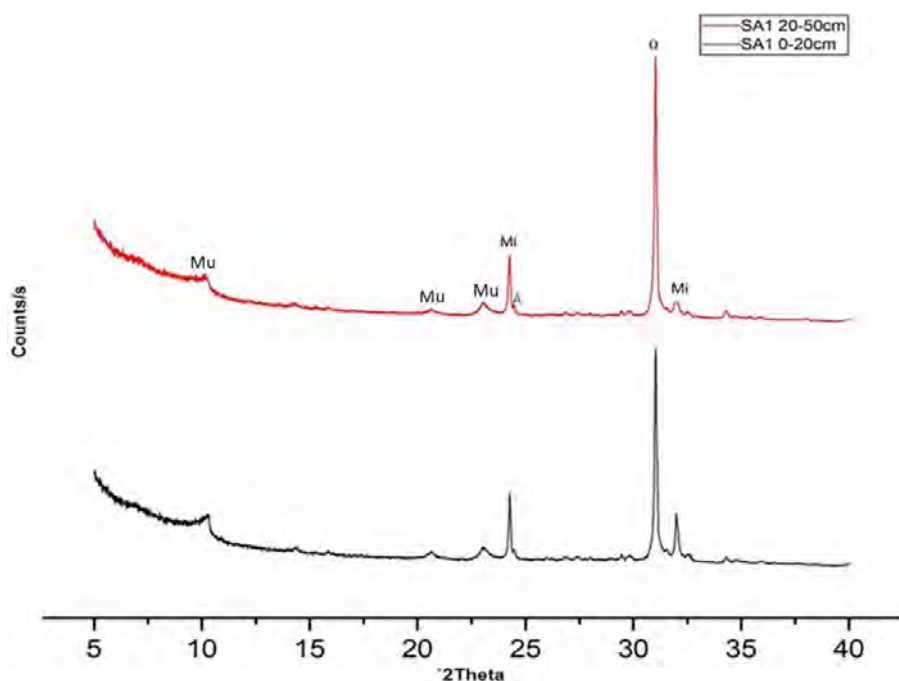


Figure 4.36: Mineral phases as determined by XRD of clay fractions of soils (SA1) developed from arkosic sandstone; Mu = muscovite, Mi = microcline, A = anatase, Q= quartz.

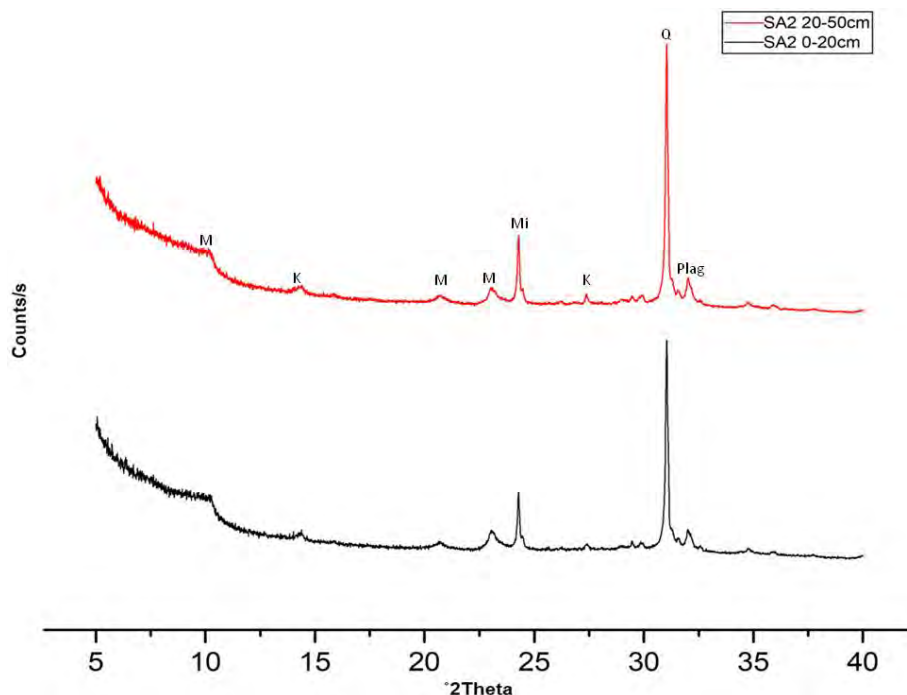


Figure 4.37: Mineral phases as determined by XRD of clay fractions of soils (SA2) developed from arkosic sandstone; M = muscovite, K = kaolinite, Mi = microcline, Q= quartz, Plag = plagioclase.

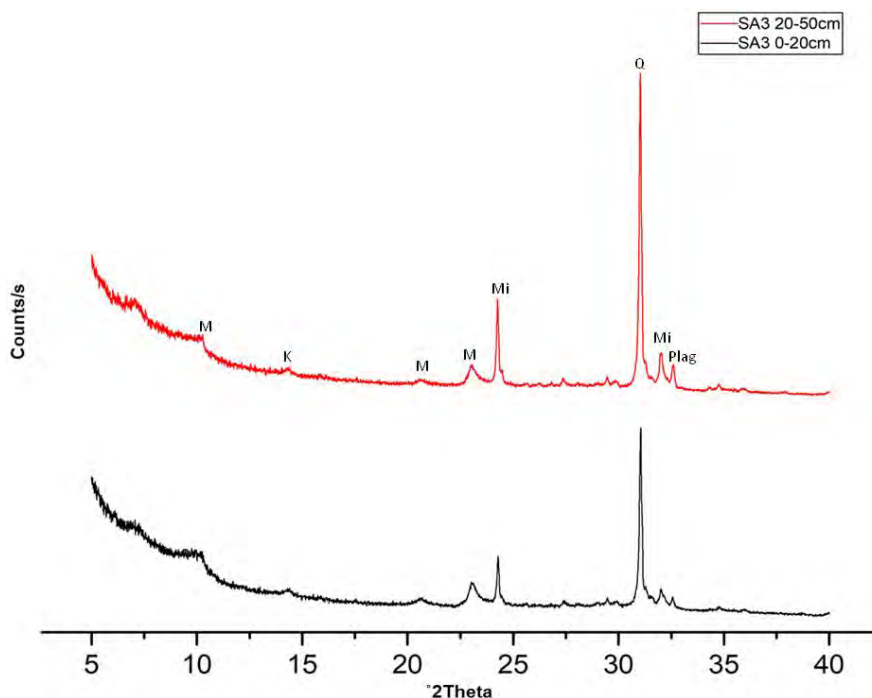


Figure 4.38: Mineral phases as determined by XRD of clay fractions of soils (SA3) developed from Arkosic sandstone; M = muscovite, K = kaolinite, Mi = microcline, Q= quartz, Plag = plagioclase.

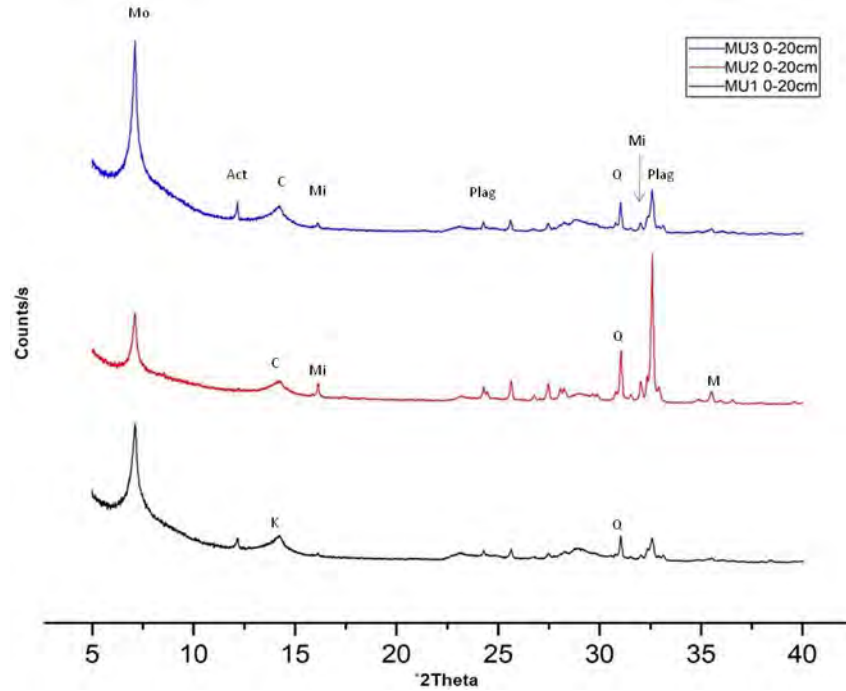


Figure 4.39: Mineral phases as determined by XRD of clay fractions of soils developed from gneiss; Mo = montmorillonite, Act = actinolite, C = chlorite, Mi = microcline, Plag = plagioclase, Q= quartz.

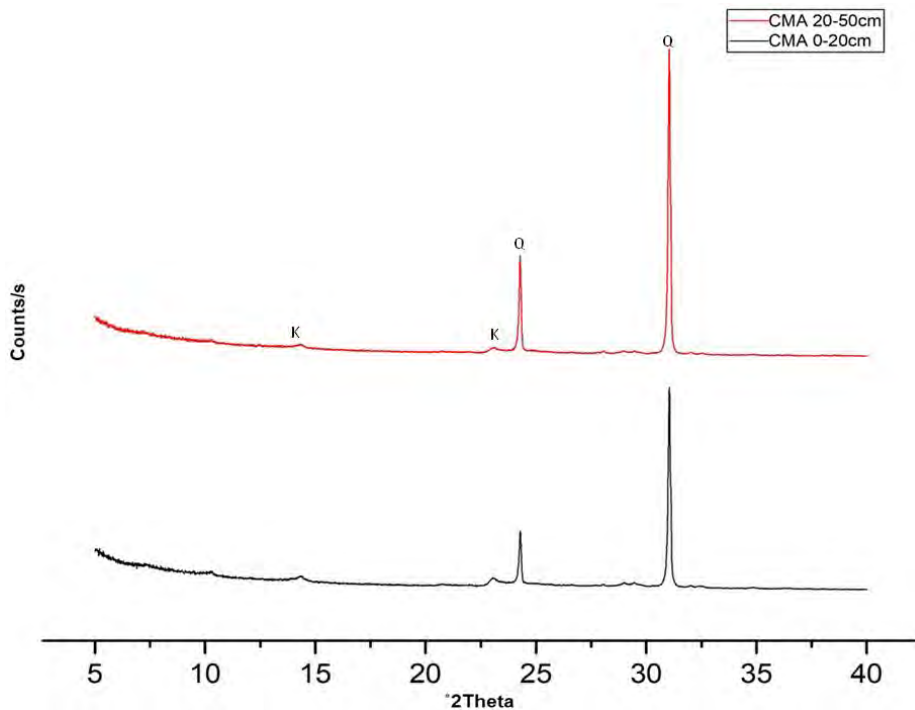


Figure 4.40: Mineral phases as determined by XRD of clay fractions of soils developed from Quartzite; K = kaolinite, Q= quartz.

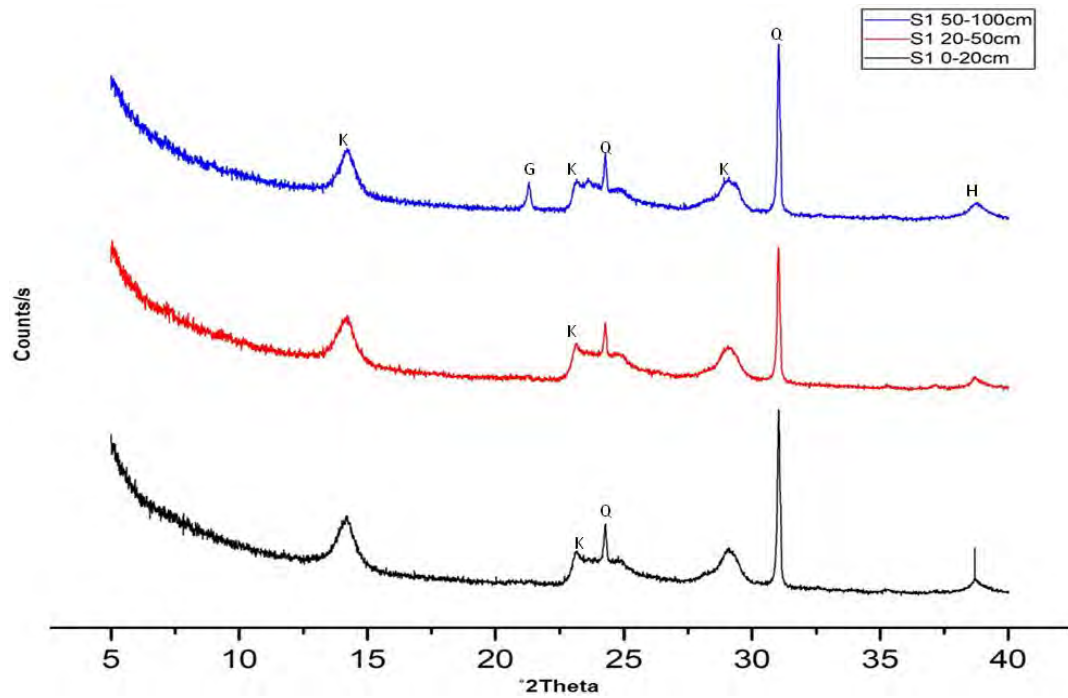


Figure 4.41: Mineral phases as determined by XRD of soil kaolins (S1) developed from basalt; K = kaolinite, Q= quartz, G =goethite, H= hematite.

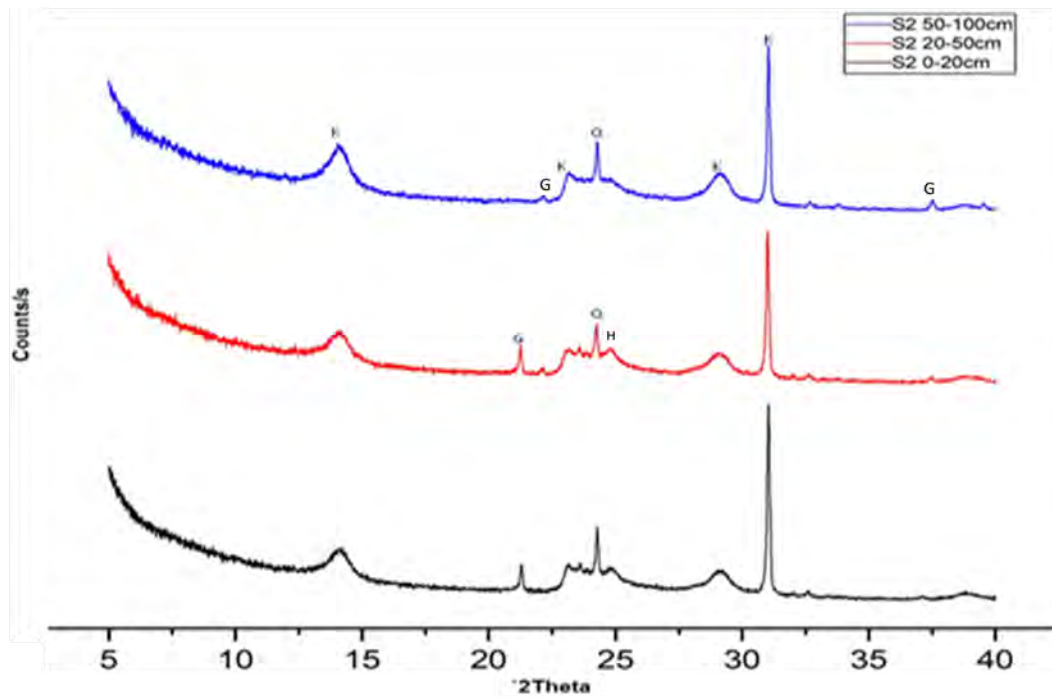


Figure 4.42: Mineral phases as determined by XRD of soil kaolins (S2) developed from basalt; K = kaolinite, G = goethite, Q= quartz, H= hematite.

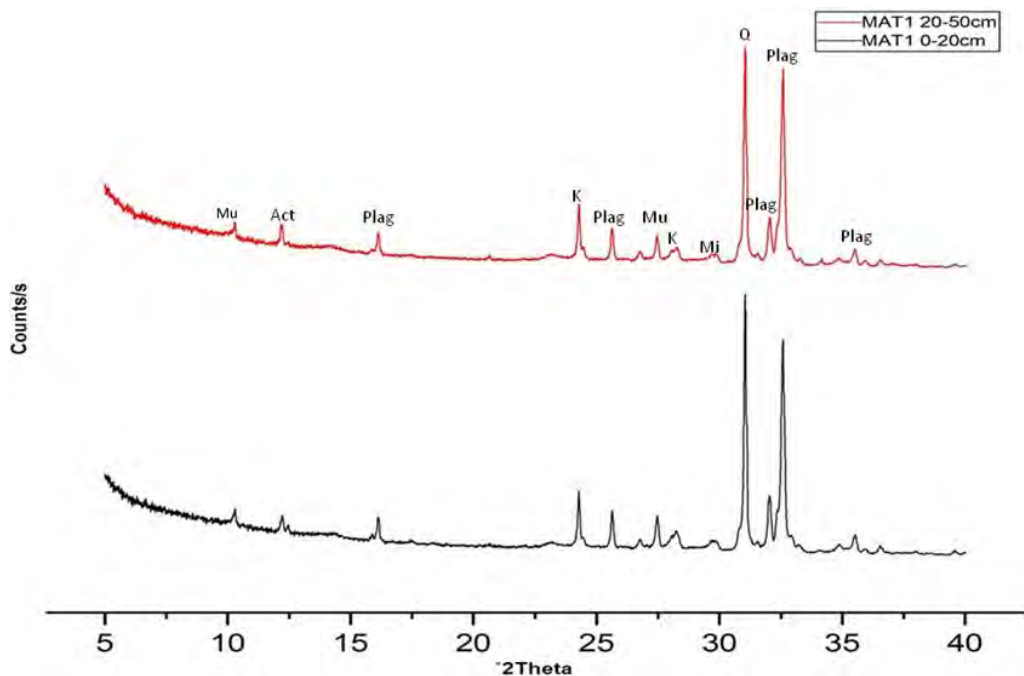


Figure 4.43: Mineral phases as determined by XRD of soil kaolins (MAT1) developed from granite; Mu = muscovite, Act = actinolite, Plag = plagioclase, K =kaolinite, Mi = microcline, Q= quartz.

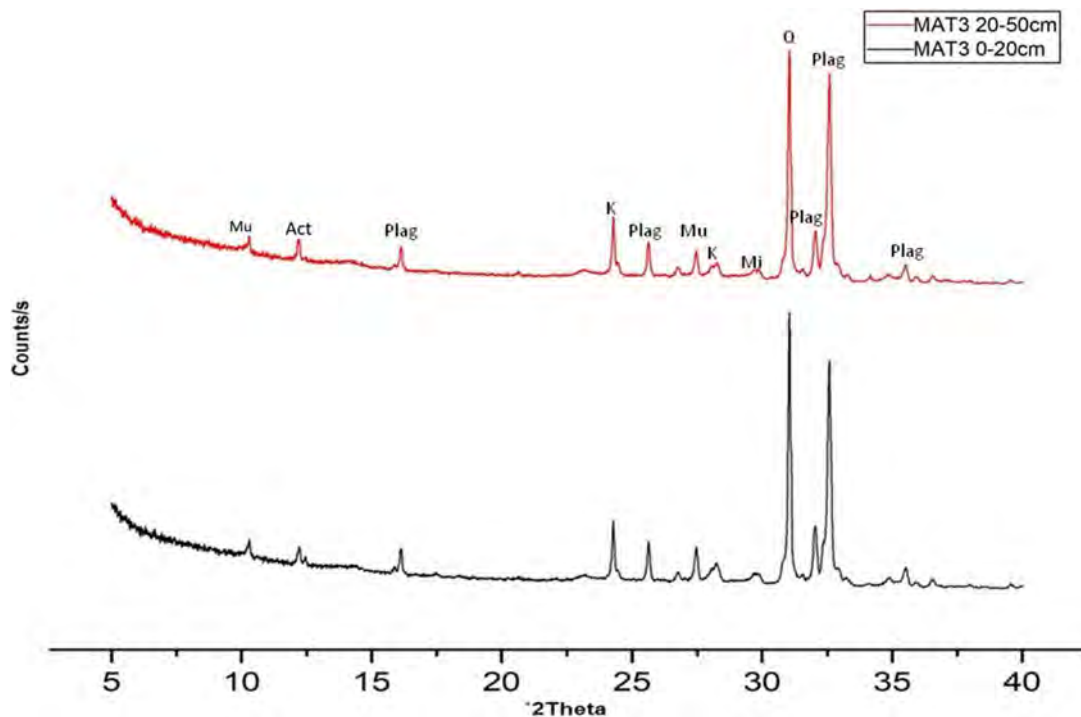


Figure 4.44: Mineral phases as determined by XRD of soil kaolins (MAT3) developed from granite; Mu = muscovite, Act = actinolite, Plag = plagioclase, K =kaolinite, Mi = microcline, Q= quartz.

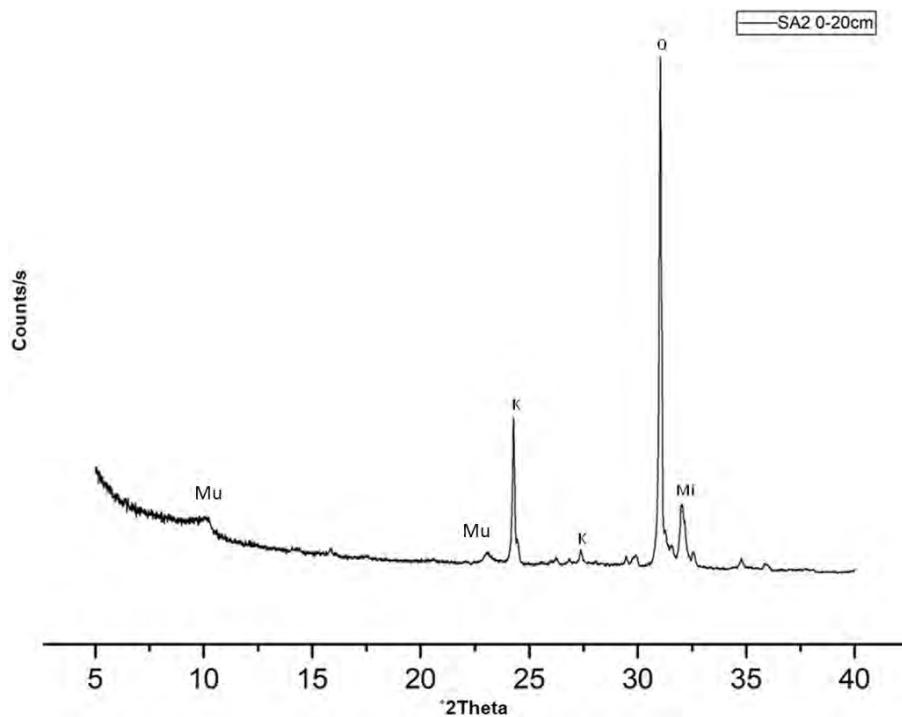


Figure 4.45: Mineral phases as determined by XRD of soil kaolins (SA2) developed from arkosic sandstone; Mu = muscovite, K = kaolinite, Q= quartz, Mi = microcline.

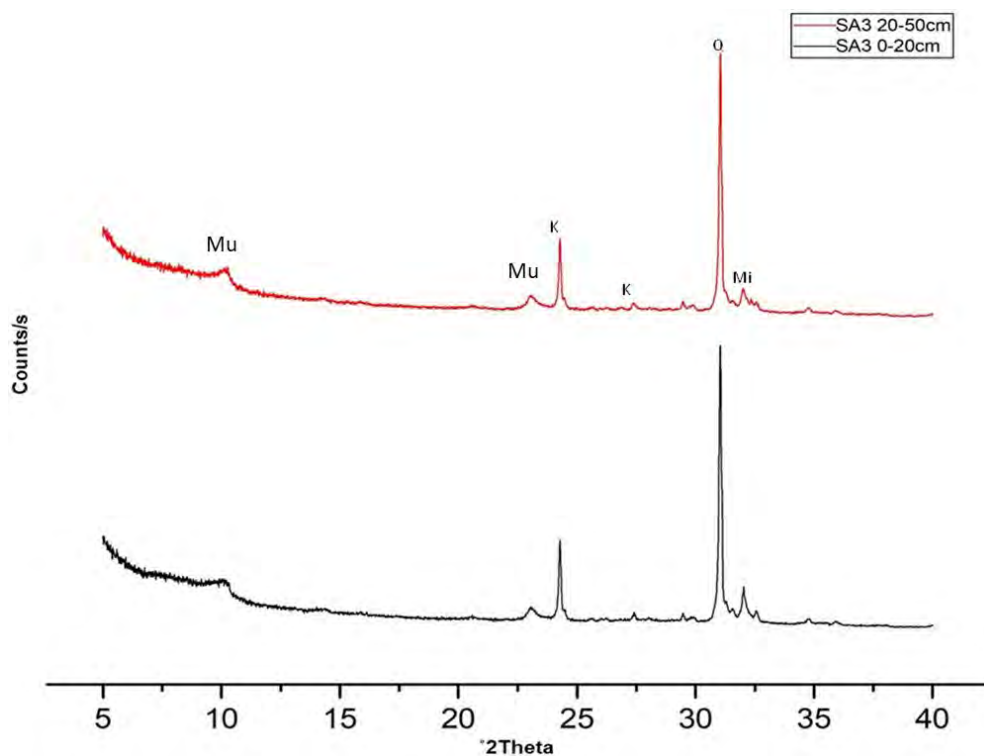


Figure 4.46: Mineral phases as determined by XRD of soil kaolins (SA3) developed from arkosic sandstone; M = muscovite, K = kaolinite, Q= quartz, Mi = microcline.

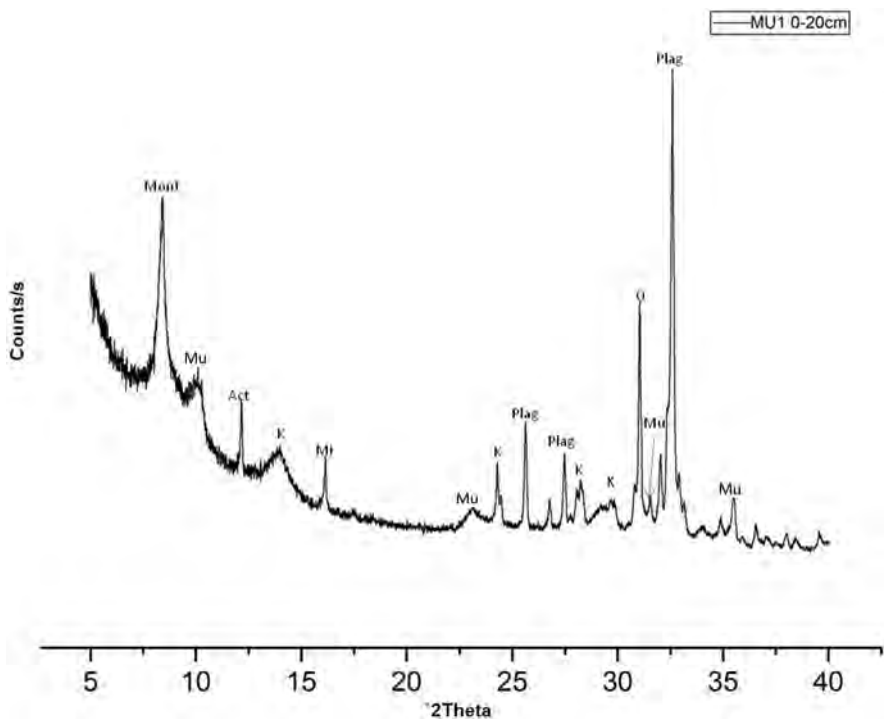


Figure 4.47: Mineral phases as determined by XRD of soil kaolins (MU1) developed from gneiss; Mont = montmorillonite, Mu = muscovite, Act = actinolite, K = kaolinite, Mi = microcline, Plag = plagioclase, Q= quartz.

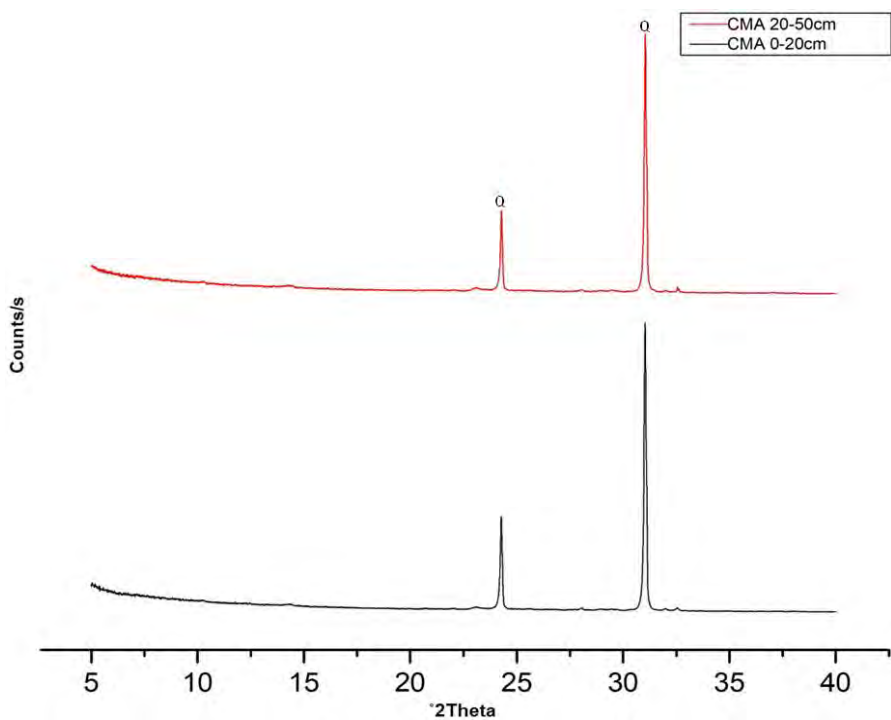


Figure 4.48: Mineral phases as determined by XRD of soil kaolins developed from quartzite; Q= quartz.

4.2.2.2 Quantitative Analyses

- **Parent Rock Samples**

The results of quantitative analyses of the various minerals present in the parent rocks are presented in Table 4.6. Basalt had plagioclase, diopside, and chlorite as the dominant mineral constituents in that order of abundances ranging from 24 to 29 wt % whereas quartz, epidote, and actinolite were present in abundances less than 10 wt %. In Granite, plagioclase, quartz, and microcline were the dominant mineral phases with abundances ranging from 30 to 33 wt % whereas, muscovite and chlorite were present in minor quantities. Arkosic sandstone had quartz as the most dominant mineral with an abundance of 77 wt % whereas, microcline and muscovite have abundances of 16 wt % and 7 wt %, respectively. The most dominant mineral in quartzite was quartz with an abundance of 97 wt % whereas, plagioclase and muscovite were in minor quantities.

Table 4.6: Results of Quantitative analyses of minerals present (wt %) in parent rocks.

Lithology	Quartz	Plagioclase	Muscovite	Microcline	Diopside	Chlorite	Epidote	Actinolite
Basalt	9	39	-	-	27	24	8	3
Granite	31	33	5	30	-	1	-	-
Ark. Sst.	77	-	7	16	-	-	-	-
Quartzite	97	1	2	-	-	-	-	-

(-) Not detected

- **Bulk (<2 mm) Samples**

The results of quantitative analyses of the various minerals present in the bulk fractions are presented in Table 4.7. Soils developed from basalt had kaolinite as the most dominant mineral constituent with abundances ranging from 45 to 50 wt %. Quartz was also present with abundances ranging between 24 and 29 wt % whereas, anatase, goethite, hematite and gibbsite have abundances less than 12 wt %. Soils developed from granite had plagioclase, quartz and microcline as the dominant mineral phases with abundances ranging from 32 to 33 wt %, 25 to 31 wt % and 19 to 21 wt %, respectively.

respectively, whereas kaolinite and muscovite were present with combined abundances between 7 and 13 wt %. Actinolite was present in trace quantities.

Soils developed from arkosic sandstone had quartz as the dominant mineral with abundances between 76 and 79 wt % whereas, kaolinite, muscovite, microcline and chlorite were present with abundances between 1 and 11 wt %. In soils developed from gneiss, the dominant mineral was plagioclase with an abundance of 50 wt %, followed by quartz with 25 wt %, montmorillonite with 11 wt %, kaolinite and actinolite with 9 wt %, respectively. Microcline and chlorite occurred in trace quantities. The dominant mineral in soils developed from quartzite was quartz with abundance between 90 to 93 wt % whereas, plagioclase and muscovite occurred in minor quantities.

- **Silt (2 – 63 μm) Fractions**

The results of quantitative analyses of the various minerals present in the silt fractions are presented in Tables 4.8. The silt fraction of soils developed from basalt had kaolinite as the most dominant mineral constituent with abundances between 49 and 53 wt % followed by quartz with 21 and 24 wt %.

Anatase, goethite, hematite and gibbsite were present in abundances less than 11 wt %. The silt fraction of soils developed from granite had plagioclase and quartz as the dominant minerals with abundances between 32 and 35 wt %. Microcline and kaolinite occurred with abundances ranging from 15 to 16 wt % and 9 to 10 wt %, respectively whereas, muscovite and actinolite occurred in amounts less than 10 wt %. The silt fraction of soil developed from gneiss had plagioclase as the dominant mineral with an abundance of 40 wt %. Montmorillonite, kaolinite, microcline, quartz, and actinolite were present with abundances of 18 wt %, 13 wt %, 12 wt %, 9 wt %, and 6 wt % respectively. Chlorite occurred in trace quantities. The silt fraction of soils developed from quartzite was dominated by quartz with an abundance of 90 wt % whereas, muscovite, kaolinite, and plagioclase occurred in quantities less than 7 wt %.

Table 4.7: Results of Quantitative Analyses of Minerals present (wt %) in the Bulk samples of the studied Soils.

Lithology	Location	Depth	Kaolinite	Quartz	Anatase	Goethite	Hematite	Plagioclase	Microcline	Muscovite	Gibbsite	Chlorite	Actinolite	Montmorillonite
Basalt	S2	0-20	45	24	5	9	9	-	-	-	8	-	-	-
		20-50	48	29	8	5	6	-	-	-	4	-	-	-
		50-100	50	24	4	10	11	-	-	-	1	-	-	-
Granite	MAT1	0-20	8	25	-	-	-	32	21	13	-	-	1	-
		20-50	7	31	-	-	-	33	19	9	-	-	1	-
Ar. Sst.		0-20	3	79	-	-	-	-	9	9	-	-	-	-
		20-50	1	76	-	-	-	-	11	8	-	3	-	-
Gneiss	MU1	0-20	9	25	-	-	-	50	6	-	-	1	-	9
Qtzite	CMA	0-20	3	93	-	-	-	1	-	3	-	-	-	-
		20-50	5	90	-	-	-	1	-	4	-	-	-	-

(-) Not detected

Table 4.8: Results of Quantitative Analyses of Minerals present (wt %) in the Silt Fractions of the studied Soils.

Lithology	Location	Depth	Kaolinite	Quartz	Anatase	Goethite	Hematite	Plagioclase	Microcline	Muscovite	Gibbsite	Chlorite	Actinolite	Montmorillonite
Basalt	S2	0-20	49	21	5	10	10	-	-	-	5	-	-	-
		20-50	50	22	6	14	-	-	-	-	8	-	-	-
		50-100	53	24	4	10	7	-	-	-	2	-	-	-
Granite	MAT1	0-20	10	32	-	-	-	35	16	6	-	-	1	-
		20-50	9	33	-	-	-	34	15	7	-	-	2	-
Ark. Sst.	SA3	0-20	1	71	-	-	1	-	15	13	-	-	-	-
		20-50	1	70	-	-	-	-	15	12	-	2	-	-
Gneiss	MU1	0-20	13	9	-	-	-	40	12	-	-	2	-	6
Qtzite	CMA	0-20	4	90	-	-	-	1	-	5	-	-	-	-
		20-50	4	90	-	-	-	-	-	6	-	-	-	-

(-) Not detected

- **Clay (<2 µm) Fractions**

The results of quantitative analyses of the various mineral present in the clay fractions are presented in Table 4.9. The clay fractions of soils developed from basalt was dominated by kaolinite followed by quartz with abundances ranging from 44 to 57 wt % and 13 to 20 wt %, respectively. Hematite, goethite, gibbsite, and anatase were present with abundances less than 18 wt %. The mineral phases dominating the clay fractions of soils developed from granite were plagioclase, kaolinite, muscovite quartz, and microcline with abundances between 7 and 38 wt % whereas, chlorite and actinolite occurred in quantities less than 6 wt %. The clay fractions of soils developed from arkosic sandstone had quartz as the dominant mineral followed by muscovite, kaolinite, and microcline with abundances varying from 30 to 55 wt %, 19 to 29 wt %, 15 to 17 wt %, and 9 to 20 wt %, respectively. Plagioclase and chlorite have quantities less than 9 wt %.

Plagioclase, montmorillonite, kaolinite, quartz, and muscovite dominate the clay fractions of soils developed from gneiss in that order with abundances between 8 and 47 wt %. Chlorite and actinolite occurred in amounts less than 7 wt %. The clay fractions of soils developed from quartzite were dominated by quartz with abundance varying from 59 to 73 wt %. Kaolinite and muscovite occurred with abundances between 9 and 18 wt % whereas, anatase and chlorite occurred in minor quantities.

- **Soil Kaolins**

The results of quantitative analyses of the various minerals present in the soil kaolins are presented in Table 4.10. Soil kaolins developed from basalt had kaolinite as the dominant mineral with a varying abundance between 62 and 85 wt % followed by quartz with an abundance varying from 7 to 22 wt %. Hematite, gibbsite, anatase and goethite were present in quantities less than 10 wt %. Soil kaolins developed from granite had kaolinite as the dominant mineral constituent with abundances btween 24 and 31 wt %. Quartz, plagioclase, muscovite and microcline were present with abundances between 9 and 32 wt % whereas, chlorite and anatase were in minor amount.

Table 4.9: Results of Quantitative Analyses of Minerals present (wt %) in the Clay Fractions of the studied Soils.

Lithology	Location	Depth	Kaolinite	Quartz	Anatase	Goethite	Hematite	Plagioclase	Microcline	Muscovite	Gibbsite	Chlorite	Actinolite	Montmorillonite
Basalt	S1	0-20	56	16	6	8	14	-	-	-	-	-	-	-
		20-50	57	13	7	10	13	-	-	-	-	-	-	-
		50-100	56	14	7	12	11	-	-	-	-	-	-	-
	S2	0-20	51	19	6	10	10	-	-	-	4	-	-	-
		20-50	50	18	7	12	8	-	-	-	5	-	-	-
		50-100	54	20	7	9	8	-	-	-	2	-	-	-
	S3	0-20	45	16	4	9	15	-	-	-	9	-	-	-
		20-50	44	14	6	10	14	-	-	-	12	-	-	-
		50-100	44	14	6	9	17	-	-	-	14	-	-	-
Granite	MAT1	0-20	22	18	-	-	-	26	10	22	-	-	2	-
		20-50	18	19	-	-	-	25	12	16	-	5	3	-
	MAT2	0-20	17	20	-	-	-	28	15	7	-	4	2	-
		20-50	14	27	-	-	-	38	9	11	-	-	1	-
	MAT3	0-20	19	20	-	-	-	37	8	14	-	-	2	-
		20-50	18	18	-	-	-	26	10	17	-	3	2	-
Ar. SST	SA1	0-20	-	49	-	-	-	-	20	29	-	2	-	-
		20-50	-	55	-	-	-	-	21	24	-	1	-	-
	SA2	0-20	15	38	-	-	-	-	19	28	-	-	-	-
		20-50	-	42	-	-	-	5	20	28	-	4	-	-
	SA3	0-20	18	30	-	-	-	5	15	24	-	5	-	-
		20-50	16	39	-	-	-	8	9	19	-	4	-	-
Gneiss	MU1	0-20	34	8	-	-	-	19	9	-	-	-	-	30
	MU2	0-20	-	20	-	-	-	47	16	-	-	3	-	12
	MU3	0-20	-	11	-	-	-	27	14	8	-	4	6	29
Qtzite	CMA	0-20	18	59	2	-	-	-	2	16	-	3	-	-
		20-50	13	73	1	-	-	-	3	9	-	1	-	-

(-) Not detected

Table 4.10: Results of Quantitative Analyses of Minerals present (wt %) in the Soil Kaolins developed from different parent rocks.

Lithology	Location	Depth	Kaolinite	Qtz	Anatase	Goethite	Hematite	Plag.	Microcline	Muscovite	Gibbsite	Chlorite	Actinolite	Montmorillonite	
Basalt	S1	0-20	62	22	8	-	8	-	-	-	-	-	-	-	
		20-50	64	18	7	4	7	-	-	-	-	-	-	-	
		50-100	82	8	2	5	-	-	-	-	3	-	-	-	
	S2	0-20	77	10	3	5	4	-	-	-	-	1	-	-	
		20-50	85	7	2	5	-	-	-	-	-	1	-	-	
		50-100	77	9	3	6	4	-	-	-	-	1	-	-	
Granite	MAT1	0-20	31	21	-	-	-	20	10	17	-	-	1	-	
		20-50	24	20	-	-	-	-	24	14	14	-	2	2	-
	MAT3	0-20	26	19	-	-	-	-	32	9	13	-	-	1	-
		20-50	29	20	-	-	-	-	22	9	14	-	4	2	-
Ark. Sst.	SA2	0-20	23	35	-	-	-	-	17	25	-	-	-	-	
	SA3	0-20	26	27	-	-	-	-	19	24	-	5	-	-	
		20-50	24	38	-	-	-	-	-	13	19	-	6	-	
Gneiss	MU1	0-20	36	8	-	-	-	22	3	5	-	-	-	26	
Qtzite	CMA	0-20	22	65	-	-	-	-	3	8	-	2	-	-	
		20-50	24	66	-	-	-	-	-	2	6	-	2	-	

(-) Not detected

Soil kaolins developed from arkosic sandstone were dominated by quartz with abundance between 27 and 38 wt % followed by kaolinite, muscovite, and microcline with abundances between 19 and 26 wt %. Chlorite occurred in minor quantities.

Kaolinite, montmorillonite, and plagioclase were the dominant minerals in soil kaolins developed from gneiss with abundances between 22 to 36 wt %. Quartz, microcline, and muscovite were present in quantities less than 10 wt %. Soil kaolins developed from quartzite were dominated by quartz with abundance between 65 and 66 wt % followed by kaolinite with abundances between 22 and 23 wt %. Microcline, muscovite and chlorite occurred in amounts less than 10 wt %.

4.2.3 Scanning Electron Microscopy with an Energy Dispersive X-ray Spectrum (SEM-EDX) studies

The different elemental maps and SEM photomicrographs are presented in Figs. 4.49 – 4.72. The soil kaolinites identified were occurring as thin plates without the identification of pseudo-hexagonal stacks to books unique to kaolins except in Figure 4.52 (Keller, 1976). The SEM/EDS results for mineral chemistry provided additional information regarding minerals present in association with the kaolinites in the soils (Table 4.11).

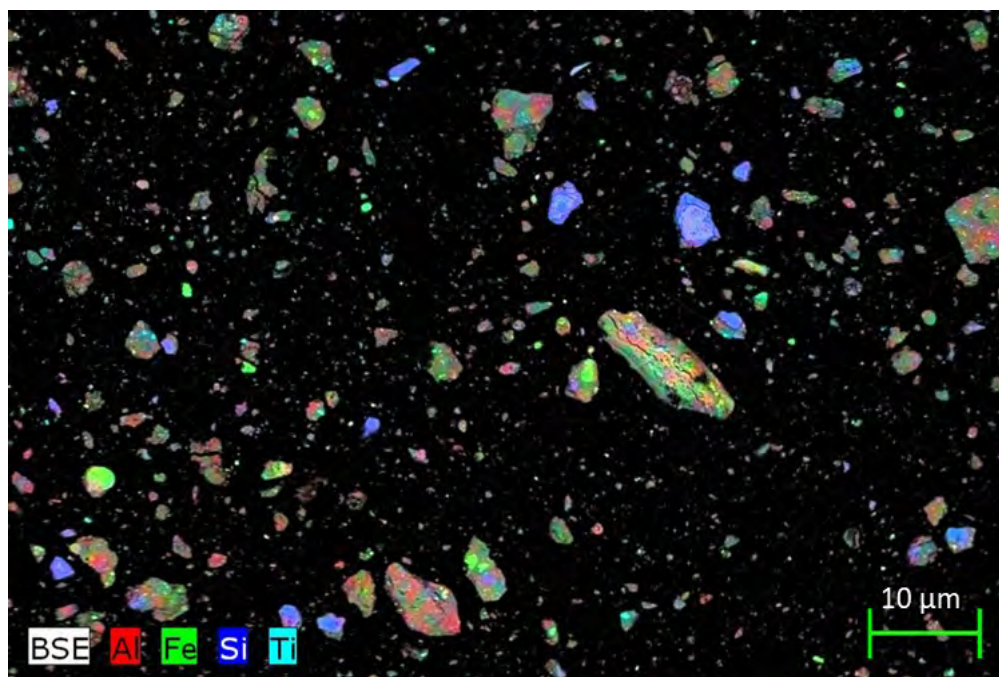


Figure 4.49: SEM elemental map of representative soil kaolin developed from basalt.

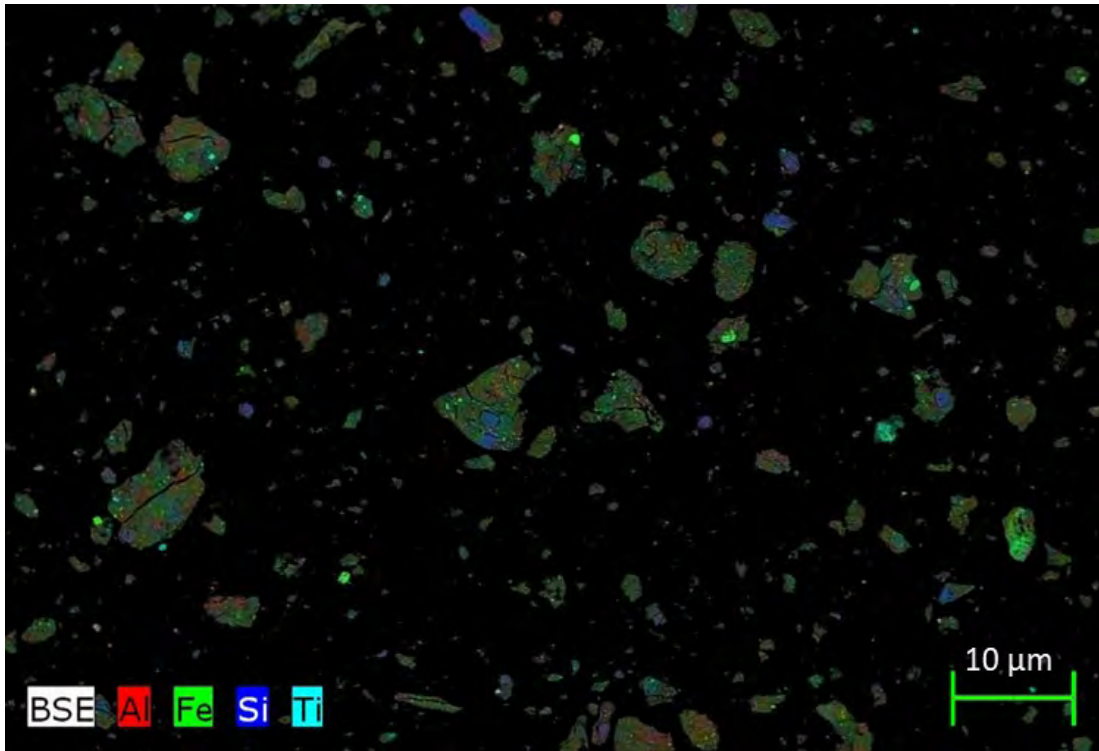


Figure 4.50: SEM elemental map of representative soil kaolin developed from basalt.

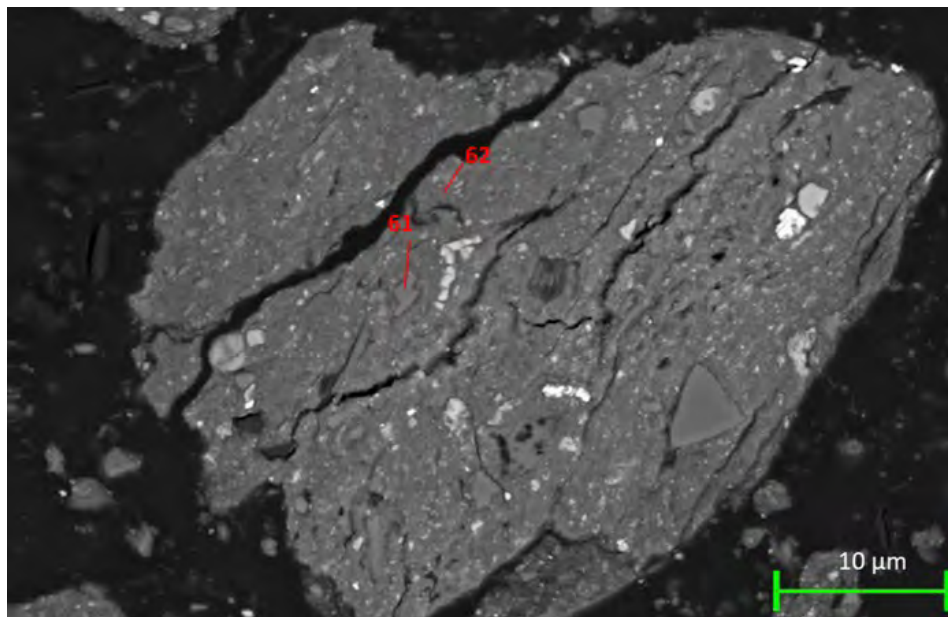


Figure 4.51: SEM image of representative soil kaolin developed from basalt (61, 62 – pyroxene/olivine).

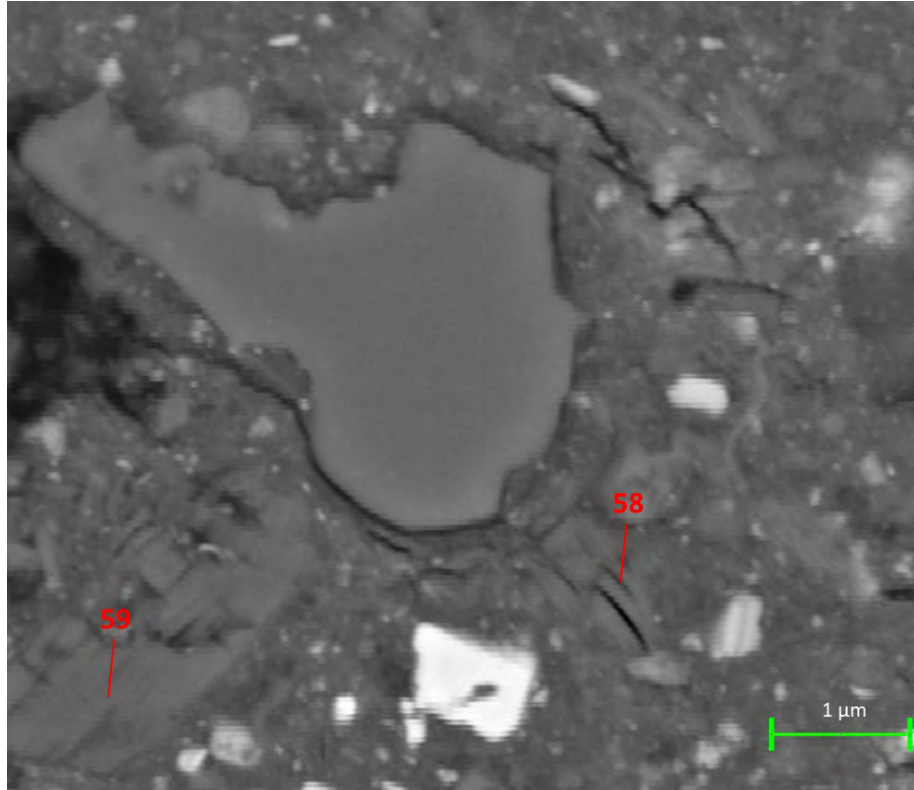


Figure 4.52: SEM image of representative soil kaolin developed from basalt showing stacks of kaolinite (58 – kaolinite; 59 – hematite).

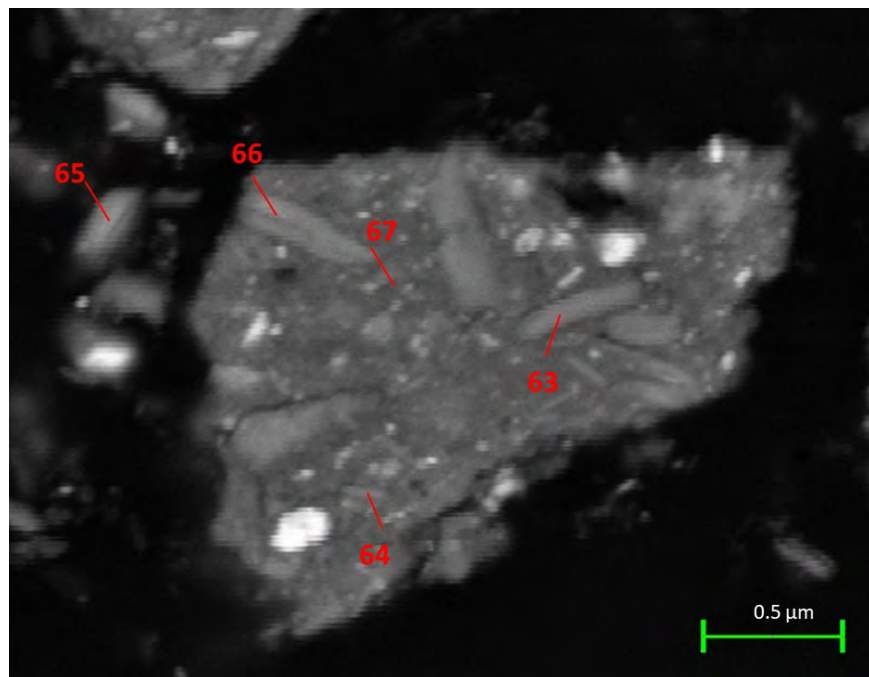


Figure 4.53: SEM image of representative soil kaolin developed from basalt showing thin platy kaolinite (63,66 – kaolinite; 64,65 – pyroxene/olivine; 67 – hematite).

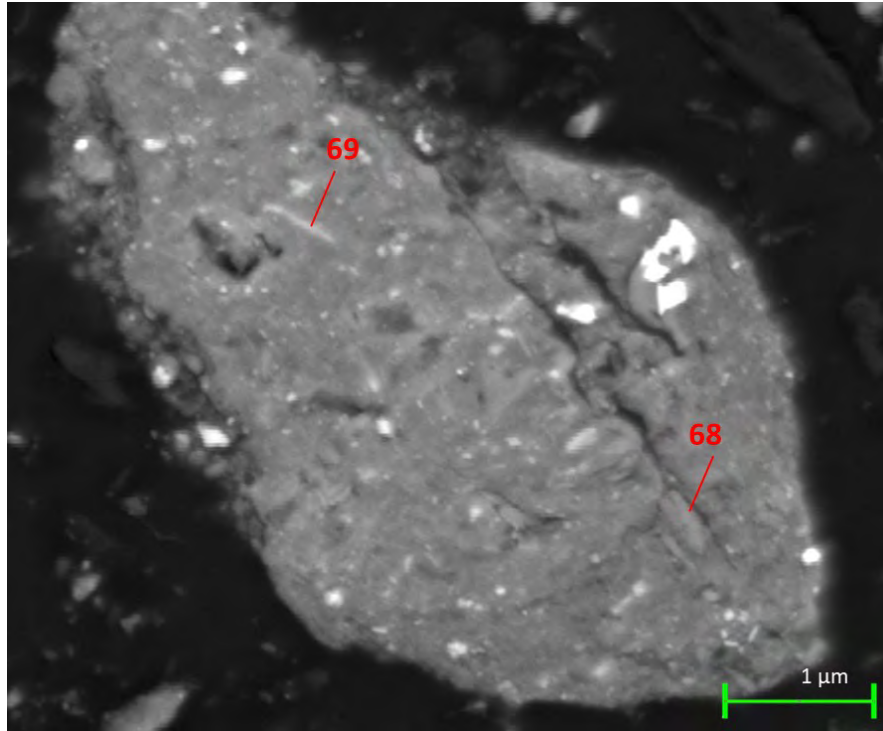


Figure 4.54: SEM image of representative soil kaolin developed from basalt (68 – hematite; 69 – pyroxene/olivine).

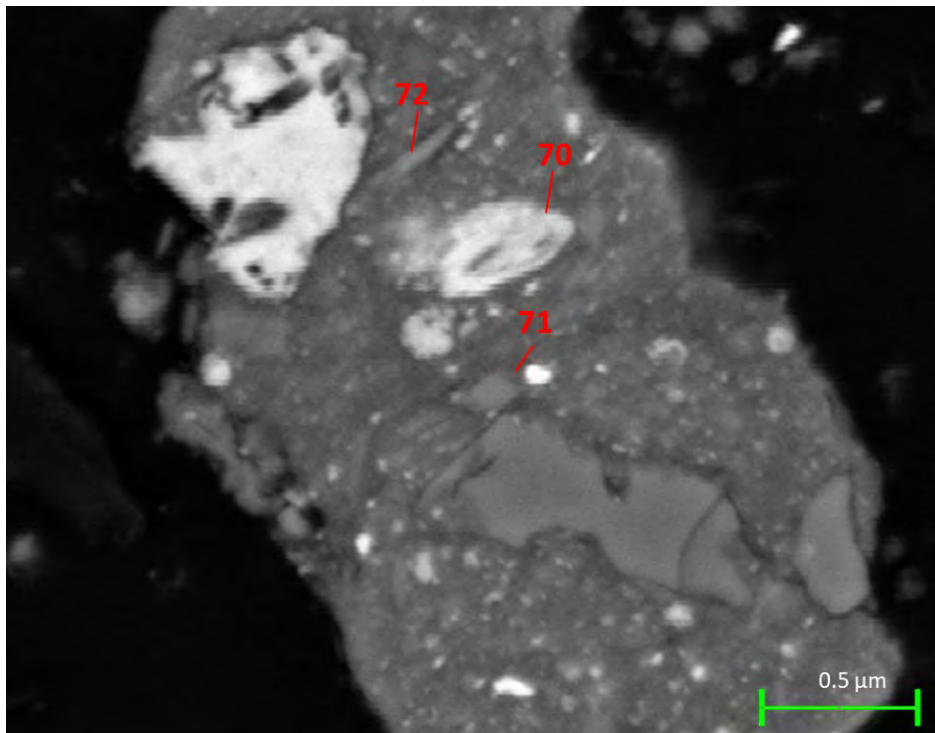


Figure 4.55: SEM image of representative soil kaolin developed from basalt showing thin platy kaolinite (70 – pyroxene/olivine; 71 – kaolinite; 72 – biotite).

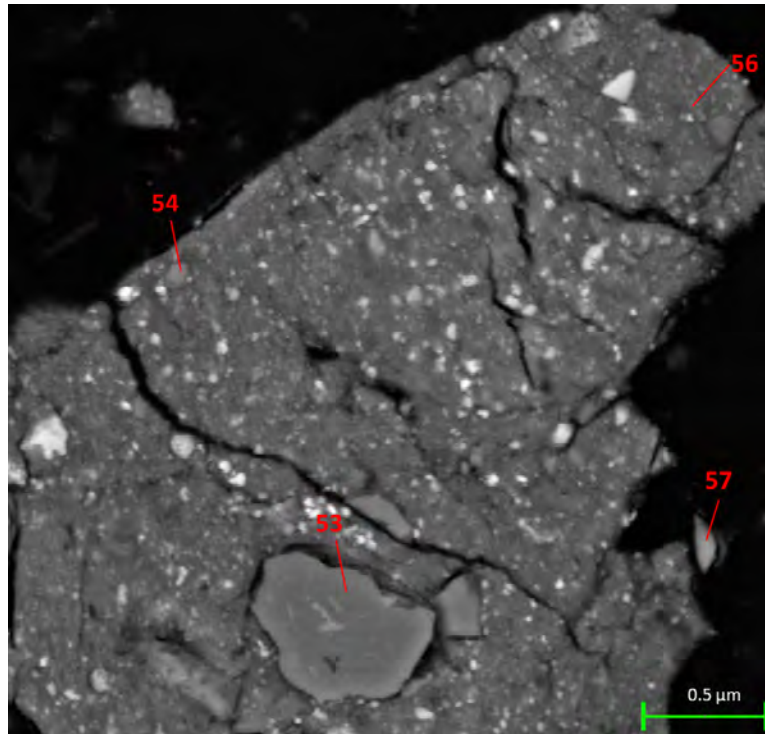


Figure 4.56: SEM image of representative soil kaolin developed from basalt (54,55 – hematite; 56 – microcline; 57 - pyroxene/olivine).

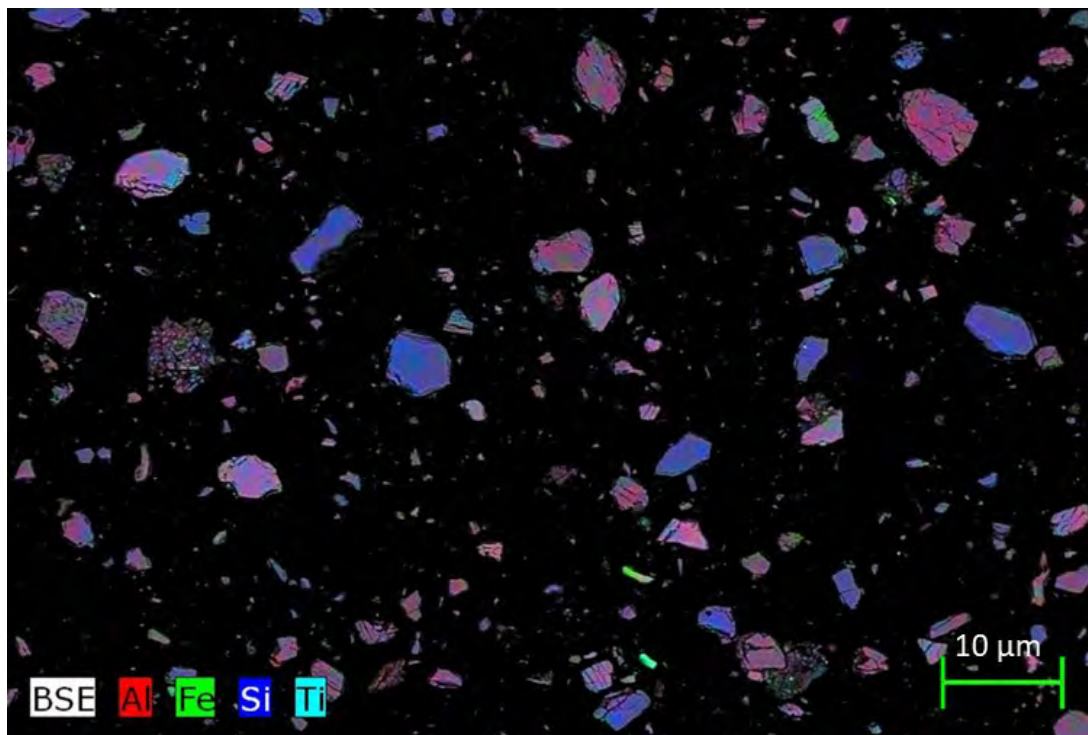


Figure 4.57: SEM elemental map of representative soil kaolin developed from granite.

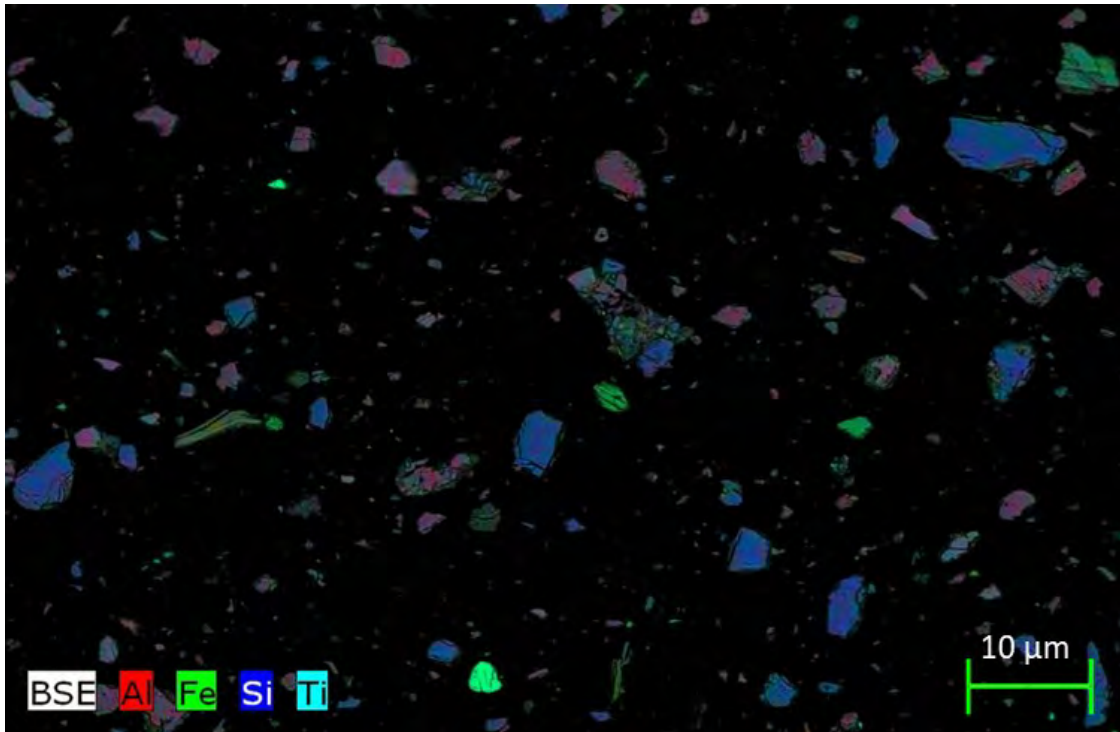


Figure 4.58: SEM elemental map of representative soil kaolin developed from granite.

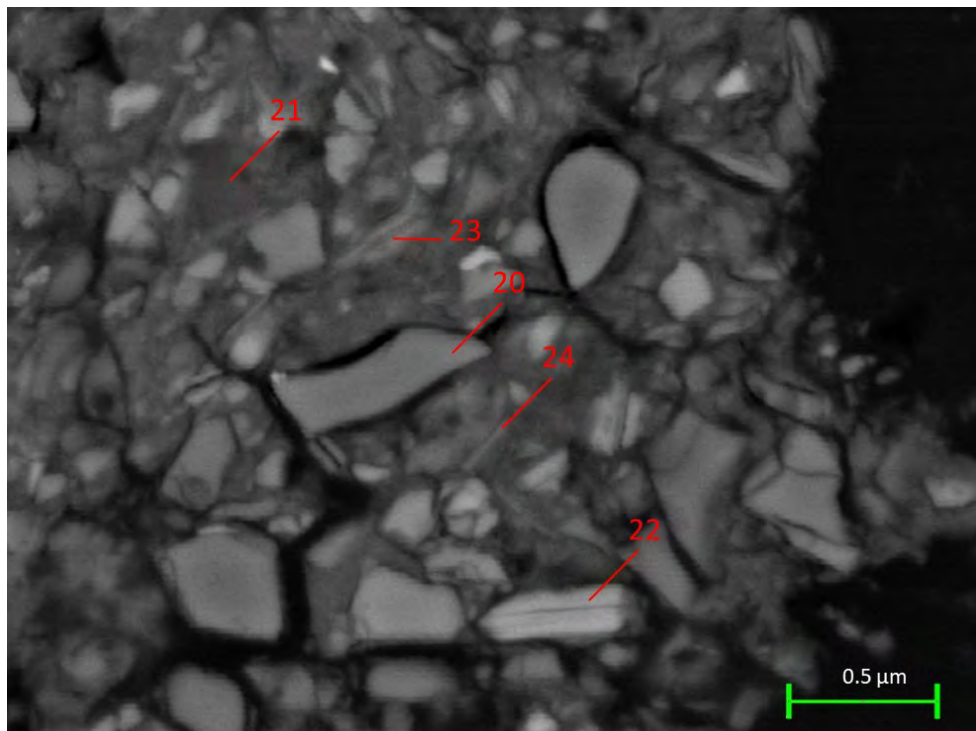


Figure 4.59: SEM image of representative soil kaolin developed from granite (20,21 – quartz; 22,23,24 – biotite).

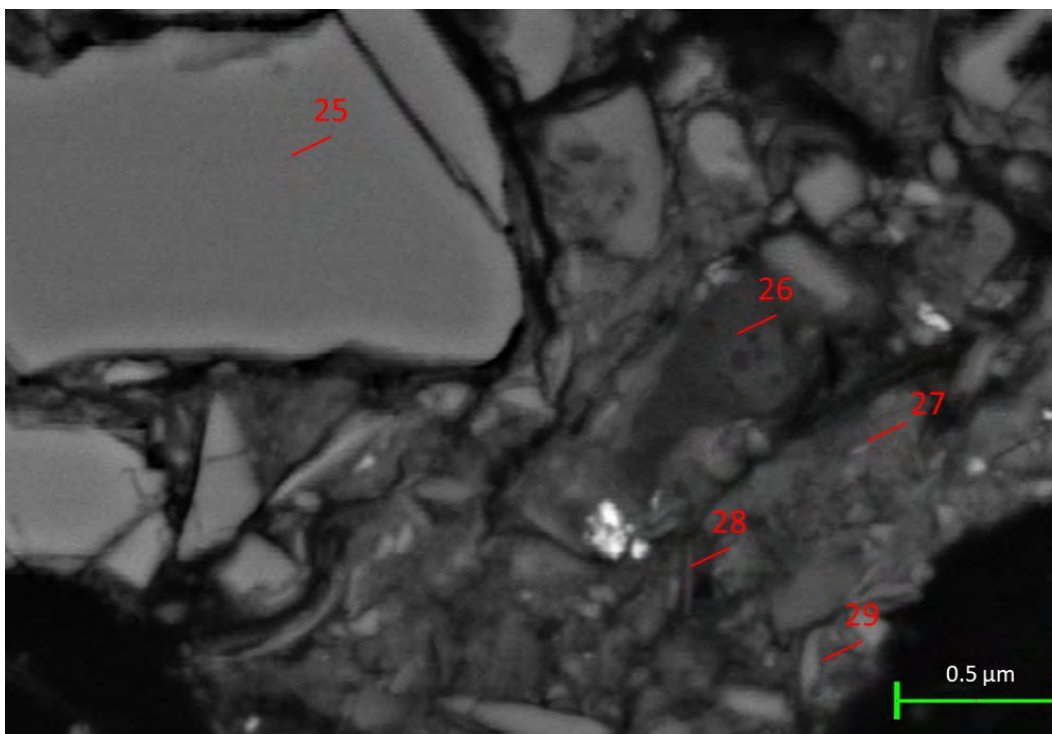


Figure 4.60: SEM image of representative soil kaolin developed from granite showing thin platy kaolinite particles (25 – plagioclase; 26 - quartz; 27,28,29 – kaolinite).

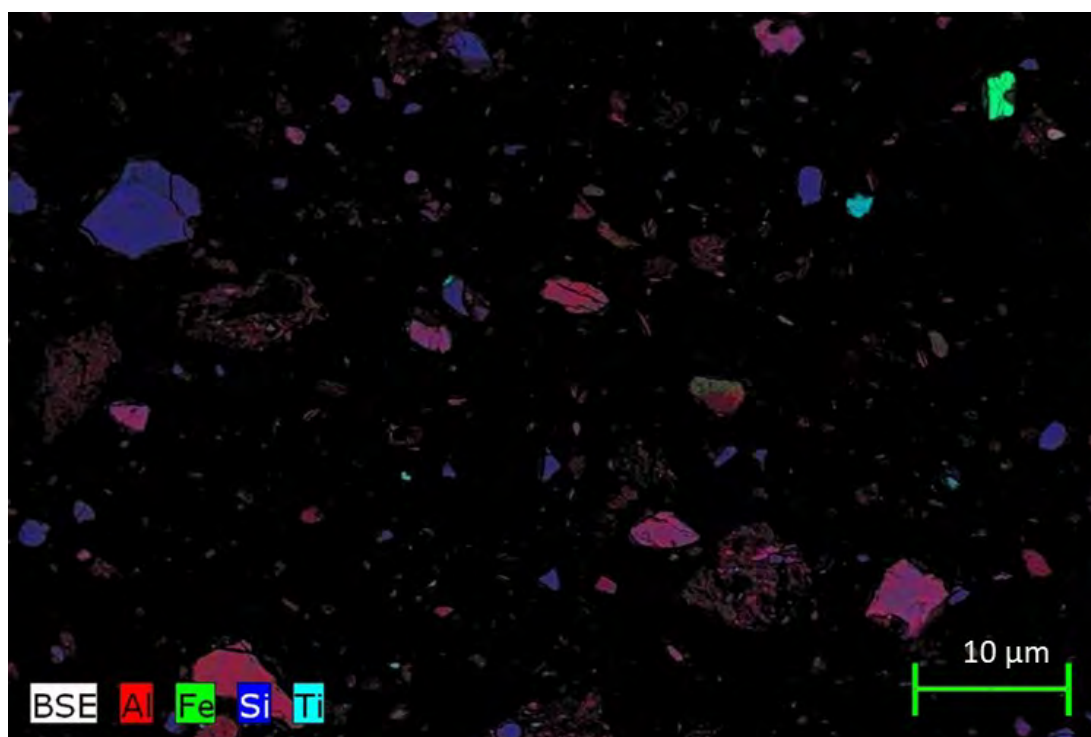


Figure 4.61: SEM elemental map of representative soil kaolin developed from arkosic sandstone.

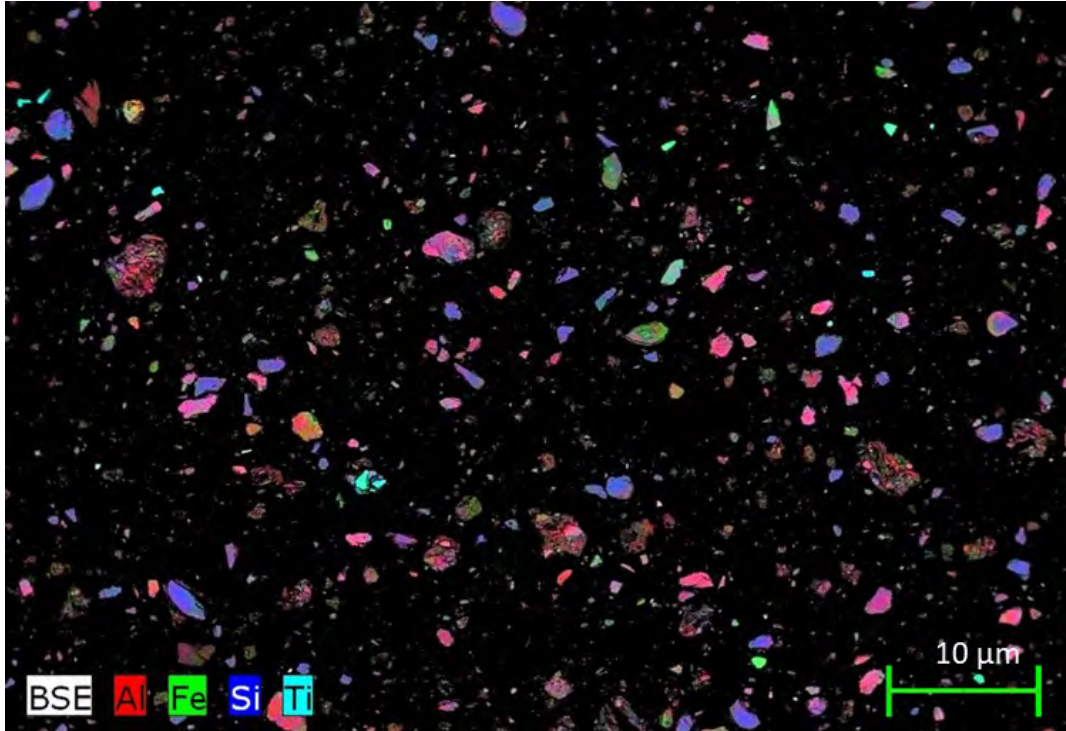


Figure 4.62: SEM elemental map of representative soil kaolin developed from arkosic sandstone.

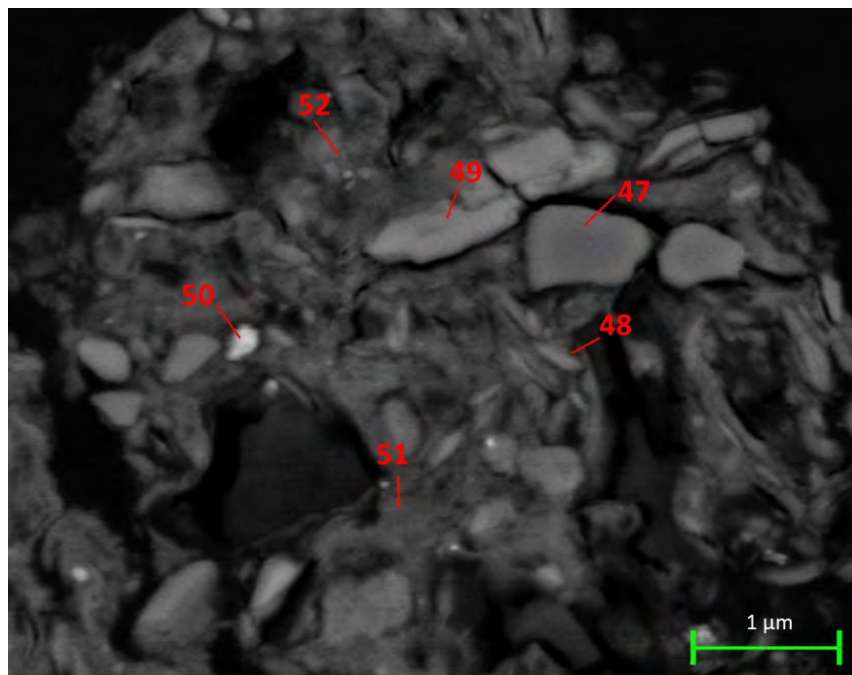


Figure 4.63: SEM image of representative soil kaolin developed from arkosic sandstone (47,50,51 – biotite; 48 – microcline, 49 – rutile; 52 – pyroxene/olivine).

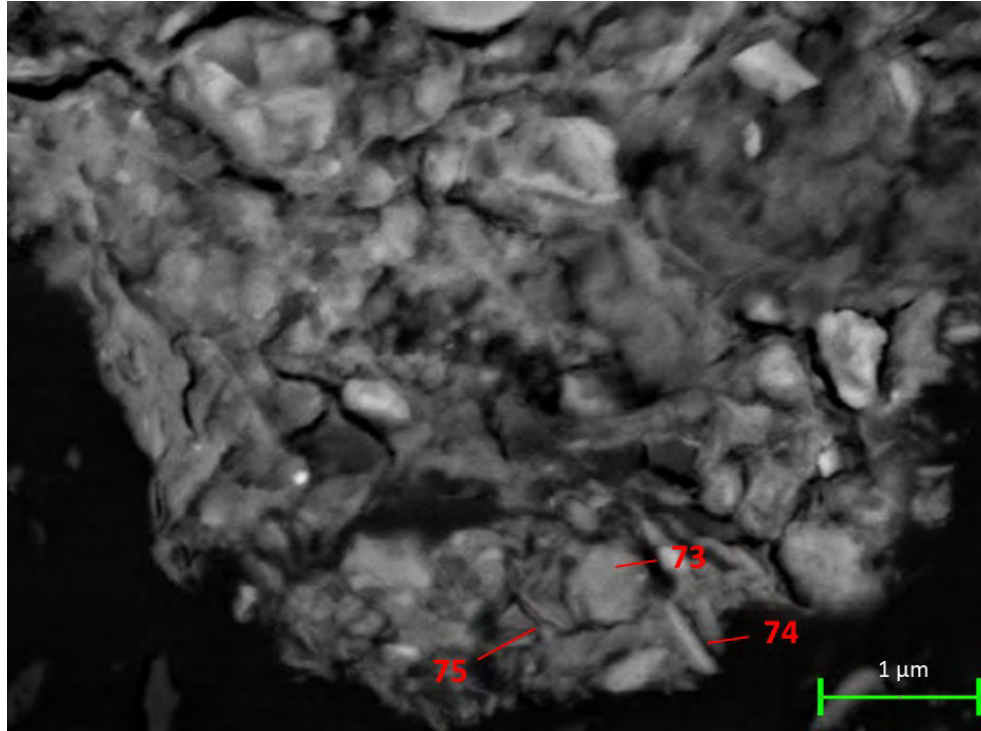


Figure 4.64: SEM image of representative soil kaolin developed from arkosic sandstone showing thin platy kaolinite (73 – biotite; 74 – kaolinite, 75 – ilmenite).

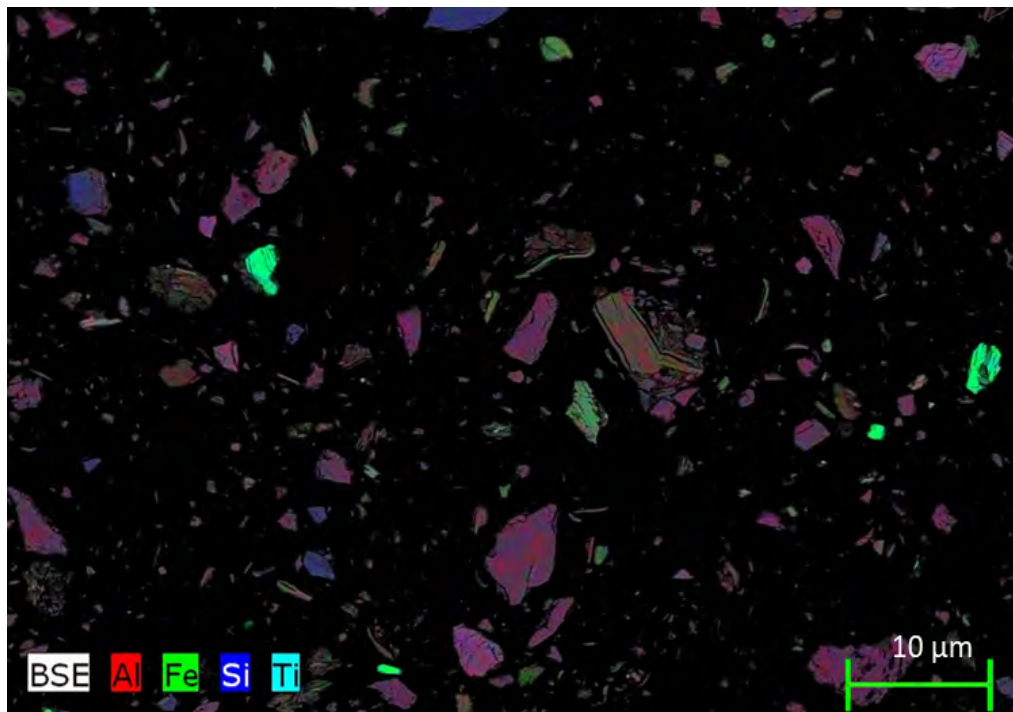


Figure 4.65: SEM elemental map of representative soil kaolin developed from gneiss.

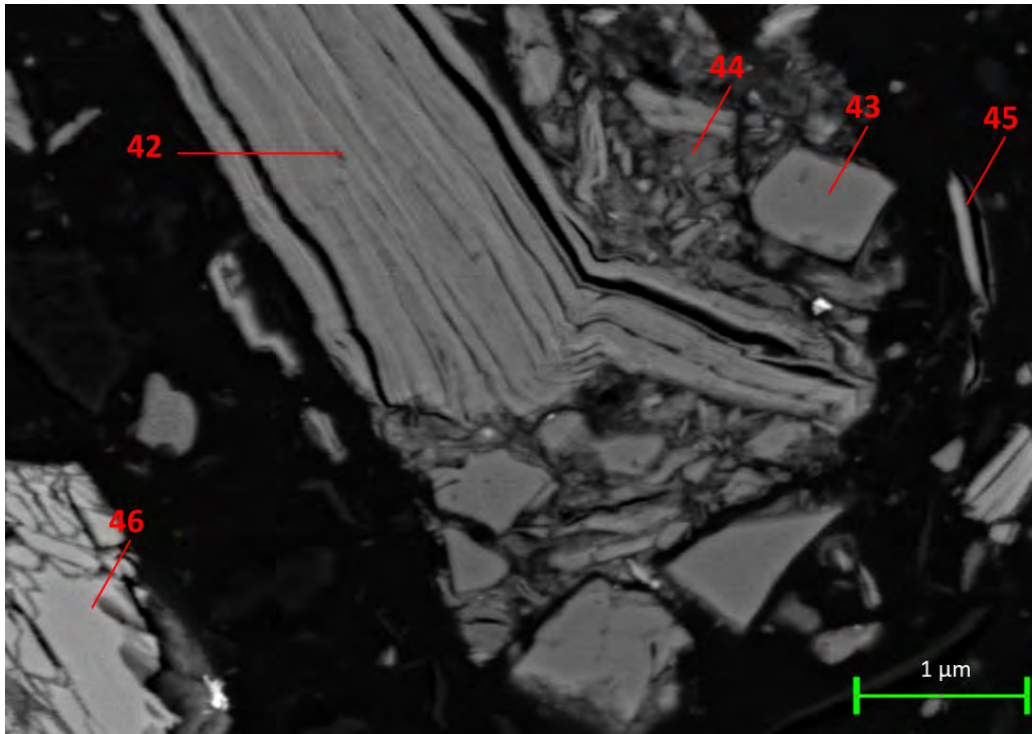


Figure 4.66: SEM image of representative soil kaolin developed from gneiss showing thin platy kaolinite particles (42 – plagioclase; 43 – pyroxene/olivine; 44 - kaolinite, 45 – biotite; 46 - quartz).

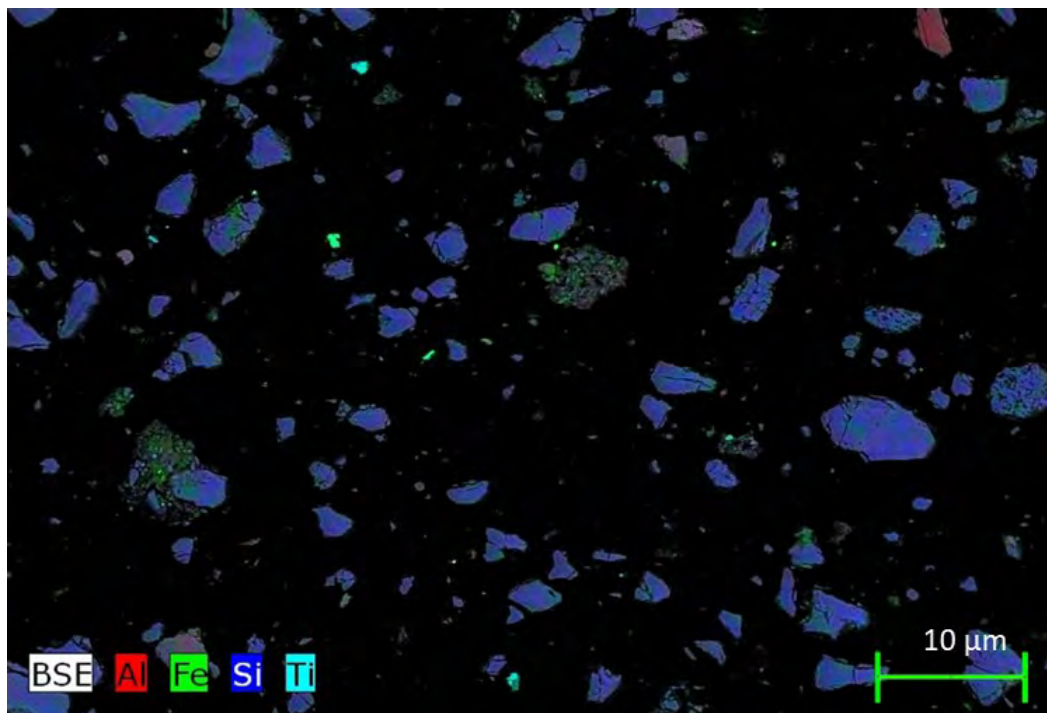


Figure 4.67: SEM elemental map of representative soil kaolin developed from quartzite.

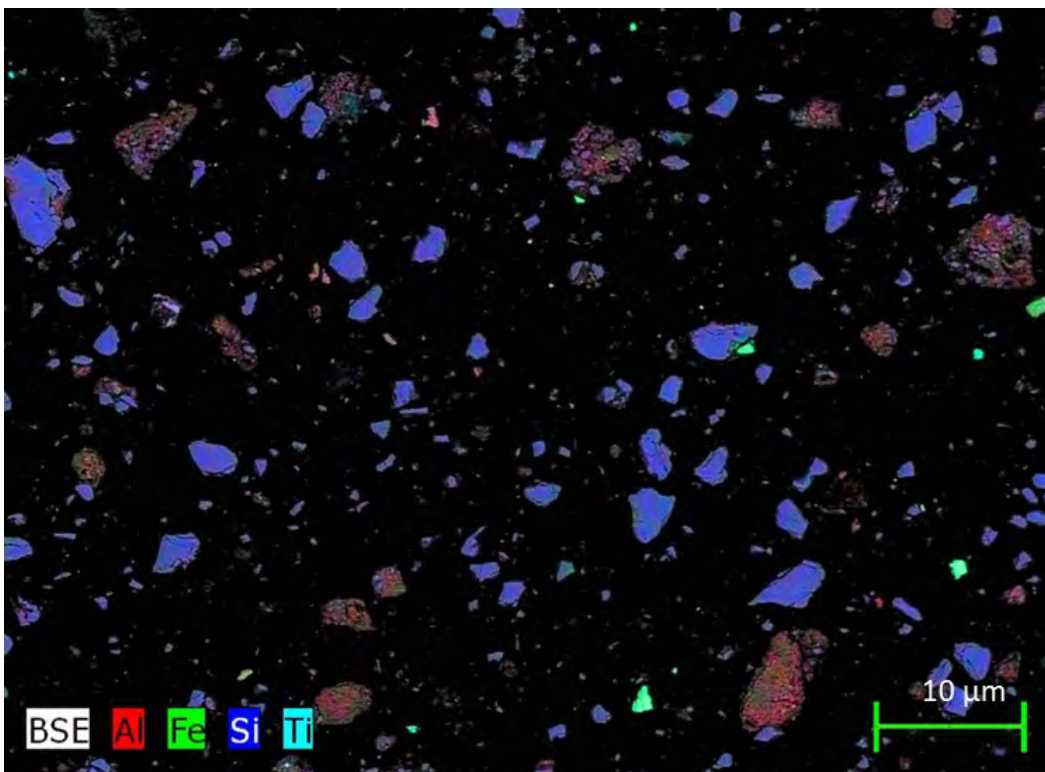


Figure 4.68: SEM elemental map of representative soil kaolin developed from quartzite.

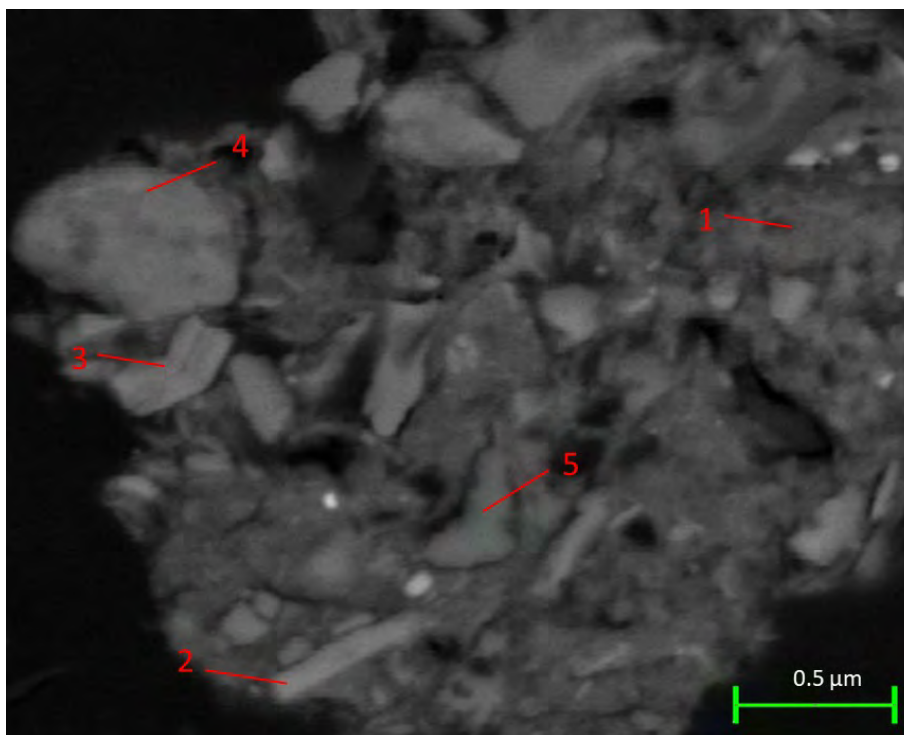


Figure 4.69: SEM image of representative soil kaolin developed from quartzite showing thin platy kaolinite particles (1 – kaolinite; 2,3,4 – biotite; 5 - quartz).

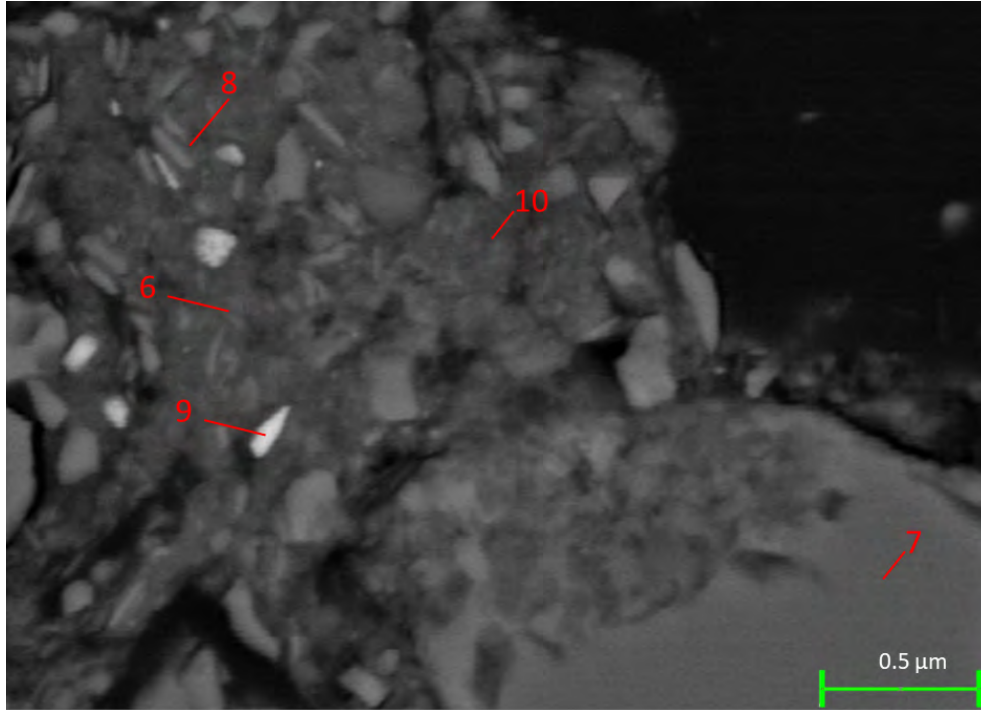


Figure 4.70: SEM image of representative soil kaolin developed from quartzite showing thin platy kaolinite particles (6,10 – kaolinite; 7 – quartz; 8 – biotite; 9 - ilmenite).

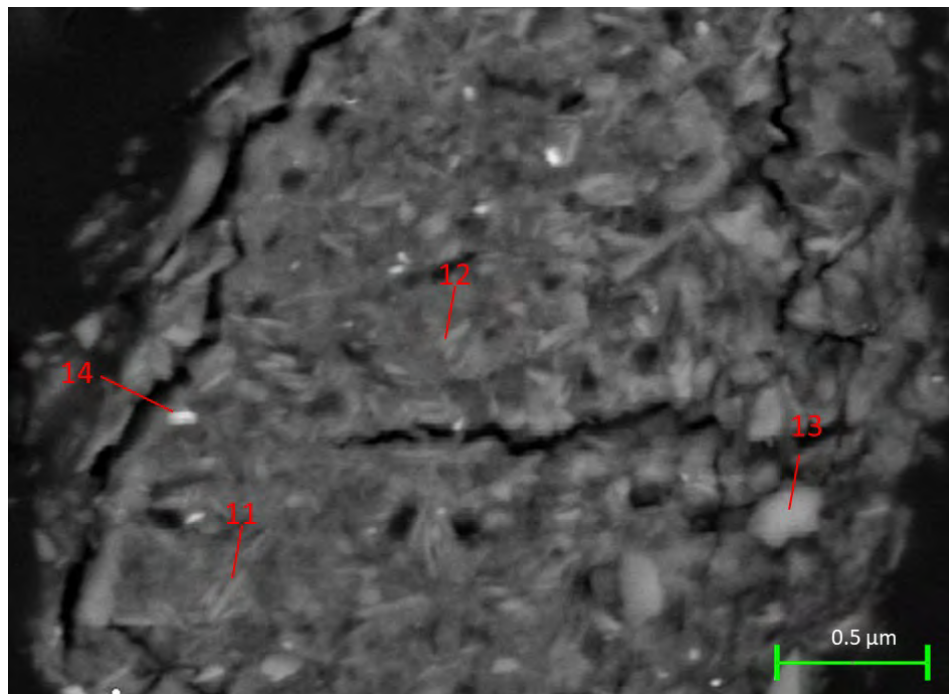


Figure 4.71: SEM image of representative soil kaolin developed from quartzite showing thin platy kaolinite particles (11,12 – kaolinite; 13 – biotite; 14 - ilmenite).

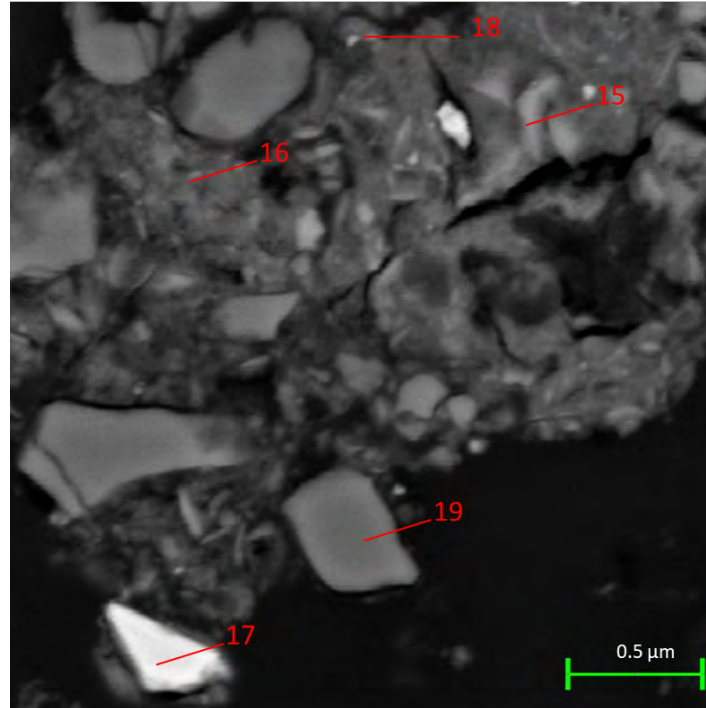


Figure 4.72: SEM image of representative soil kaolin developed from quartzite showing thin platy kaolinite particles (15 – quartz; 16 - kaolinite; 17 – ilmenite; 18 - biotite; 19 - microcline).

4.2.4 Fourier Transform Infrared Spectroscopy

The Infrared (IR) spectra for the soil kaolins are presented in Figures 4.73 – 4.80. The summary of the assignment of the adsorption bands in measured IR are presented in Appendix 4.1. The 3695, 3670, 3650, and 3620 cm^{-1} hydroxyls stretching region unique to kaolin minerals (Vaculikova *et al.*, 2011) were absent in the soil kaolins developed from basalt (except for S2 20-50 cm with 3692 and 3620 cm^{-1} , and S3 20-50 cm with 3692 and 3652 cm^{-1}), gneiss, and quartzite (control).

However, soil kaolins developed from granite (except for MAT1 20-50 cm, MAT2 20-50 cm, and MAT3 20-50 cm) and arkosic sandstone (except for SA2 20-50 cm, SA3 0-20 cm, and SA3 20-50 cm) had the four distinguishable bands present (Figures 4.73, 4.75, and 4.77).

Table 4.11: Elements in percentage present in the studied Soil kaolins obtained by SEM/EDS.

Lithology	Point Spectrum	O	Na	Mg	Al	Si	S	K	Ca	Ti	Cr	Mn	Fe	Ni	Zr	Total	Possible Mineral
Quartzite (Control)	1	49.6	0.0	0.0	19.8	27.5	0.0	3.1	0.0	0.0	0.0	0.0	0.0	0.0	0.0	100.0	Kaolinite
	2	45.2	0.0	1.3	16.8	23.0	0.0	9.5	0.0	0.0	0.0	0.0	4.2	0.0	0.0	100.0	Biotite
	3	44.3	0.0	1.2	15.8	22.6	0.0	10.7	0.0	0.0	0.0	0.0	5.4	0.0	0.0	100.0	Biotite
	4	46.3	0.0	0.0	18.9	21.1	0.0	4.2	0.0	4.9	0.0	0.0	4.5	0.0	0.0	100.0	Biotite
	5	52.9	0.0	0.0	3.4	43.8	0.0	0.0	0.0	0.0	0.0	0.0	0.0	0.0	0.0	100.0	Quartz
	6	49.2	0.0	0.0	34.9	15.9	0.0	0.0	0.0	0.0	0.0	0.0	0.0	0.0	0.0	100.0	Kaolinite
	7	53.3	0.0	0.0	0.0	46.7	0.0	0.0	0.0	0.0	0.0	0.0	0.0	0.0	0.0	100.0	Quartz
	8	45.9	0.0	1.3	18.9	21.5	0.0	6.1	0.0	1.9	0.0	0.0	4.4	0.0	0.0	100.0	Biotite
	9	35.2	0.0	0.0	3.3	3.6	0.0	0.0	0.0	30.4	0.0	0.0	27.5	0.0	0.0	100.0	Ilmenite
	10	46.7	0.0	0.0	20.5	22.4	0.0	3.0	0.0	0.7	0.0	0.0	6.6	0.0	0.0	100.0	Kaolinite
	11	48.9	0.0	0.0	15.0	29.9	0.0	2.5	0.0	0.0	0.0	0.0	3.7	0.0	0.0	100.0	Kaolinite
	12	47.1	0.0	0.0	19.7	24.0	0.0	5.2	0.0	0.0	0.0	0.0	3.9	0.0	0.0	100.0	Kaolinite
	13	46.1	0.0	1.1	19.1	22.0	0.0	1.2	0.0	0.0	0.0	0.0	10.5	0.0	0.0	100.0	Biotite
	14	42.7	0.0	0.0	11.9	12.9	0.0	1.6	0.0	21.4	0.0	0.0	9.6	0.0	0.0	100.0	Ilmenite
	15	53.3	0.0	0.0	0.0	46.7	0.0	0.0	0.0	0.0	0.0	0.0	0.0	0.0	0.0	100.0	Quartz
	16	47.5	0.0	0.0	19.4	23.5	0.0	2.8	0.0	2.5	0.0	0.0	4.3	0.0	0.0	100.0	Kaolinite
	17	31.5	0.0	0.0	0.0	0.0	0.0	0.0	0.0	31.0	0.0	0.0	37.6	0.0	0.0	100.0	Ilmenite
	18	45.9	0.0	0.8	12.2	24.4	0.0	5.0	0.0	6.3	0.0	0.0	5.5	0.0	0.0	100.0	Biotite
	19	46.0	0.0	0.0	10.7	29.6	0.0	13.8	0.0	0.0	0.0	0.0	0.0	0.0	0.0	100.0	Microcline
Granite	20	53.1	0.0	0.0	1.0	45.8	0.0	0.0	0.0	0.0	0.0	0.0	0.0	0.0	0.0	100.0	Quartz
	21	52.2	0.0	0.0	4.3	42.2	0.0	1.3	0.0	0.0	0.0	0.0	0.0	0.0	0.0	100.0	Quartz
	22	40.0	0.0	2.6	8.5	18.7	0.0	7.5	0.0	3.7	0.0	0.0	19.0	0.0	0.0	100.0	Biotite
	23	46.6	0.0	1.3	18.3	23.5	0.0	3.3	0.0	0.0	0.0	0.0	7.1	0.0	0.0	100.0	Biotite
	24	46.5	0.7	4.7	17.2	22.5	0.0	1.6	0.0	0.0	0.0	0.0	6.8	0.0	0.0	100.0	Biotite
	25	48.0	5.6	0.0	14.2	27.8	0.0	0.0	4.4	0.0	0.0	0.0	0.0	0.0	0.0	100.0	Plagioclase
	26	53.0	0.0	0.0	1.9	45.0	0.0	0.0	0.0	0.0	0.0	0.0	0.0	0.0	0.0	100.0	Quartz
	27	48.8	0.0	0.0	16.3	28.6	0.0	1.4	0.0	0.0	0.0	0.0	4.9	0.0	0.0	100.0	Kaolinite
	28	50.1	0.0	0.0	11.1	34.2	0.0	1.4	0.0	0.0	0.0	0.0	3.2	0.0	0.0	100.0	Kaolinite

Table 4.11 continued.

Lithology	Point Spectrum	O	Na	Mg	Al	Si	S	K	Ca	Ti	Cr	Mn	Fe	Ni	Zr	Total	Possible Mineral	
	29	49.2	0.0	0.0	20.6	26.2	0.0	0.9	0.0	0.0	0.0	0.0	3.0	0.0	0.0	100.0	Kaolinite	
Gneiss	30	40.9	0.0	0.0	18.9	22.9	0.0	11.8	0.0	0.0	0.0	0.0	5.6	0.0	0.0	100.0	Biotite	
	31	41.6	7.8	0.0	14.9	32.8	0.0	0.0	2.8	0.0	0.0	0.0	0.0	0.0	0.0	100.0	Plagioclase	
	32	40.2	0.0	0.0	11.5	31.2	0.0	17.1	0.0	0.0	0.0	0.0	0.0	0.0	0.0	100.0	Microcline	
	33	38.0	0.0	0.0	19.6	32.2	0.0	0.0	0.0	0.0	0.0	0.0	10.2	0.0	0.0	100.0	Pyroxene/Olivine	
	34	46.5	0.0	0.0	20.1	23.7	0.0	0.0	0.0	0.0	0.0	0.0	9.7	0.0	0.0	100.0	Pyroxene/Olivine	
	35	8.1	0.0	0.0	2.5	4.2	0.0	0.0	0.0	0.0	0.0	15.0	2.1	58.1	10.2	0.0	100.2	Hematite/Chromite
	36	47.0	0.0	6.5	10.5	24.5	0.0	0.0	4.6	0.0	0.0	0.0	6.8	0.0	0.0	100.0	Diopside	
	37	25.0	0.0	0.0	0.0	0.0	0.0	0.0	0.0	35.4	0.0	3.1	36.4	0.0	0.0	100.0	Ilmenite	
	38	40.4	0.0	0.0	0.0	0.0	0.0	0.0	0.0	29.0	0.0	1.1	29.5	0.0	0.0	100.0	Ilmenite	
	39	41.9	6.9	0.0	14.9	33.0	0.0	0.0	3.4	0.0	0.0	0.0	0.0	0.0	0.0	100.0	Plagioclase	
	40	39.5	0.0	0.0	0.0	60.5	0.0	0.0	0.0	0.0	0.0	0.0	0.0	0.0	0.0	100.0	Quartz	
	41	44.5	0.0	0.0	18.6	24.2	0.0	0.0	0.0	0.0	0.0	0.0	12.7	0.0	0.0	100.0	Pyroxene/Olivine	
	42	42.1	7.4	0.0	14.8	32.7	0.0	0.0	3.0	0.0	0.0	0.0	0.0	0.0	0.0	100.0	Plagioclase	
	43	41.7	0.0	0.0	20.0	25.3	0.0	0.0	0.0	0.0	0.0	0.0	13.0	0.0	0.0	100.0	Pyroxene/Olivine	
	44	39.1	0.0	0.0	25.3	30.3	0.0	2.1	0.0	0.0	0.0	0.0	3.1	0.0	0.0	100.0	Kaolinite	
	45	34.5	1.9	5.3	8.4	19.2	0.0	1.3	9.4	0.0	0.0	0.0	20.0	0.0	0.0	100.0	Biotite	
46	48.0	0.0	0.0	0.0	52.0	0.0	0.0	0.0	0.0	0.0	0.0	0.0	0.0	0.0	100.0	Quartz		
Ark. Sst.	47	42.2	0.0	6.5	12.4	22.0	0.0	2.9	0.0	0.0	0.0	0.0	14.1	0.0	0.0	100.0	Biotite	
	48	43.7	0.0	0.0	10.7	28.8	0.0	16.7	0.0	0.0	0.0	0.0	0.0	0.0	0.0	100.0	Microcline	
	49	42.4	0.0	0.0	3.0	4.4	0.0	0.0	0.0	48.0	0.0	0.0	2.1	0.0	0.0	100.0	Rutile	
	50	40.0	0.0	0.0	16.6	25.9	0.0	7.9	0.0	0.0	0.0	0.0	9.6	0.0	0.0	100.0	Biotite	
	51	38.8	0.0	0.0	17.5	28.9	0.0	7.2	0.0	0.0	0.0	0.0	7.5	0.0	0.0	100.0	Biotite	
	52	46.1	0.0	0.0	0.0	50.9	0.0	0.0	0.0	0.0	0.0	0.0	3.1	0.0	0.0	100.0	Pyroxene/Olivine	
Basalt	53	32.6	0.0	0.0	21.3	16.9	0.0	0.0	0.0	0.0	0.0	0.0	29.2	0.0	0.0	100.0	Pyroxene/Olivine	
	54	33.3	0.0	0.0	6.1	2.2	0.0	0.0	0.0	1.6	0.0	0.0	56.7	0.0	0.0	100.0	Hematite	

Table 4.11 continued.

Lithology	Point Spectrum	O	Na	Mg	Al	Si	S	K	Ca	Ti	Cr	Mn	Fe	Ni	Zr	Total	Possible Mineral
	55	39.6	0.0	0.0	20.4	17.0	0.0	0.0	0.0	0.0	0.0	0.0	23.0	0.0	0.0	100.0	Hematite
	56	47.4	0.0	0.0	10.9	26.2	0.0	15.5	0.0	0.0	0.0	0.0	0.0	0.0	0.0	100.0	Microcline
	57	46.4	0.0	0.0	21.6	21.1	0.0	0.0	0.0	0.0	0.0	0.0	10.8	0.0	0.0	100.0	Pyroxene/Olivine
	58	48.6	0.0	0.0	22.6	23.8	0.0	0.0	0.0	0.0	0.0	0.0	4.9	0.0	0.0	100.0	Kaolinite
	59	32.6	1.1	0.0	10.8	6.3	0.7	0.0	0.0	1.5	0.0	0.0	47.0	0.0	0.0	100.0	Hematite
	60	41.7	0.0	0.0	17.3	17.1	0.0	0.0	0.0	0.0	0.0	0.0	23.8	0.0	0.0	100.0	Hematite
	61	45.1	0.0	0.0	19.5	20.7	0.0	0.0	0.0	0.0	0.0	0.0	14.7	0.0	0.0	100.0	Pyroxene/Olivine
	62	44.6	0.0	0.0	18.5	20.1	0.0	0.0	0.0	1.3	0.0	0.0	15.5	0.0	0.0	100.0	Pyroxene/Olivine
	63	48.6	0.0	0.0	22.5	23.7	0.0	0.0	0.0	0.0	0.0	0.0	5.2	0.0	0.0	100.0	Kaolinite
	64	46.3	0.0	0.0	20.4	21.8	0.0	0.0	0.0	0.0	0.0	0.0	11.5	0.0	0.0	100.0	Pyroxene/Olivine
	65	44.2	0.0	0.0	18.8	19.8	0.0	0.0	0.0	0.0	0.0	0.0	17.3	0.0	0.0	100.0	Pyroxene/Olivine
	66	47.8	0.0	0.0	22.9	22.4	0.0	0.0	0.0	0.0	0.0	0.0	6.9	0.0	0.0	100.0	Kaolinite
	67	34.7	0.0	0.0	11.5	9.0	0.3	0.0	0.0	2.7	0.0	0.0	41.8	0.0	0.0	100.0	Hematite
	68	25.9	0.0	0.0	4.8	2.0	0.0	0.0	0.0	0.0	0.0	0.0	67.3	0.0	0.0	100.0	Hematite
	69	50.0	0.0	0.0	5.2	37.6	0.0	0.0	0.0	1.1	0.0	0.0	6.1	0.0	0.0	100.0	Pyroxene/Olivine
	70	43.5	0.0	0.0	17.7	19.5	0.0	0.0	0.0	0.0	0.0	0.0	19.4	0.0	0.0	100.0	Pyroxene/Olivine
	71	47.2	0.0	0.0	19.6	24.4	0.0	5.8	0.0	0.0	0.0	0.0	3.0	0.0	0.0	100.0	Kaolinite
	72	44.0	0.0	0.0	13.6	23.6	0.0	4.0	0.0	0.0	0.0	0.0	14.9	0.0	0.0	100.0	Biotite
Ark. Sst.	73	45.9	0.0	0.0	16.6	24.4	0.0	5.3	0.0	0.0	0.0	0.0	7.9	0.0	0.0	100.0	Biotite
	74	45.6	0.0	0.0	17.6	29.2	0.0	4.9	0.0	0.0	0.0	0.0	2.6	0.0	0.0	100.0	Kaolinite
	75	31.8	0.0	0.0	0.0	0.0	0.0	0.0	0.0	31.7	0.0	0.0	36.5	0.0	0.5	100.5	Ilmenite

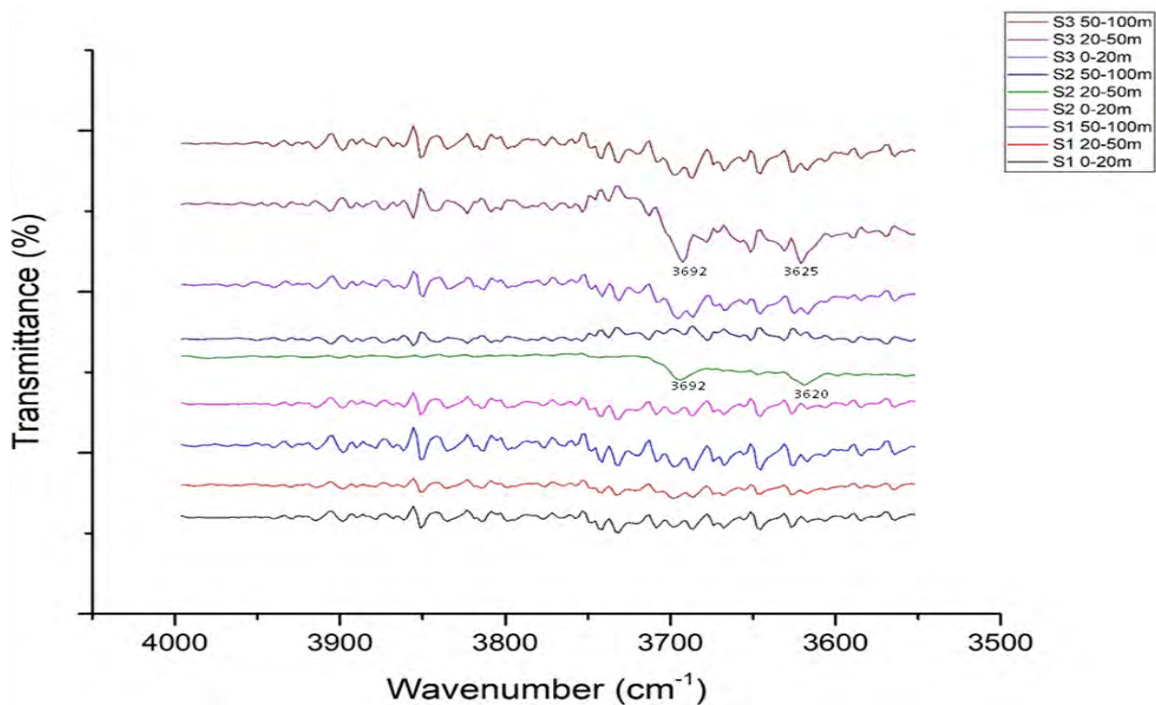


Figure 4.73: The IR spectra of soil kaolins developed from basalt between 4000 to 3500 cm^{-1} .

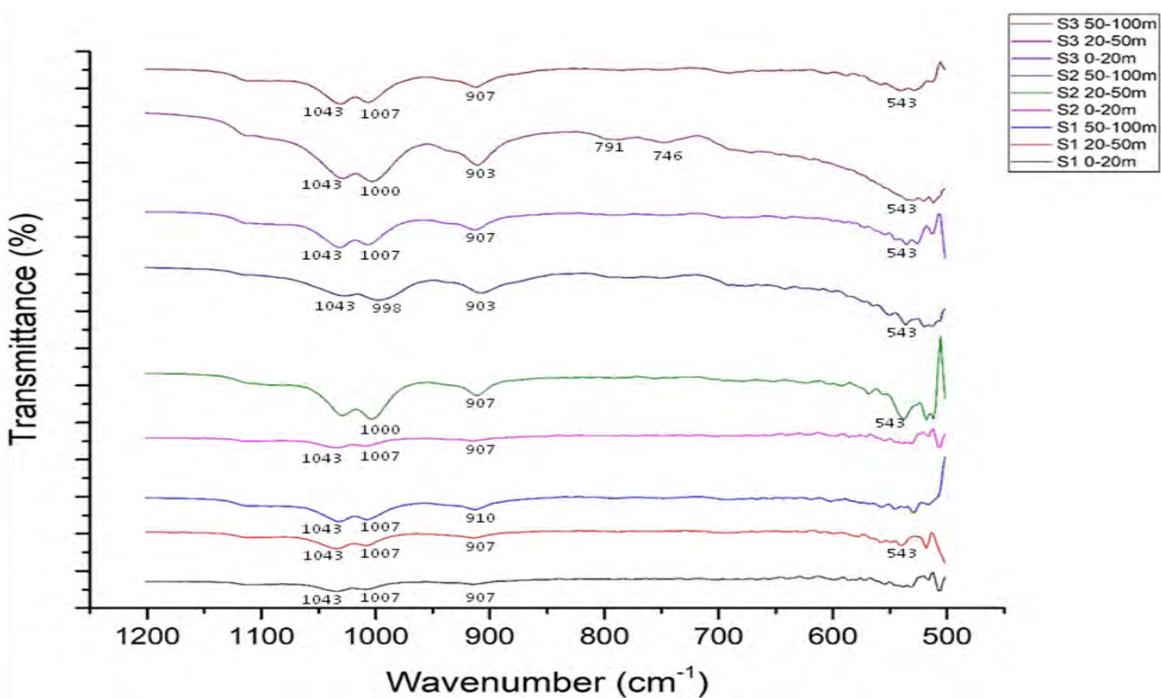


Figure 4.74: The IR spectra of soil kaolins developed from basalt between 1200 to 500 cm^{-1} .

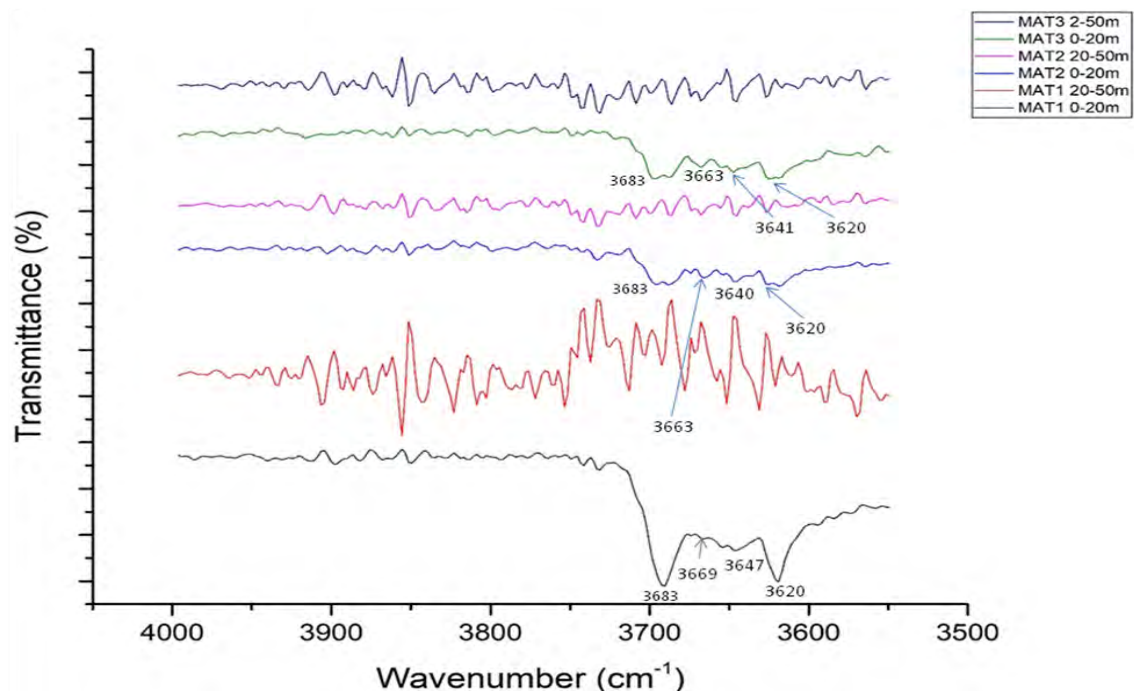


Figure 4.75: The IR spectra of soil kaolins developed from granite between 4000 to 3500 cm^{-1} .

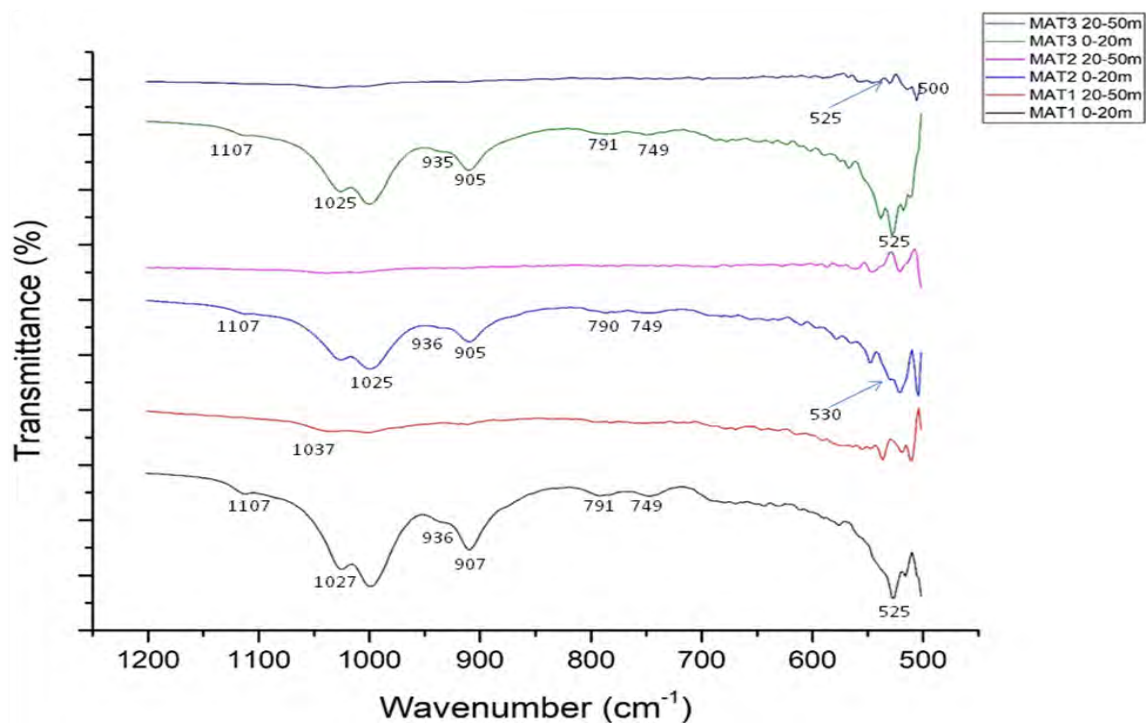


Figure 4.76: The IR spectra of soil kaolins developed from granite between 1200 to 500 cm^{-1} .

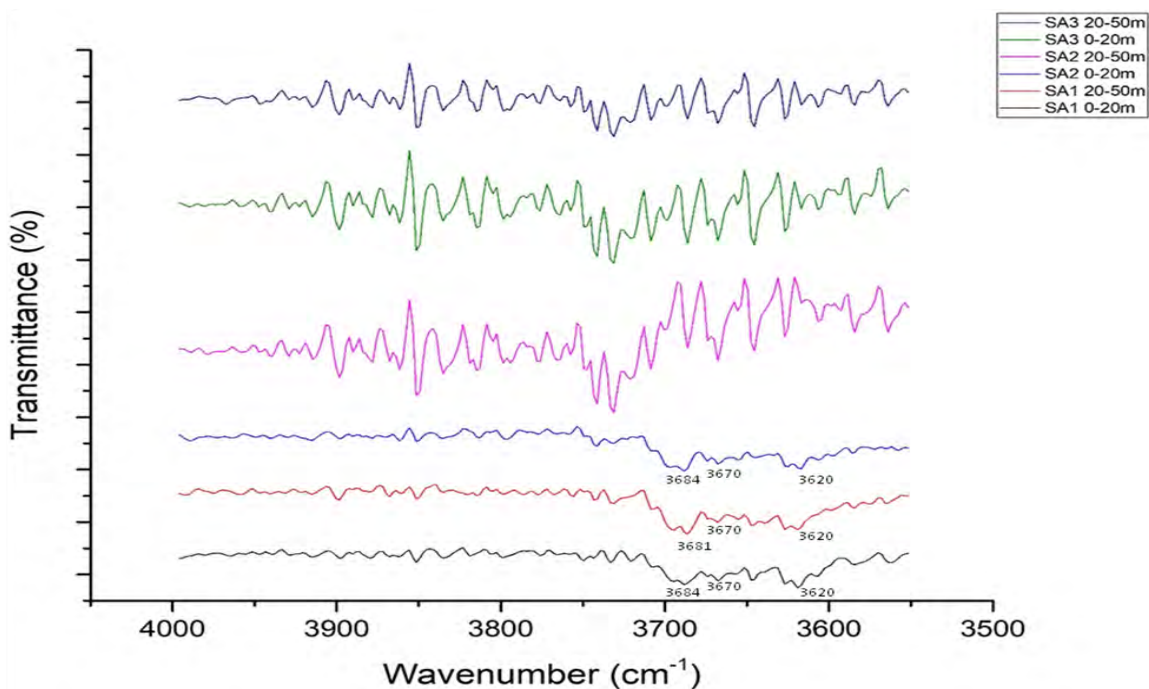


Figure 4.77: The IR spectra of soil kaolins developed from arkosic sandstone between 4000 to 3500 cm^{-1} .

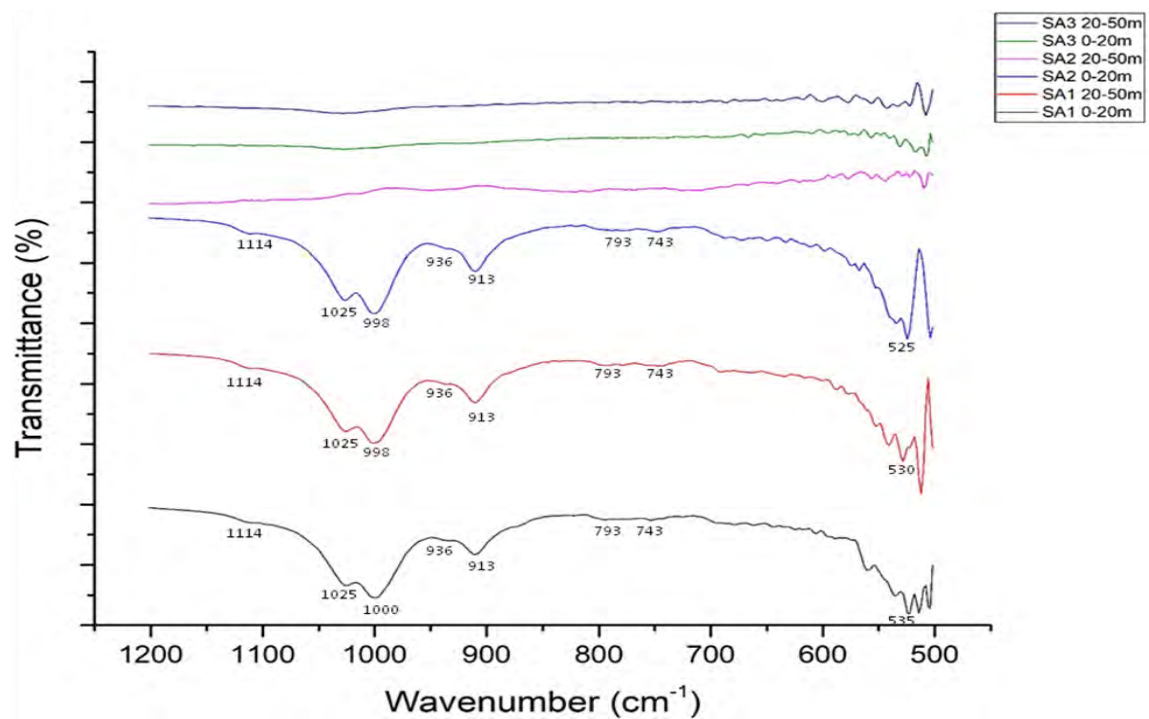


Figure 4.78: The IR spectra of soil kaolins developed from arkosic sandstone between 1200 to 500 cm^{-1} .

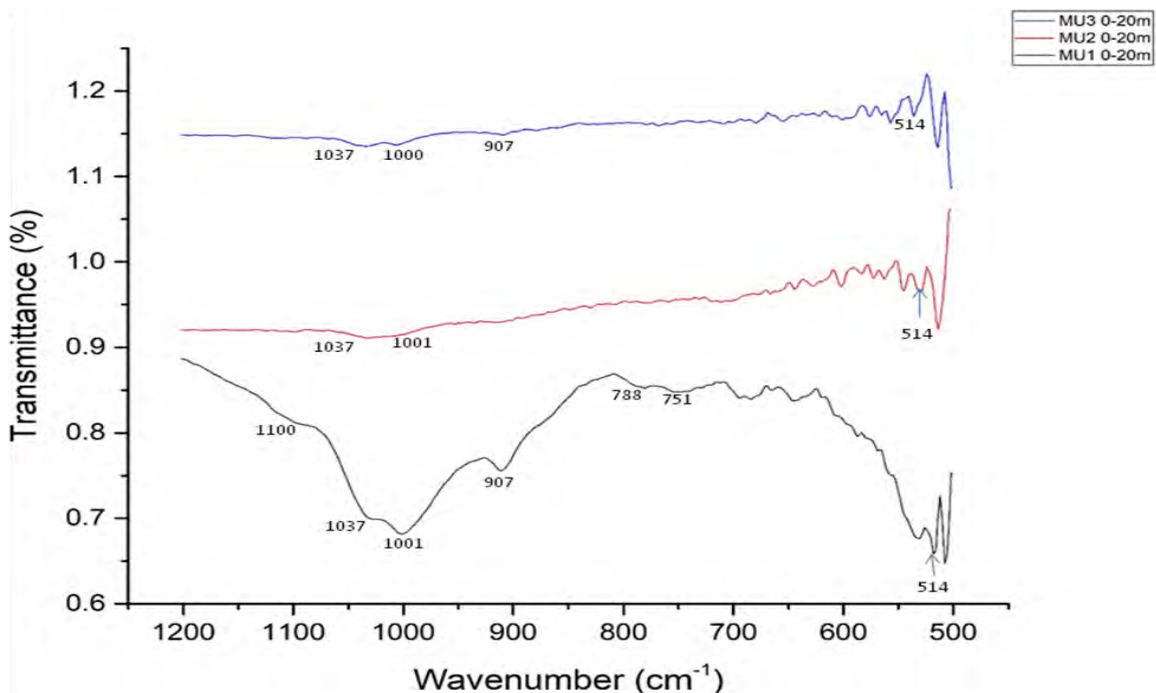


Figure 4.79: The IR spectra of soil kaolins developed from Gneiss between 1200 to 500 cm^{-1} .

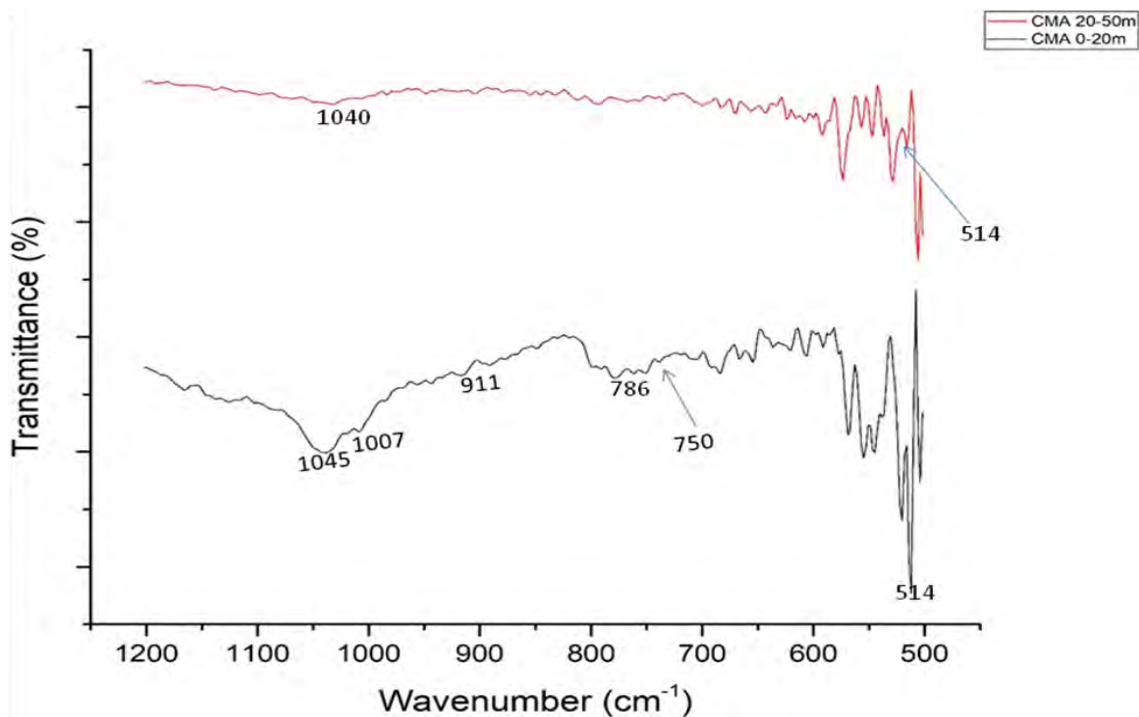


Figure 4.80: The IR spectra of soil kaolins developed from Quartzite between 1200 to 500 cm^{-1} .

Soil kaolins developed from basalt had the Si-O stretching bands at 1114, 1043, and 1007 cm^{-1} whereas, for soil kaolins developed from granite the Si-O stretching bands were identified at 1107, 1025 – 1037, and 1000 cm^{-1} (except for MAT1 20-50 cm, MAT2 20-50 cm, and MAT3 20-50 cm). Soil kaolins developed from arkosic sandstone had Si-O stretching within regions 1114, 1025, and 998-1000 cm^{-1} (except for SA2 20-50 cm, SA3 0-20 cm, and SA3 20-50 cm). Soil kaolins developed from gneiss and quartzite (control) had Si-O stretching within region 1037 -1045 and 1000 – 1007 cm^{-1} (except for CMA 20-50 cm) (Figures 4.74, 4.76, 4.77, and 4.80).

The OH deformation of inner-surface hydroxyl groups (935 – 937 cm^{-1}) was absent in all the soil kaolins developed from basalt, gneiss, and quartzite (control) whereas, OH deformation of inner hydroxyl groups (912 cm^{-1}) was present within 903 – 911 cm^{-1} bands. Soil kaolins developed from granite had OH deformation inner surface hydroxyl within region 935 – 936 cm^{-1} (except for MAT1 20-50 cm, MAT2 20-50 cm, and MAT3 20-50 cm). For soil kaolins developed from arkosic sandstone, they occurred within regions 936 and 913 cm^{-1} respectively (Figures 4.74, 4.76, 4.78, and 4.80).

The Si-O stretching and perpendicular bands (788 -798 cm^{-1} and 750 - 751 cm^{-1}) were identified in soil kaolins developed from granite (except for MAT1 20-50 cm, MAT2 20-50 cm, and MAT3 20-50 cm), arkosic sandstone (except for SA2 20-50 cm, SA3 0-20 cm, and SA3 20-50 cm), gneiss (except for MU2 0-20 cm and MU3 0-20 cm), and quartzite (control) (except for CMA 20-50 cm) within regions at 786 – 793 cm^{-1} and 743 – 751 cm^{-1} (Figures 4.74, 4.76, 4.78, and 4.80).

The Fe-O, Fe_2O_3 , Ti-O and Si-O-Al stretching were identified within regions 514 – 543 cm^{-1} and for soil kaolins developed from basalt (except for S1 0-20 cm, S1 50-100 cm, and S2 0-20 cm), granite (except for MAT1 20-50 cm, MAT2 20-50 cm, and MAT3 20-50 cm), arkosic sandstone (except for SA2 20-50 cm, SA3 0-20 cm, and SA3 20-50 cm), gneiss, and quartzite (control) (Figures 4.74, 4.76, 4.78, and 4.80).

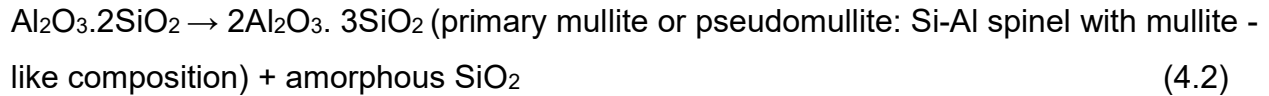
4.2.5 Thermogravimetric Analyses (TGA) and Differential Scanning Calorimetry (DSC)

Reactions accompanying the dehydroxylation and phase transformations of raw kaolin with increasing temperatures are presented in Equations 4.1 – 4.2 (Teklay *et al.*, 2014).

Between 450 – 700 °C: endothermic: dehydroxylation:



Between 900 – 1000 °C: exothermic: transformation into crystalline phases:



Dehydration occurs at temperature (T) < 100 °C due to the presence of free bound water (Teklay *et al.*, 2014) and pre-dehydroxylation at T between 200 and 450 °C (Ilic *et al.*, 2010). The TGA-DSC data and characteristic patterns for the studied soil kaolins are presented in Table 4.12 and Figures 4.81 – 4.96. In addition, exothermic reaction peak temperatures for mullite formation were identified between 867 – 958 °C for soil kaolins developed from basalt (except for S1 20-50 cm) but absent in other soil kaolins (except for MAT1 0-20 cm and SA3 0-20 cm). The reactions were accompanied with total weight losses ranging between 15.4 – 21.2 % for soil kaolins developed from basalt, 3.7 – 10.4 % for soil kaolins developed from granite, 5.1 - 9.8 % for soil kaolins developed from arkosic sandstone, gneiss, and quartzite (control) (Table 4.12).

Table 4.12: DTG/DSC/TGA Endothermic and Exothermic Peak Temperatures (with main reactions) and Total Weight Loss for the studied Soil kaolins.

Parent Rock	Sample ID	Endothermic Temperature Peaks			Exothermic Temperature Peaks ⁺	Total Weight Loss (%) [#]
		Dehydration* (T < 100 °C)	Pre-dehydroxylation* (200 - 400 °C)	Dehydroxylation* (450 - 700 °C)	Mullite Formation (900 - 1000 °C)	
Basalt	S1 0-20cm	83	250	457	867	16.2
	S1 20-50cm	83	249	467	-	21.2
	S1 50-100cm	99	256	475	958	16.2
	S2 0-20cm	99	252	467	859	17.5
	S2 20-50cm	100	275	467	870	18.1
	S2 50-100cm	83	259	475	944	15.4
Granite	MAT1 0-20cm	83	233	467	867	16.4
	MAT1 20-50cm	55	-	430	-	3.7
	MAT3 0-20cm	75	333	430	-	5.7
	MAT3 20-50cm	83	331	425	-	6.1
Ark. Sst.	SA1 0-20cm	75	336	-	-	5.1
	SA3 0-20cm	85	306	-	915	9.8
	SA3 20-50cm	80	298	-	-	9.5
Gneiss	MU1 0-20cm	60	250	440	-	6.3
Quartzite	CMA 0-20cm	85	300	425	-	6.1
	CMA 20-50cm	60	365	425	-	8.3

* From DTG curves, ⁺ From DSC curves, [#] From TGA curves, (-): No peak

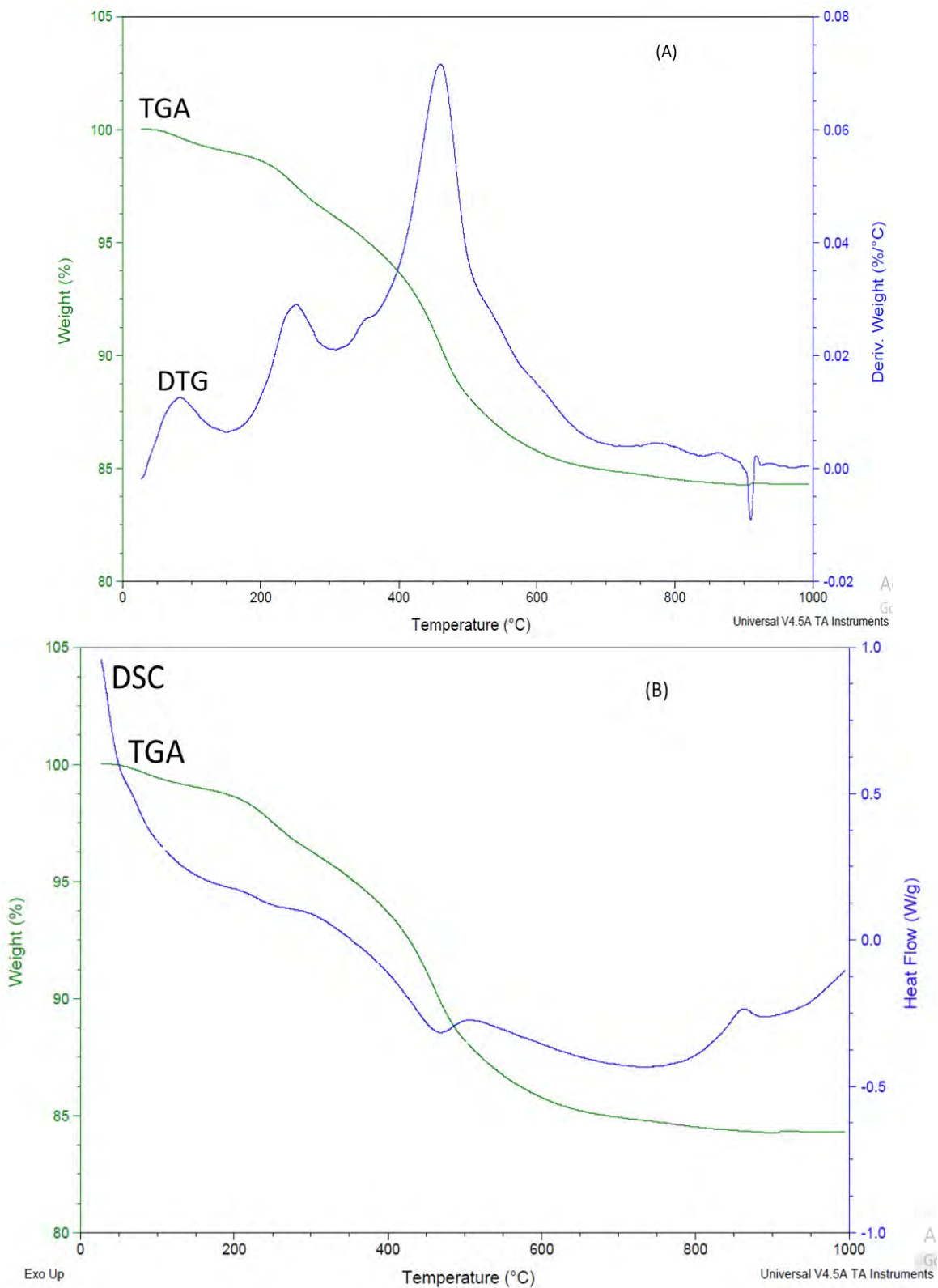


Figure 4.81: Thermal analyses of S1 0-20 cm showing: (a) TGA/DTG and (b) DSC/TGA curves.

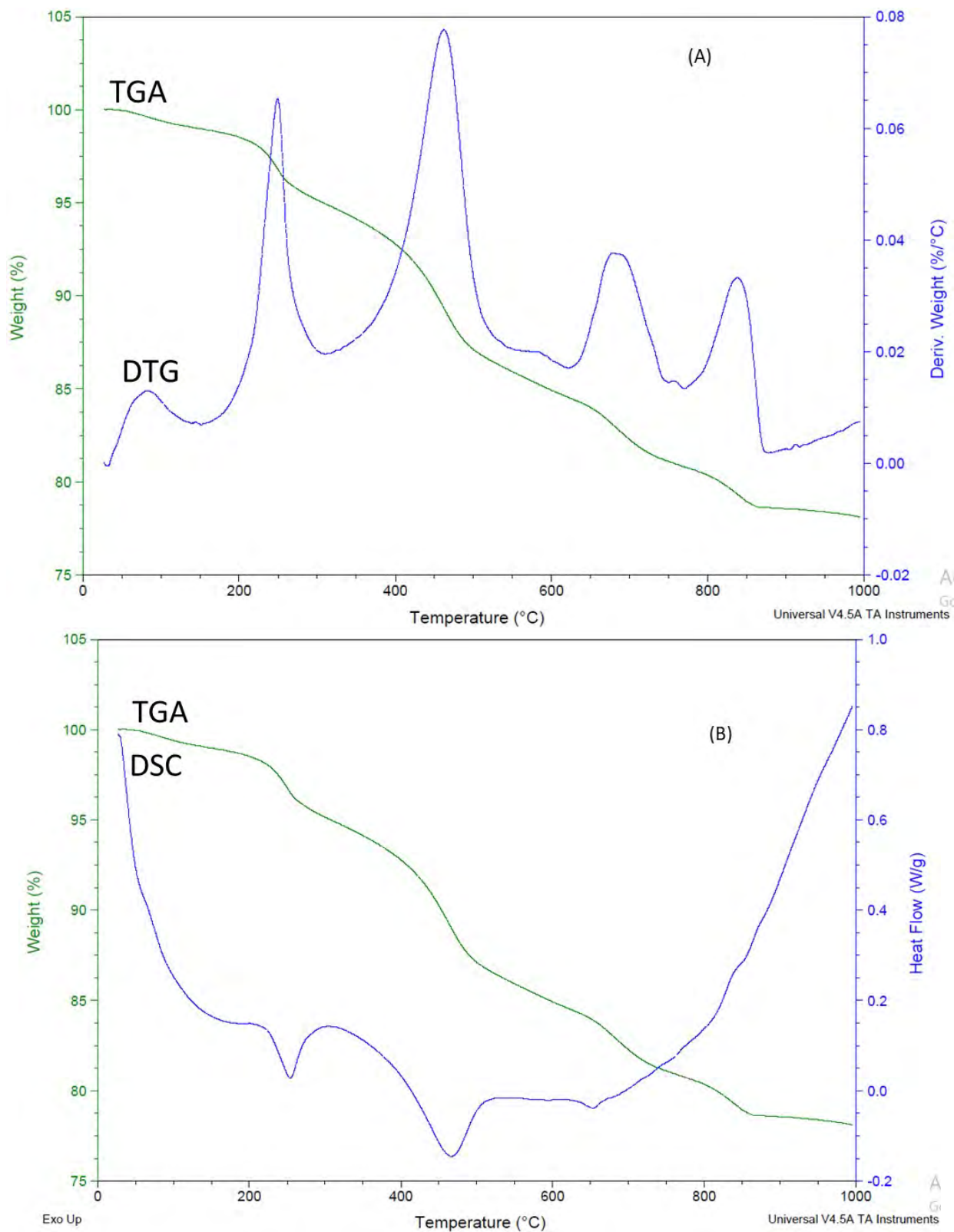


Figure 4.82: Thermal analyses of S1 20-50 cm showing: (a) TGA/DTG and (b) DSC/TGA curves.

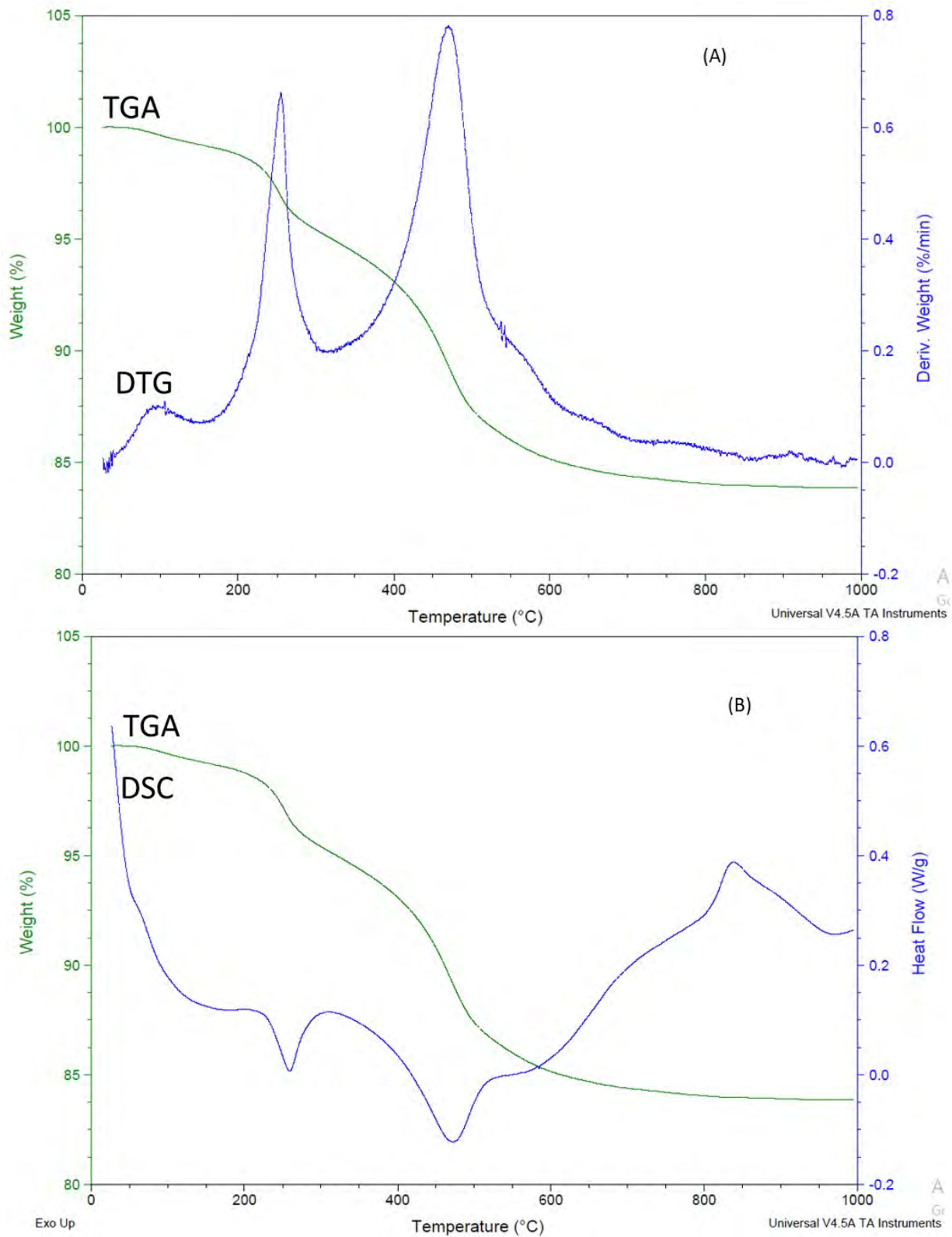


Figure 4.83: Thermal analyses of S1 50-100 cm showing: (a) TGA/DTG and (b) DSC/TGA curves.

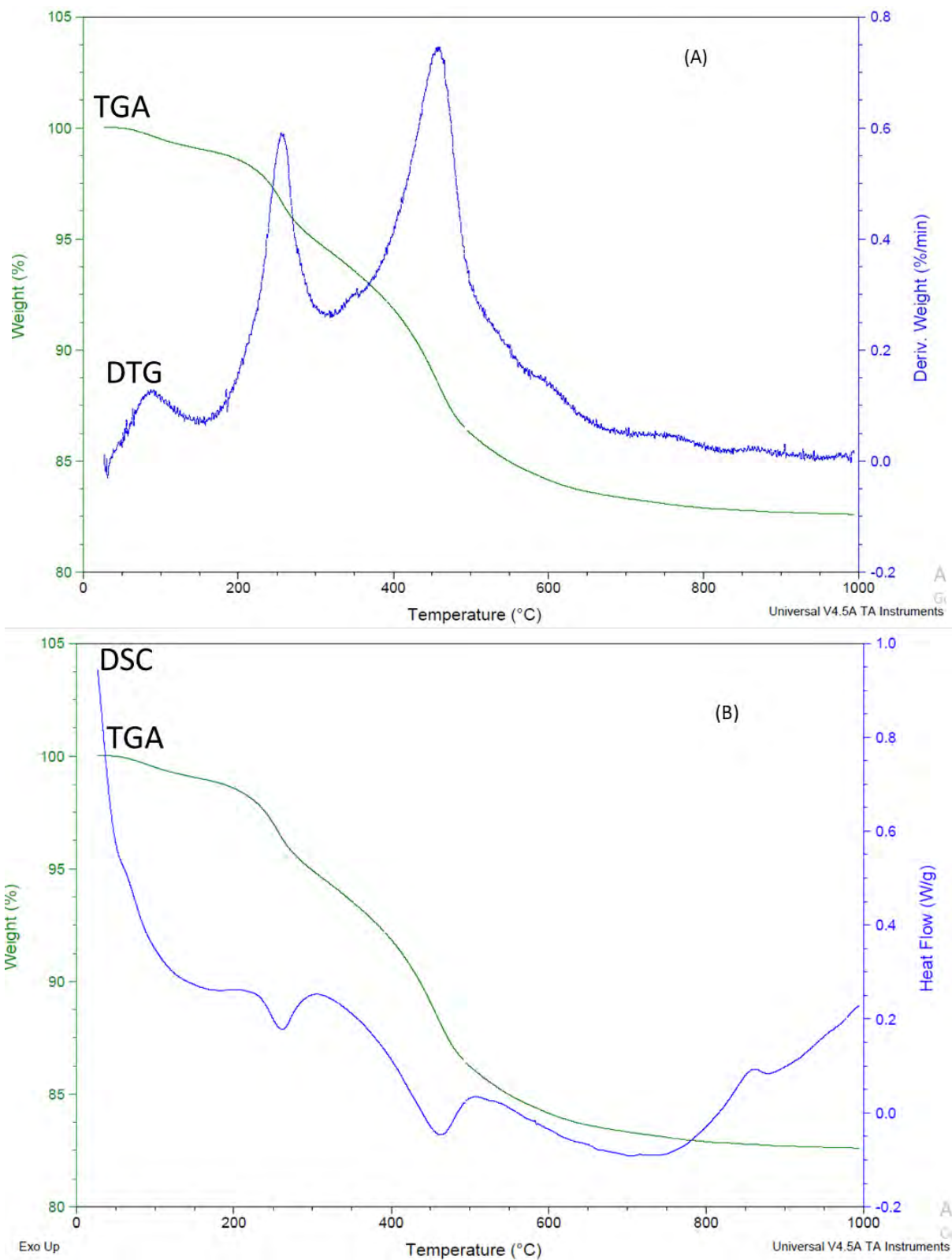


Figure 4.84: Thermal analyses of S2 0-20 cm showing: (a) TGA/DTG and (b) DSC/TGA curves.

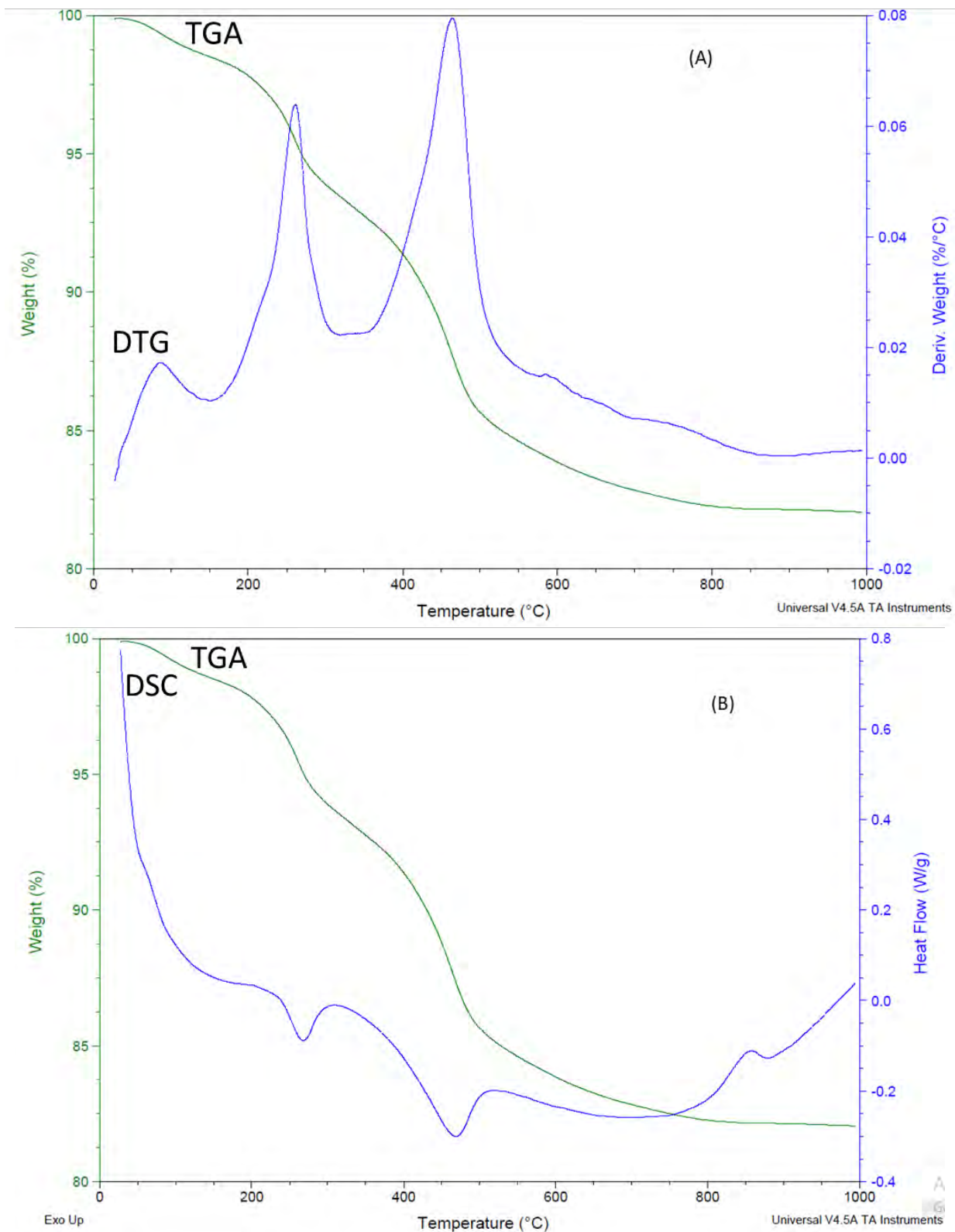


Figure 4.85: Thermal analyses of S2 20-50 cm showing: (a) TGA/DTG and (b) DSC/TGA curves.

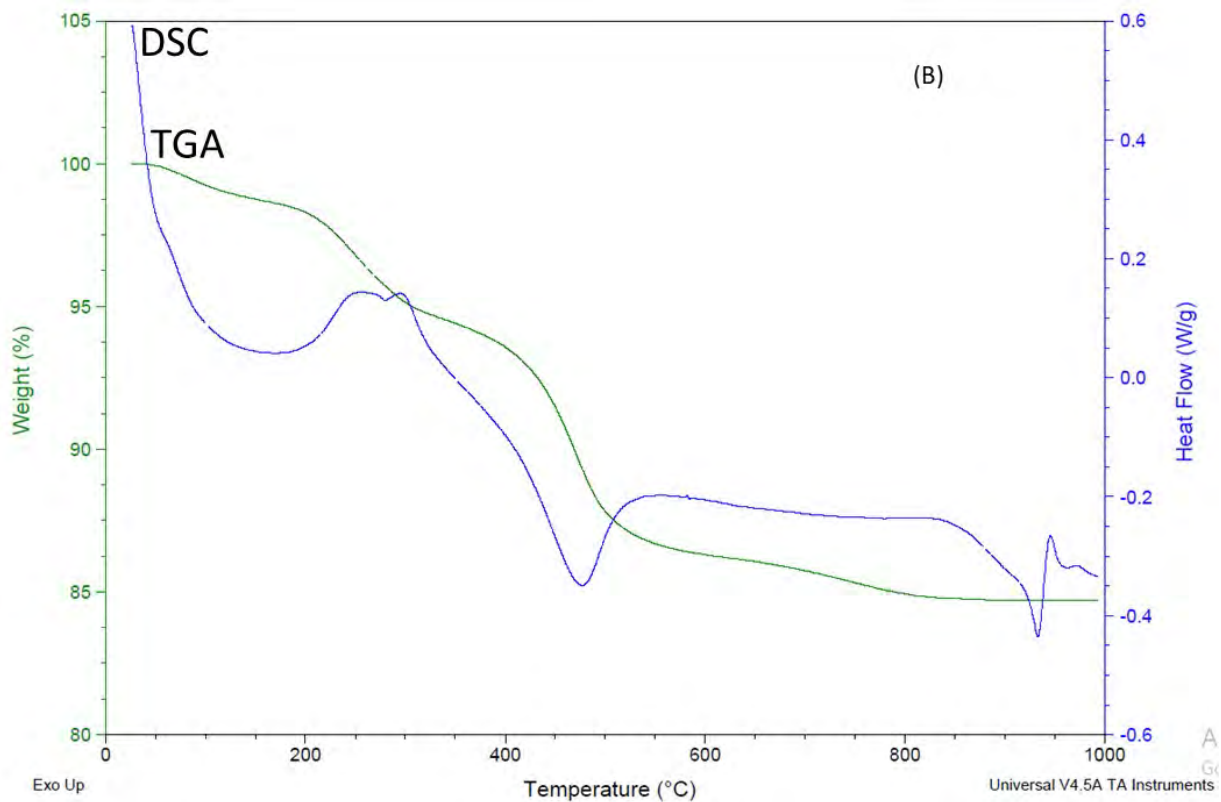
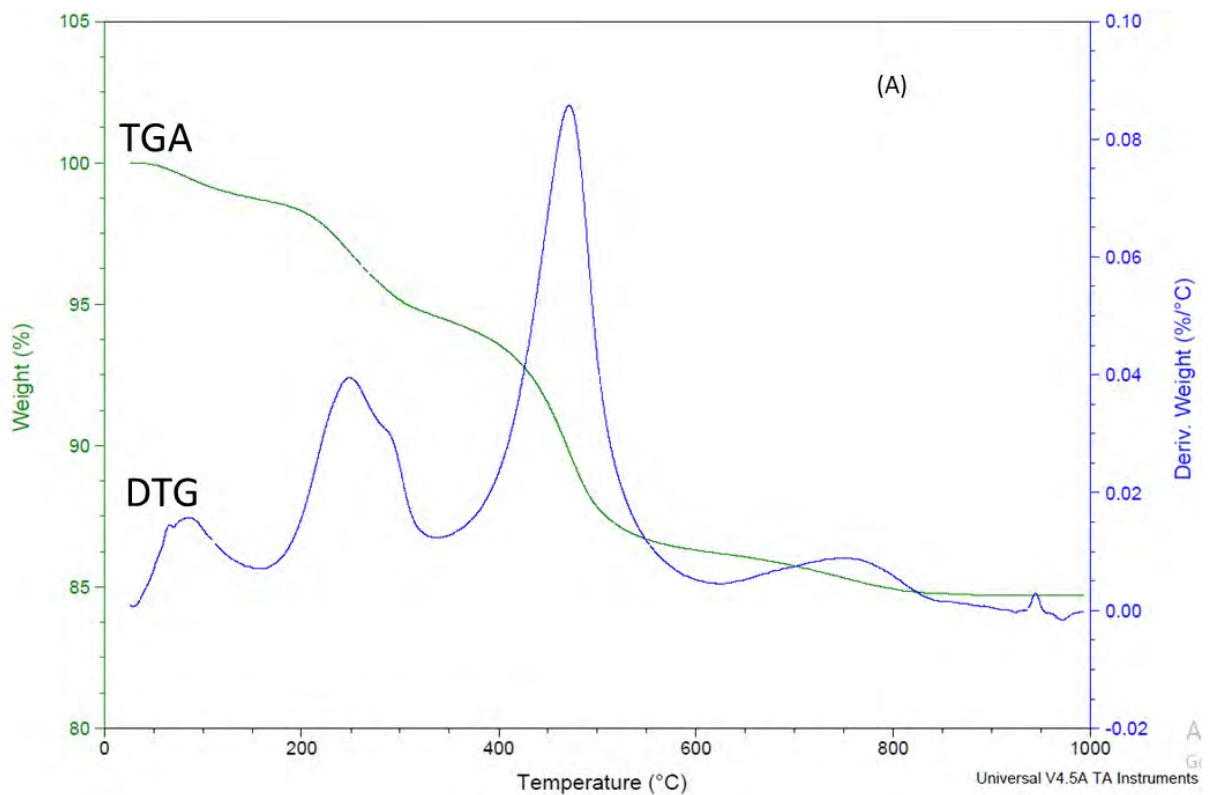


Figure 4.86: Thermal analyses of S2 50-100 cm showing: (a) TGA/DTG and (b) DSC/TGA curves.

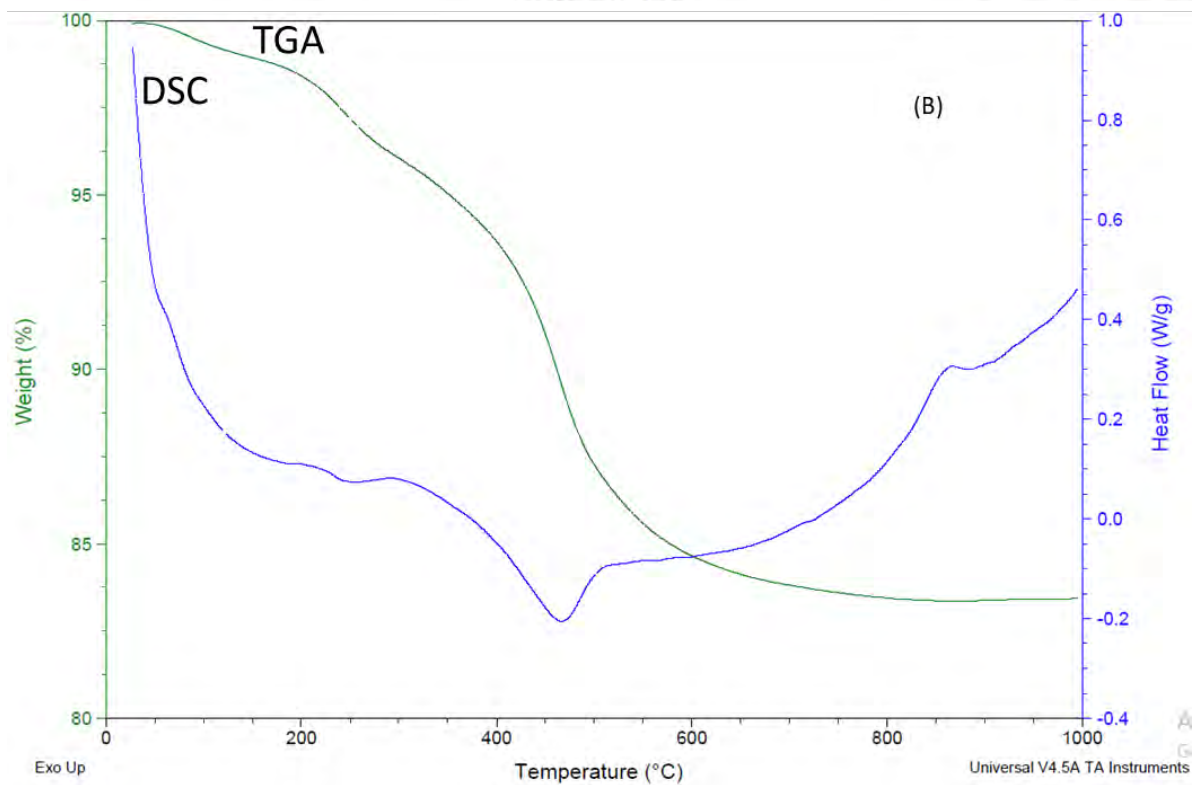
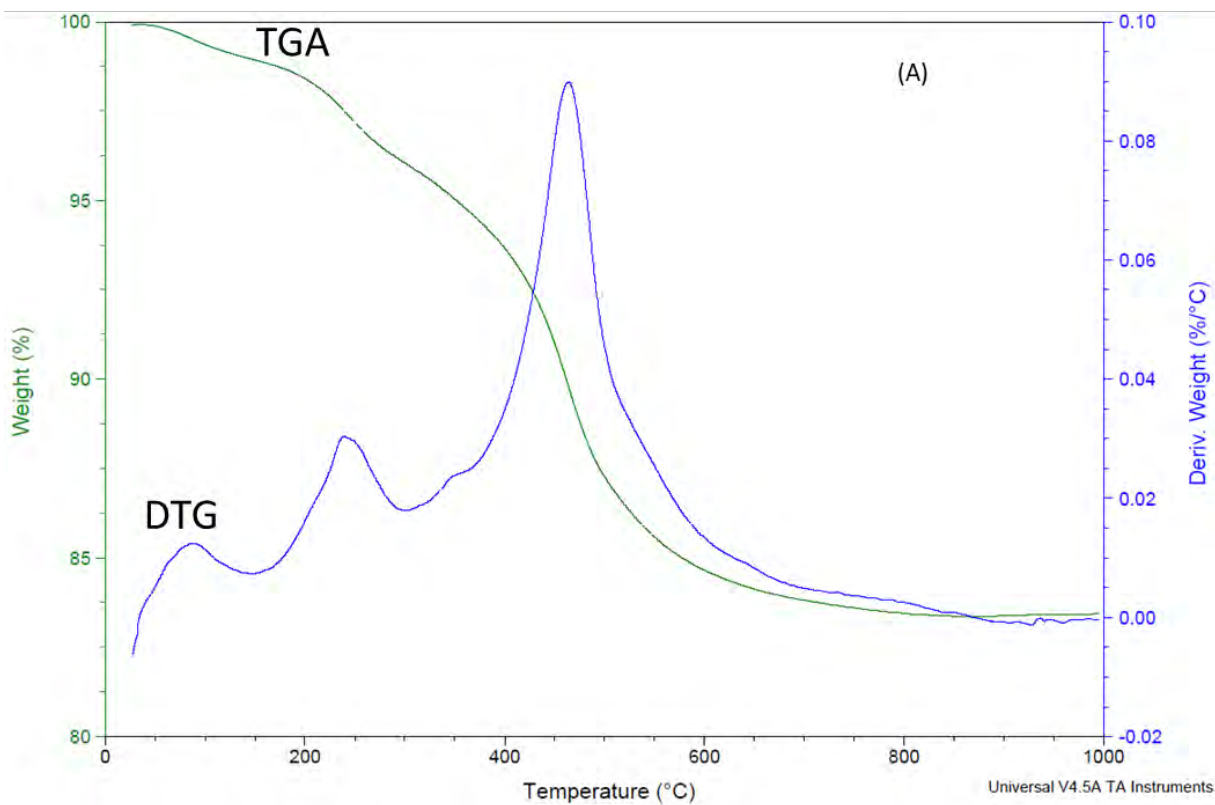


Figure 4.87: Thermal analyses of MAT1 0-20 cm showing: (a) TGA/DTG and (b) DSC/TGA curves.

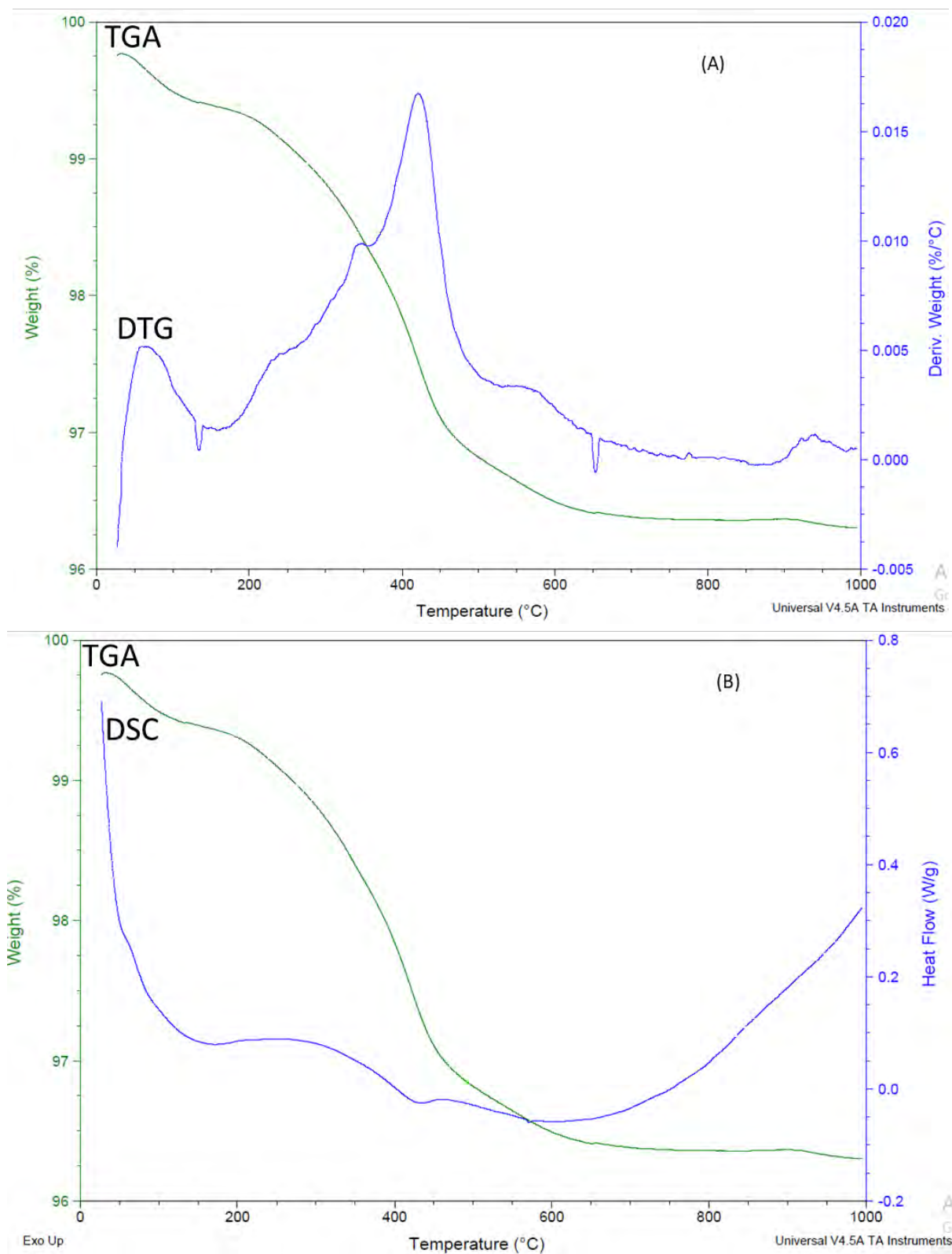


Figure 4.88: Thermal analyses of MAT1 20-50 cm showing: (a) TGA/DTG and (b) DSC/TGA curves.

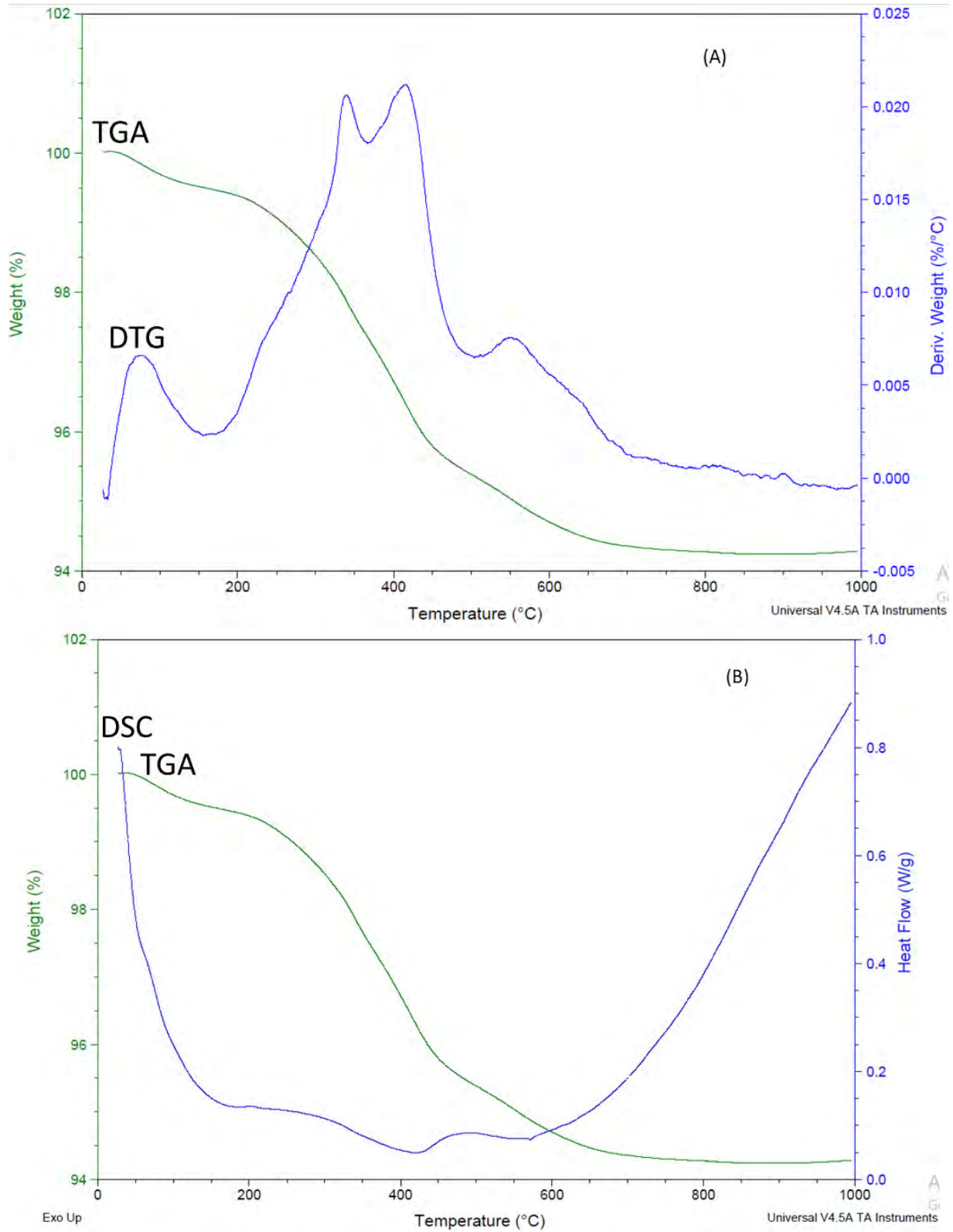


Figure 4.89: Thermal analyses of MAT3 0-20 cm showing: (a) TGA/DTG and (b) DSC/TGA curves.

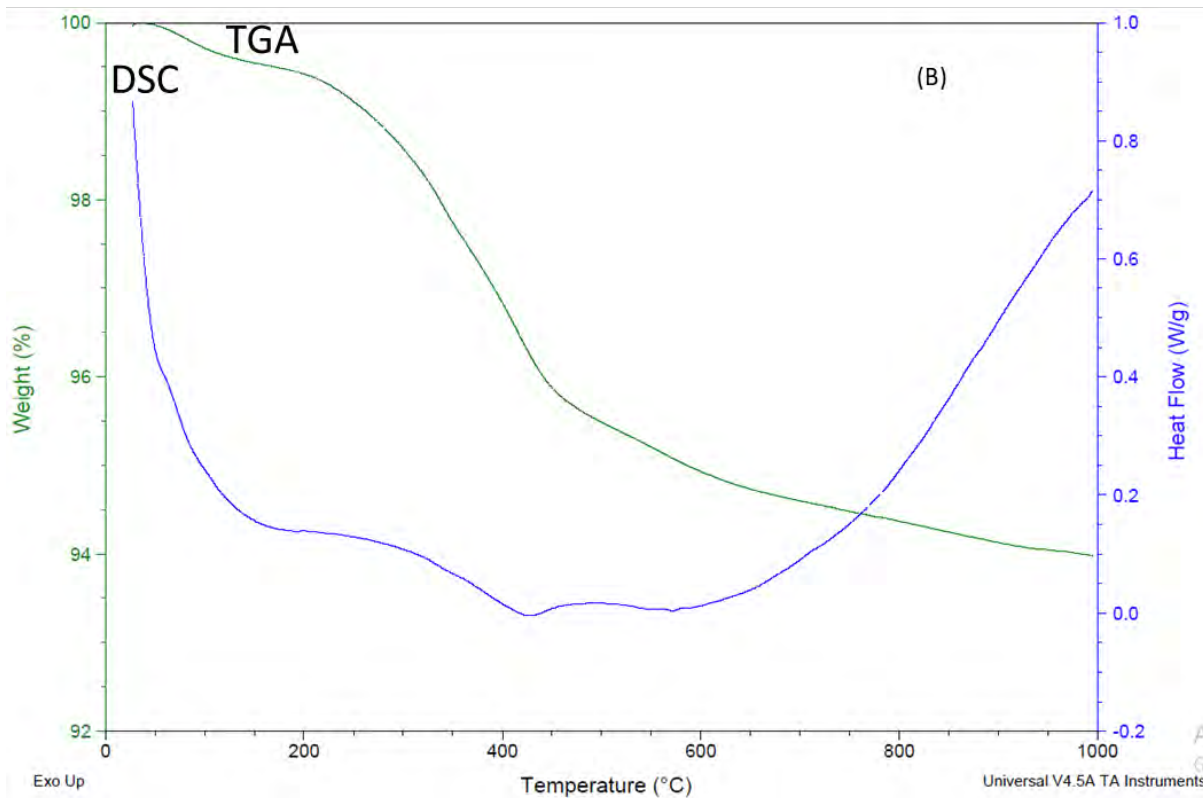
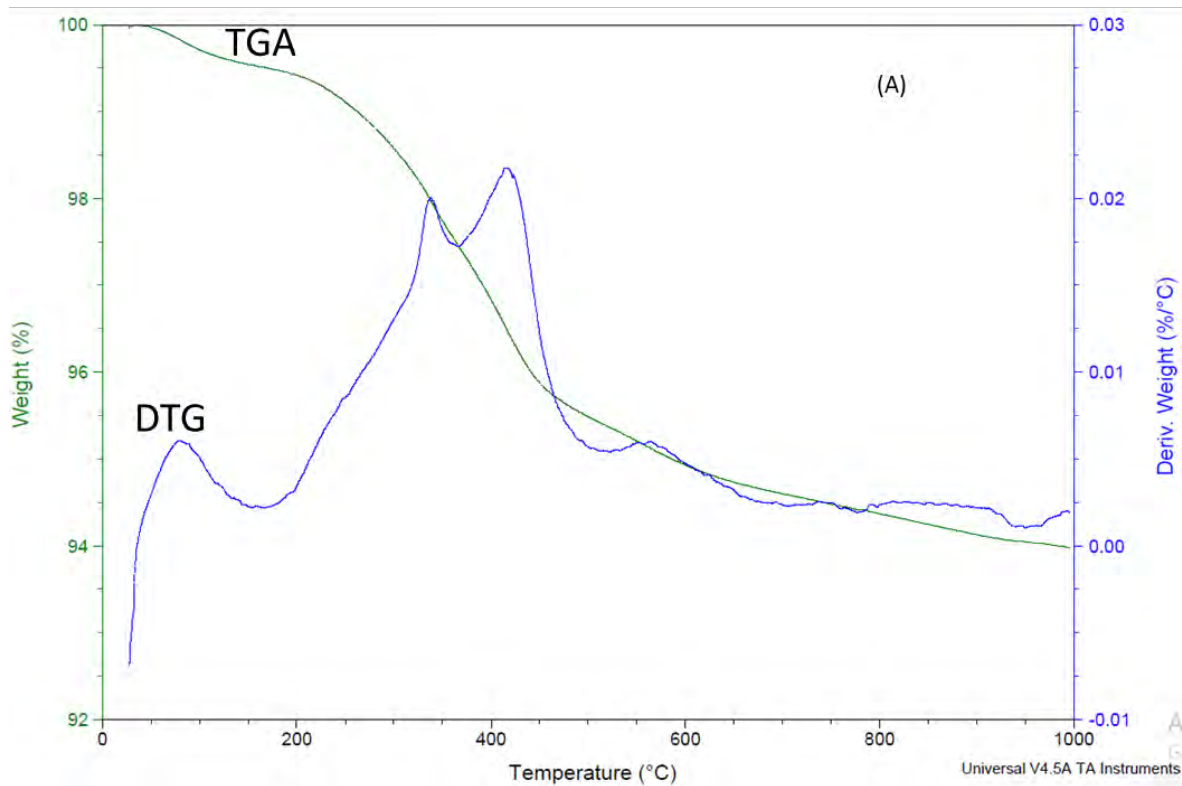


Figure 4.90: Thermal analyses of MAT3 20-50 cm showing: (a) TGA/DTG and (b) DSC/TGA curves.

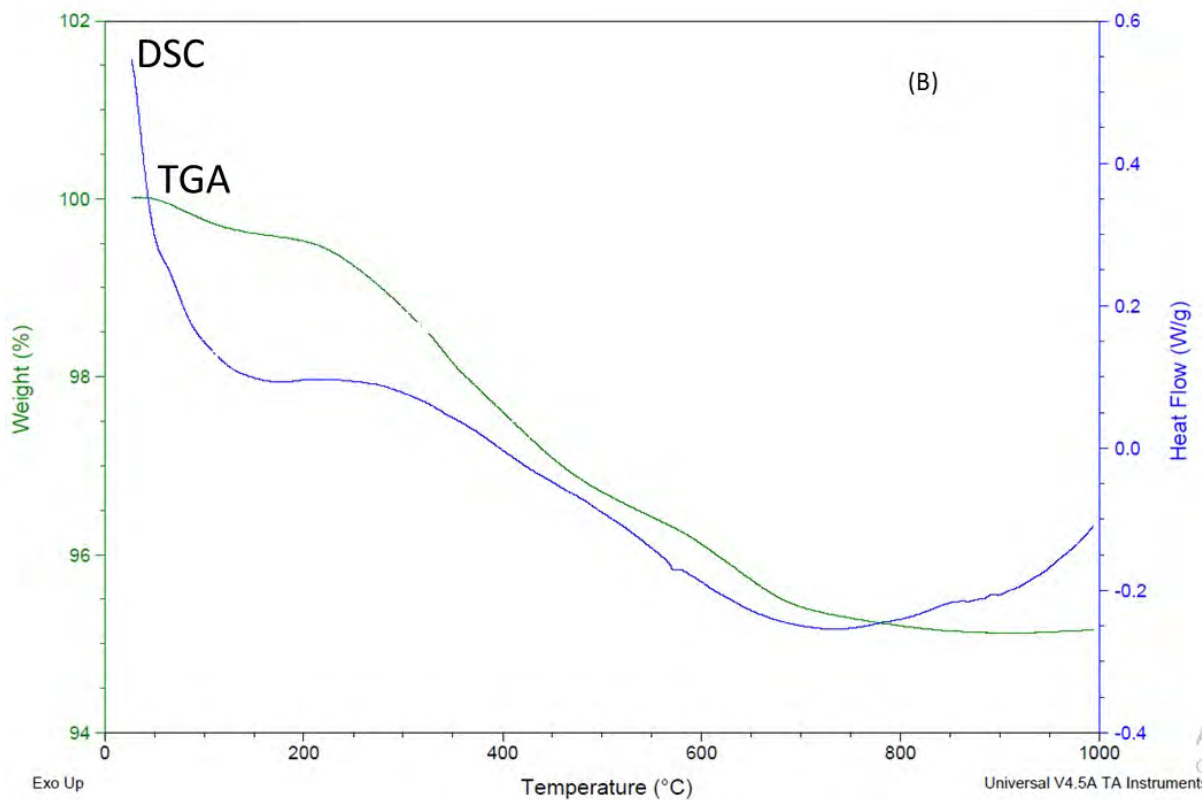
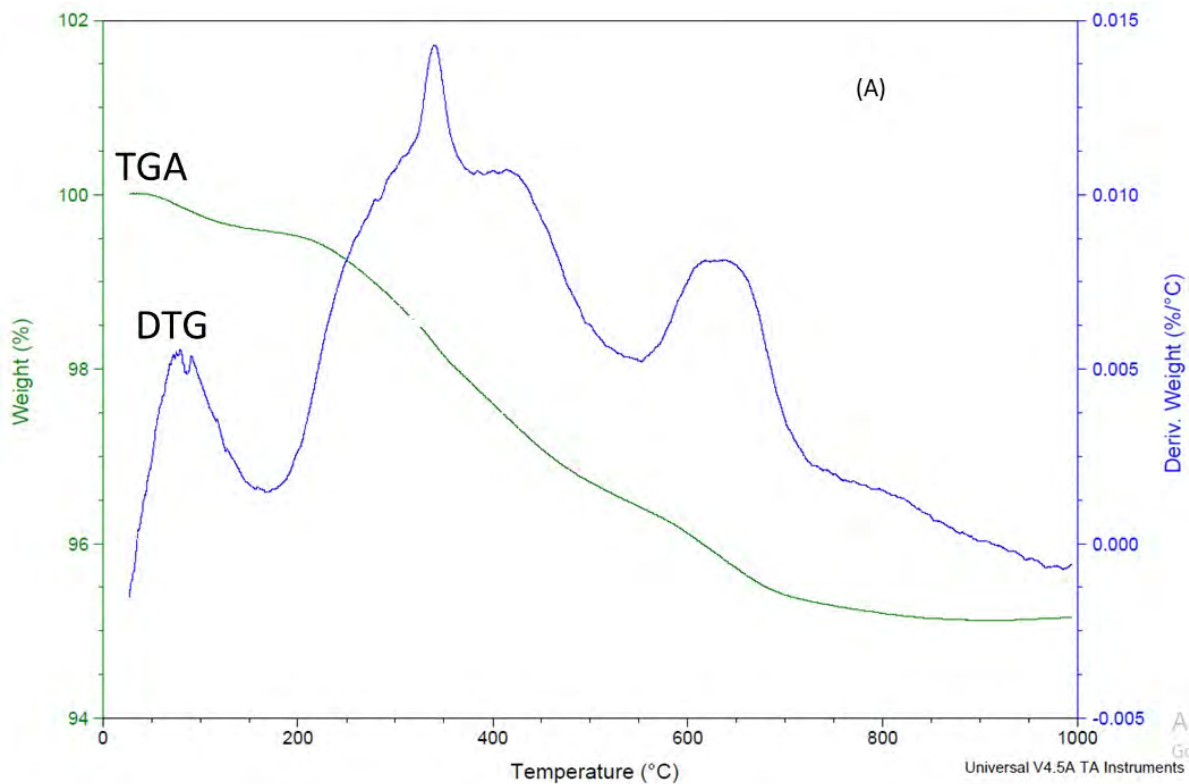


Figure 4.91: Thermal analyses of SA2 0-20 cm showing: (a) TGA/DTG and (b) DSC/TGA curves.

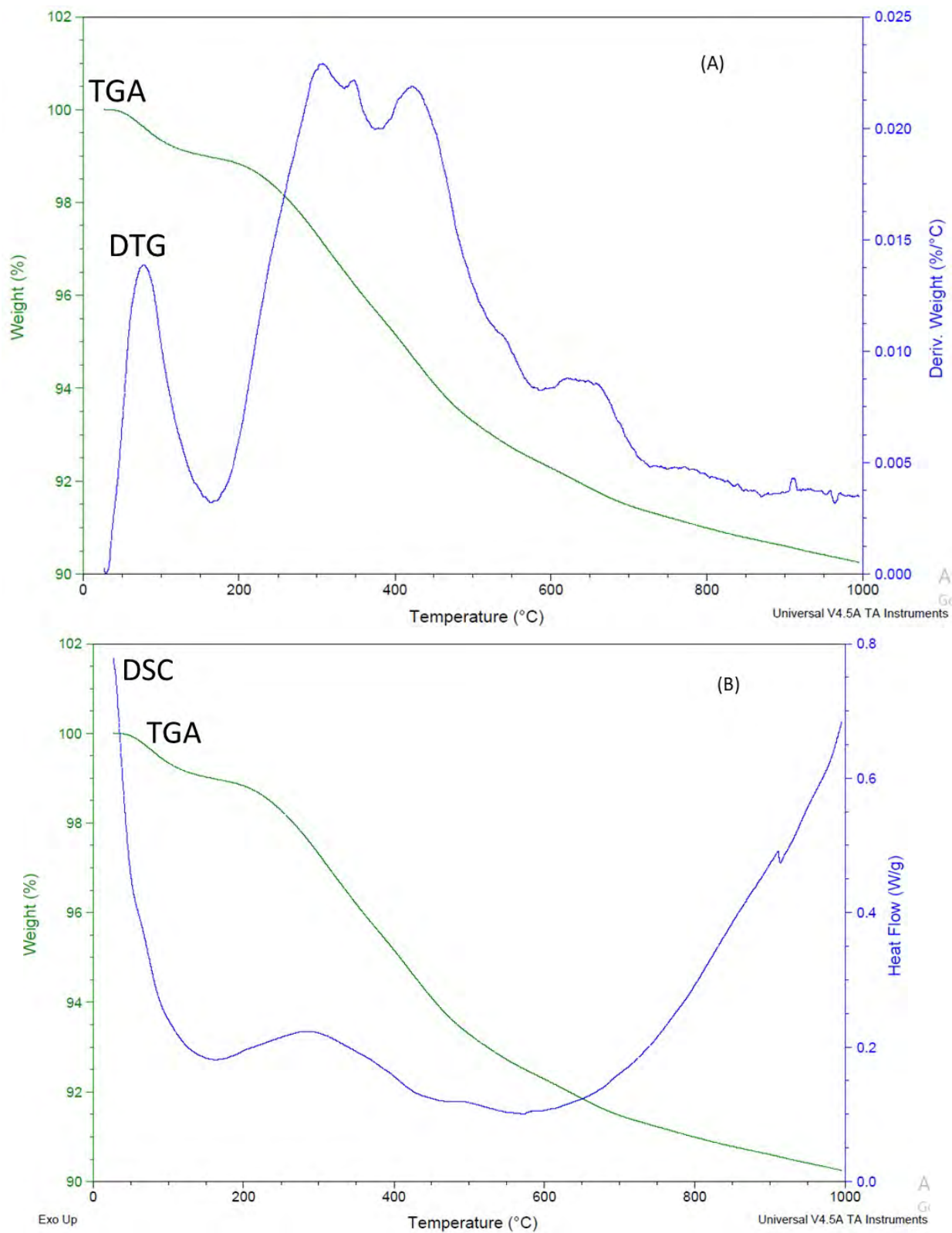


Figure 4.92: Thermal analyses of SA3 0-20 cm showing: (a) TGA/DTG and (b) DSC/TGA curves.

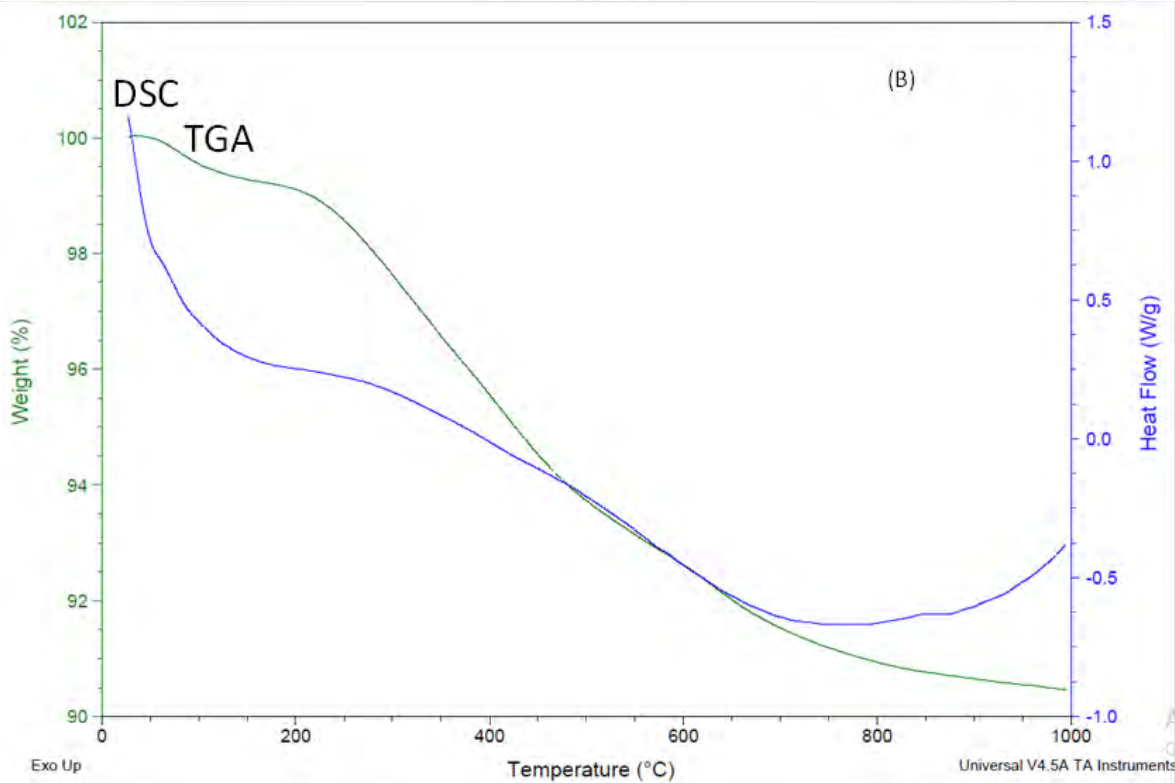
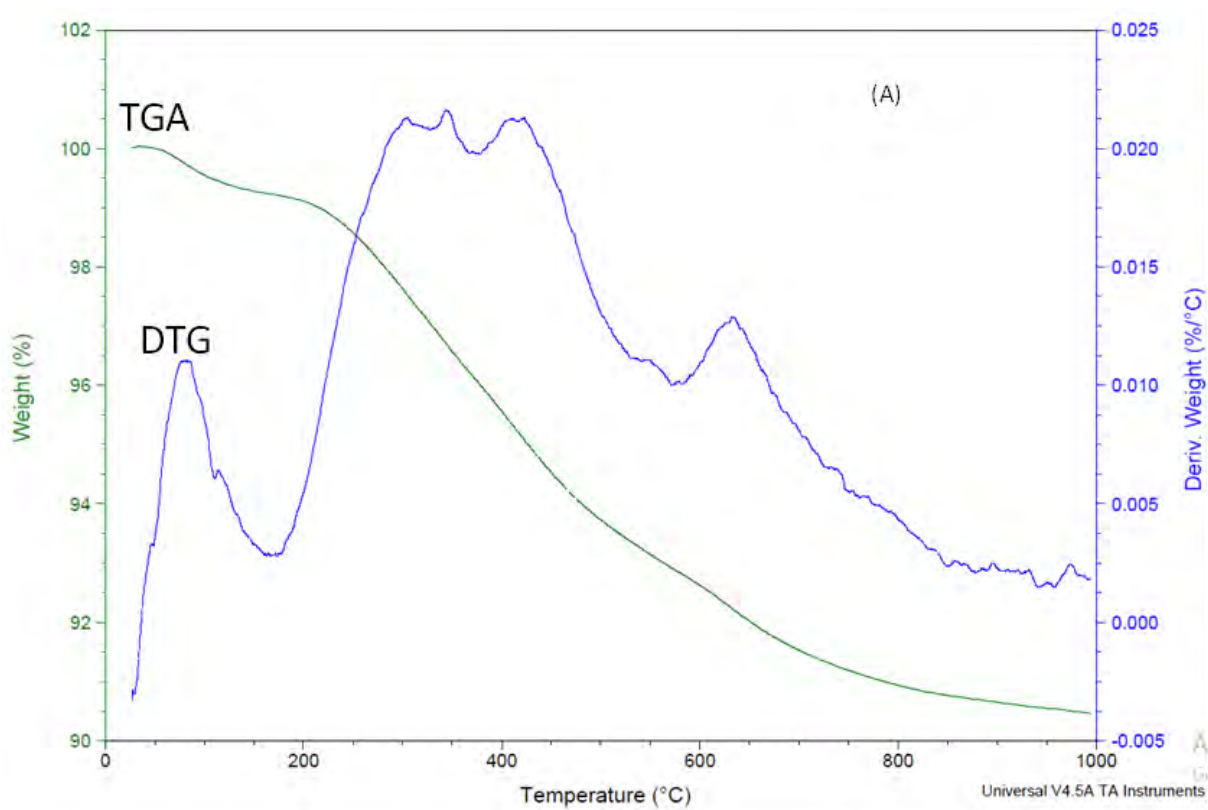


Figure 4.93: Thermal analyses of SA3 20-50 cm showing: (a) TGA/DTG and (b) DSC/TGA curves.

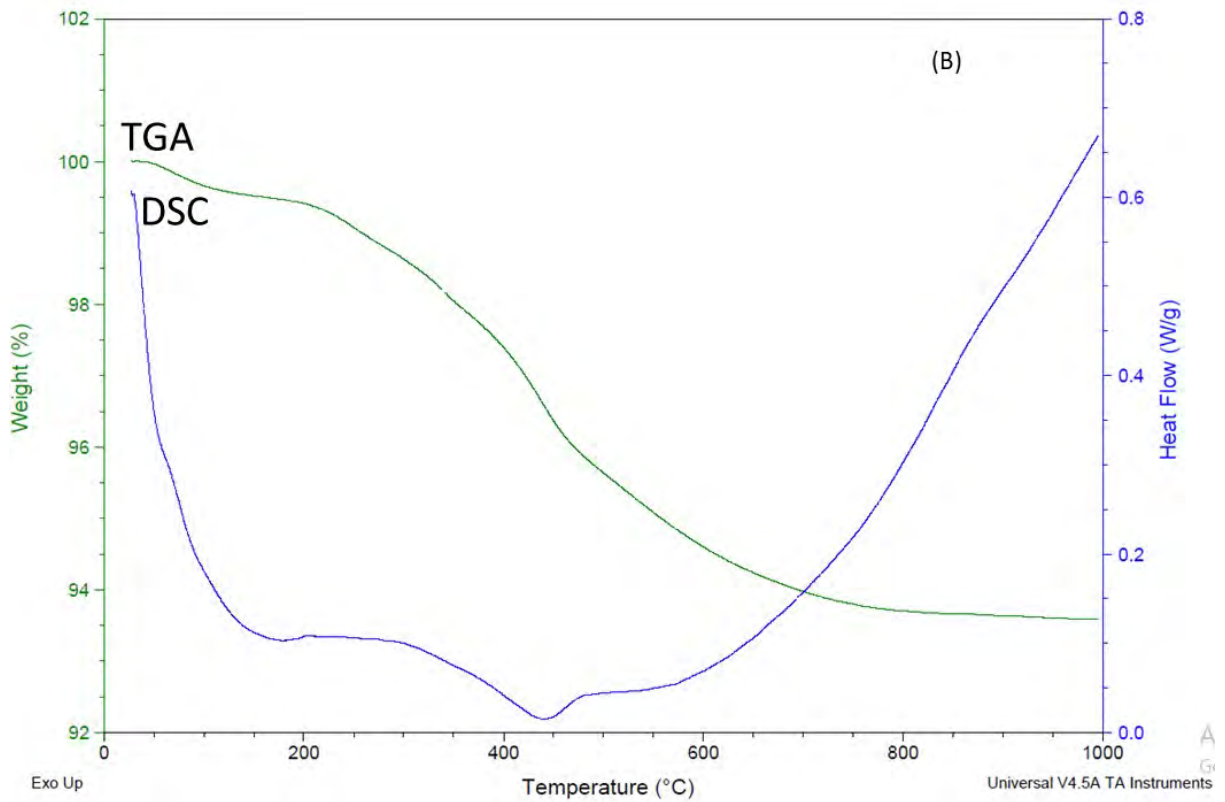
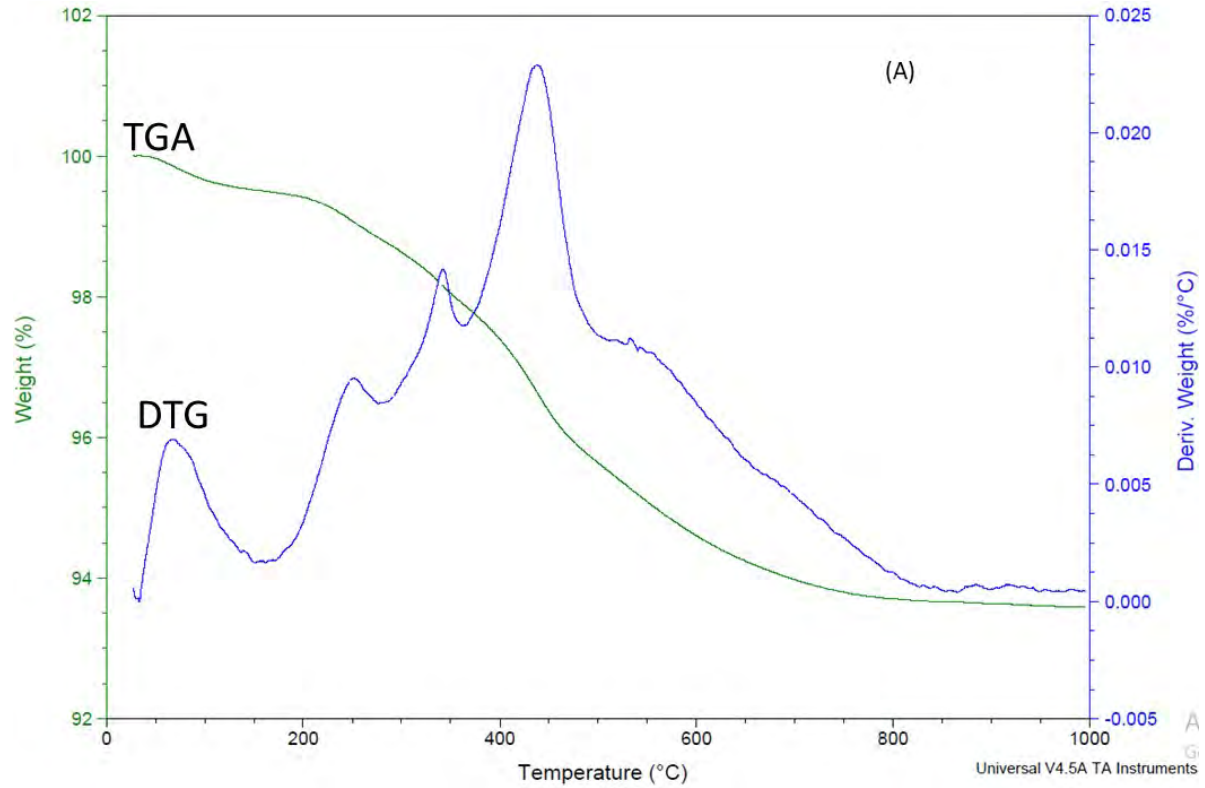


Figure 4.94: Thermal analyses of MU1 0-20 cm showing: (a) TGA/DTG and (b) DSC/TGA curves.

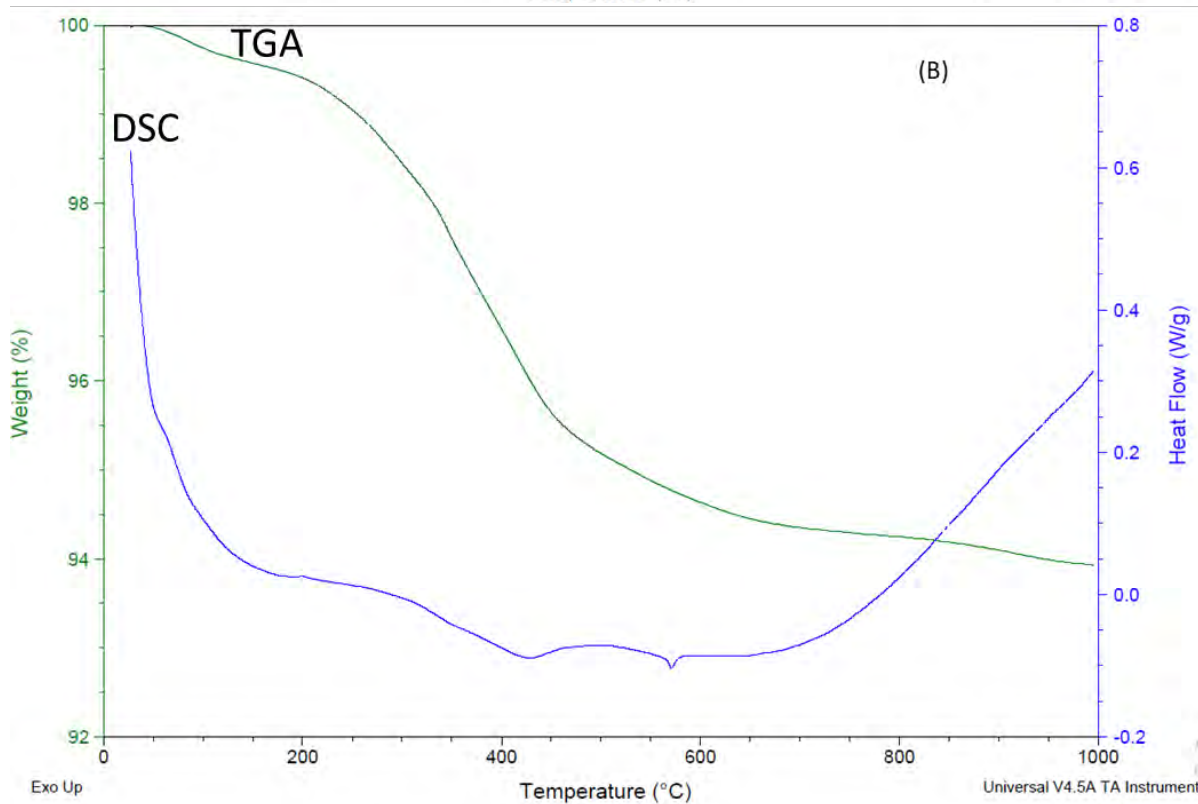
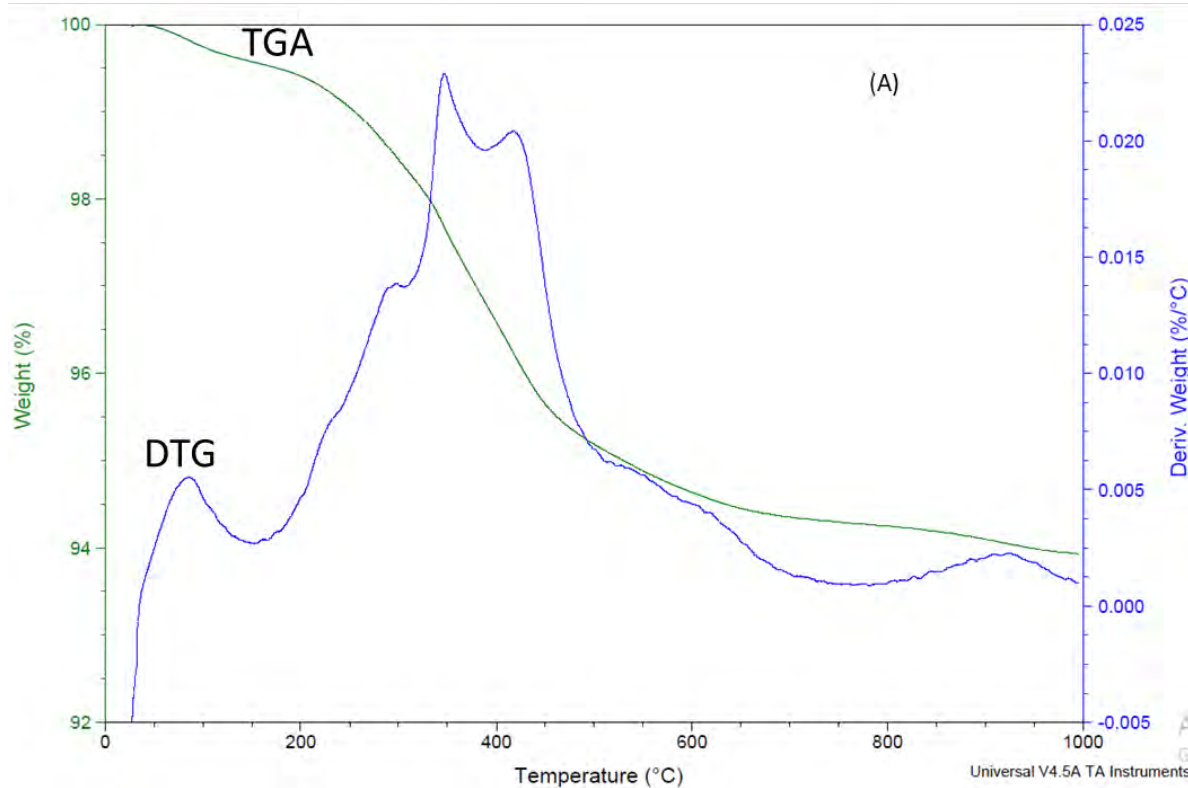


Figure 4.95: Thermal analyses of CMA 0-20 cm showing: (a) TGA/DTG and (b) DSC/TGA curves.

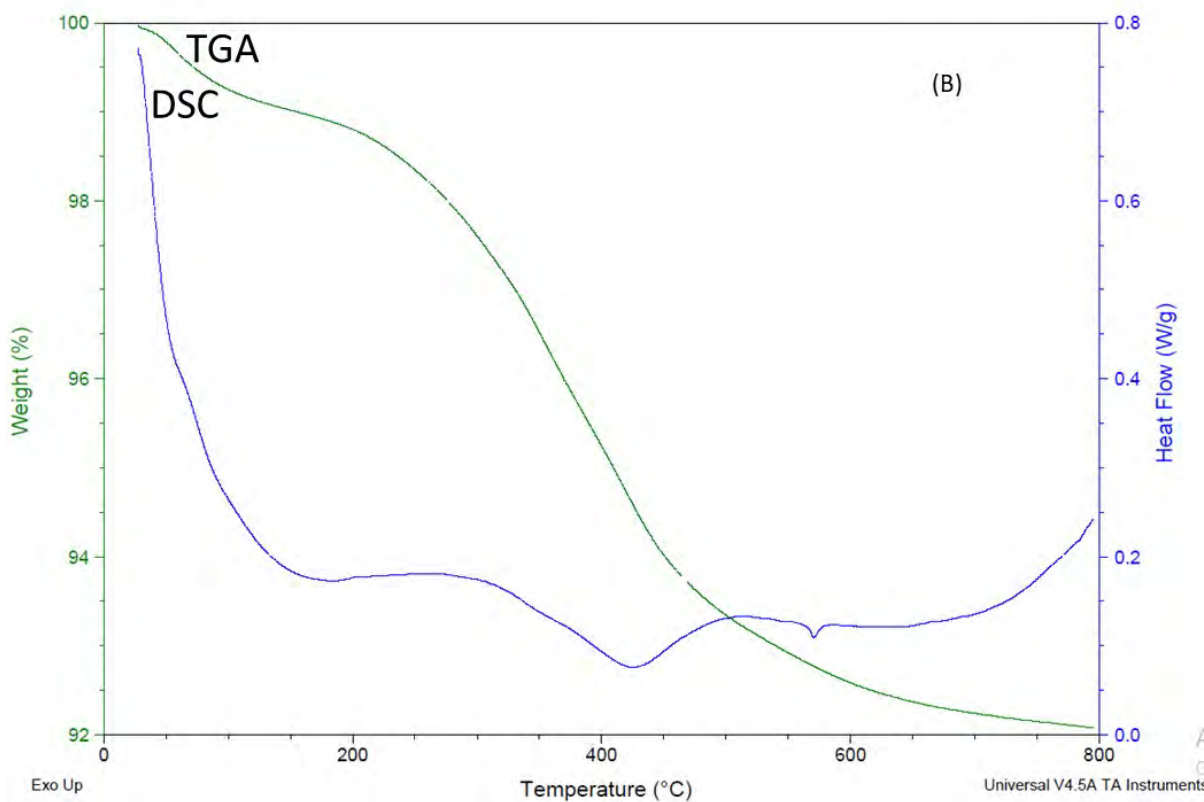
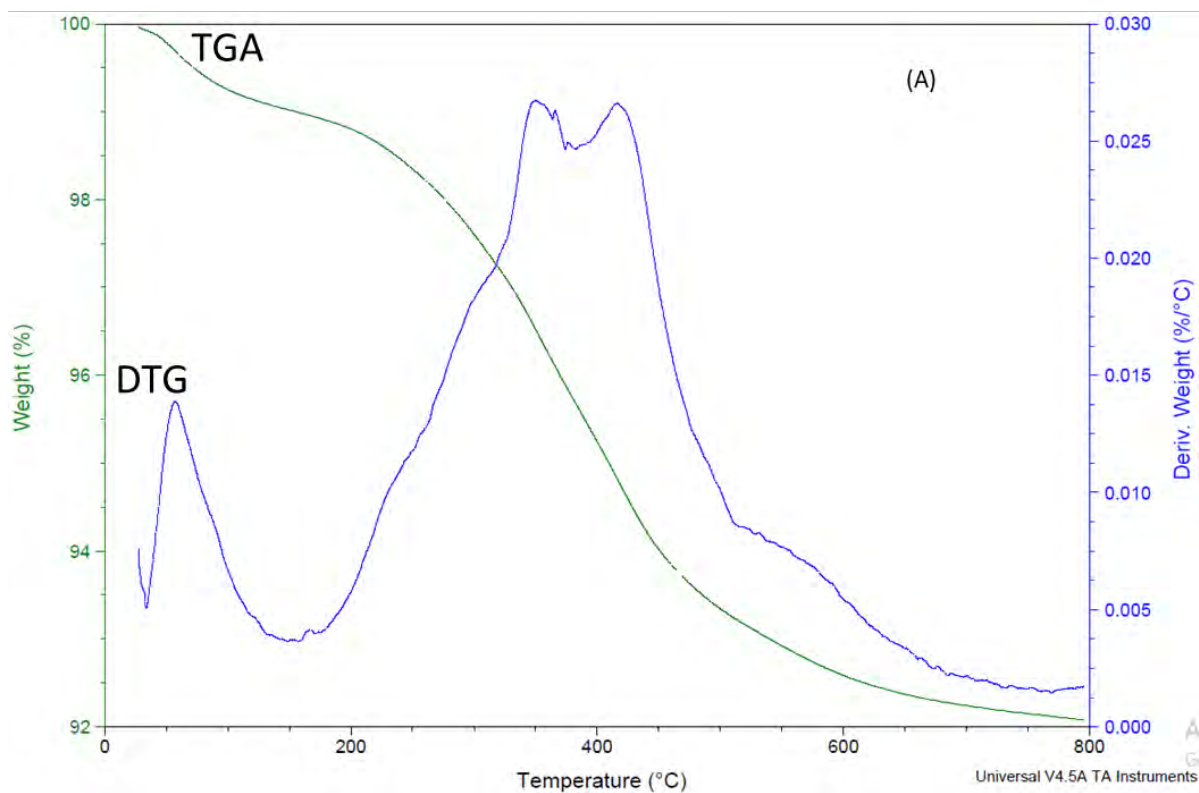


Figure 4.96: Thermal analyses of CMA 20-50 cm showing: (a) TGA/DTG and (b) DSC/TGA curves.

4.3 Geochemical Studies

Major element oxide, trace elements and REE data for the parent rocks, bulk soils, silt, clay fractions, and deferrated clay fractions (soil kaolins) for the studied soils developed from different parent rocks are presented in Tables 4.13 – 4.26.

4.3.1 Geochemical Properties of Studied Parent rocks

4.3.1.1 Major Element Oxides

Basalt has SiO₂ concentrations varying between 48.93 and 49.24 wt % and Al₂O₃ concentrations from 13.86 to 14.53 wt %. Fe₂O₃ and TiO₂ concentrations ranged from 13.44 to 14.42 wt % and 1.31 to 1.55 wt %, respectively. The concentration of K₂O varies from 0.52 to 0.99 wt % while the concentration of CaO varies from 7.87 to 9.73 wt %. Cr₂O₃ has a concentration of 0.02 wt %, MgO concentration varies from 5.40 to 6.55 wt % while Na₂O has a concentration ranging from 2.12 to 2.70 wt %. MnO, and P₂O₅ were generally below 0.7 wt %. The LOI were between 2.15 and 2.86 wt % (Table 4.13).

Granite has SiO₂ concentrations ranging between 72.23 and 72.77 wt % and Al₂O₃ concentrations from 15.54 to 15.86 wt %. Fe₂O₃ and TiO₂ concentrations ranged from 0.78 to 0.88 wt % and 0.07 to 0.11 wt %, respectively. The concentration of K₂O varies from 0.98 to 2.13 wt % while the concentration of CaO varies from 1.47 to 91.64 wt %. Cr₂O₃ was below detection limit, Na₂O has a concentration ranging from 5.73 to 6.32 wt %. MnO, MgO and P₂O₅ were generally below 0.5 wt %. The LOI were between 0.46 and 0.60 wt % (Table 4.13).

Arkosic sandstone has SiO₂ concentrations varying between 87.34 and 90.85 wt % and Al₂O₃ concentrations from 4.61 to 6.39 wt %. Fe₂O₃ and TiO₂ concentrations ranged from 0.33 to 0.61 wt % and 0.08 to 0.12 wt %, respectively. The concentration of K₂O varies from 2.54 to 3.64 wt % while the concentration of CaO varies from 1.47 to 91.64 wt %. Cr₂O₃ was below detection limit, Na₂O, MnO, MgO and P₂O₅ were generally below 0.5 wt %. The LOI were between 0.72 and 0.84 wt % (Table 4.13).

Quartzite had SiO₂ concentration of 96.21 wt % and Al₂O₃ concentration of 1.12 wt %. Fe₂O₃ and TiO₂ concentrations were 1.21 and 0.08 wt % respectively. K₂O had a

concentration of 0.21 wt % while the concentrations of CaO, MgO, MnO, and P₂O₅ were generally below 0.50 wt %. Cr₂O₃ and Na₂O were below detection limit. The LOI value was 0.69 wt % (Table 4.13).

4.3.1.2 Trace Elements

- **Compatible Trace Elements (Sc, V, Cr, Co, and Ni)**

These are trace elements whose preference is in the mineral phase usually with partition coefficient greater than 1.

The values obtained for Sc, V, Cr, Co, and Ni in basalt ranged from 3.23 to 38.59 ppm, 5.08 to 333.9 ppm, 3.81 to 192.00 ppm, 0.62 to 46.64 ppm, and 4.9 to 99.05 ppm, respectively. In granite, Sc, V, Cr, Co, and Ni concentrations varied from 4.72 to 5.39 ppm, 7.77 to 10.32 ppm, 8.85 to 17.31 ppm, 0.96 to 1.35 ppm, and 9.15 to 16.95 ppm, respectively (Table 4.14).

The Sc, V, Cr, Co, and Ni concentrations in the studied arkosic sandstone ranged from 5.44 to 6.98 ppm, 9.12 to 14.64 ppm, 6.5 to 13.35 ppm, 1.20 to 2.52 ppm, and 7.4 to 14.15 ppm, respectively. In quartzite, the Sc, V, Cr, Co, and Ni concentrations are 153.90 ppm, 1281.00 ppm, 621.40 ppm, 142.4 ppm, and 277.50 ppm, respectively (Table 4.14).

- **Incompatible Trace Elements (Rb, Sr, Y, Zr, Nb, Ba, Th, and U)**

The concentrations of Rb, Y, Th, Nb and U in basalt were generally less than 50 ppm whereas, Sr Zr, and Ba values were more than 50 ppm. In the studied granite, the concentrations of Rb (except in MAT1 and MAT2), Sr, Zr, and Ba were generally more than 50 ppm whereas, Th, U, Y and Nb were less than 10 ppm. The concentrations of Rb, Sr, Zr and Ba were generally more than 50 ppm in the arkosic sandstone whereas, Y, Nb, Th, and U were generally less than 10 ppm. In quartzite (control), the Rb, Sr, Y, Zr, Nb, Ba, Th, and U concentrations were 94.25 ppm, 27.70 ppm, 70.35 ppm, 546.85 ppm, 30.99 ppm, 249.2 ppm, 18.00 ppm and 3.65 ppm, respectively (Table 4.14).

Table 4.13: Major element oxide concentrations (wt %) in parent rocks.

Parent Rock	Sample ID	Al ₂ O ₃	CaO	Cr ₂ O ₃	Fe ₂ O ₃	K ₂ O	MgO	MnO	Na ₂ O	P ₂ O ₅	SiO ₂	TiO ₂	L.O.I.	Sum of Conc.
Basalt	RK S1	14.53	7.87	0.02	13.92	0.81	6.55	0.19	2.70	0.14	48.93	1.36	2.86	99.88
	RK S2	14.30	9.63	0.02	13.44	0.99	6.17	0.20	2.12	0.14	49.12	1.31	2.38	99.82
	RK S3	13.86	9.73	0.02	14.42	0.52	5.40	0.20	2.33	0.17	49.24	1.55	2.15	99.59
Granite	RK MAT1	15.86	1.47	bdl	0.80	2.13	0.22	0.02	5.73	0.06	72.23	0.07	0.60	99.19
	RK MAT2	15.54	1.64	bdl	0.88	0.98	0.21	0.02	6.32	0.07	72.77	0.11	0.46	99.00
	RK MAT3	15.73	1.55	bdl	0.78	1.56	0.27	0.02	6.05	0.06	72.5	0.09	0.53	99.14
Ark. Sst.	RK SA1	6.39	0.05	bdl	0.61	3.64	0.06	0.01	0.13	0.06	87.34	0.12	0.84	99.25
	RK SA2	4.61	0.08	bdl	0.34	2.45	0.15	0.01	0.05	0.02	90.85	0.12	0.77	99.45
	RK SA3	4.70	0.12	bdl	0.33	2.86	0.06	0.01	0.07	0.08	90.60	0.08	0.72	99.63
Quartzite	RK CMA	1.12	0.03	bdl	1.21	0.21	0.07	0.01	bdl	0.03	96.21	0.08	0.69	99.66

Table 4.14: Trace element concentrations (ppm) in parent rocks.

Parent Rocks	Sample ID	Sc	V	Cr	Co	Ni	Cu	Zn	Rb	Sr	Y	Zr	Nb	Mo	Cs	Ba	Hf	Ta	Pb	Th	U
Basalt	RK S1	36.12	300.15	192	46.64	99.05	180.05	101.5	36.66	146.45	25.15	102.76	5.6	0.48	0.51	202.6	2.77	0.31	4.32	2.6	0.67
	RK S2	38.59	333.85	148.1	45.11	71.7	190.2	115.55	13.02	130.5	29.59	125.2	7.12	0.74	0.24	206.7	3.6	0.41	5.02	3.4	0.75
	RK S3	3.23	5.075	3.81	0.62	4.9	3.72	15.95	32.4	373.35	1.3	15.56	1.72	0.36	1.33	637	0.33	0.17	12.7	0.56	0.32
Granite	RK MAT1	5.38	7.77	15.6	0.96	16.95	6.49	19.95	18.15	506.5	6.95	62.3	4.45	0.8	1.14	319.5	1.77	0.31	15.8	1.14	0.84
	RK MAT2	4.72	10.32	8.85	1.35	9.15	4.32	18	88.25	115.1	3.54	99.3	2.27	0.29	0.75	1042.5	2.86	0.15	18.7	3.6	0.65
	RK MAT3	5.1	8.61	17.31	1.1	15.2	5.88	19.11	22.1	44.01	4.98	67.22	4.71	0.73	1.21	297.33	1.66	0.21	16.4	1.42	0.63
Ark. Sst	RK SA1	5.62	13.17	13.35	1.51	14.15	4.32	16.15	77.25	57.35	4.08	91.8	2.57	bdl	0.74	570	2.83	0.29	14.1	3.46	0.56
	RK SA2	5.44	9.12	10.25	1.2	7.4	5.88	16.35	92.6	77.4	3.7	100.6	1.82	0.55	0.76	699	2.66	0.22	14.9	2.64	0.68
	RK SA3	6.98	14.64	6.5	2.52	7.75	9.2	43.45	41.4	915	3.74	126.35	1.42	bdl	0.95	739.5	3.35	0.03	17.7	2.59	0.25
Quartzite	RK CMA	153.9	1280.5	621.4	142.4	277.5	654.5	238.3	94.25	27.7	70.35	546.85	30.99	2.54	4.14	249.2	15.16	1.84	26.8	17.99	3.65

4.3.1.3 Rare Earth Elements (REEs)

The light REEs (LREE) are the low atomic number members of the REE series from La – Eu, while the higher atomic number members from Gd – Lu are referred to as the heavy REEs (HREE).

- **Light REEs (LREE) (La, Ce, Pr, Nd, Sm, Eu)**

Values obtained for La, Ce, Pr, Nd, Sm and Eu in basalt ranged from 8.15 to 15.80 ppm, 14.52 to 32.84 ppm, 1.44 to 4.16 ppm, 5.17 to 16.70 ppm, 0.45 to 3.80 ppm and 0.39 to 1.42 ppm, respectively. In Granite, the concentration of La, Ce, Pr, Nd, Sm and Eu concentrations varied from 11.3 to 11.15 ppm, 18.83 to 21.20 ppm, 2.03 to 2.30 ppm, 8.08 to 8.37 ppm, 0.80 to 1.40 ppm and 0.34 to 0.52 ppm, respectively.

The La, Ce, Pr, Nd, Sm and Eu concentrations in arkosic sandstone ranged from 7.50 to 16.80 ppm, 14.53 to 34.25 ppm, 1.64 to 3.87 ppm, 5.41 to 13.30 ppm, 0.84 to 1.72 ppm and 0.31 to 0.56 ppm, respectively. In quartzite, the La, Ce, Pr, Nd, Sm and Eu concentrations are 46.20 ppm, 143.30 ppm, 13.60 ppm, 57.00 ppm, 13.50 ppm and 3.96 ppm, respectively (Table 4.15).

- **Heavy REEs (HREE) (Gd, Tb, Dy, Ho, Er, Tm, Yb, Lu)**

The concentrations of HREE in the studied parent rocks were generally less than 10 ppm. Tm was below detection limit in arkosic sandstone (Table 4.15).

Table 4.15: Rare earth element concentrations (ppm) in parent rocks.

Parent Rocks	Sample ID	La	Ce	Pr	Nd	Sm	Eu	Gd	Tb	Dy	Ho	Er	Tm	Yb	Lu
Basalt	RK S1	12.35	27.07	3.36	14.30	3.50	1.21	4.09	0.68	4.37	0.92	2.49	0.40	2.62	0.44
	RK S2	15.78	32.84	4.16	16.68	3.80	1.42	5.50	0.78	5.38	1.10	2.89	0.43	3.14	0.46
	RK S3	8.15	14.52	1.44	5.17	0.45	0.39	0.58	bdl	bdl	bdl	Bdl	bdl	bdl	bdl
Granite	RK MAT1	11.50	21.20	2.03	8.10	0.80	0.34	1.64	0.18	1.16	0.18	0.74	0.09	0.88	0.10
	RK MAT2	11.53	18.83	2.30	8.37	1.40	0.52	0.88	0.12	0.70	0.14	0.33	0.06	0.24	0.06
	Rk MAT3	11.30	20.10	2.10	8.08	1.10	0.41	0.93	0.14	0.96	0.18	0.46	0.06	0.51	0.04
Ark. Sst.	RK SA1	7.50	14.53	1.64	5.41	1.07	0.31	1.03	0.13	0.72	0.17	0.36	bdl	0.44	0.06
	RK SA2	8.82	14.64	1.72	5.87	0.84	0.49	0.84	0.07	0.72	0.16	0.37	bdl	0.48	0.06
	RK SA3	16.81	34.25	3.87	13.25	1.72	0.56	1.51	0.16	0.49	0.11	0.25	bdl	bdl	bdl
Quartzite	RK CMA	46.18	143.30	13.62	57.00	13.50	3.96	13.00	2.24	14.06	2.99	8.95	1.22	8.28	1.21

4.3.2 Geochemical Properties of the Bulk soils

4.3.2.1 Major Element Oxides

Soils developed from basalt had SiO_2 concentrations varying between 32.09 and 37.88 wt % and Al_2O_3 concentrations from 22.91 to 25.75 wt %. Fe_2O_3 and TiO_2 concentrations ranged from 20.73 to 25.43 wt % and 1.90 to 2.81 wt %, respectively. The concentrations of K_2O , CaO , Cr_2O_3 , Na_2O , MnO , and P_2O_5 were generally below 0.5 wt %. The LOI were between 13.50 and 16.28 wt % (Table 4.16).

Soils developed from granite had SiO_2 concentrations ranging between 74.30 and 76.90 wt % and Al_2O_3 concentrations from 11.98 to 13.54 wt %. Fe_2O_3 and Na_2O concentrations ranged from 1.43 to 1.91 wt % and 3.38 to 3.89 wt %, respectively. The concentration of K_2O varied from 1.82 to 2.13 wt % while the concentration of CaO varied from 1.11 to 1.18 wt %. Cr_2O_3 , TiO_2 , MnO , MgO and P_2O_5 were generally below 0.7 wt %. The LOI were between 1.27 and 2.16 wt % (Table 4.16).

Soils developed from arkosic sandstone have SiO_2 concentrations varying between 79.48 and 88.11 wt % and Al_2O_3 concentrations from 3.46 to 7.16 wt %. Fe_2O_3 , K_2O and TiO_2 concentrations ranged from 1.30 to 2.51 wt %, 2.19 to 2.63 wt % and 0.77 to 1.06 wt %, respectively. CaO , Cr_2O_3 , Na_2O , MnO , MgO and P_2O_5 were generally below 1.00 wt %. The LOI were between 1.46 and 5.06 wt % (Table 4.16).

Soils developed from gneiss had SiO_2 concentrations ranging from 60.30 to 62.10 wt % and Al_2O_3 concentrations between 14.40 and 16.10 wt %. Fe_2O_3 , MgO and TiO_2 concentrations were between 6.62 and 7.31 wt %, 1.10 and 1.26 wt %, 1.31 and 1.56 wt %, respectively. K_2O concentrations ranged from 1.28 to 1.41 wt % whereas, Na_2O concentrations were between 4.28 and 6.31 wt %. The concentrations of CaO were from 2.72 to 3.46 wt % whereas, MnO , and P_2O_5 were generally below 0.50 wt %. Cr_2O_3 was below detection limit and the LOI values were between 3.10 and 3.80 wt % (Table 4.16).

Table 4.16: Major element oxide concentrations (wt %) in bulk soils.

Parent Rocks	Sample ID	Al ₂ O ₃	CaO	Cr ₂ O ₃	Fe ₂ O ₃	K ₂ O	MgO	MnO	Na ₂ O	P ₂ O ₅	SiO ₂	TiO ₂	L.O.I.	Sum of Conc.
Basalt	BK S1 0-20 cm	23.63	0.11	0.03	22.51	0.31	0.19	0.17	0.05	0.15	35.43	2.25	16.05	100.88
	BK S1 20-50 cm	24.93	0.08	0.03	22.39	0.36	0.18	0.15	0.03	0.14	35.60	2.14	14.42	100.45
	BK S1 50-100 cm	24.83	0.06	0.03	22.74	0.36	0.18	0.17	0.01	0.16	35.48	2.23	13.59	99.84
	BK S2 0-20 cm	22.91	0.20	0.04	20.73	0.15	0.21	0.20	0.07	0.16	37.23	1.99	16.28	100.17
	BK S2 20-50 cm	25.02	0.11	0.04	21.41	0.09	0.16	0.16	0.01	0.12	36.60	1.92	14.50	100.14
	BK S2 50-100 cm	24.89	0.09	0.04	21.17	0.07	0.19	0.16	0.03	0.12	37.88	1.90	13.81	100.35
	BK S3 0-20 cm	25.58	0.07	0.04	24.64	0.06	0.04	0.14	0.03	0.16	33.00	2.66	13.74	100.16
	BK S3 20-50 cm	25.63	0.06	0.04	25.05	0.05	0.03	0.14	0.01	0.15	32.09	2.76	14.17	100.18
	BK S3 50-100 cm	25.75	0.06	0.04	25.43	0.04	0.03	0.14	0.01	0.16	32.23	2.81	13.50	100.20
Granite	BK MAT1 0-20 cm	12.56	1.11	0.01	1.43	1.82	0.28	0.02	3.73	0.07	76.45	0.40	1.54	99.42
	BK MAT1 20-50 cm	13.42	1.18	0.01	1.67	1.94	0.31	0.03	3.82	0.07	74.30	0.50	1.89	99.14
	BK MAT2 0-20 cm	11.98	1.14	0.01	1.91	2.00	0.46	0.03	3.38	0.07	76.02	0.52	1.73	99.25
	BK MAT2 20-50 cm	12.96	1.15	0.01	1.77	2.13	0.39	0.02	3.65	0.07	74.77	0.51	1.76	99.19
	BK MAT3 0-20 cm	12.53	1.16	0.01	1.46	1.92	0.26	0.03	3.89	0.07	76.90	0.53	1.27	100.03
	BK MAT3 20-50 cm	13.54	1.15	0.01	1.63	1.98	0.31	0.02	3.75	0.08	75.19	0.47	2.16	100.29
Ark. Sst	BK SA1 0-20 cm	3.46	0.08	0.01	1.30	2.63	0.21	0.01	0.13	0.11	88.11	0.81	2.32	99.18
	BK SA1 20-50 cm	3.81	0.11	0.01	1.36	2.33	0.42	0.03	0.16	0.16	87.66	0.99	2.66	99.55
	BK SA2 0-20 cm	4.97	0.10	0.01	1.41	2.59	0.18	0.01	0.12	0.04	87.28	0.91	1.46	99.08
	BK SA2 20-50 cm	5.10	0.42	0.01	2.20	2.19	0.11	0.01	0.11	0.09	88.01	0.77	1.66	100.68
	BK SA3 0-20 cm	6.28	0.54	0.01	2.24	2.34	0.51	0.03	0.17	0.14	82.00	1.06	4.14	99.46
	BK SA3 20-50 cm	7.16	0.69	0.01	2.51	2.41	0.61	0.03	0.17	0.15	79.48	1.06	5.06	99.34
Gneiss	BK MU1 0-20 cm	15.47	2.72	bdl	7.31	1.28	1.19	0.09	4.28	0.19	61.87	1.56	3.65	99.61
	BK MU2 0-20 cm	16.10	3.46	bdl	6.62	1.41	1.10	0.03	6.31	0.14	60.30	1.31	3.10	99.88
	BK MU3 0-20 cm	14.40	2.93	bdl	7.03	1.33	1.26	0.07	5.41	0.10	62.10	1.47	3.80	99.90
Quartzite	BK CMA 0-20 cm	3.44	0.04	0.01	1.12	0.35	0.15	0.01	bdl	0.04	92.18	0.43	2.06	99.83
	BK CMA 20-50 cm	3.75	0.04	0.01	1.46	0.33	0.15	0.01	bdl	0.04	91.12	0.47	2.26	99.64
Duplicate	BK DS1 0-20 cm	23.51	0.11	0.03	22.31	0.31	0.17	0.17	0.02	0.16	35.32	2.27	16.11	100.49

Soils developed from quartzite (control) had SiO₂ concentrations ranging between 91.12 and 92.18 wt % and Al₂O₃ concentrations from 3.44 to 3.75 wt %. Fe₂O₃ and TiO₂ concentrations ranged from 1.12 to 1.46 wt % and 0.43 to 0.47 wt %, respectively. The concentration of K₂O, CaO, Cr₂O₃, MnO, MgO and P₂O₅ were generally below 0.5 wt %. The LOI were between 2.06 and 2.26 wt % while Na₂O was below detection limit (Table 4.16).

4.3.2.2 Trace Elements

- **Compatible Trace Elements (Sc, V, Cr, Co, and Ni)**

The values obtained for Sc, V, Cr, Co, and Ni in the bulk soils developed from basalt ranged from 49.24 to 59.95 ppm, 414.50 to 538.65 ppm, 232.75 to 300.75 ppm, 48.35 to 69.45 ppm, and 103.80 to 144.95 ppm respectively. For the soils developed on granite, Sc, V, Cr, Co, and Ni concentrations varied from 6.58 to 7.97 ppm, 25.07 to 35.18 ppm, 63.45 to 89.90 ppm, 2.55 to 4.48 ppm, and 21.95 to 34.05 ppm, respectively (Table 4.17).

The Sc, V, Cr, Co, and Ni concentrations in the studied bulk soils developed from arkosic sandstone ranged from 8.06 to 11.2 ppm, 37.46 to 64.60 ppm, 100.15 to 136.05 ppm, 3.43 to 9.11 ppm, and 25.11 to 49.85 ppm, respectively (Table 4.17).

Soils developed from gneiss had Sc, V, Cr, Co, and Ni values between 15.10 and 16.20 ppm, 131.30 and 136.9 ppm, 40.10 and 41.02 ppm, 16.42 and 17.68 ppm, 30.88 and 31.55 ppm, respectively. In soils developed from quartzite (control), the Sc, V, Cr, Co, and Ni concentrations ranged from 7.42 to 8.02 ppm, 33.70 to 41.60 ppm, 47.10 to 58.40 ppm, 1.99 to 2.24 ppm, and 17.90 to 18.40 ppm, respectively (Table 4.17).

- **Incompatible Trace Elements (Rb, Sr, Y, Zr, Nb, Ba, Th, and U)**

The concentrations of Rb, Sr, Y, Th, Nb and U in bulk soils developed from basalt were generally less than 50 ppm whereas, Zr and Ba values were more than 50 ppm. In the studied bulk soils developed from granite, the concentrations of Rb (except in MAT2), Y, Nb, Th, U were generally less than 50 ppm whereas Sr, Zr, and Ba were more than 50 ppm (Table 4.17).

In soils developed from arkosic sandstone, the concentrations of Rb, Sr, Zr and Ba were generally more than 50 ppm whereas, Y, Nb, Th, and U were less than 50 ppm (Table 4.17).

The values obtained for Sr, Zr, and Ba were more than 50 ppm whereas, Rb, Y, Nb, Th, and U were below 50 ppm in the soils developed from gneiss. In soils developed from quartzite (control), the Rb, Sr, Y, Zr, Nb, Ba, Th, and U concentrations were generally less than 50 ppm whereas, Zr and Ba were more than 50 ppm (Table 4.17).

4.3.2.3 Rare Earth Elements (REEs)

- **Light REEs (LREE) (La, Ce, Pr, Nd, Sm, Eu)**

The concentrations of La, Ce, Pr, Nd, Sm and Eu in bulk soils developed from basalt ranged from 8.96 to 17.02 ppm, 35.25 to 64.55 ppm, 2.31 to 5.02 ppm, 9.78 to 20.84 ppm, 2.40 to 4.88 ppm and 0.75 to 1.70 ppm respectively. In the bulk soils developed on granite, La, Ce, Pr, Nd, Sm and Eu concentrations varied from 19.76 to 33.38 ppm, 38.55 to 68.30 ppm, 4.36 to 7.44 ppm, 14.46 to 26.35 ppm, 2.54 to 4.88 ppm, and 0.60 to 0.84 ppm respectively (Table 4.18).

Bulk soils developed from arkosic sandstone had La, Ce, Pr, Nd, Sm and Eu concentrations ranging from 32.89 to 56.25 ppm, 66.70 to 115.50 ppm, 7.94 to 13.30 ppm, 28.25 to 50.70 ppm, 4.51 to 8.81 ppm, and 0.66 to 1.06 ppm, respectively.

The values obtained for La, Ce, Pr, Nd, Sm and Eu in the bulk soils developed from gneiss were between 21.74 to 22.10 ppm, 42.31 to 44.10 ppm, 4.63 to 6.13 ppm, 22.86 to 23.73 ppm, 4.18 to 5.61 ppm, and 1.37 to 1.71 ppm, respectively. In soils developed from quartzite, the La, Ce, Pr, Nd, Sm and Eu concentrations varied from 8.58 to 9.26 ppm, 17.14 to 19.38 ppm, 1.93 to 2.10 ppm, 7.20 to 7.31 ppm, 1.59 to 1.68 ppm and 0.35 to 0.4 ppm, respectively.

- **Heavy REEs (HREE) (Gd, Tb, Dy, Ho, Er, Tm, Yb, Lu)**

The concentrations of HREE in the studied bulk soils developed from the different parent rocks were generally less than 10 ppm (Table 4.18).

Table 4.17: Trace element concentrations (ppm) in bulk soils.

Parent Rocks	Sample ID	Sc	V	Cr	Co	Ni	Cu	Zn	Rb	Sr	Y	Zr	Nb	Mo	Cs	Ba	Hf	Ta	Pb	Th	U
Basalt	BK S1 0-20 cm	55.4	477.55	235.05	53.47	105.3	248.55	85.15	34.62	12.78	26.37	206.1	11.69	1.21	1.49	104.5	5.86	0.68	9.95	6.48	1.33
	BK S1 20-50 cm	55.3	463.95	236.3	48.35	108.95	252.75	83.7	36.1	10.5	21.17	194.7	11.13	4.56	1.62	83.85	5.39	0.67	9.72	6.05	1.36
	BK S1 50-100 cm	57.2	471.45	232.75	56	103.8	248.3	77.9	36.05	8.995	23.04	200.2	11.43	1	1.63	77.55	5.65	0.71	9.22	6.44	1.36
	BK S2 0-20 cm	49.3	417.4	284.7	69.45	132.7	243.7	91.85	12.15	18.77	25.33	167.1	9.105	0.88	0.74	151.7	4.37	0.56	18.1	4.59	1.15
	BK S2 20-50 cm	50.1	426.05	300.75	55.32	144.95	271.25	79.1	9.11	11.5	18.76	161	8.85	1.08	0.62	108.4	4.28	0.46	7.64	4.57	1.01
	BK S2 50-100 cm	49.2	414.5	265.65	53.05	137.3	270.65	75.7	7.95	11.31	16.86	158.3	8.975	0.7	0.61	102.7	4.39	0.49	8.12	4.53	0.95
	BK S3 0-20 cm	59.6	518.8	268.4	60.6	132.6	286.65	79.2	5.23	9.735	25.9	249	14.37	1.26	0.62	67	6.77	0.8	11.2	7.43	1.46
	BK S3 20-50 cm	60	524.3	270.15	57.83	128.4	289.6	83.4	4.355	9.135	23.41	256.9	14.91	1.23	0.59	57.95	6.57	0.81	12.6	7.63	1.38
BK S3 50-100 cm	59.8	538.65	275.45	54.48	135.1	292.6	79.25	3.855	8.065	22.21	258.7	14.99	1.32	0.47	53.7	6.95	0.92	11	7.45	1.51	
Granite	BK MAT1 0-20 cm	6.91	25.1	63.45	3.555	25.35	11.75	19.4	43.2	389.2	6.75	211.1	5.255	0.44	0.96	772.3	5.24	0.3	17.6	3.74	0.69
	BK MAT1 20-50 cm	7.21	27.645	73.05	4.165	29.5	14.45	24.55	45.9	417.2	9.735	322.1	6.385	0.34	1.05	880.5	8.09	0.38	19.5	4.8	1.13
	BK MAT2 0-20 cm	7.97	35.175	89.9	4.475	34.05	13.91	20.6	49.7	358.2	9.595	288.8	7.075	0.38	1.1	886.5	7.17	0.38	17.9	8.41	0.93
	BK MAT2 20-50 cm	7.53	30.16	85.9	3.485	28.55	13.455	22.4	52.15	396	8.47	341.5	6.295	0.49	1.03	959	8.54	0.33	18.5	5.04	0.98
	BK MAT3 0-20 cm	6.58	25.07	66.8	2.545	21.95	10.555	21.2	41.85	410.2	7.81	402	6.35	0.41	0.9	832.5	10.1	0.4	17.6	4.8	0.91
	BK MAT3 20-50 cm	6.88	27.515	75.75	3.2	31.7	12.65	23.9	47.7	412.9	8.02	287.2	6.045	0.62	1.24	868.5	7.6	0.37	17.9	5.42	0.96
Ark. Sst.	BK SA1 0-20 cm	9.11	37.46	111.21	4.36	28.71	18.92	23.17	78.36	82.61	19.46	532.1	9.55	0.71	1.22	637.1	13.4	0.66	19.2	17.2	2.47
	BK SA 20-50 cm	10.2	40.11	130.17	6.37	26.98	16.55	26.41	80.11	84.18	17.88	576.3	10.26	0.77	1.46	651.3	14.3	0.71	21.2	18.2	2.18
	BK SA2 0-20 cm	8.06	42.6	100.15	3.425	26.15	20.215	19.25	84.65	80.85	15.84	517.4	10.24	0.66	1.04	685.5	13	0.7	18.5	14.4	2.12
	BK SA2 20-50 cm	9.21	47.33	107.31	5.37	25.11	18.19	23.33	86.1	81.36	11.31	547.1	11.01	0.61	1.24	688.1	14.3	0.62	18.1	15.4	2.33
	BK SA3 0-20 cm	10.3	57	127.45	7.99	48.2	23.205	37.35	79.4	90.8	31.22	586.4	12.34	0.66	1.32	601.6	15.3	0.88	20.5	23.2	3.31
	BK SA3 20-50 cm	11.2	64.6	136.05	9.105	49.85	17.9	43.95	82.85	95.75	20.95	661.4	12	0.73	1.47	629	17	0.84	22.9	24.2	2.95
Gneiss	BK MU1 0-20 cm	15.7	136.9	40.985	17.68	31.55	23.34	92.45	38.1	586.9	21.35	185.2	8.99	0.61	1.48	570.3	5.04	0.48	13.8	2.52	0.47
	BK MU2 0-20 cm	15.1	133.1	40.1	17.21	30.88	23.88	92.51	37.62	581.2	22.1	187.1	7.81	0.72	1.3	560.1	5.24	0.56	13.1	2.51	0.61
	BK MU3 0-20 cm	16.2	131.3	41.02	16.42	31.01	22.33	91.01	38.51	580.2	20.1	180.1	8.5	0.52	1.68	577.2	4.78	0.33	14.3	2.72	0.77
Quartzite	BK CMA 0-20 cm	7.42	33.7	47.1	1.985	18.4	11.185	15.1	22.5	11.39	6.63	229.9	4.125	0.18	0.64	89.85	6.12	0.33	6.23	4.47	1
	BK CMA 20-50 cm	8.02	41.6	58.4	2.24	17.9	14.35	15.9	21.07	10.62	7.745	270	4.835	0.43	0.76	83.3	6.81	0.35	5.64	4.85	1.15

Table 4.18: Rare earth element concentrations (ppm) in bulk soils.

Parent Rocks	Values in ppm	La	Ce	Pr	Nd	Sm	Eu	Gd	Tb	Dy	Ho	Er	Tm	Yb	Lu
Basalt	BK S1 0-20 cm	17.02	53.08	4.92	20.51	4.88	1.70	4.99	0.82	5.41	1.02	3.21	0.48	3.11	0.46
	BK S1 20-50 cm	13.38	54.60	3.90	16.19	3.87	1.18	4.16	0.64	4.31	0.90	2.63	0.39	2.50	0.40
	BK S1 50-100 cm	14.58	55.52	4.34	18.07	4.24	1.18	4.51	0.75	4.84	0.93	3.02	0.47	2.99	0.46
	BK S2 0-20 cm	13.45	42.22	3.90	15.99	4.16	1.19	4.36	0.75	4.74	1.02	3.04	0.46	3.23	0.44
	BK S2 20-50 cm	9.38	36.44	2.45	10.32	2.47	0.77	2.98	0.53	3.33	0.70	2.29	0.37	2.37	0.36
	BK S2 50-100 cm	8.96	35.25	2.31	9.78	2.40	0.75	2.51	0.43	3.04	0.66	2.08	0.29	2.44	0.35
	BK S3 0-20 cm	16.29	61.00	5.02	20.84	4.68	1.36	5.61	0.88	5.59	1.10	3.35	0.48	3.49	0.48
	BK S3 20-50 cm	14.58	63.80	4.51	19.39	4.58	1.38	4.62	0.82	5.15	0.99	3.24	0.48	3.68	0.52
	BK S3 50-100 cm	13.39	64.55	4.15	17.59	4.25	1.19	4.56	0.72	4.79	0.91	3.02	0.46	3.22	0.46
Granite	BK MAT1 0-20 cm	19.76	38.55	4.36	14.46	2.54	0.63	2.09	0.23	1.36	0.26	0.77	0.10	0.76	0.08
	BK MAT1 20-50 cm	25.80	49.48	5.49	19.95	3.57	0.72	2.64	0.39	1.78	0.36	1.00	0.12	0.98	0.15
	BK MAT2 0-20 cm	33.38	68.30	7.44	26.35	4.88	0.84	2.96	0.36	1.95	0.37	0.89	0.13	0.93	0.14
	BK MAT2 20-50 cm	23.81	47.93	5.44	19.20	3.28	0.60	2.37	0.31	1.58	0.30	0.81	0.13	0.73	0.15
	BK MAT3 0-20 cm	22.18	42.86	4.74	16.62	2.70	0.47	1.93	0.25	1.48	0.24	0.67	0.11	0.77	0.13
	BK MAT3 20-50 cm	25.08	49.09	5.56	19.92	3.43	0.72	2.42	0.31	1.53	0.27	0.75	0.12	0.73	0.09
Ark. Sst.	BK SA1 0-20	42.11	98.31	11.71	38.31	7.56	0.81	6.51	0.78	5.71	0.76	2.88	0.19	2.31	0.63
	BK SA1 20-50	44.71	101.51	12.32	42.53	7.77	0.86	6.10	0.83	4.88	0.84	2.81	0.23	2.01	0.41
	BK SA2 0-20 cm	32.89	66.70	7.94	28.25	4.83	0.66	4.01	0.45	2.82	0.47	1.63	0.21	1.92	0.24
	BK SA2 20-50	37.11	71.33	8.56	31.71	4.51	0.69	3.97	0.61	2.91	0.41	1.51	0.31	1.81	0.14
	BK SA3 0-20 cm	51.42	108.30	12.75	46.75	8.81	0.99	6.24	0.90	5.48	0.93	3.00	0.41	2.84	0.57
	BK SA3 20-50 cm	56.25	115.50	13.31	50.70	8.55	1.06	6.27	0.81	4.46	0.80	2.09	0.30	1.79	0.27
Gneiss	BK MU1 0-20 cm	21.74	43.64	5.73	23.19	4.75	1.56	5.02	0.62	3.85	0.84	2.27	0.28	1.96	0.35
	BK MU2 0-20 cm	21.86	44.10	6.13	22.86	4.18	1.71	4.96	0.44	3.77	0.71	2.41	0.41	1.91	0.38
	BK MU3 0-20 cm	22.10	42.31	4.63	23.73	5.61	1.37	5.77	0.76	3.91	0.66	2.61	0.33	1.86	0.46
Quartzite	BK CMA 0-20 cm	8.58	17.14	1.93	7.20	1.59	0.35	1.18	0.13	1.05	0.28	0.73	0.09	0.70	0.10
	BK CMA 20-50 cm	9.26	19.38	2.10	7.31	1.68	0.42	1.41	0.25	1.28	0.24	0.86	0.15	1.12	0.16

4.3.3 Geochemical Properties of the Silt fractions of the studied Soils

4.3.3.1 Major Element Oxides

The silt fractions of soils developed from basalt had SiO_2 concentrations varying between 36.83 and 38.39 wt % and Al_2O_3 concentrations from 22.53 to 25.14 wt %. Fe_2O_3 and TiO_2 concentrations ranged from 20.72 to 21.64 wt % and 1.88 to 2.02 wt %, respectively. The concentrations of K_2O , CaO , Cr_2O_3 , Na_2O , MnO , and P_2O_5 were generally below 0.5 wt %. The LOI were between 13.85 and 16.33 wt % (Table 4.19).

The silt fractions of soils developed from granite had SiO_2 concentrations ranging between 70.03 and 70.92 wt % and Al_2O_3 concentrations from 14.58 to 15.24 wt %. Fe_2O_3 , CaO and Na_2O concentrations ranged from 2.19 to 2.25 wt %, 1.39 to 1.60 wt % and 3.96 to 4.27 wt %, respectively. The concentration of K_2O varied from 2.48 to 2.53 wt % whereas, the concentrations of TiO_2 varied from 0.91 to 1.22 wt %. Cr_2O_3 , MnO , MgO and P_2O_5 were generally below 0.7 wt %. The LOI were between 1.06 and 2.21 wt % (Table 4.19).

The silt fractions of soils developed from arkosic sandstone had SiO_2 concentrations between 71.04 and 73.94 wt % and Al_2O_3 concentrations from 8.90 to 10.23 wt %. Fe_2O_3 , K_2O and TiO_2 concentrations ranged from 3.40 to 3.56 wt %, 3.40 to 3.56 wt %, and 1.97 to 2.28 wt %, respectively. CaO , Cr_2O_3 , Na_2O , MnO , MgO and P_2O_5 were generally below 1.00 wt %. The LOI were between 5.21 and 6.58 wt % (Table 4.19).

The silt fraction of soil developed from gneiss had SiO_2 concentration of 51.70 wt % and Al_2O_3 concentration of 17.48 wt %. Fe_2O_3 , MgO and TiO_2 concentrations were 11.13, 1.50 and 3.10 wt %, respectively. K_2O had a concentration of 1.61 wt % whereas, Na_2O and CaO have concentrations of 3.55 and 2.80 wt %, respectively. The concentrations of MnO , and P_2O_5 were generally below 0.50 wt %. Cr_2O_3 was not detected and the LOI value was 6.30 wt % (Table 4.19).

The silt fractions of soils developed from quartzite had SiO_2 concentrations ranging between 87.86 and 91.53 wt % and Al_2O_3 concentrations from 3.81 to 5.20 wt %. Fe_2O_3 and TiO_2 concentrations ranged from 1.19 to 1.76 wt % and 0.49 to 0.68 wt %, respectively.

respectively. The concentrations of K_2O , CaO , Cr_2O_3 , MnO , MgO and P_2O_5 were generally below 0.5 wt %. The LOI were between 1.99 and 3.32 wt % while Na_2O was below detection limit (Table 4.19).

4.3.3.2 Trace Elements

- **Compatible Trace Elements (Sc, V, Cr, Co, and Ni)**

The values obtained for Sc, V, Cr, Co, and Ni in the silt fractions of soils developed from basalt ranged from 48.46 to 49.95 ppm, 422.25 to 427.10 ppm, 282.25 to 313.55 ppm, 53.05 to 64.14 ppm, and 128.95 to 146 ppm, respectively. In the silt fractions of soils developed on granite, Sc, V, Cr, Co, and Ni concentrations varied from 9.77 to 10.56 ppm, 38.61 to 43.10 ppm, 113.50 to 137.30 ppm, 4.99 to 5.55 ppm, and 43.5 to 48.95 ppm, respectively (Table 4.20).

The Sc, V, Cr, Co, and Ni concentrations in the silt fractions of soils developed from arkosic sandstone ranged from 14.54 to 14.72 ppm, 97.39 to 101 ppm, 215.9 to 219.2 ppm, 11.38 to 12.56 ppm, and 65.6 to 70.85 ppm, respectively (Table 4.20).

The values obtained for Sc, V, Cr, Co, and Ni in the silt fractions of soils developed from gneiss are 18.16, 205.35, 60.9, 27.29, 51.10 ppm, respectively.

In silt fractions of soils developed from quartzite, the Sc, V, Cr, Co, and Ni concentrations were between 8.58 and 9.91 ppm, 36.4 and 54.1 ppm, 39.55 and 72.1 ppm, 2.10 and 3.10 ppm, 18.6 and 25.15 ppm, respectively (Table 4.20).

- **Incompatible Trace Elements (Rb, Sr, Y, Zr, Nb, Ba, Th, and U)**

The concentrations of Rb, Sr, Y, Nb, Th, and U in the silt fractions of soils developed from basalt and quartzite (control) were generally less than 50 ppm whereas, Zr and Ba values were more than 50 ppm (Table 4.20).

In the studied silt fractions of soils developed from granite, arkosic sandstone, and gneiss, the concentrations of Rb, Sr, Zr, and Ba were generally more than 50 ppm whereas, Y, Nb, Th (except for SA3 0-20 cm), and U were less than 50 ppm (Table 4.20).

Table 4.19: Major element oxide concentrations (wt %) in the silt fractions of the studied soils.

Parent Rocks	Sample ID	Al ₂ O ₃	CaO	Cr ₂ O ₃	Fe ₂ O ₃	K ₂ O	MgO	MnO	Na ₂ O	P ₂ O ₅	SiO ₂	TiO ₂	L.O.I.	Sum of Conc.
Basalt	ST S2 0-20 cm	22.53	0.23	0.05	20.72	0.18	0.22	0.18	0.08	0.17	37.32	2.02	16.33	100.03
	ST S2 20-50 cm	25.14	0.13	0.04	21.64	0.10	0.18	0.16	0.01	0.13	36.83	1.95	14.26	100.57
	ST S2 50-100 cm	24.71	0.09	0.04	21.35	0.07	0.17	0.17	0.02	0.12	38.39	1.88	13.85	100.86
Granite	ST MAT1 0-20 cm	14.58	1.60	0.01	2.19	2.53	0.59	0.05	4.27	0.08	70.92	1.22	1.06	99.10
	ST MAT1 20-50 cm	15.24	1.39	0.01	2.25	2.48	0.51	0.04	3.96	0.09	70.03	0.91	2.21	99.12
Ark. Sst.	ST SA3 0-20 cm	8.90	0.77	0.01	3.34	3.40	0.75	0.04	0.28	0.19	73.94	2.28	5.21	99.11
	ST SA3 20-50 cm	10.23	0.99	0.01	3.56	3.56	0.91	0.05	0.29	0.20	71.04	1.97	6.58	99.39
Gneiss	ST MU1 0-20 cm	17.48	2.80	0.00	11.13	1.61	1.50	0.14	3.55	0.34	51.70	3.10	6.30	99.65
Quartzite	ST CMA 0-20 cm	3.81	0.04	0.01	1.19	0.36	0.15	0.01	bdl	0.04	91.53	0.49	1.99	99.62
	ST CMA 20-50 cm	5.20	0.05	0.01	1.76	0.44	0.17	0.01	bdl	0.05	87.86	0.68	3.32	99.55

Table 4.20: Trace element concentrations (ppm) in the silt fractions of the studied soils.

Parent Rocks	Sample ID	Sc	V	Cr	Co	Ni	Cu	Zn	Rb	Sr	Y	Zr	Nb	Mo	Cs	Ba	Hf	Ta	Pb	Th	U
Basalt	ST S2 0-20 cm	49.95	423.05	313.55	64.14	137.30	242.70	94.35	13.20	20.48	26.55	179.95	9.24	0.82	0.69	155.85	5.06	0.52	18.20	4.97	1.12
	ST S2 20-50 cm	48.46	427.10	312.85	53.05	146.00	277.10	75.30	9.08	11.12	18.30	159.90	8.90	1.02	0.61	103.70	4.40	0.49	8.10	4.70	1.01
	ST S2 50-100 cm	49.66	422.25	282.25	53.20	128.95	272.30	77.35	7.47	9.85	16.94	157.20	8.83	0.86	0.65	101.35	4.33	0.54	7.61	4.48	0.99
Granite	ST MAT1 0-20 cm	10.56	43.10	137.30	4.99	48.95	10.49	31.20	55.25	490.20	25.15	1245.50	13.22	0.41	1.01	1161.00	31.17	0.68	24.15	15.99	2.53
	ST MAT1 20-50 cm	9.77	38.61	113.50	5.55	43.50	19.76	32.30	58.65	471.50	15.89	800.95	11.07	0.50	1.37	1170.00	20.61	0.69	25.02	11.51	1.98
Ark. Sst.	ST SA3 0-20 cm	14.72	101.00	215.90	11.38	65.60	23.92	52.60	116.60	138.95	43.40	1820.50	24.59	0.74	1.95	878.50	47.50	1.73	30.39	57.08	6.60
	ST SA3 20-50 cm	14.55	97.39	219.20	12.56	70.85	19.37	58.05	124.15	149.40	30.52	1171.90	21.55	0.73	2.13	921.50	29.31	1.47	31.00	35.26	4.51
Gneiss	ST MU1 0-20 cm	18.16	205.35	60.90	27.29	51.10	54.90	133.65	57.90	530.00	28.79	266.65	17.62	0.63	2.82	770.00	6.92	0.97	16.40	3.36	0.53
Quartzite	ST CMA 0-20 cm	8.58	36.40	39.55	2.10	18.60	14.33	13.10	22.70	13.64	9.26	465.45	5.50	0.46	0.78	97.95	11.89	0.46	6.22	4.96	1.58
	ST CMA 20-50 cm	9.91	54.10	72.10	3.10	25.15	16.25	19.70	28.32	17.25	13.76	623.35	7.81	0.44	1.01	127.75	15.63	0.61	8.25	8.00	2.46

4.3.3.3 Rare Earth Elements (REEs)

- **Light REEs (LREE) (La, Ce, Pr, Nd, Sm, Eu)**

The values obtained for La, Ce, Pr, Nd, Sm and Eu in silt fractions of soils developed from basalt ranged from 8.57 to 14.60 ppm, 35.00 to 42.20 ppm, 2.29 to 3.99 ppm, 9.67 to 16.74 ppm, 2.36 to 4.41 ppm, and 0.65 to 1.35 ppm, respectively. In the silt fractions of soils developed from granite, La, Ce, Pr, Nd, Sm and Eu concentrations varied from 43.50 to 53.00 ppm, 86.60 to 109.00 ppm, 10.30 to 12.80 ppm, 36.34 to 46.35 ppm, 6.51 to 7.98 ppm, and 0.94 to 0.99 ppm, respectively (Table 4.21).

The La, Ce, Pr, Nd, Sm and Eu concentrations in the silt fractions of soils developed from arkosic sandstone ranged from 81.90 to 127.00 ppm, 166.00 to 265.00 ppm, 19.70 to 30.80 ppm, 72.75 to 114.20 ppm, 12.70 to 19.80 ppm and 1.62 to 1.68 ppm, respectively (Table 4.21).

The values obtained for La, Ce, Pr, Nd, Sm and Eu in the silt fraction of soil developed from gneiss are 27.8, 55.9, 7.26, 29.40, 5.74, and 1.98 ppm, respectively. In the silt fractions of soils developed from quartzite, the La, Ce, Pr, Nd, Sm and Eu concentrations varied from 8.38 to 13.60 ppm, 17.10 to 27.90 ppm, 1.94 to 3.08 ppm, 6.34 to 11.08 ppm, 0.92 to 2.21 ppm, and 0.35 to 0.56 ppm, respectively (Table 4.21).

- **Heavy REEs (HREE) (Gd, Tb, Dy, Ho, Er, Tm, Yb, Lu)**

The concentrations of HREE in the studied silt fractions of soils developed from the different parent rocks were generally less than 10 ppm (Table 4.21).

4.3.4 Geochemical Properties of the Clay fractions of the studied Soils

4.3.4.1 Major Element Oxides

The clay fractions of soils developed from basalt had SiO₂ concentrations varying between 36.38 and 38.51 wt % and Al₂O₃ concentrations from 22.87 to 25.01 wt %. Fe₂O₃ and TiO₂ concentrations ranged from 20.79 wt % to 21.85 and 1.90 to 1.98 wt %, respectively.

respectively. The concentrations of K₂O, CaO, Cr₂O₃, Na₂O, MnO, and P₂O₅ were generally below 0.5 wt %. The LOI were between 13.70 and 16.41 wt % (Table 4.22).

The clay fraction of soils developed from granite had SiO₂ concentrations ranging between 64.42 and 64.47 wt % and Al₂O₃ concentrations from 16.79 to 17.11 wt %. Fe₂O₃, CaO and Na₂O concentrations ranged from 3.78 to 3.86 wt %, 1.44 to 1.54 wt % and 3.45 to 3.67 wt %, respectively. The concentration of K₂O varies from 2.37 to 2.41 wt % while the concentration of TiO₂ varies from 1.17 to 1.22 wt %. Cr₂O₃, MnO, MgO and P₂O₅ were generally below 1.00 wt %. The LOI were between 4.35 and 4.55 wt % (Table 4.22).

The clay fraction of soils developed from arkosic sandstone had SiO₂ concentrations varying between 55.79 and 57.38 wt % and Al₂O₃ concentrations from 14.53 to 15.37 wt %. The concentration of K₂O is 3.98 wt %. Fe₂O₃, CaO and TiO₂ concentrations ranged from 5.73 to 5.75 wt %, 1.57 to 1.82 wt % and 1.95 to 2.28 wt %, respectively. Cr₂O₃, Na₂O, MnO, and P₂O₅ were generally below 0.50 wt %. MgO ranged from 1.29 to 1.34 wt % whereas, the LOI were between 5.21 and 6.58 wt % (Table 4.22).

Table 4.21: Rare earth element concentrations (ppm) in the silt fractions of the studied soils.

Parent Rocks	Sample ID	La	Ce	Pr	Nd	Sm	Eu	Gd	Tb	Dy	Ho	Er	Tm	Yb	Lu
Basalt	ST S2 0-20 cm	14.6	42.2	3.99	16.74	4.41	1.35	4.91	0.76	5.14	1.07	3.25	0.44	2.98	0.45
	ST S2 20-50 cm	9.42	35	2.46	10.01	2.69	0.8	2.85	0.51	3.38	0.63	2.26	0.32	2.26	0.35
	ST S2 50-100 cm	8.57	36.1	2.29	9.67	2.36	0.65	2.73	0.49	3.08	0.63	2.19	0.31	2.14	0.31
Granite	ST MAT1 0-20 cm	53	109	12.8	46.35	7.98	0.94	6.12	0.82	4.34	0.83	2.52	0.31	2.67	0.42
	ST MAT1 20-50 cm	43.5	86.6	10.3	36.34	6.51	0.99	4.61	0.56	2.98	0.55	1.71	0.2	1.8	0.28
Ark. Sst.	ST SA3 0-20 cm	127	265	30.8	114.2	19.8	1.62	13.2	1.72	8.6	1.61	4.5	0.57	4.43	0.72
	ST SA3 20-50 cm	81.9	166	19.7	72.75	12.7	1.68	9.41	1.13	6.21	1.03	3.17	0.46	3.16	0.48
Gneiss	ST MU1 0-20 cm	27.8	55.9	7.26	29.4	5.74	1.98	6.06	0.9	5.48	1.06	2.89	0.38	3	0.42
Quartzite	ST CMA 0-20 cm	8.38	17.1	1.94	6.335	0.92	0.35	1.27	0.18	1.27	0.26	1.03	0.12	0.94	0.17
	ST CMA 20-50 cm	13.6	27.9	3.08	11.08	2.21	0.56	1.88	0.34	2.75	0.49	1.53	0.23	1.81	0.26

The clay fraction of soil developed from gneiss had SiO₂ concentration of 50.65 wt % and Al₂O₃ concentration of 18.10 wt %. Fe₂O₃, MgO and TiO₂ concentrations were 11.44, 1.58, and 2.32 wt %, respectively. K₂O and Na₂O have concentrations of 1.63 and 2.95 wt %. The concentration of CaO was 2.63 wt % whereas, MnO, and P₂O₅ were generally below 0.50 wt %. Cr₂O₃ was below detection limit and the LOI value was 6.30 wt % (Table 4.22).

The clay fraction of soils developed from quartzite (control) had SiO₂ concentrations ranging between 76.47 and 78.58 wt % and Al₂O₃ concentrations from 8.74 to 9.59 wt %. Fe₂O₃ and TiO₂ concentrations ranged from 3.10 to 3.80 wt % and 1.52 to 1.54 wt % respectively. The concentration of K₂O ranged from 0.76 to 0.93 wt % whereas, CaO, Na₂O, Cr₂O₃, MnO, MgO and P₂O₅ were generally below 0.5 wt %. The LOI values were between 5.76 and 7.59 wt % (Table 4.22).

4.3.4.2 Trace Elements

- **Compatible Trace Elements (Sc, V, Cr, Co, and Ni)**

The values obtained for Sc, V, Cr, Co, and Ni in the clay fractions of soils developed from basalt ranged from 46.27 to 50.30 ppm, 406.50 to 426.70 ppm, 262.65 to 350.70 ppm, 43.40 to 56.74 ppm, and 126.75 to 140.85 ppm, respectively. In the clay fractions of soils developed from granite, Sc, V, Cr, Co, and Ni concentrations varied from 14.11 to 13.84 ppm, 59.30 to 61.35 ppm, 207.45 to 210.90 ppm, 10.51 to 10.62 ppm, and 64.30 to 64.85 ppm, respectively (Table 4.23).

The Sc, V, Cr, Co, and Ni concentrations in the clay fractions of soils developed from arkosic sandstone ranged from 18.62 to 19.18 ppm, 129.00 to 135.80 ppm, 350.45 to 397.55 ppm, 19.59 to 20.95 ppm, and 109.15 to 113.10 ppm, respectively (Table 4.23).

The values obtained for Sc, V, Cr, Co, and Ni in the clay fraction of soil developed from gneiss were 21.65, 192.00, 73.75, 27.79, and 53.20 ppm, respectively. In the clay fractions of soils developed from quartzite, the Sc, V, Cr, Co, and Ni concentrations varied from 13.35 to 13.45 ppm, 93.85 to 101.90 ppm, 169.15 to 195.80 ppm, 5.89 to 6.03 ppm, and 39.40 to 42.85 ppm, respectively (Table 4.23).

Table 4.22: Major element oxide concentrations (wt %) in the clay fractions of the studied soils.

Parent Rocks	Sample ID	Al ₂ O ₃	CaO	Cr ₂ O ₃	Fe ₂ O ₃	K ₂ O	MgO	MnO	Na ₂ O	P ₂ O ₅	SiO ₂	TiO ₂	L.O.I.	Sum of Conc.
Basalt	CF S2 0-20 cm	22.87	0.20	0.04	20.79	0.17	0.21	0.17	0.06	0.18	37.47	1.98	16.41	100.55
	CF S2 20-50 cm	25.01	0.12	0.05	21.85	0.11	0.17	0.14	0.01	0.13	36.38	1.97	14.40	100.34
	CF S2 50-100 cm	24.83	0.09	0.04	21.04	0.07	0.18	0.16	0.03	0.12	38.51	1.90	13.70	100.67
Granite	CF MAT1 0-20 cm	16.79	1.54	0.02	3.78	2.41	0.84	0.06	3.67	0.13	64.42	1.22	4.35	99.23
	CF MAT1 20-50 cm	17.11	1.44	0.03	3.86	2.37	0.83	0.06	3.45	0.12	64.47	1.17	4.55	99.46
Ark. Sst.	CF SA3 0-20 cm	14.53	1.57	0.05	5.73	3.98	1.29	0.07	0.44	0.31	57.38	2.28	12.24	99.87
	CF SA3 20-50 cm	15.37	1.82	0.04	5.75	3.98	1.34	0.08	0.39	0.33	55.79	1.95	13.43	100.27
Gneiss	CF MU1 0-20 cm	18.10	2.63	bdl	11.44	1.63	1.58	0.12	2.95	0.42	50.65	2.32	8.01	99.85
Quartzite	CF CMA 0-20 cm	9.59	0.11	0.02	3.10	0.93	0.29	0.03	0.08	0.09	76.47	1.54	7.59	99.84
	CF CMA 20-50 cm	8.74	0.11	0.02	3.80	0.76	0.23	0.03	0.10	0.09	78.58	1.52	5.76	99.74

Table 4.23: Trace element concentrations (ppm) in the clay fractions of the studied soils.

Parent Rocks	Sample ID	Sc	V	Cr	Co	Ni	Cu	Zn	Rb	Sr	Y	Zr	Nb	Mo	Cs	Ba	Hf	Ta	Pb	Th	U
Basalt	CF S2 0-20 cm	46.27	406.5	300.25	56.74	126.75	229.3	89.95	13.27	18.45	25.68	171.85	8.34	1.02	0.74	147.2	4.605	0.55	16.64	4.76	1.09
	CF S2 20-50 cm	49.75	426.7	350.7	43.4	140.85	290.6	78.05	9.46	11.01	18.22	163	9.04	0.85	0.67	107.7	4.515	0.53	7.47	4.6	0.99
	CF S2 50-100 cm	50.3	407.7	262.65	43.94	133.75	260.65	78.1	7.15	9.97	17.16	164	8.79	0.77	0.58	99.35	4.525	0.53	7.1	4.48	1.04
Granite	CF MAT1 0-20 cm	13.84	61.35	207.45	10.62	64.3	27.5	52.45	70.3	414.8	28.65	1237	15.4	0.66	2.1	1014.5	30.72	0.83	25.85	12.7	2.87
	CF MAT1 20-50 cm	14.11	59.3	210.9	10.51	64.85	23.935	51.1	71.55	401.6	27.53	1064	15	0.83	2.24	1046.5	26.42	0.83	25.65	11.7	2.5
Ark. Sst.	CF SA3 0-20 cm	19.18	135.8	397.55	19.59	113.1	32.4	88.55	141.5	181.9	40.66	874	26	0.9	3.16	1049.5	22.92	1.86	34.79	26.2	4.45
	CF SA3 20-50 cm	18.62	129	350.45	20.95	109.15	27.83	91.35	145.4	186.85	34.91	609.1	25.3	0.85	3.21	1082	16.22	1.62	35.7	19.6	3.52
Gneiss	CF MU1 0-20 cm	21.65	192	73.75	27.79	53.2	39.05	132.4	59.7	462.3	34.97	316.1	14.4	0.55	2.86	805	8.625	0.73	18.19	4.53	0.76
Quartzite	CF CMA 0-20 cm	13.45	93.85	169.15	5.89	39.4	20.705	33.3	58.45	34.645	20.1	714.35	15.9	0.92	1.85	245.45	18.7	1.21	16.46	15.2	3.43
	CF CMA 20-50 cm	13.35	101.9	195.8	6.03	42.85	27.1	29.5	45.35	32.85	21.12	766.55	15.6	0.84	1.57	207.25	20.26	1.23	14.15	15.3	3.5

- **Incompatible Trace Elements (Rb, Sr, Y, Zr, Nb, Ba, Th, and U)**

The concentrations of Rb, Sr, Y, Th, Nb and U in clay fractions of soils developed from basalt and quartzite (control) were generally less than 50ppm (except for Rb in CMA 0-20 cm) whereas, Zr and Ba values were more than 50 ppm (Table 4.23).

In the studied clay fractions of soils developed from granite, arkosic sandstone, and gneiss, the concentrations of Y, Nb, Th, U were generally less than 50 ppm whereas, Rb, Sr, Zr, and Ba were more than 50 ppm (Table 4.23).

4.3.4.3 Rare Earth Elements (REEs)

- **Light REEs (LREE) (La, Ce, Pr, Nd, Sm, Eu)**

The values obtained for La, Ce, Pr, Nd, Sm and Eu in clay fractions of soils developed from basalt ranged from 8.44 to 14.52 ppm, 32.21 to 40.41 ppm, 2.34 to 3.77 ppm, 9.42 to 16.65 ppm, 2.27 to 4.05 ppm, and 0.75 to 1.30 ppm, respectively. In the clay fractions of soils developed from granite, La, Ce, Pr, Nd, Sm and Eu concentrations varied from 55.30 to 57.17 ppm, 106.80 to 113.90 ppm, 12.53 to 13.64 ppm, 46.70 to 48.65 ppm, 8.20 to 8.94 ppm, and 1.45 to 1.49 ppm, respectively (Table 4.24).

The La, Ce, Pr, Nd, Sm and Eu concentrations in the clay fraction of soils developed from arkosic sandstone ranged from 56.97 to 69.70 ppm, 111.90 to 140.50 ppm, 13.66 to 16.82 ppm, 52.30 to 63.15 ppm, 9.26 to 11.40 ppm, and 2.09 to 2.16 ppm, respectively (Table 4.24).

The values obtained for La, Ce, Pr, Nd, Sm and Eu in the clay fraction of soil developed from gneiss were 35.38, 70.24, 9.45, 39.00, 8.03, and 2.58 ppm, respectively. In clay fractions of soils developed quartzite (control), the La, Ce, Pr, Nd, Sm and Eu concentrations varied from 25.91 to 26.56 ppm, 53.36 to 56.50 ppm, 5.54 to 6.14 ppm, 21.26 to 22.70 ppm, 4.27 to 4.38 ppm, and 0.84 to 0.95 ppm, respectively.

- **Heavy REEs (HREE) (Gd, Tb, Dy, Ho, Er, Tm, Yb, Lu)**

The concentrations of HREE in the studied clay fractions of soils developed from the different parent rocks were generally less than 10 ppm (Table 4.24).

Table 4.24: Rare earth element concentrations (ppm) in the clay fractions of the studied soils.

Parent Rocks	Sample ID	La	Ce	Pr	Nd	Sm	Eu	Gd	Tb	Dy	Ho	Er	Tm	Yb	Lu
Basalt	CF S2 0-20 cm	14.52	40.41	3.77	16.65	4.05	1.3	4.56	0.77	4.94	1.04	2.86	0.42	3.13	0.46
	CF S2 20-50 cm	9.21	32.21	2.45	10.69	2.44	0.76	2.84	0.47	3.41	0.66	2.3	0.32	2.17	0.34
	CF S2 50-100 cm	8.44	33.41	2.34	9.42	2.27	0.75	2.55	0.43	3.08	0.66	2.11	0.3	2.41	0.35
Granite	CF MAT1 0-20 cm	57.17	113.9	13.64	48.65	8.94	1.45	7.11	0.91	5.02	0.98	2.94	0.42	3.21	0.51
	CF MAT1 20-50 cm	55.3	106.8	12.53	46.7	8.2	1.49	6.49	0.84	4.77	1	2.77	0.41	3.06	0.45
Ark. Sst.	CF SA3 0-20 cm	69.7	140.5	16.82	63.15	11.4	2.16	9.63	1.19	7.65	1.42	4.32	0.56	4.44	0.64
	CF SA3 20-50 cm	56.97	111.9	13.66	52.3	9.26	2.09	8.66	1.16	6.78	1.22	3.55	0.52	3.65	0.5
Gneiss	CF MU1 0-20 cm	35.38	70.24	9.45	39	8.03	2.58	7.87	1.16	6.85	1.32	3.76	0.5	3.47	0.5
Quartzite	CF CMA 0-20 cm	25.91	53.36	5.54	21.26	4.38	0.84	3.9	0.58	3.68	0.78	2.38	0.36	2.46	0.4
	CF CMA 20-50 cm	26.56	56.5	6.14	22.7	4.27	0.95	3.88	0.65	3.9	0.75	2.41	0.35	2.55	0.43

4.3.5 Geochemical Properties of Soil Kaolins

4.3.5.1 Major Element Oxides

The soil kaolins developed from basalt had SiO₂ concentrations varying between 32.74 and 39.51 wt % and Al₂O₃ concentrations from 23.18 to 25.82 wt %. Fe₂O₃, Na₂O and TiO₂ concentrations ranged from 14.68 to 20.50 wt %, 1.55 to 2.15 wt %, and 1.90 to 2.84 wt %, respectively. The concentrations of K₂O, CaO, Cr₂O₃, MnO, and P₂O₅ were generally below 0.5 wt %. The LOI values were between 16.28 and 19.53 wt % (Table 4.25).

The soil kaolins developed from granite had SiO₂ concentrations ranging between 62.17 and 65.91 wt % and Al₂O₃ concentrations from 15.80 to 16.35 wt %. Fe₂O₃, CaO and Na₂O concentrations ranged from 2.64 to 3.40 wt %, 1.30 to 1.71 wt %, and 4.38 to 4.94 wt %, respectively. The concentration of K₂O, MgO, TiO₂ varied from 2.26 to 2.57 wt %, 0.85 to 1.32 wt %, and 1.23 to 1.40 wt %, respectively. Cr₂O₃, MnO, and P₂O₅ were generally below 0.50 wt %. The LOI values were between 3.80 and 6.96 wt % (Table 4.25).

The soil kaolins developed from arkosic sandstone had SiO₂ concentrations varying between 55.18 and 66.73 wt % and Al₂O₃ concentrations from 12.51 to 15.46 wt %. The

concentration of K_2O varied from 3.95 to 4.57 wt % whereas, MgO ranged from 0.46 to 1.20 wt %. Fe_2O_3 , CaO and TiO_2 concentrations ranged from 3.42 to 4.45 wt %, 0.39 to 0.81 wt %, and 2.13 to 2.68 wt %, respectively. Cr_2O_3 , MnO , and P_2O_5 were generally below 0.50 wt %. Na_2O concentration varied from 2.06 to 2.72 wt % and LOI values were between 6.18 and 13.45 wt % (Table 4.25).

The soil kaolins developed from gneiss had SiO_2 concentration of 52.66 wt % and Al_2O_3 concentration of 18.44 wt %. Fe_2O_3 , MgO and TiO_2 concentrations were 8.08, 1.20, and 1.89 wt % respectively. K_2O had a concentration of 1.79 wt % whereas, Na_2O had a concentration of 5.27 wt %. The concentration of CaO was 2.04 wt % with MnO , and P_2O_5 concentrations below 0.50 wt %. Cr_2O_3 was below detection limit and the LOI value was 7.82 wt % (Table 4.25).

The soil kaolins developed from quartzite (control) had SiO_2 concentrations ranging between 77.22 and 73.51 wt % and Al_2O_3 concentrations from 8.37 to 9.68 wt %. Fe_2O_3 , Na_2O and TiO_2 concentrations ranged from 2.17 to 2.29 wt %, 1.36 to 1.64 wt %, and 1.41 to 1.48 wt %, respectively. The concentration of K_2O ranged from 0.80 to 0.96 wt % and CaO , Cr_2O_3 , MnO , MgO and P_2O_5 were generally below 0.5 wt %. The LOI values were between 7.60 and 9.67 wt % (Table 4.25).

4.3.5.3 Trace Elements

- **Compatible Trace Elements (Sc, V, Cr, Co, and Ni)**

The values obtained for Sc, V, Cr, Co, and Ni in soil kaolins developed from basalt ranged from 38.31 to 47.70 ppm, 248.55 to 381.20 ppm, 187.80 to 361.20 ppm, 16.58 to 34.57 ppm, and 113.70 to 159.45 ppm, respectively. In the soil kaolins developed from granite, Sc, V, Cr, Co, and Ni concentrations varied from 8.67 to 11.54 ppm, 42.34 to 59.56 ppm, 177.05 to 229.90 ppm, 6.65 to 10.49 ppm, and 58.2 to 92.55 ppm, respectively (Table 4.26).

The Sc, V, Cr, Co, and Ni concentrations in the soil kaolins developed from arkosic sandstone ranged from 12.86 to 15.78 ppm, 106.25 to 110.85 ppm, 350.60 to 437.00 ppm, 8.93 to 12.55 ppm, and 70.10 to 104.65 ppm, respectively (Table 4.26).

Table 4.25: Major element oxide concentrations (wt %) in the soil kaolins.

Parent Rocks	Sample ID	Al ₂ O ₃	CaO	Cr ₂ O ₃	Fe ₂ O ₃	K ₂ O	MgO	MnO	Na ₂ O	P ₂ O ₅	SiO ₂	TiO ₂	L.O.I.	Sum of Conc.
Basalt	DF S1 0-20 cm	23.69	0.10	0.03	17.86	0.33	0.18	0.09	1.69	0.15	37.06	2.38	16.70	100.26
	DF S1 20-50 cm	24.99	0.06	0.02	16.50	0.39	0.18	0.07	1.97	0.13	37.12	2.21	16.28	99.92
	DF S1 50-100 cm	25.09	0.04	0.03	20.50	0.05	0.03	0.08	1.69	0.14	32.74	2.82	17.30	100.51
	DF S2 0-20 cm	23.18	0.11	0.05	17.19	0.20	0.17	0.06	2.09	0.16	36.85	2.12	17.85	100.03
	DF S2 20-50 cm	23.57	0.10	0.06	18.19	0.17	0.15	0.06	2.15	0.13	34.01	2.05	19.53	100.17
	DF S2 50-100 cm	24.54	0.04	0.03	14.68	0.08	0.13	0.06	2.10	0.11	39.51	1.90	16.86	100.04
	DF S3 0-20 cm	25.55	0.06	0.03	20.34	0.06	0.03	0.08	1.55	0.16	33.56	2.69	15.95	100.06
	DF S3 20-50 cm	25.82	0.09	0.03	19.53	0.06	0.05	0.07	1.66	0.17	33.40	2.84	16.46	100.18
	DF S3 50-100 cm	24.74	0.06	0.02	16.95	0.36	0.16	0.07	2.00	0.15	36.68	2.28	16.64	100.11
Granite	DF MAT1 0-20 cm	16.33	1.53	0.01	2.64	2.40	0.91	0.05	4.38	0.08	64.97	1.27	4.70	99.27
	DF MAT1 20-50 cm	16.25	1.31	0.01	2.85	2.28	0.85	0.05	4.94	0.08	62.17	1.25	6.96	99.00
	DF MAT2 0-20 cm	15.83	1.71	0.01	3.40	2.44	1.32	0.05	4.40	0.13	63.89	1.36	4.93	99.47
	DF MAT2 20-50 cm	15.80	1.70	0.01	2.81	2.57	1.16	0.06	4.46	0.08	65.91	1.40	3.80	99.76
	DF MAT3 0-20 cm	16.10	1.49	0.01	2.72	2.36	0.90	0.05	4.74	0.09	64.71	1.26	5.35	99.78
	DF MAT3 20-50 cm	16.35	1.30	0.01	2.88	2.26	0.86	0.05	4.85	0.09	62.34	1.23	6.94	99.16
Ark. Sst.	DF SA2 0-20 cm	12.51	0.39	0.06	3.42	4.57	0.46	0.03	2.06	0.07	66.73	2.68	6.18	99.16
	DF SA3 0-20 cm	14.94	0.81	0.05	4.42	3.95	1.17	0.04	2.11	0.27	56.43	2.17	13.45	99.81
	DF SA3 20-50 cm	15.46	0.77	0.05	4.45	4.02	1.20	0.04	2.72	0.26	55.18	2.13	13.15	99.43
Gneiss	DF MU1 0-20 cm	18.44	2.04	bdl	8.08	1.79	1.20	0.07	5.27	0.30	52.66	1.89	7.82	99.56
Quartzite	DF CMA 0-20 cm	8.37	0.09	0.02	2.29	0.80	0.23	0.03	1.36	0.07	77.22	1.48	7.60	99.56
	DF CMA 20-50 cm	9.68	0.10	0.01	2.17	0.96	0.27	0.03	1.64	0.07	73.51	1.41	9.67	99.52

Table 4.26: Trace element concentrations (ppm) in the soil kaolins.

Parent Rocks	Sample ID	Sc	V	Cr	Co	Ni	Cu	Zn	Rb	Sr	Y	Zr	Nb	Mo	Cs	Ba	Hf	Ta	Pb	Th	U
Basalt	DF S1 0-20 cm	43.52	329.95	209.3	32.6	133.3	235.45	79.4	35.08	15.4	24.2	208.7	10.69	0.84	1.49	112.75	5.42	0.735	9.68	4.34	1.17
	DF S1 20-50 cm	41.36	291.9	191.3	27.67	113.7	239.45	76.05	37.41	10.13	17.48	187.65	10.08	0.76	1.63	82.45	5.1	0.696	9.06	3.97	1.09
	DF S1 50-100 cm	47.7	384	240.6	29.4	159.45	265.45	69.9	4.04	8.13	21.47	254.35	13.21	0.99	0.48	61.9	6.95	0.894	10.77	5.59	1.36
	DF S2 0-20 cm	38.31	323.5	361.2	27.84	127.95	275	74.65	13.64	14.12	16.03	175.6	8.705	0.76	0.73	112.1	4.73	0.583	13.57	3.66	1
	DF S2 20-50 cm	40.28	335.45	398.6	24.29	135.35	300.1	67.35	11.8	9.99	13.62	166.45	8.215	0.62	0.64	98.2	4.27	0.558	7.31	3.6	1.03
	DF S2 50-100 cm	39.25	248.55	226	16.58	123.7	244.5	68.5	7.145	7.53	11.24	155.35	7.795	0.6	0.54	69.9	4.27	0.484	6.5	2.92	0.93
	DF S3 0-20 cm	46.38	381.2	232.85	34.57	138.65	298.05	73.75	5.85	9.195	27.53	248.7	12.8	0.97	0.64	74.65	6.73	0.879	10.87	5.28	1.3
	DF S3 20-50 cm	45.28	360.3	233.4	33.48	133.3	271.65	75.6	4.645	11.35	19.36	253.35	13.33	1.15	0.54	73.85	6.66	0.925	11.94	5.22	1.33
DF S3 50-100 cm	44.35	302.9	187.8	22.04	100.5	245.4	76.9	34.15	9.035	18.23	194.3	10.51	0.68	1.59	77.45	5.38	0.727	8.63	4.04	1.2	
Granite	DF MAT1 0-20 cm	8.835	42.34	177.05	6.645	58.2	26.5	48.85	69.05	413.7	22.32	1185.6	13.29	0.52	2.07	976	30	0.831	23.22	11.1	2.37
	DF MAT1 20-50 cm	8.665	43.75	178.1	6.97	59.85	29.75	50.9	70.85	372.6	21.36	1049.1	13.36	0.62	2.26	943	26.3	0.915	22.17	10.4	2.36
	DF MAT2 0-20 cm	11.54	59.555	229.9	10.49	92.55	35.7	53.5	81.3	388.1	29.94	1285.8	15.09	0.63	2.2	998.5	31.3	0.913	23.93	12.5	2.79
	DF MAT2 20-50 cm	10.21	50.05	205.55	7.165	69.6	23.95	44.9	77.1	431.5	29.88	1424.5	15.34	0.49	1.93	1127.5	34.7	0.967	22.57	14.5	3.02
	DF MAT3 0-20 cm	9.19	44.28	182.35	7.145	59.6	34.35	51.2	70.25	412.2	23.25	1264.7	13.69	0.62	1.99	981.5	30.6	0.938	24.3	11.9	2.59
	DF MAT3 20-50 cm	9.11	44.635	182.15	6.93	61.3	25.1	51.35	72.55	368.9	22.37	1039.9	13.41	0.63	2.37	941.5	26	0.865	22.92	10.8	2.42
Ark. Sst.	DF SA2 0-20 cm	12.86	110.85	437	8.925	70.1	29.65	53.05	159.3	160.6	39.51	1148.3	29.29	0.68	2.68	1220	29.5	2.23	39.59	29	5.04
	DF SA3 0-20 cm	15.52	110.3	351.45	12.19	104.65	53.65	86	138.9	147	35.37	835.15	22.71	0.88	3.04	983.5	21.6	1.798	31.98	22.9	4.19
	DF SA3 20-50 cm	15.78	106.25	350.6	12.55	90.9	40.05	82.8	144.3	146.2	33.88	733.05	22.72	0.62	3.18	1002	19.3	1.754	32.78	22.2	4.18
Gneiss	DF MU1 0-20 cm	14.58	110.95	54.05	13.9	40.45	43.6	120.1	57.05	492	19.56	367.9	10.63	0.48	2.54	720	9.57	0.658	18.05	4.4	0.83
Quartzite	DF CMA 0-20 cm	7.555	74.7	154.65	5.3	37.75	18.8	30.95	48.6	32.15	18.02	707.95	13.37	0.74	1.51	210.35	18.4	1.151	12.72	9.84	2.79
	DF CMA 20-50 cm	7.52	71.4	136.9	5.485	38.65	21.705	31.15	59.35	34.65	15.08	499.5	13.18	0.81	1.74	243.55	13.2	1.125	13.96	9.22	2.36

The values obtained for Sc, V, Cr, Co, and Ni in the soil kaolins developed from gneiss are 14.58, 110.95, 54.05, 13.90, and 40.45 ppm, respectively. In soil kaolins developed from quartzite (control), the Sc, V, Cr, Co, and Ni concentrations varied from 7.52 to 7.56 ppm, 71.40 to 74.70 ppm, 136.90 to 154.65 ppm 5.30 to 5.49 ppm, and 37.75 to 38.65 ppm, respectively (Table 4.26).

- **Incompatible Trace Elements (Rb, Sr, Y, Zr, Nb, Ba, Th, and U)**

The concentrations of Rb, Sr, Y, Th, Nb and U in soil kaolins developed from basalt and quartzite (control) were generally less than 50ppm (except for Rb in CMA 20-50 cm) whereas, Zr and Ba values were more than 50 ppm (Table 4.26).

In the studied soil kaolins developed from granite, arkosic sandstone, and gneiss, the concentrations of Y, Nb, Th, U were generally less than 50 ppm whereas, Rb, Sr, Zr, and Ba were more than 50 ppm (Table 4.26).

4.3.5.3 Rare Earth Elements (REEs)

- **Light REEs (LREE) (La, Ce, Pr, Nd, Sm, Eu)**

The values obtained for La, Ce, Pr, Nd, Sm and Eu in soil kaolins developed from basalt ranged from 6.12 to 19.27 ppm, 22.47 to 55.16 ppm, 1.39 to 4.86 ppm, 6.08 to 17.25 ppm, 1.33 to 5.35 ppm, and 0.44 to 1.52 ppm, respectively. In the soil kaolins developed on granite, La, Ce, Pr, Nd, Sm and Eu concentrations varied from 44.82 to 61.09 ppm, 84.16 to 120.40 ppm, 9.58 to 13.30 ppm, 37.95 to 52.15 ppm, 6.56 to 9.61 ppm, and 1.04 to 1.67 ppm, respectively (Table 4.27).

The La, Ce, Pr, Nd, Sm and Eu concentrations in the soil kaolins developed from arkosic sandstone ranged from 65.74 to 76.25 ppm, 123.50 to 146.20 ppm, 14.70 to 16.30 ppm, 57.80 to 64.00 ppm, 10.70 to 11.60 ppm, and 1.73 to 1.92 ppm, respectively (Table 4.27).

Table 4.27: Rare earth element concentrations (ppm) in the soil kaolins.

Parent Rocks	Sample ID	La	Ce	Pr	Nd	Sm	Eu	Gd	Tb	Dy	Ho	Er	Tm	Yb	Lu
Basalt	DF S1 0-20 cm	16.74	39.46	4.01	17.25	4.32	1.26	4.34	0.76	4.83	0.97	2.71	0.42	2.89	0.41
	DF S1 20-50 cm	12.18	37.43	2.73	12.14	2.80	0.90	3.06	0.58	3.53	0.77	2.18	0.33	2.29	0.36
	DF S1 50-100 cm	15.01	55.16	3.74	16.16	4.41	1.18	4.01	0.67	4.78	0.96	2.87	0.43	3.11	0.46
	DF S2 0-20 cm	9.75	26.60	2.23	10.30	2.47	0.73	2.76	0.54	3.05	0.68	1.93	0.29	2.26	0.35
	DF S2 20-50 cm	7.69	22.47	1.78	7.90	1.75	0.67	2.15	0.38	2.54	0.55	1.77	0.26	1.94	0.29
	DF S2 50-100 cm	6.12	23.29	1.39	6.08	1.33	0.44	1.63	0.30	2.05	0.48	1.44	0.24	1.74	0.26
	DF S3 0-20 cm	19.27	51.37	4.86	21.45	5.35	1.52	5.64	0.93	5.77	1.16	3.36	0.52	3.62	0.53
	DF S3 20-50 cm	12.53	51.82	3.17	12.98	3.34	1.02	3.62	0.62	4.17	0.85	2.44	0.39	2.91	0.47
	DF S3 50-100 cm	12.97	40.01	3.07	13.33	2.95	1.02	3.18	0.60	3.54	0.76	2.18	0.32	2.48	0.38
Granite	DF MAT1 0-20 cm	47.39	89.83	10.09	39.85	7.07	1.04	5.37	0.73	4.10	0.78	2.10	0.35	2.71	0.41
	DF MAT1 20-50 cm	44.82	84.16	9.58	37.95	6.56	1.10	5.11	0.70	3.62	0.72	2.13	0.32	2.37	0.42
	DF MAT2 0-20 cm	61.09	120.35	13.27	52.15	9.61	1.67	6.98	0.98	5.39	1.12	3.01	0.45	3.17	0.56
	DF MAT2 20-50 cm	56.78	106.60	12.56	49.50	8.60	1.46	7.02	0.88	5.03	1.01	2.91	0.50	3.50	0.52
	DF MAT3 0-20 cm	48.86	92.60	10.70	41.55	7.79	1.14	5.86	0.79	4.15	0.85	2.31	0.38	2.89	0.42
	DF MAT3 20-50 cm	45.45	85.70	9.93	38.60	6.88	1.07	4.97	0.68	4.20	0.82	2.38	0.35	2.71	0.42
Ark. Sst.	DF SA2 0-20 cm	76.25	146.15	16.32	64.00	11.62	1.73	8.82	1.24	7.31	1.42	4.06	0.64	4.42	0.66
	DF SA3 0-20 cm	67.29	125.97	14.70	59.15	10.65	1.92	8.14	1.15	6.69	1.26	3.63	0.52	3.69	0.59
	DF SA3 20-50 cm	65.74	123.53	14.78	57.80	10.85	1.89	8.34	1.14	6.37	1.35	3.50	0.48	3.62	0.55
Gneiss	DF MU1 0-20 cm	32.12	60.46	7.60	30.77	5.94	1.82	4.90	0.67	3.83	0.72	2.11	0.26	2.00	0.30
Quartzite	DF CMA 0-20 cm	21.46	40.18	4.07	15.84	3.02	0.70	2.73	0.47	3.01	0.67	2.10	0.33	2.39	0.33
	DF CMA 20-50 cm	20.47	37.33	3.82	14.91	3.07	0.68	2.64	0.44	2.76	0.57	1.64	0.26	1.85	0.30

The values obtained for La, Ce, Pr, Nd, Sm and Eu in the soil kaolins developed from gneiss were 32.12, 60.46, 7.60, 30.77, 5.94, and 1.82 ppm, respectively. In soil kaolins developed from quartzite (control), the La, Ce, Pr, Nd, Sm and Eu concentrations varied from 20.47 to 21.46 ppm, 37.33 to 40.18 ppm, 3.82 to 4.07 ppm, 14.91 to 15.84 ppm, 3.02 to 3.07 ppm, and 0.68 to 0.70 ppm, respectively (Table 4.27).

- **Heavy REEs (HREE) (Gd, Tb, Dy, Ho, Er, Tm, Yb, Lu)**

The concentrations of HREE in the studied soil kaolins developed from the different parent rocks were generally less than 10 ppm (Table 4.27).

4.4 Concluding Remarks

In this chapter, the results obtained from the various physico-chemical, mineralogical, and geochemical laboratory analyses have been presented and summarised in the form of tables and figures. The interpretations and implications of the results with respect to the specific objectives of the study are discussed in the following chapters 5, 6, 7, 8, and 9.

Chapter Five

Influence of Provenance and Degree of Weathering on Oxidic Soils Developed from different Parent Rocks in Limpopo Province, South Africa

This chapter aimed to establish the influence of provenance and degree of weathering on the mineralogy and geochemistry of oxidic soils developed from different parent rocks in Limpopo Province, South Africa (Specific Objective 1) based on Hypothesis 1. The mineralogical and geochemical characteristics of the studied soils were used to achieve specific objective 1.

5.1 Influence of Provenance

The ranges and mean values of the major oxides concentrations in both the soils and their respective bedrocks are presented in Table 5.1. The SiO_2 is the dominant component in the soils with values ranging from 32.09 to 88.11 wt %. These values were lower than the average value (91.65 wt %) obtained for the soils developed from quartzite (control). This reflects the mineralogy of the soils. The soils developed from quartzite have higher mean quartz content (91.50 wt %) relative to the soils developed from basalt (25.67 wt %), granite (28 wt %), arkosic sandstone (77 wt %), and gneiss (20 wt %) respectively. The Al_2O_3 and LOI were highest in the soils developed from basalt which could be attributed to the higher mean kaolinite content (47.67 wt %) relative to the other soils. The presence of anatase, hematite and goethite was evident from the Ti and Fe oxides present particularly in soils developed from basalt. For soils developed from granite and gneiss, the higher CaO and Na_2O contents are indicative of the presence of plagioclase feldspars present in them. In addition, K_2O was higher in soils developed from granite, arkosic sandstone, and gneiss due to microcline present in them. The Cr_2O_3 and MgO contents were comparatively lower than the other oxides in the soils. The reddish, brownish, and yellowish colours were further indications of the presence of hematite, goethite, anatase, and organic matter in the soils (Ekosse, 2001; Fernandez-Caliani and Cantano, 2010; Diko *et al.*, 2011).

Table 5.1a: Major oxides (wt %) and weathering indices (CIA, CIW, and PIA) of the studied soils and for average Upper Continental Crust (UCC).

Parent Rock		SiO ₂	TiO ₂	Al ₂ O ₃	Cr ₂ O ₃	Fe ₂ O ₃	CaO	MgO	MnO	Na ₂ O	K ₂ O	P ₂ O ₅	L.O.I.	CIA	CIW	PIA
Basalt (n=9)	Min	32.09	1.90	22.91	0.03	20.73	0.06	0.03	0.14	0.01	0.04	0.12	13.50	98.05	98.88	98.08
	Max	37.88	2.81	25.75	0.04	25.43	0.20	0.21	0.20	0.07	0.36	0.16	16.28	99.57	99.81	99.63
	Average	35.06	2.30	24.80	0.04	22.90	0.09	0.13	0.16	0.03	0.17	0.15	14.45	98.84	99.51	99.02
Granite (n=6)	Min	74.30	0.40	11.98	0.01	1.43	1.11	0.26	0.02	3.38	1.82	0.07	1.27	64.26	71.27	67.75
	Max	76.90	0.53	13.54	0.01	1.91	1.18	0.46	0.03	3.89	2.13	0.08	2.16	66.31	73.43	70.23
	Average	75.61	0.49	12.83	0.01	1.65	1.15	0.34	0.03	3.70	1.97	0.07	1.73	65.29	72.55	69.12
Ark. Sst. (n=6)	Min	79.48	0.77	3.46	0.01	1.30	0.08	0.11	0.01	0.11	2.19	0.04	1.46	54.92	57.20	60.23
	Max	88.11	1.06	7.16	0.01	2.51	0.69	0.61	0.03	0.17	2.63	0.16	5.06	68.65	69.30	71.53
	Average	85.42	0.93	5.13	0.01	1.84	0.32	0.34	0.02	0.14	2.42	0.12	2.88	63.24	65.10	68.18
Gneiss (n=3)	Min	60.30	1.31	14.40	bdl	6.62	2.72	1.10	0.03	4.28	1.28	0.10	3.10	59.02	62.23	60.06
	Max	62.10	1.56	16.10	bdl	7.31	3.46	1.26	0.09	6.31	1.41	0.19	3.80	65.14	68.85	66.97
	Average	61.42	1.45	15.32	bdl	6.99	3.04	1.18	0.06	5.33	1.34	0.14	3.52	61.33	64.80	62.69
Quartzite (n=2)	Min	91.12	0.43	3.44	0.01	1.12	0.04	0.15	0.01	bdl	0.33	0.04	2.06	89.82	98.81	98.72
	Max	92.18	0.47	3.75	0.01	1.46	0.04	0.15	0.01	bdl	0.35	0.04	2.26	91.02	98.94	98.84
	Average	91.65	0.45	3.60	0.01	1.29	0.04	0.15	0.01	bdl	0.34	0.04	2.16	90.42	98.90	98.78
UCC ¹	Average	65.89	0.50	15.17	-	4.49	4.19	2.20	0.07	3.89	3.39	0.20	-	-	-	-

¹ Taylor and McLennan (1985) and bdl = below detection limit

Table 5.1b: Major element oxides (wt %) and weathering indices (CIA, CIW, PIA) of the parent rocks.

Parent Rock		SiO ₂	TiO ₂	Al ₂ O ₃	Cr ₂ O ₃	Fe ₂ O ₃	CaO	MgO	MnO	Na ₂ O	K ₂ O	P ₂ O ₅	L.O.I.	CIA	CIW	PIA
Basalt (n=3)	Min	48.93	1.31	13.86	0.02	13.44	7.87	5.40	0.19	2.12	0.52	0.14	2.15	52.42	53.47	52.83
	Max	49.24	1.55	14.53	0.02	14.42	9.73	6.55	0.20	2.70	0.99	0.17	2.86	56.08	57.89	56.48
	Av.	49.10	1.41	14.23	0.02	13.93	9.08	6.04	0.20	2.38	0.77	0.15	2.46	53.79	55.42	54.23
Granite (n=3)	Min	72.23	0.07	15.54	bdl	0.78	1.47	0.21	0.02	5.73	0.98	0.06	0.46	62.96	66.13	64.65
	Max	72.77	0.11	15.86	bdl	0.88	1.64	0.27	0.02	6.32	2.13	0.07	0.60	63.48	68.78	65.60
	Av.	72.50	0.09	15.71	bdl	0.82	1.55	0.23	0.02	6.03	1.56	0.06	0.53	63.22	67.44	65.12
Ark. Sst. (n=3)	Min	87.34	0.08	4.61	bdl	0.33	0.05	0.06	0.01	0.05	2.45	0.02	0.72	60.65	64.31	62.65
	Max	90.85	0.12	6.39	bdl	0.61	0.12	0.15	0.01	0.13	3.64	0.08	0.84	64.12	66.19	66.32
	Av.	89.60	0.11	5.23	bdl	0.43	0.08	0.09	0.01	0.08	2.98	0.05	0.78	62.45	65.29	64.94
Quartzite		96.21	0.08	1.12	bdl	1.21	0.03	0.07	0.01	bdl	0.21	0.03	0.69	82.35	87.20	90.20

bdl = below detection limit

The minerals present in the soils were also present in their respective parent rocks except for additional secondary minerals such as kaolinite, anatase, goethite, hematite, and gibbsite due to the weathering of the primary minerals (Fig. 5.1).

Kaolinite as the dominant clay mineral in the soils account for the low CEC. Average exchangeable cations in the soils were in order of $\text{Ca} > \text{Mg} > \text{K} > \text{Na}$ (except for soils developed from gneiss having $\text{Na} > \text{K}$). This order is consistent with the mineralogy since Ca, K, and Na are present essentially in feldspars. Calcium having the highest concentration among the exchangeable cations can be contributed to its high mobility during weathering (Flantis *et al.*, 2010). It is easily mobilised even at low degree of weathering of feldspars and hence provided significant additions to the soil exchangeable cation pool. In addition, exchangeable Mg are controlled by the relative abundance of Mg-bearing minerals such as muscovite, chlorite, actinolite, and montmorillonite (Weil and Brady, 2017).

The soils developed from basalt and gneiss from this study show higher averages in Al_2O_3 and Fe_2O_3 relative to the Upper Continental Crust (UCC). However, UCC show depletion in TiO_2 and relative enrichments in CaO, K_2O , MgO, Na_2O , and P_2O_5 when compared with the averages obtained for soils from this study (Table 5.1).

The ratios of the major elements in the soils were estimated with respect to their underlying fresh bedrocks to have a better understanding of the elemental distribution within the respective soils (Table 5.2). The geochemical data for UCC given by McLennan *et al.* (1993) were used to represent the parent rock for gneiss as its fresh bedrock was not exposed in the area studied. Soils developed from granite, arkosic sandstone, and gneiss showed enrichment in CaO, K_2O , MgO, MnO, and Na_2O relative to their depletion in soils developed from basalt. However, Fe_2O_3 and TiO_2 were enriched within all the soils. In addition, the soil developed from quartzite (control) showed enrichment in all the major elements except for SiO_2 . The striking loss of the alkalis (CaO, K_2O , MgO, and Na_2O), enrichment of sesquioxides (Al_2O_3 , Fe_2O_3 , and TiO_2), and increasing water as reflected by the LOI in the soils developed from basalt is a clear indication of geochemical change accompanying the chemical weathering of the primary minerals present in the parent rock (Price and Velbel, 2003; Tijani *et al.*, 2006).

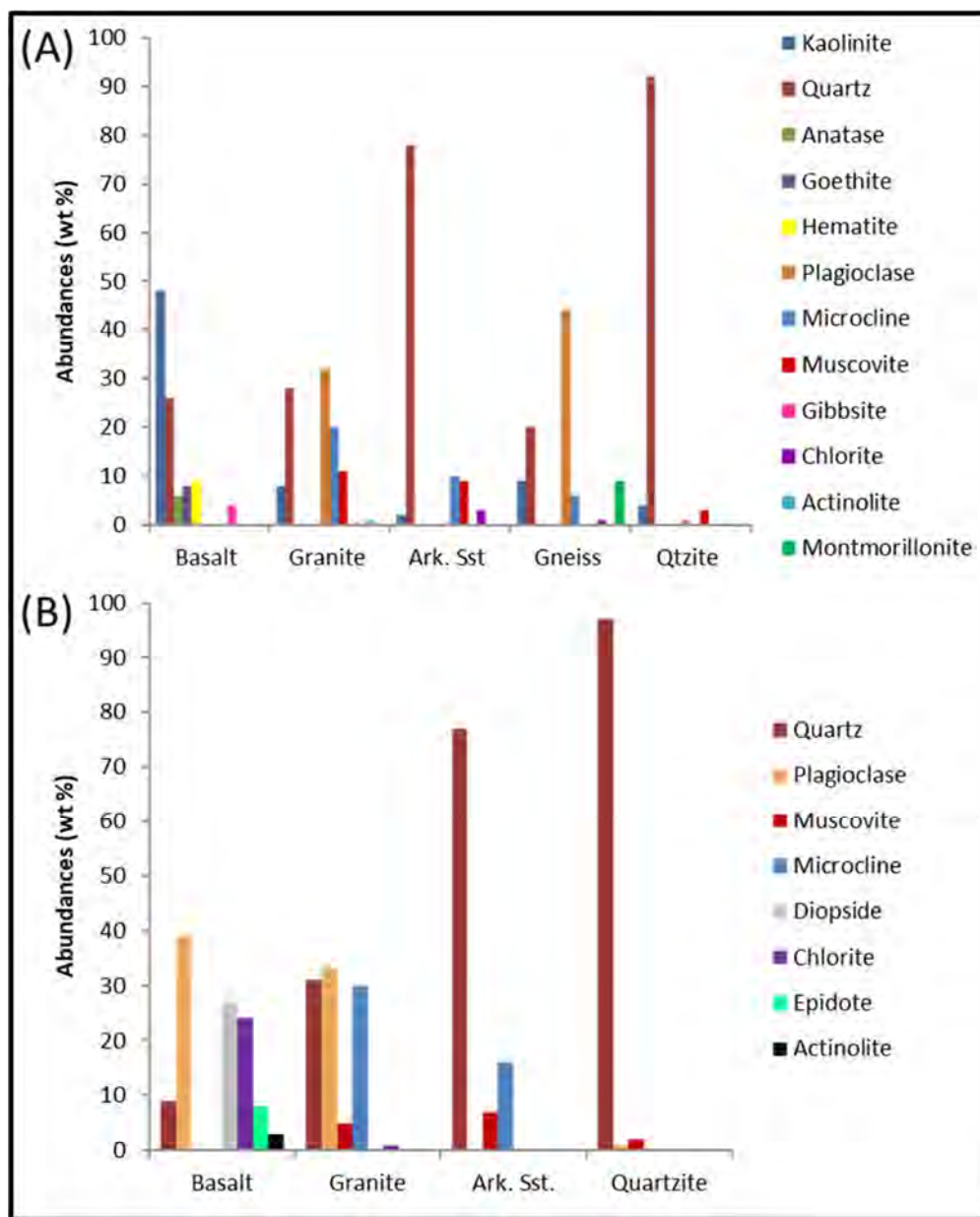


Figure 5.1: Mineral abundances in the soils (A) and parent rocks (B).

Table 5.2: Major oxide ratios between the soils and their respective parent rocks.

Parent Rock	SiO ₂	TiO ₂	Al ₂ O ₃	Cr ₂ O ₃	Fe ₂ O ₃	CaO	MgO	MnO	Na ₂ O	K ₂ O	P ₂ O ₅	L.O.I.
Basalt	0.71	1.63	1.74	1.83	1.64	0.01	0.02	0.81	0.01	0.21	0.98	5.86
Granite	1.04	5.43	0.82	-	2.01	0.74	1.44	1.25	0.61	1.26	1.13	3.24
Arkosic Sandstone	0.95	8.75	0.98	-	4.30	3.88	3.78	2.00	1.72	0.81	2.16	3.70
Gneiss	0.93	2.89	1.01	-	1.56	0.72	0.54	0.90	1.37	0.40	0.72	-
Quartzite	0.95	5.63	3.21	-	1.07	1.33	2.14	1.00	-	1.62	1.33	3.11

The ranges and mean concentrations of the trace elements in both the soils and their respective bedrocks are presented in Table 5.3. From the mean concentrations, soils developed from basalt have highest values for Sc, V, Cr, Co, Ni, Cu, Y, Nb, and Mo whereas, soils developed from granite had highest concentrations for Ba (due to the weathering of plagioclase feldspar). In addition, soils developed from arkosic sandstone have highest concentrations for Rb, Zr, Hf, Ta, Pb, Th, and U whereas, soils developed from gneiss have highest concentrations for Zn, Sr, and Cs. These trace element trends are similar in their respective fresh bedrocks. This suggests lithogenic release of the respective trace elements through weathering process (Tijani *et al.*, 2006). The mean values indicate that the concentrations of trace element in the soils are more enriched relative to the soils developed from quartzite (control) except for V, Cr, Zr, Hf, Th, U that have values similar to some of the soils.

The soils show lower averages in Th (except for soils developed from arkosic sandstone), Ni, Cu, Y (except for soils developed from basalt), Rb, Nb, Mo, Cs, U and Ta when compared with the UCC (Table 5.3a). Trace element mean concentrations for V (except for soils developed from basalt and gneiss), Cr (except for soils developed from basalt and arkosic sandstone), Co, Ni, Cu (except for soils developed from basalt), Zn, Mo and Pb were not enough to be considered hazardous (Table 5.3a).

The soil/bedrock trace element ratios show that most of the trace elements were enriched (Table 5.4) except for Rb, Sr, and Ba for soils developed from basalt; Mo for soils developed from granite; Sr and Ba for soils developed from arkosic sandstone; and Cr, Ni, and Cu for soils developed from gneiss. The distribution of Rb, Sr, and Ba are controlled by the weathering of plagioclase feldspar (Deepthy, 2008). Soils developed from quartzite (control) showed depletion for all the trace elements. This suggests minimal weathering-induced release of trace elements from the bedrock and hence points to the fact that the primary metasedimentary mineralogy is devoid of weatherable minerals, due to pre-metamorphic sedimentary processes (Tijani *et al.*, 2006).

To better assess the enrichment and loss of trace elements (mobility), the immobile element approach was applied using Titanium (Ti) as the reference element. Titanium has been successfully used by several authors (Tijani *et al.*, 2006; Deepthy, 2008;

Yousefifard *et al.*, 2012) because it causes lesser error in mass loss/gain calculations compared to V and Sr (Yousefifard *et al.*, 2012). Titanium remains relatively unaffected during chemical weathering. The enrichment factor (EF) normalized with respect to Ti was calculated for each selected trace elements in the soil. The EF is expressed as:

$$EF = \left\{ \frac{(Me/Ti)_{\text{soil}}}{(Me/Ti)_{\text{bedrock}}} \right\} \text{ (Tijani *et al.*, 2006)} \quad (5.2)$$

Where, Me = concentration of the respective trace element of interest and Ti = concentration of the reference immobile element in the soil on the one hand and bedrock on the other. An EF value approximately 1.0 for any element implies a concentration representing the lithogenic input; EF > 1.0 and EF < 1.0 imply enrichment and depletion of the element in consideration (Tijani *et al.*, 2006).

Table 5.5 shows the summary of the Ti-normalised EF for the soils. The soils developed from basalt and gneiss have enrichment factor (EF) >1 for all the trace elements with exception of Rb, Sr, and Ba in soils developed from basalt. The mobile elements (Rb, Sr, and Ba) which are depleted in the soils developed from basalt are derived from leachable minerals such as feldspar, mica, and apatite due to intense chemical weathering. For soils developed from granite and arkosic sandstone, the trend is reversed with EF < 1 except for Cr in soils developed from granite, and Cr and Ta in soils developed from arkosic sandstone having EF > 1. This suggests little or no lithogenic release of these elements through weathering processes.

A combination of the previous observations from weathering indices and enrichment trend suggests that the trace element geochemistry of the soils is controlled by the intensity of chemical weathering. The soils developed from quartzite (control) showed similar enrichment trend with soils developed from granite and arkosic sandstone with EF < 1 for all the trace elements. This trend suggests low absolute concentrations of the trace elements in quartzite and hence, little or no lithogenic release by weathering processes.

Table 5.3a: Trace element concentrations (ppm) of oxidic soils developed from different parent rocks in Limpopo Province, South Africa and for average Upper Continental Crust (UCC) and Critical Concentrations.

Parent Rock		Sc	V	Cr	Co	Ni	Cu	Zn	Rb	Sr	Y	Zr	Nb	Mo	Cs	Ba	Hf	Ta	Pb	Th	U
Basalt (n=9)	Min	49.24	414.50	232.75	48.35	103.80	243.70	75.70	3.86	8.07	16.86	158.30	8.85	0.70	0.47	53.70	4.28	0.46	7.64	4.53	0.95
	Max	59.95	538.65	300.75	69.45	144.95	292.60	91.85	36.10	18.77	26.37	258.65	14.99	4.56	1.63	151.65	6.95	0.92	18.15	7.63	1.51
	Av.	55.11	472.52	263.24	56.50	125.46	267.12	81.69	16.60	11.20	22.56	205.75	11.72	1.47	0.93	89.68	5.58	0.68	10.84	6.13	1.28
Granite (n=6)	Min	6.58	25.07	63.45	2.55	21.95	10.56	19.40	41.85	358.20	6.75	211.10	5.26	0.34	0.90	772.30	5.24	0.30	17.60	3.74	0.69
	Max	7.97	35.18	89.90	4.48	34.05	14.45	24.55	52.15	417.15	9.74	402.00	7.08	0.62	1.24	959.00	10.06	0.40	19.46	8.41	1.13
	Av.	7.18	28.44	75.81	3.57	28.52	12.80	22.01	46.75	397.28	8.40	308.75	6.23	0.45	1.05	866.55	7.78	0.36	18.17	5.37	0.93
Arkosic Sst (n=6)	Min	8.06	37.46	100.15	3.43	25.11	16.55	19.25	78.36	80.85	11.31	517.35	9.55	0.61	1.04	601.55	13.03	0.62	18.11	14.40	2.12
	Max	11.20	64.60	136.05	9.11	49.85	23.21	43.95	86.10	95.75	31.22	661.40	12.34	0.77	1.47	688.10	17.01	0.88	22.95	24.23	3.31
	Av.	9.68	48.18	118.72	6.10	34.17	19.16	28.91	81.91	85.93	19.44	570.10	10.90	0.69	1.29	648.76	14.57	0.74	20.07	18.77	2.56
Gneiss (n=3)	Min	15.10	131.30	40.10	16.42	30.88	22.33	91.01	37.62	580.20	20.10	180.10	7.81	0.52	1.30	560.10	4.78	0.33	13.11	2.51	0.47
	Max	16.20	136.90	41.02	17.68	31.55	23.88	92.51	38.51	586.85	22.10	187.10	8.99	0.72	1.68	577.20	5.24	0.56	14.30	2.72	0.77
	Av.	15.67	133.77	40.70	17.10	31.15	23.18	91.99	38.08	582.75	21.18	184.13	8.43	0.62	1.49	569.20	5.02	0.46	13.74	2.58	0.62
Quartzite (n=2)	Min	7.42	33.70	47.10	1.99	17.90	11.19	15.10	21.07	10.62	6.63	229.85	4.13	0.18	0.64	83.30	6.12	0.33	5.64	4.47	1.00
	Max	8.02	41.60	58.40	2.24	18.40	14.35	15.90	22.50	11.39	7.75	270.00	4.84	0.43	0.76	89.85	6.81	0.35	6.23	4.85	1.15
	Av.	7.72	37.65	52.75	2.11	18.15	12.77	15.50	21.79	11.00	7.19	249.93	4.48	0.31	0.70	86.58	6.46	0.34	5.94	4.66	1.08
UCC ¹	Av.	13.60	107.00	83.00	17.00	44.00	25.00	71.00	112.00	350.00	22.00	190.00	12.00	1.50	4.60	550.00	5.80	1.00	17.00	10.70	2.80
CC ²			50- 100	75- 100	25- 50	<100	60- 125	70- 400						2- 30					2- 300		

¹ McLennan, 2001; ² Critical concentrations (Alloway, 1995).

Table 5.3b: Trace element concentrations (ppm) of different parent rocks in Limpopo Province, South Africa.

Parent Rock		Sc	V	Cr	Co	Ni	Cu	Zn	Rb	Sr	Y	Zr	Nb	Mo	Cs	Ba	Hf	Ta	Pb	Th	U
Basalt (n=3)	Min	3.23	5.08	3.81	0.62	4.90	3.72	15.95	13.02	130.50	1.30	15.57	1.72	0.40	0.24	202.60	0.33	0.17	4.32	0.56	0.30
	Max	38.60	333.90	192.00	46.60	99.05	190.20	115.60	36.66	373.40	29.60	125.20	7.12	0.70	1.33	637.00	3.60	0.41	12.67	3.40	0.80
	Av.	26.00	213.00	114.62	30.80	58.55	124.70	77.67	27.36	216.80	18.70	81.18	4.81	0.50	0.69	348.77	2.23	0.30	7.33	2.19	0.60
Granite (n=3)	Min	4.72	7.77	8.85	0.96	9.15	4.32	18.00	18.15	115.10	3.54	62.30	2.27	0.30	0.75	297.33	1.66	0.15	15.75	1.15	0.60
	Max	5.39	10.32	17.31	1.35	16.95	6.48	19.95	88.25	506.50	6.95	99.30	4.71	0.80	1.21	1042.50	2.87	0.31	18.70	3.60	0.80
	Av.	5.07	8.90	13.92	1.14	13.77	5.56	19.02	42.83	353.90	5.16	76.27	3.81	0.60	1.03	553.11	2.10	0.22	16.96	2.06	0.70
Arkositic Sst (n=3)	Min	5.44	9.12	6.50	1.20	7.40	4.32	16.15	41.40	57.35	3.70	91.80	1.42	0.60	0.74	570.00	2.67	0.03	14.05	2.59	0.20
	Max	6.98	14.64	13.35	2.52	14.15	9.20	43.45	92.60	915.00	4.08	126.40	2.57	0.60	0.95	739.50	3.35	0.29	17.74	3.47	0.70
	Av.	6.01	12.31	10.03	1.74	9.77	6.47	25.32	70.42	349.90	3.84	106.30	1.94	0.60	0.81	669.50	2.95	0.18	15.56	2.90	0.50
Quartzite (n=1)		154.00	1281.00	621.40	142.00	277.50	654.50	238.30	94.25	27.70	70.40	546.90	31.00	2.50	4.14	249.20	15.20	1.84	26.80	18.00	3.60

Table 5.4: Trace element ratios between the soils and their respective parent rocks.

Parent Rock	Sc	V	Cr	Co	Ni	Cu	Zn	Rb	Sr	Y	Zr	Nb	Mo	Cs	Ba	Hf	Ta	Pb	Th	U
Basalt	2.12	2.22	2.30	1.84	2.14	2.14	1.05	0.61	0.05	1.21	2.53	2.43	2.79	1.35	0.26	2.50	2.27	1.48	2.80	2.20
Granite	1.42	3.20	5.45	3.14	2.07	2.30	1.16	1.09	1.12	1.63	4.05	1.64	0.73	1.01	1.57	3.71	1.61	1.07	2.61	1.32
Ark. Sst.	1.61	3.92	11.83	3.50	3.50	2.96	1.14	1.16	0.25	5.07	5.37	5.63	1.25	1.59	0.97	4.94	4.15	1.29	6.47	5.13
Gneiss	1.15	1.25	0.49	1.01	0.71	0.93	1.30	0.34	1.67	0.96	0.97	0.70	0.41	0.32	1.03	0.87	0.46	0.81	0.24	0.22
Quartzite	0.05	0.03	0.08	0.01	0.07	0.02	0.07	0.23	0.40	0.10	0.46	0.14	0.12	0.17	0.35	0.43	0.18	0.22	0.26	0.29

Table 5.5: Ti-normalised enrichment factor of trace elements for oxidic soils developed from different parent rocks in Limpopo Province, South Africa.

Parent Rock		Sc	V	Cr	Co	Ni	Cu	Zn	Rb	Sr	Y	Zr	Nb	Mo	Cs	Ba	Hf	Ta	Pb	Th	U
Basalt (n=9)	Min	0.89	0.92	0.71	0.63	0.62	0.80	0.45	0.06	0.01	0.46	1.03	1.00	0.77	0.18	0.04	0.94	0.90	0.43	1.05	1.03
	Max	9.76	54.06	37.30	51.69	14.31	40.69	2.66	0.73	0.11	10.58	8.46	4.42	5.81	2.40	0.57	10.84	2.73	2.82	7.08	2.38
	Av.	3.82	18.41	12.95	16.49	5.33	13.94	1.21	0.41	0.05	3.52	3.53	2.21	1.87	1.42	0.26	4.23	1.61	1.19	3.15	1.53
Granite (n=6)	Min	0.18	0.44	0.56	0.39	0.21	0.25	0.13	0.13	0.11	0.13	0.47	0.16	0.06	0.12	0.20	0.41	0.13	0.15	0.39	0.11
	Max	0.44	0.80	2.67	0.78	0.87	0.86	0.34	0.40	0.95	0.66	1.02	0.76	0.46	0.38	0.54	1.03	0.61	0.27	0.70	0.42
	Av.	0.28	0.60	1.28	0.58	0.47	0.48	0.22	0.28	0.37	0.36	0.76	0.38	0.19	0.21	0.36	0.71	0.36	0.20	0.53	0.26
Arkasic Sst (n=6)	Min	0.14	0.23	0.74	0.30	0.14	0.22	0.09	0.08	0.01	0.33	0.47	0.30	-	0.14	0.08	0.38	0.19	0.11	0.40	0.29
	Max	0.26	0.81	2.39	0.70	0.74	0.48	0.22	0.23	0.16	0.84	0.85	0.97	-	0.26	0.15	0.84	3.18	0.19	1.07	1.35
	Av.	0.18	0.46	1.45	0.40	0.44	0.35	0.14	0.14	0.09	0.54	0.60	0.69	-	0.18	0.11	0.55	1.23	0.14	0.73	0.72
Gneiss (n=3)	Min	4.22	7.64	4.49	19.94	4.16	1.95	9.08	9.43	209.98	10.56	7.86	12.75	-	17.17	14.75	7.28	5.73	4.70	1.56	1.53
	Max	5.23	9.36	5.46	24.38	5.06	2.27	10.81	11.37	252.49	12.39	9.26	17.47	-	23.92	17.88	8.47	9.17	5.89	1.86	2.26
	Av.	4.78	8.38	4.97	21.61	4.58	2.06	9.84	10.40	229.50	11.24	8.42	15.06	-	21.45	16.34	7.72	7.97	5.38	1.74	1.82
Quartzite (n=2)	Min	0.01	0.00	0.01	0.00	0.01	0.00	0.01	0.04	0.07	0.02	0.07	0.02	0.01	0.03	0.06	0.07	0.03	0.04	0.04	0.05
	Max	0.01	0.01	0.02	0.00	0.01	0.00	0.01	0.04	0.07	0.02	0.09	0.03	0.03	0.03	0.06	0.08	0.03	0.04	0.05	0.06
	Av.	0.01	0.01	0.01	0.00	0.01	0.00	0.01	0.04	0.07	0.02	0.08	0.03	0.02	0.03	0.06	0.07	0.03	0.04	0.05	0.05

The enrichment of the trace elements in soils developed from basalt and gneiss coupled with the little or no lithogenic release for soils developed from granite and arkosic sandstone imply that these elements are not mobilised except for Rb, Sr, and Ba for soils developed from basalt. This clearly signifies no potential environmental impact of chemical weathering-induced release of trace elements under the current weathering and climatic conditions on both surface drainage and shallow groundwater system interacting with the soil profiles (Tijani *et al.*, 2006). In the same sense, trace element soil to plant transfer will be minimal and hence, food quality and safety is guaranteed.

The absolute REE ranges and mean values in the soils and parent rocks are listed in Table 5.6. The absolute mean Σ REE concentrations were in decreasing order of soils developed from arkosic sandstone > gneiss > granite > basalt > quartzite (control), respectively. The chondrite-normalised REE patterns are shown in Figs. 5.2 - 5.6. The absolute REE contents of the soils and parent rocks were normalised to chondrite values (Haskin *et al.*, 1971) to remove the Oddo-Harkin's effect.

Similar trend between the soils developed from basalt and the parent rocks was observed (Fig. 5.2) except for pronounced positive Ce anomaly in the soils with relatively flat HREE. This suggests there has been no dominant control of heavy minerals on crustal composition from a HREE-fractionating phase like garnet (McLennan, 1989). REE fractionation during weathering of the parent rock could have possibly caused the enrichment of Ce in the soils (McLennan, 1989; Caspari *et al.*, 2006). However, zircon can also cause positive Ce anomalies but its presence would have given rise to HREE enrichment (Ayres and Harris, 1997). For soils developed from granite (Fig. 5.3), the soils showed similar trend to the parent rocks with no pronounced Eu anomaly but with a steep LREE pattern which is due to a partial melting of mantle or crustal rocks leading to an overall enrichment of large ion lithophile (LIL) elements such as K, Ba, Sr, Rb, and Pb (McLennan, 1989).

The soils developed from arkosic sandstone also showed similar trend with the parent rocks except for pronounced negative Eu anomaly in the soils which can be attributed to the substitution of Ca^{2+} by Eu^{2+} in feldspars (McLennan, 1989). Furthermore, the soils displayed REE enrichment relative to their parent rocks (Fig. 5.4) except for the absence of Tm in the parent rocks because it was below detection limits.

Table 5.6a: Rare earth element (REE) concentrations (ppm) and elemental ratios of oxidic soils developed from different parent rocks in Limpopo Province, South Africa.

Parent Rock		La	Ce	Pr	Nd	Sm	Eu	Gd	Tb	Dy	Ho	Er	Tm	Yb	Lu	LREE/HREE	Eu/Eu*
Basalt (n=9)	Min	8.96	35.25	2.31	9.78	2.40	0.75	2.51	0.43	3.04	0.66	2.08	0.29	2.37	0.35	4.48	0.82
	Max	17.02	64.55	5.02	20.84	4.88	1.70	5.61	0.88	5.59	1.10	3.35	0.48	3.68	0.52	5.85	1.06
	Average	13.45	51.83	3.94	16.52	3.94	1.19	4.25	0.70	4.58	0.91	2.87	0.43	3.00	0.44	5.27	0.89
Granite (n=6)	Min	19.76	38.55	4.36	14.46	2.54	0.47	1.93	0.23	1.36	0.24	0.67	0.10	0.73	0.08	14.17	0.63
	Max	33.38	68.30	7.44	26.35	4.88	0.84	2.96	0.39	1.95	0.37	1.00	0.13	0.98	0.15	18.32	0.84
	Average	25.00	49.37	5.50	19.42	3.40	0.66	2.40	0.31	1.61	0.30	0.81	0.12	0.81	0.12	15.87	0.72
Arkosic Sst (n=6)	Min	32.89	66.70	7.94	28.25	4.51	0.66	3.97	0.45	2.82	0.41	1.51	0.19	1.79	0.14	10.06	0.36
	Max	56.25	115.50	13.31	50.70	8.81	1.06	6.51	0.90	5.71	0.93	3.00	0.41	2.84	0.63	14.62	0.50
	Average	44.08	93.61	11.10	39.71	7.00	0.84	5.52	0.73	4.38	0.70	2.32	0.28	2.11	0.38	12.12	0.43
Gneiss (n=3)	Min	21.74	42.31	4.63	22.86	4.18	1.37	4.96	0.44	3.77	0.66	2.27	0.28	1.86	0.35	6.10	0.74
	Max	22.10	44.10	6.13	23.73	5.61	1.71	5.77	0.76	3.91	0.84	2.61	0.41	1.96	0.46	6.73	1.16
	Average	21.90	43.35	5.50	23.26	4.85	1.55	5.25	0.61	3.84	0.74	2.43	0.34	1.91	0.40	6.49	0.96
Quartzite (n=2)	Min	8.58	17.14	1.93	7.20	1.59	0.35	1.18	0.13	1.05	0.24	0.73	0.09	0.70	0.10	7.36	0.80
	Max	9.26	19.38	2.10	7.31	1.68	0.42	1.41	0.25	1.28	0.28	0.86	0.15	1.12	0.16	8.67	0.85
	Average	8.92	18.26	2.01	7.25	1.63	0.39	1.29	0.19	1.16	0.26	0.79	0.12	0.91	0.13	8.01	0.82

$$\text{Eu}/\text{Eu}^* = \text{Eu}_N / (\text{Sm}_N \times \text{Gd}_N)^{0.5}$$

Table 5.6b: Rare earth element (REE) concentrations (ppm) in the different parent rocks in Limpopo Province, South Africa.

Parent Rock		La	Ce	Pr	Nd	Sm	Eu	Gd	Tb	Dy	Ho	Er	Tm	Yb	Lu
Basalt (n=3)	Min	8.15	14.52	1.44	5.17	0.45	0.39	0.58	bdl	bdl	bdl	bdl	bdl	bdl	bdl
	Max	15.78	32.84	4.16	16.68	3.80	1.42	5.50	0.78	5.38	1.10	2.89	0.43	3.14	0.46
	Average	12.09	24.81	2.99	12.05	2.58	1.01	3.39	0.73	4.88	1.01	2.69	0.42	2.88	0.45
Granite (n=3)	Min	11.30	18.83	2.03	8.08	0.80	0.34	0.88	0.12	0.70	0.14	0.33	0.06	0.24	0.04
	Max	11.53	21.20	2.30	8.37	1.40	0.52	1.64	0.18	1.16	0.18	0.74	0.09	0.88	0.10
	Average	11.44	20.04	2.14	8.18	1.10	0.42	1.15	0.15	0.94	0.17	0.51	0.07	0.54	0.07
Arkosic Sst (n=3)	Min	7.50	14.53	1.64	5.41	0.84	0.31	0.84	0.07	0.49	0.11	0.25	bdl	bdl	bdl
	Max	16.81	34.25	3.87	13.25	1.72	0.56	1.51	0.16	0.72	0.17	0.37	bdl	0.48	0.06
	Average	11.04	21.14	2.41	8.18	1.21	0.45	1.12	0.12	0.64	0.15	0.33	bdl	0.46	0.06
Quartzite (n=1)		46.18	143.30	13.62	57.00	13.50	3.96	13.00	2.24	14.06	2.99	8.95	1.22	8.28	1.21

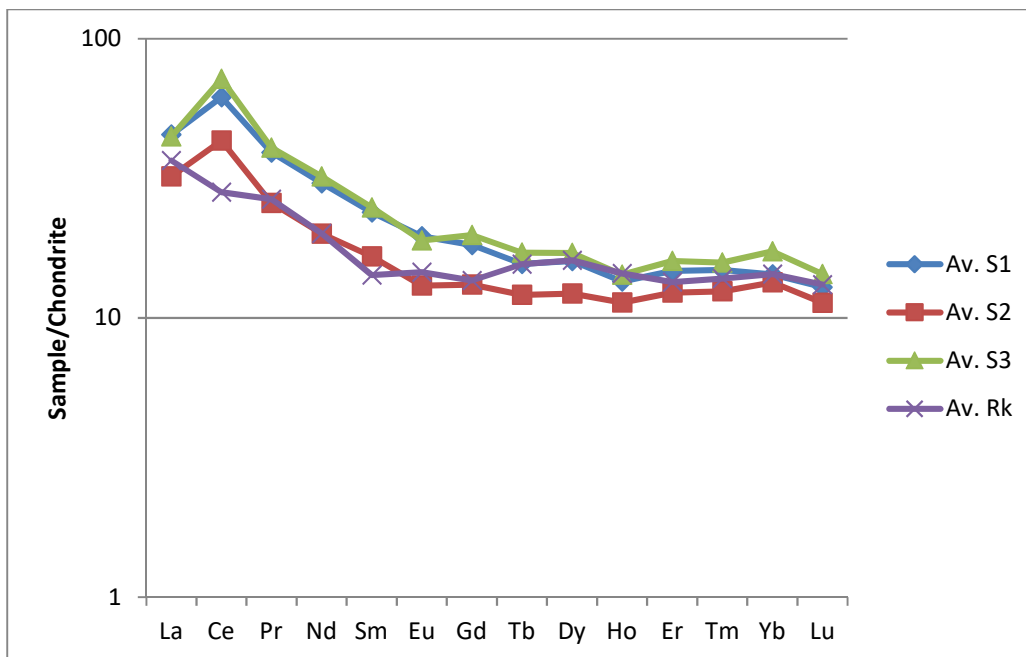


Figure 5.2: Chondrite-normalised REE pattern of average of the soils developed from basalt and their parent rocks.

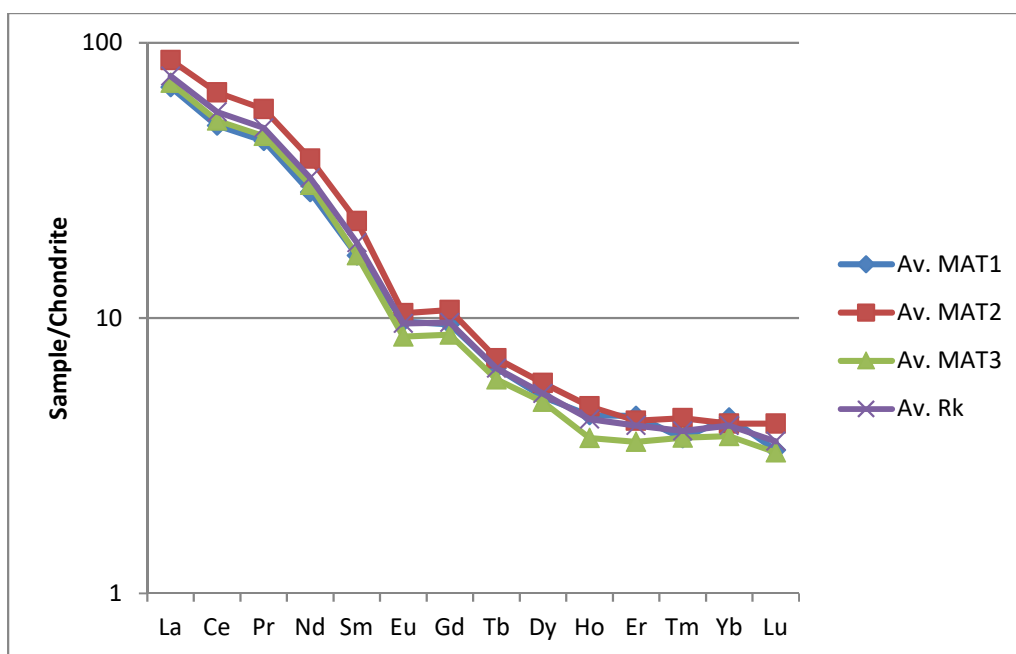


Figure 5.3: Chondrite-normalised REE pattern of average of the soils developed from granite and their parent rocks.

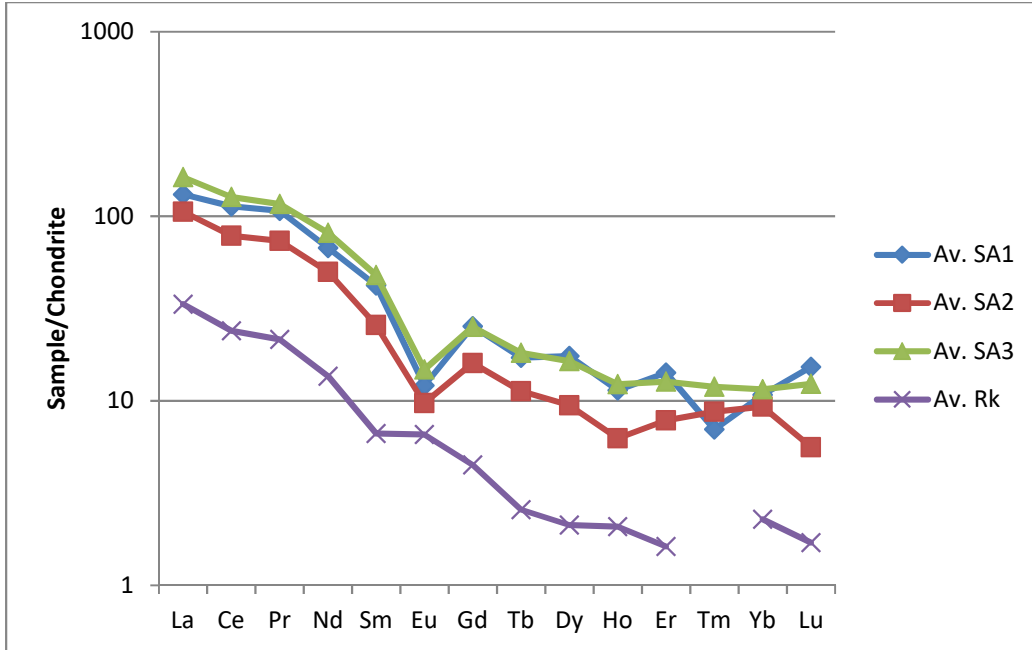


Figure 5.4: Chondrite-normalised REE pattern of average of the soils developed from arkosic sandstone and their parent rocks.

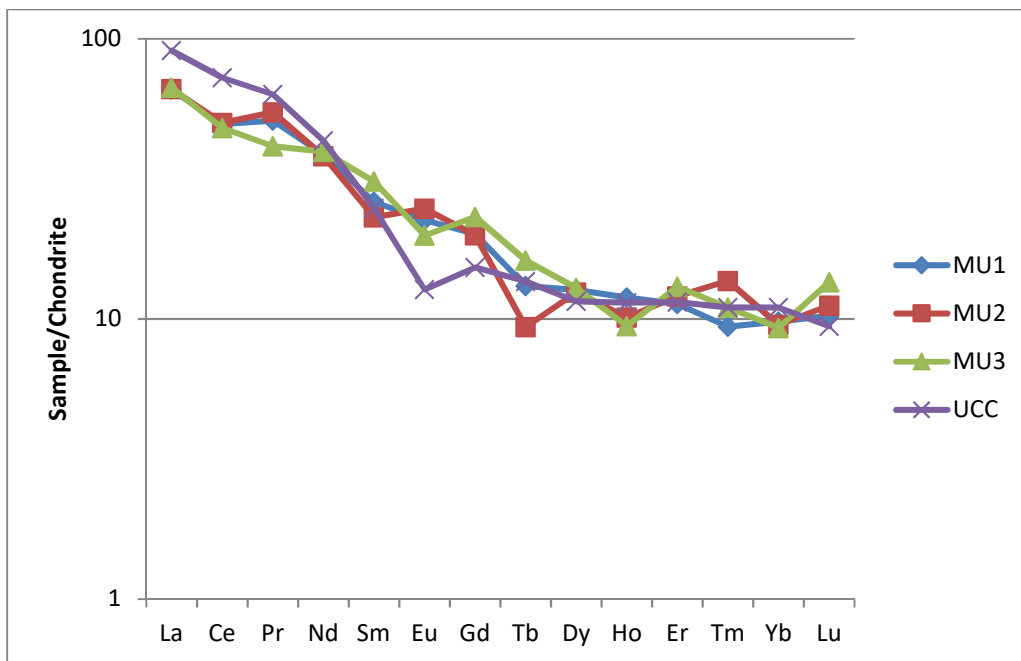


Figure 5.5: Chondrite-normalised REE pattern of average of the soils developed from gneiss and their parent rocks.

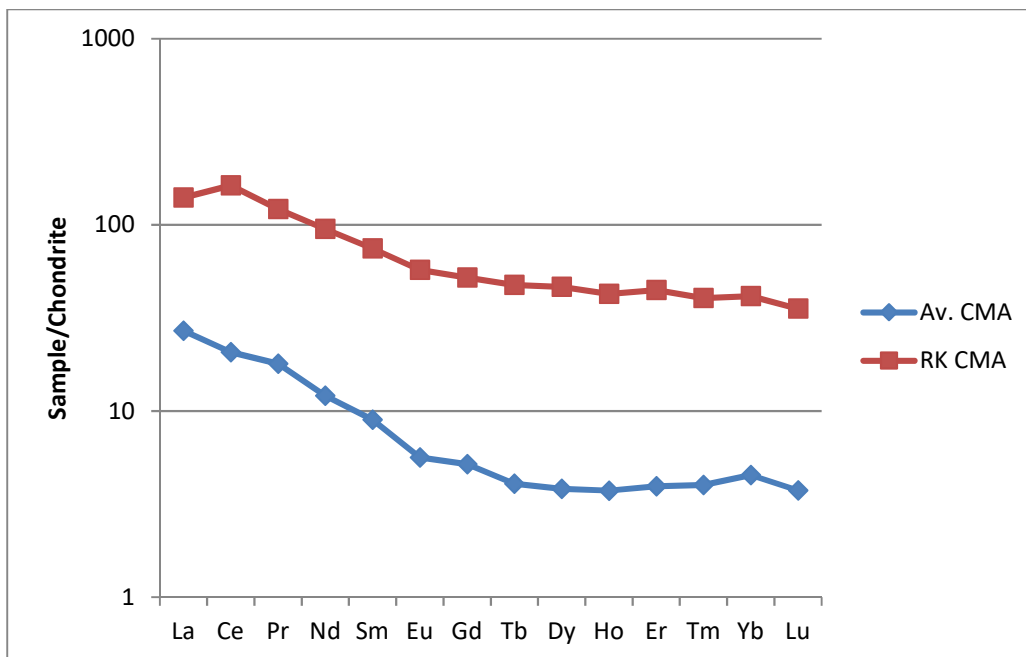


Figure 5.6: Chondrite-normalised REE pattern of average of the soils developed from quartzite and their parent rock.

Soils developed from gneiss showed LREE enrichment relative to the HREE (Fig. 5.5), whereas the soils developed from quartzite (control) showed similar trend with the parent rock except for the REE depletion in the soils relative to the parent rock (Fig. 5.6). Low REE concentrations in the soils can be attributed to the dominance of quartz (Gouveia *et al.*, 1993).

The LREE/HREE ratios (Table 5.6a) for the soils show that the content of LREE was generally higher than that of HREE. The average Eu/Eu* ratios greater than 0.85 obtained for the soils developed from basalt and gneiss confirm their mafic provenance, whereas Eu/Eu* less than 0.85 obtained for soils developed granite, arkosic sandstone, and quartzite (control) indicate their felsic provenance (Condie *et al.*, 1992).

5.2 Degree of Weathering

The present-day applications of weathering indices include among others, soil fertility evaluation and development (Delvaux *et al.*, 1989; Hamdan and Burnham, 1996),

demonstrating the impact of climate on bedrock weathering, quantifying the engineering properties of regolith (Duzgoren-Aydin *et al.*, 2002), and assessing elemental mobility during weathering (de Jayawardena and Izawa, 1994). The mineralogy of the parent rocks from the present study has feldspar as one of the dominant minerals and therefore the CIA, CIW, and PIA were found to be more applicable as they measure the extent of the conversion of feldspars to clays (Price and Velbel, 2003).

From the CIA values (Table 5.1a and Fig. 5.7), soils developed from basalt have the highest mean value (98.84), whereas soils developed from granite, arkosic sandstone, and gneiss have close mean values between 61.33 and 65.29. The soils developed from quartzite (control) have mean value of 90.42. The CIA values for the soils developed from basalt were higher than those of their bedrocks; and soils developed from granite and arkosic sandstone have similar CIA values close to that of their bedrocks (Tables 5.1a and b). According to Nesbitt and Wilson (1992), CIA values ranging from 50 to 70 suggest low-to-moderate degree of weathering and 70 to 100 suggest moderate-to-high degree of chemical weathering. Therefore, the soils developed from basalt have undergone intense chemical weathering whereas, those soils developed from granite, arkosic sandstone, and gneiss have experienced low degree of chemical weathering (Fig. 5.7).

The CIW and PIA indices also showed similar trends like the CIA for all the soils (Table 5.1a). However, CIW and PIA have slightly higher values relative to CIA which could be attributed to the exclusion of K_2O from the former (Hofer *et al.*, 2013). Soils that have experienced high degree of weathering are usually dominated by clays. Hence, the particle size distribution of the soils developed from basalt classified dominantly as clays relative to others classified dominantly as sandy loam reflects their weathering intensities (Velde and Meunier, 2008).

The ternary diagram with $Al_2O_3 - (CaO^* + Na_2O) - K_2O$ (A-CN-K) was used for evaluating the weathering trend of rocks containing plagioclase and orthoclase feldspars (Nesbitt and Young, 1984; 1989). Furthermore, to assess the relationship between the felsic (leucocratic) and mafic (melanocratic) constituents in the weathering profiles, $Al_2O_3 - (CaO^* + Na_2O + K_2O) - (FeO+MgO)$ (A-CNK-FM) diagram (Nesbitt and

Young, 1989) was also used. In the case of A-CN-K, fresh and unaltered granitic rocks with CIA values of about 50 would plot along the plagioclase-K-feldspar line (Fig. 5.8). The breakdown of plagioclase feldspar at the initial stages of weathering causes the composition of the weathered materials to shift away from the CN corner parallel to the A-CN due to the loss of Ca and Na with a corresponding increase in Al_2O_3 .

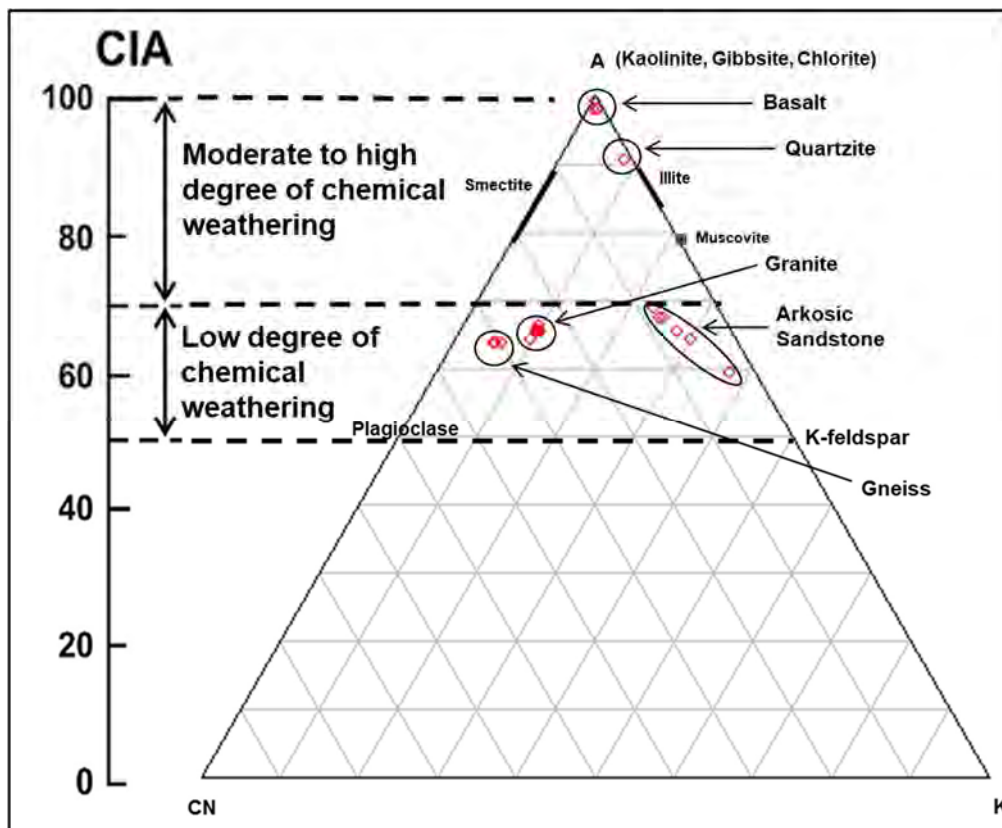


Figure 5.7: CIA ternary diagram for the studied soils (Fields after Nesbitt and Young, 1982; Hofer *et al.*, 2013).

However, as the weathering becomes more intense, K would be lost from the weathered materials and the compositional plot will move away from K corner and eventually plot towards the Al_2O_3 corner for highly weathered clay-rich materials with CIA values of about 100 (Nesbitt and Young, 1989; Sharma and Rajamani, 2000). The A-CN-K diagrams for the various soils developed from parent rocks are given in Figures 5.9 – 5.13.

For soils developed from basalt (Fig. 5.9), the parent rocks plotting close to the plagioclase composition indicate the dominance of plagioclase over k-feldspar in the original rock. The direct movement of the trend towards the A-apex without intersecting the A-K line also indicates very low initial values of K in the parent rocks. The observed weathering trend parallel to the A-CN line with all the samples plotting around the Al_2O_3 apex show that they have undergone the maximum degree of chemical weathering as earlier confirmed from their CIA values. This implies near total depletion of Ca, Na, and K and enrichment of Fe and Al since all the major silicate minerals have reached the end stage of chemical weathering and are replaced by secondary mineral phases in the soils. The mineralogy of the soils also supports these observations.

Figure 5.10 represents the compositional weathering trend of the soils developed from granite. The trend is subparallel to the A-CN boundary indicating higher rate of removal of Ca and Na than K primarily by weathering of plagioclase as expected for a granitic parent rock. The soils have not suffered intense chemical weathering as the weathering trend has not progressed to the A-K line which suggests incomplete dissolution of plagioclase (Deepthy, 2008).

The plot of the parent rocks for soils developed from arkosic sandstone close to the A-K line suggests the dominance of K-feldspar in the original rock (Fig. 5.11). The weathering trend towards the Al_2O_3 apex corresponds to the dissolution of K-feldspar. It therefore indicates that the chemical composition of the soils and their elemental distribution depends not only on the extent and nature of weathering alone but on the mineralogy of the parent rock.

The compositional weathering trend for soils developed from gneiss parallel to the A-CN line towards the A-apex indicates the removal of Na and Ca due to the dissolution of plagioclase (Fig. 5.12). The trend further suggests that the soils have not suffered intense chemical weathering as the trend has neither reached the A-K line nor the A-apex.

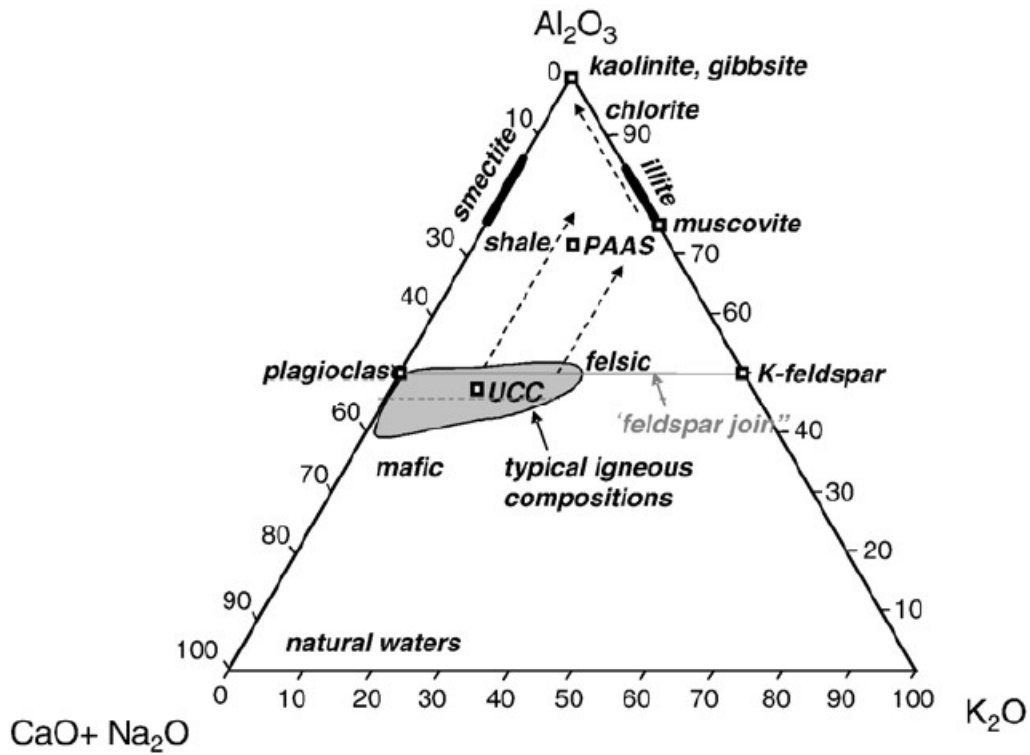


Figure 5.8: A-CN-K ternary diagram showing location of common minerals, UCC, PAAS and possible weathering trends (After Nesbitt and Young, 1984).

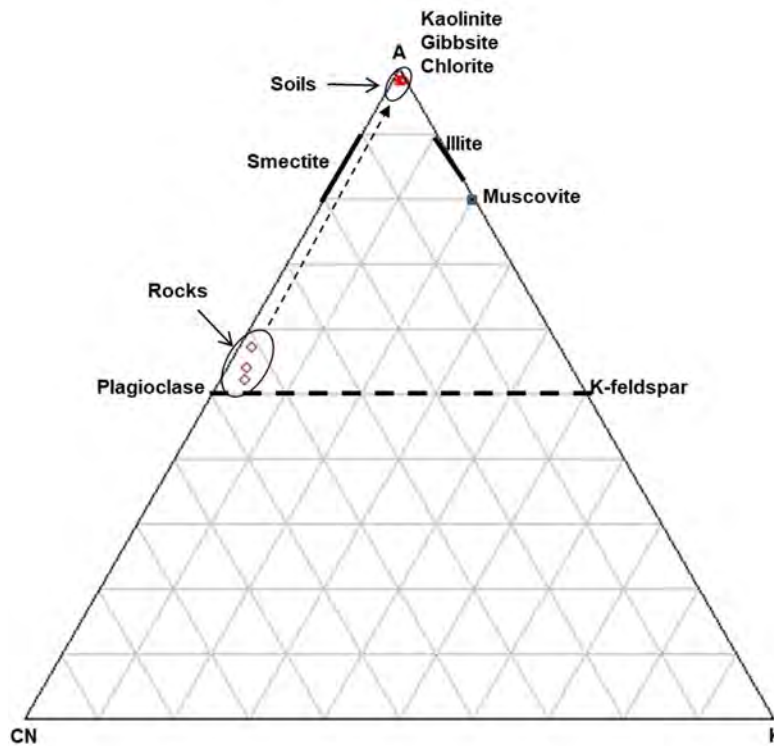


Figure 5.9: A-CN-K ternary diagram for soils developed from basalt.

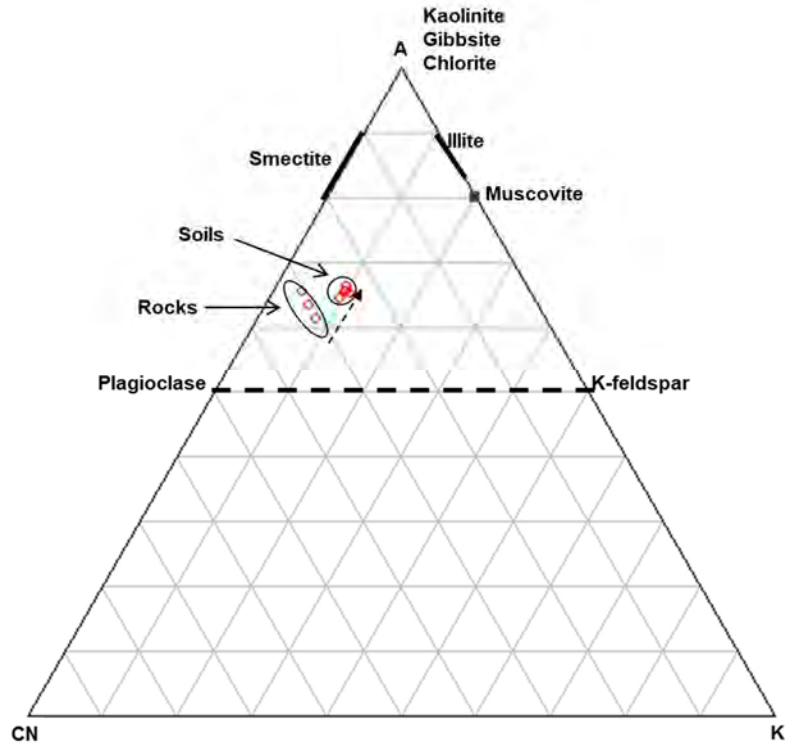


Figure 5.10: A-CN-K ternary diagram for soils developed from granite.

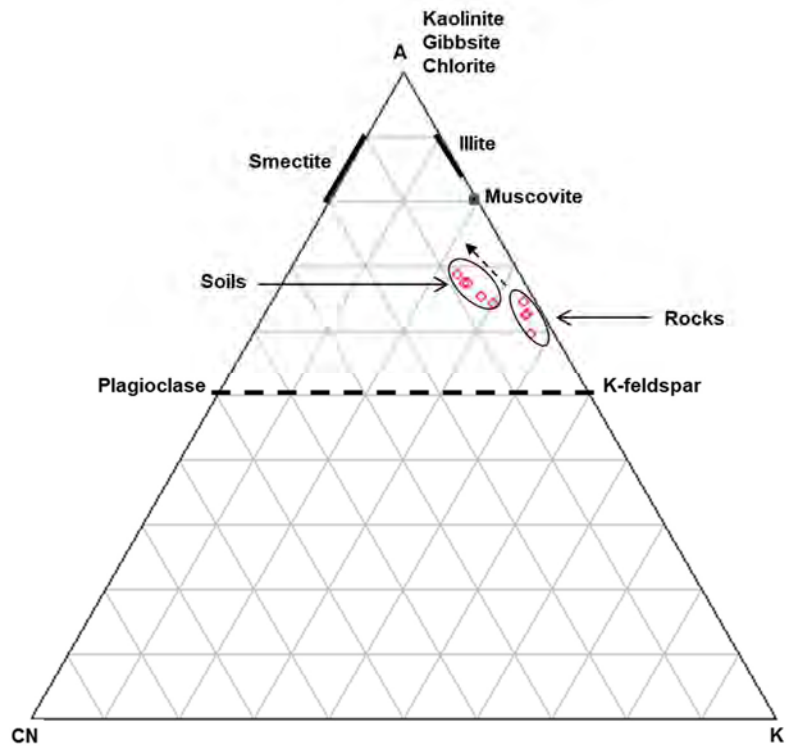


Figure 5.11: A-CN-K ternary diagram for soils developed from arkosic sandstone.

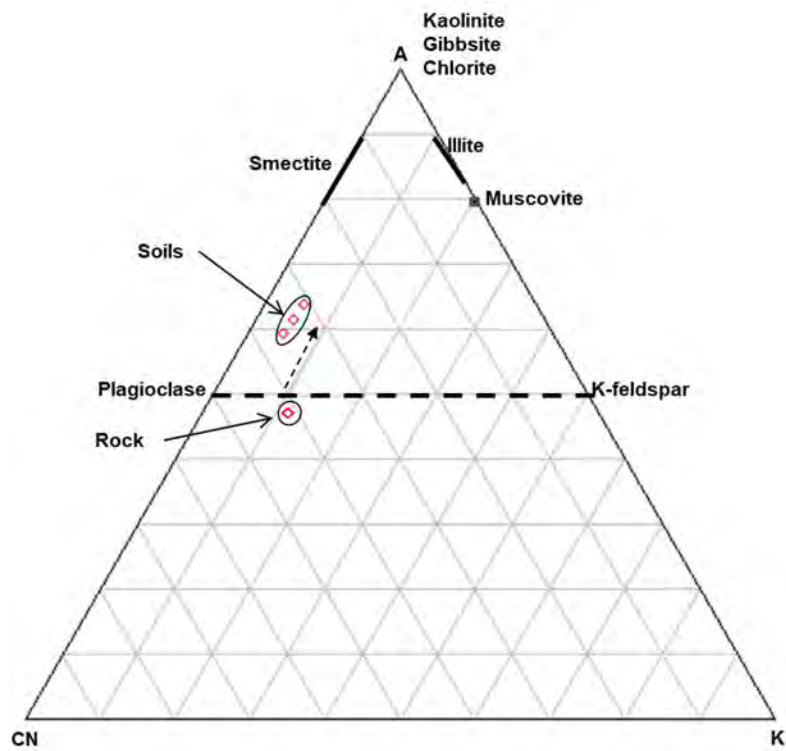


Figure 5.12: A-CN-K ternary diagram for soils developed from gneiss.

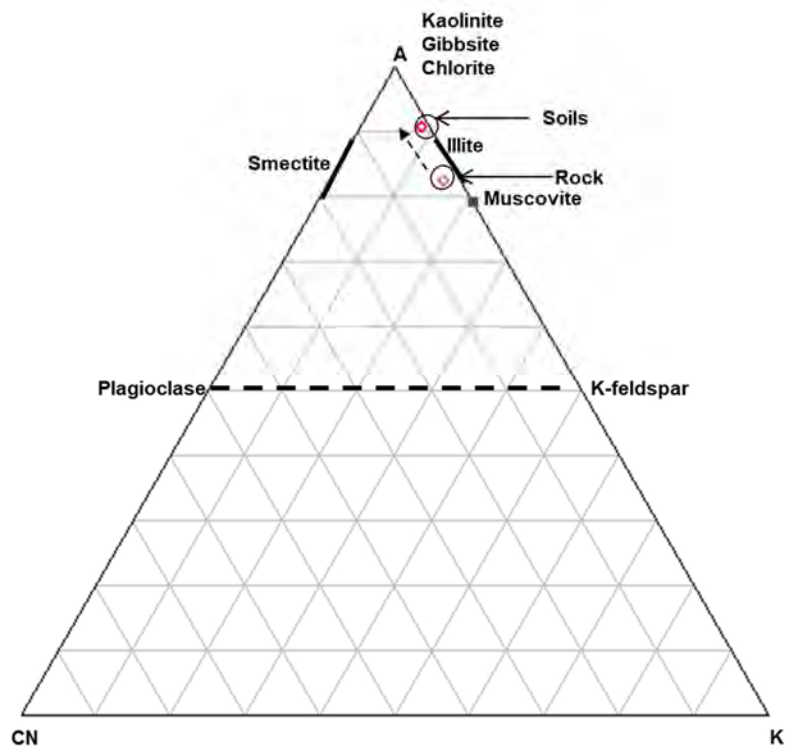


Figure 5.13: A-CN-K ternary diagram for soils developed from quartzite (control).

The parent rock for soils developed from quartzite (control) plotted close to the A-K line towards the A-apex suggesting the depletion of K in the original rock due to intense chemical weathering (Fig. 5.13). The parent rock having CIA value of 80.35 can only be possibly attributed to pre-metamorphism history of weathering, differential erosion, and chemical maturation (Tijani *et al.*, 2006). Metamorphosed sedimentary rocks might exhibit 'weathered' chemical signatures; hence, application of A-CN-K ternary diagram to meta-sedimentary units should be interpreted with caution. The diagram and CIA value is likely to be a reflection of the pre-metamorphic weathering history of the primary material rather than the prevailing weathering regime and trend. In addition, the rainfall regime around Matoks/Sagole axis could not have favoured intense chemical weathering.

In the case of A-CNK-FM, the parent rocks for the soils developed from basalt plotted along the line between feldspar and FM apex (Fig. 5.14). This reflects equal preference for felsic and mafic components. The compositional weathering trend has reached the A-FM line following the leaching of alkali elements in preference to Fe and Mg and marking the beginning of a trend towards the Al_2O_3 apex. The soils developed from basalt are characterised by the presence of Ti and Fe oxides compared to other soils in this study.

The parent rocks for soils developed from granite plotting along the line between muscovite and feldspar reflects felsic composition (Fig. 5.15). The weathering trend shows a shift towards the A-FM line. This indicates that the weathering has not progressed enough to leach all the alkali elements. The weathering trend pointing towards the FM apex suggests Fe and Mg gain which is supported by their relative enrichments in the soil (Table 5.2).

Felsic nature of the parent rocks for soil developed from arkosic sandstone (Fig. 5.16) was evident from their plots between muscovite and feldspar just like in the case of granite. The weathering trend not reaching the A-FM line suggests low chemical weathering and more alkalis are still present.

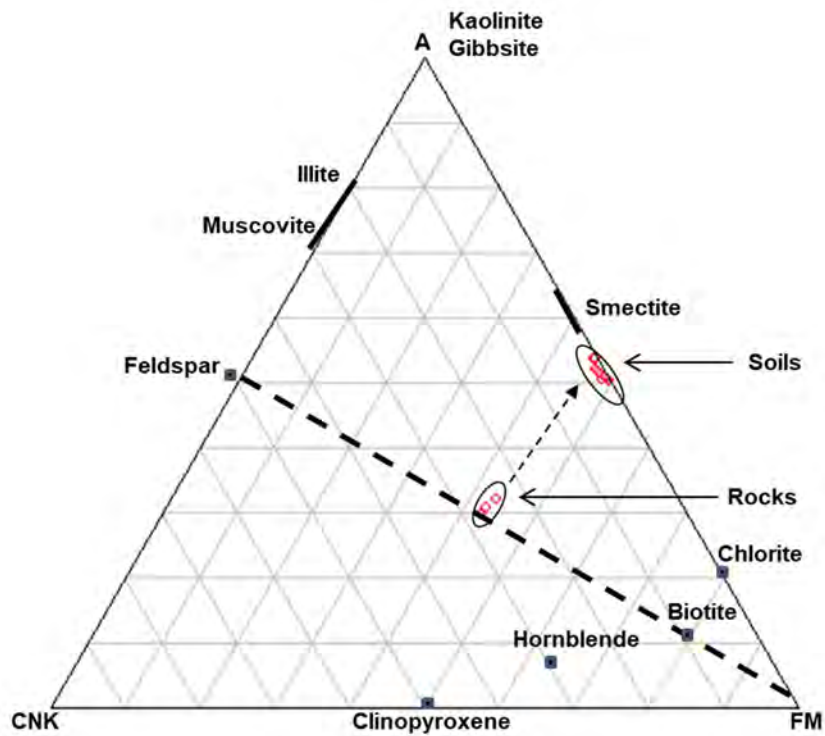


Figure 5.14: A-CNK-FM ternary diagram for soils developed from basalt.

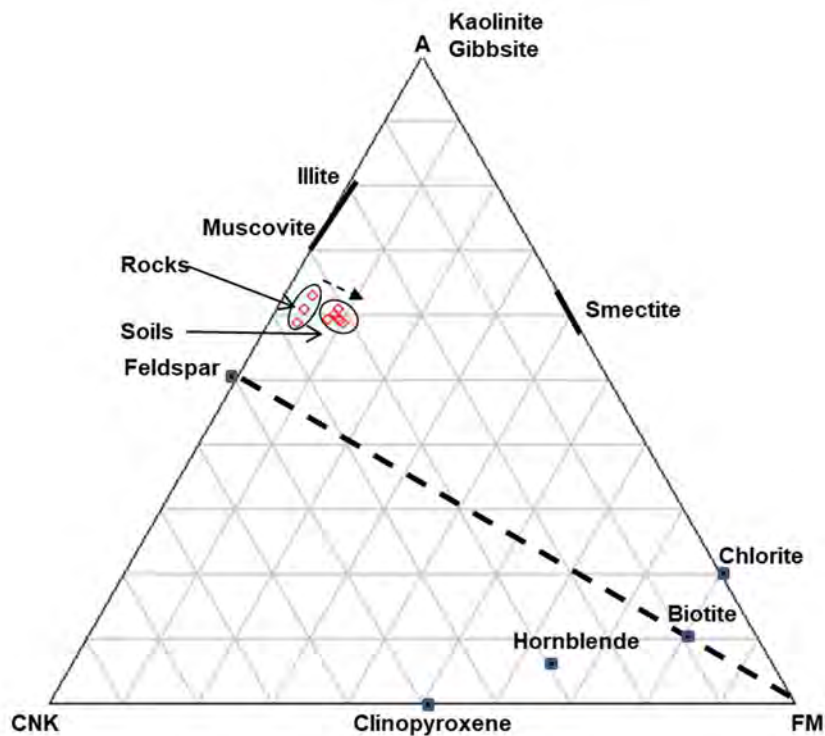


Figure 5.15: A-CNK-FM ternary diagram for soils developed from granite.

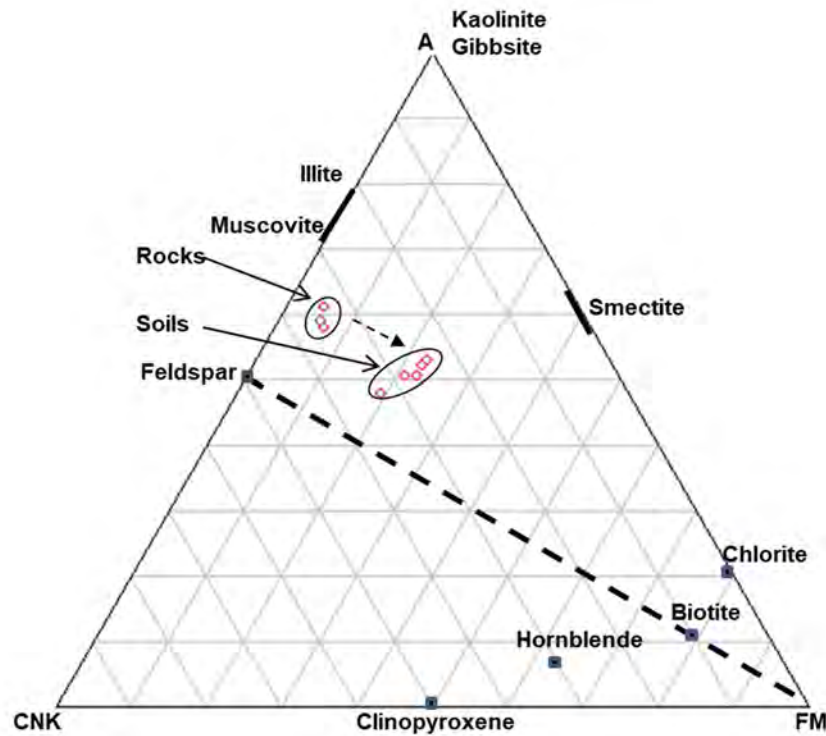


Figure 5.16: A-CNK-FM ternary diagram for soils developed from arkosic sandstone.

The weathering trend towards the A-FM line but still close to the feldspar-FM line for soils developed from gneiss (Fig. 5.17). This also indicates low degree of chemical weathering which is evident with the presence of primary minerals in the soils.

For soils developed from quartzite (control) (Fig. 5.18), the parent rock plotted close to the A-FM line suggesting depletion in the alkali which can be attributed to advanced stage of weathering. As earlier mentioned, this would possibly be due to its pre-metamorphic history of weathering rather than the current weathering regime in the area. The compositional weathering trend towards the A-apex indicates relative enrichment in Al compared to Fe in the residual phases.

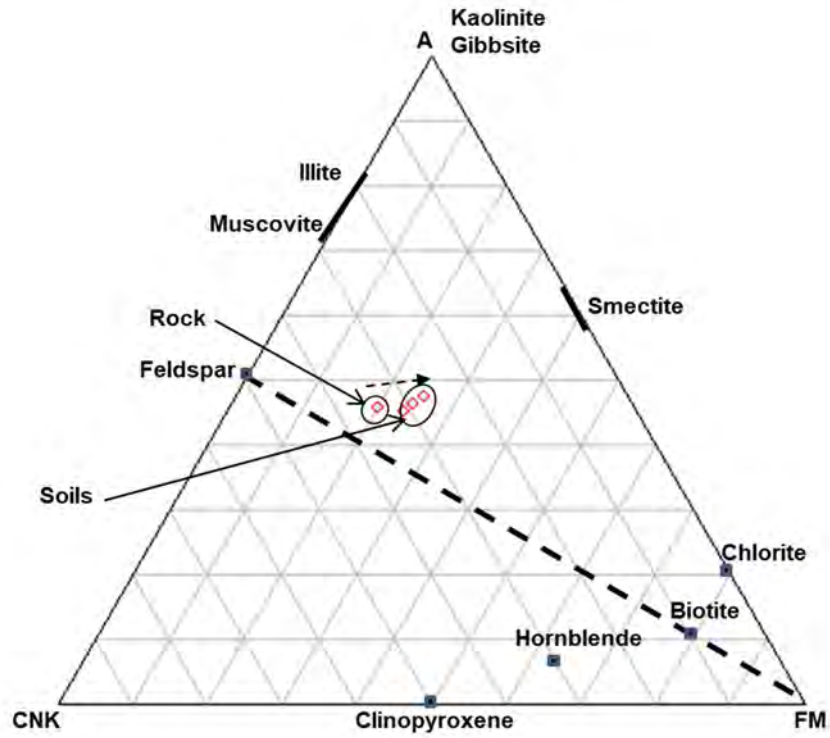


Figure 5.17: A-CNK-FM ternary diagram for soils developed from gneiss.

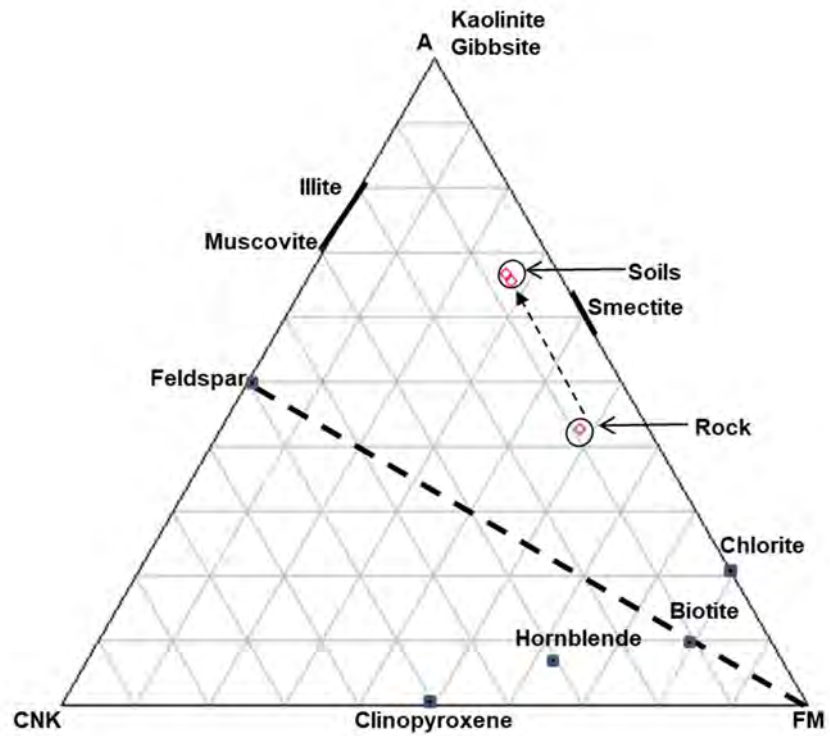


Figure 5.18: A-CNK-FM ternary diagram for soils developed from quartzite (control).

5.3 Statistical Analyses

Principal component analysis was conducted to identify variables of similar geochemical behaviour in the soils developed from different parent rocks. Factor analyses were extended to include the major element oxides, LOI, trace elements, LREE, HREE, and CIA data. The factor analyses of gneiss and quartzite were carried out together because of their small sample sizes for a more reliable resulting factor (Davis, 2002). Based on the Scree plots (Figures 5.19 – 5.22), three factors explained 94.90 % of the variation in the data for soils developed from basalt (Table 5.7) whereas, four factors each accounted 97.57 % and 98.66 % of the data variability in the soils developed from granite and arkosic sandstone, respectively (Tables 5.8 and 5.9). In addition, a factor explained 94.80 % of variation in the data for gneiss and quartzite (control). Hence, the rotated component matrix cannot be computed due to the high loading single factor (Davis, 2002).

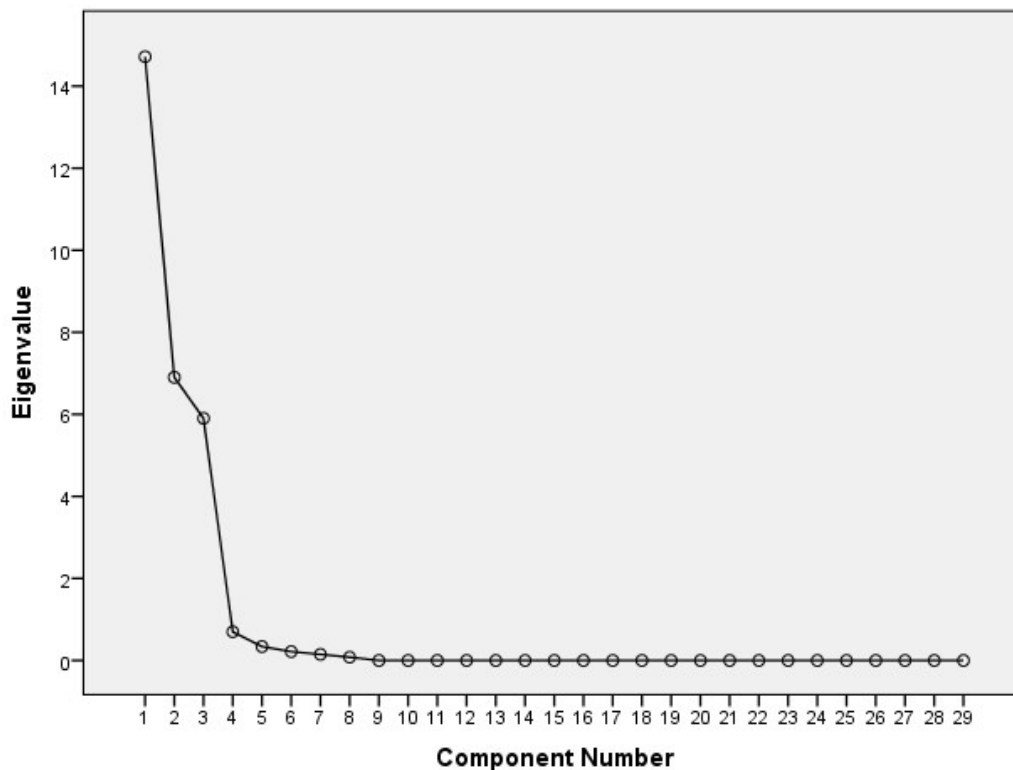


Figure 5.19: Scree plot of the studied Soils developed from basalt.

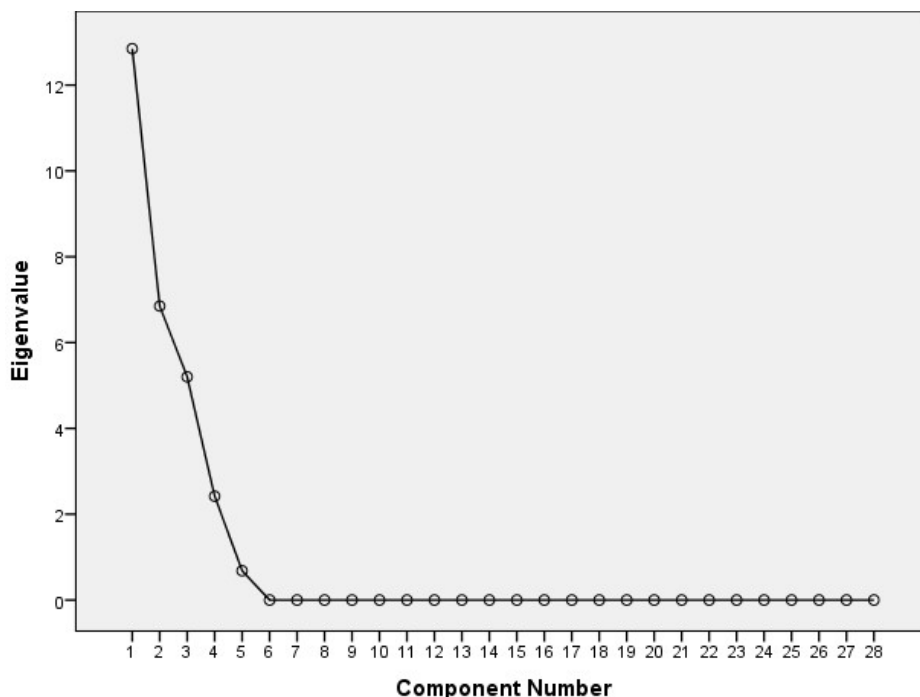


Figure 5.20: Scree plot of the studied Soils developed from granite.

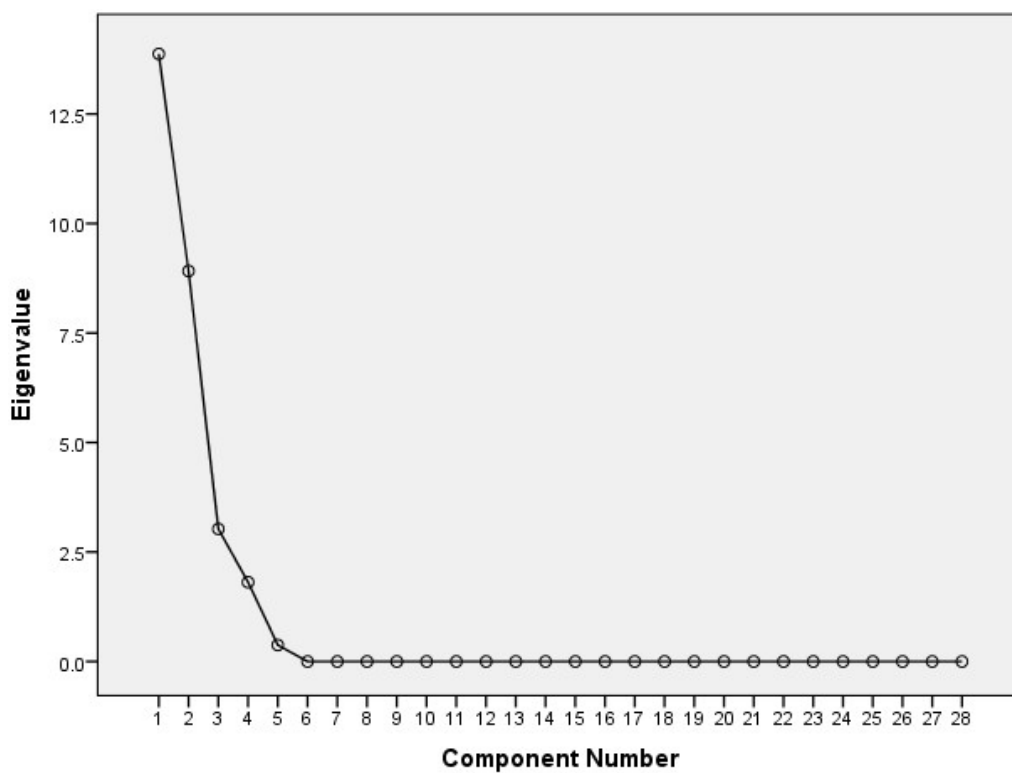


Figure 5.21: Scree plot of the studied Soils developed from arkosic sandstone.

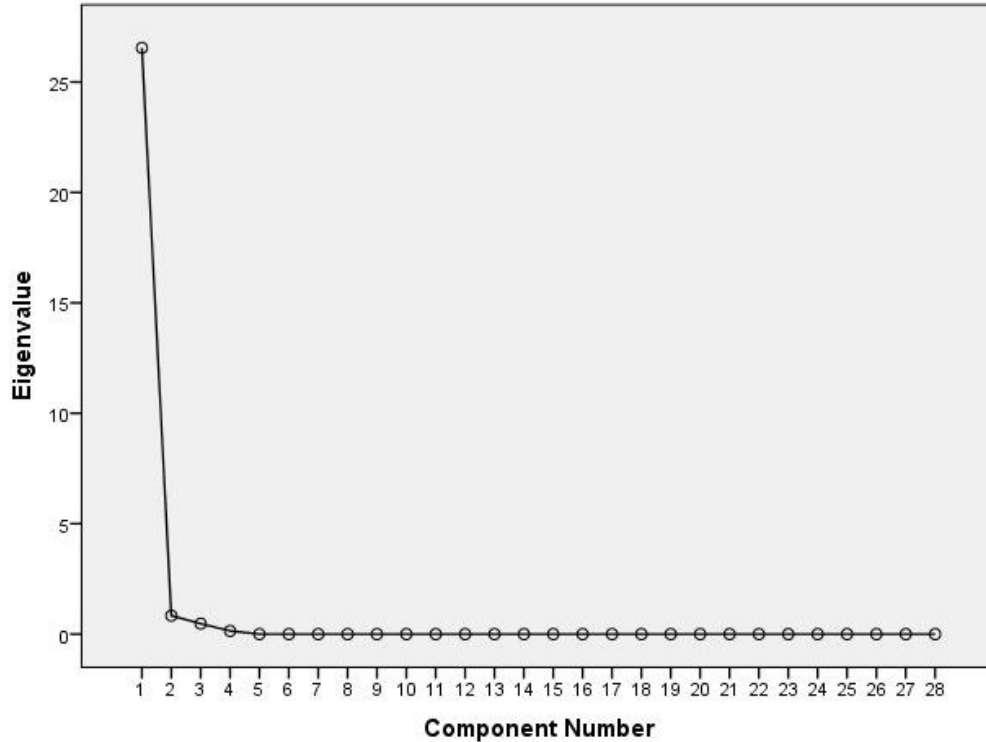


Figure 5.22: Scree plot of the studied Soils developed from gneiss and quartzite.

For the soils developed from basalt, the calculated factors 1, 2, and 3 explained 50.75, 23.80, and 20.35 % respectively, of the variance. Factor 1 shows significant positive factor loadings (Table 5.8, bold numbers indicate significant factor loadings > 0.500) with Zr, V, Th, TiO₂, Sc, Fe₂O₃, U, P₂O₅, LREE, Cu and negative factor loadings with SiO₂, MgO, Ba, Sr, CaO, and MnO. Factor 2 has positive factor loadings with Ba, Zn, LOI, Pb, Sr, CaO, HREE, Na₂O, Co, and MnO and negative factor loadings with Al₂O₃ only. Factor 3 has positive factor loadings with Ni, Cr₂O₃, Cr, CIA, LREE, and Cu and negative factor loadings with MgO, Rb, and K₂O. Factor 1 represents the weathering factor which shows the depletion of SiO₂, MgO, Ba, Sr, CaO, and MnO due to the weathering of plagioclase and diopside. The inverse relationship between Al₂O₃ and Ba, Zn, LOI, Pb, Sr, CaO, HREE, Na₂O, Co, and MnO represents the kaolinite factor relating to its derivation from the alteration of felsic and ferromagnesian minerals. Factor 3 also represents the weathering factor.

Table 5.7: Factor Loadings obtained from Principal Component Analysis of the studied Soils developed from basalt.

	Factors		
	1	2	3
Zr	.986	-.103	.116
V	.983	-.166	.064
Th	.980	-.155	-.092
TiO ₂	.972	-.096	.197
SiO ₂	-.963	.135	-.203
Sc	.960	-.219	-.109
Fe ₂ O ₃	.948	-.256	.185
U	.934	.042	-.237
MgO	-.819	.243	-.511
Ba	-.764	.640	-.023
P ₂ O ₅	.708	.471	-.198
Zn	.020	.930	-.129
LOI	-.281	.865	-.192
Pb	.172	.855	.173
Sr	-.533	.835	.024
CaO	-.545	.826	.117
HREE	.478	.818	-.318
Na ₂ O	-.291	.816	-.201
Al ₂ O ₃	.482	-.786	.333
Co	-.015	.740	.404
MnO	-.607	.676	-.238
Ni	-.213	-.049	.969
Cr ₂ O ₃	-.020	.047	.964
Rb	-.127	.040	-.955
Cr	-.212	.164	.952
K ₂ O	-.135	.083	-.945
CIA	.323	-.473	.798
LREE	.679	-.129	.722
Cu	.533	-.446	.699
Eigenvalues	14.72	6.90	5.90
Cumulative Variance (%)	50.75	74.55	94.90

Table 5.8: Factor Loadings obtained from Principal Component Analysis of the studied Soils developed from granite.

	Factors			
	1	2	3	4
LREE	.966	.178	-.023	.159
HREE	.945	-.255	.174	.052
V	.927	.128	-.336	.095
Th	.888	.402	-.081	.175
Sc	.887	-.070	-.396	-.063
Ni	.863	-.204	-.150	-.081
Co	.855	-.285	.041	-.393
Cr	.806	-.031	-.503	.310
Cu	.788	-.612	-.056	-.024
Sr	-.628	-.517	.384	.381
LOI	.077	.970	.205	-.029
CIA	.121	.962	.213	.063
Al ₂ O ₃	.129	.868	.470	-.082
P ₂ O ₅	.284	.856	.220	.349
Pb	.324	-.848	.239	.231
Fe ₂ O ₃	-.494	.804	.307	-.114
MgO	-.611	.742	.271	-.048
Zn	.126	-.714	.268	.515
K ₂ O	-.466	.666	.441	-.378
Na ₂ O	.056	.236	.966	.089
TiO ₂	-.265	.155	.933	-.189
SiO ₂	-.116	.004	.903	.411
CaO	-.186	.436	.879	.049
MnO	-.279	-.151	.796	.516
Rb	.614	-.316	-.678	.221
Zr	-.125	.095	.130	.942
U	.415	-.542	.298	.667
Ba	.466	-.398	-.477	.628
Eigenvalues	12.85	6.85	5.20	2.42
Cumulative Variance (%)	45.90	70.35	88.93	97.57

Table 5.9: Factor Loadings obtained from Principal Component Analysis of the studied Soils developed from arkosic sandstone.

	Factors			
	1	2	3	4
Zr	.988	-.013	-.029	-.122
Co	.982	.036	.052	.048
Zn	.977	.051	.105	.169
LREE	.966	.145	.108	.184
Sr	.962	.107	.119	.156
Sc	.948	-.043	.178	-.193
Th	.932	.131	.283	.183
Cr	.894	.161	.266	-.267
Pb	.891	.218	.191	-.323
V	.885	.015	-.249	.377
Ni	.875	.165	.175	.402
HREE	.863	-.098	-.417	-.211
U	.730	.051	.308	.601
LOI	.054	.982	-.068	.154
MgO	.116	-.980	-.107	.103
MnO	.137	-.978	-.089	-.043
Na ₂ O	.175	-.974	-.097	-.049
TiO ₂	.180	.973	-.098	-.050
Al ₂ O ₃	-.043	.958	.224	.154
P ₂ O ₅	.167	.954	.224	.060
CaO	-.133	-.917	.325	.169
CIA	-.033	.861	.468	.011
Fe ₂ O ₃	-.170	.837	.473	.143
K ₂ O	.477	-.746	.031	.454
Rb	-.124	-.200	-.962	.067
SiO ₂	.424	-.046	.843	.318
Ba	-.640	-.193	-.686	-.272
Cu	-.022	.381	.178	.904
Eigenvalues	13.87	8.92	3.03	1.81
Cumulative Variance (%)	49.54	81.38	92.19	98.66

The four calculated factors for soils developed from granite explained 45.90, 25.46, 18.58, and 8.64 % respectively, of the variance. Factor 1 shows significant positive factor loadings with V, Sc, Cr, LREE, Th, Rb, Ni, HREE, Co, and Cu, and negative loadings with Sr, Rb, and MgO. Factor 2 shows significant positive loadings with TiO₂, Al₂O₃, LOI, CIA, K₂O, Fe₂O₃, P₂O₅, and MgO, and negative loadings with Sr, U, Cu, Zn, and Pb. Factor 3 shows significant positive loadings with Na₂O, TiO₂, SiO₂, CaO, and MnO, and negative factor loadings with Rb and Cr. Factor 4 shows significant positive loadings with Zn, MnO, Zr, U, and Ba. The factor 1 represents the weathering factor which shows the removal of bases and silica (such as K₂O, CaO, MgO, Na₂O, MnO with significant factor loadings < 0.500 except for Na₂O). Factors 2, 3, and 4 are the provenance factors which show the felsic input from plagioclase, muscovite, microcline, and quartz.

The calculated factors 1, 2, 3, and 4 explained 49.54, 31.84, 10.81, and 6.47 % of the variance respectively in soils developed from arkosic sandstone. Factor 1 shows significant positive loadings with Zr, Zn, Sr, Co, LREE, Sc, Th, Pb, Cr, Ni, V, HREE, and U, and negative loadings with Ba only. Factor 2 shows significant positive loadings with LOI, TiO₂, Al₂O₃, P₂O₅, Fe₂O₃, and CIA, and negative loadings with MgO, MnO, Na₂O, CaO, and K₂O. Factor 3 shows significant positive loadings with SiO₂ and negative factor loadings with Rb and Ba. Factor 4 shows significant positive loadings with Cu and U. Factor 1 represents the provenance factor with the trace elements and REEs associated with the survival of abrasion – resistant accessory mineral such as zircon rich in Zr. Factor 2, 3, and 4 represents the weathering factor with the enrichment of U, LOI, TiO₂, Al₂O₃, P₂O₅, and Fe₂O₃ as weathering intensify.

Influences of parent rocks and degree of weathering have also been reported in explaining principal factors responsible for similar geochemical association of elements in soils (Miko *et al.*, 2001; Melegy and El-Agami, 2004; Bam *et al.*, 2011; Silva *et al.*, 2016). Provenance discriminating factor due to inputs from quartz, orthoclase, biotite, and muscovite explained the geochemical associations of major and trace elements in Croatian, Czech, and Thai soils (Miko *et al.*, 2001; Melegy and El-Agami, 2004; Kanket, 2006). Furthermore, major geogenic elemental association in soils developed on

Croatian Karst was termed as the 'clay factor' due to the inverse relationship between Al and other alkali metals (Miko *et al.*, 2001). Geochemical association of major and trace elements in Brazillian soils were attributed to the degree of weathering intensity which was as well described as the 'weathering factor'. This was inferred from the accumulation of some elements relative to others that were leached as weathering intensity increases (Silva *et al.*, 2016).

5.4 Concluding Remarks

Based on the mineralogical and geochemical considerations, the following deductions have been made:

- a. The soils developed from granite, arkosic sandstone, and gneiss had undergone low degree of chemical weathering whereas, soils developed from basalt experienced intense chemical weathering.
- b. The mineralogical and geochemical characteristics of the parent rocks and intensity of weathering both played vital roles in the overall mineralogical and geochemical characteristics of the soils.
- c. Enrichment factor with reference to immobile Ti showed accumulation of trace elements in soils developed from basalt and gneiss (except for Rb, Sr, and Ba in soils developed from basalt) in contrast to depletion due to little or no lithogenic release by weathering processes for soils developed from granite, arkosic sandstone, quartzite except for Cr and Ta.
- d. Geochemical characteristics of the soils suggest minimal potential of trace element risk to plant.

Chapter Six

The Nature of Soil Kaolins Developed from different Parent Rocks in Limpopo Province, South Africa

This chapter aimed to establish the variations in the mineralogy and geochemistry of soil kaolins developed from different parent rocks in Limpopo Province, South Africa (Specific Objective 2) based on Hypothesis 2. The mineralogical and geochemical characteristics of the studied soil kaolins were used to achieve specific objective 2.

6.1 Mineralogical Characteristics

6.1.1 Mineral Identification and Quantification

The soil kaolins developed from basalt were mainly composed of kaolinite, quartz, anatase, goethite, hematite, and gibbsite. Kaolinite and quartz were the dominant components ranging from 82 to 92 wt % with > 60 wt % kaolinite (Fig. 6.1). The non-clay minerals constituted < 18 wt % in all the samples with Ti-bearing mineral, anatase, Fe-bearing minerals, goethite and hematite dominating. Gibbsite was present mainly in minor amounts. The dominance of kaolin coupled with the presence of gibbsite is consistent with the highly weathered state of the soils and similar observations have been made for highly weathered soils from other parts of the world (Kanket, 2006). The presence of anatase, goethite and hematite could be attributed to the relative abundance of Ti and Fe in mafic rocks which are concentrated considerably during weathering (Wiriyakitnatekul *et al.*, 2010). From the mineralogy of the parent rock (basalt), the formation of kaolinite must have been because of the weathering of plagioclase feldspar following the two steps earlier discussed (Eqns. 2.1 and 2.2). Further interaction of kaolinite with water led to the formation of gibbsite (Eqn. 2.5).

The minerals present in soil kaolins developed from granite were kaolinite, quartz, plagioclase feldspar, muscovite, chlorite, and actinolite. Kaolinite dominated the clay minerals (> 24 wt %) with chlorite present in minor amounts. The non-clay minerals constituted > 69 wt % in all the samples. The presence of greater % of weatherable

minerals could be associated with low chemical weathering due to low rainfall regime around Matoks area based on the climatic zone. The parent rock (granite) has plagioclase feldspar, quartz, microcline, muscovite, and chlorite as the primary minerals. It is evident that the weathering of plagioclase feldspar, microcline, and muscovite led to the formation of the kaolinite following equations 2.1 - 2.5, respectively.

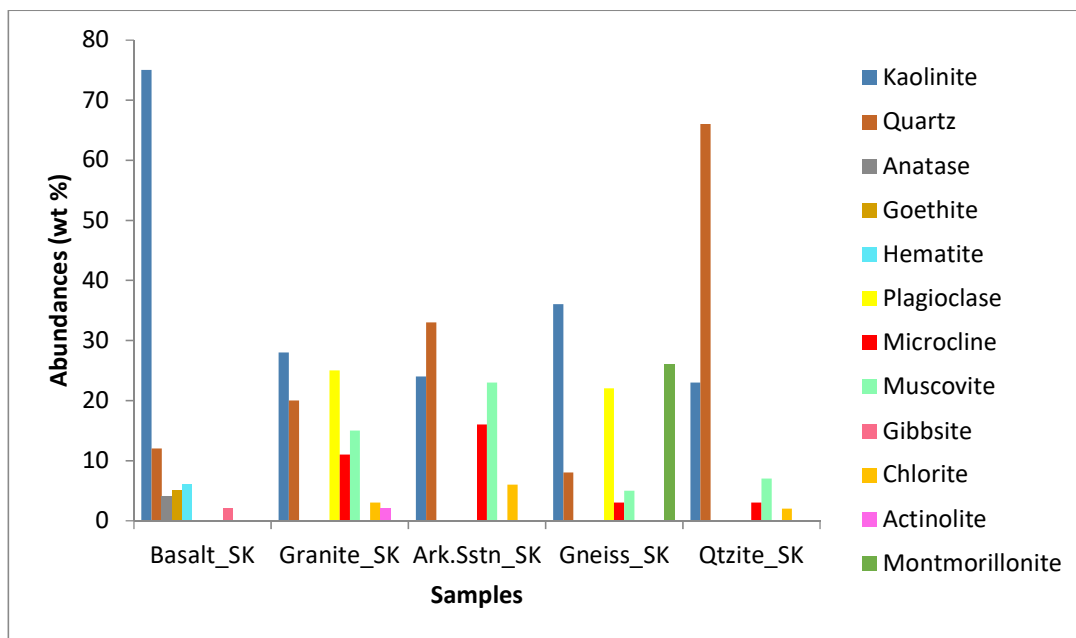


Fig. 6.1: Mineral abundances (wt %) in the soil kaolins developed from different parent rocks.

Quartz was the dominant mineral (> 27 wt %) followed by kaolinite in soil kaolins developed from arkosic sandstone. The non-clay minerals constituted > 69 wt % with weatherable minerals like muscovite and microcline present. The prevailing arid climate around Sagole area could not have allowed intense weathering of the primary minerals to form kaolinite. However, the weathering of muscovite and microcline in the arkosic sandstone would have resulted in the formation of kaolinite following equations 2.3 and 2.4.

Kaolinite and montmorillonite are the clay minerals present in the soil kaolins developed from gneiss. Plagioclase feldspar, quartz, muscovite, and microcline constituted the

non-clay minerals. The plagioclase feldspar, microcline, and muscovite are relatively abundant in the parent rock (Robb *et al.*, 2006) and hence their weathering will result in the formation of kaolinite following equations 2.1 - 2.5, respectively.

The soil kaolins developed from quartzite (control) were characterised by kaolinite (dominant clay mineral), quartz (> 65 wt %), muscovite, microcline, and chlorite. Kaolinite must have been formed from the weathering of microcline, plagioclase feldspar, and muscovite present in the parent rock, quartzite following equations 2.1 - 2.5, respectively.

The average abundances of kaolinite from this study which ranges between 23 and 75 wt % were lower than the average values obtained for kaolinites in Thai (95 wt %) and Brazillian (85 wt %) soils (Kanket, 2006). This could be attributed to the advanced soil developmental stages in the Thai and Brazillian soils due to more leaching and oxidation associated with greater moisture regime (Kheoruenromne and Suddhiprakarn, 1984; Kanket, 2006).

6.1.2 Kaolinite Crystallinity

Kaolinite crystal structural defects have been linked to large number of stacking faults that may appear during its formation and growth (Aparicio and Galan, 1999). X-ray diffraction based determination of soil kaolinite crystallinity cannot be successfully used in studying these soil kaolins since almost pure kaolin samples with little or no impurities are required (Hughes *et al.*, 2009). Hence, the infrared (IR) spectroscopy and DTA based approaches were applied in this study.

The soil kaolinite crystallinity was determined from IR spectra. According to the IR-E classification, kaolinite structure is considered ordered, if the four OH stretching and bending bands (3691/3689, 3669, 3651/3650, and 3619) were clearly resolved; partially ordered, if the individual OH bands at 3669, 3651/3650 and 937/935 cm^{-1} could be identified but intensities were low; and poorly ordered, if only one band near 3660 cm^{-1} or inflexions near 3669 cm^{-1} , 3651/3650 cm^{-1} and 937/935 cm^{-1} were observed in the spectra (Madejova *et al.*, 1997; Vaculikova *et al.*, 2011).

Characteristic bands at 3691-89, 3669, 3651, and 3619 were observed in the studied soil kaolinites in MAT1 0-20 cm, MAT2 0-20 cm, MAT3 0-20 cm, SA1 0-20 cm, SA1 20-50 cm, and SA2 0-20 cm, respectively (Appendix 4.1). The IR spectra of soil kaolinites developed from basalt, gneiss, granite (MAT1 20-50 cm, MAT2 20-50 cm, and MAT3 20-50 cm), and quartzite (control) showed very weak or no inflexion at the bands typical of kaolins. Based on these observations according to the IR-E approach, the soil kaolinites can possibly be grouped into two classes; partially ordered and poorly ordered. The first class is represented by some soil kaolinites developed from granite and arkosic sandstone which are MAT1 0-20 cm, MAT2 0-20 cm, MAT3 0-20 cm, SA1 0-20 cm, SA1 20-50 cm, and SA2 0-20 cm, respectively. The IR spectra of those developed from basalt, gneiss, granite (MAT1 20-50 cm, MAT2 20-50 cm, and MAT3 20-50 cm), and quartzite (control) belong to the second class because of the absence of the typical kaolin bands.

The IR-N approach is based on crystallinity indices Cl_1 and Cl_2 defined as $Cl_1 = I(v_1)/I(v_3)$ and $Cl_2 = I(v_4)/I(v_1)$ where $I(v_1)$ and $I(v_4)$ are intensities of OH stretching bands at 3691/3689 cm^{-1} and 3619 cm^{-1} , respectively, and $I(v_3)$ is the intensity of OH bending band at 912 cm^{-1} . The kaolinite structures are classified as poorly ordered, if $Cl_1 < 0.7$ and $Cl_2 > 1.2$; partially ordered; if $0.7 < Cl_1 < 0.8$ and $0.9 < Cl_2 < 1.2$; and ordered, if $Cl_1 > 0.8$ and $Cl_2 < 0.9$ (Russell and Fraser, 1994; Madejova and Komadel, 2001). The calculated Cl_1 and Cl_2 values obtained for the soil kaolinites are presented in Table 6.1. They correspond to partially ordered structures based on the IR-N classification (Table 6.1). The IR-N classification corresponds well with the first class from IR-E. However, the discrepancy between IR-N and the second class of IR-E could either be due to Fe^{3+} substituting for Al in the octahedral sheet of the kaolinite structure which could cause lower crystallinity value (Russell and Fraser, 1994) or the presence of montmorillonite which can contribute to the increase of both OH bending adsorption at 915 cm^{-1} and OH stretching adsorption at 3695 cm^{-1} . Higher contributions to the adsorption at 915 cm^{-1} relative to adsorption at 3695 cm^{-1} causes the crystallinity value to be erroneously high for the kaolinites (Neal and Worrall, 1977; Vaculikova *et al.*, 2011; Oyebanjo *et al.*, 2018).

Table 6.1: Structural order of kaolinities in soils developed from different Parent Rocks using IR-N classification.

Parent Rock	Sample ID	V1	V3	V4	Cl ₁	Cl ₂	Degree of Crystallinity
Basalt	S1 0-20cm	0.92	0.93	0.92	0.99	1.00	Pao
	S1 20-50cm	0.94	0.93	0.94	1.00	1.00	Pao
	S1 50-100cm	0.84	0.82	0.84	1.01	1.00	Pao
	S2 0-20cm	0.92	0.93	0.92	0.99	1.00	Pao
	S2 20-50cm	0.95	0.87	0.95	1.09	0.99	Pao
	S2 50-100cm	1.04	0.89	1.05	1.17	1.00	Pao
	S3 0-20cm	0.84	0.81	0.85	1.04	1.00	Pao
	S3 20-50cm	0.99	0.73	0.99	1.35	1.00	Pao
	S3 50-100cm	0.83	0.80	0.83	1.04	1.00	Pao
	Min				0.99	0.99	
	Max				1.35	1.00	
Average				1.08	1.00	Pao	
Granite	MAT1 0-20cm	0.92	0.70	0.92	1.32	1.00	Pao
	MAT1 20-50cm	1.08	0.96	1.07	1.13	0.99	Pao
	MAT2 0-20cm	0.97	0.84	0.97	1.16	1.00	Pao
	MAT2 20-50cm	0.97	0.98	0.97	0.99	1.00	Pao
	MAT3 0-20cm	0.97	0.81	0.96	1.20	1.00	Pao
	MAT3 20-50cm	0.95	0.96	0.95	0.99	1.00	Pao
	Min				0.99	0.99	
	Max				1.32	1.00	
	Average				1.13	1.00	Pao
	Arkosic Sandstone	SA1 0-20cm	0.98	0.84	0.97	1.17	1.00
SA1 20-50cm		0.97	0.82	0.97	1.17	1.00	Pao
SA2 0-20cm		0.97	0.81	0.97	1.20	1.00	Pao
SA2 20-50cm		0.89	0.96	0.90	0.92	1.02	Pao
SA3 0-20cm		0.87	0.91	0.89	0.95	1.01	Pao
SA3 20-50cm		0.92	0.94	0.93	0.98	1.01	Pao
Min					0.92	1.00	
Max					1.20	1.02	
Average					1.07	1.01	Pao
Gneiss		MU1 0-20cm	0.85	0.76	0.86	0.98	1.02
	MU2 0-20cm	0.85	0.91	0.87	0.98	1.02	Pao
	MU3 0-20cm	0.93	0.95	0.94	0.99	1.01	Pao
	Min				0.98	1.01	
	Max				0.99	1.02	
	Average				0.98	1.02	Pao
Quartzite	CMA 0-20cm	0.93	0.93	0.94	1.00	1.01	Pao
	CMA 20-50cm	1.02	1.00	1.01	1.02	1.00	Pao
	Average				1.01	1.00	Pao

(pa-o): Partially ordered.

DTA curves for kaolinite based on their respective decomposition peak temperatures were used to determine the degree of structural order. Well-ordered kaolinities have T_d

between 561 and 570 °C, poorly ordered samples have T_d between 546 and 560 °C, and disordered samples have $T_d < 545$ °C (Vaculikova *et al.*, 2011). The T_d values obtained for the soil kaolinites were < 545 °C (Table 4.12) which corresponds to extremely disordered samples. Nevertheless, the determination of kaolinite structural order by thermal analysis cannot be applied in all circumstances unless the analysis was carried out under these conditions: heating rate 10 °C/min, sample fraction under 5 μm , and sample mass about 50 mg. This is crucial because the T_d values can vary under different conditions, so that the T_d interval of disorder can differ too (Guggenheim and van Gross, 2001; Vaculikova *et al.*, 2011). Hence, the T_d kaolinite structural order classification will not be considered. The average dehydroxylation temperature (DT) ranging from 425 to 468 °C for the soil kaolinites were lower when compared to the averages for kaolinites in Brazilian soils (510 °C) (Melo *et al.*, 2001) and West Australian soils (489 °C) (Singh and Gilkes, 1992) and are 50 – 90 °C lower than values for reference kaolinite (520 - 544 °C) (Hart *et al.*, 2002). This reduction in DT may be probably due to the small crystal size and the presence of Fe. The presence of Fe and small crystal size has been identified as a cause for the decrease in DT which invariably induces structural disorder (Singh and Gilkes, 1992; Hart *et al.*, 2002).

6.1.3 Kaolinite Morphology

The identified kaolinite crystals in soils developed from basalt clearly demonstrate small subhedral – euhedral and platy morphology with elongated laths (Fig. 6.2) whereas, those developed from granite, arkosic sandstone, gneiss, and quartzite (control) were generally small subhedral – anhedral crystals with platy morphology. The longest dimension of the sizes of the platy kaolinite crystals ranged from 0.06 – 0.2, 0.08 – 0.15, 0.2, 0.15, and 0.15 – 0.25 μm for soils developed from basalt, granite, arkosic sandstone, gneiss, and quartzite, respectively. These sizes are smaller relative to those in the reference Georgia kaolins (0.4 – 0.8 μm) (Wiriakitnatekul *et al.*, 2010).

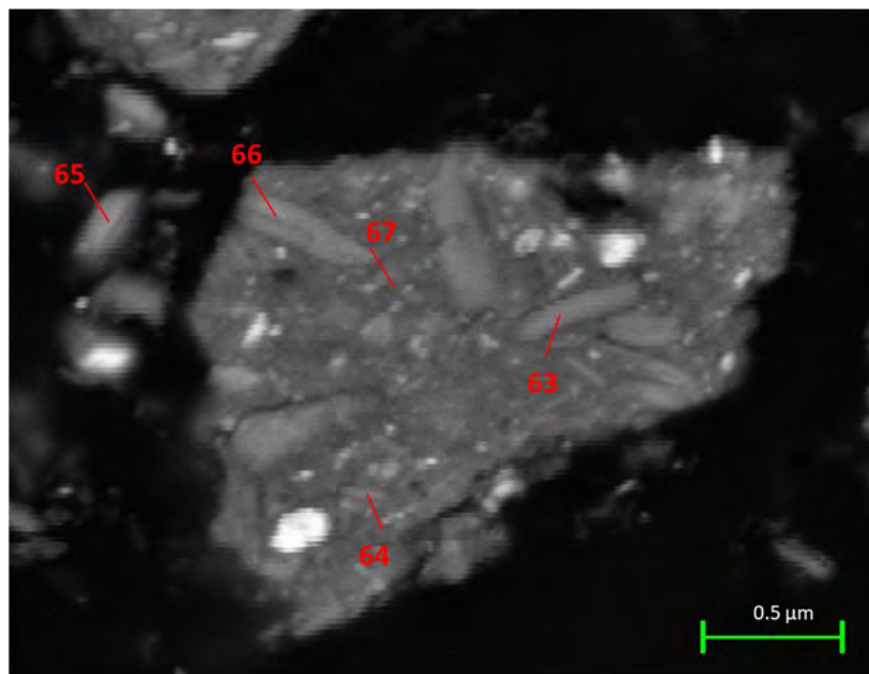


Figure 6.2: SEM image of representative soil kaolins developed from basalt showing thin platy particles with elongated laths (63,66 – kaolinite; 64,65 – pyroxene/olivine; 67 – hematite).

6.2 Geochemical Characteristics

6.2.1 Major Oxides

The mean values and ranges of the major oxides concentrations are given in Table 5.2. The SiO_2 mean values obtained for the soil kaolins (35.66 – 64.00 wt %) were higher than that of ideal kaolin (46.54 wt %) and lower for those in the control sample (75.37 wt %). However, the mean Al_2O_3 value for the ideal kaolin (39.50 wt %) was higher substantially than those obtained for the soil kaolins (16.11 – 24.57 wt %) and the control sample (9.03 wt %). The mean $\text{SiO}_2/\text{Al}_2\text{O}_3$ ratios for the soil kaolins ranged between 1.45 and 4.23 which were greater than the value of 1.18 for ideal kaolin, 1.20 for Georgia kaolin, 1.38 for Thailand Ultisols, and 1.16 for Brazilian Ultisols (Table 6.2). This could be attributed to the presence of quartz as indicated from the XRD results and partly due to some Al in soil kaolin being replaced by Fe (Melo *et al.*, 2001; Kanket, 2006).

Table 6.2: Major element oxides (wt %) of soil kaolins developed from different Parent rocks in Limpopo Province, South Africa and for average Ideal and Georgia kaolins, Thailand and Brazilian Ultisols.

Parent Rock		SiO ₂	TiO ₂	Al ₂ O ₃	Cr ₂ O ₃	Fe ₂ O ₃	CaO	MgO	MnO	K ₂ O	Na ₂ O	P ₂ O ₅	L.O.I.	SiO ₂ /Al ₂ O ₃
Basalt (n=9)	Min	32.74	1.9	23.18	0.02	14.68	0.04	0.03	0.06	0.05	1.55	0.11	15.95	1.41
	Max	39.51	2.84	25.82	0.06	20.5	0.11	0.18	0.09	0.39	2.15	0.17	19.53	1.53
	Average	35.66	2.37	24.57	0.03	17.97	0.07	0.12	0.07	0.19	1.88	0.14	17.06	1.45
Granite (n=6)	Min	62.17	1.23	15.8	0.01	2.64	1.3	0.85	0.05	2.26	4.38	0.08	3.80	3.93
	Max	65.91	1.4	16.35	0.01	3.4	1.71	1.32	0.06	2.57	4.94	0.13	6.96	4.03
	Average	64.00	1.30	16.11	0.01	2.88	1.51	1.00	0.05	2.39	4.63	0.09	5.45	3.97
Arkosic Sst (n=3)	Min	55.18	2.13	12.51	0.05	3.42	0.39	0.46	0.03	3.95	2.06	0.07	6.18	3.57
	Max	66.73	2.68	15.46	0.06	4.45	0.81	1.2	0.04	4.57	2.72	0.27	13.45	5.33
	Average	59.45	2.33	14.30	0.05	4.10	0.66	0.94	0.04	4.18	2.30	0.20	10.93	4.23
Gneiss (n=1)		52.66	1.89	18.44	bdl	8.08	2.04	1.2	0.07	1.79	5.27	0.3	7.82	2.86
Quartzite (n=2)	Min	73.51	1.41	8.37	0.01	2.17	0.09	0.23	0.03	0.8	1.36	0.07	7.60	7.59
	Max	77.22	1.48	9.68	0.02	2.29	0.1	0.27	0.03	0.96	1.64	0.07	9.67	9.23
	Average	75.37	1.45	9.03	0.02	2.23	0.10	0.25	0.03	0.88	1.50	0.07	8.64	8.41
Ideal Kaolin ¹	Average	46.54	-	39.50	-	-	-	-	-	-	-	-	-	1.18
Georgia Kaolin (MP#5) ¹	Average	53.2	1.64	44.2	-	0.69	0.13	0.01	-	0.12	-	0.08	-	1.20
Thailand Ultisols ¹	Average	55.0	1.56	40.3	-	2.53	0.09	0.05	-	0.46	-	0.03	-	1.38
Brazilian Ultisols ²	Average	41.5	0.31	35.85	-	1.91	-	0.09	-	0.03	-	-	-	1.16

¹ Kanket *et al.* (2005), ² Melo *et al.* (2001) and bdl= below detection limit

Soil kaolins developed from basalt have the lowest $\text{SiO}_2/\text{Al}_2\text{O}_3$ ratios which are consistent with the mineralogy, since they have more kaolinite than the other soil kaolins developed from granite, arkosic sandstone, gneiss, and quartzite (control). TiO_2 is present in all the soil kaolins but higher in those developed from basalt and arkosic sandstone. This is due to the presence of anatase as observed by XRD and ilmenite by SEM.

The significant difference between the soil kaolins and Georgia kaolin was the higher amount of Fe in the soil kaolins with mean values between 2.88 and 17.97 wt % against 0.69 wt % for Georgia kaolins. This shows the presence of considerable Fe despite the removal of some iron oxides by DCB treatment. However, the Fe_2O_3 mean value for the soil kaolins developed from granite (2.88 wt %) is comparable to those for kaolins from other soils, from Thailand ultisols, 2.53 wt %; Western Australia, 2.57 wt %; Indonesia, 2.54 wt %; Rwanda, 2.32 wt % (Mestdagh *et al.*, 1980; Kanket, 2006) but higher to those from Nigeria, 1.86 wt %; Brazillian ultisols, 1.91 wt % (Mestdagh *et al.*, 1980; Melo *et al.*, 2001). The relationship of Fe with kaolinite has been mentioned in several previous studies (Singh and Gilkes, 1992; Hart *et al.*, 2002).

Using several independent techniques, Fe has been proven to be present in the form of Fe^{3+} and substitutes for Al in the octahedral sheet of the kaolinite (Herbillon *et al.*, 1976; Singh and Gilkes, 1992; Darunsontaya *et al.*, 2010).

The lowest levels of CaO, MgO, K_2O , and Na_2O were obtained for soil kaolins developed from basalts and quartzite (control) with lower percentages of weatherable minerals. On the other hand, the soil kaolins from the other soils with higher percentage of weatherable minerals contain higher amounts of CaO, MgO, K_2O , and Na_2O as indicated from the XRD results.

The cation exchange capacity (CEC) of the soil kaolins ranged from 6.09 to 37.3 cmol/kg. These values were higher than those from Thai (14.4 – 17.4 cmol/kg) and Indonesian (5.2 – 12.9 cmol/kg) soil kaolins and similar to values of 9.3 to 30.5 cmol/kg and 16 to 34 cmol/kg for Queensland soil kaolins and high defect kaolins of sedimentary origin respectively (Koppi and Skjemstad, 1981; Ma and Eggleton, 1999). In addition, the CECs for reference kaolins (typically between 0.4 and 4.6 cmol/kg) were

significantly lower relative to the values obtained for the studied soil kaolins. This has been attributed to the smaller crystal size of soil kaolins as there is a general trend for CEC to increase with decreasing crystal size. The CEC is primarily due to pH-dependent charge arising from broken bonds along the edges of crystals with some contribution from basal surfaces. The charge becomes more abundant as the crystal size of kaolin decreases (Hart *et al.*, 2002; Darunsontaya *et al.*, 2010).

6.2.2 Trace Elements

The mean values and ranges of trace elements in the soil kaolins are presented in Table 6.3. The soil kaolins developed from basalt contain higher amounts of Sc, V, Co, Ni, and Cu whereas, soil kaolins developed from granite have higher concentrations of Zr. Kaolins from arkosic sandstone derived soils contain higher concentrations of Cr, Rb, Ba, Pb, Th, and U whereas, kaolins from gneissic soil have higher concentrations of Zn and Sr.

The soil kaolins in this study were enriched significantly in Co, Ni, Cu, Zn, and Pb respectively, relative to kaolins in Thailand ultisols (Table 6.3). This could be attributed to the presence of other weatherable and accessory minerals in the soil kaolins from this study. The retention of appreciable proportions of trace elements in the soil kaolins has significant implications for soil fertility (Kanket *et al.*, 2005).

6.2.3 Rare Earth Elements (REEs)

The REE abundances in the soil kaolins are listed in Table 6.4. The absolute mean LREE and HREE concentrations were in decreasing order of soil kaolins developed from arkosic sandstone > granite > gneiss > basalt > quartzite (control), respectively. The average UCC generally showed relative depletion in the REEs in comparison to the average soil kaolins developed from granite, arkosic sandstone, and gneiss.

Table 6.3: Trace elements concentrations (ppm) of soil kaolins developed from different Parent rocks in Limpopo Province, South Africa and for average Thailand Ultisols.

Parent Rock		Sc	V	Cr	Co	Ni	Cu	Zn	Rb	Sr	Zr	Ba	Pb	Th	U	Th/U
Basalt (n=9)	Min	38.31	248.55	187.80	16.58	100.50	235.45	67.35	4.04	7.53	155.35	61.90	6.50	2.92	0.93	3.12
	Max	47.70	384.00	398.60	34.57	159.45	300.10	79.40	37.41	15.40	254.35	112.75	13.57	5.59	1.36	4.13
	Average	42.93	328.64	253.45	27.61	129.54	263.89	73.57	17.08	10.54	204.94	84.81	9.81	4.29	1.16	3.68
Granite (n=6)	Min	8.67	42.34	177.05	6.65	58.20	23.95	44.90	69.05	368.85	1039.85	941.50	22.17	10.44	2.36	4.43
	Max	11.54	59.56	229.90	10.49	92.55	35.70	53.50	81.30	431.45	1424.50	1127.50	24.30	14.53	3.02	4.81
	Average	9.59	47.44	192.52	7.56	66.85	29.23	50.12	73.52	397.82	1208.24	994.67	23.18	11.87	2.59	4.58
Arkosic Sst (n=3)	Min	12.86	106.25	350.60	8.93	70.10	29.65	53.05	138.90	146.20	733.05	983.50	31.98	22.23	4.18	5.32
	Max	15.78	110.85	437.00	12.55	104.65	53.65	86.00	159.25	160.55	1148.30	1220.00	39.59	29.00	5.04	5.76
	Average	14.72	109.13	379.68	11.22	88.55	41.12	73.95	147.47	151.23	905.50	1068.50	34.78	24.72	4.47	5.52
Gneiss (n=1)		14.58	110.95	54.05	13.90	40.45	43.60	120.05	57.05	491.95	367.90	720.00	18.05	4.40	0.83	5.28
Quartzite (n=2)	Min	7.52	71.40	136.90	5.30	37.75	18.80	30.95	48.60	32.15	499.50	210.35	12.72	9.22	2.36	3.53
	Max	7.56	74.70	154.65	5.49	38.65	21.71	31.15	59.35	34.65	707.95	243.55	13.96	9.84	2.79	3.91
	Average	7.54	73.05	145.78	5.39	38.20	20.25	31.05	53.98	33.40	603.73	226.95	13.34	9.53	2.57	3.72
Thailand Ultisols (n=9)	Average	-	-	-	0.36	4.20	2.40	4.90	-	-	-	-	2.60	-	-	-

Table 6.4: Rare Earth Elements concentrations (ppm) of soil kaolins developed from different Parent rocks in Limpopo Province, South Africa and for average Upper Continental Crust (UCC).

Parent Rock		La	Ce	Pr	Nd	Sm	Eu	Gd	Tb	Dy	Ho	Er	Tm	Yb	Lu	LREE/HREE	Eu/Eu*
Basalt (n=9)	Min	6.12	22.47	1.39	6.08	1.33	0.44	1.63	0.30	2.05	0.48	1.44	0.24	1.74	0.26	4.28	0.85
	Max	19.27	55.16	4.86	21.45	5.35	1.52	5.64	0.93	5.77	1.16	3.36	0.52	3.62	0.53	5.53	1.06
	Average	12.47	38.62	3.00	13.06	3.19	0.97	3.37	0.60	3.80	0.80	2.32	0.35	2.58	0.39	4.97	0.92
Granite (n=6)	Min	44.82	84.16	9.58	37.95	6.56	1.04	4.97	0.68	3.62	0.72	2.10	0.32	2.37	0.41	11.03	0.52
	Max	61.09	120.35	13.27	52.15	9.61	1.67	7.02	0.98	5.39	1.12	3.01	0.50	3.50	0.56	11.98	0.63
	Average	50.73	96.54	11.02	43.27	7.75	1.24	5.88	0.79	4.41	0.88	2.47	0.39	2.89	0.46	11.60	0.56
Arkosic Sst (n=3)	Min	65.74	123.53	14.70	57.80	10.65	1.73	8.14	1.14	6.37	1.26	3.50	0.48	3.62	0.55	10.83	0.52
	Max	76.25	146.15	16.32	64.00	11.62	1.92	8.82	1.24	7.31	1.42	4.06	0.64	4.42	0.66	11.07	0.63
	Average	69.76	131.88	15.27	60.32	11.04	1.84	8.43	1.18	6.79	1.34	3.73	0.55	3.91	0.60	10.93	0.59
Gneiss (n=1)		32.12	60.46	7.60	30.77	5.94	1.82	4.90	0.67	3.83	0.72	2.11	0.26	2.00	0.30	9.39	1.04
Quartzite (n=2)	Min	20.47	37.33	3.82	14.91	3.02	0.68	2.64	0.44	2.76	0.57	1.64	0.26	1.85	0.30	7.10	0.73
	Max	21.46	40.18	4.07	15.84	3.07	0.70	2.73	0.47	3.01	0.67	2.10	0.33	2.39	0.33	7.69	0.75
	Average	20.97	38.75	3.94	15.37	3.04	0.69	2.68	0.46	2.88	0.62	1.87	0.29	2.12	0.31	7.39	0.74
UCC ¹	Average	30	64	7.1	26	4.5	0.9	3.8	0.64	3.5	0.8	2.3	0.33	2.2	0.3	7.38	0.65

¹ McLennan (2001); $Eu/Eu^* = Eu_N / (Sm_{NX}Gd_N)^{0.5}$

However, average REEs obtained for UCC were enriched relative to soil kaolins developed from basalt and quartzite (control) (Table 6.4). When the average REE contents of the soil kaolins and UCC were normalised to chondrite values (Haskin *et al.*, 1971) (Fig. 6.3), soil kaolins developed from arkosic sandstone and granite showed pronounced Eu anomalies whereas, those developed from basalt, gneiss, and quartzite (control) lack distinct Eu anomaly. However, they all showed a general trend of REE fractionation with the enrichment of LREE relative to HREE. The absence of negative Ce anomaly in the trends suggest that the alteration of the primary minerals in the parent rocks took place under suboxic conditions since minerals formed in equilibrium with oxic marine waters are likely to show a negative Ce anomaly (Jeans *et al.*, 2000; Arslan *et al.*, 2006).

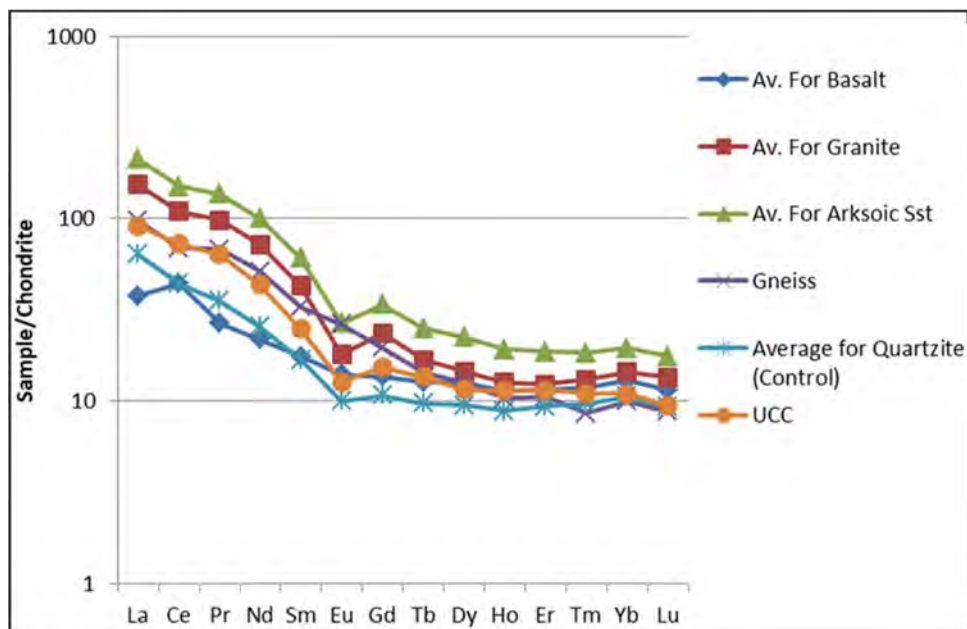


Figure 6.3: Chondrite-normalised REE pattern of average of the soil kaolins developed from different Parent rocks in Limpopo Province, South Africa and for average UCC.

Low LREE/HREE ratio and no Eu anomalies reflect mafic source area composition, while high LREE/HREE and Eu anomalies reflect felsic source area composition (Cullers and Graf, 1983; Cullers, 1994). Hence, the high LREE/HREE ratios and EU

anomalies in the soil kaolins developed from arkosic sandstone and granite are traceable to felsic source whereas, the low LREE/HREE ratios and absence of EU anomalies for soil kaolins developed from basalt, gneiss, and quartzite (control) are traceable to mafic source. In addition, the average Eu/Eu^* ratios of 0.56, 0.59, and 0.74 obtained for soil kaolins developed from granite, arkosic sandstone, and quartzite (control) also indicated felsic sources since negative Eu anomaly ($\text{Eu}/\text{Eu}^* < 0.85$) are typical of felsic rocks (Table 6.4) due to lithospheric or intercrustal feldspar fractionation or breakdown of feldspars during weathering processes (Condie *et al.*, 1992). Average Eu/Eu^* ratios of 0.92 and 1.02 for soil kaolins developed from basalt and gneiss further confirm mafic sources for them.

6.2.4 Statistical Analyses of Geochemical and Mineralogical Data

Factor analyses were extended to include the major element oxides, LOI, trace elements, LREE, HREE, Eu, % kaolinite, and % quartz data. The factor analyses of arkosic sandstone, gneiss, and quartzite were carried out together because of their small sample sizes for a more reliable resulting factor (Davis, 2002). Based on the Scree plots (Figures 6.4 - 6.6), four factors explained 92.92 % of the variation in the data for soil kaolins developed from basalt (Table 6.5), whereas three factors accounted 96.15 % of the data variability in the soil kaolins developed from granite (Table 6.6). In addition, three factors explained 99.15 % of variation in the data for arkosic sandstone, gneiss, and quartzite (control) (Table 6.7).

For the soil kaolins developed from basalt, the calculated factors 1, 2, 3, and 4 explained 48.94, 20.72, 17.72, and 4.54 % respectively, of the variance. Factor 1 show significant positive factor loadings (Table 6.5, bold numbers indicate significant factor loadings > 0.500) with Th, LREE, HREE, Zr, TiO_2 , Eu, U, Fe_2O_3 , Co, V, Sc, MnO, P_2O_5 , Ni, and % kaolinite and negative factor loadings with Na_2O , SiO_2 , MgO, % quartz. Factor 2 has positive factor loadings with Cu, Cr, Cr_2O_3 , and LOI, and negative factor loadings with MgO, Rb, Zn, K_2O , and SiO_2 .

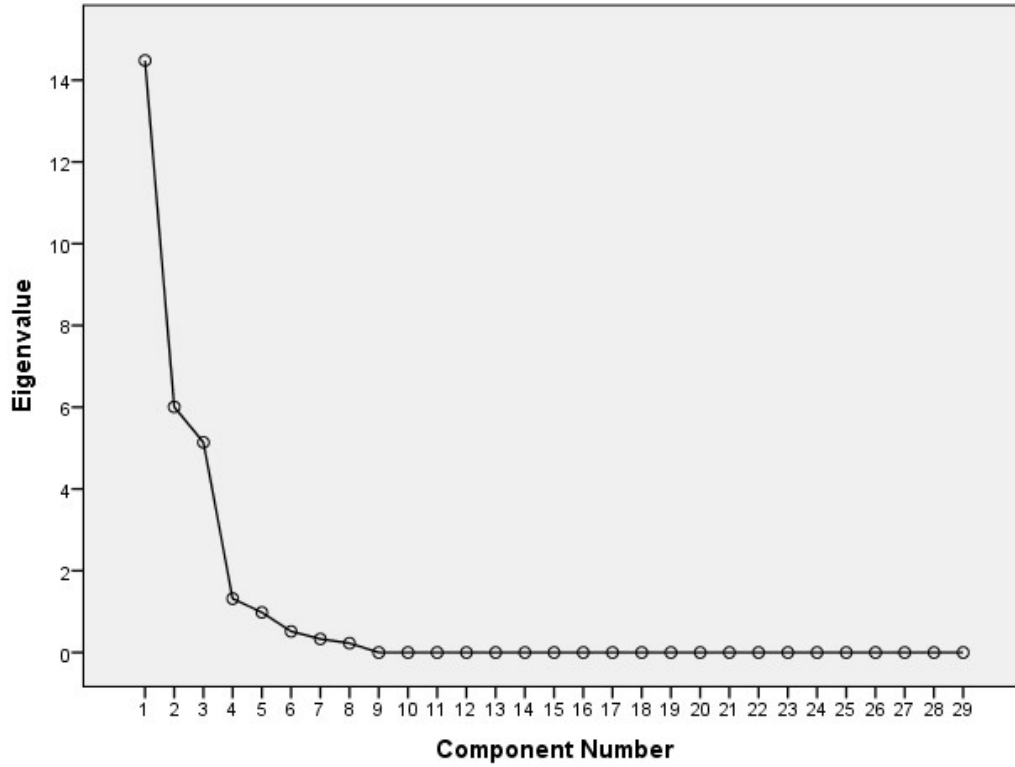


Figure 6.4: Scree plot of the studied soil kaolins developed from basalt.

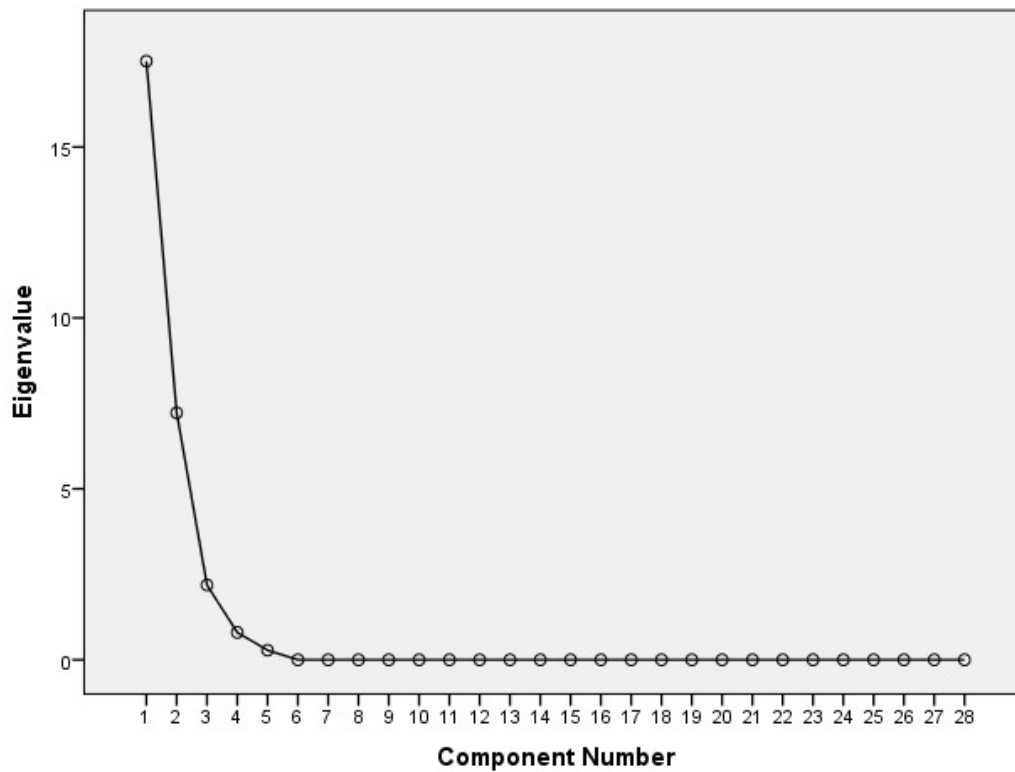


Figure 6.5: Scree plot of the studied soil kaolins developed from granite.

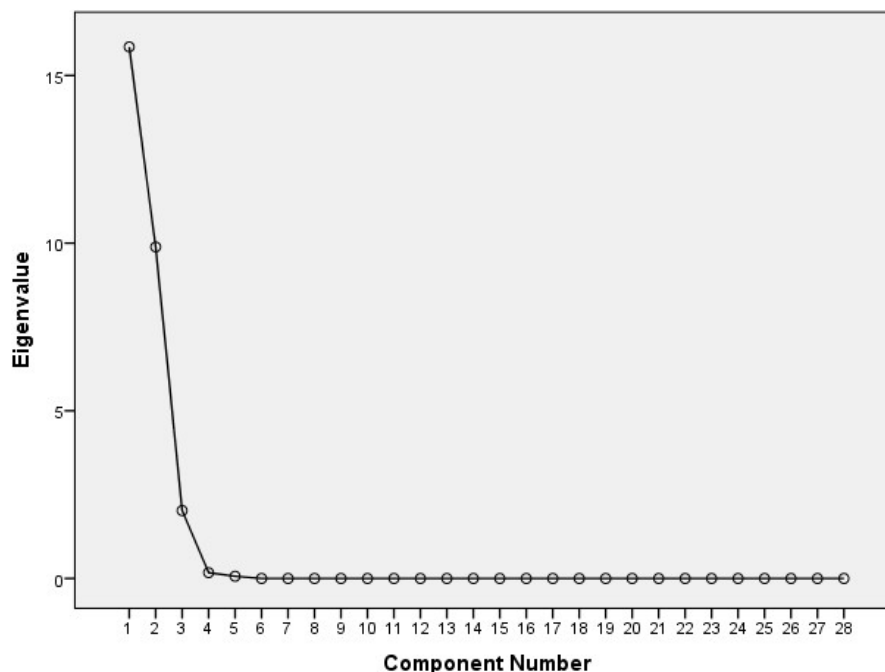


Figure 6.6: Scree plot of the studied soil kaolins developed from arkosic sandstone, gneiss, and quartzite (control).

Factor 3 has positive factor loadings with LOI, Al_2O_3 , and % kaolinite and negative factor loadings with MgO, Cr, Cr_2O_3 , Ba, CaO, and Sr. Factor 4 has positive factor loadings with LOI and negative factor loadings with CaO. The factor 1 represents the weathering factor which shows the removal of bases and silica by ferralitisation through leaching and desilication of the primary minerals to form kaolinite (van Breeman and Buurman, 2003). The mineralogical transformation by alteration of kaolinite to gibbsite also results in the loss of considerable silica and consequent increase in Al_2O_3 . Factors 2 and 4 also represents the weathering factor. However, factor 3 represents the kaolinite factor relating to its derivation from the alteration of ferromagnesian minerals.

The three calculated factors for soil kaolins developed from granite explained 62.54, 25.80, and 7.81 % respectively, of the variance. Factor 1 shows significant positive factor loadings with V, Ni, Rb, Fe_2O_3 , Cr, Sc, Co, Eu, P_2O_5 , Ba, K_2O , SiO_2 , U, TiO_2 , CaO, HREE, LREE, MgO, and % quartz and negative loadings with LOI, Al_2O_3 , and % kaolinite. Factor 2 shows significant positive loadings with CaO, Zn, HREE, TiO_2 , U, Na_2O , Th, SiO_2 , Sr, Zr, K_2O , Ba, LREE, and MnO and negative loadings with LOI and

Al₂O₃. Factor 3 shows significant positive loadings with % kaolinite and negative loadings with CaO and MnO. The inverse relationships between % kaolinite, Al₂O₃ and the other variables as expressed by the factors suggest kaolinite factors due to the weathering of the felsic minerals.

Table 6.5: Factor Loadings obtained from Principal Component Analysis of the studied soil kaolins developed from basalt.

	Factors			
	1	2	3	4
Eu	.938	-.175	-.033	.112
LREE	.938	-.122	-.246	.180
HREE	.937	-.084	-.074	.182
Th	.921	.184	-.230	.206
Na ₂ O	-.908	.038	.228	-.208
Zr	.892	.147	-.305	.276
U	.891	.055	-.316	.182
Sc	.888	.017	-.399	-.023
TiO ₂	.875	.170	-.287	.294
MnO	.872	-.392	.037	-.143
Fe ₂ O ₃	.871	.453	.009	.133
V	.852	.463	.114	.171
Co	.831	.039	.235	.411
SiO ₂	-.713	-.599	.017	-.076
MgO	-.582	-.563	-.557	-.141
Rb	-.060	-.888	.309	-.151
Cu	.179	.844	.174	.136
K ₂ O	-.161	-.815	.384	-.114
Zn	.340	-.774	.218	.482
Cr	-.306	.717	-.614	.008
Cr ₂ O ₃	-.272	.701	-.654	-.049
Ni	.556	.651	-.062	-.176
LOI	.346	.590	.572	.645
Ba	-.160	-.185	-.949	.132
CaO	-.043	.089	-.870	-.798
Al ₂ O ₃	.437	.002	.821	.201
Sr	.135	-.290	-.805	.404
Pb	.409	.154	.222	.373
P ₂ O ₅	.559	.030	.222	.256
% Kaolinite	.754	.443	.636	.356
% Quartz	-.502	-.257	.187	.367
Eigenvalues	14.48	6.01	5.14	1.32
Cumulative Variance (%)	48.94	20.72	17.72	4.54

Table 6.6: Factor Loadings obtained from Principal Component Analysis of the studied soil kaolins developed from granite.

	Factors		
	1	2	3
V	.972	.198	.121
Ni	.967	.139	.182
Rb	.967	.217	-.103
Fe ₂ O ₃	.959	-.212	.180
Cr	.948	.306	.072
Sc	.929	.330	.136
Co	.921	.000	.379
Eu	.919	.386	.014
MgO	.878	.463	.049
P ₂ O ₅	.848	-.106	.505
LREE	.846	.521	.109
HREE	.772	.622	-.029
Al ₂ O ₃	-.734	-.606	.080
SiO ₂	.647	.995	.078
Sr	-.177	.982	.005
LOI	-.594	-.965	-.059
Zr	.351	.921	.002
K ₂ O	.561	.907	-.183
Ba	.504	.849	-.433
Th	.444	.823	-.285
CaO	.557	.806	-.638
Na ₂ O	-.326	.742	-.224
U	.600	.712	-.237
TiO ₂	.649	.708	-.250
MnO	.152	.694	-.688
Zn	.318	.684	.433
Pb	.166	.249	.390
Cu	.407	-.130	.374
% Kaolinite	-.616	-.367	.568
% Quartz	.547	.451	.278
Eigenvalues	17.51	7.22	2.19
Cumulative Variance (%)	62.54	88.34	96.15

Table 6.7: Factor Loadings obtained from Principal Component Analysis of the studied Soil kaolins developed from arkosic sandstone, gneiss, and quartzite.

	Factors		
	1	2	3
Fe ₂ O ₃	.996	-.064	-.058
CaO	.992	-.117	-.039
Zn	.979	.097	.174
Al ₂ O ₃	.960	.209	.162
Sr	.958	-.086	-.269
Na ₂ O	.958	-.191	-.178
MnO	.955	-.289	-.059
Co	.907	.310	.278
SiO ₂	-.889	-.391	-.343
P ₂ O ₅	.860	.043	.400
MgO	.838	.227	.491
Sc	.751	.570	.328
V	.742	.666	.025
Eu	.740	.645	.190
Cu	.738	.353	.502
Pb	.160	.980	.078
Th	-.180	.974	.133
HREE	.188	.970	.151
Rb	.057	.969	.214
Cr	-.201	.965	.166
LREE	.218	.963	.158
K ₂ O	.226	.957	.168
TiO ₂	.302	.938	-.166
U	-.393	.899	.180
Ba	.432	.899	.026
Zr	-.368	.896	-.552
Ni	.149	.760	.625
LOI	.105	.139	.981
% Kaolinite	.689	.217	.179
% Quartz	-.528	-.180	-.235
Eigenvalues	15.85	9.89	2.02
Cumulative Variance (%)	56.61	91.92	99.15

The calculated factors 1, 2 and 3 explained 56.61, 35.31, and 7.23 % of the variance respectively in soil kaolins developed from arkosic sandstone, gneiss, and quartzite (control). Factor 1 shows significant positive loadings with Fe₂O₃, CaO, Na₂O, Al₂O₃, Zn, Sr, MnO, Co, P₂O₅, MgO, Sc, Eu, V, Cu, and % kaolinite and negative loadings with SiO₂ and % quartz. Factor 2 shows significant positive loadings with Sc, Eu, V, Pb, Th,

HREE, Rb, Cr, LREE, K₂O, TiO₂, Zr, U, Ba, and Ni, and weak negative loadings with SiO₂. Factor 3 shows significant positive loadings with Cu, Ni, and LOI and negative loadings with Zr. The negative correlation between SiO₂ and the other variables in factors 1 and 2 represents desilication and possible input from both ferromagnesian and felsic minerals. Factor 3 represents the release of Cu and Ni with the weathering of accessory mineral such as zircon rich in Zr.

Similar work on the factor analyses of kaolins in soils from different parent rocks showed that the geochemical associations of major and trace elements were linked to derivations from the felsic and ferromagnesian minerals present in the parent materials (Darunsontaya *et al.*, 2010). Formations of kaolin minerals and gibbsite in soils by ferralitisation as weathering intensifies have also been reported by earlier workers (Driessen *et al.*, 2001; Kleber *et al.*, 2007; Nguyen and Egashira, 2007; Jien *et al.*, 2016). The loss of cations and silica through leaching and desilication of the primary minerals due to hydrolysis favour the development of clay minerals in soils (Jien *et al.*, 2016).

6.3 Concluding Remarks

Based on the mineralogical and geochemical considerations, the following deductions have been made:

- a. Kaolinite dominated the clay minerals present in the soil kaolins. The higher percentage of weatherable minerals present in soil kaolins developed from granite, arkosic sandstone, gneiss, and quartzite (control) accounted for the greater amounts of CaO, MgO, K₂O, and Na₂O relative to soil kaolins developed from basalt.
- b. The crystallinity based on FTIR showed that the soil kaolinites have partially to poorly structural order. The average dehydroxylation temperatures ranged from 425 – 468 °C for the soil kaolinites as obtained from their respective decomposition peak temperatures. The soil kaolinites have platy morphology with smaller sizes relative to reference kaolinites.

- c. Statistical geochemical evaluation established a great influence of the parent rocks on the geochemical characteristics of the soil kaolins. In addition, kaolinite was formed from the primary minerals through leaching and desilication.

Chapter Seven

Phosphorus Sorption in Soils and Soil Kaolins Developed from different Parent Rocks in Limpopo Province, South Africa

This chapter aimed to assess the relationship between the phosphorus sorption capacities of soils and soil kaolins (deferated clay fraction) developed from different parent rocks in Limpopo Province, South Africa (Specific Objective 3) based on Hypothesis 3. The Langmuir, Freundlich, Redlich-Peterson, and Sips models were used to achieve specific objective 3.

7.1 Soils and Soil Kaolins Phosphorus Adsorption Isotherms Characteristics

Data obtained from the phosphorus adsorption analyses of soil and soil kaolin samples developed from different parent rocks are presented in Appendix 7.1. The non-linear adsorption isotherms gotten from these data are graphically shown in Figures 7.1 and 7.2 for soil and soil kaolin samples respectively.

The phosphorus (P) adsorption isotherm graphs of the soils and soil kaolins developed from different parent rocks presented in Figures 7.1 and 7.2 showed strong P-adsorption. The overall shapes of the average isotherm curves were remarkably similar despite the noticeable variation in the amount of P adsorbed for equilibrium solution. This implies that the soils and soil kaolins adsorb phosphorus alike. According to Giles *et al.* (1960) and Njoyim *et al.* (2016), these isotherms are of the H-type, showing that the soils and soil kaolins have a high affinity for phosphorus. P adsorption was observed to be very high at the beginning and this value increased with an increase in the concentration of added P. The figures show that highest P was adsorbed by soils and soil kaolins developed from basalt (Figs. 7.1 and 7.2).

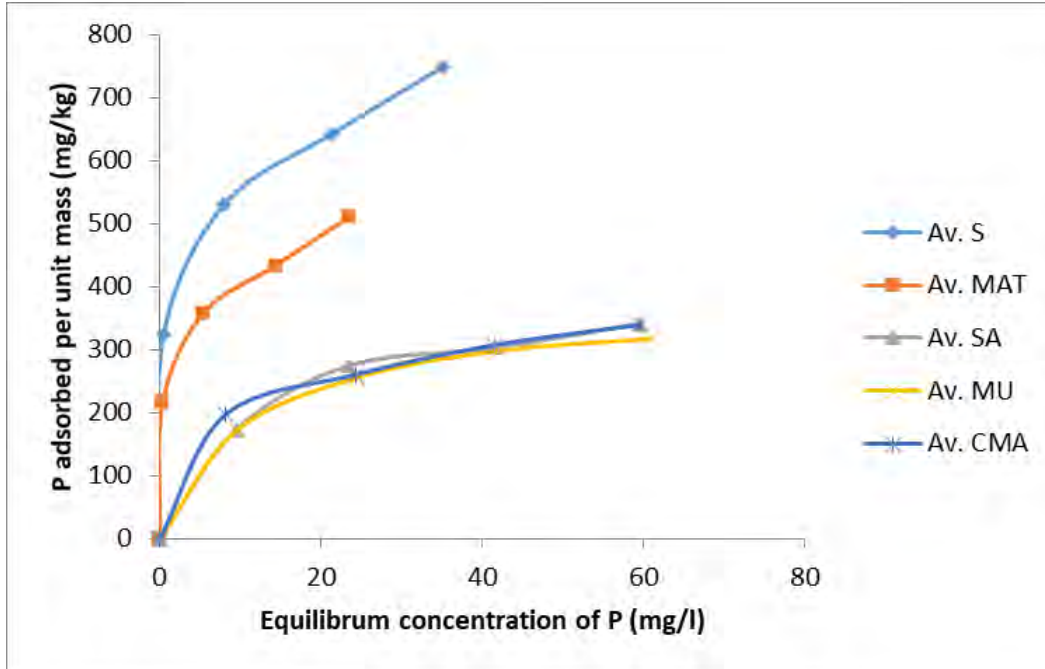


Figure 7.1: Phosphorus adsorption isotherms for soils developed from different parent rocks in Limpopo Province, South Africa.

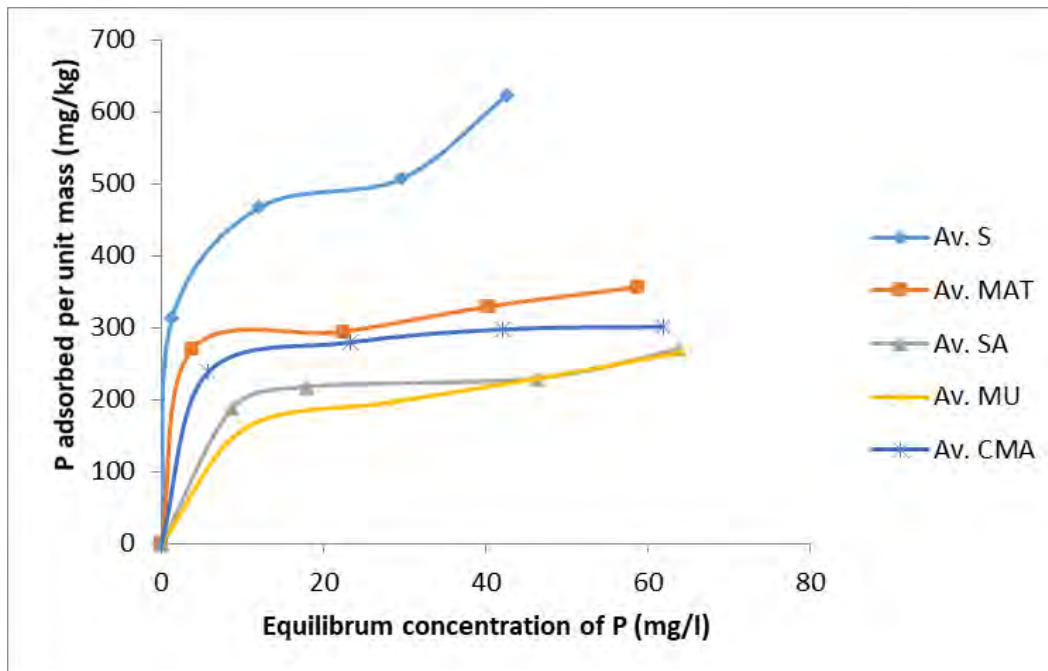


Figure 7.2: Phosphorus adsorption isotherms for soil kaolins developed from different parent rocks in Limpopo Province, South Africa.

The average maximum P adsorption values were in decreasing order of soils developed from basalt > granite > arkosic sandstone > quartzite (control) > gneiss respectively whereas, for soil kaolins is basalt > granite > quartzite (control) > arkosic sandstone > gneiss respectively.

7.2 Adsorption Parameters

7.2.1 Langmuir Adsorption Parameters for Soils

The Langmuir adsorption isotherms for the soils along with the adsorption equation and coefficient of determination values (R^2) are presented in Figures 7.3 – 7.7. The highly significant value of R^2 ranging from 0.95 to 0.98 indicated that the data fitted well to Langmuir model for the soils developed from all the parent rocks. The isotherms were linear even at the highest amount of added P in soils from all the parent rocks. This perhaps shows that in these soils, the P adsorption sites were not completely occupied (Poswa, 2016).

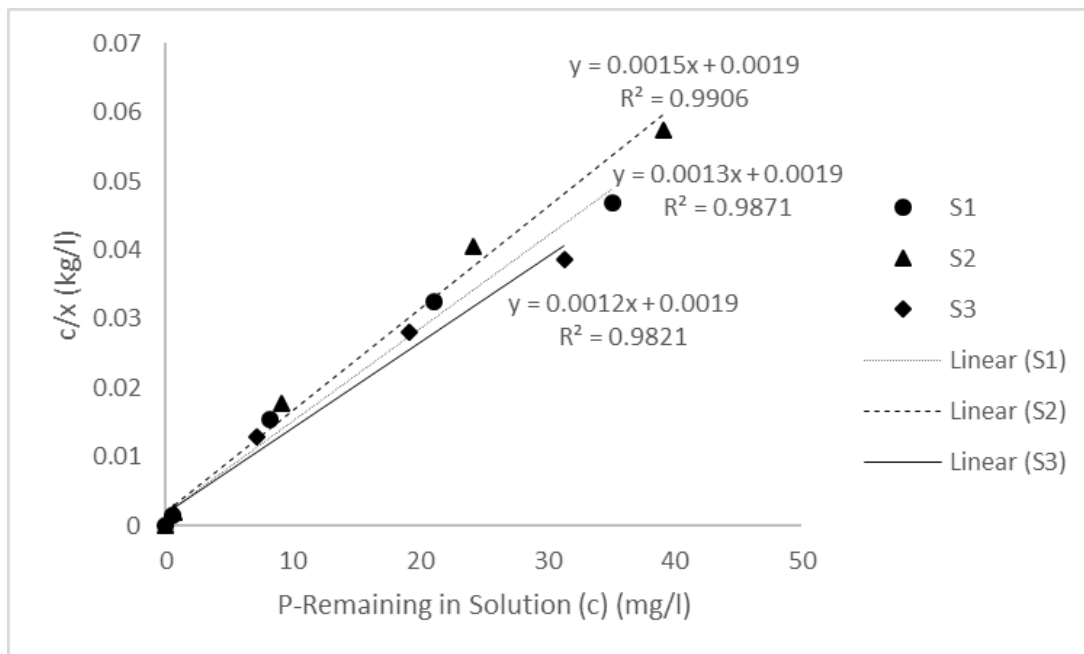


Figure 7.3: Langmuir adsorption isotherm for soils (0-20 cm) developed from basalt.

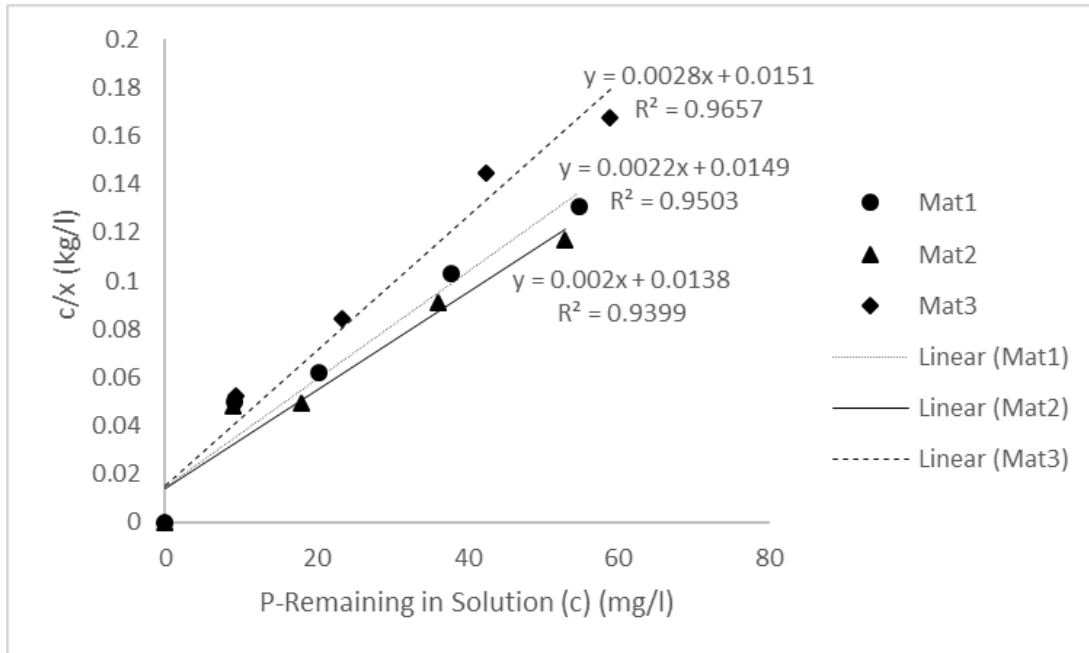


Figure 7.4: Langmuir adsorption isotherm for soils (0-20 cm) developed from granite.

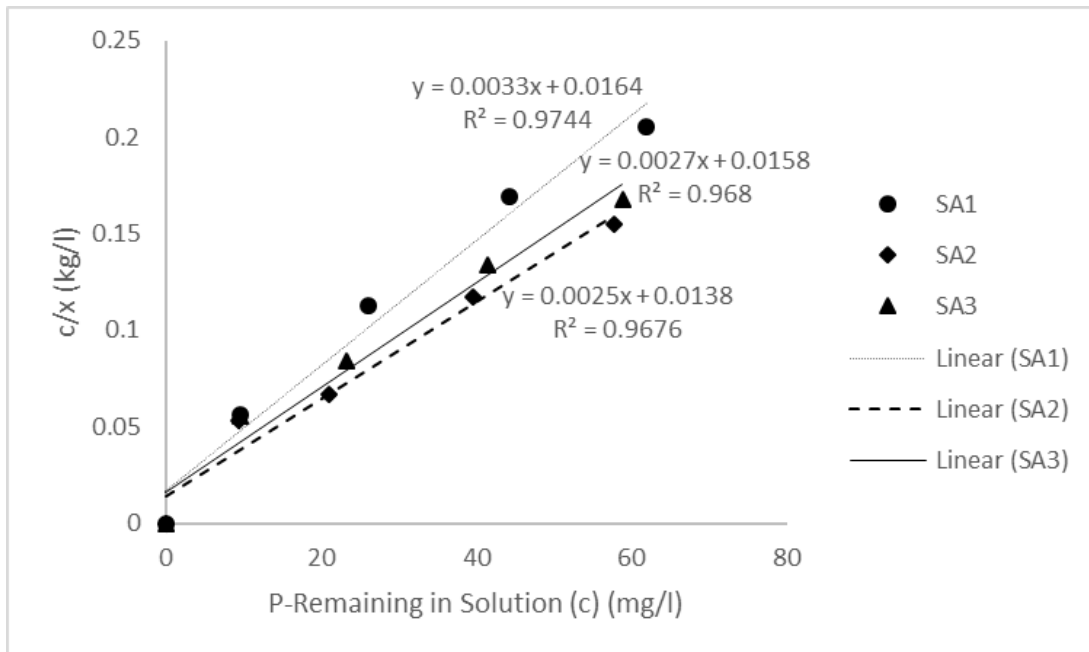


Figure 7.5: Langmuir adsorption isotherm for soils (0-20 cm) developed from arkosic sandstone.

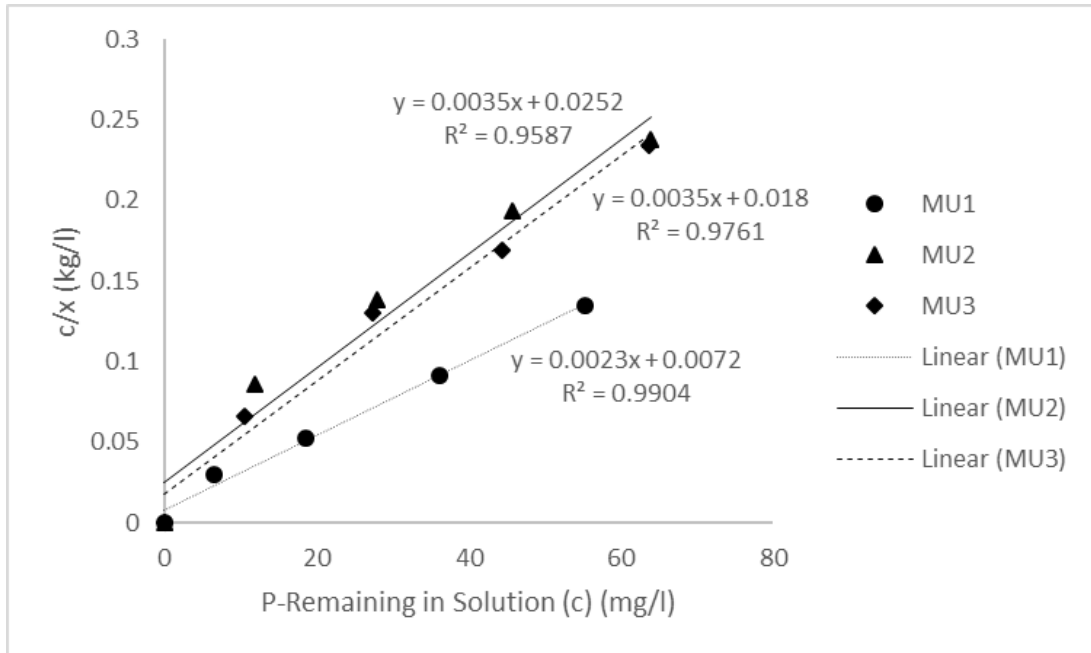


Figure 7.6: Langmuir adsorption isotherm for soils (0-20 cm) developed from gneiss.

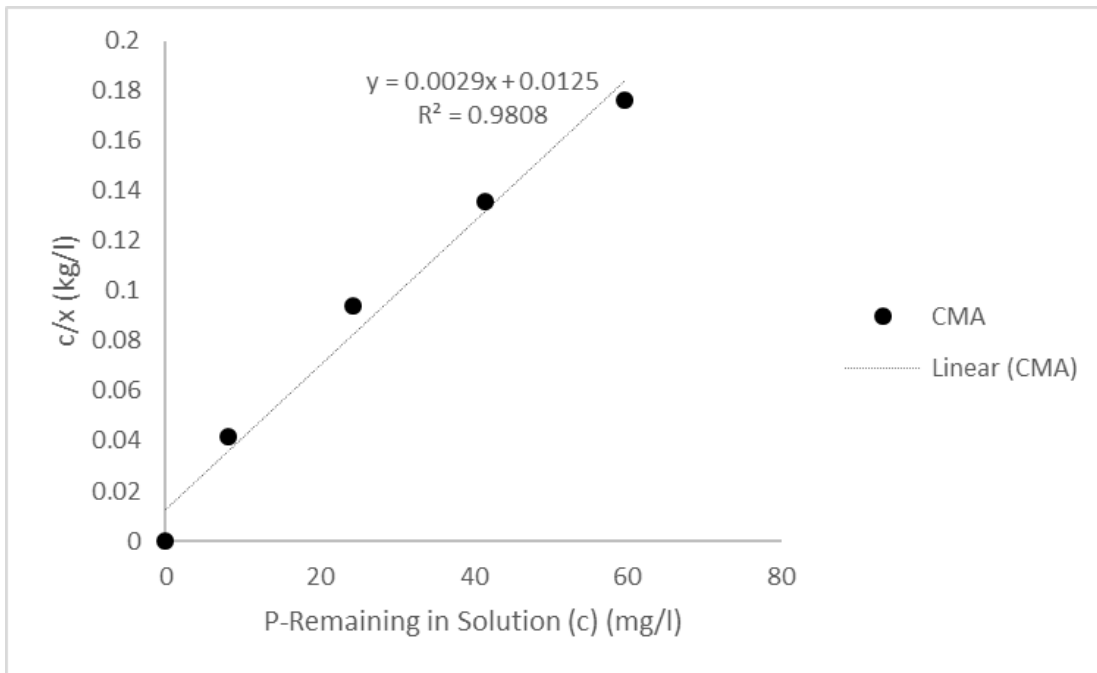


Figure 7.7: Langmuir adsorption isotherm for soil (0-20 cm) developed from quartzite.

The phosphorus adsorption maxima (X_m) mean values of the soils ranged from 285.71 to 833.33 mg/kg (Table 7.1) and were in increasing order of gneiss < quartzite (control) < arkosic sandstone < granite < basalt. These values were higher than X_m values between 127 and 185 mg/kg for Hutton soils at Groblersdal (Henry and Smith, 2002) but fall within the reported values for several acid soils developed from different parent materials in Indonesia with X_m values ranging from 294 to 1430 mg/kg (Hartono *et al.*, 2005; Wolde and Haile, 2015). However, Fontes (1988) reported an average X_m value of 4482 mg/kg for Brazilian oxisols developed from sandstone, claystone, mafic rock and schist. Clearly, the Brazilian oxisols are extremely high P fixing soils relative to the soils from this study which are moderately P fixing (Wolde and Haile, 2015).

The bounding energy (a) was highest for soils developed from basalt followed by soils developed from gneiss, arkosic sandstone and was the least for soils developed from granite in that order (Table 7.1). Bounding energy is one of such factors that indicate the energy of adsorption and the higher its value, the higher will be the tenacity of P adsorption (Munhoz *et al.*, 2011; Wolde and Haile, 2015). In soils with binding strengths less than 0.07 l/mg, P is subject to loss in subsurface flow (Mcdowell *et al.*, 2002). The soils having average “ a ” value > 0.07 l/mg suggest lesser or no susceptibility to P losses due to subsurface flow. The soil developed from basalt had the highest value of “ a ” (0.70 l/mg) (Table 7.1), this implies that the soil is high P sorbing with a strong bounding energy relative to the other soils and can retain more nutrients than others (Umoh *et al.*, 2014).

The maximum buffering capacity (aX_m) measures the ability of the soil to replenish phosphate ions when depleted by plant uptake. This reflects the ability of the soil to moderate change in solution P concentration when P is added to or withdrawn by plant from soil system (Umoh *et al.*, 2014). Table 7.1 revealed that buffering capacities of the soils were in an increasing order of arkosic sandstone < granite < gneiss < quartzite (control) < basalt. The buffering capacity values thus obtained indicate that to maintain a given intensity of P in solution, maximum quantity of P in the solid phase would be required for soils developed from basalt, followed by quartzite (control), gneiss, granite

and arkosic sandstone. Relative to other soils developed from different parent rocks within the studied area, soils developed from basalt (with more clay content) had higher capacity and buffer power for P adsorption (Poswa, 2016).

Table 7.1: Phosphorus adsorption parameters for soils developed from different parent rocks in Limpopo Province, South Africa.

Parent Rock		Langmuir Isotherm				Freundlich Isotherm		
		a (l/mg)	X _m (mg/kg)	aX _m (l/kg)	R ²	1/b (l/kg)	K (mg/kg)	R ²
Basalt (n=3)	Minimum	0.63	666.67	253.08	0.98	0.17	351.88	0.99
	Maximum	0.79	833.33	526.67	0.99	0.21	370.42	0.99
	Average	0.70	756.41	524.91	0.98	0.19	362.13	0.99
Granite (n=3)	Minimum	0.14	357.14	67.11	0.93	0.35	73.19	0.85
	Maximum	0.19	500.00	70.00	0.96	0.45	83.21	0.95
	Average	0.16	437.23	68.33	0.95	0.42	77.54	0.91
Arkosic sandstone (n=3)	Minimum	0.17	303.03	60.61	0.96	0.30	75.86	0.87
	Maximum	0.20	400.00	72.00	0.97	0.39	84.51	0.99
	Average	0.18	357.80	65.19	0.96	0.35	84.51	0.94
Gneiss (n=3)	Minimum	0.14	285.71	39.99	0.95	0.29	58.89	0.93
	Maximum	0.32	434.78	139.13	0.99	0.39	134.83	0.99
	Average	0.22	335.40	77.80	0.97	0.33	89.91	0.96
Quartzite (n=1)		0.23	344.83	79.31	0.98	0.28	108.74	0.99

7.2.2 Freundlich Adsorption Parameters for Soils

The Freundlich adsorption isotherms along with the equation and value of R² are presented in Figures 7.8 – 7.12. The highly significant value of R² (0.91 – 0.99) obtained for Freundlich equation indicated that the data fitted well to Freundlich equation for all the soils developed from the different parent rocks.

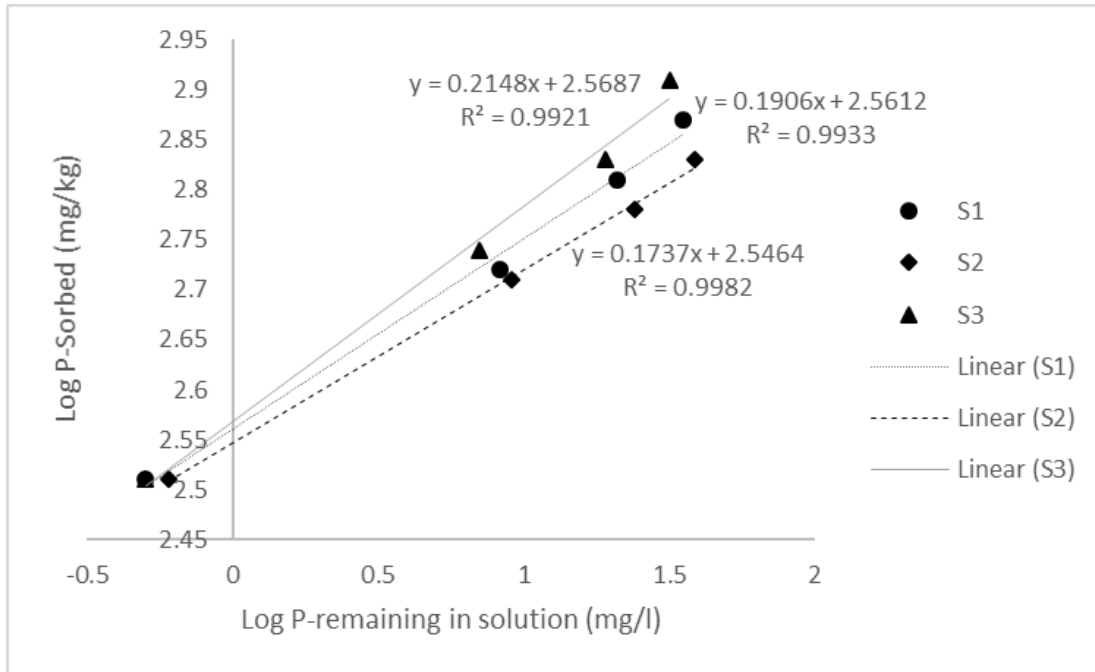


Figure 7.8: Freundlich adsorption isotherms for soils (0-20 cm) developed from basalt.

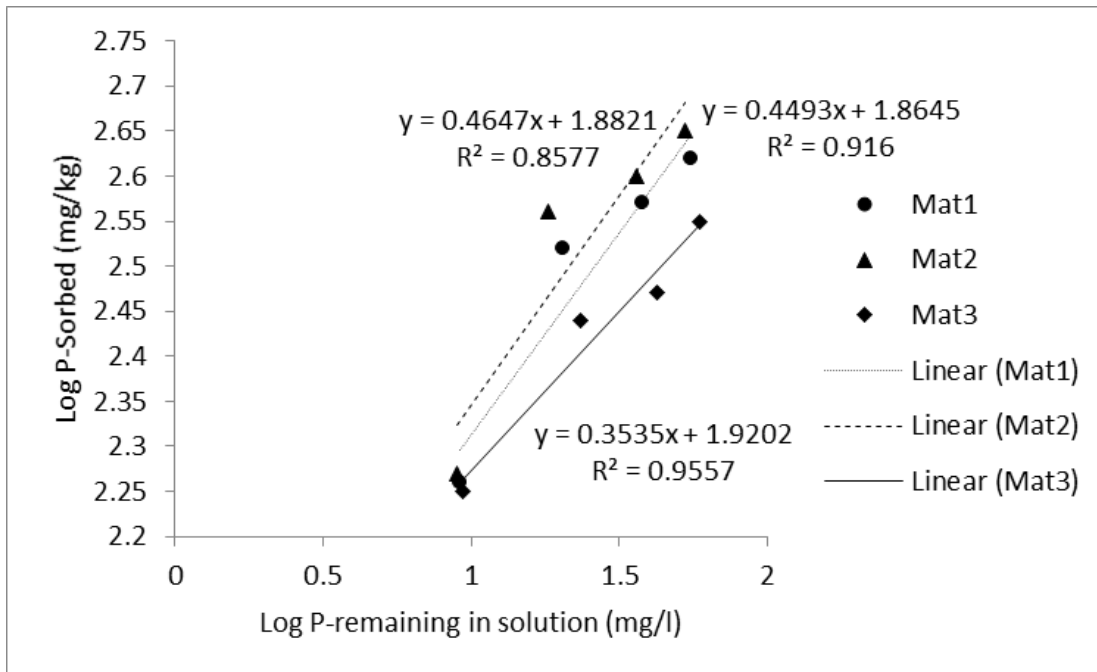


Figure 7.9: Freundlich adsorption isotherms for soils (0-20 cm) developed from granite.

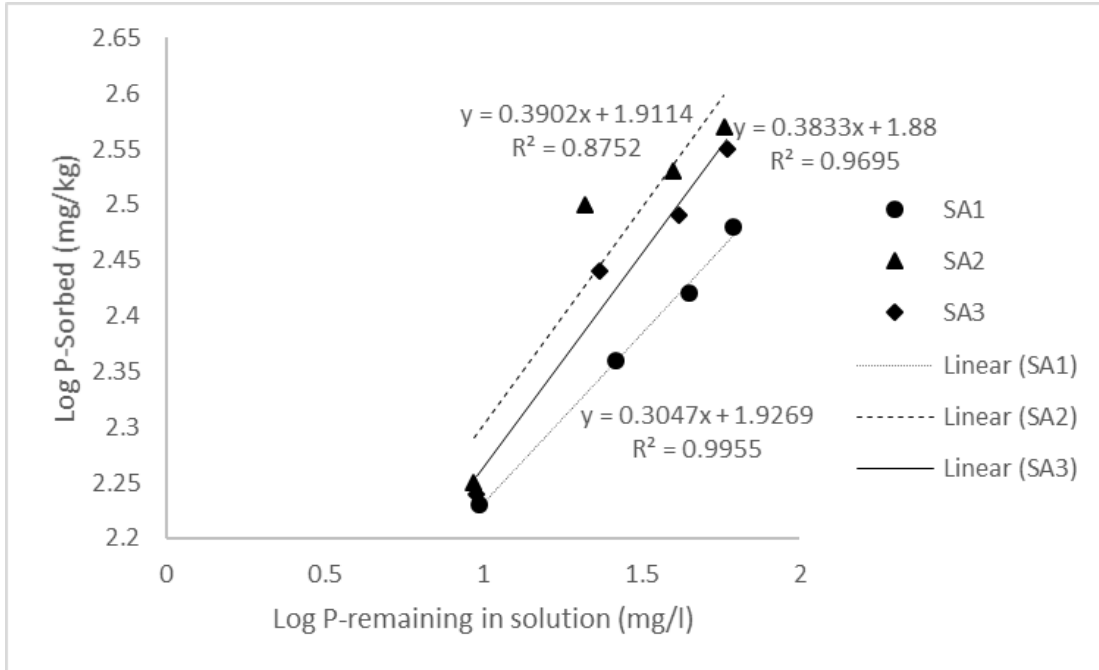


Figure 7.10: Freundlich adsorption isotherms for soils (0-20 cm) developed from arkosic sandstone.

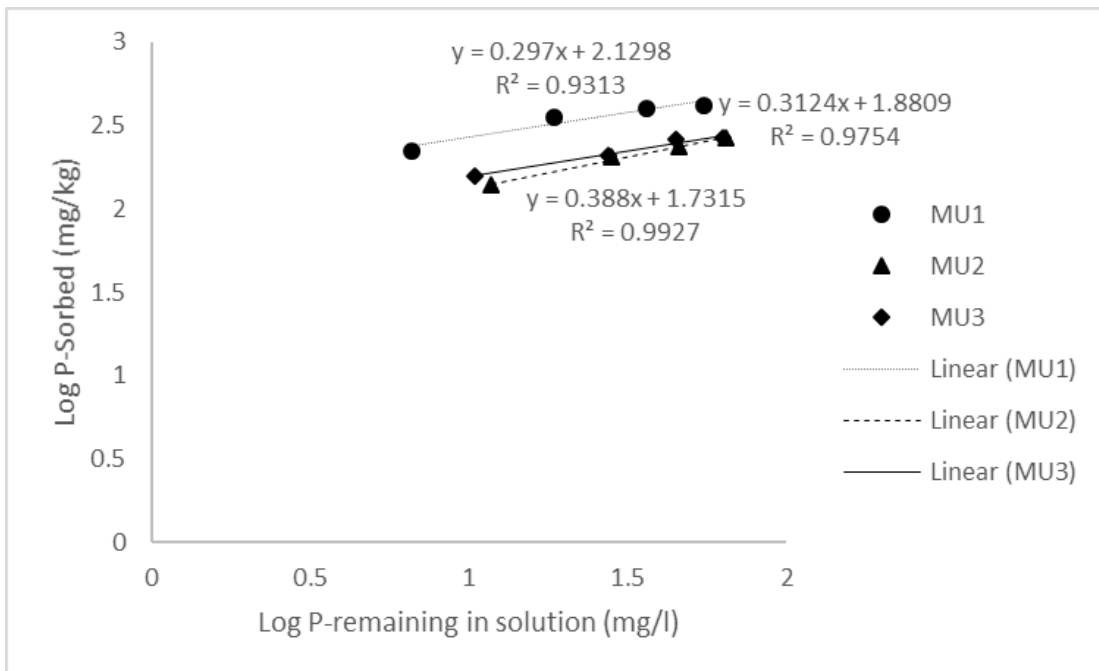


Figure 7.11: Freundlich adsorption isotherms for soils (0-20 cm) developed from gneiss.

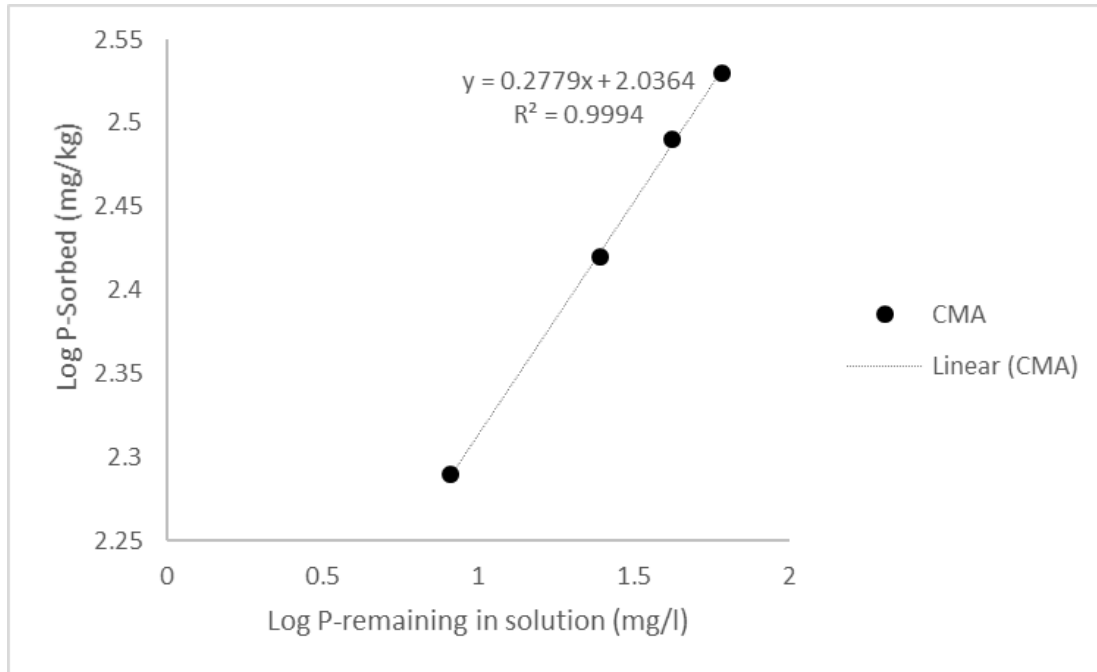


Figure 7.12: Freundlich adsorption isotherm for soil (0-20 cm) developed from quartzite.

The values of sorption energy ($1/b$) showed an increasing order of basalt < quartzite (control) < gneiss < arkosic sandstone < granite, whereas, the values of sorption capacity (K) showed a decreasing trend in the same order (i.e basalt > quartzite (control) > gneiss > arkosic sandstone > granite) (Table 7.1). This implies that as K increased, there was a corresponding decrease in the value of $1/b$. This agrees with Bolland *et al.* (2003) that as sorption of P increases, there is a slow decrease in the value of $1/b$. The heterogeneity factor ($1/b$) with values between 0.17 and 0.45 l/kg closer to zero suggests that the surface mechanism for P adsorption is heterogenous in nature (Saruchi and Kumar, 2016). In addition, the $1/b$ values < 1 implies that the P adsorption process in the soil was chemical (Sieczka and Koda, 2016). The findings agree with the results of Yousuf *et al.* (2019).

The soil P adsorption data were further tested with the Redlich-Peterson (R-P) and Sips isotherms. The isotherm plots are presented in Appendix 7.2, whereas the R-P (b_R) and Sips ($1/n$) model exponents are presented in Table 7.2. The b_R and $1/n$ for the soils

were generally between 0.70 and 0.92, and 0.70 and 0.90, respectively (Table 7.2). These values closer to unity (1) suggests closeness to the Langmuir isotherm. In addition, the higher R^2 values obtained for the R-P model relative to the Sips model indicates that the R-P model has better fitting with the experimental data (Table 7.2).

Table 7.2: Redlich-Peterson (b_R) and Sips ($1/n$) model exponents for the studied soils and soil kaolins.

Parent Rock		Soils				Soil Kaolins			
		Redlich-Peterson		Sips		Redlich-Peterson		Sips	
		b_R	R^2	$1/n$	R^2	b_R	R^2	$1/n$	R^2
Basalt (n=3)	Minimum	0.89	0.97	0.80	0.76	0.82	0.95	0.84	0.96
	Maximum	0.92	0.98	0.90	0.83	0.93	0.98	0.89	0.99
	Average	0.90	0.97	0.85	0.79	0.86	0.96	0.86	0.97
Granite (n=3)	Minimum	0.71	0.88	0.71	0.76	0.90	0.97	0.80	0.71
	Maximum	0.79	0.95	0.81	0.97	0.92	0.98	0.85	0.88
	Average	0.75	0.91	0.76	0.89	0.91	0.98	0.82	0.81
Arkosic sandstone (n=3)	Minimum	0.70	0.92	0.75	0.75	0.83	0.93	0.83	0.83
	Maximum	0.80	0.94	0.81	0.96	0.87	0.95	0.94	0.95
	Average	0.74	0.93	0.78	0.88	0.85	0.94	0.88	0.91
Gneiss (n=3)	Minimum	0.70	0.90	0.70	0.93	0.71	0.97	0.74	0.65
	Maximum	0.71	0.93	0.78	0.98	0.85	0.99	0.81	0.77
	Average	0.70	0.92	0.73	0.95	0.78	0.98	0.77	0.71
Quartzite (n=1)		0.73	0.92	0.72	0.82	0.90	0.97	0.77	0.87

7.2.3 Langmuir Adsorption Parameters for Soil Kaolins (Deferated Clay Fraction)

The average R^2 values derived from the Langmuir isotherms (Figures 7.13 – 7.17) ranged from 0.98 – 0.99 indicating that the P adsorption data of the studied kaolins in soils were well described by Langmuir model. Based on the Langmuir equation, the P adsorption maxima (X_m) values of the soil kaolin were in a decreasing order of basalt > quartzite (control) > gneiss > arkosic sandstone (Table 7.3). Singh and Gilkes (1992) studied the maximum P sorption of soil kaolins from South Western Australia and

reported it to be between 486 and 654 mg/kg with an average of 556.43 mg/kg. Thus, it appears that soil kaolins from South Western Australia have a much higher capacity to sorb P than the soil kaolins investigated in this study. This could be attributed to the higher kaolinite percentage in the former relative to the latter.

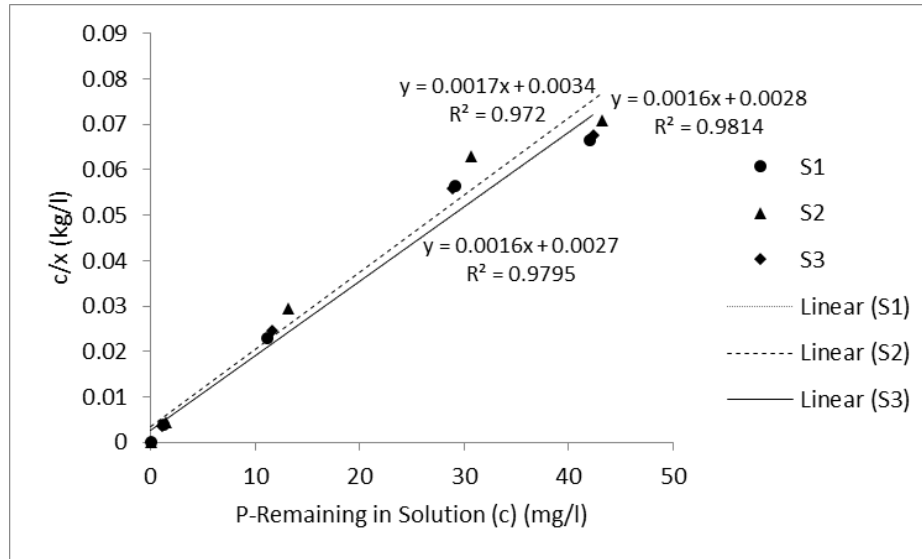


Figure 7.13: Langmuir adsorption isotherms for soil kaolins (0-20 cm) developed from basalt.

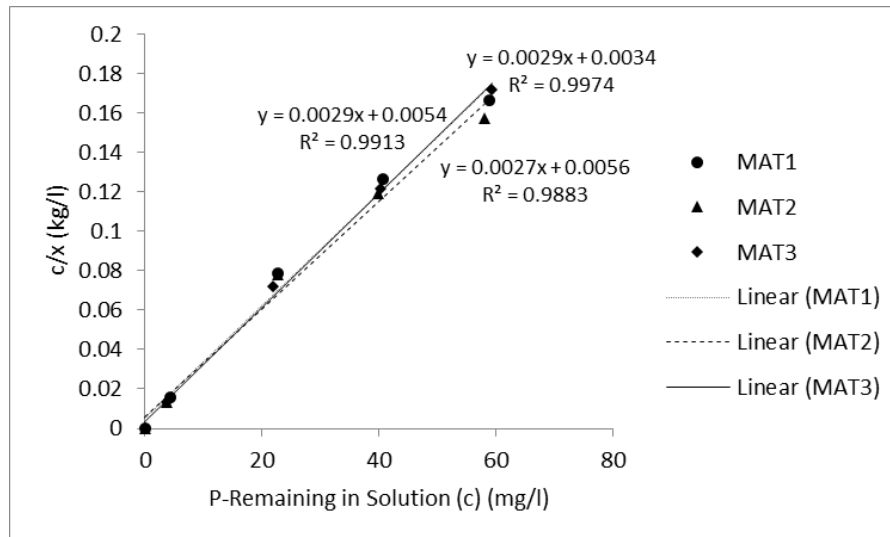


Figure 7.14: Langmuir adsorption isotherms for soil kaolins (0-20 cm) developed from granite.

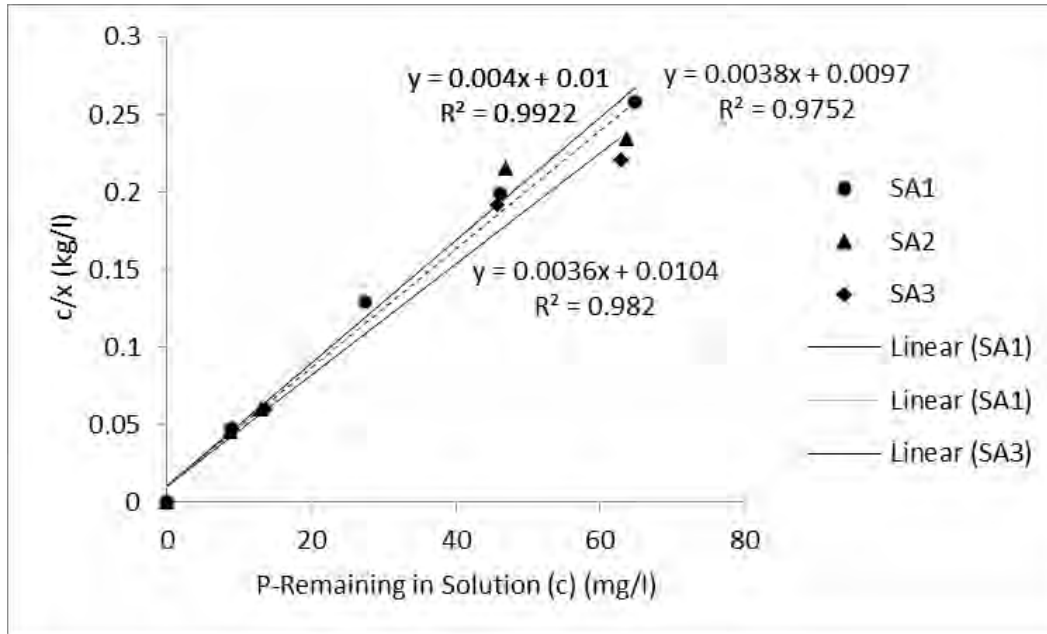


Figure 7.15: Langmuir adsorption isotherms for soil kaolins (0-20 cm) developed from arkosic sandstone.

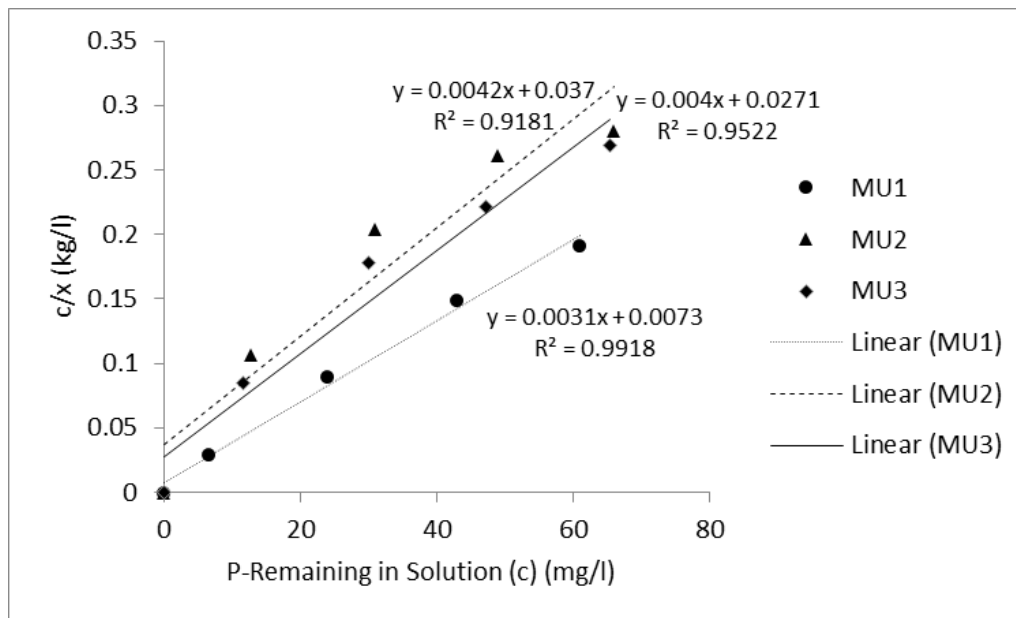


Figure 7.16: Langmuir adsorption isotherms for soil kaolins (0-20 cm) developed from gneiss.

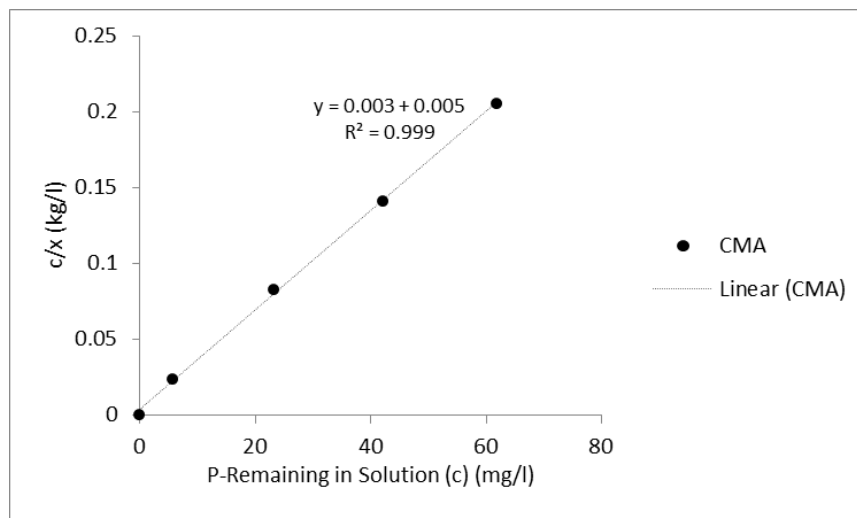


Figure 7.17: Langmuir adsorption isotherm for soil kaolin (0-20 cm) developed from quartzite.

Table 7.3: Phosphorus Adsorption Parameters for soil kaolins developed from different parent rocks in Limpopo Province, South Africa.

Parent Rock		Langmuir Isotherm				Freundlich Isotherm		
		a (l/mg)	X_m (mg/kg)	aX_m (l/kg)	R^2	1/b (l/kg)	K (mg/kg)	R^2
Basalt (n=3)	Minimum	0.50	588.24	294.12	0.97	0.17	287.81	0.94
	Maximum	0.59	625.00	368.75	0.98	0.18	303.60	0.96
	Average	0.55	612.75	339.71	0.97	0.18	299.79	0.95
Granite (n=3)	Minimum	0.48	344.83	177.78	0.98	0.08	222.18	0.77
	Maximum	0.85	370.37	293.11	0.99	0.10	243.78	0.95
	Average	0.62	353.34	219.03	0.98	0.09	233.37	0.86
Arkosic sandstone (n=3)	Minimum	0.36	250.00	100.00	0.97	0.13	134.68	0.71
	Maximum	0.40	277.78	103.09	0.99	0.17	147.40	0.97
	Average	0.38	263.65	101.03	0.98	0.15	139.34	0.83
Gneiss (n=3)	Minimum	0.11	238.09	26.19	0.91	0.15	42.55	0.94
	Maximum	0.42	322.58	135.48	0.99	0.39	166.88	0.97
	Average	0.23	270.22	66.39	0.95	0.25	89.72	0.95
Quartzite (n=1)		0.60	333.33	200.01	0.99	0.10	200.40	0.98

Bounding energy (a) of soil kaolins developed from basalt, granite, and quartzite (control) were marginally similar with average values between 0.55 and 0.62 whereas, soils developed from gneiss had the least average value of 0.23 of all the soil kaolins studied (Table 7.3). The maximum buffering capacity (aX_m) of the soil kaolins were in a decreasing order of basalt > granite > quartzite (control) > arkosic sandstone > gneiss.

7.2.4 Freundlich Adsorption Parameters for Soil Kaolins (Deferated Clay Fraction)

The goodness of fit of the Freundlich model was ascertained by looking at the R^2 values. All the plots (Figures 7.18 – 7.21) correlated well with R^2 values > 0.80 indicating apparent high conformity of the P adsorption data to the Freundlich model. Soil kaolins developed from basalt had the highest P sorption capacity (K) value, followed by granite, quartzite (control), arkosic sandstone, and gneiss soil kaolins in that order (Table 7.3). The P adsorption energy ($1/b$) values of soil kaolins studied were in an increasing order of granite < quartzite (control) < arkosic sandstone < basalt < gneiss.

The values of $1/b$ close to zero also suggest heterogenous nature and chemical process of P adsorption in the soil kaolins. However, like in the bulk soils, the R-P and Sips model exponent values close to 1 demonstrate that the Langmuir isotherm is more satisfactory. This further confirms that the P adsorption was homogenous in nature. The R^2 values of R-P model were also higher relative to Sips model. The values of R^2 for all the isotherm parameters from the models (Tables 7.1 – 7.3) were compared and the Langmuir model had the highest value. Thus, Langmuir model indicated the homogenous distribution of the P adsorption sites in the soils and soil kaolins in this present study. This is consistent with earlier recommendation by Henry and Smith

(2002) that Langmuir Isotherm is more suitable in modelling P sorption in South African soils.

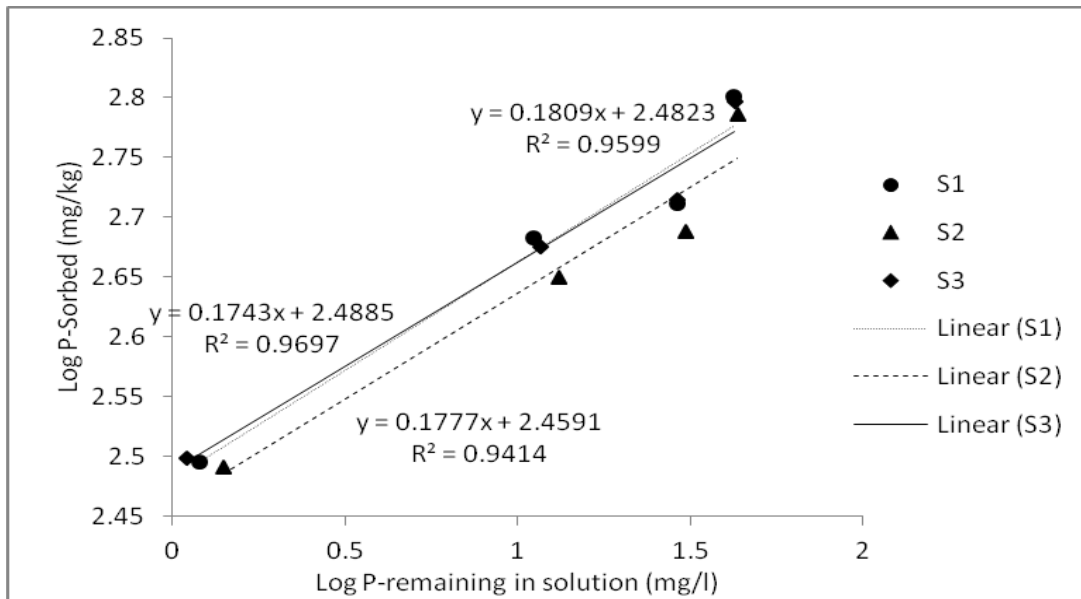


Figure 7.18: Freundlich adsorption isotherms for soil kaolins (0-20 cm) developed from basalt.

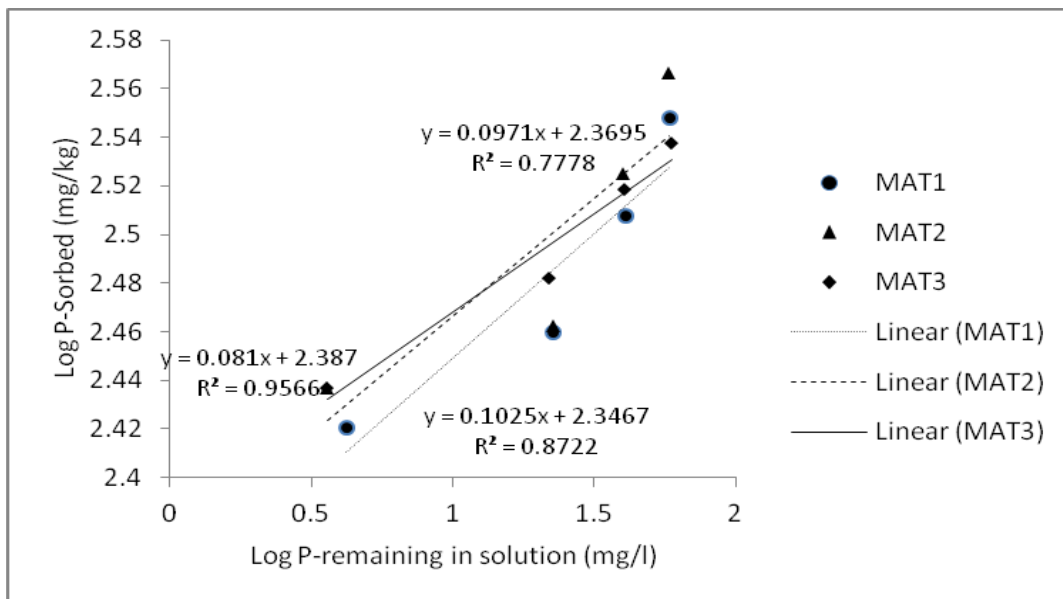


Figure 7.19: Freundlich adsorption isotherms for soil kaolins (0-20 cm) developed from granite.

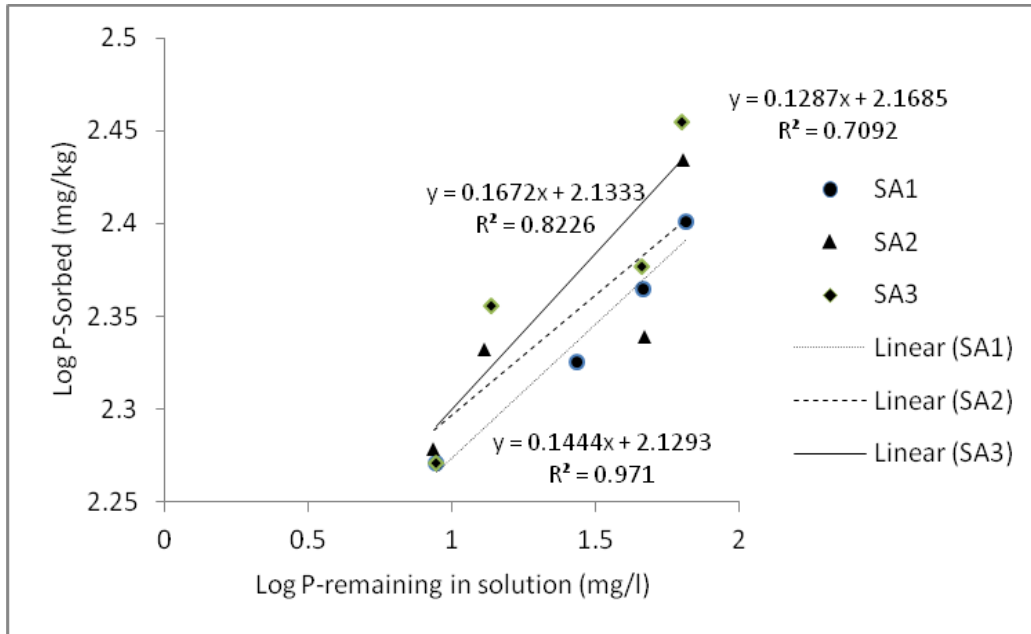


Figure 7.20: Freundlich adsorption isotherms for soil kaolins (0-20 cm) developed from arkosic sandstone.

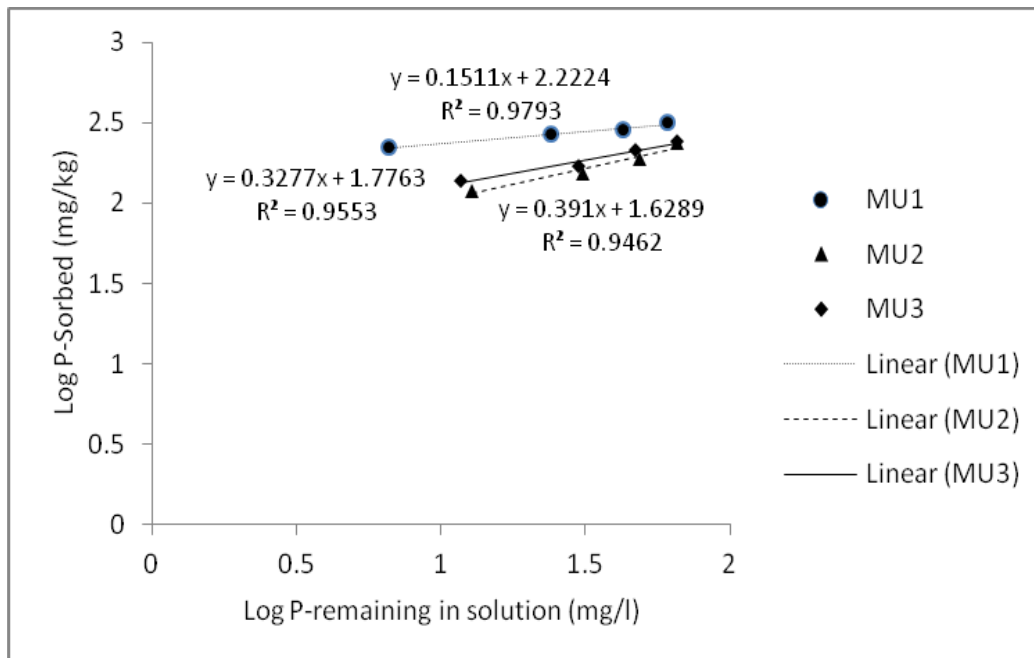


Figure 7.21: Freundlich adsorption isotherms for soil kaolins (0-20 cm) developed from gneiss.

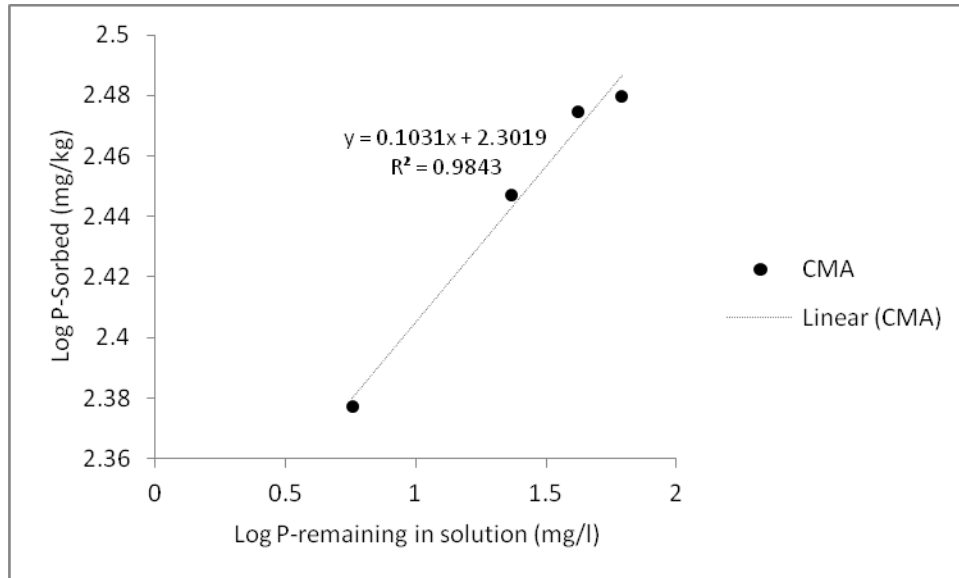


Figure 7.22: Freundlich adsorption isotherm for soil kaolins (0-20 cm) developed from quartzite.

7.3 External Phosphorus Requirements (EPR)

The amounts of added P required to maintain a concentration of 0.2 mgP/l in solution (EPR) based on Langmuir model were in a decreasing order of basalt > quartzite (control) > gneiss > granite > arkosic sandstone (Table 7.4) in soils and basalt > granite > quartzite (control) > arkosic sandstone > gneiss in soil kaolins whereas, based on the Freundlich model, the EPR values were in a decreasing order of basalt > quartzite (control) > gneiss > arkosic sandstone > granite in soils and basalt > granite > quartzite (control) > arkosic sandstone > gneiss in soil kaolins (Table 7.5).

Gichangi *et al.* (2008) studied the EPR of the different surface soil of Transkei, South Africa using the Langmuir model and reported it to be in the range of 2 – 123 mgP/kg with a mean value of 29 mgP/kg. In line with this, the studied soils had EPR values within this range. Of all soils and soil kaolins studied, soils developed from basalt had the highest EPR (267.90 mgP/kg).

Table 7.4: External Phosphorus Requirements (EPR) values for soils developed from different parent rocks in Limpopo Province, South Africa.

Parent Rock		EPR (mgP/kg)	
		Langmuir Isotherm	Freundlich Isotherm
Basalt (n=3)	Minimum	90.80	262.15
	Maximum	92.91	267.90
	Average	91.83	256.37
Granite (n=3)	Minimum	13.05	35.51
	Maximum	13.59	47.11
	Average	12.76	39.57
Arkosic sandstone (n=3)	Minimum	11.65	40.94
	Maximum	13.89	51.75
	Average	12.57	45.40
Gneiss (n=3)	Minimum	7.78	31.54
	Maximum	26.25	83.59
	Average	15.16	69.53
Quartzite (n=1)		69.53	15.16

Table 7.5: External Phosphorus Requirements (EPR) values for soil kaolins (deferated clay fraction) developed from different parent rocks in Limpopo Province, South Africa.

Parent Rock		EPR (mgP/kg)	
		Langmuir Isotherm	Freundlich Isotherm
Basalt (n=3)	Minimum	53.47	216.91
	Maximum	65.85	232.63
	Average	61.17	225.25
Granite (n=3)	Minimum	32.62	188.39
	Maximum	50.10	213.98
	Average	38.76	200.89
Arkosic sandstone (n=3)	Minimum	18.52	103.86
	Maximum	19.13	119.82
	Average	18.77	110.14
Gneiss (n=3)	Minimum	5.13	22.68
	Maximum	24.99	130.85
	Average	12.47	62.92
Quartzite (n=1)		35.71	169.79

Determination of EPR based on sorption models is important to discriminate soils into high and low P sorbing categories. In this regard, Juo and Fox (1977) proposed a classification system (Table 7.6) in which the P sorbed at 0.2 mgP/l is referred to as standard P requirement. According to this guideline, soils developed from granite, arkosic sandstone, gneiss and quartzite (control) which had average EPR values from both Langmuir and Freundlich models within the range 10 - 100 mgP/kg, are classified as low P sorbing soils except for soils developed from basalt classified as medium P sorbing soils with values within 100 – 500 mgP/kg for Freundlich model (Table 7.6).

Table 7.6: The magnitude of P adsorption in the soils studied (After Juo and Fox, 1977).

Standard P requirement (mgP/kg soil)	Scale	Studied soils	
		EPRL	EPRF
< 10	Very low	-	-
10 – 100	Low	Soils developed from basalt, granite, arkosic sandstone, gneiss, and quartzite (control)	Soils developed from granite, arkosic sandstone, gneiss, and quartzite (control)
100 – 500	Medium	-	Soils developed from basalt
500 -1000	High	-	-
> 1000	Very high	-	-

The low EPR values of the soils developed from granite, arkosic sandstone, gneiss and quartzite (control) indicate possible early P saturation for these soils following their available P contents. These could lead to elevated P levels in the soil solution with time which could contribute to the eutrophication of fresh water bodies with repeated applications of P fertilisers to the soils. Based on the United States Environmental Protection Agency (USEPA) 1 mgP/l in surface runoff (USEPA, 1986), EPR calculated on this criterion for the different soils using their averages ranged from 53.98 to 308.77 mgP/kg for Langmuir model and 77.54 to 362.13 mgP/kg for Freundlich model. These

values are equivalent to 107.96 to 617.54 kgP/ha and 155.08 to 724.26 kgP/ha respectively. Fertiliser P applications in South Africa ranges between 21 and 160 kgP/ha depending on the crop group (FAO, 2005). This suggest that the application of P fertiliser could pose significant threat to water quality in the region if a blanket fertiliser application recommended is applied above the EPR values. Hence, a site-specific P fertiliser application management strategy is important.

7.4 Variability of Adsorption Parameters

The values of P adsorption parameters in the soils and soil kaolins developed from different parent rocks within the study areas showed variability. Generally, soils especially those developed from basalt showed higher values of P adsorption parameters than soil kaolins. This can be attributed to the fact that apart from kaolins being a major constituent in soil providing an important contribution to P sorption, other oxides such as Fe_2O_3 and Al_2O_3 are also capable of adsorbing much P (Gichangi *et al.*, 2008).

Considering the R^2 values derived from the Langmuir and Freundlich models for soils and soil kaolins, the Langmuir model had slightly higher values (except for soils developed from basalt and quartzite) relative to the Freundlich model (Tables 7.1 and 7.3). Consequently, only adsorption parameters derived from Langmuir model were considered for assessing the influence of provenance and degree of weathering, and the test of significance (T-test and F-test (one-way ANOVA)).

7.4.1 Correlation between Sorption parameters, Provenance, and degree of weathering

To evaluate the influence of provenance and degree of weathering on the various P sorption Langmuir parameters (a , X_m , aX_m , and EPR) in the studied soils, Pearson correlation coefficients were calculated. Variables selected to assess the influence of

provenance were major oxides such as Al_2O_3 , Fe_2O_3 , and CaO which have been known to be responsible for P sorption in soils (Poswa, 2016). The SiO_2 contents and CIA of the soils were used to assess the influence of desilication and degree of weathering on P sorption in the soils (Scheffe and Tymms, 2013).

All the P sorption parameters showed significant correlations with Al_2O_3 , Fe_2O_3 , SiO_2 , and CIA except for CaO (Table 7.7). The lack of significant correlation with CaO could be attributed to the non-calcareous nature of the soils (Yousuf *et al.*, 2019). The positive correlations between Al_2O_3 , Fe_2O_3 , and sorption parameters suggest increases in the sorption parameters with increases in Al_2O_3 and Fe_2O_3 (Poswa, 2016). In addition, the positive correlation of CIA and negative correlation of SiO_2 with the P sorption parameters indicate that as weathering and the removal of SiO_2 increases, more P is sorbed due to the corresponding increase in Al_2O_3 and Fe_2O_3 in the soils. The positive correlations between Al_2O_3 , Fe_2O_3 , and CIA (Table 7.7) suggest that the weathering intensities in the soils played a major role in their P sorption (Scheffe and Tymms, 2013).

Table 7.7: Pearson Correlation Coefficients between Sorption parameters, Provenance, and degree of weathering.

	a	Xm	aXm	EPR	Al_2O_3	SiO_2	Fe_2O_3	CaO	CIA
a	1								
Xm	.864**	1							
aXm	.983**	.932**	1						
EPR	.981**	.936**	.991**	1					
Al_2O_3	.776**	.780**	.813**	.814**	1				
SiO_2	-.849**	-.794**	-.872**	-.872**	-.977**	1			
Fe_2O_3	.937**	.914**	.962**	.962**	.896**	-.957**	1		
CaO	-.129*	-.171*	-.135*	-.136*	.121*	-.053*	-.201*	1	
CIA	.870**	.831**	.882**	.883**	.603**	-.655**	.801**	-.544**	1

* Correlation is significant at the 0.05 level (2-tailed); ** Correlation is significant at the 0.01 level (2-tailed).

7.4.2 Test of Hypothesis

Null Hypothesis: There is no difference between the P sorption parameters for soils and soil kaolins (deferated clay fraction) developed from different parent rocks in Limpopo Province, South Africa.

Using both the independent sample T-test and F-test, Table 7.8 reveals that the significant level (P-value) is greater than 0.05 for bounding energy ($p = 0.06$), sorption capacity ($p = 0.17$), maximum buffering capacity ($p = 0.84$), and EPR ($p = 0.84$). Hence, the null hypothesis is accepted. This suggest that the sorption parameters obtained for soil kaolins could as well be taken as a good predictor for P sorption and buffering in the soils (Raty and Peltovuori, 2008).

Several experimentally proven studies have reported significant positive relationships between P sorption in Australian, Natal, Finnish, Thai, and North American soils and their respective deferated clay fractions (Singh and Gilkes, 1992; Bainbridge *et al.*, 1995; Raty and Peltovuori, 2008; Wiryakitnateekul *et al.*, 2005; Gilkes and Prakongkep, 2016; Brenner *et al.*, 2019). These various studies corroborated that sufficient information regarding P sorption parameters in soils can be deduced from their deferated clay fractions.

Table 7.8: T-test for significance of difference in P sorption parameters between soils and soil kaolins (deferated clay fraction) developed from different parent rocks in Limpopo Province, South Africa (at 5 % significant level).

Parameter		Mean (n=13)	SD	t-value	p- value	F- value	p- value
Bounding energy	Soil	0.31	0.23	-1.94	0.06	3.76	0.06
	Soil kaolin	0.48	0.23				
Sorption Capacity	Soil	461.95	182.76	1.43	0.17	2.04	0.17
	Soil kaolin	369.46	144.85				
Maximum buffering capacity	Soil	176	161.19	-0.21	0.84	0.04	0.84
	Soil kaolin	189.49	117.18				
EPR	Soil	31.74	28.51	-0.2	0.84	0.04	0.84
	Soil kaolin	33.96	20.59				

7.5 Concluding Remarks

Based on the phosphorus adsorption analyses of soils and soil kaolins (deferated clay fraction) developed from different parent rocks within the studied area, the following deductions have been made:

- a. The studied soils and soil kaolins within the study area have high affinity for phosphorus since they were generally characterised by H-type P adsorption isotherm curves.
- b. The Langmuir and Freundlich isotherms were linear for soils and soil kaolins developed from all studied parent rocks, signifying that in these soils and soil kaolins, the P adsorption sites were not completely occupied. The P adsorption in the soils and soil kaolins were homogenous in nature and by chemical processes. In addition, Langmuir model is most suited for describing the adsorption of P by soil and soil kaolin developed from the different parent rocks within the studied area.
- c. Phosphorus fixing capacity is at the maximum in soils and soil kaolins developed from basalt and minimum in soils developed from gneiss and soil kaolins developed from arkosic sandstone respectively. The standard P requirements for the soils were generally classified as low based on the Langmuir model. Blanket P fertiliser application in the region should be discouraged to avoid underfertilisation or overfertilisation problems.
- d. The statistical independent T-test and F-test evaluations revealed that the P sorption and buffering parameters for the bulk soils can be deduced from the P sorption of the soil kaolins.

Chapter Eight

Properties of Oxidic Soils Developed from different Parent Rocks in Limpopo Province, South Africa: Implications on Fertility and Phosphorus Adsorption

This chapter aimed to establish the influence of soil properties on the fertility of oxidic soils developed from different parent rocks in Limpopo Province, South Africa (Specific Objective 4) based on Hypothesis 4. The soil properties at plow depth (0-20 cm) were used to achieve specific objective 4.

8.1 Soil Properties and Fertility

The physico-chemical characteristics, soil fertility indices (SFI), and soil evaluation factor (SEF) of the soils are presented in Table 8.1. The pH of the soils was between 5.30 and 8.17 indicating a moderately acidic to moderately alkaline conditions. The soils developed from granite had the least pH average value of 5.69 whereas, soils developed from arkosic sandstone had the highest pH average value of 7.53. These pH values are satisfactory for most plant requirements except for water melon and potato that requires a strongly acidic condition (Table 8.2). The soil developed from quartzite (control) also has a moderate acidic condition.

The average electrical conductivity (EC) was highest and least for soils developed from arkosic sandstone and gneiss with values of 81.77 and 13.72 $\mu\text{S}/\text{cm}$, respectively. The EC value of 17.80 $\mu\text{S}/\text{cm}$ obtained for the soil developed from quartzite (control) was within this range. Those with higher EC values suggest higher soluble salt concentrations. However, these EC values are sufficiently low and can be taken as negligible since they are within the 0 – 2000 $\mu\text{S}/\text{cm}$ (Table 8.3). In addition, the soils are not classified as saline since their EC values were greatly lower than 4 dS/m (40×10^6 $\mu\text{S}/\text{cm}$). Hence, the concentrations of soluble salts in the soils were not sufficient to seriously interfere with the growth of most plants. The presence of soluble salts affects plant uptake of P, Na, K, and especially Ca (Manicus, 2009; Weil and Brady, 2017).

Table 8.1: Physico-chemical parameters, fertility indices (SFI), and evaluation factors (SEF) of Oxidic Soils developed from different parent rocks in Limpopo Province, South Africa.

Parent Rock		pH	EC	OM	Clay	Silt	Sand	CEC	Avai. P	Ca	K	Mg	Na	Al	SFI	SEF
Basalt (n=3)	Min	5.30	14.96	0.41	54.00	12.00	10.00	13.22	0.01	2.61	0.10	0.95	0.07	0.76	9.73	6.40
	Max	6.50	56.40	3.62	78.00	20.00	26.00	18.30	0.01	5.14	0.29	1.91	0.11	1.12	13.67	25.03
	Average	6.07	30.42	1.55	64.33	16.33	19.33	15.01	0.01	3.83	0.17	1.57	0.09	0.90	12.29	13.57
Granite (n=3)	Min	5.58	17.50	2.90	10.00	6.00	62.00	2.93	15.33	0.74	0.21	0.48	0.04	0.17	27.06	8.96
	Max	5.90	21.60	4.55	18.00	14.00	80.00	4.12	26.41	1.06	0.25	0.68	0.05	0.33	36.05	12.66
	Average	5.69	19.17	3.83	14.00	10.00	72.67	3.58	22.02	0.85	0.23	0.55	0.04	0.25	32.91	10.91
Arkosic Sandstone (n=3)	Min	6.41	40.60	2.59	10.00	5.00	77.00	5.09	0.01	1.50	0.29	1.41	0.03	0.23	25.60	13.78
	Max	8.17	114.40	4.76	16.00	10.00	80.00	11.57	54.99	13.92	0.63	2.29	0.07	0.41	67.24	67.18
	Average	7.53	81.77	3.38	13.00	8.33	78.67	9.31	20.65	8.57	0.47	1.80	0.05	0.34	42.06	43.24
Gneiss (n=3)	Min	6.49	12.60	2.79	16.00	5.00	73.00	4.87	0.01	2.87	0.07	1.68	0.09	0.18	15.64	26.55
	Max	7.10	15.31	4.76	22.00	8.00	76.00	10.70	0.01	7.24	0.09	3.88	0.20	0.31	22.00	52.03
	Average	6.81	13.72	3.93	18.67	7.00	74.33	7.53	0.01	5.03	0.08	2.91	0.13	0.24	18.53	35.45
Quartzite		5.13	17.80	4.45	14.00	5.00	81.00	2.57	0.97	0.09	0.03	0.60	0.06	0.04	11.23	8.13

Note: The unit for electrical conductivity (EC) is $\mu\text{S}/\text{cm}$; the unit for organic matter (OM), clay, silt, and sand is percent; the unit for cation exchange capacity (CEC) is cmol/kg ; the unit for available phosphorus (avai. P) is mg/kg ; the unit for exchangeable cations (Ca, K, Mg, Na, and Al) is cmol/kg ; SFI: soil fertility indices; and SEF: soil evaluation factor.

Table 8.2: pH requirements for plants (After Hazelton and Murphy, 2007).

Crop/vegetable	pH range
Watermelon, Potato	Strongly acidic (4 – 5)
Carrots, tomato, maize, cowpeas	Moderately acidic to neutral (5 – 7)
Cucumber	Moderately acidic to slightly acidic (5 – 7)
Spinach, beetroot	Slightly acidic to neutral (6 – 7)
Onion	Slightly acidic (6 – 7)

Table 8.3: Soil conductivity limits (After Patiram *et al.*, 2007).

Conductivity ($\mu\text{S}/\text{cm}$)	
0 - 2000	Salinity effects negligible
2000 - 4000	Very sensitive crops affected
4000 - 8000	Many crops affected
8000 - 16000	Yields of only salt-tolerant crops satisfactory
>16000	Yields of only very salt-tolerant crops satisfactory

Organic matter (OM) content of the soils ranged from 0.41 % in soils developed from basalt to 4.76 % in soils developed from gneiss. The control sample had higher OM content (4.45 %) relative to the averages of the other soils. The obvious influence of soil OM reflects more in the colouration which is usually brownish. The average OM values obtained for the soils were above the threshold of 3.4 % below which potentially serious decline in soil quality will occur (Loveland and Webb, 2003) except for soils developed from basalt. The OM showed strong positive correlation with sand content ($r = 0.70$) and negative correlation with silt and clay contents ($r = -0.73$ and -0.63) (Table 8.4). Ideally, the influence of soil texture on OM could be attributed to its effect on the water holding capacity (Weil and Brady, 2017). Small particles (Clay and silt) have a much larger surface area than the larger sand particles which allows the former to hold a greater quantity of water. In addition, there will be increase in humidity needed for bacterial growth which will eventually increase the OM content (Azlan *et al.*, 2012). However, kaolinite as the main clay mineral in the soils has smaller specific surface than most other clay minerals. Therefore, the soils dominated with kaolins contain considerably fewer clay-humus complexes and the unprotected unstable humic substances are vulnerable to decomposition under appropriate soil moisture conditions (FAO, 2005).

Among the different soil fractions, the clay content was the highest in soils developed from basalt and were classified as clays whereas, the sand content was highest in the soils developed from granite, arkosic sandstone, gneiss, and quartzite (control) and were classified dominantly as sandy loam. Soils in which chemical weathering dominates relative to mechanical weathering tend to be richer in clays (Plummer *et al.*, 2016). In addition, the presence of less resistant minerals such as plagioclase and

diopside in basalt relative to more resistant minerals like quartz and potassium feldspar in granite, arkosic sandstone, gneiss, and quartzite, respectively also accounts for the differences in soil texture (Ibarra *et al.*, 2016). Hence, the variation in the soil texture reflects the differences in the weathering intensities of the various minerals present in the parent rocks (Umoh *et al.*, 2014).

Table 8.4: Pearson correlation matrix for linear relationships between parameters for Oxidic Soils developed from different parent rocks in Limpopo Province, South Africa.

	pH	EC	OM	Clay	Silt	Sand	CEC	Avai. P	Al	SFI	SEF
pH	1										
EC	0.61*	1									
OM	-0.09	0.19	1								
Clay	-0.17	-0.11	-0.63*	1							
Silt	-0.22	-0.12	-0.73**	0.61*	1						
Sand	0.22	0.13	0.7**	-0.98**	-0.75**	1					
CEC	0.3	0.41	-0.4	0.73**	0.54	-0.7**	1				
Avai. P	-0.21	-0.05	-0.02	-0.4	0.01	0.32	-0.49	1			
Al	-0.07	0.19	-0.52	0.88**	0.75**	-0.91**	0.88**	-0.31	1		
SFI	0.11	0.21	0.07	-0.52	-0.14	0.46	-0.38	0.94**	-0.35	1	
SEF	0.77**	0.71**	0.41	-0.28	-0.37	0.34	0.36	-0.34	-0.05	-0.01	1

* Correlation is significant at the 0.05 level (2-tailed); ** Correlation is significant at the 0.01 level (2-tailed).

Available P contents were extremely lower (<0.01 mg/kg) in soils developed from basalt, gneiss and quartzite (control) whereas, soils developed from granite and arkosic sandstone have averages > 20 mg/kg. The available P levels in soils developed from granite and arkosic sandstone were higher than the critical level of 12 – 15 mg/kg proposed for most crops (Weil and Brady, 2017). The parent rocks do not have primary P minerals such as apatite, strengite, and variscite which could have weathered to release much P into the soil. However, exogenous materials such as dust and organic matter could be possible sources for substantial P to be added to the soils relative to what is derived from parent rock weathering (Porder and Ramachandran, 2012). This suggest that provenance would only have more influence on the adsorption and desorption of available P in the soils due to the presence of Fe and Al secondary minerals (Poswa, 2016).

The order of the average exchangeable cations for the soils was $\text{Ca} > \text{Mg} > \text{K} > \text{Na}$, respectively. The soils developed from quartzite (control) had lower concentrations relative to other soils and thus could be attributed to the highly sandy nature of the former (Weil and Brady, 2017). The weathering of feldspar and ferromagnesian minerals in the parent rocks determines the variability of exchangeable cations in the soils. The order of prevalence of exchangeable cations in the soils is favourable for crop production (Havlin *et al.*, 2014). The range of critical values for optimum crop production for Ca, Mg, and K are from 1.25 – 2.5, 0.25 – 0.5, and 0.28 – 0.51 cmol/kg soil, respectively (Sims, 2000). The exchangeable Ca and Mg in the soils were above the critical values (except for Ca in soils developed from granite and quartzite). In addition, the exchangeable K in all the soils was below the critical value except for soils developed from arkosic sandstone.

The exchangeable Al ranged from 0.17 cmol/kg in soils developed from granite to 1.12 cmol/kg in soils developed from basalt. Exchangeable Al correlated negatively ($r = -0.52$) with OM content. This suggests that the amount of exchangeable Al decreases with increase in OM content. Organic matters form complexes with Al in soils and hence, Al are not available in exchangeable sites. Hence, soil acidity damage to crops due to Al toxicity will be minimal in the soils with higher OM content (Hoyt, 1977; Palleiro *et al.*, 2016). Relationship existed between exchangeable Al and soil texture which suggested that the texture played important role on the availability of exchangeable Al in the soils. The strong positive correlation between exchangeable Al and clay content ($r = 0.88$) and silt content ($r = 0.75$) implied that the exchangeable Al in the soils increased with increasing clay and silt contents. Small particles (clay and silt) have much larger surface area than larger sand particles. High correlation is often found between specific surface area and CEC (Weil and Brady, 2017).

The CEC of the soils developed from basalt was higher than other soils. The higher the CEC values in soil was due to high clay content and hence higher surface area (Manicus, 2009). According to the rating of Hazelton and Murphy (2007), the CEC averages of the soils can be classified as very low except for soils developed from basalt rated as medium (Table 8.5). The soils with low CEC are more likely to be

susceptible to leaching and loss of the exchangeable cations (Manicus, 2009). The higher the clay content, the more the CEC ($r = 0.73$) in the soils. Clay minerals with their negatively charged sites on their surfaces absorb and hold positively charged ions (cations) by electrostatic force in the soils (Mckenzie *et al.*, 2004). This accounts for the lesser susceptibility of the soils to cation leaching.

Table 8.5: Soil CEC classification (After Hazelton and Murphy, 2007).

Rating	CEC range (cmol/kg)
Very low	<6
Low	6 - 12
Moderate	12 - 25
High	25 - 40
Very high	>40

8.1.1 Evaluation of the Soil Fertility Status

Table 8.1 shows the SFI and SEF ranges and average values obtained for the different soils. Soils developed from arkosic sandstone had the highest SFI average value followed by soils developed from granite, gneiss, basalt, and quartzite (control), respectively. The SFI exhibited strong positive correlation with available P ($r = 0.94$) and a negative correlation with clay content ($r = -0.52$) (Table 8.4). The average SEF values ranged from 6.40 for soils developed from basalt to 6.72 for soils developed from arkosic sandstone. According to Lu *et al.* (2002), SEF value < 5 indicates extremely poor soil fertility whereas, SEF value > 5 indicates higher soil fertility. All the SEF average values estimated were all greater than 5 indicating that they are not of poor soil fertility. Based on their average SEF values, the order of increasing soil fertility is soils developed from quartzite (control) < granite < basalt < gneiss < arkosic sandstone. Results of the correlation analyses of SEF with soil properties showed strong positive correlation between SEF and pH ($r = 0.77$), SEF and EC ($r = 0.71$) (Table 8.4). The soil pH affects the plant nutrient availability by controlling the chemical forms of the nutrients as well as their availability in the soil (Weil and Brady, 2017).

8.2 Relationship between Sorption Parameters and Soil Properties

Correlation analysis between sorption parameters such as bounding energies (a), sorption maximum (Xm), maximum buffering capacity (aXm), and external phosphorus requirement (EPR) and soil properties was conducted to identify the key variables influencing P sorption in the soils. Table 8.6 shows the correlation coefficients with significant positive correlations (> 0.50) for clay content, silt content, CEC, Al₂O₃, and Fe₂O₃ whereas, OM, sand content were negative correlated with the sorption parameters. In addition, pH and avai. P were weakly and not significantly correlated with the sorption parameters. The correlation results suggest that several variables can influence the P sorption capacity of the soils. Hence, multiple linear regressions were used to describe the relationship between the sorption parameters and soil properties. Assumptions of linearity, independence of errors, homoscedasticity, unusual points and normality of residuals were examined.

Table 8.6: Pearson correlation matrix for linear relationships between sorption parameters and properties of Oxidic Soils developed from different parent rocks in Limpopo Province, South Africa.

	pH	OM	Clay	Silt	Sand	CEC	Avai. P	Al ₂ O ₃	Fe ₂ O ₃	a	Xm	aXm	EPR
pH	1												
OM	-0.09	1											
Clay	-0.17	-0.63*	1										
Silt	-0.22	-0.73**	0.61*	1									
Sand	0.22	0.7**	-0.98**	-0.75**	1								
CEC	0.3	-0.4	0.73**	0.54	-0.7**	1							
Avai. P							1						
P	-0.21	-0.02	-0.4	0.01	0.32	-0.49							
Al ₂ O ₃	-0.25	-0.51	0.82**	0.64*	-0.84**	0.55	-0.40	1					
Fe ₂ O ₃	-0.12	-0.67	0.94	0.71**	-0.94**	0.75**	-0.45	0.90**	1				
a	-0.22	-0.59	0.93	0.74**	-0.94**	0.81**	-0.38	0.78**	0.94**	1			
Xm	-0.26	-0.66	0.86	0.74**	-0.87**	0.62*	-0.19	0.78**	0.87**	0.86**	1		
aXm	-0.22	-0.66	0.95	0.76**	-0.96**	0.77**	-0.34	0.81**	0.96**	0.98**	0.93**	1	
EPR	-0.21	-0.66	0.95	0.77**	-0.96**	0.77**	-0.34	0.81**	0.96**	0.98**	0.93**	1.00**	1

*Correlation is significant at the 0.05 level (2-tailed); **Correlation is significant at the 0.01 level (2-tailed).

8.2.1 Bounding Energy and Soil Properties

The regression coefficients and statistics summary of each prediction model of bounding energy (a) values depending on soil properties as developed using stepwise

multiple linear regression are presented in Table 8.7. Out of all the variables entered, only sand content, CEC, pH, OM, and clay content are useful in predicting the bounding energy. The models having F value > 1 suggest that they significantly improve the ability to predict the bounding energy (Table 8.8). In Table 8.9, the unstandardised coefficients indicate the individual contributions of each predictor (sand content, CEC, pH, OM, and clay content) to the model. Significant values < 0.05 suggests that the predictor is making statistically significant contribution to the model. Hence, it is obvious that CEC, pH, OM, and clay content are significant predictors of the bounding energy. Table 8.10 showing significant values > 0.05 corroborated the fact that the excluded variables (silt content, available P, Al_2O_3 , and Fe_2O_3) would not have had a significant impact statistically on the model's ability to predict the bounding energy. From t- statistics, CEC and clay content have slightly more impact than pH and OM based on model 6 and their impact in increasing order is $\text{pH} < \text{OM} < \text{clay content} < \text{CEC}$ following the standardised beta values measured in standard deviation units (Table 8.9). This suggests that CEC is the most important variable for the bounding energy in the soils. Sand content was excluded from model 6 since it has the highest significant level (0.11, model 4). No removals in model 6 since all the remaining variables (CEC, pH, OM, and clay content) have significant level < 0.05 (Table 8.9). The variance inflation factor (VIF) values not exceeding 10 implies that the associated regression coefficients are not poorly estimated due to multilinearity (Montgomery, 2001) (Table 8.9).

In all the six (6) models, the multiple correlations between the bounding energy values and predictors (sand content, CEC, pH, OM, and clay content) are strong with R varying from 0.942 to 0.995 and increase slightly while one specific soil property is added to the previous model (Table 8.11). The Durbin-Watson (d) = 1.70 (Table 8.11), which lies between $1.5 < d < 2.5$ suggest that there is no first order autocorrelation in the multiple linear regression data. Values of d outside the critical values in regression could imply an underestimation of the level of statistical significance for F and t – statistics (Montgomery, 2001).

Table 8.7: Variables entered/removed for each of the models where bounding energy is the dependent variable.

Model	Variables Entered	Variables Removed	Method
1	Sand		Stepwise (Criteria: Probability-of-F-to-enter \leq .050, Probability-of-F-to-remove \geq .100).
2	CEC		Stepwise (Criteria: Probability-of-F-to-enter \leq .050, Probability-of-F-to-remove \geq .100).
3	pH		Stepwise (Criteria: Probability-of-F-to-enter \leq .050, Probability-of-F-to-remove \geq .100).
4	OM		Stepwise (Criteria: Probability-of-F-to-enter \leq .050, Probability-of-F-to-remove \geq .100).
5		Sand	Stepwise (Criteria: Probability-of-F-to-enter \leq .050, Probability-of-F-to-remove \geq .100).
6	Clay		Stepwise (Criteria: Probability-of-F-to-enter \leq .050, Probability-of-F-to-remove \geq .100).

Table 8.8: ANOVA of the models with bounding energy as the dependent variable.

Model	Sum of Squares	df	Mean Square	F	Sig.
1 Regression	.566	1	.566	87.225	.000
Residual	.071	11	.006		
Total	.637	12			
2 Regression	.594	2	.297	68.961	.000
Residual	.043	10	.004		
Total	.637	12			
3 Regression	.622	3	.207	122.179	.000
Residual	.015	9	.002		
Total	.637	12			
4 Regression	.628	4	.157	138.265	.000
Residual	.009	8	.001		
Total	.637	12			
5 Regression	.624	3	.208	147.417	.000
Residual	.013	9	.001		
Total	.637	12			
6 Regression	.631	4	.158	197.943	.000
Residual	.006	8	.001		
Total	.637	12			

Table 8.9: Regression coefficients of the models when each soil variable was removed with bounding energy as the dependent variable.

Model	Unstandardized Coefficients		Standardized Coefficients	t	Sig.	Collinearity Statistics	
	B	Std. Error	Beta			Tolerance	VIF
1 (Constant)	.844	.062		13.716	.000		
Sand	-.009	.001	-.942	-9.339	.000	1.000	1.000
2 (Constant)	.611	.104		5.888	.000		
Sand	-.007	.001	-.734	-6.341	.000	.505	1.981
CEC	.014	.005	.296	2.562	.028	.505	1.981
3 (Constant)	.817	.083		9.888	.000		
Sand	-.004	.001	-.490	-5.195	.001	.299	3.342
CEC	.026	.004	.555	5.739	.000	.285	3.506
pH	-.069	.017	-.285	-4.048	.003	.538	1.859
4 (Constant)	.894	.075		11.884	.000		
Sand	-.002	.001	-.237	-1.786	.112	.101	9.915
CEC	.032	.005	.694	7.003	.000	.181	5.511
pH	-.097	.018	-.399	-5.278	.001	.311	3.214
OM	-.029	.013	-.185	-2.334	.048	.284	3.520
5 (Constant)	.929	.081		11.497	.000		
CEC	.039	.002	.849	15.840	.000	.772	1.296
pH	-.124	.012	-.509	-10.298	.000	.907	1.103
OM	-.048	.008	-.300	-5.852	.000	.843	1.186
6 (Constant)	.723	.095		7.607	.000		
CEC	.031	.003	.681	9.499	.000	.243	4.116
pH	-.099	.012	-.409	-7.951	.000	.473	2.114
OM	-.032	.008	-.205	-4.003	.004	.477	2.096
Clay	.002	.001	.240	2.820	.023	.172	5.803

Table 8.10: Regression coefficients of the excluded variables for models with bounding energy as the dependent variable.

Model	Beta In	t	Sig.	Partial Correlation	Collinearity Statistics			
					Tolerance	VIF	Minimum Tolerance	
1	pH	-.018	-0.171	0.868	-0.054	0.952	1.05	0.952
	OM	.140	0.99	0.346	0.299	0.51	1.961	0.51
	Clay	.304	0.638	0.538	0.198	0.048	21.051	0.048
	Silt	.063	0.395	0.701	0.124	0.433	2.311	0.433
	CEC	.296	2.562	0.028	0.63	0.505	1.981	0.505
	Avai. P	-.086	-0.796	0.445	-0.244	0.897	1.115	0.897
	Al ₂ O ₃	-.048	-0.248	0.809	-0.078	0.296	3.379	0.296
	Fe ₂ O ₃	.438	1.579	0.145	0.447	0.116	8.598	0.116
2	pH	-.285	-4.048	0.003	-0.803	0.538	1.859	0.285
	OM	.087	0.721	0.489	0.234	0.491	2.036	0.294
	Clay	.057	0.14	0.892	0.046	0.044	22.561	0.044
	Silt	.059	0.455	0.66	0.15	0.433	2.311	0.306
	Avai. P	.000	-0.004	0.997	-0.001	0.763	1.31	0.43
	Al ₂ O ₃	-.008	-0.05	0.961	-0.017	0.293	3.416	0.212
	Fe ₂ O ₃	.236	0.896	0.394	0.286	0.099	10.08	0.099
3	OM	-.185	-2.334	0.048	-0.636	0.284	3.52	0.101
	Clay	.108	0.419	0.686	0.146	0.044	22.618	0.043
	Silt	.020	0.242	0.815	0.085	0.426	2.347	0.231
	Avai. P	-.017	-0.274	0.791	-0.097	0.76	1.317	0.266
	Al ₂ O ₃	-.041	-0.413	0.691	-0.144	0.291	3.442	0.173
	Fe ₂ O ₃	.242	1.596	0.149	0.491	0.099	10.081	0.099
4	Clay	.375	1.97	0.089	0.597	0.036	27.606	0.021
	Silt	-.153	-2.06	0.078	-0.614	0.229	4.365	0.091
	Avai. P	-.094	-1.985	0.088	-0.6	0.581	1.72	0.083
	Al ₂ O ₃	.000	0.002	0.998	0.001	0.275	3.63	0.068
	Fe ₂ O ₃	.196	1.564	0.162	0.509	0.097	10.358	0.068
5	Clay	.240	2.82	0.023	0.706	0.172	5.803	0.172
	Silt	-.185	-2.475	0.038	-0.659	0.253	3.951	0.253
	Avai. P	-.115	-2.658	0.029	-0.685	0.706	1.416	0.571
	Al ₂ O ₃	.068	0.911	0.389	0.306	0.41	2.438	0.41
	Fe ₂ O ₃	.246	2.473	0.039	0.658	0.143	6.975	0.143
	Sand	-.237	-1.786	0.112	-0.534	0.101	9.915	0.101
6	Silt	-.095	-1.012	0.345	-0.357	0.141	7.09	0.091
	Avai. P	-.077	-1.849	0.107	-0.573	0.557	1.796	0.136
	Al ₂ O ₃	-.012	-0.173	0.867	-0.065	0.311	3.214	0.131
	Fe ₂ O ₃	.128	1.034	0.335	0.364	0.081	12.273	0.081
	Sand	.198	0.796	0.452	0.288	0.021	47.169	0.021

Table 8.11: Statistics summary of each regression model with bounding energy as the dependent variable.

Model	R	R Square	Adjusted R Square	Std. Error of the Estimate	Durbin-Watson
1	.942	.888	.878	.08053	
2	.966	.932	.919	.06562	
3	.988	.976	.968	.04118	
4	.993	.986	.979	.03369	
5	.990	.980	.973	.03757	
6	.995	.990	.985	.02822	1.703

For model development, four factors have been selected as the predictors of bounding energy (a) to build the regression equation based on Model 6 (Table 8.9):

$$a = 0.72 + 0.031 \text{ CEC} - 0.099 \text{ pH} - 0.032 \text{ OM} + 0.02 \text{ Clay content} \quad (8.1)$$

The R^2 is 0.99, that is, the variation of CEC, pH, OM, and clay content in the soils accounts for 99 % bounding energy (a) variation (Table 8.11).

8.2.2 Sorption Maximum and Soil Properties

Table 8.12 presents the stepwise multiple linear regression of the prediction model for sorption maximum (X_m). Iron oxide (Fe_2O_3) was the only variable that was found useful in predicting X_m excluding pH, OM, soil texture, CEC, available P, and Al_2O_3 with no statistically significant impact on the model with significant levels > 0.05 (Table 8.13). The model with $F > 1$ indicates that the ability to predict X_m is significantly improved (Table 8.14) by the predictor with significant level < 0.05 (Table 8.15). The VIF value (Table 8.15) not exceeding 10 suggests that the associated regression coefficient is a better estimate.

For model development, the Fe_2O_3 is the most important factor affecting X_m in the soils. Therefore, the factor is taken as the predictor of X_m (Table 8.15) to build up the regression equation:

$$X_m = 328.83 + 18.01 \text{ Fe}_2\text{O}_3 \quad (8.2)$$

The R^2 is 0.76, that is, the variation of Fe_2O_3 in the soil accounts for 76 % X_m variation (Table 8.16) and the remaining 24 % can only be attributed to other variables. Hydrous oxide of Fe and Al has been found to occur as fine coatings on the surface of clay minerals in soils. For soils from various part of the world P sorption has been related to different forms of Fe and Al which provides additional sites for sorption (Singh and Gilkes, 1992; Gilkes and Prakongkep, 2016). In this study, Fe oxide plays more superior and important role in the overall P sorption of the oxidic soils.

Table 8.12: Variables entered/removed for the model where sorption maximum (X_m) is the dependent variable.

Model	Variables Entered	Variables Removed	Method
1	Fe_2O_3		Stepwise (Criteria: Probability-of-F-to-enter $\leq .050$, Probability-of-F-to-remove $\geq .100$).

Table 8.13: Regression coefficients of the excluded variables for the model with sorption maximum (X_m) as the dependent variable.

Model		Beta In	t	Sig.	Partial Correlation	Collinearity Statistics		
						Tolerance	VIF	Minimum Tolerance
1	pH	-.162	-1.106	.295	-.330	.986	1.014	.986
	OM	-.138	-.684	.510	-.211	.553	1.809	.553
	Clay	.281	.615	.553	.191	.109	9.136	.109
	Silt	.246	1.199	.258	.355	.493	2.029	.493
	Sand	-.437	-1.017	.333	-.306	.116	8.598	.116
	CEC	-.102	-.441	.669	-.138	.431	2.321	.431
	Avai. P	.255	1.671	.126	.467	.796	1.256	.796
	Al_2O_3	-.015	-.043	.967	-.013	.197	5.079	.197

Table 8.14: ANOVA of the model with sorption maximum as the dependent variable.

Model		Sum of Squares	df	Mean Square	F	Sig.
1	Regression	305886.940	1	305886.940	35.451	.000
	Residual	94911.784	11	8628.344		
	Total	400798.724	12			

Table 8.15: Regression coefficients of the model with sorption maximum as the dependent variable.

Model		Unstandardized Coefficients		Standardized Coefficients	t	Sig.	Collinearity Statistics	
		B	Std. Error	Beta			Tolerance	VIF
1	(Constant)	323.828	34.668		9.341	.000		
	Fe ₂ O ₃	18.008	3.024	.874	5.954	.000	1.000	1.000

Table 8.16: Statistics summary of the regression model with sorption maximum as the dependent variable.

R	R Square	Adjusted R Square	Std. Error of the Estimate	Durbin-Watson
.874	.763	.742	92.88888	1.479

8.2.3 Maximum Buffering Capacity, External Phosphorus Requirements, and Soil Properties

Out of all the variables entered, only sand content and Fe₂O₃ are useful in predicting the maximum buffering capacity (aXm) and external phosphorus requirements (EPR) (Table 8.17) whereas, pH, OM, clay content, silt content, CEC, avai. P, and Al₂O₃ were excluded since the significant level > 0.05 suggest that they will not contribute significantly to the models abilities to predict aXm and EPR respectively (Table 8.18). The VIF < 10 suggest no problem with respect to independence of errors and multicollinearity (Montgomery, 2001) (Table 8.19). The unstandardised and standardised coefficients indicate the greater contribution of Fe₂O₃ relative to sand

content as predictor in the models with Fe_2O_3 having positive coefficient and sand content with negative coefficient (Table 8.19). This suggests that Fe_2O_3 is the most important factor for the aXm and EPR in the oxidic soils.

Table 8.17: Variables entered/removed for the models where aXm and EPR are the dependent variables.

Model	Variables Entered	Variables Removed	Method
1	Sand		Stepwise (Criteria: Probability-of-F-to-enter <= .050, Probability-of-F-to-remove >= .100).
2	Fe_2O_3		Stepwise (Criteria: Probability-of-F-to-enter <= .050, Probability-of-F-to-remove >= .100).

Table 8.18a: Regression coefficients of the excluded variables for the models with aXm as the dependent variable.

Model	Beta In	t	Sig.	Partial Correlation	Collinearity Statistics			
					Tolerance	VIF	Minimum Tolerance	
1	pH	-.007	-.076	.941	-.024	.952	1.050	.952
	OM	.025	.212	.837	.067	.510	1.961	.510
	Clay	.270	.712	.493	.220	.048	21.051	.048
	Silt	.091	.729	.483	.225	.433	2.311	.433
	CEC	.183	1.751	.110	.484	.505	1.981	.505
	Avai. P	-.039	-.439	.670	-.137	.897	1.115	.897
	Al_2O_3	.016	.105	.919	.033	.296	3.379	.296
	Fe_2O_3	.481	2.448	.034	.612	.116	8.598	.116
2	pH	-.054	-.737	.480	-.239	.889	1.125	.105
	OM	.035	.359	.728	.119	.509	1.965	.107
	Clay	.005	.015	.989	.005	.042	24.046	.042
	Silt	.087	.840	.422	.270	.433	2.312	.102
	CEC	.110	1.092	.303	.342	.431	2.322	.099
	Avai. P	.053	.643	.537	.209	.704	1.421	.091
	Al_2O_3	-.238	-1.723	.119	-.498	.197	5.082	.077

Table 8.18b: Regression coefficients of the excluded variables for the models with EPR as the dependent variable.

Model	Beta In	t	Sig.	Partial Correlation	Collinearity Statistics			
					Tolerance	VIF	Minimum Tolerance	
1	pH	-.005	-.053	.959	-.017	.952	1.050	.952
	OM	.013	.104	.919	.033	.510	1.961	.510
	Clay	.264	.681	.511	.210	.048	21.051	.048
	Silt	.095	.744	.474	.229	.433	2.311	.433
	CEC	.178	1.655	.129	.464	.505	1.981	.505
	Avai. P	-.038	-.419	.684	-.131	.897	1.115	.897
	Al ₂ O ₃	.023	.143	.889	.045	.296	3.379	.296
	Fe ₂ O ₃	.495	2.485	.032	.618	.116	8.598	.116
2	pH	-.053	-.716	.492	-.232	.889	1.125	.105
	OM	.023	.230	.823	.077	.509	1.965	.107
	Clay	-.011	-.031	.976	-.010	.042	24.046	.042
	Silt	.090	.864	.410	.277	.433	2.312	.102
	CEC	.102	.986	.350	.312	.431	2.322	.099
	Avai. P	.057	.687	.509	.223	.704	1.421	.091
	Al ₂ O ₃	-.236	-1.675	.128	-.488	.197	5.082	.077

Table 8.19a: Regression coefficients of the models with aXm as the dependent variable.

Model		Unstandardized Coefficients		Standardized Coefficients	t	Sig.	Collinearity Statistics	
		B	Std. Error	Beta			Tolerance	VIF
1	(Constant)	651.722	42.795		15.229	.000		
	Sand	-7.579	.635	-.963	-11.930	.000	1.000	1.000
2	(Constant)	345.308	130.114		2.654	.024		
	Sand	-4.024	1.545	-.512	-2.604	.026	.116	8.598
	Fe ₂ O ₃	10.856	4.435	.481	2.448	.034	.116	8.598

Table 8.19b: Regression coefficients of the models with EPR as the dependent variable.

Model		Unstandardized Coefficients		Standardized Coefficients	t	Sig.	Collinearity Statistics	
		B	Std. Error	Beta			Tolerance	VIF
1	(Constant)	113.622	7.530		15.090	.000		
	Sand	-1.304	.112	-.962	-11.670	.000	1.000	1.000
2	(Constant)	59.198	22.762		2.601	.026		
	Sand	-.673	.270	-.496	-2.490	.032	.116	8.598
	Fe ₂ O ₃	1.928	.776	.495	2.485	.032	.116	8.598

For model development, two factors (Fe₂O₃ and sand content) from model 2 (Table 8.19) have been considered as the predictors of aX_m and EPR to build up regression equations:

$$aX_m = 345.31 - 4.02 \text{ Sand content} + 10 \text{ Fe}_2\text{O}_3 \quad (8.3)$$

$$\text{EPR} = 59.20 - 0.67 \text{ Sand content} + 1.93 \text{ Fe}_2\text{O}_3 \quad (8.4)$$

The R² values are 0.96 and 0.95 (Table 8.20) for Eqns. 8.5 and 8.6 respectively. These imply that the variations of Fe₂O₃ and sand contents in the soils account for 96 % aX_m and 95 % EPR variations respectively.

 Table 8.20a: Statistics summary of the regression model with aX_m as the dependent variable.

Model	R	R Square	Adjusted R Square	Std. Error of the Estimate	Durbin-Watson
1	.963	.928	.922	56.00674	
2	.977	.955	.946	46.45035	1.841

Table 8.20b: Statistics summary of the regression model with EPR as the dependent variable.

Model	R	R Square	Adjusted R Square	Std. Error of the Estimate	Durbin-Watson
1	.962	.925	.918	9.85426	
2	.977	.954	.945	8.12605	1.801

8.3 Concluding Remarks

Based on the soil properties, the following deductions have been made:

- a. The pH of the soils were moderately acidic to moderately alkaline with soluble salt concentrations not sufficient to seriously interfere with the growth of most plants.
- b. The order of prevalence of exchangeable cations (Ca, Mg, K, and Na) in the soils is favourable for crop production except for exchangeable K which is lower than the critical value.
- c. The soil texture played a major role on the soil OM, exchangeable Al, and CEC dynamics.
- d. Soil fertility index (SFI) and soil evaluation factor (SEF) varied from 9.73 and 6.40 in soils developed from basalt to 67.24 and 67.18 in soils developed from arkosic sandstone, respectively. This suggests a better soil quality. SFI and SEF had significant correlations with soil properties such as available P, clay content, pH, and CEC.
- e. From the various model equations developed between P sorption and soil properties, the critical soil variables explaining the variations in the P sorption and buffering capacity of the soils were CEC, pH, OM, sand and clay contents, and Fe₂O₃. However, Fe oxide played the most important role in the soil P sorption dynamics.

Chapter Nine

Kaolins in Oxidic Soils Developed from different Parent Rocks in Limpopo Province, South Africa: Influence on Some Soil Fertility Parameters

9.0 Background

Factors limiting crop yield in South Africa are attributed to prolonged drought, longer dry spells, limited water and nutrient availability, degraded soils and inefficient farming practices (Myeni *et al.*, 2019). In previous chapters, the mineralogical, geochemical, and P adsorption characteristics of the soils and soil kaolins have been discussed. In chapter eight, the influence of the soil properties on the soil fertility and P adsorption was examined. However, it is important to investigate the nature of relationship between the soil kaolins and soil properties with major soil fertility implications. Clay mineralogy – soil fertility relationship is an important component in understanding and managing soil fertility for sustaining crop production (Mandiringana *et al.*, 2005; Abe *et al.*, 2006). To make visible links that exist between the soil kaolins and soil fertility, linear correlation coefficients (r) and principal component analysis (PCA) between the % kaolinite and nutrient supply and availability, organic matter, physico-chemical properties, SFI, SEF, and EPR are established and discussed (Tables 9.1, 9.2, and Figs. 9.1 – 9.4).

9.1 Influence of soil kaolins on some soil fertility parameters

Through the weathering of primary minerals such as plagioclase, microcline, and muscovite in the soil kaolins, plant nutrients are released into the soil solution. This indicated that these weatherable primary minerals will act as an important reservoir for elements such as K, Ca, Mg, Fe, Na, and Si (Blanco-Canqui and Lal, 2008) on a long-term especially in the young soils with low CIA. The presence of oxides and hydroxides of Fe and Al such as hematite, goethite, gibbsite in addition to kaolinite have major influence on the adsorption and precipitation processes in the soil. These minerals possess high specific surface area which provides adsorption sites for both cationic and

anionic elements in the soils (Kome *et al.*, 2019). Goethite and hematite present in the soil kaolins developed from basalt are known to have substantial structural substitution for trace elements including Mn, Ni, Zn, and Cu (Singh and Sculze, 2015). The exchangeable cations in the soils showed positive correlation ($r= 0.185 - 0.965$) (Fig. 9.1) with the % kaolinite except for K ($r= -0.107$) (Fig. 9.1) (Table 9.1).

This implies increase in the exchangeable Ca, Mg, Na, and Al and decrease in K with increase in the kaolinite content as weathering progresses ($r= 0.749$) (Fig. 9.2). The increase in CEC as the kaolinite content increases ($r= 0.856$) (Fig. 9.2) suggest that the ability of the soils to hold positively charged ions is directly linked to the % kaolinite in them. Isomorphous substitutions within the crystal lattice give rise to the negative charges on the surfaces of kaolin crystals and contribute to the CEC. It is well known that the negative charge caused by substitutions for Si and Al by Fe within the lattice structure of kaolins is pH dependent (Churchman and Lowe, 2012). Higher pH values give rise to more negative charges (Ma and Eggleton, 1999). Therefore, more incorporation of Fe in the soil kaolinite structure at higher pH leads to a higher CEC value relative to theoretical kaolinite. The microchemical result from SEM-EDX showed that Fe was present in the soil kaolinite octahedral sites.

Soils with high CEC generally have greater water holding capacity than the ones with low CEC (CUCE, 2007). The ability of the soils to retain the water received from rainfall or irrigation and then release this water to plants in response to the demands of the growing plant will increase with % kaolinite present in them (Gilkes and Prakongkep, 2016). Hence, the oxidic soils developed from basalt with more kaolinite content will be less sensitive to drought conditions and water will be used efficiently.

An assessment of the overall relationship of the % kaolinite with soil fertility with respect to SFI and SEF showed that, the soil fertility decreases with increase in the % kaolinite content ($r= -0.505$ and -0.064) (Table 9.1 and Fig. 9.2). This is consistent with earlier submission by Juo and Franzluebbbers (2003) that kaolinitic soils usually have low nutrient reserve, and high phosphate fixation capacity causing serious major agronomic constraints. Hence, large quantities of external inputs, including chemical fertilisers and lime, are needed to promote and sustain optimum crop yield (Juo and Franzluebbbers, 2003).

Table 9.1: Pearson correlation matrix for linear relationships between % kaolinite and some soil properties for Oxidic Soils developed from different parent rocks in Limpopo Province, South Africa

	pH	CEC	Ca	K	Mg	Na	Al	OM	%Kaolinite	Al ₂ O ₃	Fe ₂ O ₃	CIA	SFI	SEF	EPR
pH	1.000														
CEC	.295	1.000													
Ca	.877	.638	1.000												
K	.612	.248	.539	1.000											
Mg	.653	.596	.783	.091	1.000										
Na	.295	.816	.556	-.159	.669	1.000									
Al	-.063	.880	.266	.122	.225	.681	1.000								
OM	.030	-.204	.113	.263	.014	-.511	-.431	1.000							
%Kaolinite	-.182	.856	.185	-.107	.241	.731	.965	-.415	1.000						
Al₂O₃	.083	.800	.358	.002	.375	.700	.887	-.487	.878	1.000					
Fe₂O₃	-.003	.875	.318	-.137	.385	.884	.921	-.556	.958	.878	1.000				
CIA	-.368	.545	-.050	-.330	-.069	.627	.653	-.385	.749	.423	.756	1.000			
SFI	.134	-.464	-.276	.269	-.137	-.525	-.393	-.087	-.505	-.350	-.510	-.698	1.000		
SEF	.801	.436	.904	.598	.738	.250	.019	.484	-.064	.080	.000	-.303	-.145	1.000	
EPR	-.152	.807	.166	-.188	.218	.810	.923	-.584	.967	.834	.983	.831	-.514	-.154	1.000

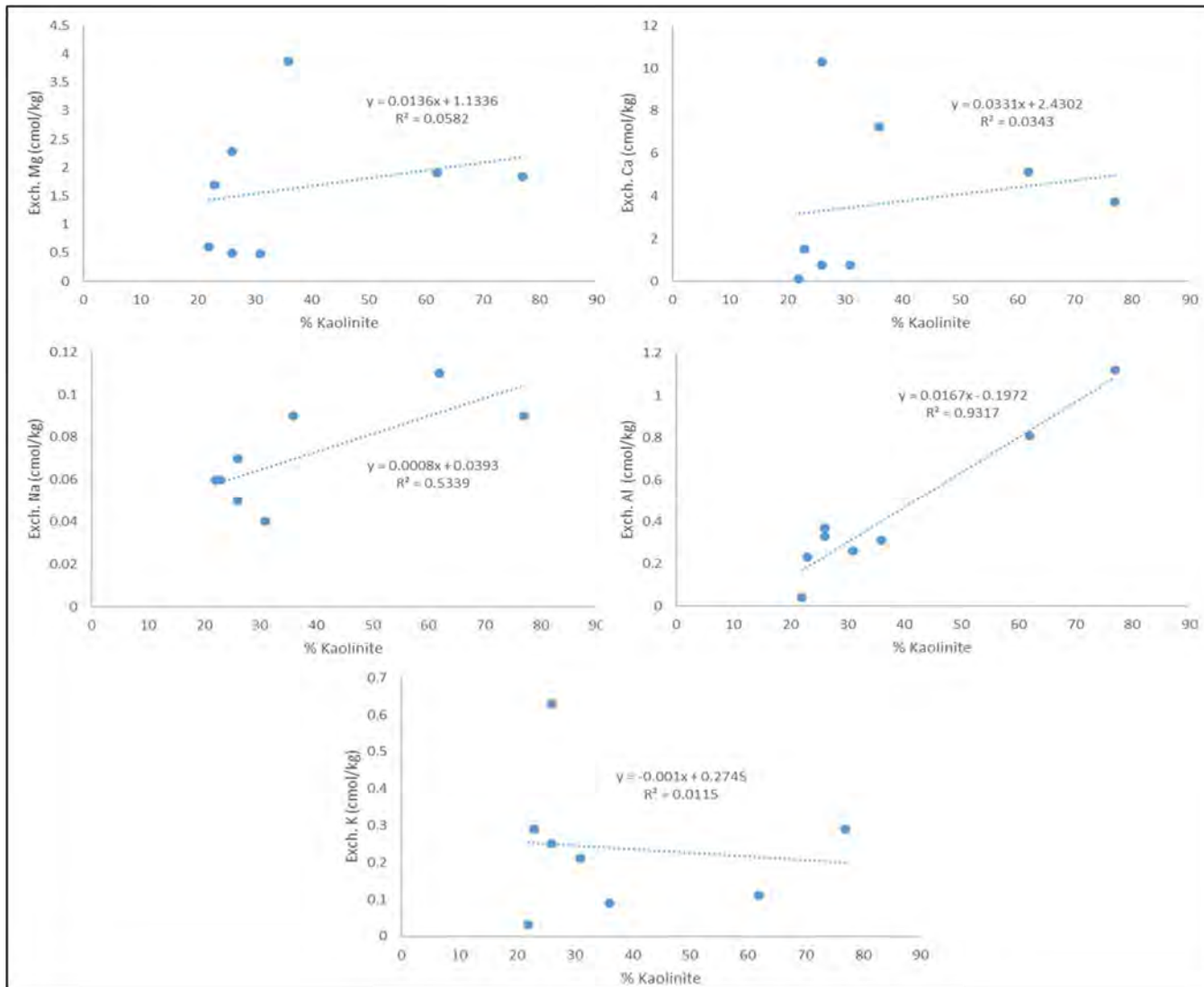


Figure 9.1: Binary diagram showing relationship between % kaolinite, exch. Mg, Ca, Na, Al, and K.

Organic matter is both a source and a sink of plant nutrients (Kome *et al.*, 2019). The type and quantity of clay minerals in soils determine the retention of the organic C and N added to the soils (Christensen, 1992; Cheshire *et al.*, 2000). The organic matter content correlated negatively with the kaolinite content ($r = -0.415$) as well as Fe_2O_3 ($r = -0.556$) and Al_2O_3 ($r = -0.487$) (Table 9.1 and Fig. 9.2) in the soils.

This accounted for the small amounts of organic matter in soils developed from basalt. Several studies have corroborated that Fe and/or Al oxides have larger influence on the retention of organic matter in soils than kaolinite (Jindaluang *et al.*, 2010; Kaiser *et al.*, 2002). However, other factors such as temperature and moisture could play a critical role in the organic matter dynamics in the soils (Singh *et al.*, 2017).

Juo and Franzluebbbers (2003) and FAO (2017) suggested that the amount of organic input in kaolinitic soils can be maximised by multiple cropping, cover crops, green manure, and planted fallow. Hence, the use of minimum tillage for seedbed preparation and weed control, return of crop residues to the soil as a mulch, and use of composts, manures, household and municipal wastes are recommended.

Soil properties such as texture, structure, moisture content, pore size distribution, plasticity, shrink-swell potential, soil strength and erodibility affect every aspect of soil fertility and productivity (Osman, 2013). Soil erodibility is lower in soils with more kaolinite (non-expansive clay) relative to those with montmorillonite (expansive clay) which are more susceptible to surface soil loss (Schulten and Leinweber, 2000). Hence, the soils developed from gneiss with montmorillonite will be more susceptible to erosion, leading to the reduction in topsoil thickness.

The soil pH influences the soil health. The soil pH showed negative correlation with the kaolinite content ($r = -0.182$) (Fig. 9.3). Therefore, the soil becomes more acidic with increase in the kaolinite content. At lower pH (<5.5), aluminosilicate clays such as kaolinite and Al hydroxide minerals begin to dissolve hereby releasing Al^{3+} into the soil solution which could cause Al toxicity (McBride, 1994). This phenomenon accounted for the highest exchangeable Al in the soils developed from basalt relative to others. This as well causes the unavailability of phosphorus for plant uptake (Eqn. 9.1) (Hopkins, 2015).

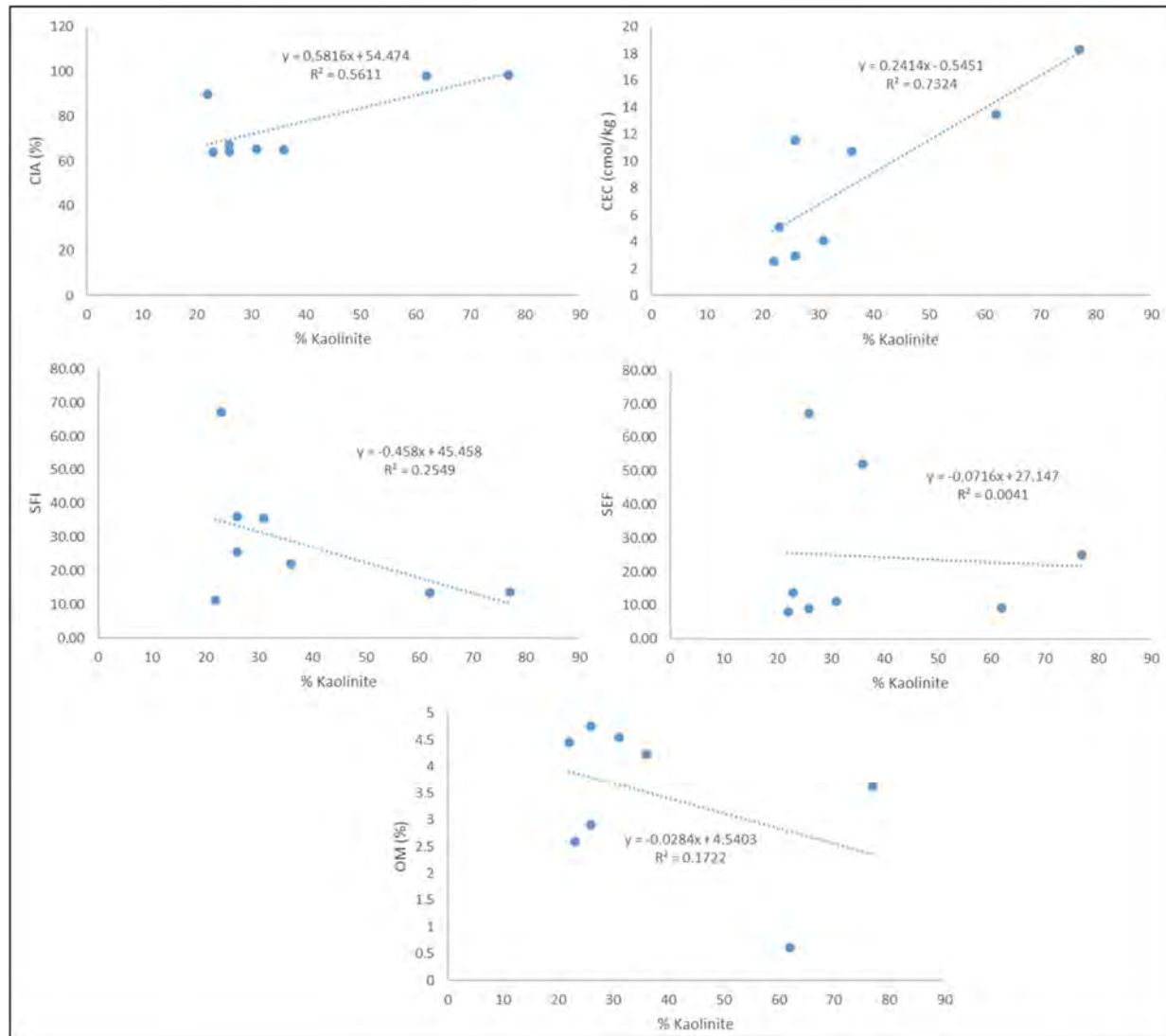
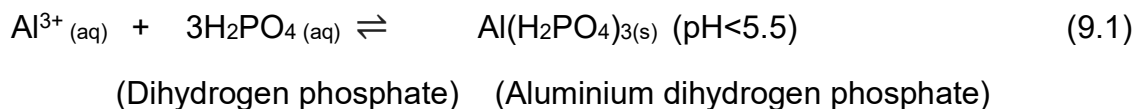
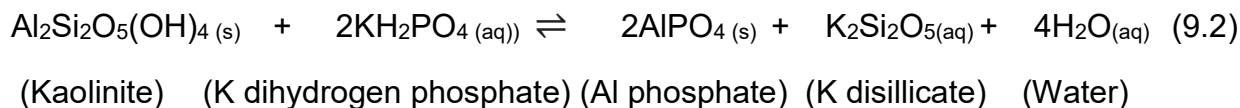


Figure 9.2: Binary diagram showing relationship between % kaolinite, CIA, CEC, SFI, SEF, and OM.



In addition, Al originating from kaolinite with exposed Al-OH group react very fast with the phosphate in the soils as shown in eqn. 9.2 (Bohn *et al.*, 2001).



These explained the strong positive correlation between kaolinite content and the EPR ($r = 0.967$) (Fig. 9.3) as well as negative correlation with pH. Hence, soils with higher kaolinite content requires larger amount of fertiliser with low available phosphorus.

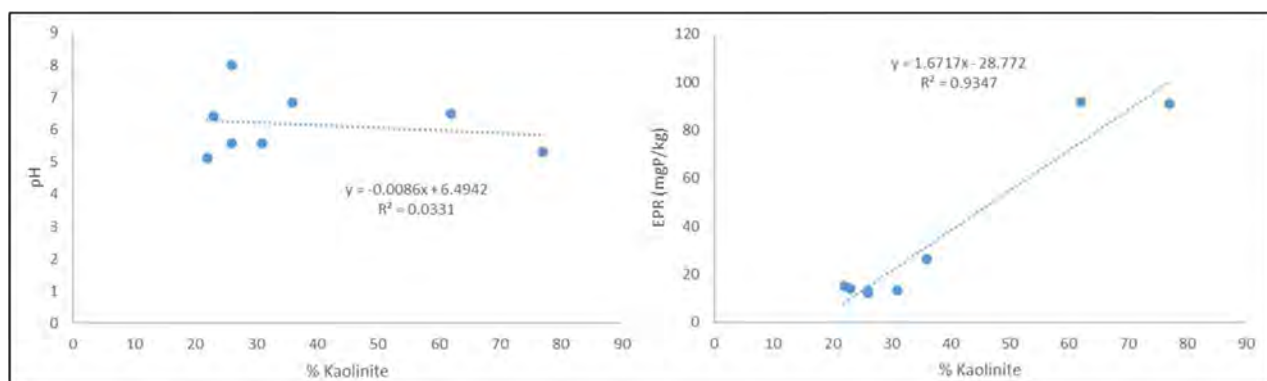


Figure 9.3: Binary diagram showing relationship between % kaolinite, pH, and EPR.

The principal component analysis from the Scree plot (Fig. 9.4) showed that three factors explained 86.70 % of the variation in the data for the soil properties (Table 9.2). The calculated factors 1, 2, and 3 explained 50.42, 27.34, and 8.94 % respectively, of the variance. Factor 1 shows significant positive factor loadings (Table 9.2, bold numbers indicate significant factor loadings > 0.500) with % kaolinite, Fe₂O₃, EPR, exch. Al, Na, CEC, Al₂O₃, CIA, and negative factor loading with OM. Factor 2 has positive factor loadings with SEF, Ca, pH, Mg, and K. Factor 3 has positive factor loading with CIA and

negative factor loading with SFI only. Factor 1 which accounts for the highest variance represents the weathering factor which invariably determines the % kaolinite in the soils whereas, factor 2 shows that SEF depends on Ca, pH, Mg, and K in the soils. However, the inverse relationship between CIA and SFI indicates that degree of weathering plays a role in the overall soil fertility status of the soils.

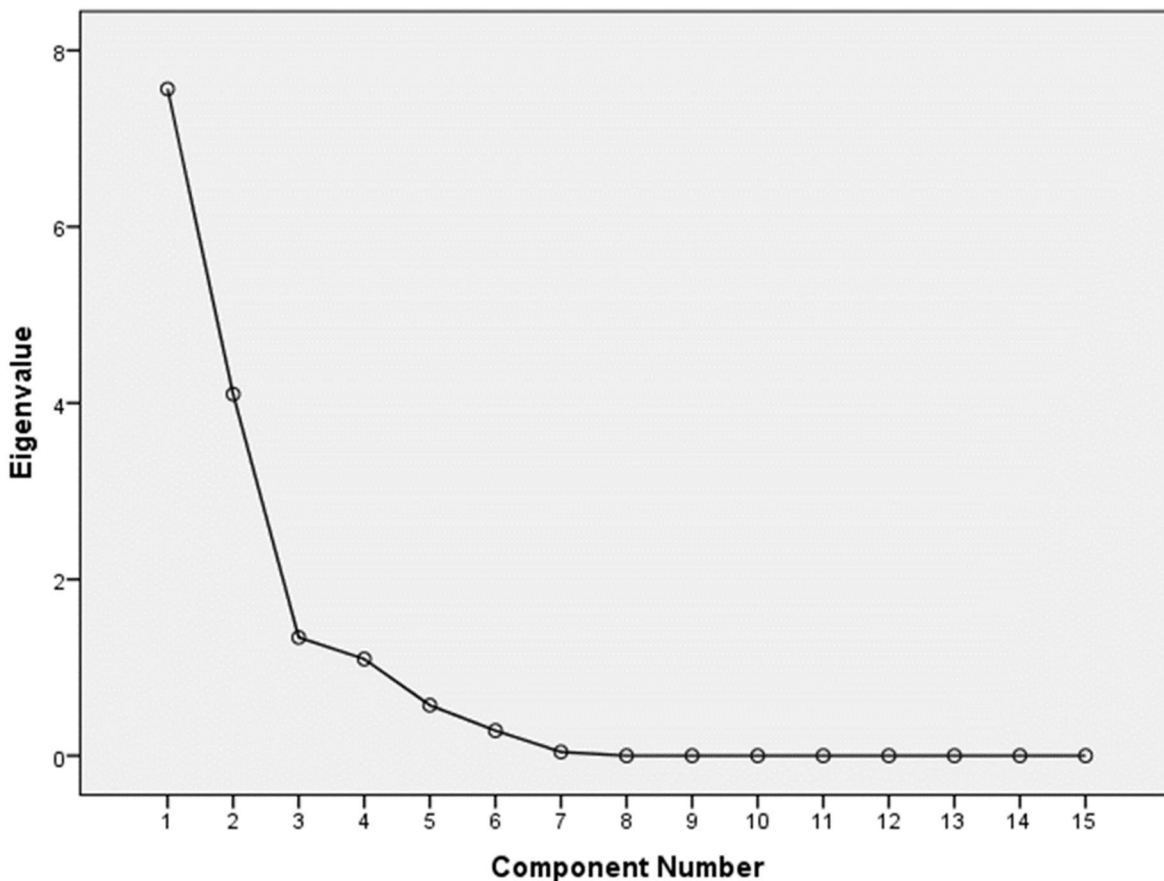


Figure 9.4: PCA Scree plot of % kaolinite and some soil properties.

Table 9.2: Factor loadings obtained from Principal Component Analysis of % kaolinite and some soil properties.

	Factors		
	1	2	3
Fe ₂ O ₃	.970	.039	.204
EPR	.967	-.122	.219
% Kaolinite	.963	-.020	.193
Al	.956	.082	.077
Al ₂ O ₃	.884	.170	.005
CEC	.853	.470	.197
Na	.781	.255	.296
CIA	.685	-.366	.558
OM	-.584	.407	.282
SEF	-.072	.983	.160
Ca	.224	.899	.200
pH	-.051	.821	-.127
Mg	.304	.768	.019
K	-.051	.634	-.253
SFI	-.325	-.026	-.937
Eigenvalues	7.46	4.10	1.24
Cumulative Variance (%)	50.42	77.76	86.70

9.2 Concluding Remarks

The influence of soil kaolins on the soil fertility through its direct impacts on soil physical and chemical properties have been demonstrated. The following deductions have been made:

- The mineralogical status of the soil kaolins suggest that some of the weatherable minerals could supply K, Ca, Mg, Fe, Na, and Si particularly on long-term basis.
- The % kaolinite showed positive correlation with CEC, exch. Ca, Mg, Na, Al, CIA, and EPR and negative correlation with K, pH, OM, SFI, and SEF with various degree of agronomic implications.
- The various statistical relationships showed that the degree of weathering which determines the % kaolinite in the soils indirectly determines the soil fertility status

of the soils. As such, the soil fertility decreases with increase in the degree of weathering.

- d. For sustainable agricultural management of the soils, careful conservative tillage, mulching, and use of fertilisers are required.

Chapter Ten

Conclusions and Recommendations

10.1 Conclusions

This study examined the mineralogy, geochemistry, phosphorus adsorption (Chapters five, six, and seven), and fertility implications of oxidic soils and soil kaolins developed from different parent rocks in Limpopo Province, South Africa (Chapters eight and nine). To achieve these objectives, the physico-chemical, mineralogical, geochemical, and phosphorus adsorption characteristics of the soils and soil kaolins were determined using latest available techniques. The results were interpreted to arrive at the following important conclusions:

1. Kaolinite dominated minerals in soils developed from basalt whereas, quartz was dominant mineral in soils developed from arkosic sandstone and quartzite (control). Plagioclase dominated the minerals present in soils developed from granite and gneiss. The studied soils had undergone low to high degree of chemical weathering. The compositional changes accompanying the chemical weathering of the primary minerals present in the parent rocks were evident with the enrichment of Fe_2O_3 and TiO_2 in all the soils. Trace elements were accumulated in soils developed from basalt and gneiss (except for Rb, Sr, and Ba in soils developed from basalt) but depleted in soils developed from granite, arkosic sandstone, and quartzite (except Cr and Ta) due to little or no lithogenic release by weathering processes. The overall mineralogical and geochemical characteristics of the soils were influenced by the characteristics of the parent rocks and intensity of weathering.
2. Kaolinite dominated the clay minerals present in the soil kaolins. The kaolinites were formed through the leaching and desilication of the primary mafic and felsic minerals. The presence of greater percentage of weatherable minerals in the soil kaolins developed from granite, arkosic sandstone, gneiss, and quartzite could

be attributed to the low degree of chemical weathering relative to soil kaolins developed from basalt. The appreciable amounts of trace elements in the soil kaolins suggest the likely role for kaolins to serve as host for minor elements as structural ions which has significant implications on soil fertility. The soil kaolinites were characterised by platy morphology with partial to poor structural order. Relative to reference kaolinites, the studied soil kaolinites have smaller sizes, lower dehydroxylation temperatures, and higher CEC and Fe_2O_3 .

3. The soils and soil kaolins were characterised by H-type P adsorption with linear Langmuir and Freundlich isotherms. The Langmuir model provided a suitable description of P adsorption dynamics in the soils and soil kaolins. Phosphorus adsorption in the soils and soil kaolins was by chemisorption. Sorption maximum was highest in soils and soil kaolins developed from basalt and lowest in soils developed from gneiss and soil kaolins developed from arkosic sandstone. Hence, soils developed from basalt will require higher P fertilisation. The external P requirements obtained for the soils suggested that the application of blanket P fertiliser could pose threat to water quality in the region. The results further showed that P sorption of the soil kaolins could successfully be used to predict the P sorption dynamics of the soils in the area.
4. The pH and EC of the soils were within most plant growth requirements. The soil fertility status indicated a better quality with significant relationship with soil properties such as available P, clay content, pH, and EC. The CEC of the soils were generally low (except for soils developed from basalt with medium status). The order of prevalence of exchangeable cations (Ca, Mg, K, and Na) was favourable for crop production except for K in soils developed from arkosic sandstone. The soil fertility based on SFI was highest in soils developed from arkosic sandstone, followed by granite, gneiss, basalt, and quartzite, respectively. The P sorption dynamics of the soils were closely related to CEC, pH, OM, sand and clay contents, and Fe_2O_3 . Stepwise regression models

indicated that 95 % and 96 % of the variability in the maximum buffering capacity and external P requirements, respectively could be explained by a combination of Fe_2O_3 and sand contents. However, Fe_2O_3 is the most important parameter in predicting the P sorption dynamics in the soils. In addition, kaolinite content appears to be one of the most important indicators of soil quality.

The study has contributed to the body of knowledge in Applied Clay Mineralogy and Soil Fertility Management in the following ways:

1. Kaolins in soils

- Novel understanding of the characteristics of kaolins in oxidic soils developed from different parent rocks in Limpopo Province where such studies have not been carried out.
- The genesis of the soil kaolins were better unraveled to be related to leaching and desilication processes.
- Differences between the properties of soil kaolins in the region and reference kaolins have been established.

2. Soil Mineralogy

- Valid mineralogical and geochemical data contributed to better understanding of the influence of parent rock characteristics and the degree of weathering on the overall mineralogical and geochemical characteristics of the soils.

3. Soil fertility management

- The understanding on the overall fertility status of oxidic soils developed from different parent rocks has been advanced.
- External P requirements based on the contrasting P fixing capacities of the soils have been reported which will greatly promote increase in agricultural production without compromising water quality in the region. The findings will provide guidance to policy makers on setting baselines for P fertiliser applications.

- Based on statistical analyses, the P sorption properties of the whole soils can be deduced from information on sorption properties of kaolins present in them.
- Models have been postulated to estimate P sorption parameters for the soils in the area, thereby reducing the need for elaborate P isotherm studies.
- Proper knowledge on kaolins in oxidic soils has practical implications on soil fertility management.

10.2 Recommendations

The following are recommendations for further actions:

1. It is recommended that careful conservative tillage could be promoted to increase the soil organic matter, particularly in soils developed from basalt. This will also effectively improve the CEC in the soils. However, future studies must focus on sustainable approaches to effectively enhance the soil organic matter and CEC with respect to their parent rocks.
2. The use of site-specific P fertiliser application management strategy is needed to minimise underfertilisation and overfertilisation problems.
3. Considering the remarkable differences in soil kaolin properties, there is a need to further evaluate the properties of kaolins in other major soil groups where it is the dominant clay mineral in South Africa. This is important since it has the potential to influence the overall soil properties.
4. Phosphorus sorption association with the crystalline and non-crystalline iron oxides in the soils should be carried out.
5. To validate the efficacy of the models, it would be important for studies under field conditions to be conducted. This will greatly help to correlate the model estimates with the actual field P sorption parameters under cropped conditions.

REFERENCES

- Abe, S.S., Masunaga, T., Yamamoto, S., Honna, T. and Wakatsuki, T. (2006). Comprehensive Assessment of the Clay Mineralogical Composition of Lowland Soils in West Africa. *J. Soil Sci. Plant Nutr.*, 52, 479-488.
- Agricultural Research Council – Institute for Soil, Climate and Water (ARC–ISCW) (2006). Land types and soil inventory databases of South Africa. Pretoria: ARC – ISCW.
- Alloway B.J. (1995). Heavy Metals in Soils. 2nd edition, Blackie Academic and Professional, Chapman & Hall, London. 368 pages.
- Amrani, M., Westfall, D.G., and Moughli, L. (1999). Improving the soil test phosphorus calibration for calcareous soils. *Commun. Soil Sci. Plant Anal.* 30: 129–144.
- Arslan, M., Kadir, S., Abdioglu, E., and Kolayli, H. (2006). Origin and formation of kaolin minerals in saprolite of Tertiary alkaline volcanic rocks, Eastern Pontides, NE Turkey. *Clay Miner.* 41, 597-617.
- Ayawei, N., Ebelegi, A.N., and Wankasi, D. (2017). Modelling and Interpretation of Adsorption Isotherms. *J. Chem.*, Article ID 3039817, 11 pages.
- Ayres, M. and Harris, N. (1997). REE fractionation and Nd-isotope disequilibrium during crustal anatexis: constraints from Himalayan leucogranites. *Chem. Geol.* 139 (1–4), 249–269.
- Azlan, A., Aweng, E.R., Ibrahim, C.O., and Noorhaidah, A. (2012). Correlation between Soil Organic Matter, Total Organic Matter and Water Content with Climate and Depths of Soil at Different Land use in Kelantan, *Malaysia. J. Appl. Sci. Environ. Manage.* 16 (4): 353-358.
- Bainbridge, S. H., Miles, N., Praan, R., and Johnston, M. A. (1995). Phosphorus sorption in Natal soils; *S. Afr. J. Plant & Soil*; 12(2):59–64.
- Bam, E.K., Akiti, T.T., Osaе, S.D., Ganyaglo, S.Y., and Gibrilla, A. (2011). Multivariate cluster analysis of some major and trace elements distribution in an unsaturated zone profile, Densu river basin, Ghana. *Afr. J. Environ. Sci. Technol.* 5(3), pp. 155-167.

- Barker, O.B., Brandl, G., Callaghan, C.C., Eriksson, P.G., and Van der Neut, M. (2006). The Soutpansberg and Waterberg Groups and the Blouberg Formation. In: Johnson, M.R., Anhaeusser, C.R., and Thomas, R.J., eds., *The Geology of South Africa: Johannesburg, Geological Society of South Africa and Pretoria, Council for Geoscience*, p. 301-318.
- Barton Jr., J.M., Doig, R., Smith, B.C., Bohlender, F. and van Reenen, D.D. (1992). Isotopic and REE characteristics of the intrusive charnoenderbite and enderbite geographically associated with the Matok Pluton, Limpopo Belt, Southern Africa. *Precambrian Res.*, 55, 451-467.
- Bird, M.I. and Chivas, A.R. (1988). Stable isotope evidence for low temperature kaolinite weathering and post-formational hydrogen isotope exchange in Permian kaolinite. *Chem. Geol.* 72, 249–265.
- Bish, D.L. and Post, J.E. (1993). Quantitative mineralogical analysis using the Rietveld full-pattern fitting method. *Am. Miner.*, 78, 932-940.
- Blanco-Canqui, H. and Lal, R. (2008). *Principles of Soil Conservation and Management*. Springer, Berlin, 564 pages.
- Bohn, H., McNeal, B. and O'Connor, G. (2001). *Soil Chemistry*. 3rd Edition, Wiley Inter-Science, New York, 206-259.
- Bolland, M. D., Allen, D. G., and Barrow, N. J. (2003). Sorption of phosphorus by soils: how it is measured in Western Australia. Department of Agriculture and Food, Western Australia, Perth. Bulletin 4591.
- Brady, N.C., and Weil, R.R. (1999). *The Nature and Properties of Soils*. Twelfth ed. Prentice Hall., Upper Saddle River, NJ, 881 pp.
- Brandl, G., (1981). The geology of the Messina area, Explanation of Sheet 2230, Geological Survey of South Africa, 35 p.
- Brandl, G. (1999). Soutpansberg Group. Catalogue of South African Lithostratigraphic Units, SA Committee for Stratigraphy, Council of Geoscience, pp. 6-39 – 6-41.
- Brenner, J., Porter, W., Phillips, J. R., Childs J., Yang, X., Mayes, M. A. (2018). Phosphorus sorption on tropical soils with relevance to Earth system model needs. *Soil Res.* 57, 17-27.

- Buhmann, D. (1988). An occurrence of authigenetic nacrite. *Clays Clay Miner.*, 36:137-140.
- Buhmann, C. (1994). Parent material and pedogenic processes in South Africa. *Clay Miner.*, 29, 239-246.
- Bühmann, C., Escott, B.J., and Hughes, J.C. (2004). Soil mineralogy research in South Africa, 1978 to 2002 - a review, *S. Afr. J. Plant & Soil*, 21:5, 316-329.
- Bulska, E. and Ruszczyńska, A. (2017). Analytical techniques for trace element determination. *Phys. Sci. Rev*, 2 (5). 14 pages.
- Buol, S.W., Southard, R.J., Graham, R.C., and McDaniel, P. A. (2011). Soil Genesis and Classification. Wiley-Blackwell Publishers, 6th Edition. 543 pages.
- Caspari, T., Bäumler, R., Norbu, C., Tshering, K., and Baillie, I. (2006). Geochemical investigation of soils developed in different lithologies in Bhutan, Eastern Himalayas. *Geoderma* 136: 436-458.
- Chen, P.Y., Wang, M.K., and Yang, D.S. (2001). Mineralogy of dickite and nacrite from Northern Taiwan. *Clays Clay Miner.*, 49 (6), 586-595.
- Chen, P.Y., Wang, M.K., Yang, D.S., and Chang, S.S. (2004). Kaolin minerals from Chinmen Island (Quemoy). *Clays and Clay Minerals* 52, 130–137.
- Cheney, E.S., Barton, J.M., and Brandl, G. (1990). Extent and age of the Soutpansberg sequence of South Africa. *S Afr J Geol.*, 93(4): 664–675.
- Cheshire, M.V., Dumat, C., Fraser, A.R., Hiller, S. and Staunton, S. (2000) The Interaction between Soil Organic Matter and Soil Clay Minerals by Selective Removal and Controlled Addition of Organic Matter. *Eur. J. Soil Sci.*, 51, 497-509.
- Chittleborough, D.J. and Walker, P.H. (1988). Crystallinity of soil kaolinites in relation to clay particle-size and soil age. *J. Soil Sci.* 39, 81–86.
- Chorover, J. and Sposito, G. (1995). Surface charge characteristics of kaolinitic tropical soils. *Geochim. et Cosmochim. Acta*, 59 (5), 875-884.
- Christensen, B.T. (1992). Physical Fractionation of Soil and Organic Matter in Primary Particle Size and Density Separates. In: Stewart, B.A., Eds., *Advances in Soil Science*. *Adv. Soil Sci.*, 20, Springer, New York, 1-90.

- Churchman, G.J. (1990). Relevance of different intercalation tests for distinguishing halloysite from kaolinite in soils. *Clays Clay Miner.* 38: 591-599.
- Churchman, G.J. and Gilkes, R.J. (1989). Recognition of intermediates in the possible transformation of halloysites to kaolinites in weathering profiles. *Clay Miner.*, 24, 579-590.
- Churchman, G.J. and Lowe, D.J. (2012). Alteration, formation, and occurrence of minerals in soils. In: Huang, P.M., Li, Y., Summer, M.E. (editors) "Handbook of Soil Sciences. 2nd edition, vol. 1: Properties and Processes". CRC Press (Taylor and Francis), Boca Raton, FL., 20.1 – 20.72.
- Churchman, G.J., Pontifex, I.R., and McClure, S.G. (2010). Factors influencing the formation and characteristics of halloysites or kaolinites in granitic and tuffaceous saprolites in Hong Kong. *Clays Clay Miner.* 58: 122-139.
- Condie, K.C., Boryta, M.D., Liu, J., Quian, X. (1992). The origin of Khondalites: geochemical evidence from the archean to Early Proterozoic granulitic belt in the North China craton: *Precambrian Res.*, 59(3-4), 207-223.
- Conradie, D.C.U. (2012). South Africa's Climatic Zones: Today, Tomorrow. Paper presented at the International Green Building Conference and Exhibition, Sandton, South Africa. 9 pages.
- Costanza, R., McGlade, J., Lovins, H., and Kubiszewski, I. (2014). An Overarching Goal for the UN Sustainable Development Goals. *Solutions*, Vol. 5 (4), 13-16.
- Council of Geoscience (2003). Simplified geologic map of South Africa by C.J. Vorster.
- Cullers, R.L. (1994). The controls on the major and trace element variation of shales, siltstone and sandstones of Pennsylvanian – Permian age from uplifted continental blocks in Colorado to platform sediment in Kansas, USA: *Geochim. Cosmochim. Acta*, 58(22), 4955-4972.
- Cullers, R.L. and Graf, J. (1983). Rare earth elements in igneous rocks of the continental crust: intermediate and silicic rocks, ore petrogenesis. In: Henderson, P. (Ed.), Rare Earth Geochemistry. Elsevier, Amsterdam, pp. 275–312.
- Cullers, R.L. (2000). The geochemistry of shales, siltstones and sandstones of Pennsylvanian-Permian age, Colorado, U.S.A.: implications for provenance and metamorphic studies: *Lithos*, 51, 305-327.

- Cullers, R.L. and Podkovyrov, V.N. (2000). Geochemistry of the Mesoproterozoic Lakhanda shales in southeastern Yakutia, Russia: implications for mineralogical and provenance control, and recycling. *Precambrian Res.*, 104 (1-2), 77-93.
- DA (2003). Annual report of the Department of Agriculture, Republic of South Africa. 203 pgs.
- Darunsontaya, T., Suddhiprakarn, A., Kheoruenromne, I., Gilkes, R.J., 2010. Geochemical properties and the nature of kaolin and iron oxides in upland oxisols and ultisols under a tropical monsoonal climate, Thailand. *Thai. J. Agric. Sci.* 43, 197–215.
- Davis, J.C. (2002). *Statistics and Data Analysis in Geology*, New York: John Wiley & Sons Inc., 3rd edition, 638 pp.
- Deepthy, R. (2008). Clay mineralogical and geochemical studies on the weathering profiles developed on either side of Western Ghats, Karnataka, India. Unpublished PhD Thesis, Pondicherry University, 165 pp.
- de Jayawardena, U.S. and Izawa, E. (1994). A new chemical index of weathering for metamorphic silicate rocks in tropical regions: a study from Sri Lanka. *Eng. Geol.*, 36, 303-310.
- Delvaux, B., Herbillon, A.J., and Vielvoye, L. (1989). Characterization of a weathering sequence of soils derived from volcanic ash in Cameroon. Taxonomic, mineralogical and agronomic implications. *Geoderma* 45, 375–388.
- Diko, M.L., Ekosse, G.E., Ayonghe, S.N., and Ntasin, E. (2011). Physical characterization of clayey materials from Tertiary volcanic cones in Limbe (Cameroon) for ceramic applications. *Appl. Clay Sci.*, 51: 380–384.
- Diko, M. L. and Ekosse, G. E. (2013). Characterisation of two kaolin facies from Ediki, Southwest Cameroon. *Sci. Res. Essays*, 8(18), 698-704.
- Diko M., Ekosse G. and Ogola J. (2016). Fourier transform infrared spectroscopy and thermal analyses of kaolinitic clays from South Africa and Cameroon. *Acta Geodyn. Geomater.*, 13 (2), xx1–x10.

- Dixon, J.B. (1989). Kaolin and Serpentine Group Minerals. Pp. 467-525 in: *Minerals in Soil Environments* (J.B. Dixon & S.B. Weed, editors). Soil Sci. Soc. America, Madison, Wisconsin.
- Driessen, P.M., Deckers, J.A., Spaargaren, O.C., And Nachtergaele, F.O. (2001). Lecture Notes on the Major Soils of the World. Food and Agricultural Organization of the United Nations, Rome.
- Duzgoren-Aydin, N.S., Aydin, A., and Malpas, J. (2002). Re-assessment of chemical weathering indices: case study of pyroclastic rocks of Hong Kong. *Eng. Geol.* 63, 99–119.
- Ekosse, G. (2001). Provenance of the Kgwakgwe kaolin deposit, southeastern Botswana and its possible utilization. *Appl. Clay Sci.* 20, 137–152.
- Ekosse, G. (2005). X-ray Powder diffraction patterns of clays and clay minerals in Botswana. Associated printers, Gaborone, Botswana. 78 pages.
- Ekosse, G. (2007). Thermoanalytical characterisation, stable isotope and paleoenvironmental considerations of kaolinite from two genetic sources. *Fresen. Environ. Bull.*, 16 (12), 1-15.
- Ekosse, G.E. and Anyangwe, S. (2012). Mineralogical and particulate morphological characterization of geophagic clayey soils from Botswana. *Bull. Chem. Soc. Ethiop.*, 26(3): 373-382.
- EPA (2010). *Methane and Nitrous Oxide Emissions from Natural Sources*. U.S. Environmental Protection Agency, Washington, DC, USA.
- Etame, J., Gerard, M., Suh, C.E., and Bilong, P. (2009). Halloysite neoformation during the weathering of nephelinitic rocks under humid tropical conditions at Mt Etinde, Cameroon. *Geoderma* 154: 59-68.
- Fedo, C.M., Nesbitt, H.W., and Young, G.M. (1995). Unravelling the effects of potassium metasomatism in sedimentary rocks and paleosols, with implications for paleoweathering conditions and provenance. *Geology*, 23, 921-924.
- Fernández-Caliani, J.C. and Cantano, M. (2010). Intensive kaolinization during a lateritic weathering event in South-West Spain Mineralogical and geochemical inferences from a relict paleosol. *Catena*, 80: 23–33.

- Fey, M.V. (2010). A short guide to the soils of South Africa, their distribution and correlation with World Reference Base soil groups. 19th World Congress of Soil Science, Soil Solutions for a Changing World. pp. 32-35.
- Filippelli, G.M (2002) The Global Phosphorus Cycle. *Rev. Miner. Geochem.* 48: 391 – 425.
- Fiantis, D., Nelson, M., Shamshuddin, J., Goh, T.B. and Van Ranst, E. (2010). Determination of the geochemical weathering indices and trace elements content of new volcanic ash deposits from Mt Talang (West Sumatra) Indonesia. *Eura. Soil Sci.*, 43 (13), 1477-1485.
- Fontes, M.P. (1988). Iron oxide mineralogy in some Brazilian Oxisols. PhD thesis. NCSU-Raleigh, North Carolina, USA.
- Foo, K.Y. and Hameed, B.H. (2010). “Insights into the modeling of adsorption isotherm systems,” *Chem. Eng. J.*, 156:1, 2–10.
- Food and Agricultural Organization (FAO) (2005). Fertilizer Use by Crop in South Africa, First Version; FAO: Rome, Italy.
- Food and Agriculture Organization of the United Nations (FAO) (2017). The state of food and agriculture. ISBN 978-92-5-109873-8.
- Fox, R.L. and Kamprath, E.J. (1970). Phosphate sorption isotherms for evaluating the phosphate requirements of soils. *Soil Sci. Soc. Am. Proc.*, 34: 902-907.
- Gaspe, A., Messer, P., and Young, P. (1994). Selection and preparation of clay bodies for stove manufacture. Clay testing. A manual on clay/non-clay ratio measurement technique. 10 pages.
- Georges, K. K, Roger, K. E., Fritz, O. T., and Bernard, P. K. (2019). Influence of Clay Minerals on Some Soil Fertility Attributes: A Review. *Open J. Soil Sci.*, 9, 155-188.
- Gichangi, E.M., Mnkeni, P.N., and Muchaonyerwa, P. (2008). Phosphate Sorption Characteristics and External P Requirements of Selected South African Soils. *J. Agr. Rural Dev. Trop.*, 109 (2), 139–149.
- Giles, C. H., MacEvan, T. H., Nakhwa, S. N. and Smith, D. (1960). Studies on adsorption—XI. *J. Chem. Soc.*, 111: 3973-3993.

- Gilkes, R.J. and Suddhiprakarn, A. (1979). Biotite alteration in deeply weathered granite. I and II. *Clays Clay Miner.* 27: 349-367.
- Gilkes, R.J. and Prakongkep, N. (2016). How the unique properties of soil kaolin affect the fertility of tropical soils, *Appl. Clay Sci.*, 131: 100 -106
- Goemaere, E. (2004). Dickite and nacrite from the Liege Coal Basin (Belgian coal measures group, Westphalian, Upper Carboniferous), *Geol. Belg.*, 7 (3-4), 285-311.
- Gouveia, M. A., Prudêncio, M. I., Figueiredo, M. O., Pereira, L. C., Waerenborgh, J. C., Morgado, I., Pena, T., Lopes, A. (1993): Behavior of REE and other trace and major elements during weathering of granitic rocks, Évora, Portugal. *Chem. Geol.* 107, 293–296.
- Gregory, D.I. and Bumb, B.L. (2006). Factors Affecting Supply of Fertilizer in Sub-Saharan Africa. The World Bank Agriculture and Rural Development Discussion Paper 24, 81 pp.
- Grim, R.E. (1968). *Clay Mineralogy*. McGraw-Hill, New York. 596 pp.
- Guggenheim, S. and Koster van Groos, A.F. (2001). Baseline studies of the clay minerals society source clays: thermal analysis. *Clays Clay Miner.*, 49 (5), 433–443.
- Günther, D. and Hattendorf, B. (2005). Solid sample analysis using laser ablation inductively coupled plasma mass spectrometry, *Trends Anal. Chem.*, 24(3), 255-265.
- Hall, R., Wisborg, P., Shirinda, S., and Zamchiya, P. (2013). Farm Workers and Farm Dwellers in Limpopo Province, South Africa. *J. Agra. Chang.* 13 (1), 47–70.
- Hamdan, J. and Burnham, C.P. (1996). The contribution of nutrients from parent material in three deeply weathered soils of Peninsular Malaysia. *Geoderma* 74, 219–233
- Hamdi, W., Pelster, D., and Seffen, M. (2014). Phosphorus sorption kinetics in different types of alkaline soils. *Arch. Agron. Soil Sci.*, 60: 577-586.
- Haq, A., Iqbal, Y., and Khan, M. (2008). Historical development in the classification of kaolin subgroup. *J Pak Mater Soc* 2 (1), 44-49.

- Hart, R.D., Gilkes, R.J., Siradz, S., Singh, S. (2002). The nature of soil kaolins from Indonesia and Western Australia. *Clay Clay Miner.* 50, 198–207.
- Hart, R.D., Wiryakitnateekul, W., Gilkes, R.J. (2003). Properties of soil kaolins from Thailand. *Clay Miner.* 38, 71–94.
- Hartono, A., Funakawa, S., and Kosaki, T. (2005). Phosphorus Sorption-Desorption Characteristics of Selected Acid Upland Soils in Indonesia, *Soil Sci. Plant Nutr.*, 51:6, 787-799.
- Haskin L. A., Helmke P. A., Paster T. P., and Allen R. O. (1971). "Rare earths in meteoritic, terrestrial, and lunar matter" In Activation Analysis in Geochemistry and Cosmochemistry, A. Brunfelt and E. Steinnes, eds., Proc. NATO Conf. on Activation Analysis in Geochemistry, pp. 201-218, Universitetsforlaget, Oslo.
- Havlin, J., Beaton, J.D., Tisdale, S.L., and Nelson, W.L. (2014). Soil fertility and fertilizers: An introduction to nutrient management. 8th ed. Pearson Prentice Hall, Upper Saddle River, NJ.
- Hazelton, P.A. and Murphy, B. (2007). Interpreting Soil Test Results, What Do All The Numbers Mean?, Commonwealth Scientific and Industrial Research Organization Publishing (CSIRO), 152 pp.
- Henry, P.C. and Smith. M.F. (2002). Phosphorous sorption study of selected South African soils. *S. Afr. J. Plant & Soil*, 19:2, 61-69.
- Herbillon, A. J., Mestdagh, M. M., Vielvoye, L. and Derouane. E. (1976). Iron in kaolinite with special reference to kaolinite from tropical soils. *Clay Miner.* 11: 201-220.
- Heckman, K. and Rasmussen, C. (2011). Lithologic controls on regolith weathering and mass flux in forested ecosystems of the Southwestern USA, *Geoderma* 164 (3), 99-111.
- Hofer, G., Wagreich, M., and Neuhuber, S. (2013). Geochemistry of fine-grained sediments of the upper Cretaceous to Paleogene Gosau Group (Austria, Slovakia): Implications for paleoenvironmental and provenance studies *Geosci. Front.* 4, 449-468.
- Holford, I.C. and Mattingly, G.E. (1976). A model for the behavior of labile phosphate in soil. *Plant and Soil* 44: 219–229.

- Holzer, L., Frei, R., Baeton, J.M., and Kramers, J.D. (1998). Unraveling the record of successive high-grade events in the Central Zone of the Limpopo Belt using Pb single phase dating of metamorphic minerals. *Precambrian Res.* 87, 87–115.
- Hopkins, B.G. (2015). Phosphorus in plant nutrition. In *Plant nutrition handbook*. eds. D.J. Pilbeam and A.V. Barker, 2nd ed., Ch. 3, 65–26. Boca Raton, FL: CRC Press, Taylor & Francis Group.
- Hoyt, P. B. (1977). Effects of organic matter content on exchangeable Al and pH-dependent acidity of very acid soils. *Can. J. Soil Sci.* 57:221–222.
- Huang, P.M., Li, Y., and Sumner, M.E. (2011). *Handbook of Soil Sciences: Properties and Processes* (2nd ed.) Taylor & Francis, 1442 pp.
- Hughes, J.C. and Brown, G. (1979). A crystallinity index for soils kaolins and its relation to parent rock, climate and soils maturity. *J. Soil Sci.* 30, 557–563.
- Hughes, J.C., Gilkes, R.J., and Hart, R.D. (2009). Intercalation of reference and soil kaolins in relation to physico-chemical and structural properties. *Appl. Clay Sci.* 45, 24–35.
- Hunter, D.R., Johnson, M.R., Anhaeusser, C. R. and Thomas, R.J. (2006). Introduction. (In: Johnson, M.R., Anhaeusser, C.R. and Thomas, R.J. (Eds), *The Geology of South Africa*. Geological Society of South Africa, Johannesburg/Council for Geoscience, Pretoria, 585-604.
- Ibarra, D., Caves Rugenstein, J., Moon, S., Thomas, D., Hartmann, J., Chamberlain, C. and Maher, K. (2016). Differential weathering of basaltic and granitic catchments from concentration-discharge relationships. *Geochim. Cosmochim. Acta* 190: 265–293.
- Imasuen, O.I. and Onyeobi, T.U.S. (2013). Chemical Compositions of Soils in Parts of Edo State, Southwest Nigeria and their Relationship to Soil Productivity. *J. Appl. Sci. Environ. Manage.* 17 (3): 379-386.
- International Centre for Diffraction Data (2002). *Mineral Powder diffraction file data book*. 941p.
- ISSS Working Group R.B. (1998). World reference base for soil resources: atlas. In: Bridges, E.M., Batjes, N.H., Nachtergaele, F.O. (Eds.), *ISRIC-FAO-ISSS-Acco*. Leuven, Belgium, p. 79.

- IUSS Working Group WRB (2006). World Reference Base for Soil Resources 2nd edition. World Soil Resources Reports 103. FAO, Rome.
- Jakubowska, J. (2007). *Effects of irrigation water type on soil organic matter (SOM) fractions and their interactions with hydrophobic compounds*. PhD Thesis, Martin-Luther-Universität Halle-Wittenberg, Halle, Germany. 196 pages.
- Jackson, M.L. (1979). Soil chemical analysis- Advanced course, 2nd edition, 11th printing, published by the author, Madison, WI, USA, 895 pp.
- Jeans, C.V., Wray, D.S., Merriman, R.J., and Fisher, M.J. (2000). Volcanogenic clays in Jurassic and Cretaceous strata of England and the North Sea Basin. *Clay Miner.*, 35, 25-55.
- Jenny, H. (1994). *Factors of Soil Formation. A System of Quantitative Pedology*. New York: Dover Press. (Reprint, with Foreword by R. Amundson, of the 1941 McGraw-Hill publication).
- Jepson, W. B. and Rowse, J. B. (1975). The composition of kaolinite--an electron microscope microprobe study: *Clays Clay Miner.*, 23, 310-317.
- Jien, S.H., Baillie, I., Huang, W.S., Chen, Y.Y., and Chiu, C.Y. (2016). Incipient ferralization and weathering indices along a soil chronosequence in Taiwan. *Eur. J. Soil Sci.*, 67, 583–596.
- Jindaluang, W., Kheoruenromne, I., Suddhiprakarn, A., Singh, B.P. and Singh, B. (2010). Relationships between Mineralogical Properties and Carbon and Nitrogen Retention in Upland Soils of Thailand. 19th World Congress of Soil Science, Soil Solutions for a Changing World, Brisbane, Australia, 1-6 August 2010.
- Johnson, M.R., Anhaeusser, C.R., and Thomas, R.J. (2006). *The Geology of South Africa*. Johannesburg: Geological Society of SA / Pretoria: Council of Geoscience. 691 pgs.
- Jongkind, A.G. and Buurman, P. (2006). The effect of kauri (*Agathis australis*) on grain size distribution and clay mineralogy of andesitic soils in the Waitakere Ranges, New Zealand. *Geoderma* 134, 171-186.

- Joussein, E., Petit, S., Churchman, J., Theng, B., Righi, D., and Delvaux, B. (2005). Halloysite clay minerals - a review. *Clay Miner.*, 40, 383-426.
- Juo, A. R. and Fox, R. L. (1977). Phosphate sorption characteristics of some benchmark soils of West Africa; *J. Soil Sci.*; 124:370–376.
- Juo, A.S. and Franzluebbbers, K. (2003). Tropical Soils. Properties and Management for Sustainable Agriculture. Oxford University Press, New York. 281 pgs.
- Kaiser, K. and Guggenberger, G. (2003). Mineral Surfaces and Soil Organic Matter. *Eur. J. Soil Sci.*, 54, 219-236.
- Kanket, W. (2006). Properties of the Clay Fraction of Alfisols and Ultisols in Thailand PhD Thesis Kasetsart University, Bangkok, Thailand.
- Kanket, W., Suddhiprakarn, A., Kheoruenromne, I., Gilkes, R.J. (2005). Chemical and crystallographic properties of kaolin from ultisols in Thailand. *Clay Clay Miner.* 53, 478–489.
- Keller, W.D. (1976). Scan electron micrographs of kaolins collected from diverse environments of origin--I. *Clays Clay Miner.*, 24, 107-113.
- Khawmee, K., Suddhiprakarn, A., Kheoruenromne, I., and Singh, B. (2010). Charge properties of kaolinite in acidic soils from Thailand. 19th World Congress of Soil Science, Soil Solutions for a Changing World. pp. 30-32.
- Kheoruenromne, I. and Suddhiprakarn, A. (1984). Ecology, classification and effect of management of selected sandy soils in Thailand, pp. 207-224. In Ecology and Management of Problem Soils in Asia. FFTC Book Series No. 27. Taipei, Taiwan.
- Kissinger, H.M. (1956). Variation of peak temperature with heating rate in differential thermal analysis. *J. Res. Natl. Bur. Stand.*, 57 (4), 217-221.
- Kleber, M., Schwenendenmann, L., Veldkamp, E., Roessner, J. and Jahn, J. (2007). Halloysite versus gibbsite: silicon cycling as a pedogenetic process in two lowland neotropical rain forest soils of La Selva, Costa Rica. *Geoderma*, 138, 1–11.

- Kome, G.K., Enang, R.K., Tabi, F.O., and Yerima, B.P. (2019). Influence of clay minerals on some soil fertility attributes; a review. *J Soil Sci* 9: 155-188.
- Koppi, A.J. and Skjemstad, J.O. (1981). Soil kaolins and their genetic relationships in southeast Queensland, Australia. *J. Soil Sci.* 32: 661–672.
- Kramers, J.D., McCourt, S., and Van Reenen, D.D. (2006). The Limpopo Belt. In: Johnson, M.R., Anhaeusser, C.R., and Thomas, R.J., eds., *The Geology of South Africa: Johannesburg, Geological Society of South Africa and Pretoria, Council for Geoscience*, pp. 209-236.
- Kumara, N.T., Hamdan, N., Petra, M.I. Tennakoon, U., and Ekanayake, P. (2014). Equilibrium Isotherm Studies of Adsorption of Pigments Extracted from Kuduk-kuduk (*Melastoma malabathricum* L.) Pulp onto TiO₂ Nanoparticles. *J. Chem.*, Article ID 468975, 6 pages.
- Kutu, F.R. and Diko, M.L. (2011). Mineralogical considerations in soil fertility management on selected farmlands in Limpopo and Northwest Provinces, South Africa. In: GIE Ekosse, L de Jager & VM Ngole (eds.) *An Innovative Perspective on the Role of clays and clay minerals and Geophagia on Economic development. Book of Conference Proceeding of the 1st International Conference of Clays and Clay Minerals in Africa and 2nd International Conference on Geophagia in Southern Africa*, pp.124-130.
- Lanson, B., Beaufort, D., Berger, G., Bauer, A., Cassagnabere, A., and Meunier, A. (2002). Authigenic kaolin and illitic minerals during burial diagenesis of sandstones: a review, *Clay Miner.* 37, 1-22.
- Larkin, P. (2011). *Infrared and Raman spectroscopy: principles and spectral interpretation*. Elsevier, London. 228 pages.
- Lee, S.Y., Jackson, M.L., and Brown, J.L. (1975). Micaceous occlusions in kaolinite observed by ultramicrotomy and high resolution electron microscopy. *Clays Clay Miner.* 23: 125–129.
- Leonard, D. N., Chandler, G. W. and Seraphin, S. (2012). Scanning Electron Microscopy. *Character. Mater.*, 1–16.
- Loveland, P. and Webb, J. (2003). Is there a critical level of organic matter in the agricultural soils of temperate regions: a review. *Soil Till. Res.*, 70: 1–18.

- Lu, D., Moran, E., and Mausel, P. (2002). Linking Amazonian secondary succession forest growth to soil properties. *Land Degrad. Dev.* 13:331–343.
- Ma, C. and Eggleton, R.A. (1999). Surface layer types of kaolinite: a high resolution transmission electron microscope study. *Clays Clay Miner.* 47: 181-191.
- MacCallum, R.C., Widaman, K.F., Zhang, S., and Hong, S. (1999). Sample size in factor analysis. *Psychol. Methods* 4:1, 84-99.
- Madejová, J., Kraus, I., Tunega, D. and Šamajová, E. (1997). Fourier transform infrared spectroscopic characterization of kaolin group minerals from the main Slovak deposits. *Geologica Carpathica – Series Clays*, 6(1), 3–10.
- Madejová, J. and Komadel, P. (2001). Baseline studies of the clay minerals source society: infrared methods. *Clays and Clay Miner.*, 49, 410–432.
- Magdoff, F. and Weil, R.R. (2004). *Soil Organic Matter in Sustainable Agriculture*. CRC Press, 398 pp.
- Mana, S.C., Hanafiah, M.M. and Chowdhury, A.J. (2017). Environmental characteristics of clay and clay-based minerals, *Geol. Ecol. Landsc.*, 1:3, 155-161.
- Mandiringana, O.T., Mnkeni, P.N.S., Mkile, Z., van Averbeke, W., Van Ranst, E. and Verplancke, H. (2005). Mineralogy and Fertility Status of Selected Soils of the Eastern Cape Province, South Africa. *Commun. Soil Sci. Plant Anal.*, 36, 2431-2446.
- Manicus, R.A. (2009). Evaluation of soil fertility in the Sekhukhune district South Africa. *J. Dev. Sustain. Agric.*, 4 (2), 141-148.
- Maponya, P. and Mpandeli, S. (2015). Climate Change Status in the Mutale Local Municipality: A Case Study of the Smallholder Farmers in Vhembe District, Limpopo Province. *J Hum Ecol*, 52(1, 2): 1-8.
- Matthews, M.W, and Bernard, S. (2015). Eutrophication and cyanobacteria in South Africa’s standing water bodies: A view from space. *S Afr J Sci.* 111(5/6), 8 pages.
- McBride, M.B. (1994). *Environmental Chemistry of Soils*. Oxford University Press, New York, 406 pgs.
- Mcdowell, R., Sharpley, A., and Withers, P. (2002). Indicator to predict the movement of phosphorus from soil to subsurface flow. *Environ. Sci. Tech.* 36(7): 1505–1509.

- McLennan, S.M. (1989). Rare earth elements in sedimentary rocks: influence of provenance and sedimentary processes. In Lipin, B.R., and McKay, G.A., eds., *Geochemistry and Mineralogy of Rare Earth Elements*: Mineralogical Society of America, *Reviews in Mineralogy*, 21, 169–200.
- McLennan, S.M., Hemming, S., McDaniel, D.K., and Hanson, G.N. (1993). Geochemical approaches to sedimentation, provenance, and tectonics. In Johnsson, M.J., and Basu, A., eds., *Processes Controlling the Composition of Clastic Sediments*: Geological Society of America, Special Paper 284, 21–40.
- McLennan, S. M. (2001). Relationships between the trace element composition of sedimentary rocks and upper continental crust, *Geochem. Geophys. Geosyst.*, 2, 1021.
- McKenzie, N.J., Jacquier, D.J., Isbell, R.F., Brown, K.L. (2004). *Australian Soils and Landscapes. An Illustrated Compendium* CSIRO Publishing: Collingwood, Victoria, 416 pgs.
- Mehra, O.P. and Jackson, M.L. (1960). Iron oxide removal from soils and clays by a dithionite-citrate system buffered with sodium bicarbonate. *Clays Clay Miner.* 7, 317-327.
- Melegy, A.A. and El-Agami, N.L. (2004). Factors controlling the chemistry and mineralogy of selected soil types of the Czech Republic and Egypt. *Bull. Geosci.*, 79 (1), 71–79.
- Melo, V.F., Singh, B., Schaefer, C.E.G.R., Novais, R.F., and Fontes, M.P.F. (2001). Chemical and mineralogical properties of kaolinite-rich Brazilian soils. *Soil Sci. Soc. Am. J.* 65, 1324–1333.
- Meyer, J.H., Wood, R.A., Schumann, A.W., Schroeder, B.L., Rampersad, A.L., and Nixon, D.J. (2004). The SASEX Fertilizer Advisory Service: A review of 50 years dedicated service to the South African Sugar Industry. *Proc. S. Afr. Sug. Technol. Ass.* 78: 359–372.
- Mestdagh, M.M., Vielvoye, L., and Herbillon, A.J. (1980). Iron in kaolinite: II. The relationship between kaolinite crystallinity and iron content. *Clay Miner.*, 15, 1-13.
- Millot, G. (1965). *Geologie des Argiles*. Masson, Paris. 499 pgs.

- Miko, S., Halami, J., Peh, Z., and Galovi, L. (2001). Geochemical Baseline Mapping of Soils Developed on Diverse Bedrock from Two Regions in Croatia. *Geol. Croat.*, 54/1: 53 – 118.
- Mnthambala, F., Maida, J. H., Lowole, M. W., and Kabambe, V.H. (2015). Phosphorus sorption and external phosphorus requirements of ultisols and oxisols in Malawi, *J. Soil Sci. Environ. Manage* 6(3), 35-41.
- Moncharoen, L. (1992). Red soils of Thailand. G. Zitong (Ed.), Proceedings of International Symposium on Management and Development of Red Soils in Asia and Pacific Region, Science Press, New York, pp. 21–26.
- Montgomery, D. C. (2001). Design and Analysis of Experiments. 5th Edition. John Wiley and Sons, Inc., 684 pgs.
- Munhoz, R.O., Berton, R.S. and Camargo, O.A. (2011). Phosphorus sorption and redistribution on soil solid phase in a Brazilian Haplorthox Amended with Biosolids. *Appl. Environ. Soil Sci.* 10:1-7.
- Murray, H.H. (2007). Applied Clay Mineralogy. Occurrences, Processing and Application of Kaolins, Bentonites, Palygorskite–Sepiolite, and Common Clays, 1st ed. Elsevier, Oxford. 189 pp.
- Myeni, L., Moeletsi, M., Thavhana, M., Randela, M., and Mokoena, L. (2019). Barriers Affecting Sustainable Agricultural Productivity of Smallholder Farmers in the Eastern Free State of South Africa. *Sustainability*, 11, 3003.
- Neal, M. and Worrall, W.E. (1977). Mineralogy of Fireclays: part 1. The crystallinity of kaolinite in fireclays. *Trans. Bri. Ceram. Soc.*, 76, 57– 61.
- Nelson, D.W. and Sommers, L.E. (1996). Total carbon, organic carbon, and organic matter. p. 961-1010. In D.L Sparks et al. (eds.) Methods of soil analysis. Part 3. Chemical Methods. SSSA Book Series No. 5, SSSA and ASA, Madison, WI.
- Nesbitt, H.W. and Young, G.M. (1982). Early Proterozoic climates and plate motions inferred from major elemental chemistry of lutites. *Nature*, 299, 715-717.
- Nesbitt, H.W. and Young, G.M. (1984). Prediction of some weathering trends of plutonic and volcanic rocks based on thermodynamic and kinetic considerations. *Geochim. Cosmochim. Acta* 48, 1523- 1534.

- Nesbitt, H. W. and Young, G. M. (1989). Formation and Diagenesis of weathering profiles. *J. Geol.*, 97(2), pp. 129-147.
- Nesbitt, H.W. and Wilson, R.E. (1992). Recent chemical weathering of basalts. *Am. J. Sci.* 292, 740–777.
- Nguyen, Q. H. and Egashira, K. (2007). Clay mineralogy of ferralitic soils derived from sedimentary and metamorphic rocks in Vietnam. *Clay Sci.*, 13, 139-148.
- Njoyim, E.B., Mvondo-Zé, A.D., Mofor, N.A., Onana, A.A. (2016). Phosphorus Adsorption Isotherms in Relation to Soil Characteristics of Some Selected Volcanic Affected Soils of Foubot in the West Region of Cameroon. *Int. J. Soil Sci.*, 11: 19-28.
- Non-Affiliated Soil Analysis Working Group (1990). Handbook of standard soil testing methods for advisory purposes. Soil Science Society of South Africa, PO Box 65217, Erasmusrand, Pretoria, 0001.
- Olsen, S. R. and Watanabe, F. S. (1957). A method to determine a phosphorus adsorption maximum of soils as measured by the Langmuir isotherm. *Soil Sci. Soc. Amer. Proe.* 21: pp. 144-149.
- Olsen, S. R. and Sommers, L. E. (1982). Phosphorus. In Page et al., (ed) Methods of soil analysis, 2nd ed. *Agronomy* 9:403-430.
- Oyebanjo, O.M., Ekosse, G.E., and Odiyo, J.O. (2018). Mineral Constituents and Kaolinite Crystallinity of the <math> < 2\mu\text{m}</math> Fraction of Cretaceous-Paleogene/Neogene Kaolins from Eastern Dahomey and Niger Delta Basins, Nigeria. *Open Geosci.* 10, 157–166.
- Osman, K.T. (2013) Physical Properties of Forest Soils. In: Forest Soils, Springer, Cham, 19-44.
- Palleiro, L., Patinha, C., Rodríguez-Blanco, M. L., Taboada-Castro M.M., and Taboada-Castro, M.T. (2016). Aluminum Forms in Solid Phase of Soils Developed over

- Schists as a Function of Land Use. *Commun. Soil Sci. Plant Anal.*, 47:sup1, 90-96
- Papoulis, D., Tsolis-Katagas, P. and Katagas C. (2004). Progressive stages in the formation of kaolin minerals of different morphologies in the weathering of plagioclase. *Clays Clay Miner.*, 52: 275-286.
- Papoulis, D., Tsolis-Katagas, P., Tsikouras B. and Katagas, C. (2005). An FT-Raman, Raman and FTIR study in Hydrothermally altered volcanic rocks from Kos island (Southeastern Aegean, Greece). *Dev. Volcan.*, 7 (C), pp. 293-304.
- Parker, A. (1970). An index of weathering for silicate rocks. *Geological Magazine*, 107, 501-504.
- Patiram, B., Azad Thakur, N.S. and Ramesh, T. (2007). Soil Testing and Analysis: Plant, Water and Pesticide Residues. New India Publishing Agency, New Delhi, 220 pp.
- Pedro, G. (1982). The conditions of formation of secondary constituents. Pp. 63-81 in: *Constituents' and Properties' of Soils* (M. Bonneau & B. Souchier, editors) Academic Press, London.
- Plummer, C., Carlson, D., and Hammersley, L. (2016). Physical Geology 14th Edition. McGraw-Hill publishers. 672 pages.
- Porder, S. and Ramachandran, S. (2012). The phosphorus concentration of common rocks - a potential driver of ecosystem P status. *Plant Soil*. DOI 10.1007/s11104-012-1490-2.
- Poswa, L.Z. (2016). Factors Affecting Phosphorus Requirements for the Soils of South African Sugar Industry. M.Sc Thesis, University of KwaZulu-Natal, South Africa. 82 pp.
- Poujol, M., Robb, L.J., Anhaeusser, C.R. and Gericke, B. (2003). "A review of the geochronological constraints on the evolution of the Kaapvaal Craton, South Africa", *Precambrian Res.*, 127 (1-3), 181-213.
- Price, J.R. and Velbel, M.A. (2003). Chemical weathering indices applied to weathering profiles developed on heterogeneous felsic metamorphic parent rocks. *Chem. Geol.* 202, 397- 416.

- Puget, P., Chenu, C. and Balesdent, J.B. (2000). Dynamics of Soil Organic Matter Associated with Particle-Size Fractions of Water-Stable Aggregates. *Eur. J. Soil Sci.*, 51, 595-605.
- Räty, M. and Peltovuori, T. (2008). Sorption of phosphate phosphorus in ultrasound-separated particle-size fractions from arable soils. Phosphorus management in Nordic-Baltic agriculture reconciling productivity and environmental protection: NJF Seminar 401 Uppsala, Sweden, 22-23 September 2008, NJF Report, 4, Nordic Association of Agricultural Scientists, Stockholm, pp. 147-151.
- Rayment, G.E. and Higginson, F.R. (1992). 'Australian laboratory handbook of soil and water chemical methods.' Inkarta Press: Melbourne. 330 pgs.
- Reddy, K.R., Kadlec, R.H., Flaig, E. and Gale, P.M. (1999). Phosphorus retention in streams and wetlands--a review. *Crit. Rev. Environ. Sci. Tech.*, 29:86-146.
- Reeves, G.M., Sims, I., and Cripps, J.C. (2006). Formation and alteration of clay materials; Geological Society, London, Engineering Geology Special Publications 21: 29-71.
- Robb, L.J., Brandl, G., Anhaeusser, C.R., and Poujol, M. (2006). Archaean granitoid intrusions, in Johnson, M.R., Anhaeusser, C.R., and Thomas, R.J., eds., *The Geology of South Africa: Johannesburg, Geological Society of South Africa and Pretoria, Council for Geoscience*, p. 57-94.
- Robertson, I.D.M. and Eggleton, R.A. (1991). Weathering of granitic muscovite to kaolinite and halloysite and of plagioclase-derived kaolinite to halloysite. *Clays Clay Miner.* 39: 113-126.
- Ruck, L. and Brown, C.T. (2015). Quantitative analysis of Munsell color data from archeological ceramics *J. Archaeol. Sci.: Reports* 3, 549-557.
- Ruiz Cruz, M.D. and Andreo, B. (1996). Tosudite in very low-grade metamorphic graywackes from the Malaga area (Betic Cordilleras, Spain), *Eur. J. Miner.*, 8: 1391-1399.
- Russell, J.D. and Fraser, A.R. (1994). in: M.J. Wilson (Ed.), *Clay Mineralogy: Spectroscopic and Chemical Determinative Methods*, Chapman & Hall, London, UK, 11 pgs.

- SACS (South African Committee for Stratigraphy) (1980). Stratigraphy of South Africa, Pt. 1. Compiled by L.E. Kent. Handbook of the Geological Survey.
- Sandeep, S. and Sujatha, M.P. (2014). Mineralogy of kaolin clays in different forest ecosystems of southern Western Ghats, India. *Curr. Sci.*, 107 (5), pp. 875-882.
- Saruchi and Kumar, P. (2016). Adsorption kinetics and isotherms for the removal of rhodamine B dye and Pb^{+2} ions from aqueous solutions by a hybrid ion-exchanger. *Arab. J. Chem.* 12, 316–329.
- Schefe, C. R. and Tymms, K. (2013). Phased addition of organic and phenolic acids with phosphate fertiliser increases P availability in an acid soil. *Soil Res.*, 51:437–446.
- Schoumans, O.F., Chardon, W.J., Bechmann, M.E., Gascuel-Oudou, C., Hofman, G. and Kronvang, B. (2014). Mitigation options to reduce phosphorus losses from the agricultural sector and improve surface water quality: A review. *Sci. Total Environ.*, 468–469, 1255–1266.
- Schulten, H.R. and Leinweber, P. (2000). New insights into organic-mineral particles: Composition, properties and models of molecular structure. *Biol. Fertil. Soils*, 30, 399-432.
- Schulze, R.E. (1997). South African Atlas of Agrohydrology and Climatology. Water Research Commission, Pretoria Report TT82/96.
- Schwertmann, U. and Herbillon, A.J. (1992). Some aspects of fertility associated with the mineralogy of highly weathered tropical soils. Pp. 47-59 in: Myths and Science of Soils of the Tropics (R. Lal, editor). Special Publication 29, Soil Science Society of America, Madison, Wisconsin.
- Shange, L.P. and Conradie, W.J. (2012). Effects of Soil Parent Material and Climate on the Performance of *Vitis vinifera* L. cvs. Sauvignon blanc and Cabernet Sauvignon - Part I. Soil Analysis, Soil Water Status, Root System Characteristics, Leaf Water Potential, Cane Mass and Yield. *S. Afr. J. Enol. Vitic.*, 33 (2), 161-173.
- Sharma, A. and Rajamani, V. (2000). Weathering of gneissic rocks in the upper reaches of Cauvery River, South India: implications to neotectonics of the region. *Chem. Geol.* 166, 203–223.

- Sieczka, A. and Koda, E. (2016). Kinetic and Equilibrium Studies of Sorption of Ammonium in the Soil-Water Environment in Agricultural Areas of Central Poland. *Appl. Sci.*, 6, 269.
- Silva, Y. J., Nascimento, C. W., Biondi, C. M., Van Straaten, P., Souza Júnior, V. S., and Ferreira, T. O. (2016). Weathering rates and carbon storage along a climosequence of soils developed from contrasting granites in northeast Brazil. *Geoderma*, 284, 1-12.
- Sims, J.T. (2000). Soil fertility evaluation. In: Sumner, M.E. (Ed.), Handbook of Soil Science. CRC Press, Boca Raton, FL, D-113– D-127.
- Singer, A., Zarei, M., Lange, F.M., and Stahr, K. (2004). Halloysite characteristics and formation in the northern Golan Heights, *Geoderma*, 123, 279–295.
- Singh, B. and Gilkes, R.J. (1992). Properties of soil kaolins from south-western Australia. *J. Soil Sci.* 43, 645-667.
- Singh, B. and Schulze, D.G. (2015). Soil Minerals and Plant Nutrition. *Nat. Educ. Knowl.*, 6, 1-10.
- Singh, M., Sarkar, B., Biswas, B., Bolan, N.S. and Churchman, G.J. (2017) Relationship between Soil Clay Mineralogy and Carbon Protection Capacity as Influenced by Temperature and Moisture. *Soil Bio. Biochem.*, 109, 95-106.
- Siradz, S. (2000). Mineralogy and Chemistry of Red Soils of Indonesia, Ph.D. Thesis, The University of Western Australia, Perth, Australia.
- Siradz, S.A. (2008). Mineralogy and chemistry of red soils of Indonesia: I. General soil properties. *J. Ilmu Tanah Lingk.*, 8: 16–32.
- Smith, M., Thompson, K., and Lennard, F. (2017). A literature review of analytical techniques for materials characterisation of painted textiles—Part 2: spectroscopic and chromatographic analytical instrumentation, *J. Inst. Conserv.*, 40 (3), 252-266.
- Soil Classification Working Group (1991) Soil Classification – a Taxonomic System for South Africa. Memoirs on the Agricultural Natural Resources of South Africa No. 15. Department of Agricultural Development, Pretoria.

- Soil Survey Staff (2014). Soil Survey Field and Laboratory Methods Manual. Soil Survey Investigations Report No. 51, Version 2.0. R. Burt and Soil Survey Staff (ed.). U.S. Department of Agriculture, Natural Resources Conservation Service. 487 pp.
- St. Pierre, T.G., Singh, B., Webb, J., Gilkes, R.J. (1992). Mössbauer spectra of soil kaolins from south-western Australia. *Clay Clay Miner.* 40, 341–346.
- Statistics South Africa (2014). Mid-year population estimates 2014 P 0302. 19 pages.
- Statistics South Africa (2017). Mid-year population estimates 2017 P 0302. 22 pages.
- Steel, R.G., Torrie, J.H., and Dickey, D.A. (1997). Principles and procedures of statistics: a biometrical approach. 3rd ed. New York: MacGraw Hill. 666 pgs.
- Strawn, D.G., Bohn, H.L., and O'Connor, G.A. (2015). *Soil Chemistry* 4th. ed. Wiley Blackwell Publisher, New York. 390 pgs.
- Suslick, K.S. and Price, G.J. (1999). Applications of Ultrasound to Materials Chemistry. *Annu. Rev. Mater. Sci.* 29:295–326.
- Tan, K.H. (2011). Principles of Soil Chemistry Fourth Edition. CRC Press, Taylor and Francis Group, p. 362.
- Taylor, S.R. and McLennan, S.M. (1985). The Continental Crust: Its Composition and Evolution. Blackwell Scientific Publications, Oxford, 312 pp.
- Teklay, A., Yin, C., Rosendahl, L., and Bøjer, M. (2014). Calcination of kaolinite clay particles for cement production: a modeling study, *Cem. Concr. Res.* 61–62: 11–19.
- Tijani, M. N., Okunola, O. A. and Abimbola, A. F. (2006). Lithogenic concentrations of trace metals in soils and saprolite over crystalline basement rocks: A case study from SW Nigeria. *J. Afr. Earth Sci.* 46: 427-238.
- Trakoonyingcharoen, P., Kheoruenromne, I., Suddhiprakarn, A., and Gilkes, R.J. (2006). Properties of kaolins in red oxisols and red ultisols in Thailand. *Appl. Clay Sci.* 32, 25–39.
- Umoh, F.O., Osodeke, V.E., Edem, I.D., and Effiong, G.S. (2014). Application of Langmuir and Freundlich Models in Phosphate Sorption Studies in Soil of Contrasting Parent Materials in South-Eastern Nigeria. *Open Access Library Journal*, 1: e989.

- United States Department of Agriculture, (2010). From the Surface Down. An Introduction to Soil Surveys for Agronomic Use, Second Edition. 34 pages.
- United States Environmental Protection Agency (1986). Environmental indicators of water quality in the United States. EPA 841-R-96-002; Office of Water (4503F), Washington, DC.
- Vaculíková, L., Plevová, E., Vallová, S., and Koutník, I. (2011). Characterization and differentiation of kaolinites from selected Czech deposits using infrared spectroscopy and differential thermal analysis. *Acta Geodyn. Geomater.*, 8 (1) (161), 59–67.
- Van Breeman, N. and Buurman, P. (2003). Soil formation. 2nd edition. Kluwer Academic Publishers, New York, USA. 413 pgs.
- Van Reeuwijk, L.P. (2002). Procedures for soil analysis. International Soil Reference and Information Centre, Wageningen, The Netherlands, Tech. Paper 9, 100 pp.
- Van Reenen, D.D., Roering, C., and Brandl, G. (1990). The granulite facies rocks of the Limpopo belt, southern Africa. In: Vielzeuf, D., Viadal, Ph. (Eds.), *Granulites and Crustal Evolution*. Klumer, Dordrecht, pp. 1257–1289.
- Varajão, A.F., Gilkes, R.J., and Hart, R.D. (2001). The relationships between kaolinite crystal properties and the origin of materials for a Brazilian kaolin deposit. *Clay Clay Miner.* 49, 44–59.
- Velde, B. (1985). *Clay Minerals; A Physico-Chemical Exploration of their Occurrence*. Developments in Sedimentology, 40. Elsevier, Amsterdam, 427 pp.
- Velde, B. and Meunier, A. (2008): *The Origin of Clay Minerals in Soils and Weathered Rocks*. Springer-Verlag, Berlin, Heidelberg. 406 pp.
- Velde, B. and Barre, P. (2010). *Soils, Plants and Clay Minerals: Mineral and Biological Interactions*. Springer – Verlag Berlin Heidelberg. 349 pages.
- Verma, S.P., SantaCruz, R., Girón, P., and Velasco, F. (1996). Calibración preliminar de Fluorescencia de Rayos X para análisis cuantitativo de elementos traza en rocas ígneas: *Actas INAGEQ 2*, 231-242.

- Walkley, A. and Black, I. A. (1934). An examination of Degtjareff method for determining soil organic matter and a proposed modification of the chromic acid titration method. *Soil Sci.* 37: 29-37.
- Watanabe, T., Shinya, F., and Takashi, K. (2006). Clay mineralogy and its relationship to soil solution composition in soils from different weathering environments of humid Asia: Japan, Thailand and Indonesia. *Geoderma* 136: 51-63.
- Weil, R.R. and Brady, N.C. (2017). The nature and properties of soils. 15th ed. Pearson, Columbus, OH. 1104 pgs.
- Wilson, S.A. (1997). The collection, preparation, and testing of USGS reference material BCR-2, Columbia River, Basalt: U.S. Geological Survey Open-File Report 98-xxx.
- Wilson, M.J., Oyegoke, C., and Fraser, A.R. (1997). Occurrence of trioctahedral clay mica in some Nigerian alluvial soils. *11th Int. Clay Conf. Ottawa, Canada. Abstracts.* p. A83.
- Wilson, M.J. (1999). The origin and formation of clay minerals in soils: Past, present and future perspectives. *Clay Miner.* 34, pp. 7-25.
- Wilson, M.J. (2013). Rock-Forming Minerals, Vol. 3c, Sheet Silicates–Clay Minerals, 2nd edition. The Geological Society, London, 724 pp.
- Wiryakitnateekul, W., Suddhiprakarn, A., and Kheuruenromne, I. (2005). Extractable iron and aluminium predict the P sorption capacity of Thai soils. *Aust. Soil Res.* 43:757-766.
- Wiryakitnateekul, W., Suddhiprakarn, A., Kheuruenromne, I., Saunders, M., and Gilkes, R.J. (2010). Characteristics of soil kaolin on various parent materials in Thailand. 19th World Congress of Soil Science, Soil Solutions for a Changing World. pp. 18-21.
- Wolde, Z. and Haile, W. (2015). Phosphorus sorption isotherms and external phosphorus requirements of some soils of Southern Ethiopia. *Afr. Crop Sci. J.*, 23 (2):89-99.

- Yoothong K, Moncharoen L, Vijarnsorn P, Eswaran H (1997) Clay mineralogy of Thai soils. *Appl. Clay Sci.* 11, 357-371.
- Young, A. (1976). *Tropical Soils and Soil Survey*. University Press, Cambridge, p. 468.
- Yousefifard, M., Ayoubi, S., Jalalian, A., Khademi, H., and Makkizadeh, M. (2012). Mass balance of major elements in relation to weathering in soils developed on igneous rocks in a Semiarid Region, Northwestern Iran. *J. Mt. Sci.*, 9: 41–58.
- Yousuf, T. S., Hossain, M. E., Afsar, M. Z., and Osman, K. T. (2019). Phosphate Sorption indices as Affected by the Calcareousness of Soils. 28(1): 93-110.
- Zabala, S.M., Conconi, M.S., Alconada, M., and Sanchez, R.M. (2007). The Rietveld method applied to the quantitative mineralogical analysis of some soil samples from Argentina. *Ciencia del suelo*, 25 (1): 65-73.
- Zhao, G., Cawood, P.A., Wilde, S.A., and Sun, M. (2002). Review of global 2.1–1.8 Ga orogens: implications for a pre-Rodinia supercontinent. *Earth-Sci. Rev.* 59: 125 – 162.
- Zimmermann, F.J. (2004). *Estatística aplicada à experimentação agrícola*. 2a ed. Santo Antônio de Goiás: Embrapa Arroz e Feijão.

APPENDICES

Appendix 4.1: Position and assignment of IR bands of the soil kaolins and theoretical kaolinite.

Basalt

Theoretical Kaolinite	S1 0-20	S1 20-50	S1 50-100	S2 0-20	S2 20-50	S2 50-100	S3 0-20	S3 20-50	S3 50-100	Assignment
3691 - 89	-	-	-	-	3692	-	-	3692	-	Al---O-H stretching of inner surface hydroxyl groups
3669	-	-	-	-	-	-	-	-	-	Al---O-H stretching of inner surface hydroxyl groups
3651	-	-	-	-	-	-	-	-	-	Al---O-H stretching of inner surface hydroxyl groups
3619	-	-	-	-	3620	-	-	3625	-	Al---O-H stretching of inner hydroxyl groups
1115 - 14	1114	-	-	-	-	-	-	-	1114	Si-O stretching (Longitudinal mode)
1028 - 27	1043	1043	1043	1043	1043	1043	1043	1043	1043	In-plane Si-O stretching
1005 - 04	1007	1007	1007	1007	1000	998	1007	1000	1007	In-plane Si-O stretching
912	907	907	910	907	907	903	907	903	907	OH deformation of inner surface hydroxyl groups
789 - 788	-	-	-	-	-	-	-	791	-	OH deformation of inner hydroxyl groups
751 - 750	-	-	-	-	-	-	-	746	-	OH deformation linked to Al, Mg
541	-	543	-	-	543	543	543	543	543	Si-O perpendicular Fe-O, Fe ₂ O ₃ , Ti-O; Si-O-Al stretching

Granite

Theoretical Kaolinite	MAT1 0-20	MAT1 20-50	MAT2 0-20	MAT2 20-50	MAT3 0-20	MAT3 20-50	Assignment
3691 - 89	3683	-	3683	-	3683	-	Al---O-H stretching of inner surface hydroxyl groups
3669	3689	-	3663	-	3663	-	Al---O-H stretching of inner surface hydroxyl groups
3651	3647	-	3640	-	3641	-	Al---O-H stretching of inner surface hydroxyl groups
3619	3620	-	3620	-	3620	-	Al---O-H stretching of inner hydroxyl groups
1115 - 14	1107	-	1107	-	1107	-	Si-O stretching (Longitudinal mode)
1028 - 27	1025	1037	1025	-	1025	-	In-plane Si-O stretching
1005 - 04	1000	1000	1000	-	1000	-	In-plane Si-O stretching
937 - 935	936	-	936	-	935	-	OH deformation of inner surface hydroxyl groups
912	907	-	905	-	905	-	OH deformation of inner hydroxyl groups
789 - 788	791	-	790	-	791	-	OH deformation linked to Al, Mg
751 - 750	749	-	749	-	749	-	Si-O perpendicular
541	525	-	530	-	525	-	Fe-O, Fe ₂ O ₃ , Ti-O; Si-O-Al stretching

Arkosic Sandstone

Theoretical Kaolinite	SA1 0-20	SA1 20-50	SA2 0-20	SA2 20-50	SA3 0-20	SA3 20-50	Assignment
3691 - 89	3684	3684	3684	-	-	-	Al---O-H stretching of inner surface hydroxyl groups
3669	3670	3670	3670	-	-	-	Al---O-H stretching of inner surface hydroxyl groups
3651	3645	-	-	-	-	-	Al---O-H stretching of inner surface hydroxyl groups
3619	3620	3620	3620	-	-	-	Al---O-H stretching of inner hydroxyl groups
1115 - 14	1114	1114	1114	-	-	-	Si-O stretching (Longitudinal mode)
1028 - 27	1025	1025	1025	-	-	-	In-plane Si-O stretching
1005 - 04	1000	999	998	-	-	-	In-plane Si-O stretching
937 - 935	936	936	936	-	-	-	OH deformation of inner surface hydroxyl groups
912	913	913	913	-	-	-	OH deformation of inner hydroxyl groups
789 - 788	793	793	793	-	-	-	OH deformation linked to Al, Mg
751 - 750	743	743	743	-	-	-	Si-O perpendicular
541	525	530	525	-	-	-	Fe-O, Fe ₂ O ₃ , Ti-O; Si-O-Al stretching

Gneiss and Quartzite

Theoretical Kaolinite	MU1 0-20	MU2 0-20	MU3 0-20	CMA 0-20	CMA 20-50	Assignment
3691 - 89	-	-	-	-	-	Al---O-H stretching of inner surface hydroxyl groups
3669	-	-	-	-	-	Al---O-H stretching of inner surface hydroxyl groups
3651	-	-	-	-	-	Al---O-H stretching of inner surface hydroxyl groups
3619	-	-	-	-	-	Al---O-H stretching of inner hydroxyl groups
1115 - 14	1100	-	-	-	-	Si-O stretching (Longitudinal mode)
1028 - 27	1037	1037	1037	1045	1040	In-plane Si-O stretching
1005 - 04	1001	1001	1000	1007	-	In-plane Si-O stretching
912	907	-	907	911	-	OH deformation of inner surface hydroxyl groups
789 - 788	788	-	-	786	-	OH deformation linked to Al, Mg
751 - 750	751	-	-	750	-	Si-O perpendicular
541	514	514	514	514	514	Fe-O, Fe ₂ O ₃ , Ti-O; Si-O-Al stretching

Appendix 7.1: Phosphorus Adsorption Raw Data

Bulk Soils

Parent Rock	Sample ID	IC	C	PA	IC	C	PA	IC	C	PA	IC	C	PA	IC	C	PA
Basalt	S1 0-20 cm	0	0	0	20	0.5	19.5	40	8.2	31.8	60	21.1	38.9	80	35.1	44.9
	S2 0-20 cm	0	0	0	20	0.6	19.4	40	9.1	30.9	60	24.2	35.8	80	39.1	40.9
	S3 0-20 cm	0	0	0	20	0.5	19.5	40	7.1	32.9	60	19.1	40.9	80	31.3	48.7
Granite	MAT1 0-20 cm	0	0	0	20	9.1	10.9	40	20.3	19.7	60	41.3	18.7	80	67.4	12.6
	MAT2 0-20 cm	0	0	0	20	8.9	11.1	40	18.1	21.9	60	36.1	23.9	80	69.1	10.9
	MAT3 0-20 cm	0	0	0	20	9	11	40	23.4	16.6	60	42.4	17.6	80	71.3	8.7
Arkoscic Sandstone	SA1 0-20 cm	0	0	0	20	9.7	10.3	40	26.1	13.9	60	46.3	13.7	80	70.1	9.9
	SA2 0-20 cm	0	0	0	20	9.4	10.6	40	21.1	18.9	60	43.4	16.6	80	68.3	11.7
	SA3 0-20 cm	0	0	0	20	9.6	10.4	40	23.3	16.7	60	41.4	18.6	80	66.4	13.6
Gneiss	MU1 0-20 cm	0	0	0	20	6.6	13.4	40	16.2	23.8	60	42.5	17.5	80	69.5	10.5
	MU2 0-20 cm	0	0	0	20	6.8	13.2	40	19.3	20.7	60	44.3	15.7	80	67.6	12.4
	MU3 0-20 cm	0	0	0	20	6.5	13.5	40	18.1	21.9	60	42.3	17.7	80	65.3	14.7
Quartzite	CMA 0-20 cm	0	0	0	20	4.2	15.8	40	15.6	24.4	60	37.4	22.6	80	66.1	13.9

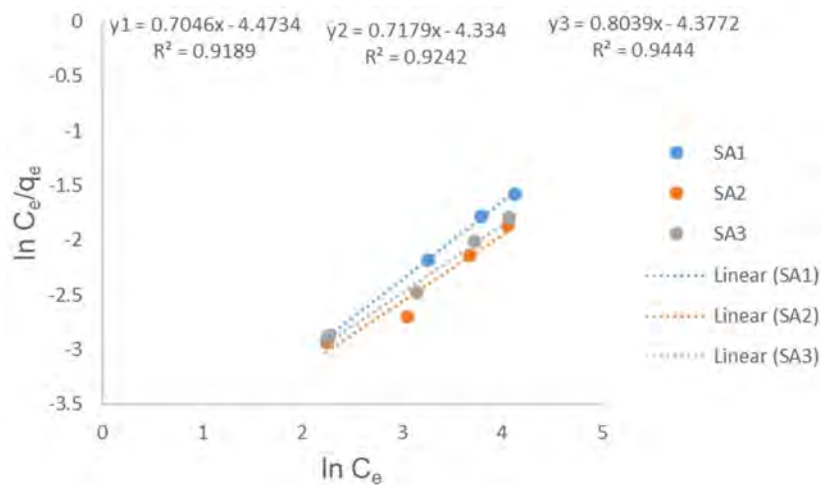
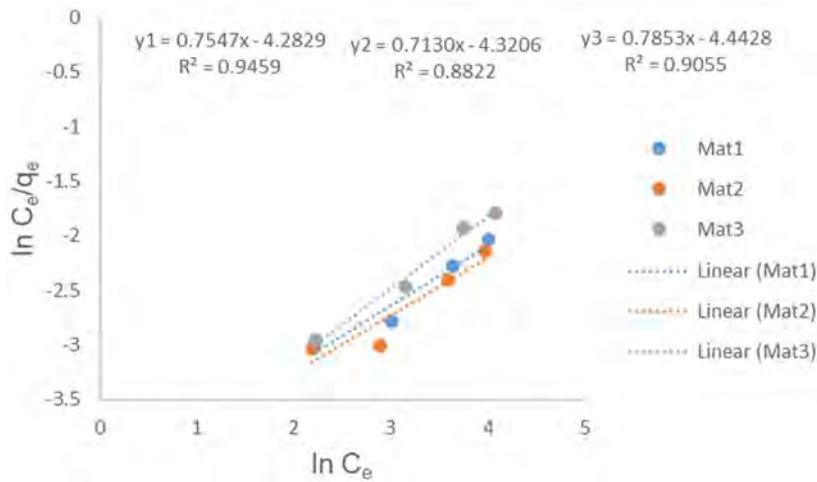
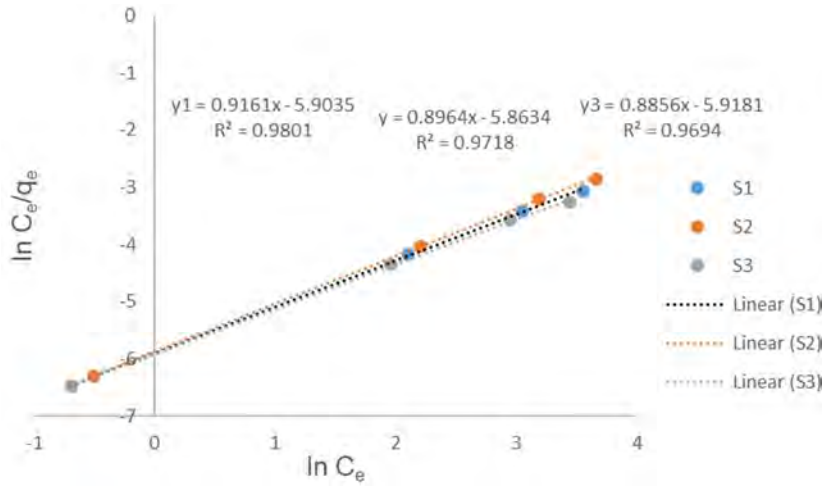
Where, IC = Initial P concentration in solution, C = P concentration left in solution at equilibrium, PA = Amount of P adsorbed.

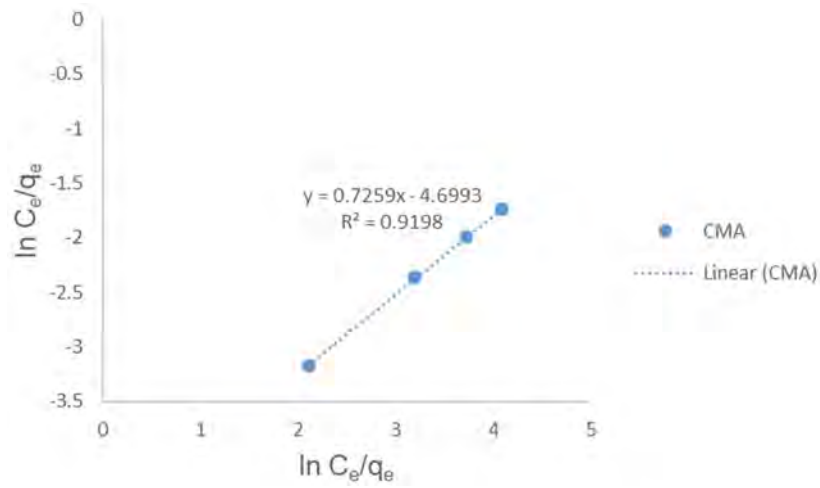
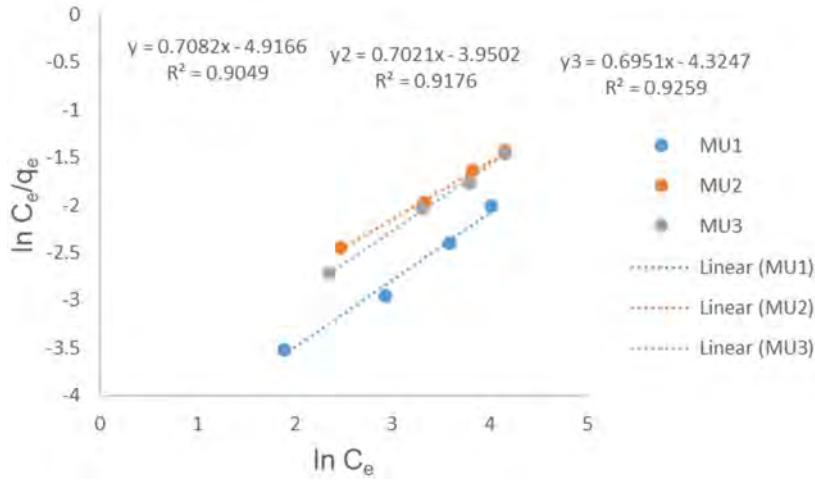
Soil Kaolins

Parent Rock	Sample ID	IC	C	PA	IC	C	PA	IC	C	PA	IC	C	PA	IC	C	PA
Basalt	S1 0-20 cm	0	0	0	20	1.2	18.8	40	11.1	28.9	60	37.1	22.9	80	42.1	37.9
	S2 0-20 cm	0	0	0	20	1.4	18.6	40	13.2	26.8	60	36.4	23.6	80	43.3	36.7
	S3 0-20 cm	0	0	0	20	1.1	18.9	40	11.6	28.4	60	36.1	23.9	80	42.4	37.6
Granite	MAT1 0-20 cm	0	0	0	20	3.7	16.3	40	24.2	15.8	60	47.3	12.7	80	66.2	13.8
	MAT2 0-20 cm	0	0	0	20	3.6	16.4	40	23.1	16.9	60	44.1	15.9	80	67.4	12.6
	MAT3 0-20 cm	0	0	0	20	3.6	16.4	40	24.5	15.5	60	46.3	13.7	80	69.1	10.9
Arkositic Sandstone	SA1 0-20 cm	0	0	0	20	6.8	13.2	40	27.3	12.7	60	47.4	12.6	80	70.3	9.7
	SA2 0-20 cm	0	0	0	20	6.6	13.4	40	27.1	12.9	60	48.2	11.8	80	72.3	7.7
	SA3 0-20 cm	0	0	0	20	6.8	13.2	40	26.4	13.6	60	46.1	13.9	80	71.1	8.9
Gneiss	MU1 0-20 cm	0	0	0	20	6.6	13.4	40	25.7	14.3	60	46.5	13.5	80	72.4	7.6
	MU2 0-20 cm	0	0	0	20	6.6	13.4	40	24.3	15.7	60	46.3	13.7	80	70.1	9.9
	MU3 0-20 cm	0	0	0	20	6.8	13.2	40	26.1	13.9	60	47.2	12.8	80	72.3	7.7
Quartzite	CMA 0-20 cm	0	0	0	20	5.7	14.3	40	23.2	16.8	60	42.1	17.9	80	63.1	16.9

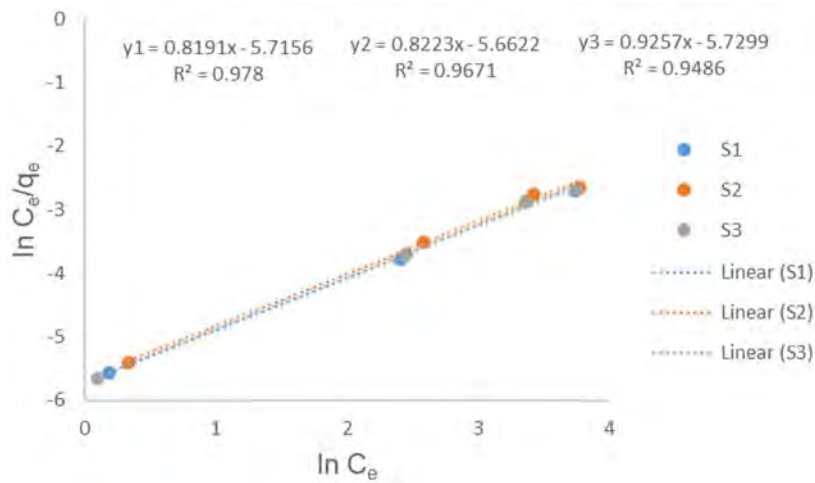
Appendix 7.2a: Redlich-Peterson Isotherm Plots

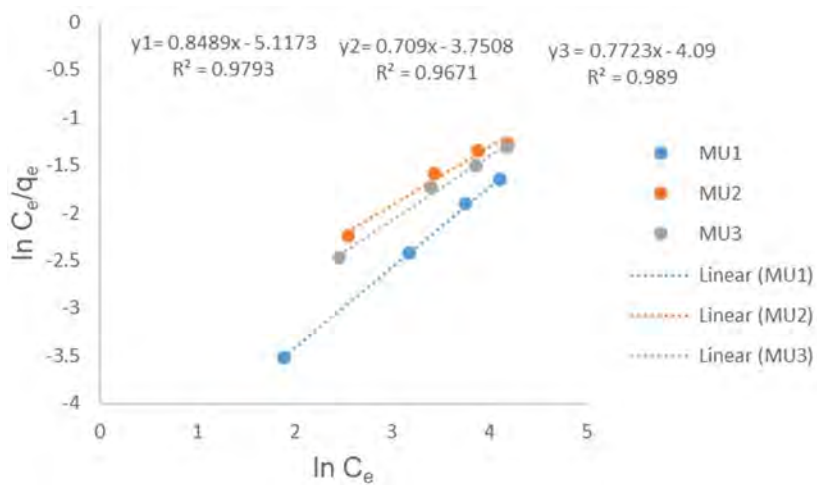
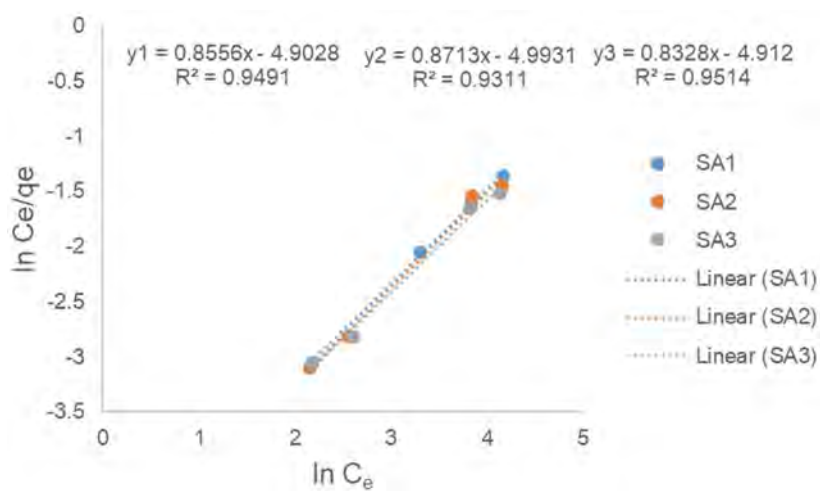
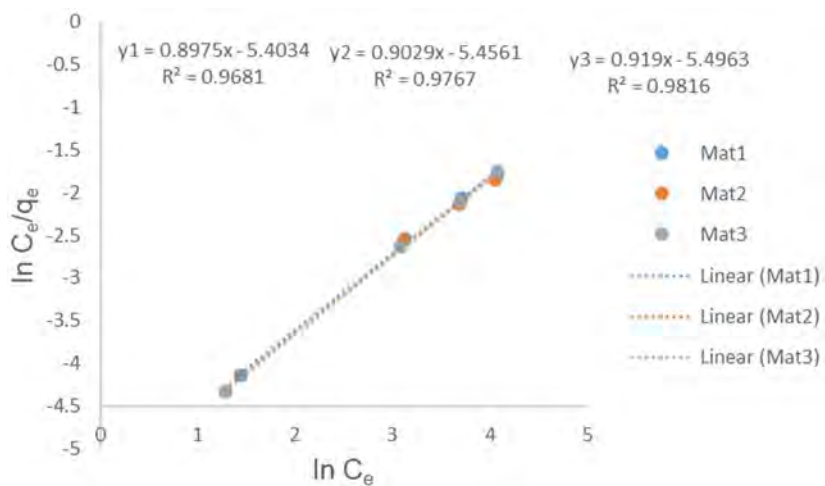
- Soils

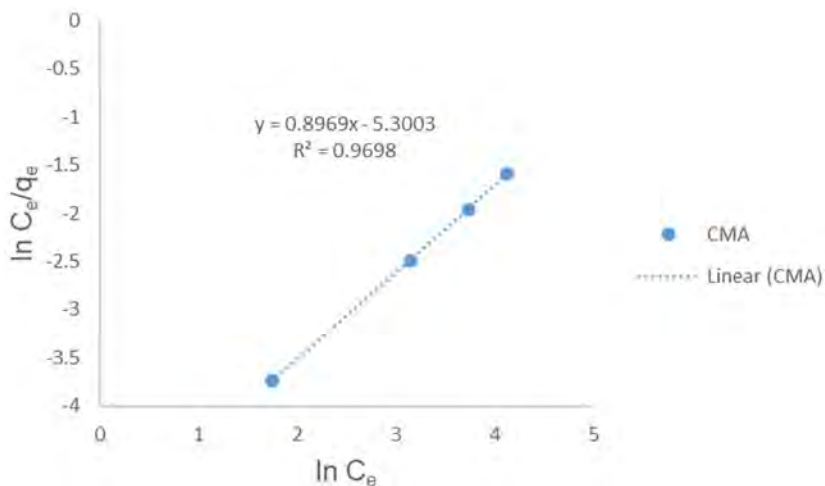




• **Soil kaolins**

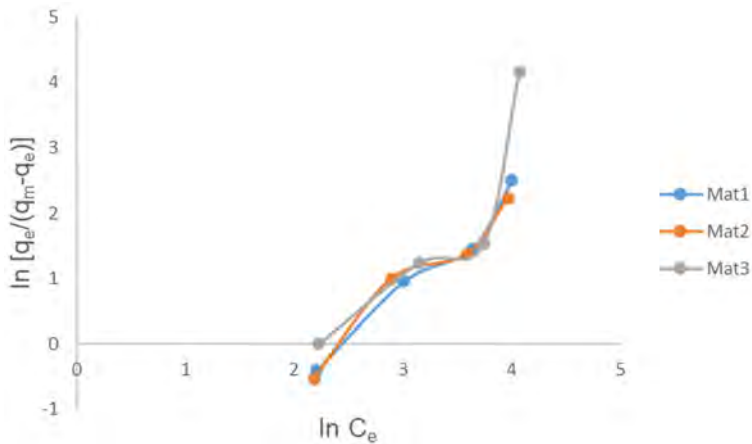
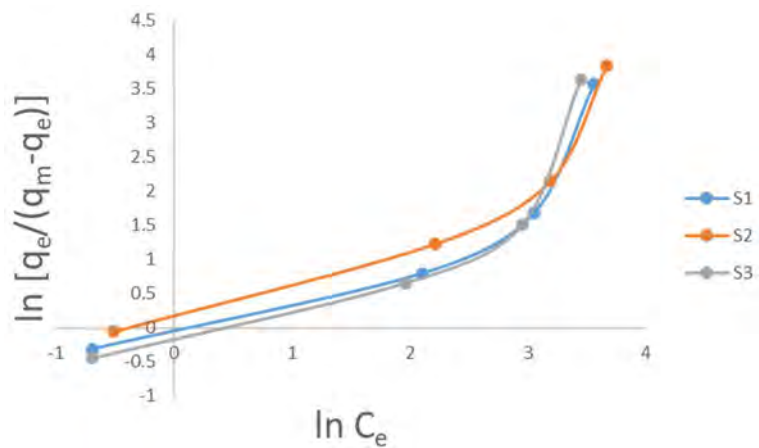


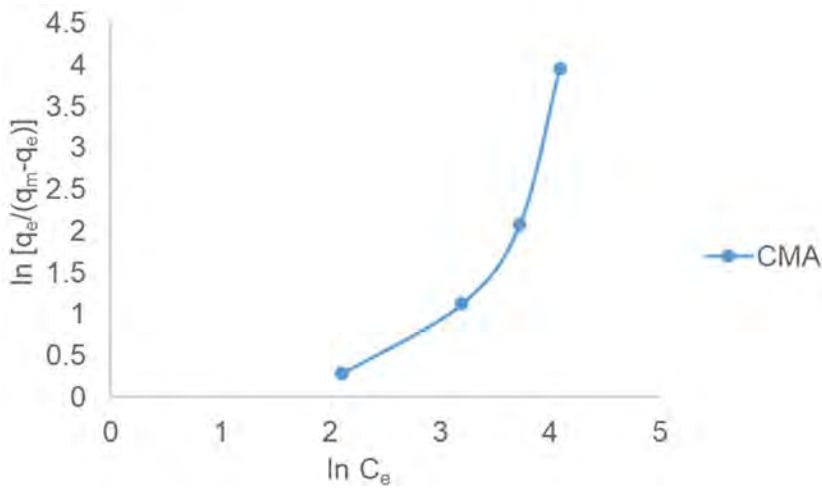
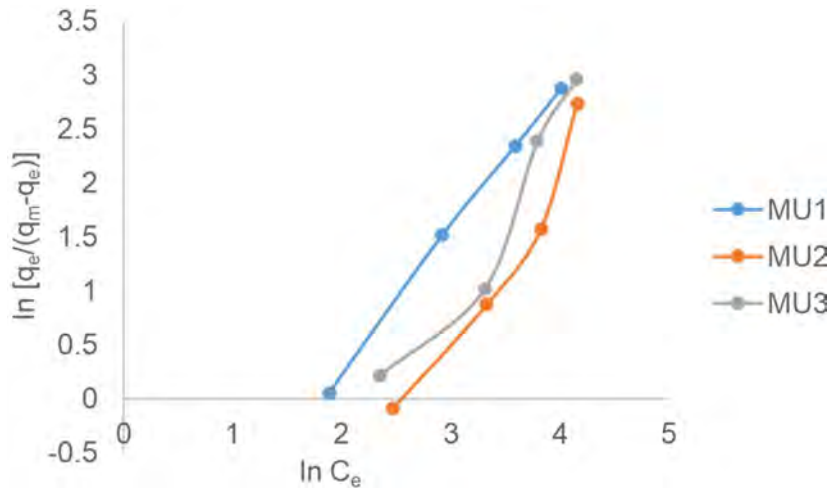
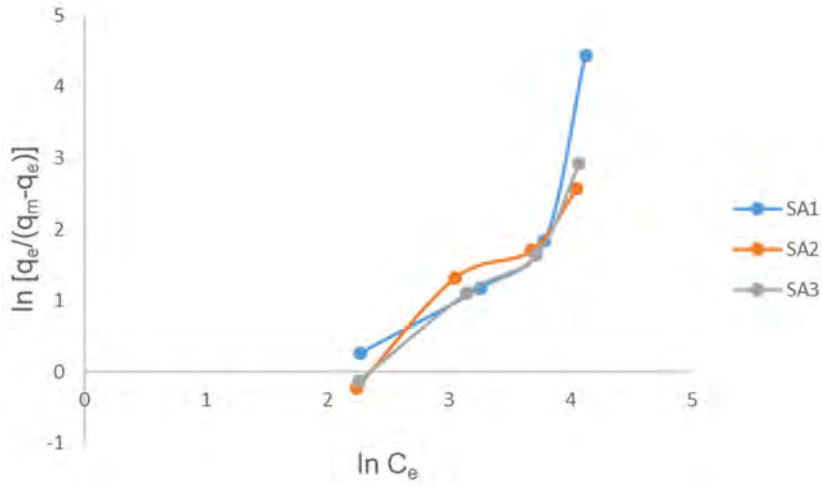




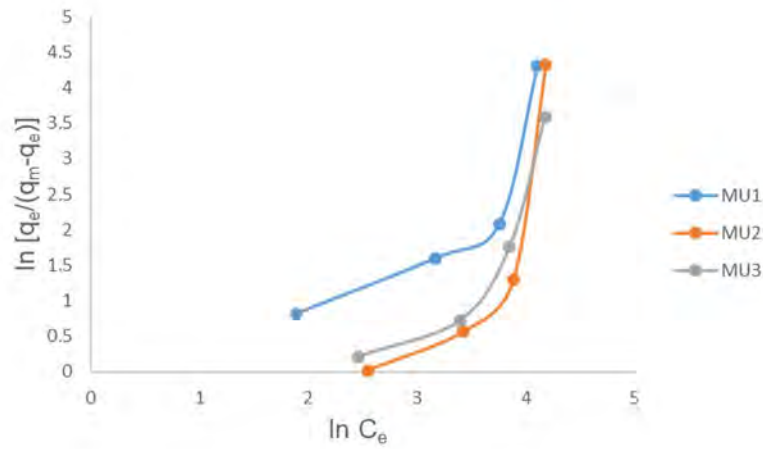
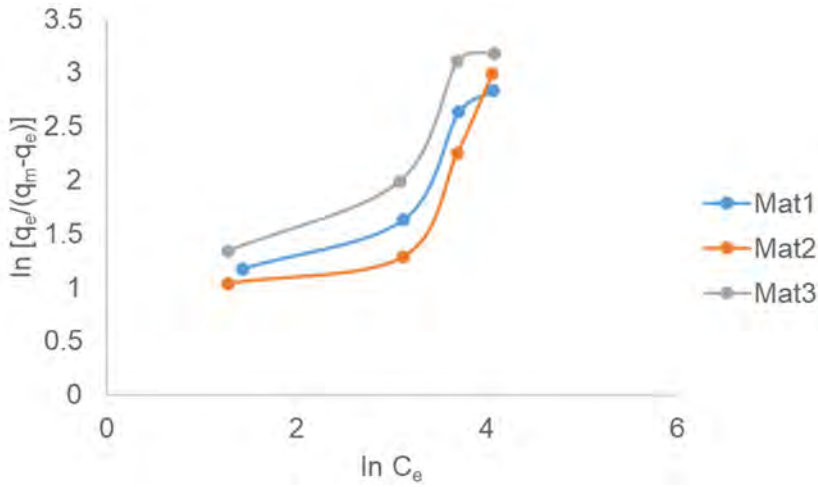
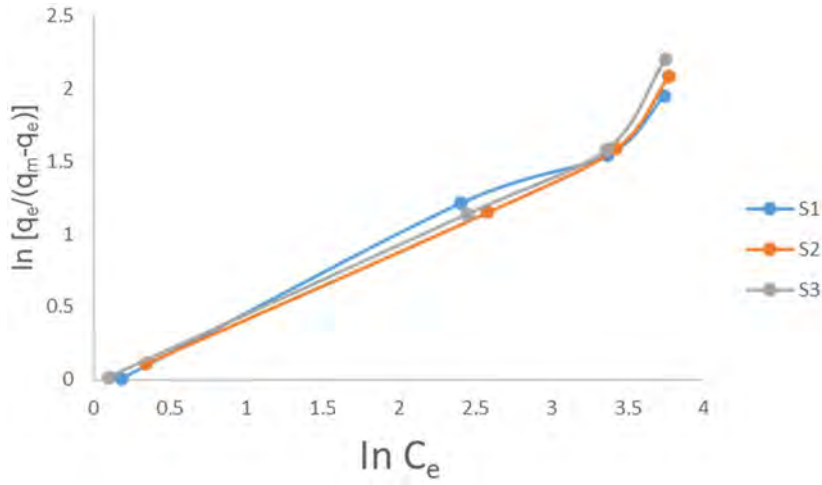
Appendix 7.2b: Sips Isotherm Plots

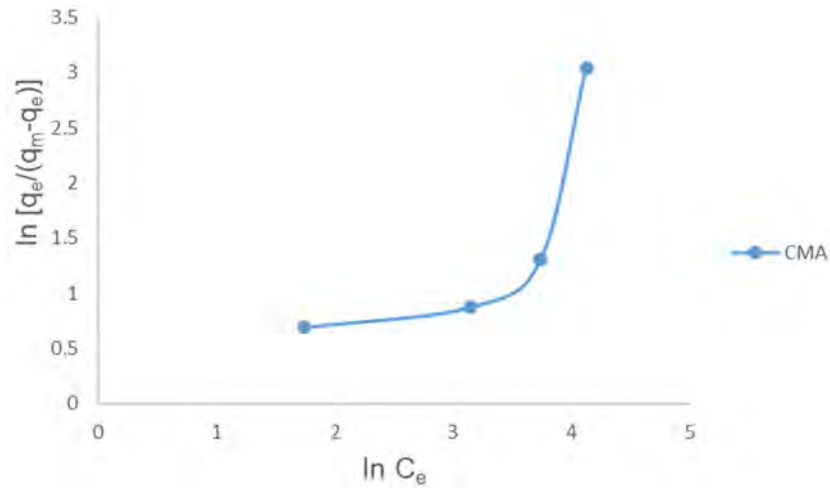
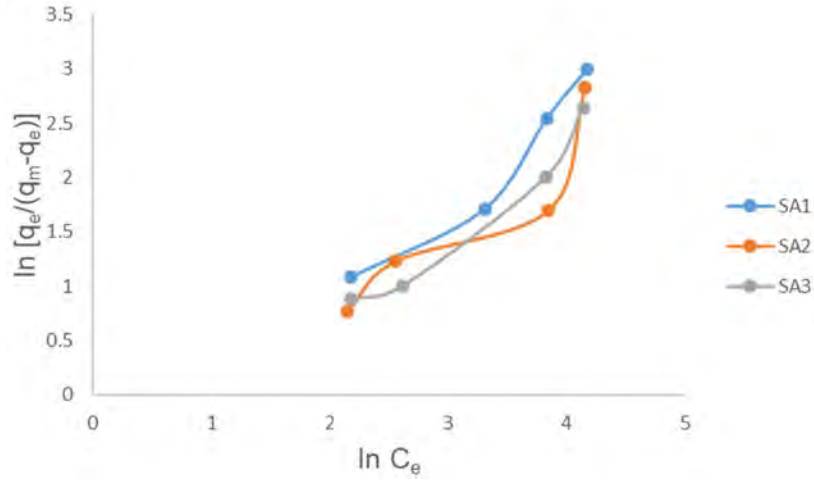
- Soils





- Soil kaolins





Research Outputs

Published

- OO Oyebanjo, GE Ekosse, and JO Odiyo (2020): Geochemistry of oxidic soils developed from different parent rocks in the Limpopo Province, South Africa. Transactions of the Royal Society of South Africa. DOI: 10.1080/0035919X.2020.1765430

Under Review

- Oyebanjo OO, Ekosse GE, and Odiyo JO. Kaolins in Tropical soils: A Review of their Mineralogy, Geochemistry, and implications on agriculture. Open Geosciences.
- Oyebanjo OO, Ekosse GE, and Odiyo JO. Mineralogy and Geochemistry of Clay Fractions and Nature of Soil Kaolins Developed from different Parent Rocks in Limpopo Province, South Africa. Heliyon
- Oyebanjo OO, Ekosse GE, and Odiyo JO. Phosphorus Sorption in Soils and Soil Kaolins Developed from different Parent Rocks in Limpopo Province, South Africa. African Journal of Science, Technology, Innovation and Development.

In Preparation

- Oyebanjo OO, Ekosse GE, and Odiyo JO. Properties of Oxidic Soils Developed from different Parent Rocks in Limpopo Province, South Africa: Implications on Fertility and Phosphorus Adsorption.

Conference

- Oyebanjo OO, Ekosse GE, and Odiyo JO (2016). Kaolins in Tropical Soils: Their Mineralogy. 2nd UNIVEN-WSU International Research Conference, Book of programme and abstracts, The Ranch Polokwane, South Africa, 5-7 October 2016.